Rev 4. (2)

MAR 26 1997

ENGINEERING DATA TRANSMITTAL

Page 1 of 1

1. EDT 607684

2. To: (Receiving Organization)	3. From: (Originating Organization)	4. Related EDT No.:
Functional Review Group	Nuclear Safety and Engineering	N/A
5. Proj./Prog./Dept./Div.:	6. Design Authority/ Design Agent/Cog. Engr.:	7. Purchase Order No.:
Spent Nuclear Fuel Project	B.D. Lorenz	N/A
8. Originator Remarks:		9. Equip./Component No.:
This document is being submitted to DOE-RL for review and approval.		N/A
		10. System/Bldg./Facility:
		N/A
11. Receiver Remarks: 11A. Design Baseline Document? [ ] Yes [X] No		12. Major Assm. Dwg. No.:
		N/A
		13. Permit/Permit Application No.:
		N/A
		14. Required Response Date:

15. DATA TRANSMITTED

(A) Item No.	(B) Document/Drawing No.	(C) Sheet No.	(D) Rev. No.	(E) Title or Description of Data Transmitted	(F) Approval Desig-nator	(G) Reason for Trans-mittal	(H) Origi-nator Dispo-sition	(I) Receiv-er Dispo-sition
1	~~WHC~~ HNF-SD-SNF-SARR-005		0	"Multicanister Overpack Topical Report"	E,S,Q	1	1	

16. KEY

Approval Designator (F)	Reason for Transmittal (G)	Disposition (H) & (I)
E, S, Q, D or N/A (see WHC-CM-3-5, Sec.12.7)	1. Approval 4. Review 2. Release 5. Post-Review 3. Information 6. Dist. (Receipt Acknow. Required)	1. Approved 4. Reviewed no/comment 2. Approved w/comment 5. Reviewed w/comment 3. Disapproved w/comment 6. Receipt acknowledged

17. SIGNATURE/DISTRIBUTION
(See Approval Designator for required signatures)

(G) Reason	(H) Disp.	(J) Name	(K) Signature	(L) Date	(M) MSIN	(G) Reason	(H) Disp.	(J) Name	(K) Signature	(L) Date	(M) MSIN
1	1	Design Authority LH Goldmann		12/23/96		1	1	Operations CA Thompson		12/20/96	
	1	RW Rasmussen		12/19/96		1	1	Sub Proj. Mgr. KE Smith		12/19/96	
1	1	Cog.Eng. BD Lorenz		12/19/96		1	1	Proj. Mgr. AS Daughtridge		12/19/96	
1	1	Cog. Mgr. LJ Garvin		12/19/96		1	2	Dsg. Authority GD Bazinet		12/19/96	
1	1	QA JI Diehl	DW Smith for	12/20/96		1	1	Sub Proj. Mgr. JE Filip		12/20/96	
1	1	Safety C. Defigh-Price		12/19/96		1	1	Dsg. Authority JJ Irwin		12/20/96	
1	1	Env. JE Turnbaugh		12/20/96		1	1	Dsg. Authority CR Miller		12/19/96	
1	2	FDH Oversight EJ Krejci		12/20/96		1	1	Sub Proj. Mgr. PW Bradshaw		12/20/96	

18.	19.	20.	21. DOE APPROVAL (if required) Ctrl. No.
Signature of EDT Originator — Date: 12.20.96	Authorized Representative for Receiving Organization — Date: 12/19/96	Design Authority/ Cognizant Manager — Date: 12/23/96	[ ] Approved [ ] Approved w/comments [ ] Disapproved w/comments

BD-7400-172-2 (05/96) GEF097 DISTRIBUTION Project Files R3-11

BD-7400-172-1 (07/91)

INSTRUCTIONS FOR COMPLETION OF THE ENGINEERING DATA TRANSMITTAL

(USE BLACK INK OR TYPE)

BLOCK	TITLE	
(1)*	EDT	• Pre-assigned EDT number.
(2)	To: (Receiving Organization)	• Enter the individual's name, title of the organization, or entity (e.g., Distribution) that the EDT is being transmitted to.
(3)	From: (Originating Organization)	• Enter the title of the organization originating and transmitting the EDT.
(4)	Related EDT No.	• Enter EDT numbers which relate to the data being transmitted.
(5)*	Proj./Prog./Dept./Div.	• Enter the Project/Program/Department/Division title or Project/Program acronym or Project Number, Work Order Number or Organization Code.
(6)*	Cognizant Engineer	• Enter the name of the individual identified as being responsible for coordinating disposition of the EDT.
(7)	Purchase Order No.	• Enter related Purchase Order (P.O.) Number, if available.
(8)*	Originator Remarks	• Enter special or additional comments concerning transmittal, or "Key" retrieval words may be entered.
(9)	Equipment/Component No.	• Enter equipment/component number of affected item, if appropriate.
(10)	System/Bldg./Facility	• Enter appropriate system, building or facility number, if appropriate.
(11)	Receiver Remarks	• Enter special or additional comments concerning transmittal.
(12)	Major Assm. Dwg. No.	• Enter applicable drawing number of major assembly, if appropriate.
(13)	Permit/Permit Application No.	• Enter applicable permit or permit application number, if appropriate.
(14)	Required Response Date	• Enter the date a response is required from individuals identified in Block 17 (Signature/Distribution).
(15)*	Data Transmitted	
	(A)* Item Number	• Enter sequential number, beginning with 1, of the information listed on EDT.
	(B)* Document/Drawing No.	• Enter the unique identification number assigned to the document or drawing being transmitted.
	(C)* Sheet No.	• Enter the sheet number of the information being transmitted. If no sheet number, leave blank.
	(D)* Rev. No.	• Enter the revision number of the information being transmitted. If no revision number, leave blank.
	(E) Title or Description of Data Transmitted	• Enter the title of the document or drawing or a brief description of the subject if no title is identified.
	(F)* Impact Level	• Enter the appropriate Impact Level (Block 15). Also, indicate the appropriate approvals for each item listed, i.e., SQ, ESQ, etc. Use NA for non-engineering documents.
	(G) Reason for Transmittal	• Enter the appropriate code to identify the purpose of the data transmittal (see Block 16).
	(H) Originator Disposition	• Enter the appropriate disposition code (see Block 16).
	(I) Receiver Disposition	• Enter the appropriate disposition code (see Block 16).
(16)	Key	• Number codes used in completion of Blocks 15 (G), (H), and (I), and 17 (G), (H) (Signature/Distribution).
(17)	Signature/Distribution	
	(G) Reason	• Enter the code of the reason for transmittal (Block 16).
	(H) Disposition	• Enter the code for the disposition (Block 16).
	(J) Name	• Enter the signature of the individual completing the Disposition 17 (H) and the Transmittal.
	(K)* Signature	• Obtain appropriate signature(s).
	(L)* Date	• Enter date signature is obtained.
	(M)* MSIN	• Enter MSIN. Note: If Distribution Sheet is used, show entire distribution (including that indicated on Page 1 of the EDT) on the Distribution Sheet.
(18)	Signature of EDT Originator	• Enter the signature and date of the individual originating the EDT (entered prior to transmittal to Receiving Organization). If the EDT originator is the cognizant engineer, sign both Blocks 17 and 18.
(19)	Authorized Representative for Receiving Organization	• Enter the signature and date of the individual identified by the Receiving Organization as authorized to approve disposition of the EDT and acceptance of the data transmitted, as applicable.
(20)*	Cognizant Manager	• Enter the signature and date of the cognizant manager. (This signature is authorization for release.)
(21)*	DOE Approval	• Enter DOE approval (if required) by letter number and indicate DOE action.

*Asterisk denote the required minimum items check by Configuration Documentation prior to release; these are the minimum release requirements.

Multicansiter Overpack Topical Report

B.D. Lorenz
DESH, Richland, WA 99352
U.S. Department of Energy Contract DE-AC06-96RL13200

EDT/ECN: 607684 UC: 2070
Org Code: 2T640 Charge Code: LE020
B&R Code: EW7040000 Total Pages: 914

Key Words: Multicanister Overpack (MCO), Topical

Abstract: The Spent Nuclear Fuel MCO is a single-use container that consists of a cylindrical shell, five to six fuel baskets, a shield plug, and features necessary for maintaining the structural integrity of the MCO while providing criticality control and fuel processing capability.

ABACUS is a trademark of Swanson Analysis Systems, Inc.

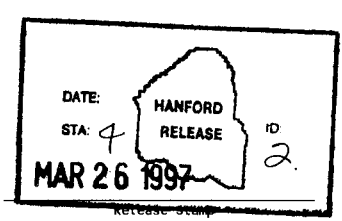

Release Approval 3/25/97 Date

Release Stamp

Approved for Public Release

CONTENTS

CONTENTS (Continued)

CONTENTS (Continued)

CONTENTS (Continued)

LIST OF FIGURES

LIST OF FIGURES (Continued)

LIST OF FIGURES (Continued)

LIST OF FIGURES (Continued)

LIST OF TABLES

LIST OF TABLES (Continued)

LIST OF TABLES (Continued)

LIST OF TERMS

ALARA	as low as reasonably achievable
CSB	Canister Storage Building
CVDF	Cold Vacuum Drying Facility
DBA	design basis accident
DOE	U.S. Department of Energy
HCS	Hot Conditioning System
HEPA	high-efficiency particulate air
HVAC	heating, ventilating, and air conditioning
LCO	limiting conditions for operation
MCO	multicanister overpack
MHM	multicanister overpack handling machine
MTU	metric ton of uranium
NCT	normal conditions of transport
NPH	natural phenomena hazard
NRC	U.S. Nuclear Regulatory Commission
PCB	polychlorinated biphenyl
PMF	probable maximum flood
PMP	probable maximum precipitation
SAR	safety analysis report
SARP	safety analysis report for packaging
SNF	spent nuclear fuel
SSC	structure, system, and component
SPR	single pass reactor
t	metric ton

This page intentionally left blank.

1.0 GENERAL DESCRIPTION

1.1 INTRODUCTION

In February 1995, the U.S. Department of Energy (DOE) approved the Spent Nuclear Fuel (SNF) Project's "Path Forward" recommendation for resolution of the safety and environmental concerns associated with the deteriorating SNF stored in the Hanford Site's K Basins (Hansen 1995). The recommendation included an aggressive series of projects to construct and operate systems and facilities to permit the safe retrieval, packaging, transport, conditioning, and interim storage of the K Basins' fuel. The facilities that are currently proposed include a Cold Vacuum Drying Facility (CVDF) in the 100 K Area of the Hanford Site and a Canister Storage Building (CSB) with a Hot Conditioning System (HCS) Annex in the 200 East Area. The intent is for the K Basins' SNF to be cleaned, repackaged in multicanister overpacks (MCOs), removed from the K Basins, and transported to the CVDF for initial drying. The MCOs would then be moved to the CSB for staging (short-term storage) before hot conditioning in the HCS Annex, followed by interim storage (40 to 75 years) in the CSB.

One of the major tasks associated with the Path Forward activities is the development and maintenance of the safety documentation. In addition to meeting the construction needs for no fewer than three new structures, the safety documentation for each must be generated. A common thread that was found to run among and between each of the structures was the MCO. Each of the structures will exist for the specific purpose of accommodating the MCO and its contents in one way or another. This would normally result in an extensive amount of MCO documentation being generated for each of the facility reports. However, the expedited schedule for removing spent fuel from the K Basins requires that effort be minimized and repetitious activities be eliminated. Therefore, a topical report is being prepared to address those aspects of the MCO that will be of interest to each of the facilities. In this way, the MCO may be included in each facility's safety documentation by reference for all but the facility-specific aspects associated primarily with accident analyses and handling. By capturing the design of the MCO in a single document, repetition, inconsistency, and duplication of effort may be minimized. As changes are made to the MCO, only a single report may need to be updated. By submitting the topical report for early review and approval, it may be possible to eliminate one step in the final review process.

The topical report approach is not new. The U.S. Nuclear Regulatory Commission (NRC) has used a Topical Report Program for quite some time, primarily for the review and approval of hardware, methodology, or analysis codes that vendors propose to market to a number of different customers. The concept is simple: review and approve once and incorporate by reference thereafter. Such an application can represent significant savings in the preparation of the Path Forward safety documentation.

Very little substantive guidance relative to the design or fabrication of the primary storage container was found in Title 10, *Code of Federal Regulations*, Part 72, "Licensing Requirements for the Independent Storage of Spent Nuclear Fuel and High-Level Radioactive Waste" (10 CFR 72), or in Regulatory Guide 3.48, *Standard Format and Content for the Safety Analysis Report for an Independent Spent Fuel Storage Installation or Monitored Retrievable Storage Installation (Dry Storage)* (NRC 1989b). However, NRC Regulatory Guide 3.61, *Standard Format and Content for a Topical Safety*

Analysis Report for a Spent Fuel Dry Storage Cask (NRC 1989a), contains a significant amount of guidance that is appropriate for the MCO. Regulatory Guide 3.61 (NRC 1989a) therefore has been used in preparing format and content guidance for the MCO Topical Report. Direct applicability to the MCO is not anticipated in all areas. Regulatory Guide 3.61 (NRC 1989a) deals with a dry storage cask design that is very much a complete system by itself. The MCO, however, never functions independently, as it is continually dependent upon other systems or facility features. Despite the differences, the regulatory guide does provide the most direct guidance of any of the documents reviewed. A topical report prepared utilizing such guidance, and incorporating pertinent modifications that will undoubtedly be forthcoming throughout the process, should result in a referenceable source of MCO-related information.

1.2 GENERAL DESCRIPTION OF THE MULTICANISTER OVERPACK

The SNF MCO is a single-use container that consists of a cylindrical shell, five to six fuel baskets, a shield plug, and features necessary for maintaining the structural integrity of the MCO while providing criticality control and fuel processing capability. These structural features are depicted in Figure 1-1.

The safety basis of the MCO is to provide required confinement and containment of SNF and to maintain the SNF in a critically safe configuration. The MCO provides "confinement" when it is vented and "containment" when it is sealed. The MCO's structural design has been developed to meet the intent of the *Boiler and Pressure Vessel Code* (ASME 1995a), Section III, "Rules for Construction of Nuclear Power Plant Components," Subsection NB. Any deviations from these rules in the structural design or analyses are documented and justified. NRC requirements for a 10 CFR 72 licensed facility would allow for application of either Subsection NB or NC (NRC 1996), 3.IV.1.b(1)(b)) of the Boiler and Pressure Vessel Code (ASME 1995a).

1.2.1 Shell

The MCO shell is a stainless steel cylindrical vessel with access at the top end that is closed with a carbon steel shield plug. The shell is fabricated from 61-cm- (24-in.-) diameter, schedule 80S pipe with a wall thickness of 1.3 cm (0.5 in.) (Figure 1-2), and it has an overall length of 406 cm (160 in.). The MCO cavity is approximately 58 cm (23 in.) in diameter and 368 cm (145 in.) long. The MCO has a forged bottom closure plate that has a constant thickness of 4.45 cm (1.75 in.) except in the center region, where it is 2.2 cm (0.88 in.) thick (Figure 1-3). The MCO's bottom plate and basket support plates allow free water to move to the long process tube pickup point for removal. The vessel holds the fuel, fuel fragments, fuel baskets, and incidental equipment. Incidental equipment includes criticality control features such as the support tube nesting feature on the shield plug and bottom plate, two process tubes connected to shield plug process ports, and sealing features. The design of the MCO vessel meets service level A requirements for normal operating loads and service level D requirements for accident conditions under the Boiler and Pressure Vessel Code, Section III, Subsection NB (ASME 1995a). The MCO specification conservatively requires all normal and off-normal conditions to meet service level A allowable limits, which are more stringent than service level B or C allowable limits.

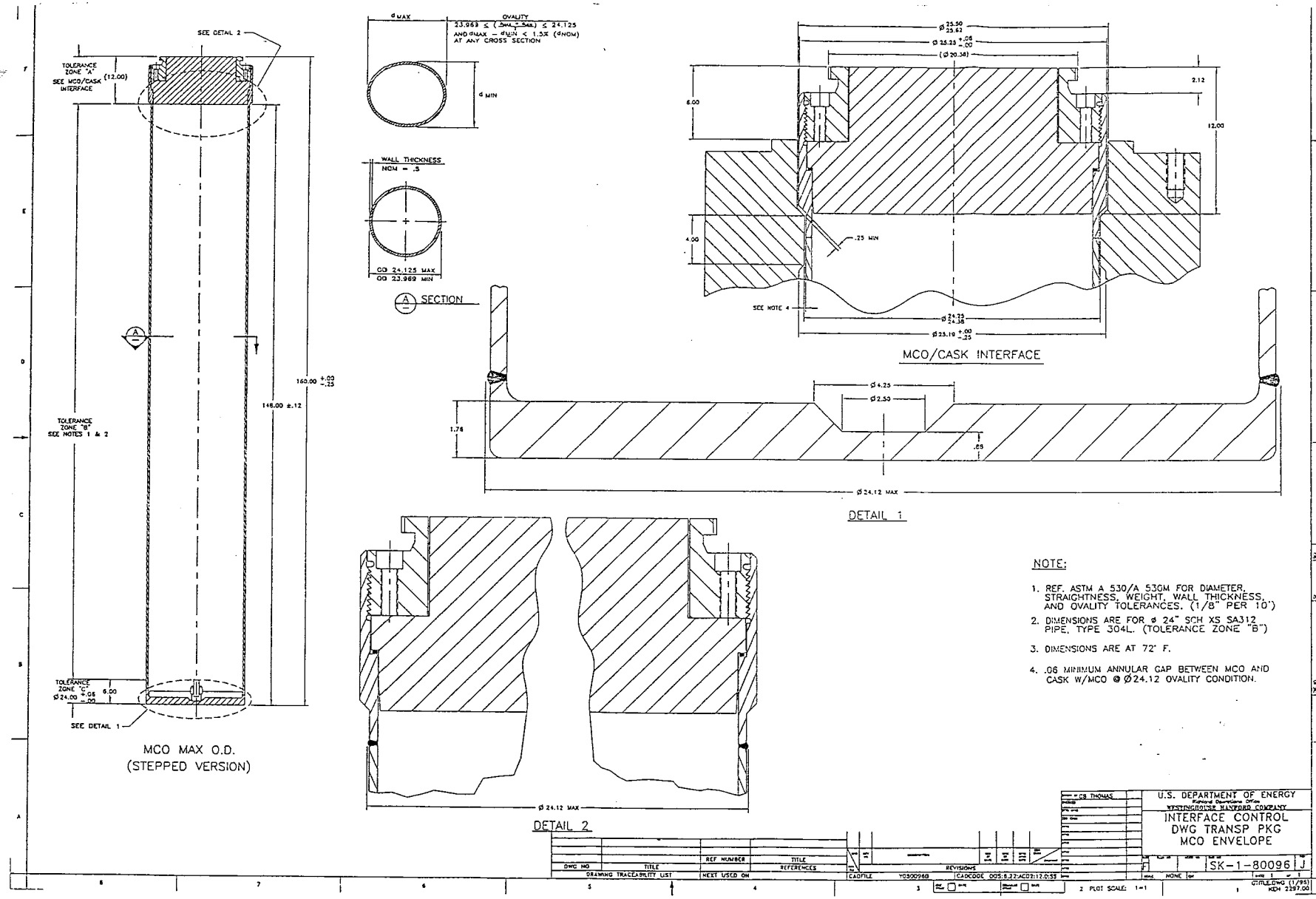

Figure 1-1. Multicanister Overpack.

THIS PAGE INTENTIONALLY
LEFT BLANK

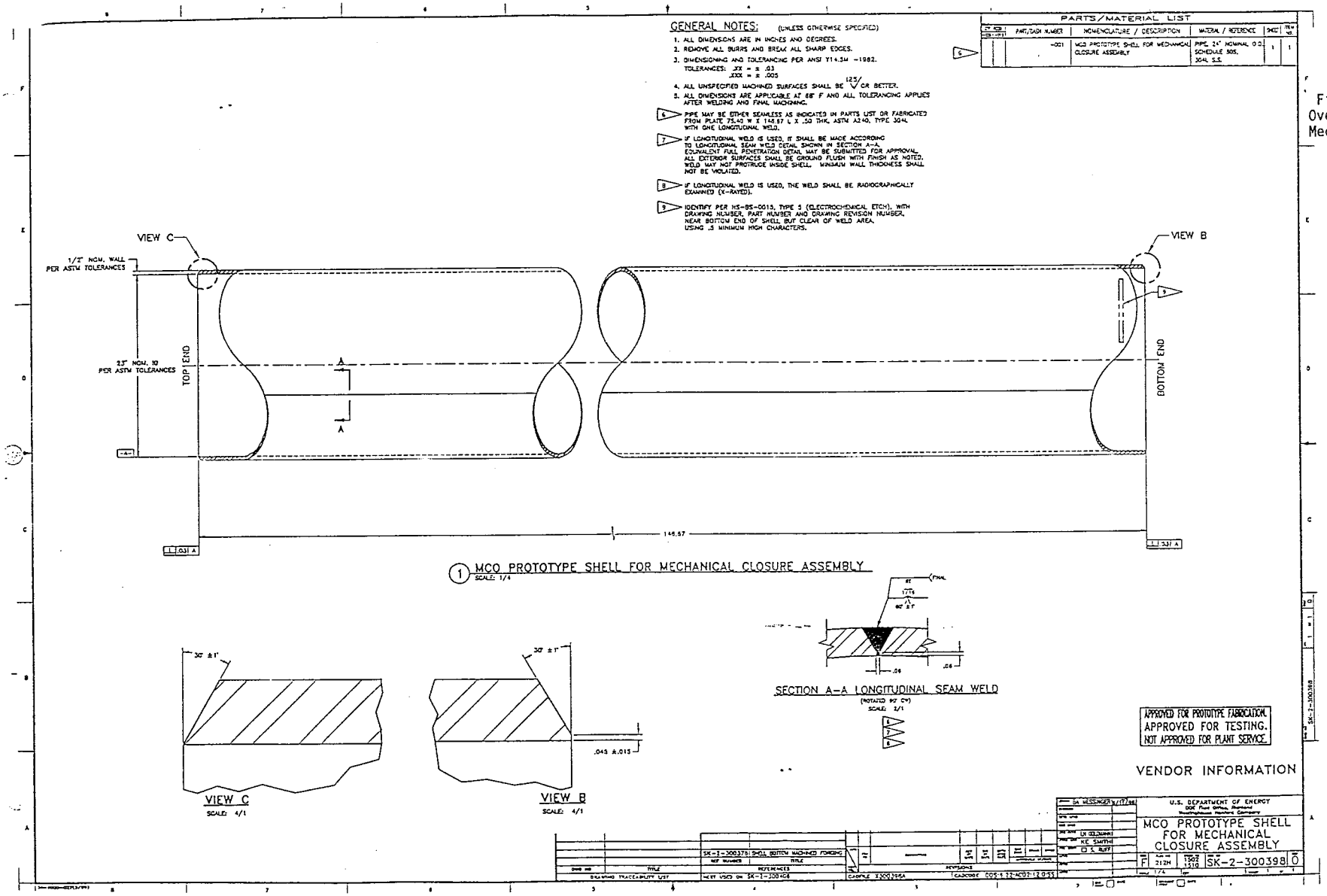

Figure 1-2. Multicanister Overpack Prototype Shell for Mechanical Closure Assembly.

THIS PAGE INTENTIONALLY
LEFT BLANK

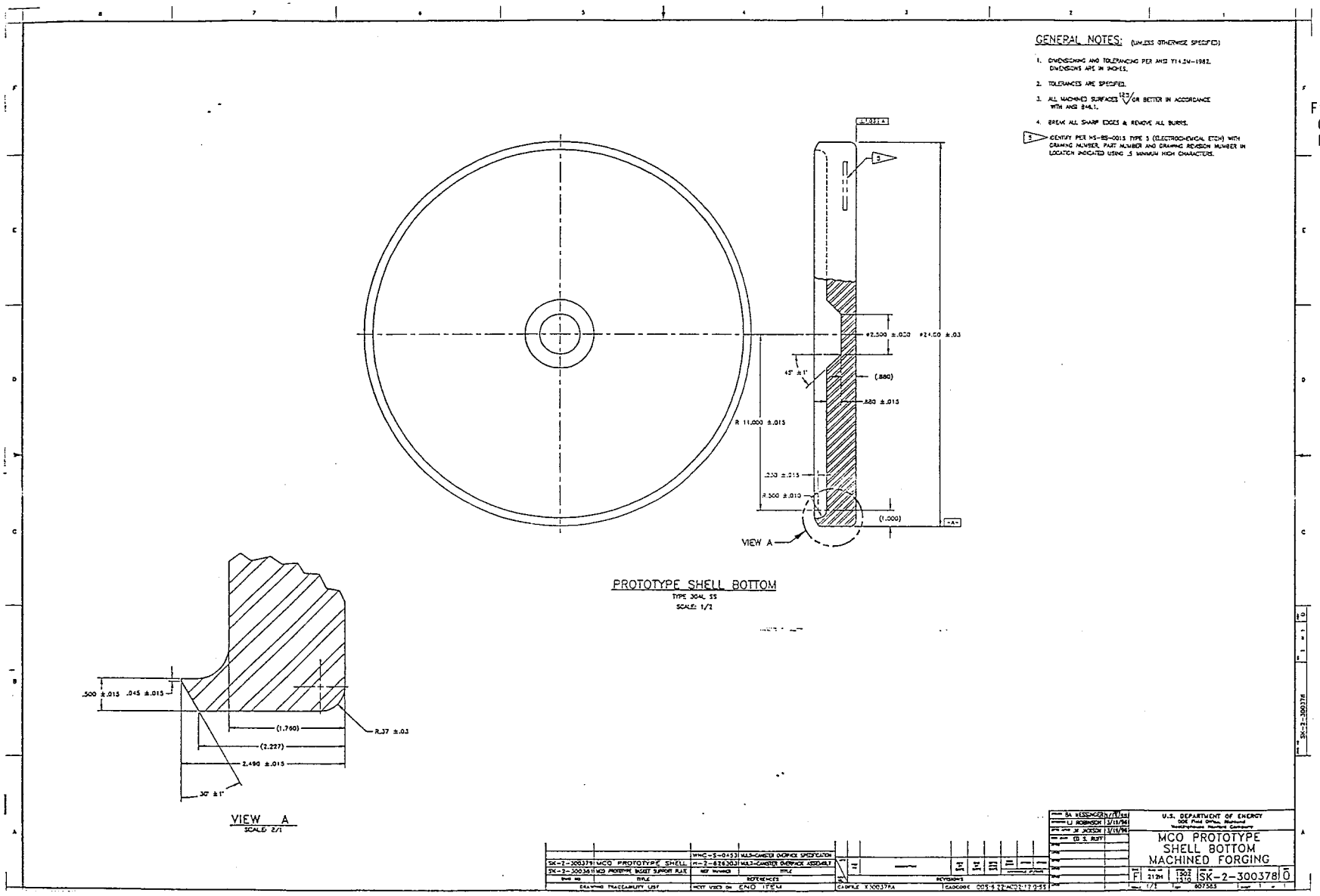

Figure 1-3. Multicanister Overpack Prototype Shell Bottom Machined Forging.

THIS PAGE INTENTIONALLY
LEFT BLANK

1.2.2 Fuel Baskets

All baskets are annular open-top containers with a maximum outer dimension of 57.5 cm (22.6 in.) at 25 °C (77 °F). All baskets will support the fuel at 1.0 *g* while at 375 °C (700 °F). All basket designs incorporate a center support tube for axial support during lifting and for protection of a long process tube.

Each basket is loaded, in the upright position, by the fuel retrieval system equipment in the K Basin pool; stored, still upright, in a loading queue; and loaded into the MCO. The loaded baskets can be easily and safely handled in the basin water, reliably loaded and nested into the cask-MCO assembly in the K Basin load-out pits, and engaged with the shield plug shield/guard plate and axial stabilizer (the shield plate and stabilizer are not pictured in Figure 1-1).

The baskets stack inside the MCO with the baskets' centerlines coincident with the MCO's centerline. While stacked inside the MCO, the baskets provide for insertion of a long process tube down the MCO centerline for water draining and gas transport, as needed. The baskets can drain freely and will not capture or retain excessive water during bulk water removal at the CVDF.

Basket design accounts for differential thermal expansion when subjected to processing temperatures inside the MCO. The baskets support heat transfer into and out of the fuel while in the gaseous and vacuum environments inside the MCO. The primary heat transfer modes are radiation and conduction during the static (storage/staging) state. Forced flow (convective) cooling of the fuel in the MCO baskets (particularly the scrap baskets) is a very large and essential component of heat transfer during the hot conditioning process and is facilitated by the basket design.

The baskets support the gas flows needed to properly dry and condition intact fuel and scrap fuel during the vacuum drying and hot conditioning processes. The baskets are compatible with the fuel and the MCO containment materials during the expected temperatures, pressures, and atmospheres inside the MCO during handling, shipping, storage, and processing.

The MCO fuel baskets are categorized into two major types: intact fuel element baskets and scrap fuel (fragment) baskets (Figures 1-4 through 1-7 [the grapples are not shown as they will be one-piece construction in combination with the basket structure and will nest with adjoining baskets]). The Mark IA fuel and scrap baskets meet the intent of the Boiler and Pressure Vessel Code, Section III, Subsection NG (ASME 1995a) under the component safety group as guided by the NUREG/CR 3854, *Fabrication Criteria for Shipping Containers* (NRC 1984). The design is being finalized and exceptions are not expected. Mark IA fuel has a higher ^{235}U enrichment than Mark IV fuel. Structural integrity is required of the Mark IA basket for criticality control whereas structural integrity is not required for the Mark IV fuel basket. Therefore, the more stringent Section III, Subsection NG requirements (ASME 1995a) are applied to the construction of the Mark IA fuel and scrap baskets. The grapple mating features and basket interface features, however, are not designed to Subsection NG (ASME 1995a) requirements.

This page intentionally left blank.

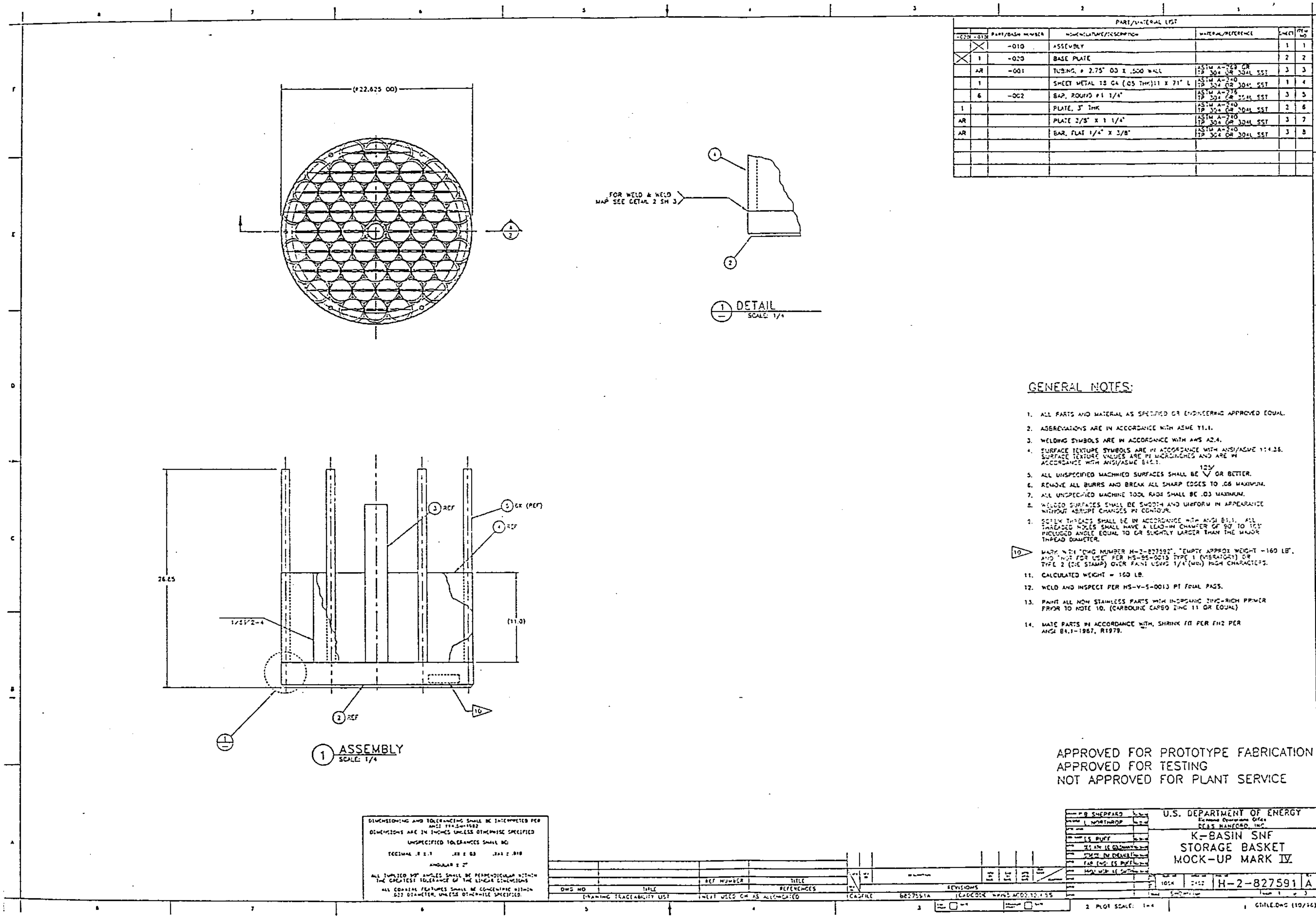

Figure 1-4. K Basin Spent Nuclear Fuel Storage Basket Mock-Up Mark IV. (3 sheets)

THIS PAGE INTENTIONALLY
LEFT BLANK

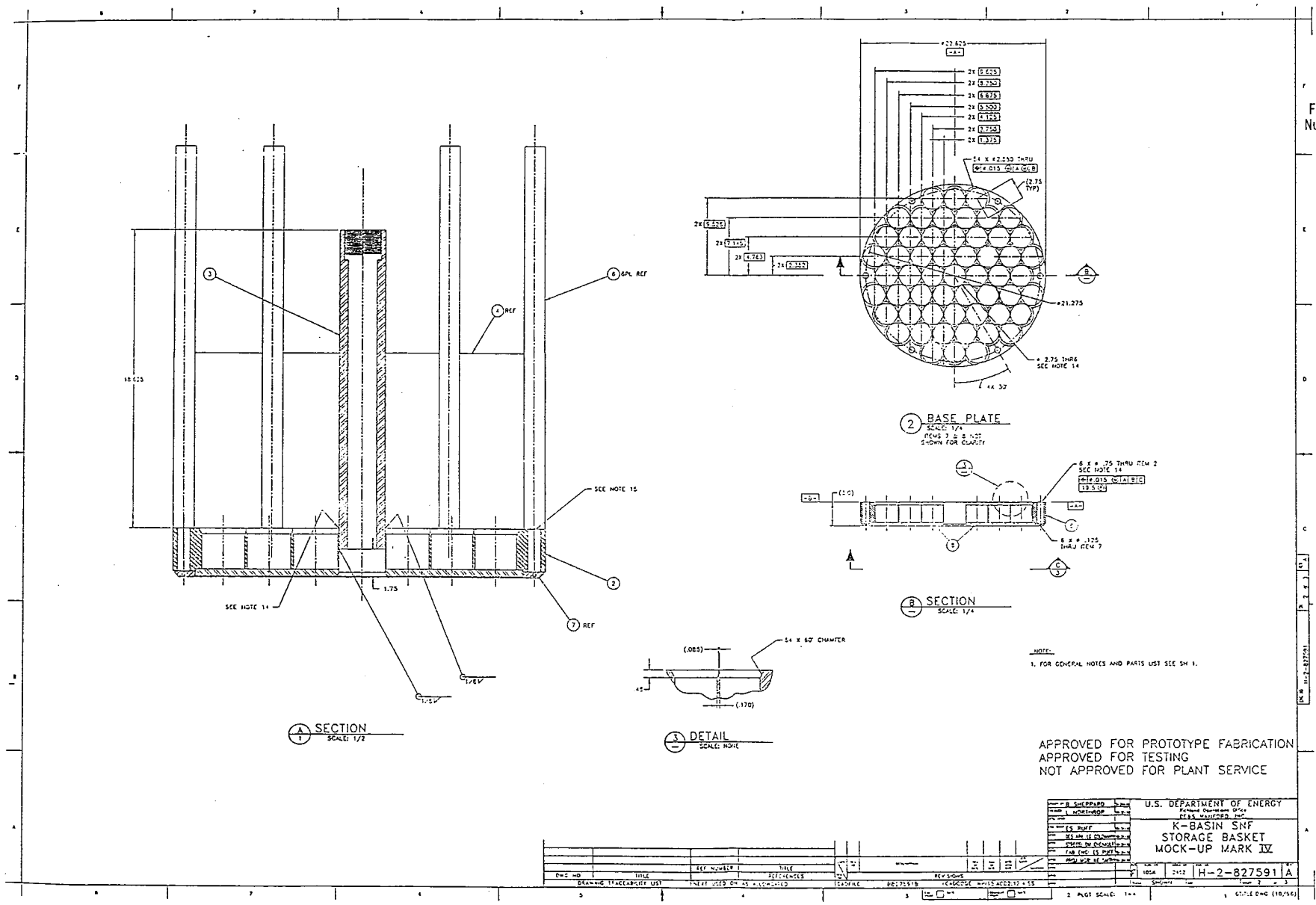

Figure 1-4. K Basin Spent Nuclear Fuel Storage Basket Mock-Up Mark IV. (3 sheets)

THIS PAGE INTENTIONALLY
LEFT BLANK

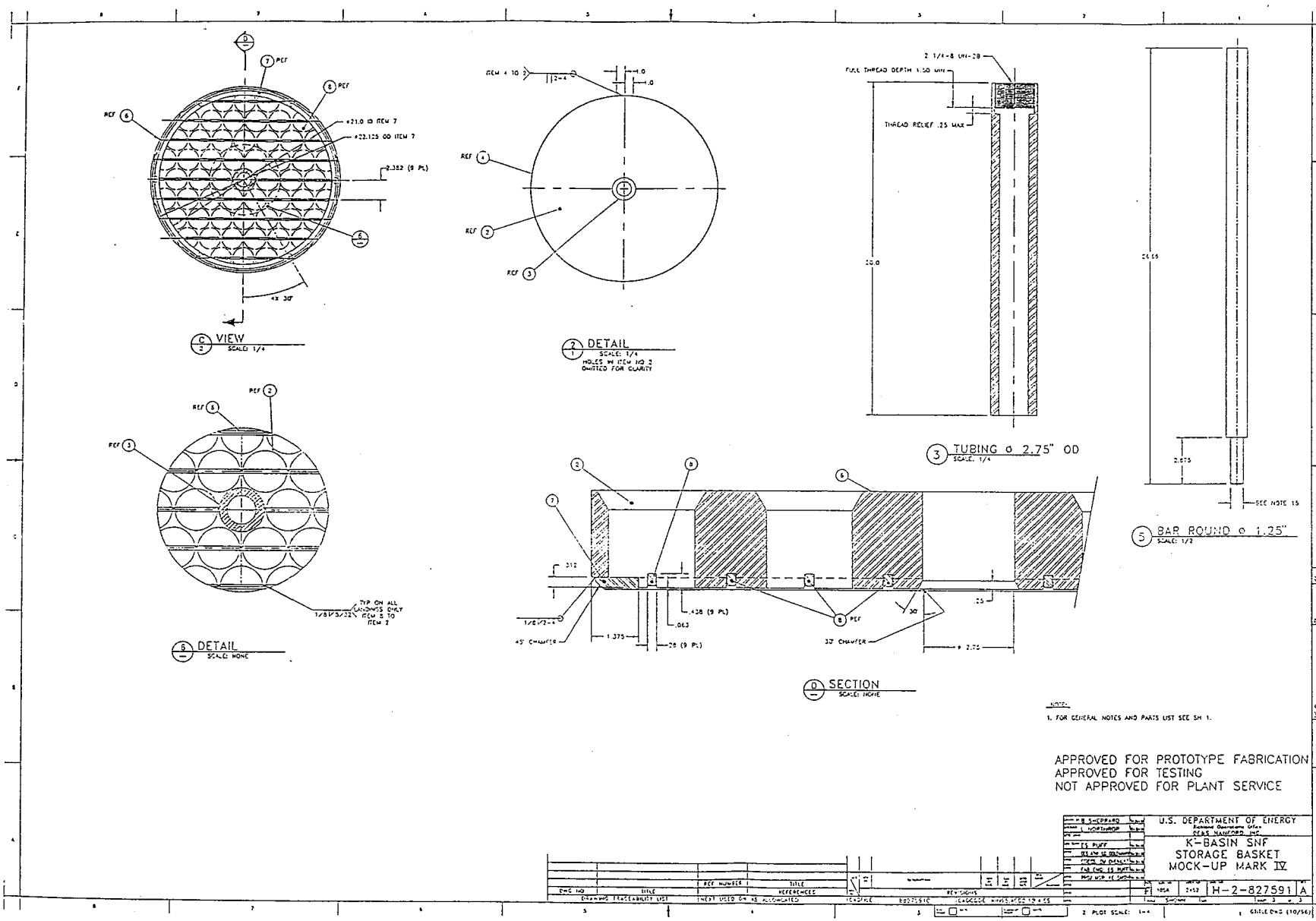

Figure 1-4. K Basin Spent Nuclear Fuel Storage Basket Mock-Up Mark IV. (3 sheets)

THIS PAGE INTENTIONALLY
LEFT BLANK

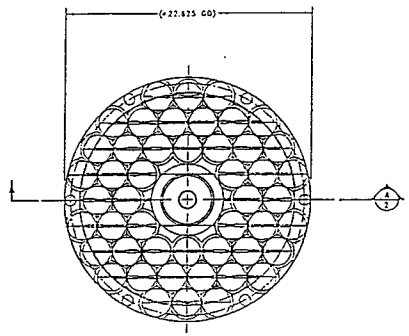

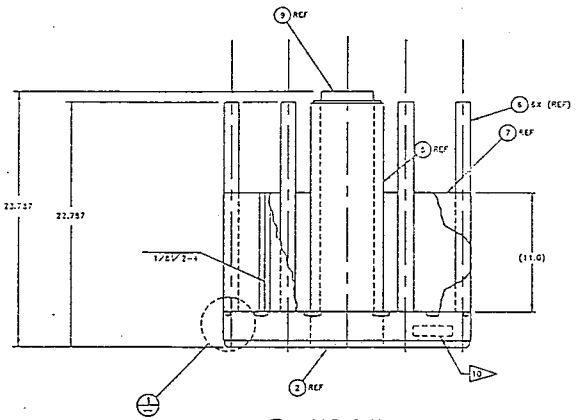

1 ASSEMBLY
SCALE: 1/4

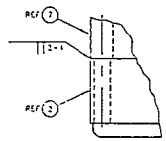

1 DETAIL
SCALE: 1/2

PART/MATERIAL LIST

ITEM	PART/DASH NUMBER	NOMENCLATURE/DESCRIPTION	MATERIAL/REFERENCE	QTY	ITEM NO.
X	-010	ASSEMBLY		1	1
X	3 -020	BASE PLATE		2	2
					3
					4
AR		PIPE, 6" SCHED XXS (.864 WALL) SMLS	ASTM A-312 GR TP 304 OR 304L SMLS SST	3	5
6		BAR, ROUND 1 3/8"	ASTM A-276 TP 304 OR 304L SST	3	6
1		SHEET METAL, 18 (.05 THK) GA X 11" X 71" L	ASTM A-240 TP 304 OR 304L SST	1	7
1		BUSHING, BAR ROUND 5" X 10" L	ASTM A-276 TP 304 OR 304L SST	3	8
1		COUPLING, BAR ROUND 7 X 6 1/4" X 3" L	ASTM A-276 TP 304 OR 304L SST	4	8
1		PLATE, 3" THK	ASTM A-240 TP 304 OR 304L SST	2	13
AR		PLATE 1 3/8" X 5/8"	ASTM A-240 TP 304 OR 304L SST	3	11
					12
AR		BAR, FLAT 1/4" X 1/2"	ASTM A-276 TP 304 OR 304L SST	3	13

GENERAL NOTES:

1. ALL PARTS AND MATERIAL AS SPECIFIED OR ENGINEERING APPROVED EQUAL.
2. ABBREVIATIONS ARE IN ACCORDANCE WITH ASME Y1.1.
3. WELDING SYMBOLS ARE IN ACCORDANCE WITH AWS A2.4.
4. SURFACE TEXTURE SYMBOLS ARE IN ACCORDANCE WITH ANSI/ASME Y14.36. SURFACE TEXTURE VALUES ARE IN MICROINCHES AND ARE IN ACCORDANCE WITH ANSI/ASME B46.1.
5. ALL UNSPECIFIED MACHINED SURFACES SHALL BE 125/ OR BETTER.
6. REMOVE ALL BURRS AND BREAK ALL SHARP EDGES TO .05 MAXIMUM.
7. ALL UNSPECIFIED MACHINE TOOL RADII SHALL BE .03 MAXIMUM.
8. WELDED SURFACES SHALL BE SMOOTH AND UNIFORM IN APPEARANCE WITHOUT ABRUPT CHANGES IN CONTOUR.
9. SCREW THREADS SHALL BE IN ACCORDANCE WITH ANSI B1.1. ALL TAPPED HOLES SHALL HAVE A LEADING CHAMFER OF 82 TO 120° INCLUDED ANGLE EQUAL TO OR SLIGHTLY LARGER THAN THE MAJOR THREAD DIAMETER.
10. MARK WITH "DWG NUMBER H-2-827589", "EMPTY APPROX WEIGHT = XXX LB", AND "NOT FOR USE" PER HS-85-0015 TYPE 1 (VIBRATORY) OR TYPE 2 (DIE STAMP) OVER PAINT USING 1/4" (MIN) HIGH CHARACTERS.
11. CALCULATED WEIGHT = XXX LB.
12. WELD AND INSPECT PER HS-V-S-0013 PT FINAL PASS.
13. PAINT ALL NON STAINLESS PARTS WITH INORGANIC ZINC-RICH PRIMER PRIOR TO NOTE 10. (CARBOLINE CARBO ZINC 11 OR EQUAL)
14. MATE PARTS IN ACCORDANCE WITH, SHRINK FIT PER FN2 PER ANSI B4.1-1967, R1979.

APPROVED FOR PROTOTYPE FABRICATION
APPROVED FOR TESTING
NOT APPROVED FOR PLANT SERVICE

DIMENSIONING AND TOLERANCING SHALL BE INTERPRETED PER ANSI Y14.5M-1982
DIMENSIONS ARE IN INCHES UNLESS OTHERWISE SPECIFIED
UNSPECIFIED TOLERANCES SHALL BE:
DECIMAL .X ± .1 .XX ± .03 .XXX ± .010
ANGULAR ± 2°
ALL TAPPED 90° ANGLES SHALL BE PERPENDICULAR WITHIN THE GREATEST TOLERANCE OF THE LINEAR DIMENSIONS
ALL CIRCULAR FEATURES SHALL BE CONCENTRIC WITHIN .005 DIAMETRAL UNLESS OTHERWISE SPECIFIED.

DWG NO | TITLE | REF NUMBER | TITLE
DRAWING TRACEABILITY LIST | NEXT USED ON AS ALLOCATED | ICN/FILE 827589S4 | CAD/CODE WHES ACCD 12.4.55

REVISIONS

U.S. DEPARTMENT OF ENERGY
Richland Operations Office
K-BASIN SNF
STORAGE BASKET
MOCK-UP MARK IA

SIZE A | CAGE 1054 | DWG NO H-2-827589 | REV A
SCALE: SHOWN | SHEET 1 OF 1
3 PLOT SCALE: 1=4
1 CUTTLE DWG (10/90)

Figure 1-5. K Basin Spent Nuclear Fuel Storage Basket Mock-Up Mark IA. (4 sheets)

THIS PAGE INTENTIONALLY
LEFT BLANK

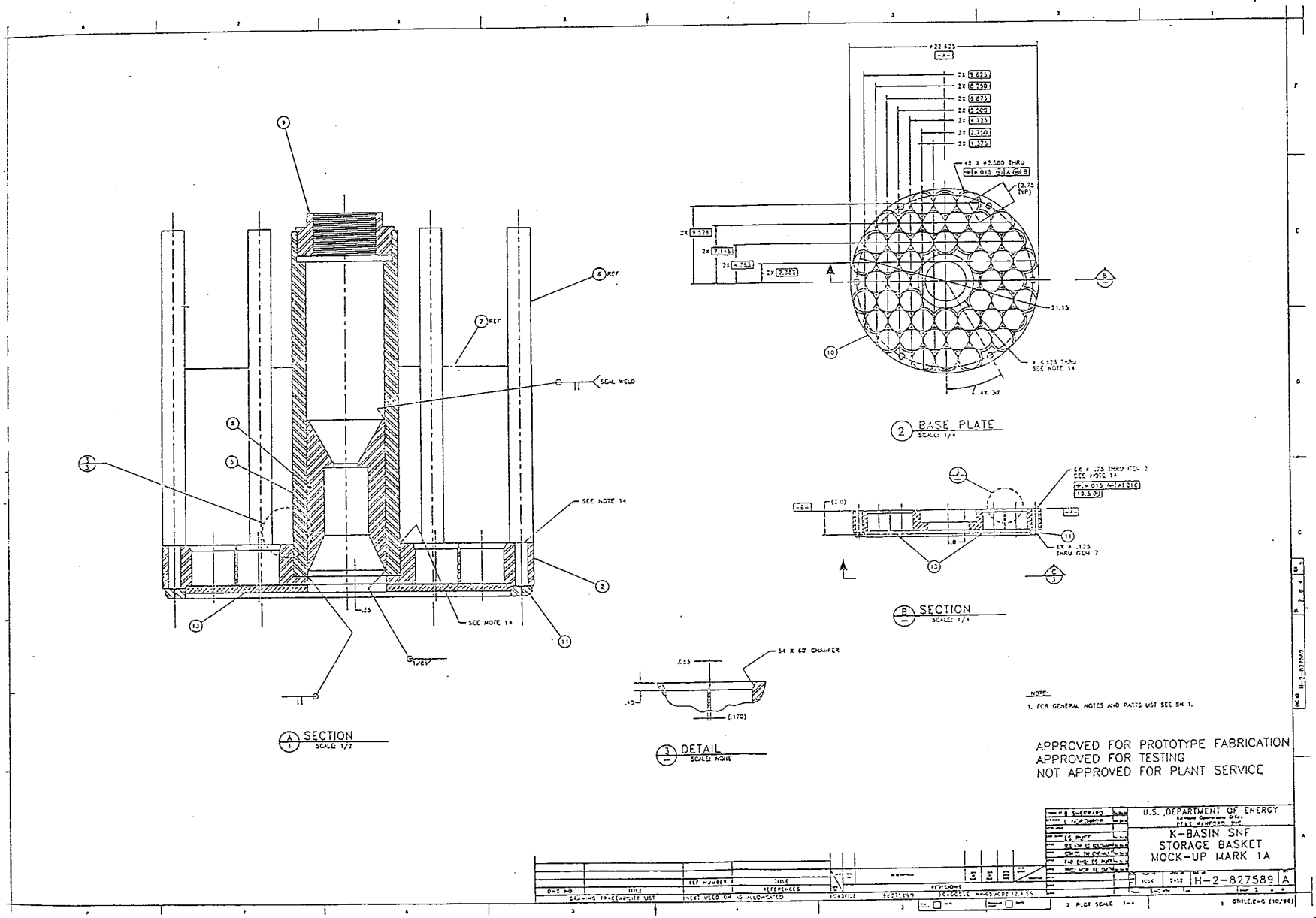

Figure 1-5. K Basin Spent Nuclear Fuel Storage Basket Mock-Up Mark IA. (4 sheets)

THIS PAGE INTENTIONALLY
LEFT BLANK

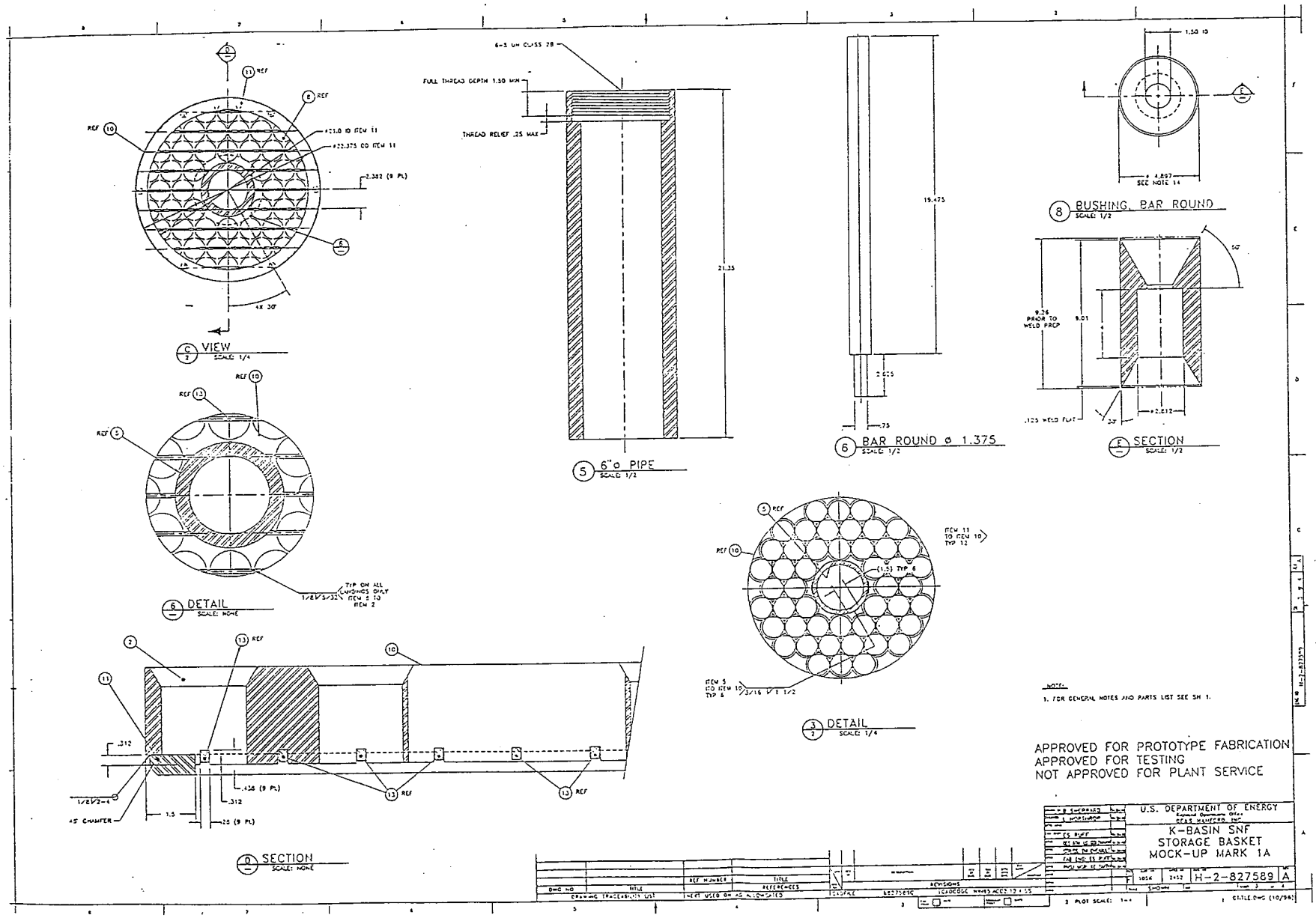

Figure 1-5. K Basin Spent Nuclear Fuel Storage Basket Mock-Up Mark IA. (4 sheets)

THIS PAGE INTENTIONALLY
LEFT BLANK

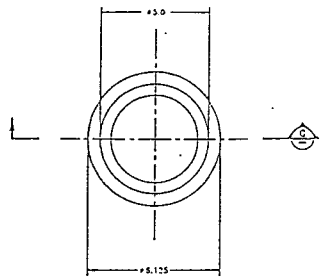

(9) BAR ROUND ⌀ 6 1/4"
SCALE: 1/2

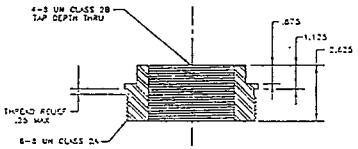

(C) SECTION
SCALE: 1/2

NOTE:
1. FOR GENERAL NOTES AND PARTS LIST SEE SH 1.

APPROVED FOR PROTOTYPE FABRICATION
APPROVED FOR TESTING
NOT APPROVED FOR PLANT SERVICE

U.S. DEPARTMENT OF ENERGY
K-BASIN SNF
STORAGE BASKET
MOCK-UP MARK 1A
H-2-827589 A

Figure 1-5. K Basin Spent Nuclear Fuel Storage Basket Mock-Up Mark IA. (4 sheets)

THIS PAGE INTENTIONALLY
LEFT BLANK

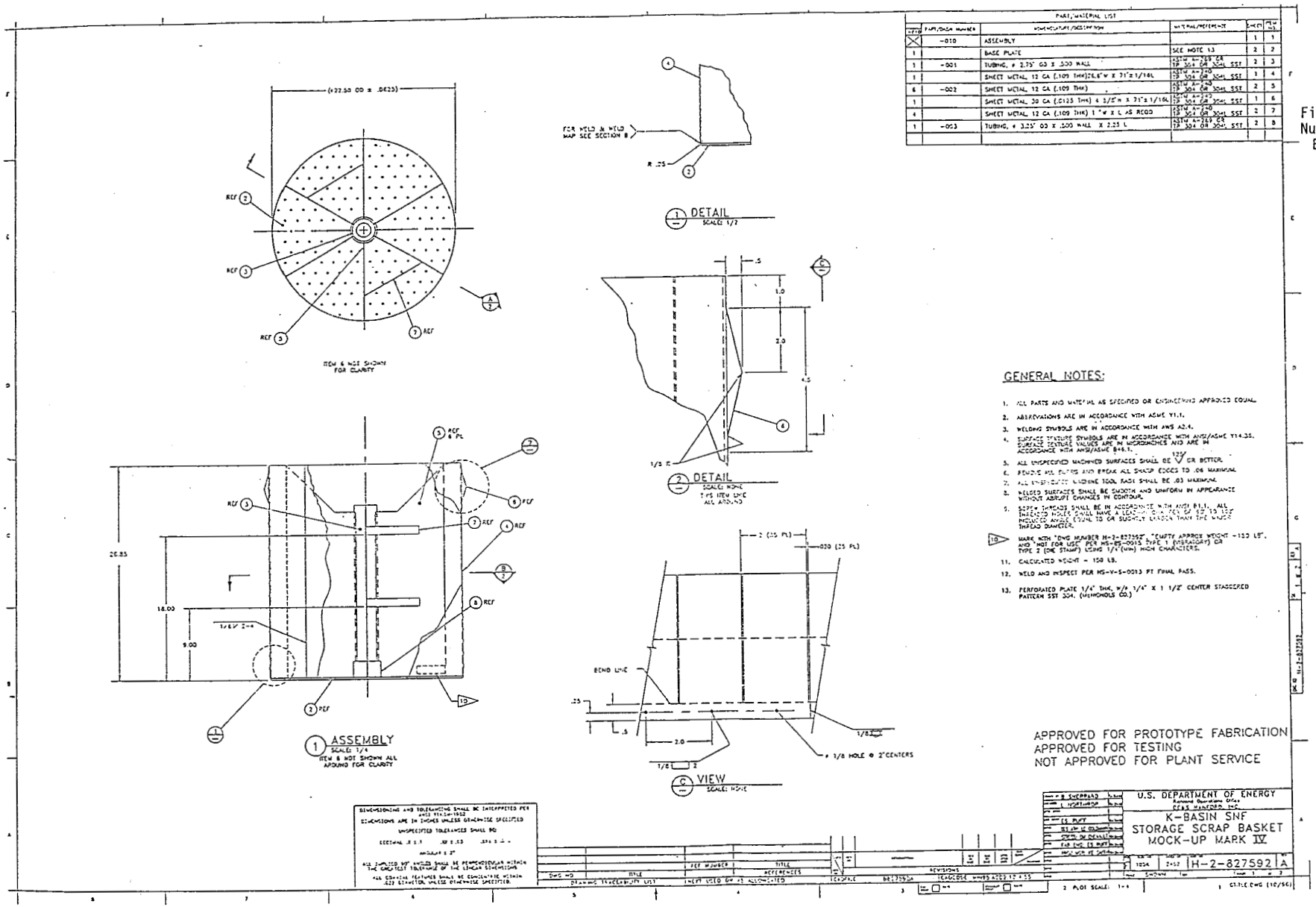

Figure 1-6. K Basin Spent Nuclear Fuel Storage Scrap Basket Mock-Up Mark IV. (2 sheets)

THIS PAGE INTENTIONALLY
LEFT BLANK

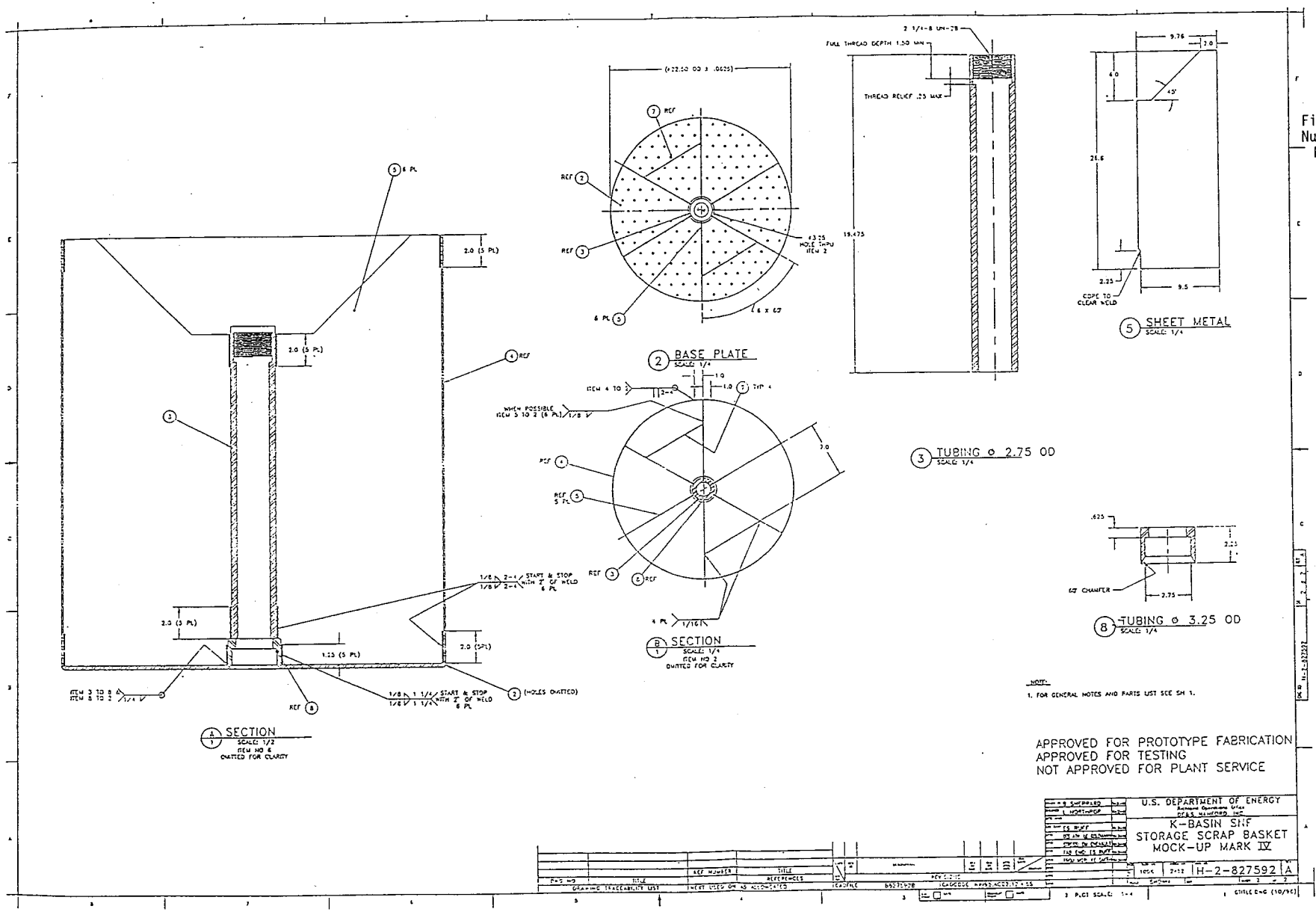

Figure 1-6. K Basin Spent Nuclear Fuel Storage Scrap Basket Mock-Up Mark IV. (2 sheets)

THIS PAGE INTENTIONALLY
LEFT BLANK

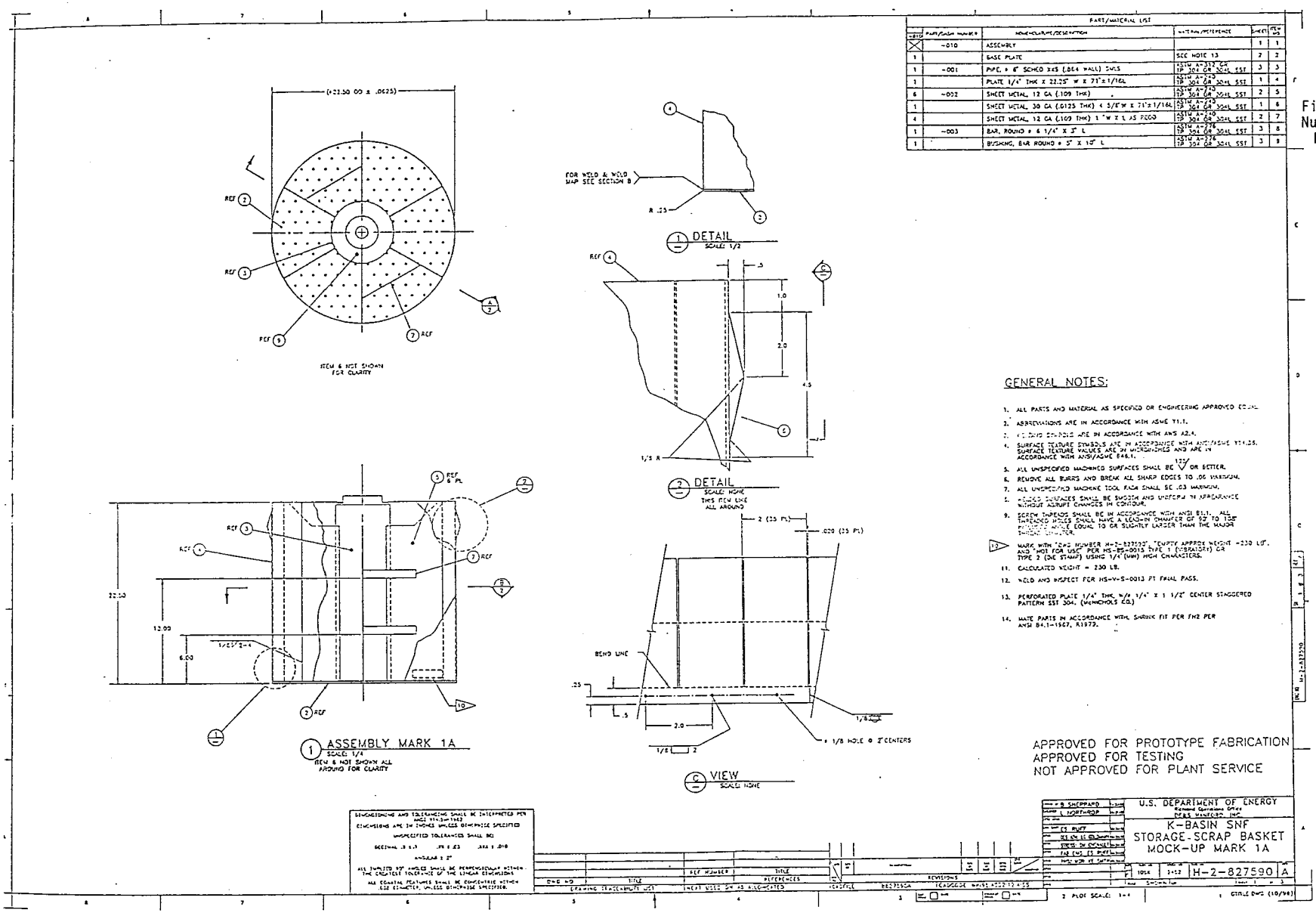

Figure 1-7. K Basin Spent Nuclear Fuel Storage Scrap Basket Mock-Up Mark IA. (3 sheets)

THIS PAGE INTENTIONALLY
LEFT BLANK

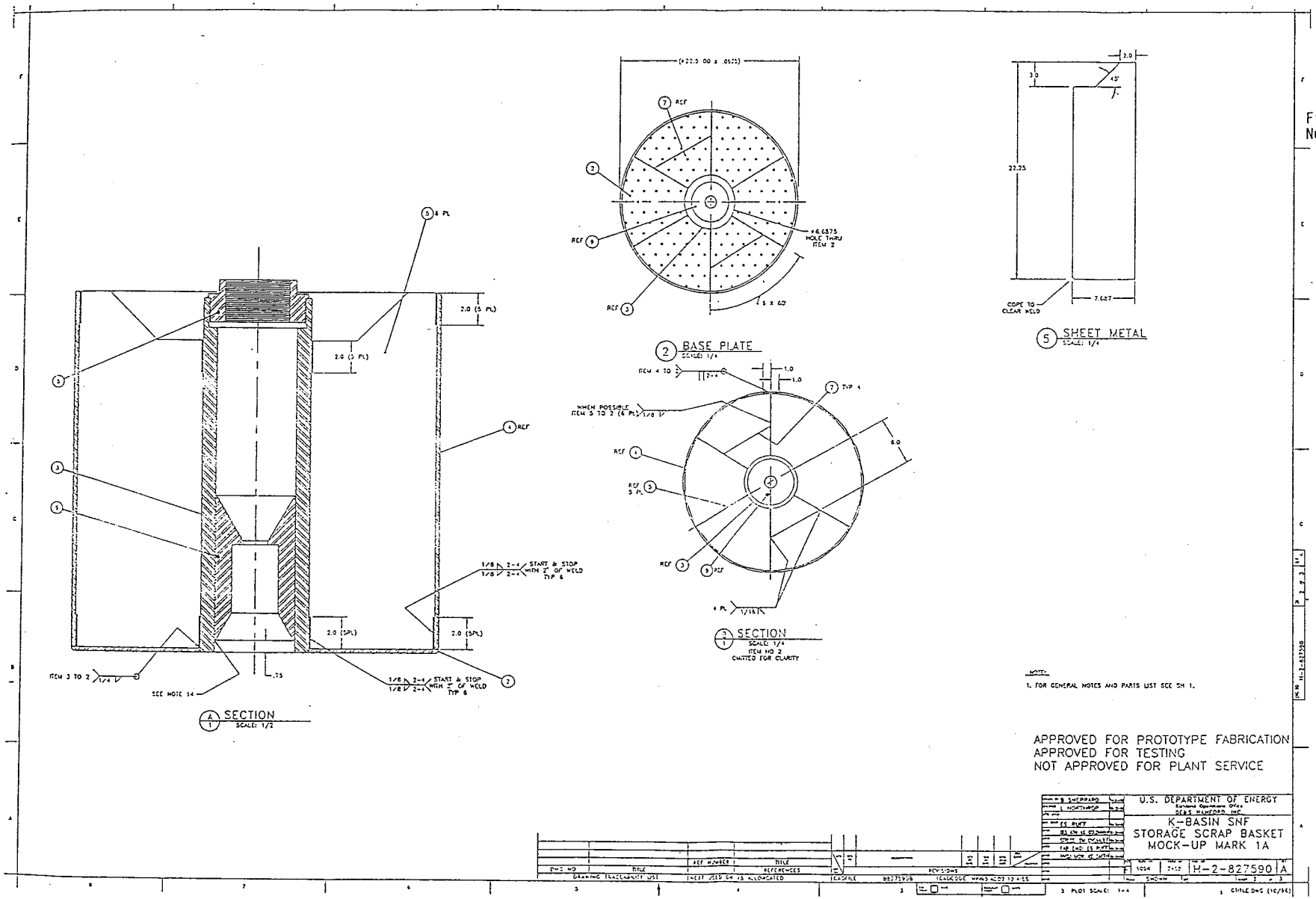

Figure 1-7. K Basin Spent Nuclear Fuel Storage Scrap Basket Mock-Up Mark IA. (3 sheets)

THIS PAGE INTENTIONALLY
LEFT BLANK

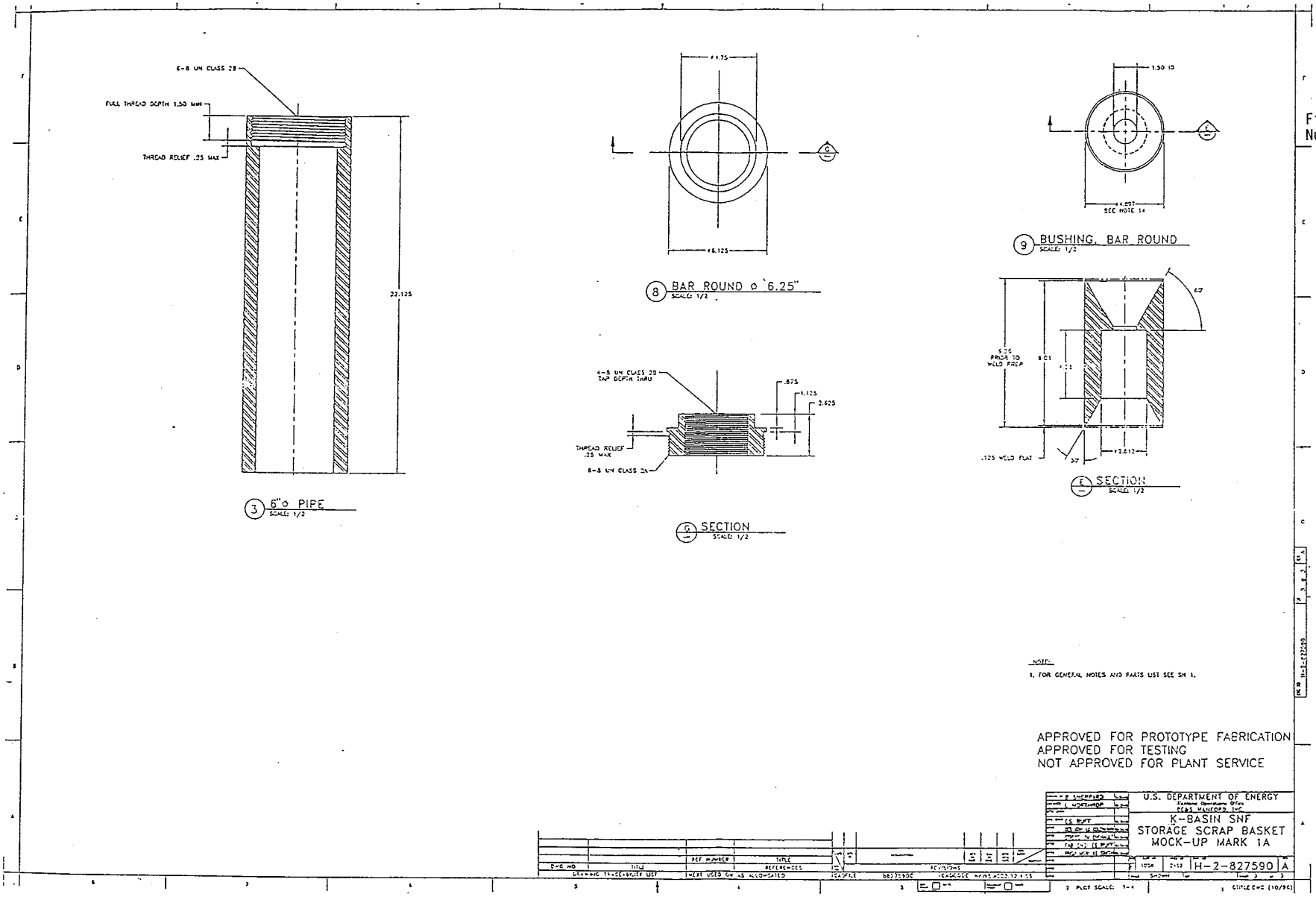

Figure 1-7. K Basin Spent Nuclear Fuel Storage Scrap Basket Mock-Up Mark IA. (3 sheets)

THIS PAGE INTENTIONALLY
LEFT BLANK

For clarification, the Mark IV fuel and scrap baskets do not have to be designed to meet the intent of the Boiler and Pressure Vessel Code (ASME 1995a). Mark IV fuel has a lower ^{235}U enrichment than Mark IA fuel. Analyses indicate that the Mark IV fuel cannot achieve criticality in an MCO under normal operating conditions or accident scenarios. It follows that the basket's structural integrity is not required for Mark IV criticality control. Therefore, the stringent Section III, Subsection NG requirements (ASME 1995a) are not required for the construction of the Mark IV fuel and scrap baskets.

During accident conditions the baskets designed for Mark IA fuel and for Mark IA fuel scrap shall maintain the criticality control features in accordance with WHC-SD-SNF-CSER-005, *Criticality Safety Evaluation Report for Spent Nuclear Fuel Processing and Storage Facilities* (Schwinkendorf 1996). For the handling of both loaded and unloaded Mark IA and Mark IV baskets, the design meets the safety factors required by ANSI N14.6-1986, *For Radioactive Materials — Special Lifting Devices for Shipping Containers Weighing 10,000 Pounds (4500 kg) or More* (ANSI 1986) for non-critical loading.

The baskets will maintain their structural integrity (with specified exceptions) during expected internal MCO environmental conditions, normal MCO handling situations, and after accidents (Mark IA baskets only). This structural integrity is required to maintain criticality safety in the MCO when loaded with Mark IA baskets as required in WHC-SD-SNF-CSER-005 (Schwinkendorf 1996). The baskets are sufficiently strong to preserve the processing ability of the MCO for the bulk water removal, vacuum drying, and hot conditioning processes during normal MCO handling, for various internal MCO environments, and after MCO design basis accidents (DBAs).

The baskets will not introduce any additional gas-producing materials into the MCO that significantly increase the pressure in the MCO during storage. Nor will the baskets introduce any materials that will appreciably accelerate corrosion of, or significantly alter the properties of, the MCO containment boundary.

1.2.3 Shield Plug

The MCO shield plug is a solid cylinder designed to mate with the open end of the MCO shell (Figure 1-8). The shield plug shields workers against photons and neutrons emanating from the inside of the MCO. This shielding maintains an average dose across the top of the shield plug of 0.3 mSv/h (30 mrem/h) on contact (5 cm [2 in.]) for the average MCO fuel inventory. The 0.3 mSv/h (30 mrem/h) limit includes radiation streaming between the MCO shield plug and MCO shell and streaming around penetrations; streaming emanating from between the MCO and cask is not included. Streaming shall be minimized. For the worst-case MCO, the average dose across the top of the shield plug on contact (5 cm [2 in.]) shall not exceed 1.0 mSv/h (100 mrem/h).

The MCO shielding design meets as low as reasonably achievable (ALARA) requirements in accordance with Title 10, *Code of Federal Regulations*, Part 835, "Occupational Radiation Protection" (10 CFR 835), Subpart K; DOE Order 5480.11, *Radiation Protection for Occupational Workers*, Paragraph 9a; HSRCM-1, *Hanford Site Radiological Control Manual*, Sections 111 and 311; WHC-IP-1043, *WHC Occupational ALARA Program* (WHC 1995), Section 8.0;

This page intentionally left blank.

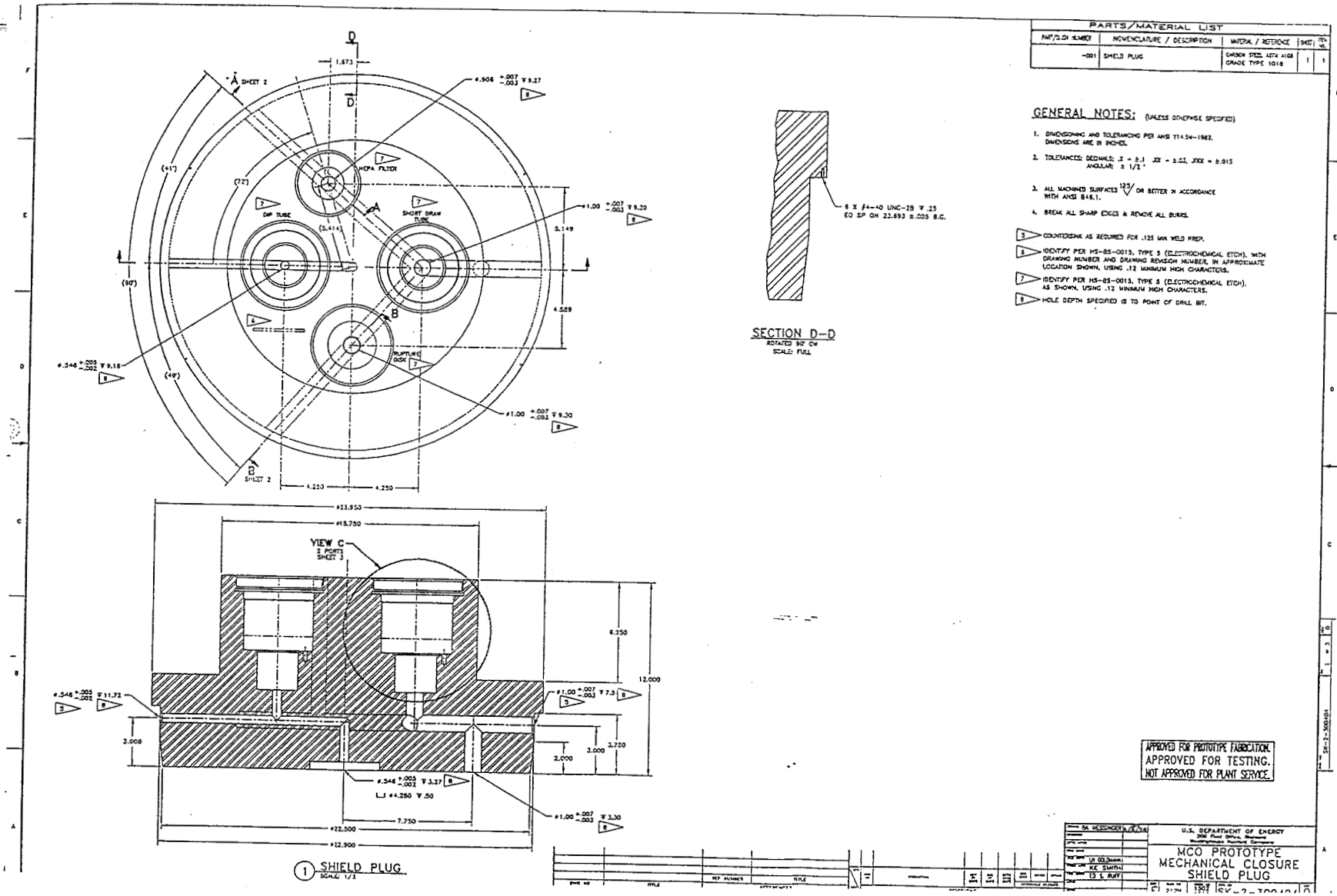

Figure 1-8. Multicanister Overpack Prototype Mechanical Closure Shield Plug. (3 sheets)

THIS PAGE INTENTIONALLY
LEFT BLANK

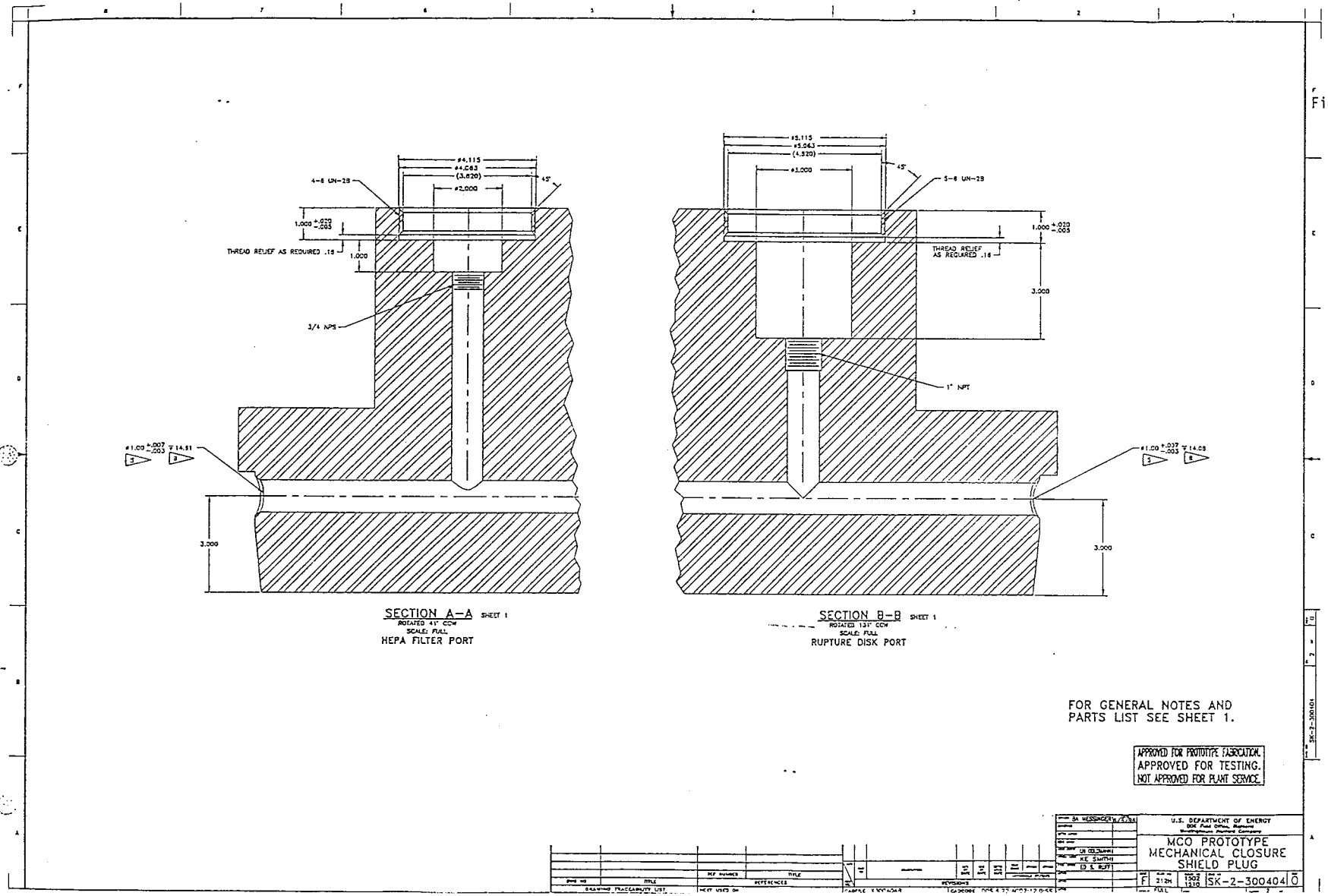

Figure 1-8. Multicanister Overpack Prototype Mechanical Closure Shield Plug. (3 sheets)

THIS PAGE INTENTIONALLY
LEFT BLANK

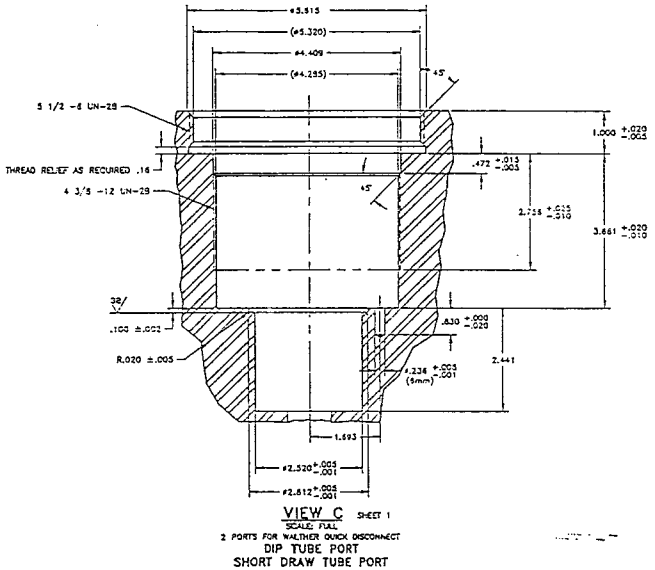

VIEW C SHEET 1
SCALE: FULL
2 PORTS FOR WALTHER QUICK DISCONNECT
DIP TUBE PORT
SHORT DRAW TUBE PORT

Figure 1-8. Multicanister Overpack Prototype Mechanical Closure Shield Plug. (3 sheets)

FOR GENERAL NOTES AND PARTS LIST SEE SHEET 1.

APPROVED FOR PROTOTYPE FABRICATION.
APPROVED FOR TESTING.
NOT APPROVED FOR PLANT SERVICE.

U.S. DEPARTMENT OF ENERGY

MCO PROTOTYPE MECHANICAL CLOSURE SHIELD PLUG

SK-2-300404 0

THIS PAGE INTENTIONALLY
LEFT BLANK

and Regulatory Guide 8.8, *Information Relevant to Ensuring that Occupational Radiation Exposures at Nuclear Power Stations will be As Low as is Reasonably Achievable* (NRC 1978), Section C.2.b, "Radiation Shields and Geometry," and Section C.2.f, "Isolation and Decontamination."

The shield plug is closed using a mechanical closure assembly. The mechanical closure assembly holds the shield plug in place using a threaded locking ring that is put into the MCO neck extension after the shield plug is inserted. Once assembled, the eight jacking bolts in the locking ring are tightened down into the shield plug's back side to push the shield plug into the seal between the MCO shell and the shield plug. The MCO shield plug also mates with the end effector on the top SNF fuel basket. The MCO has a minimum target height of 5.0 cm (2 in.) of free space between the top of the SNF materials and the bottom of the guard plate on the shield plug. This distance may be less as allowed by the process needs of the CVDF and HCS.

The shield plug provides access to the interior of the MCO via a minimum of three penetrations (Figure 1-9). The penetrations accommodate two process ports with valve mechanisms to permit processing connections, a rupture disk port, and a combination pressure relief valve and low-flow, high-efficiency particulate air (HEPA) filter port. The two process ports accommodate connections to external equipment and are integral to the shield plug. These process ports connect internally to two process tubes. One process tube (1.3 cm [0.5 in.] diameter) extends down the MCO's axis to the bottom, and the second (2.5 cm [1 in.] diameter) extends to internal process filters mounted on the shield plug's underside. A third tube (2.5 cm [1 in.] diameter) extends from the rupture disk to the space between the bottom of the shield plug and the top of the guard plate. The 1.3-cm- (0.5-in.-) diameter long process tube and the short tube for the rupture disk have 2-mm debris strainers/screens around the ends (Figure 1-9). The connections leading to the long or short process tubes are designed to be easily differentiated by a worker looking at either the top or bottom of the shield plug. The design of the penetrations, ports, and valve mechanism implements the following criteria:

- Provisions for pressurizing the MCO interior with an inert gas
- Provisions for purging gas from the MCO interior
- Provisions for leak rate testing, where applicable
- Provisions for making or breaking all connections while continuing to maintain SNF containment with minimal spread of contamination
- Connections designed to facilitate their decontamination
- Ports and connections accessible to the operator from the top face of the MCO
- Penetrations and connections that do not appreciably reduce or impair MCO shielding

Figure 1-9. Schematic Diagram of Multicanister Overpack Passages.

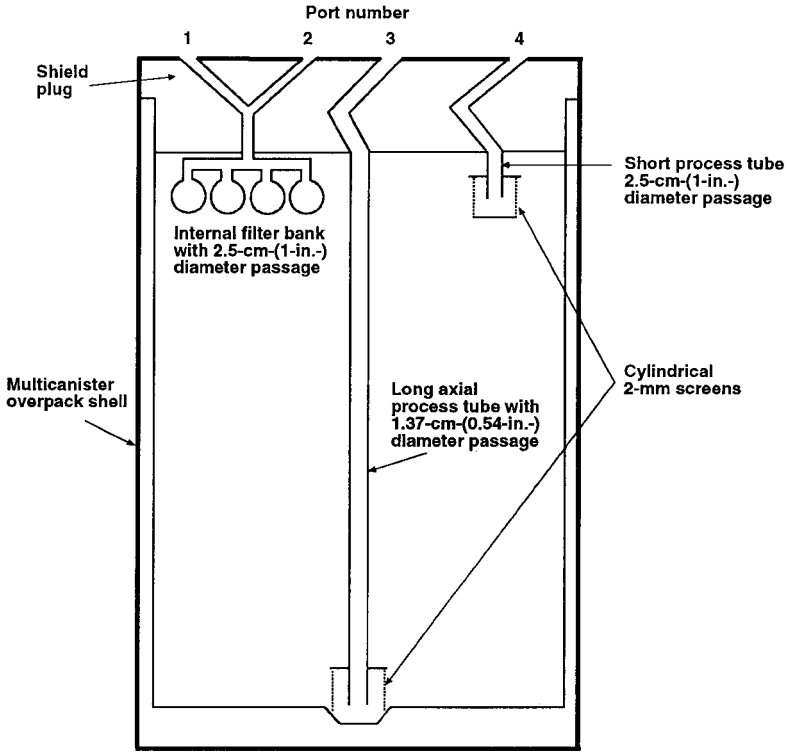

Port number	Function
1	Filtered process pressure relief
2	Filtered process exit port
3	Long axial process tube
4	Safety-class rupture disk

SK-LHG102296
10/22/96

2G96100101.1
MCO

- Provisions for removal or reinstallation of sealing mechanisms as required to cover process connections, pressure relief devices, and a low-flow HEPA filter (these sealing mechanisms, including fasteners, cannot extend above the top of the shield plug)
- Provisions for bleed down, in a controlled way into the process piping, internal MCO pressure after process connections are made
- Penetrations and connections designed to facilitate remote operation via long-handled tools and via a manipulator
- Provisions for orifice plates (0.6 cm [0.25 in.] to limit relief flow on ports for pressure relief devices when appropriate.

The shield plug features an integrally machined axisymmetric lifting ring with a 10.9-metric ton (t) (12-ton) lifting capacity when gripped with six equally spaced grippers. The ring facilitates handling of the MCO package when unloading from the transport cask, CSB storage tubes, and process cells with the MCO handling machine (MHM). The MCO lifting ring design must exhibit the safety factors (for noncritical lifts) required by ANSI N14.6-1986 (ANSI 1986). This standard requires that any handling or lift features required to perform non-critical lifts shall be capable of demonstrating a safety factor of three on material yield and five on material ultimate strength.

1.2.4 Additional Features

The MCO has internal process filters to support the vacuum drying and hot conditioning outflows from the MCO. These filters are installed between the shield plug bottom and the guard/shield plate. The internal process filters prevent fuel particulate corrosion products from leaving the MCO (thereby reducing dose in the processing facility). These internal process filters may be HEPA filters if adequate flow capacity is achieved through the filter bank to support process needs. These filters are not required to meet the requirements of DOE Order 6430.1A, *General Design Criteria*.

To summarize the key features, the MCO is a stainless steel shell that is mechanically sealed to a carbon steel shield plug. On top of the shield plug are four ports, three of which are valved to support process functions. The ports access three penetrations, two of which terminate in screened process tubes. The long process tube allows water pickup and gas transport as needed. The short process tube port doubles as the location for the safety-class pressure relief device (rupture disk). The remaining two ports are connected to a bank of four internal HEPA filters. These two ports are reserved for a process port for filtered exit and for a non-safety class pressure relief device and a valved process location. The ports are all capable of being sealed using either bolted or threaded closure plates. Additional information is provided throughout this report.

1.3 MULTICANISTER OVERPACK CHARACTERISTICS

1.3.1 Design and Fabrication

The MCO will be designed, fabricated, inspected, and examined to meet the intent of the Boiler and Pressure Vessel Code (ASME 1995a), Section III, Subsection NB, for all components except the plate and shell supports, which must meet Subsection NF, and the spent fuel basket assembly, which must meet Subsection NG for the Mark IA fuel. All MCO welds will be completed and examined in accordance with the Boiler and Pressure Vessel Code (ASME 1995a), Section III, Subsection NB. Exceptions to NB and other Subsections are discussed in the exceptions report that will be released after the design is final.

The following structural materials are used to fabricate the MCO:

- ASME SA-108, type 1018 carbon steel for the shield plug and the locking and lifting ring
- ASME SA-312, type 304L stainless steel for the MCO shell
- ASME SA-182, type 304L stainless steel for the bottom forging assembly
- Jacking bolts
- Silver-plated stainless steel for Helicoflex[1] closure seal
- Grafoil[2] flexible graphite with 304L stainless steel retainers for the port covers.

The MCO will have a maximum decay heat load of 835 W, plus any allowable margin.

The mechanical properties of the MCO's structural materials are presented in Section 3.4. The listed properties are Boiler and Pressure Vessel Code (ASME 1995a) minimums and in some instances higher property usage may be justified. The expected weights and centers of gravity of the MCO, its contents, and ancillary equipment after drying are presented in Section 3.3. The operational features of the MCO will be limited to the lifting attachments, closure design, pressure relief connections, process connections, and the internal bank of four HEPA filters located on the underside of the shield plug.

---

[1]Helicoflex is a trademark of Helicoflex Corporation.

[2]Grafoil is a trademark of Union Carbide Corporation.

1.3.2 Confinement/Containment Boundary

The MCO is to be the long-term storage container for the spent fuel and is relied upon as the primary containment and confinement boundary (see Section 1.2). The MCO confinement/containment boundary consists of the following items (Figure 1-1):

- Shield plug
- MCO shell
- MCO bottom
- Weld connecting shell to bottom
- Shield plug to shell mechanical closure and Helicoflex gasket
- Four port cover flanges and Grafoil gaskets
- Port cover closure bolts
- MCO cover cap (when the MCO is seal welded as shown on Figure 1-10).

The MCO shield plug assembly will be mechanically sealed to maintain a low leakage rate. Figure 1-10 provides the details of the mechanical closure assembly. A containment weld will be made to attach the MCO shell to the MCO bottom forging assembly. Welds will be made in conformance with the intent of the *Boiler and Pressure Vessel Code* (ASME 1995a), Section III, Subsection NB. The shell to bottom forging assembly weld is examined in accordance with the intent of the Boiler and Pressure Vessel Code (ASME 1995a), Section III, Subsection NB-5300. Details of the MCO locking and lifting ring as well as the MCO cover are provided in Figure 1-11.

The MCO will not be vented during transportation, with the possible exception of the transfer between the K Basins and the CVDF. Each port will be covered by a port cover flange and a flexible graphite gasket that can maintain a leaktight seal if required.

1.4 MULTICANISTER OVERPACK CONTENTS

The fuel to be stored in the MCOs is presently located in the K Basins storage pools. The 105 K East fuel storage basin contains 51,073 fuel assemblies (which may or may not be intact), elements, or pieces. The 105 K West fuel storage basin contains 53,964 fuel assemblies, elements, or pieces. The total mass of the fuel elements at the 105 K East fuel storage basin is approximately 1,233 t (1,359 ton); the total mass of the fuel elements in the 105 K West fuel storage basin is approximately 1,038 t (1,144 ton). This total includes approximately 1,143,600 kg (2,521,200 lb) of *uranium* and 2,155 kg (4,750 lb) of *plutonium* in the 105 K East fuel storage basin and approximately 951,900 kg (2,098,500 lb) of uranium and 1,875 kg (4,135 lb) of plutonium in the 105 K West fuel storage basin.

This page intentionally left blank.

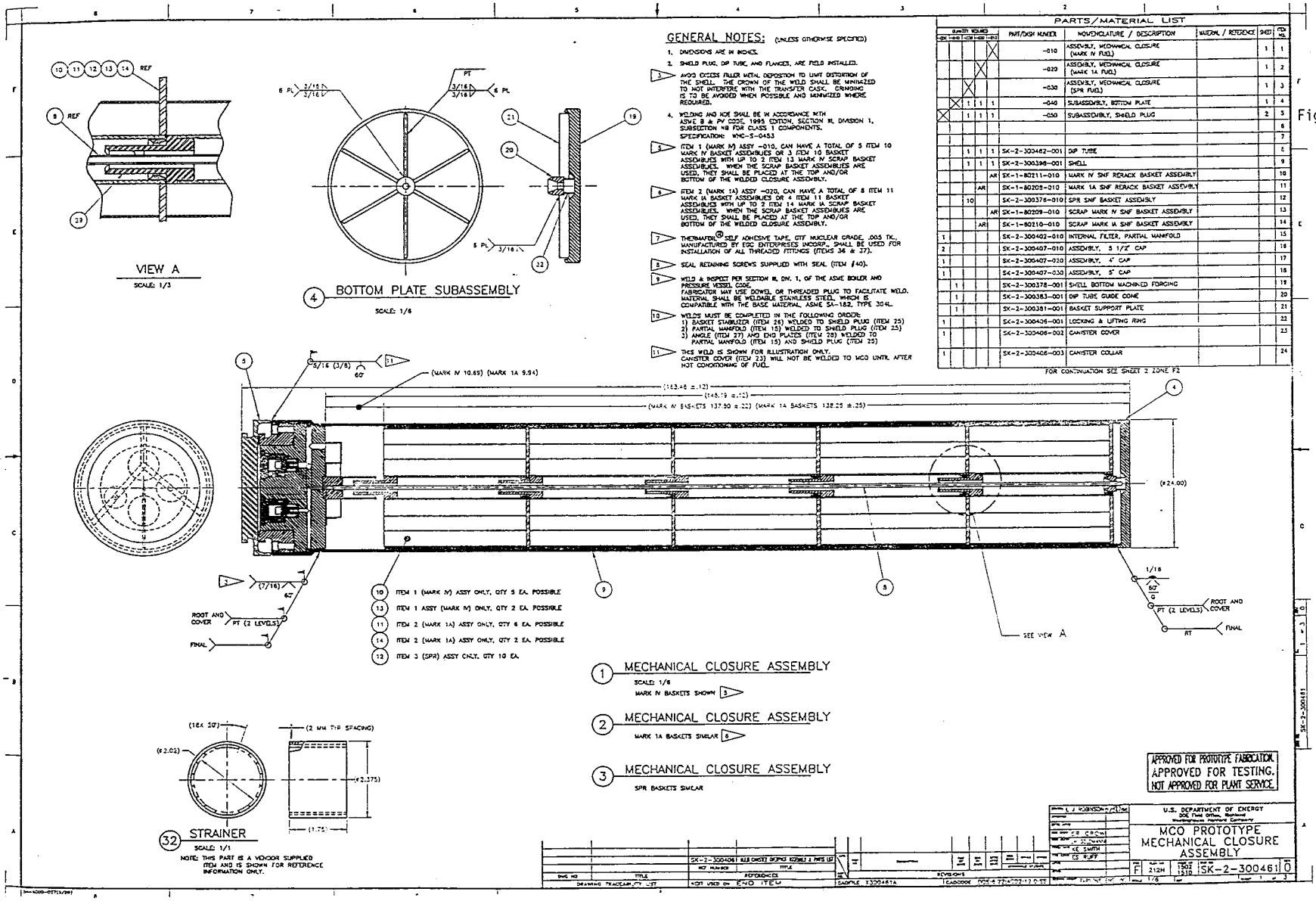

Figure 1-10. Multicanister Overpack Prototype Mechanical Closure Assembly. (3 sheets)

THIS PAGE INTENTIONALLY
LEFT BLANK

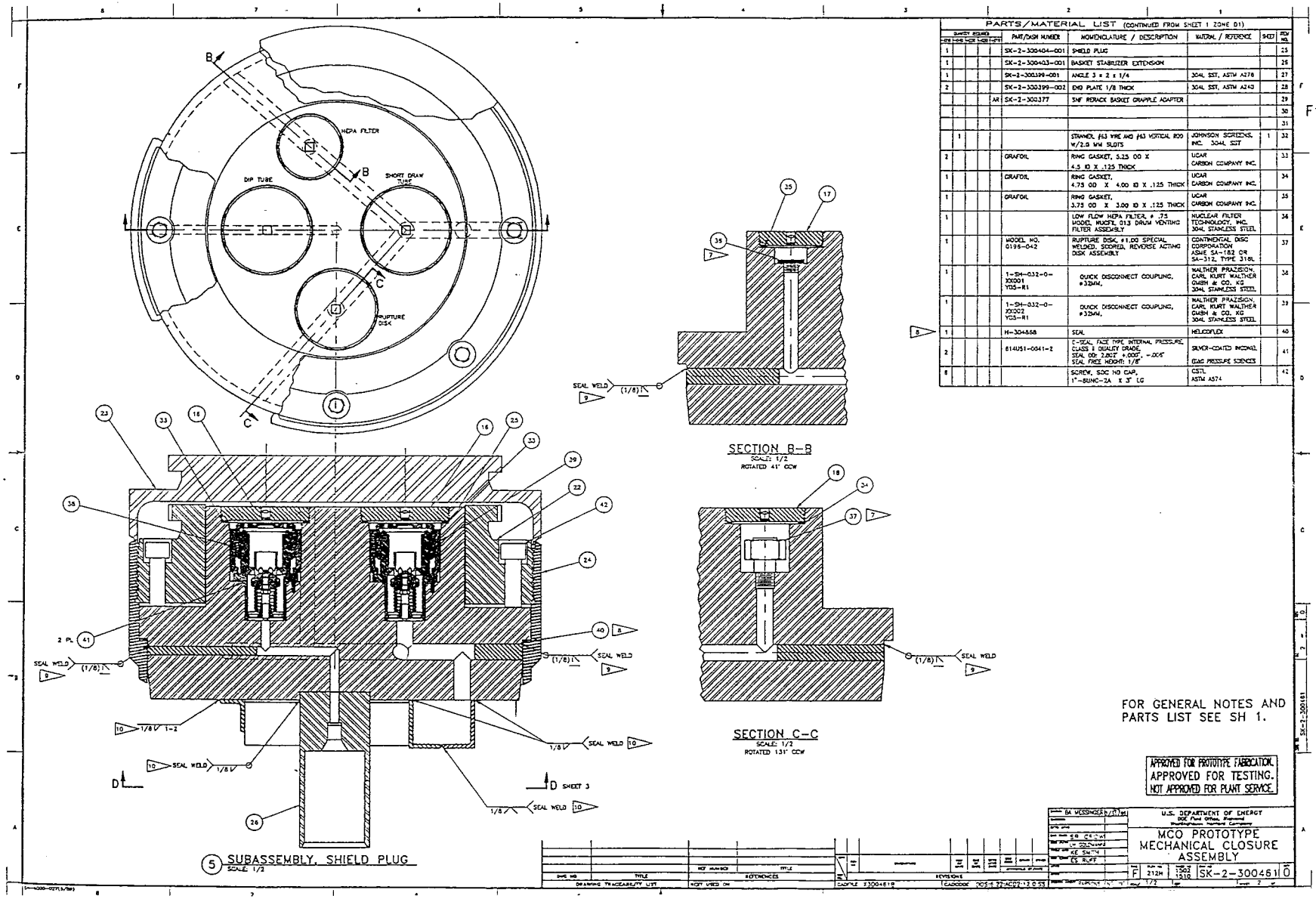

Figure 1-10. Multicanister Overpack Prototype Mechanical Closure Assembly. (3 sheets)

THIS PAGE INTENTIONALLY
LEFT BLANK

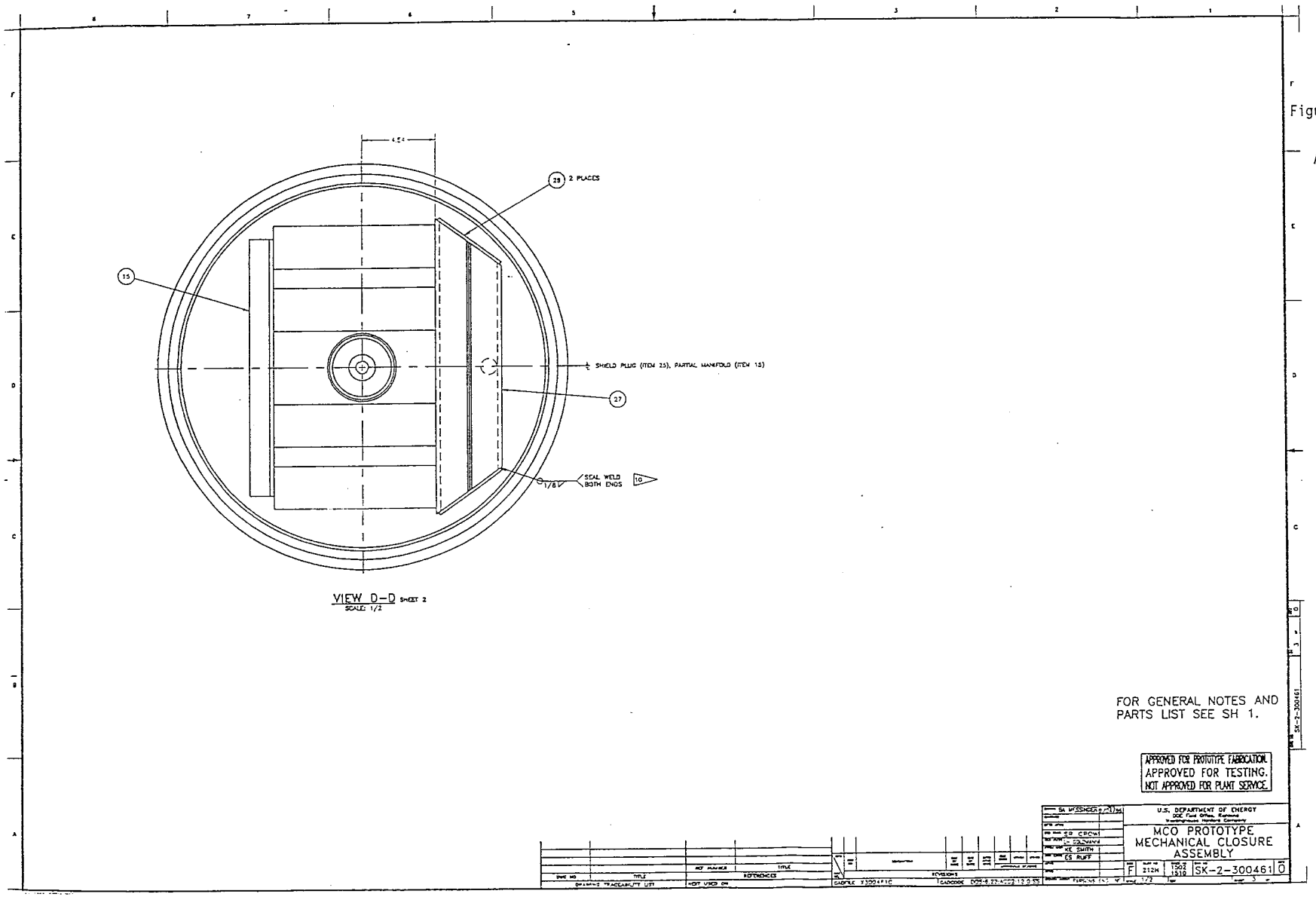

Figure 1-10. Multicanister Overpack Prototype Mechanical Closure Assembly. (3 sheets)

THIS PAGE INTENTIONALLY
LEFT BLANK

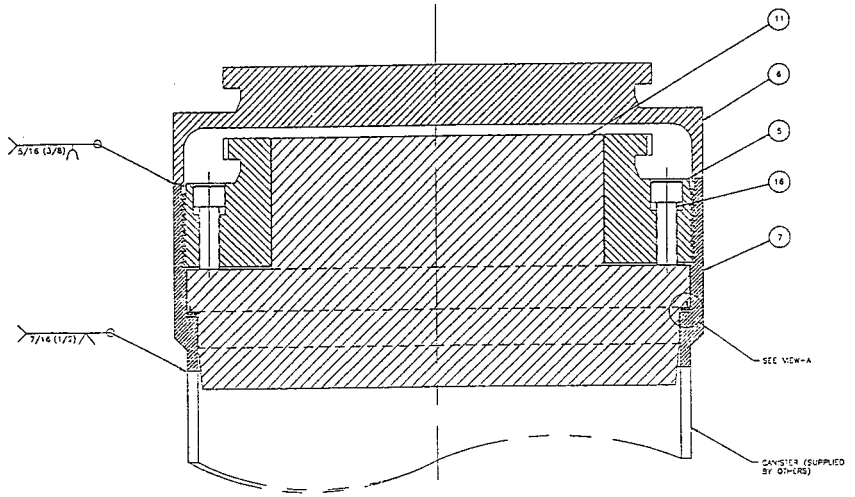

1 ASSEMBLY
SCALE: 1/2

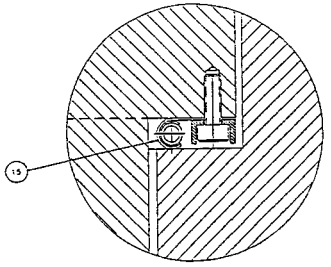

VIEW-A

PARTS/MATERIAL LIST

QTY REQ'D 2009 4826		PART/DASH NUMBER	NOMENCLATURE/DESCRIPTION	MATERIAL/REFERENCE	SHEET	ITEM NO.
	X	-000	ASSEMBLY		1	1
						2
						3
						4
	1	-001	LOCKING & LIFTING RING	CSTL 4140	2	5
	1	-002	CANISTER COVER	SST SA 182 F304L	3	6
	1	-003	CANISTER COLLAR	SST SA 182 F304L	4	7
						8
						9
						10
	1	SK-2-300404 -001	SHIELDING PLUG			11
						12
						13
						14
	1	H-204868	SEAL	HELICOFLEX		15
	8		SCREW, SOC HD CAP, 1"-8UNC-2A x 3" LG	CSTL ASTM A574		16

GENERAL NOTES: (UNLESS OTHERWISE SPECIFIED)

1. DIMENSIONING AND TOLERANCING PER ANSI Y14.5M-82. DIMENSIONS ARE IN INCHES.
2. TOLERANCES: DECIMAL: .XX= ±.03, .XXX = ±.005
   FRACTIONS: ± 1/16
   ANGULAR: ± 1°
3. ALL MACHINED SURFACES SHALL BE 125 OR BETTER IN ACCORDANCE WITH ANSI B46.1.
4. BREAK ALL SHARP EDGES & REMOVE ALL BURRS.
5. MACHINED FILLET RADII SHALL BE .03 MAX.
6. SEAL RETAINING SCREWS SUPPLIED WITH SEAL (ITEM #12).

PROTOTYPE

U.S. DEPARTMENT OF ENERGY

MULTI CANISTER OVERPACK ASSEMBLY & PARTS LIST

SK-2-300406 | 0

Figure 1-11. Multicanister Overpack Cover, Locking and Lift Ring Detail. (4 sheets)

THIS PAGE INTENTIONALLY
LEFT BLANK

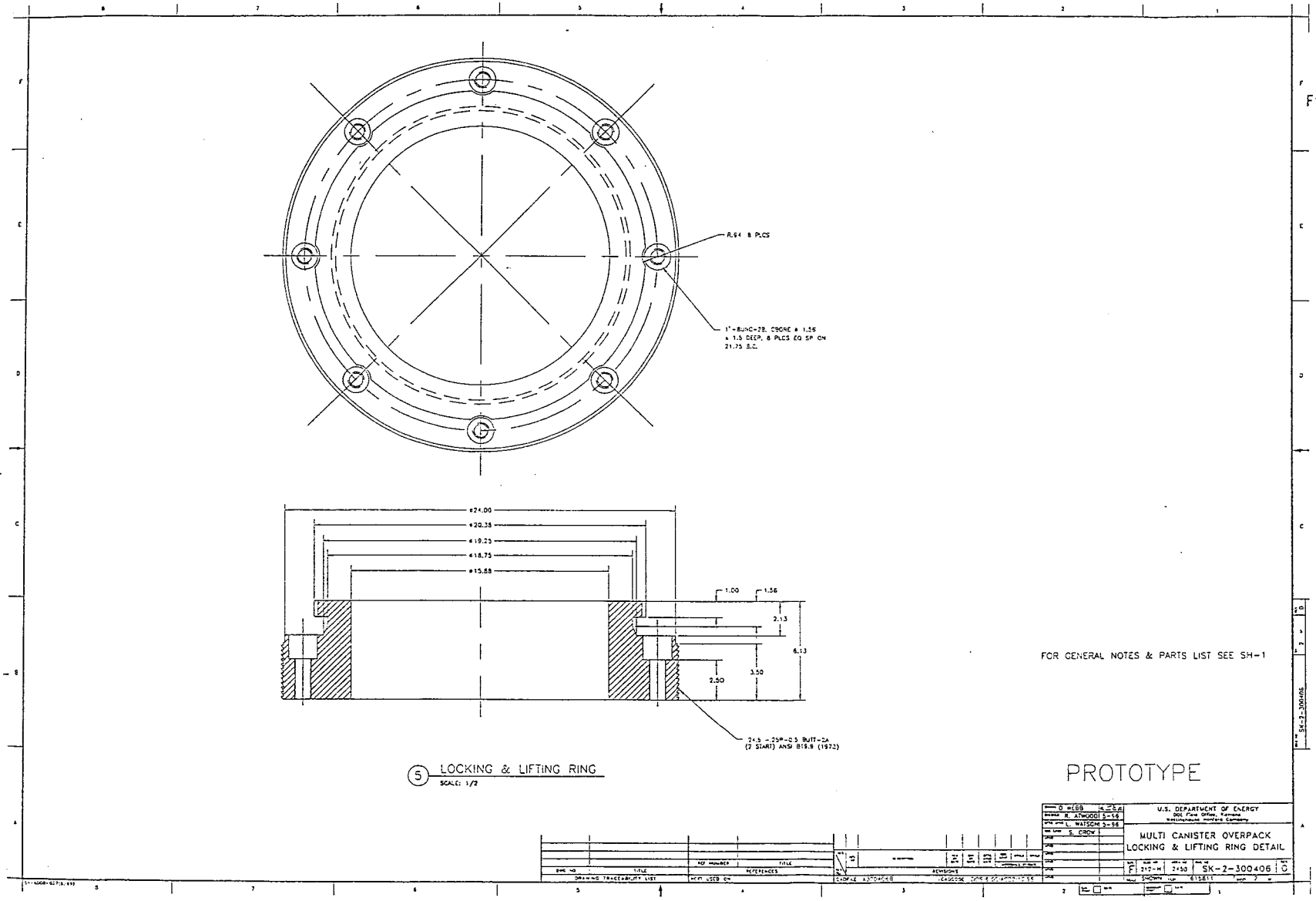

Figure 1-11. Multicanister Overpack Cover, Locking and Lift Ring Detail. (4 sheets)

THIS PAGE INTENTIONALLY
LEFT BLANK

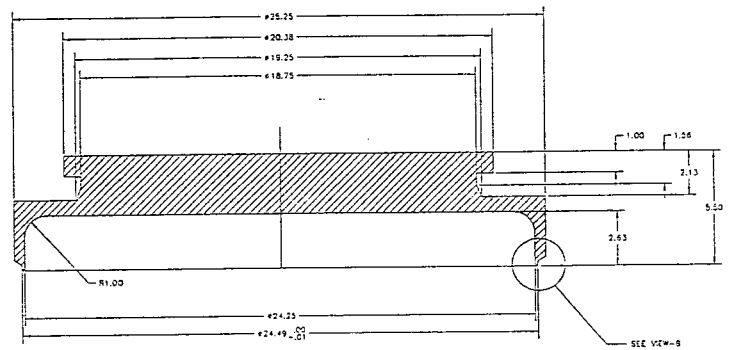

6 CANISTER COVER
SCALE: 1/2

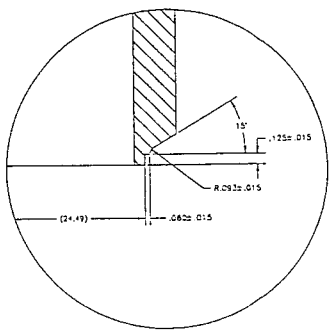

VIEW-B

FOR GENERAL NOTES & PARTS LIST SEE SH-1

PROTOTYPE

U.S. DEPARTMENT OF ENERGY
DOE Field Office, Richland
Westinghouse Hanford Company

MULTI CANISTER OVERPACK
CANISTER COVER DETAIL

SK-2-300406 0

Figure 1-11. Multicanister Overpack Cover, Locking and Lift Ring Detail. (4 sheets)

THIS PAGE INTENTIONALLY
LEFT BLANK

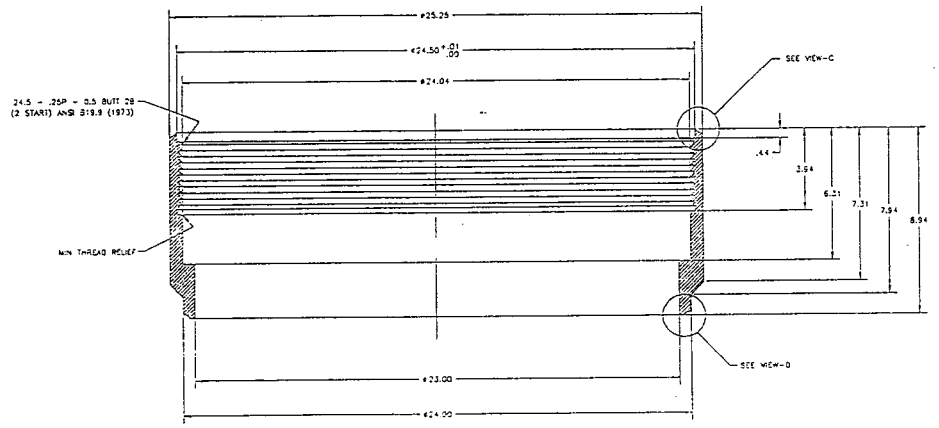

7 CANISTER COLLAR
SCALE: 1/2

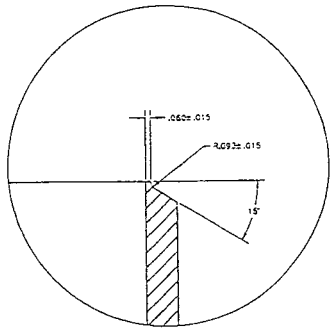

VIEW-C

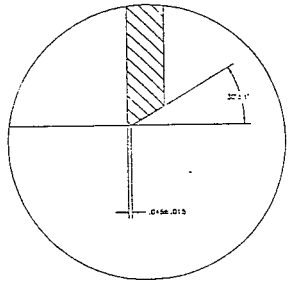

VIEW-D

FOR GENERAL NOTES & PARTS LIST SEE SH-1

PROTOTYPE

DRAWN D. WEBB 5-29-96	U.S. DEPARTMENT OF ENERGY		
DESIGN R. ATWOOD 5-96			
ENGINEER L. GAISON 5-96			
QUALITY S. CROW	MULTI CANISTER OVERPACK CANISTER COLLAR DETAIL		
	SIZE F	FSCM NO. 21210-H	SCALE 1=50	DWG NO. SK-2-300406	REV 0
	SHEET 1 OF 4		

1-61/1-62

Figure 1-11. Multicanister Overpack Cover, Locking and Lift Ring Detail. (4 sheets)

THIS PAGE INTENTIONALLY
LEFT BLANK

The cladding on a significant amount of the fuel, due to normal handling, was damaged during discharge from the reactor or during subsequent fuel handling. Video imaging indicates that the outer elements as well as the inner elements have breached cladding. As a result, the uranium in some elements was exposed to water and has oxidized during storage. This oxidation causes the fuel elements to swell, leading to further cladding damage, which exposes fresh uranium to the basin water and further oxidation. The loss of cladding integrity and the oxidation of the uranium allows soluble and gaseous fission products to dissolve into the Basin and canister water. Characterization in the basins suggests that approximately 3,800 kg (8,375 lb) of uranium in the K East Basin and 700 kg (1,545 lb) of uranium in the K West Basin have corroded.

The fuel assemblies and scrap (pieces greater than 0.6 cm [0.25 in.] in diameter) will be contained in one of five or six baskets (depending on fuel type), placed one on top of another, in the vertical MCO. The baskets will have an optimum carrying capacity in terms of weight as well as criticality considerations. More information regarding the basket structural design and analyses is presented in Section 3.0 of this report.

1.5 *IDENTIFICATION OF AGENTS AND CONTRACTORS*

Agents and contractors responsible for the design and fabrication of the MCO and the baskets are as follow:

- Duke Engineering Services Hanford

  Responsibility: Duke Engineering Services Hanford is responsible for the overall management and execution of the MCO subproject. This includes development of the subproject functions and requirements, performance specification, safety documentation, design review and approval, quality assurance, procurement, budget, schedule, and coordination with interfacing subprojects and with the DOE, Richland Operations Office.

- Parsons Infrastructure and Technology Group, Inc.

  Responsibility: Parsons Infrastructure and Technology Group, Inc. is the design agent for the MCO subproject and is tasked with development of the MCO design in accordance with the specification criteria. Parsons is responsible for the professional quality, technical accuracy, and cost-effectiveness of the design media to be used for fabrication of the MCOs.

- Fabricator - to be determined

  Responsibility: The MCO fabricator is responsible for materials, fabrication, welding, examination, shop testing, quality assurance, documentation, packaging, and shipping for the MCOs in accordance with the requirements of the fabrication specification. This includes development of a manufacturing plan, schedule, fabrication drawings, material certificates, fabrication and welding procedures, examination reports, and test reports to verify that the materials and completed work conforms to the specification requirements.

This page intentionally left blank.

2.0 PRINCIPAL DESIGN CRITERIA

2.1 SPENT FUEL TO BE STORED

Chapter 1.0 of this topical report provided background information related to the MCO and a description of the MCO and its general characteristics. When fully loaded, each MCO will house five or six baskets, each basket containing prescribed amounts of SNF and incidental fuel corrosion products that have been retrieved from the K Basins. The following materials describe the fuel that will be contained in any one of those baskets at any given time. A knowledge of the fuel types and characteristics will enable the reader to view health and safety concerns in the proper perspective as additional details pertaining to the MCO are presented in this report. The following paragraphs and tables contain physical descriptions of the fuel currently in the K Basins, give a fuel burnup summary, and provide details of the chemical and radionuclide inventories of SNF. The information presented also is useful in supporting the chapters in this report that discuss radiological protection, shielding, and criticality.

N Reactor fuel assemblies consist of two concentric tubes made of uranium metal coextruded into Zircaloy-2 cladding. The two basic types of fuel assemblies are differentiated by their uranium enrichment. Mark IV fuel assemblies have a pre-irradiation enrichment of 0.947% ^{235}U in both tubes and an average uranium weight of 22.7 kg (50 lb). The Mark IV assemblies have an outside diameter of 6.1 cm (2.42 in.) and lengths of 44.2 cm, 58.9 cm, 62.5 cm, or 66.3 cm (17.4, 23.2, 24.6, or 26.1 in.). Mark IA fuel assemblies have a pre-irradiation enrichment of 1.25% ^{235}U in the outer tube and 0.947% ^{235}U in the inner tube. The Mark IA assemblies have an average uranium weight of 16.3 kg (35.9 lb). Mark IA fuel assemblies have an outside diameter of 6.1 cm (2.40 in.) and lengths of 37.8 cm, 49.8 cm, 53.1 cm, or 66.3 cm (14.9, 19.6, 20.9, or 26.1 in.). A small amount of fuel with 0.71% ^{235}U content was designated as Mark IVB fuel. The Mark IVB fuel has the same dimensions and weights as the 66.3-cm- (26.1-in.-) long Mark IV fuel. Table 2-1 contains a detailed physical description of the fuel.

Exposure level, or fuel burnup, and time since discharge determine the radionuclide content of a fuel assembly or group of assemblies. The K Basin inventory of N Reactor fuel is composed of elements that experienced a range of exposure levels and were discharged from the reactor between January 1971 and April 1987. The exposure levels ranged from unburned fuel (0 MW) to approximately 6,000 MWd per metric ton of uranium (MTU). Burnup is related to the weight fraction of the isotope ^{240}Pu that exists within the total quantity of plutonium in a particular fuel element. The ^{240}Pu content is commonly used to indicate fuel burnup and ranges from approximately 0 wt% ^{240}Pu up to 16.72 wt% ^{240}Pu for the N Reactor fuel in inventory.

Accountability records have been used as the basis for estimating the radionuclide content of N Reactor fuel. The accountability record run data, dated November 17, 1994, includes discharge date, fuel type, ^{240}Pu content, and other information for 497 groups of fuel elements (the groups are also known as keys). Each group, or key, includes elements of the same type, with the same burnup, that were discharged from the reactor at the same time.

Table 2-1. 105-N Reactor Fuel Assembly Description.

	Mark IV				Mark IA			
Pre-irradiation enrichment of ^{235}U	0.947% enriched				1.25-0.947% enriched			
Type-length code[a]	E	S	A	C	E	M	T	F
Length (cm)	66.3	62.5	58.9	44.2	66.3	53.1	49.8	37.8
Element diameter (cm)								
1. Outer of outer	6.15				6.10			
2. Inner of outer	4.32				4.50			
3. Outer of inner	3.25				3.18			
4. Inner of inner	1.22				1.11			
Cladding mass (kg)								
1. Outer element	1.09	1.04	0.99	0.79	1.07	0.88	0.83	0.66
2. Inner element	0.55	0.52	0.50	0.40	0.66	0.54	0.51	0.40
Mass of uranium in outer element (kg)								
1. 0.947% ^{235}U	16.0	15.0	14.1	10.5				
2. 1.25% ^{235}U					13.8	11.1	10.4	7.85
Mass of uranium in inner element (kg) 0.947% ^{235}U	7.48	7.03	6.62	4.94	6.84	5.49	5.12	3.90
Weighted average of uranium in element (kg)	22.7				16.3			
Ratio of Zircaloy-2 to uranium (kg/MTU)	70.0	70.8	71.6	77.1	83.8	85.5	86.3	90.4
Weighted average (kg/MTU)	70.3				85.7			
% of total elements	63				37			
% of length type of each fuel	78	10	7	5	0.03[b]	87	10	3
Displacement volume (l/MTU)	67				67			

[a]Letter codes differentiate the different lengths of the Mark IV or Mark IA fuel elements (i.e., a type "E" element is 66.3 cm long).
[b]There are only 12 of the 66.3-cm Mark IA assemblies.

MTU = metric ton of uranium.

The mass of uranium associated with each key varies from 2.37 x 10^{-3} MTU to 67.4 MTU. The accountability database that forms the inventory basis, and which takes precedence over this topical report in fuel inventory matters, is shown in Appendix A of WHC-SD-SNF-TI-009, *105-K Basin Material Design Basis Feed Description for Spent Nuclear Fuel Project Facilities* (Willis 1995). Tables 2-2 and 2-3 present breakdowns of the fuel burnup listed in the accountability database for Mark IV and Mark IA fuel.

Table 2-2. N Reactor Mark IV Fuel Burnup Summary.

Percent ^{240}Pu (range)	Mass (MTU)	Percent of total mass
≤5	166.94	11.35
>5 - 7	125.25	8.51
>7 - 9	0.059761	0.00
>9 - 11	62.988	4.28
>11 - 13	270.56	18.39
>13 - 15	714.01	48.54
>15	131.29	8.92
Total	1471.1	100

MTU = metric ton of uranium.

Table 2-3. N Reactor Mark IA Fuel Burnup Summary.

Percent ^{240}Pu (range)	Mass (MTU)	Percent of total mass
≤5	36.124	5.75
>5 - 7	3.3729	0.54
>7 - 9	0	0.00
>9 - 11	68.008	10.83
>11 - 13	118.59	18.88
>13 - 15	401.88	64.00
>15	0	0.00
Total	627.98	100

MTU = metric ton of uranium.

The chemical content of the fuel on a pre-irradiation basis is derived by applying the reported pre-irradiation concentration range to the total uranium (2,100,000 kg), zirconium (145,000 kg), and brazing filling (3,000 kg) in N Reactor fuel. In the post-irradiation fuel, a small percentage of the

uranium will have been fissioned or converted to plutonium, and some of the other constituents will have been activated by neutron bombardment; this is particularly true for the boron and hafnium, which have relatively high neutron capture cross sections. Table 2-4 lists kilogram quantities of the chemical inventory of N Reactor fuel currently stored in the K Basins (Willis 1995).

Tables 2-5, 2-6, and 2-7 contain the radionuclide inventory of the N Reactor fuel in storage at the K Basins. Table 2-5 contains an inventory estimate for the combined total for both basins. Table 2-6 contains an inventory estimate specific to the K East Basin, and Table 2-7 contains an inventory estimate specific to the K West Basin. The ^{85}Kr data provided in each table assumes this gaseous nuclide has not been released from the fuel.

2.2 DESIGN CRITERIA FOR ENVIRONMENTAL CONDITIONS AND NATURAL PHENOMENA HAZARDS

Natural phenomena hazard (NPH) loads applicable to the MCOs are specified in this section. The DOE NPH requirements are based on DOE Order 5480.28, *Natural Phenomena Hazards Mitigation*; and supporting standards, DOE-STD-1020-94, *Natural Phenomena Hazards Design and Evaluation Criteria for Department of Energy Facilities*; DOE-STD-1022-94, *Natural Phenomena Hazards Site Characteristics Criteria*; and DOE-STD-1023-95, *Natural Phenomena Hazards Assessment Criteria*. DOE regulatory policy for SNF Project activities also requires a level of nuclear safety comparable to that of NRC-licensed facilities (Grumbly 1995). The NRC NPH requirements are based on 10 CFR 72.

DOE Order 5480.28 requires that each structure, system, and component (SSC) be assigned to one of five performance categories based on safety class and hazard category. Each performance category has an associated NPH goal that serves as a measure of the level of protection against potential natural phenomena. The CSB has been given an interim designation as a hazard category 2 facility (Kummerer 1995; Sellers 1996). It is expected that the CVDF and HCS Annex also will be designated as hazard category 2 facilities. With these classifications, safety-class SSCs within these facilities will be designated performance category 3 SSCs.

An MCO must maintain its structural integrity so as to perform the following functions for all credible events:

- Limit the release path for particulate material to the penetrations associated with the rupture disk and vent path (facility specific)
- Limit the path for oxygen ingress to these same two paths (common to all facilities [see Section 11.3])
- Maintain the geometry and physical controls assumed in the criticality safety evaluation report (common to all facilities [see Chapter 6.0]).

The SSCs required to ensure these MCO functions are maintained must be designed to performance category 3 requirements.

Table 2-4. Chemical Inventory of N Reactor Fuel Currently Stored in the K Basins.

Element	Uranium alloy 601 (kg)	Zircaloy-2 cladding (kg)	Brazing filler (kg)	Totals (kg)*
Al	1,480 - 1,900	11.1	0.411	1,700
B	0.530	0.074	0.00142	0.605
Be	21.0	--	142	163
C	769 - 1,550	40.7	1.42	1,200
Cd	0.530	0.074	0.00142	0.605
Co	--	1.48	0.0567	1.54
Cr	137	74 - 222	1.42 - 4.26	288
Cu	158	7.40	0.170	166
Fe	632 - 843	104 - 296	1.70 - 5.96	941
H	4.22	3.70	0.142	8.06
Hf	--	29.6	0.567	30.2
Mg	52.7	2.96	0.170	55.8
Mn	52.7	7.40	0.170	60.3
Mo	--	7.40	0.142	7.54
N	158	11.8	0.567	170
Na	--	2.96	0.0567	3.02
Ni	211	44.4 - 118	0.851 - 2.27	294
O	--	--	6.53	6.53
Pb	--	14.8	0.369	15.2
Si	261	14.8	0.709	277
Sn	--	1,780 - 2,520	32.3 - 48.2	2,190
Ti	--	7.40	0.142	7.54
V	--	7.40	0.142	7.54
W	--	7.40	0.284	7.68
Zr	137	145,000	2,780	148,000
Actinides				
U	2,100,000	0.518	0.0113	2,100,000
Np	87.2	--	--	87.2
Pu	4,030	--	--	4,030
Am	83.3	--	--	83.3
Cm	0.171	--	--	0.171
Fission products				
Se	1.11	--	--	1.11
Sr	73.3	--	--	73.3
Tc	152	--	--	152
Pd	26.4	--	--	26.4
Kr	75.8	--	--	75.8
I	31.6	--	--	31.6
Cs	207	--	--	207
Pm	1.14	--	--	1.14
Sm	6.39	--	--	6.39
Xe	986	--	--	986

*For the values with a range, the midpoint of the range is used (includes preburnup and postburnup values).

Table 2-5. Radionuclide Inventory of N Reactor Fuel Currently Stored in the K Basins.

Isotope	Activity (Ci)	Mass (kg)	Heat generation (W)	Isotope	Activity (Ci)	Mass (kg)	Heat generation (W)
Fission and activation products							
^{3}H	3.74 E+04	3.88 E-03	1.26 E+00	^{123}Sn	3.91 E-05	4.76 E-12	1.22 E-07
^{14}C	6.93 E+02	1.55 E-01	2.02 E-01	^{126}Sn	1.56 E+02	5.50 E+00	4.78 E-02
^{55}Fe	2.05 E+03	8.20 E-04	6.83 E-02	^{124}Sb	1.73 E-17	9.89 E-25	2.28 E-19
^{60}Co	4.18 E+03	3.70 E-03	6.45 E+01	^{125}Sb	3.72 E+04	3.60 E-02	1.17 E+02
^{59}Ni	4.10 E+01	5.41 E-01	1.63 E-03	^{126}Sb	2.18 E+01	2.61 E-07	3.96 E-01
^{63}Ni	4.51 E+03	7.31 E-02	4.54 E-01	^{126m}Sb	1.56 E+02	1.99 E-09	2.00 E+00
^{79}Se	8.62 E+01	1.24 E+00	2.66 E-02	^{123m}Te	6.61 E-11	7.45 E-18	9.58 E-14
^{85}Kr	6.06 E+05	1.54 E+00	9.08 E+02	^{125m}Te	9.07 E+03	5.04 E-04	7.65 E+00
^{89}Sr	5.75 E-17	1.98 E-24	1.98 E-19	^{127}Te	2.48 E-06	9.40 E-16	3.34 E-09
^{90}Sr	1.02 E+07	7.48 E+01	1.19 E+04	^{127m}Te	2.53 E-06	2.68 E-13	1.25 E-09
^{90}Y	1.02 E+07	1.87 E-02	5.65 E+04	^{129}Te	0.00	0.00	0.00
^{91}Y	1.33 E-13	5.42 E-21	4.78 E-16	^{129m}Te	0.00	0.00	0.00
^{93}Zr	4.00 E+02	1.59 E+02	4.61 E-02	^{129}I	6.37 E+00	3.61 E+01	2.99 E-03
^{95}Zr	8.65 E-12	4.03 E-19	4.35 E-14	^{134}Cs	1.83 E+04	1.41 E-02	1.87 E+02
^{93m}Nb	2.45 E+02	8.67 E-04	4.39 E-02	^{135}Cs	7.75 E+01	6.73 E+01	2.59 E-02
^{95}Nb	1.92 E-11	4.91 E-19	9.20 E-14	^{137}Cs	1.33 E+07	1.53 E+02	1.34 E+04
^{95m}Nb	6.41 E-14	1.68 E-22	8.46 E-17	^{137m}Ba	1.26 E+07	2.34 E-05	4.95 E+04
^{99}Tc	2.88 E+03	1.70 E+02	1.44 E+00	^{141}Ce	0.00	0.00	0.00
^{103}Ru	0.00	0.00	0.00	^{144}Ce	1.32 E+03	4.14 E-04	8.73 E-01
^{106}Ru	2.42 E+03	7.23 E-04	1.44 E-01	^{143}Pr	0.00	0.00	0.00
^{103m}Rh	0.00	0.00	0.00	^{144}Pr	1.30 E+03	1.72 E-08	9.55 E+00
^{106}Rh	2.42 E+03	6.80 E-10	2.31 E+01	^{144m}Pr	1.58 E+01	8.71 E-11	5.33 E-03
^{107}Pd	1.63 E+01	3.17 E+01	8.94 E-04	^{147}Pm	5.15 E+05	5.55 E-01	1.89 E+02
^{110}Ag	4.32 E-04	1.04 E-16	3.25 E-09	^{148}Pm	0.00	0.00	0.00
^{110m}Ag	3.25 E-02	6.84 E-09	5.39 E-04	^{148m}Pm	0.00	0.00	0.00
^{113m}Cd	3.62 E+03	1.67 E-02	3.98 E+00	^{151}Sm	1.76 E+05	6.69 E+00	2.07 E+01
^{115m}Cd	0.00	0.00	0.00	^{152}Eu	9.65 E+02	5.58 E-03	4.37 E+00
^{113m}In	5.32 E-07	3.18 E-17	1.23 E-09	^{154}Eu	1.11 E+05	4.11 E-01	9.96 E+02
^{113}Sn	5.32 E-07	5.30 E-14	8.82 E-11	^{155}Eu	2.34 E+04	5.03 E-02	1.69 E+01
^{119m}Sn	4.54 E-01	1.01 E-07	2.34 E-04	^{153}Gd	1.97 E-04	5.59 E-11	1.78 E-07
^{121m}Sn	8.00 E+01	1.35 E-03	8.41 E-02	^{160}Tb	1.18 E-14	1.05 E-21	9.41 E-17
Fission and activation product totals					2.68 E+07	7.09 E+02	1.34 E+05
Actinides							
^{234}U	8.74 E+02	1.40 E+02	2.47 E+01	^{241}Pu	5.66 E+06	5.50 E+01	1.75 E+02
^{235}U	3.37 E+01	1.56 E+04	9.14 E-01	^{242}Pu	5.49 E+01	1.44 E+01	1.60 E+00
^{236}U	1.27 E+02	1.96 E+03	3.40 E+00	^{241}Am	3.70 E+05	1.08 E+02	1.22 E+04
^{238}U	6.96 E+02	2.07 E+06	1.73 E+01	^{242}Am	1.95 E+02	2.41 E-07	1.62 E+00
^{237}Np	5.72 E+01	8.11 E+01	1.65 E+00	^{242m}Am	1.96 E+02	2.02 E-02	2.99 E-01
^{238}Pu	1.12 E+05	6.54 E+00	3.66 E+03	^{243}Am	1.20 E+02	6.02 E-01	3.81 E+00
^{239}Pu	2.14 E+05	3.44 E+03	6.59 E+03	^{242}Cm	1.62 E+02	4.90 E-05	5.86 E+00
^{240}Pu	1.19 E+05	5.22 E+02	3.71 E+03	^{244}Cm	1.47 E+03	1.82 E-02	5.04 E+01
Actinide totals					7.70 E+06	2.09 E+06	2.82 E+04

Note: 2/12/96 RUN for the N Fuel in the combined K Basins, results decayed to 12/31/97. Total mass 2.10 E+03 t uranium; total activity 5.56 E+07 Ci; total heat generation 1.62 E+05 W (5.53 E+05 Btu/h).

Table 2-6. Radionuclide Inventory of N Reactor Fuel Currently Stored in the K East Basin.

Isotope	Activity (Ci)	Mass (kg)	Heat (W)	Isotope	Activity (Ci)	Mass (kg)	Heat (W)
Fission and activation products							
^{3}H	1.84 E+04	1.90 E-03	6.19 E-01	^{123}Sn	3.29 E-05	4.00 E-12	1.03 E-07
^{14}C	3.62 E+02	8.12 E-02	1.06 E-01	^{126}Sn	8.07 E+01	2.84 E+00	2.48 E-02
^{55}Fe	1.08 E+03	4.32 E-04	3.57 E-02	^{124}Sb	1.41 E-17	8.06 E-25	1.87 E-19
^{60}Co	1.96 E+03	1.73 E-03	3.02 E+01	^{125}Sb	1.88 E+04	1.82 E-02	5.89 E+01
^{59}Ni	2.11 E+01	2.79 E-01	8.38 E-04	^{126}Sb	1.13 E+01	1.35 E-07	2.05 E-01
^{63}Ni	2.31 E+03	3.74 E-02	2.34 E-01	^{126m}Sb	8.07 E+01	1.03 E-09	1.03 E+00
^{79}Se	4.35 E+01	6.24 E-01	1.34 E-02	^{123m}Te	5.58 E-11	6.29 E-18	8.09 E-14
^{85}Kr	2.92 E+05	7.44 E-01	4.37 E+02	^{125m}Te	4.57 E+03	2.54 E-04	3.86 E+00
^{89}Sr	4.58 E-17	1.58 E-24	1.58 E-19	^{127}Te	2.06 E-06	7.80 E-16	2.79 E-09
^{90}Sr	5.01 E+06	3.67 E+01	5.83 E+03	^{127m}Te	2.11 E-06	2.24 E-13	1.04 E-09
^{90}Y	5.01 E+06	9.21 E-03	2.77 E+04	^{129}Te	0.00	0.00	0.00
^{91}Y	1.07 E-13	4.36 E-21	3.81 E-16	^{129m}Te	0.00	0.00	0.00
^{93}Zr	2.01 E+02	7.98 E+01	2.30 E-02	^{129}I	3.26 E+00	1.85 E+01	1.52 E-03
^{95}Zr	6.96 E-12	3.24 E-19	3.49 E-14	^{134}Cs	7.99 E+03	6.17 E-03	8.15 E+01
^{93m}Nb	1.24 E+02	4.39 E-04	2.22 E-02	^{135}Cs	3.96 E+01	3.44 E+01	1.32 E-02
^{95}Nb	1.55 E-11	3.95 E-19	7.40 E-14	^{137}Cs	6.61 E+06	7.60 E+01	6.68 E+03
^{95m}Nb	5.16 E-14	1.35 E-22	6.80 E-17	^{137m}Ba	6.25 E+06	1.16 E-05	2.45 E+04
^{99}Tc	1.45 E+03	8.55 E+01	7.27 E-01	^{141}Ce	0.00	0.00	0.00
^{103}Ru	0.00	0.00	0.00	^{144}Ce	1.09 E+03	3.42 E-04	7.21 E-01
^{106}Ru	1.84 E+03	5.50 E-04	1.10 E-01	^{143}Pr	0.00	0.00	0.00
^{103m}Rh	0.00	0.00	0.00	^{144}Pr	1.08 E+03	1.43 E-08	7.91 E+00
^{106}Rh	1.84 E+03	5.17 E-10	1.76 E+01	^{144m}Pr	1.31 E+01	7.22 E-11	4.40 E-03
^{107}Pd	8.59 E+00	1.67 E+01	4.72 E-04	^{147}Pm	2.73 E+05	2.94 E-01	1.00 E+02
^{110}Ag	3.46 E-04	8.30 E-17	2.60 E-09	^{148}Pm	0.00	0.00	0.00
^{110m}Ag	2.60 E-02	5.47 E-09	4.31 E-04	^{148m}Pm	0.00	0.00	0.00
^{113m}Cd	1.84 E+03	8.48 E-03	2.02 E+00	^{151}Sm	8.95 E+04	3.40 E+00	1.05 E+01
^{115m}Cd	0.00	0.00	0.00	^{152}Eu	4.77 E+02	2.76 E-03	2.16 E+00
^{113m}In	4.39 E-07	2.62 E-17	1.02 E-09	^{154}Eu	5.48 E+04	2.03 E-01	4.92 E+02
^{113}Sn	4.39 E-07	4.37 E-14	7.30 E-11	^{155}Eu	1.19 E+04	2.56 E-02	8.61 E+00
^{119m}Sn	3.82 E-01	8.53 E-08	1.97 E-04	^{153}Gd	1.48 E-04	4.20 E-11	1.33 E-07
^{121m}Sn	4.03 E+01	6.82 E-04	4.23 E-02	^{160}Tb	9.75 E-15	8.64 E-22	7.79 E-17
Fission and activation product totals					1.33 E+07	3.56 E+02	6.79 E+04
Actinides							
^{234}U	4.66 E+02	7.46 E+01	1.32 E+01	^{241}Pu	2.60 E+06	2.52 E+01	8.06 E+01
^{235}U	1.77 E+01	8.19 E+03	4.81 E-01	^{242}Pu	3.07 E+01	8.04 E+00	8.94 E-01
^{236}U	6.61 E+01	1.02 E+03	1.77 E+00	^{241}Am	2.03 E+05	5.91 E+01	6.68 E+03
^{238}U	3.80 E+02	1.13 E+06	9.46 E+00	^{242}Am	1.14 E+02	1.41 E-07	9.46 E-01
^{237}Np	3.02 E+01	4.28 E+01	8.70 E-01	^{242m}Am	1.14 E+02	1.17 E-02	1.75 E-01
^{238}Pu	6.07 E+04	3.55 E+00	1.98 E+03	^{243}Am	7.12 E+01	3.57 E-01	2.25 E+00
^{239}Pu	1.15 E+05	1.84 E+03	3.54 E+03	^{242}Cm	9.42 E+01	2.85 E-05	3.40 E+00
^{240}Pu	6.38 E+04	2.80 E+02	1.99 E+03	^{244}Cm	8.84 E+02	1.09 E-02	3.05 E+01
Actinide totals					3.96 E+06	9.51 E+05	1.52 E+04

Note: 02/12/96 RADNUC 2A test run for K East Basin N fuels, results decayed to 12/31/97. Total mass 1.146 E+03 t uranium; total activity 2.76 E+07 Ci; total heat generation 8.12 E+04 W (2.77 E+05 Btu/h).

Table 2-7. Radionuclide Inventory of N Reactor Fuel Currently Stored in the K West Basin.

Isotope	Activity (Ci)	Mass (kg)	Heat (W)	Isotope	Activity (Ci)	Mass (kg)	Heat (W)
Fission and activation products							
^{3}H	1.91 E+04	1.97 E-03	6.39 E-01	^{123}Sn	6.19 E-06	7.53 E-13	1.93 E-08
^{14}C	3.31 E+02	7.43 E-02	9.67 E-02	^{126}Sn	7.50 E+01	2.64 E+00	2.30 E-02
^{55}Fe	9.77 E+02	3.91 E-04	3.25 E-02	^{124}Sb	3.10 E-18	1.77 E-25	4.10 E-20
^{60}Co	2.22 E+03	1.96 E-03	3.43 E+01	^{125}Sb	1.85 E+04	1.79 E-02	5.80 E+01
^{59}Ni	1.99 E+01	2.63 E-01	7.88 E-04	^{126}Sb	1.05 E+01	1.26 E-07	1.90 E-01
^{63}Ni	2.19 E+03	3.55 E-02	2.22 E-01	^{126m}Sb	7.50 E+01	9.55 E-10	9.61 E-01
^{79}Se	4.28 E+01	6.14 E-01	1.32 E-02	^{123m}Te	1.03 E-11	1.16 E-18	1.49 E-14
^{85}Kr	3.15 E+05	8.03 E-01	4.72 E+02	^{125m}Te	4.50 E+03	2.50 E-04	3.80 E+00
^{89}Sr	1.17 E-17	4.03 E-25	4.01 E-20	^{127}Te	4.14 E-07	1.57 E-16	5.60 E-10
^{90}Sr	5.22 E+06	3.83 E+01	6.07 E+03	^{127m}Te	4.23 E-07	4.48 E-14	2.09 E-10
^{90}Y	5.22 E+06	9.59 E-03	2.89 E+04	^{129}Te	0.00	0.00	0.00
^{91}Y	2.67 E-14	1.09 E-21	9.55 E-17	^{129m}Te	0.00	0.00	0.00
^{93}Zr	2.01 E+02	7.98 E+01	2.30 E-02	^{129}I	3.11 E+00	1.76 E+01	1.46 E-03
^{95}Zr	1.70 E-12	7.90 E-20	8.55 E-15	^{134}Cs	1.03 E+04	7.96 E-03	1.05 E+02
^{93m}Nb	1.20 E+02	4.25 E-04	2.15 E-02	^{135}Cs	3.79 E+01	3.29 E+01	1.27 E-02
^{95}Nb	3.77 E-12	9.63 E-20	1.80 E-14	^{137}Cs	6.71 E+06	7.71 E+01	6.77 E+03
^{95m}Nb	1.26 E-14	3.31 E-23	1.66 E-17	^{137m}Ba	6.34 E+06	1.18 E-05	2.49 E+04
^{99}Tc	1.43 E+03	8.43 E+01	7.18 E-01	^{141}Ce	0.00	0.00	0.00
^{103}Ru	0.00	0.00	0.00	^{144}Ce	2.28 E+02	7.15 E-05	1.51 E-01
^{106}Ru	5.76 E+02	1.72 E-04	3.43 E-02	^{143}Pr	0.00	0.00	0.00
^{103m}Rh	0.00	0.00	0.00	^{144}Pr	2.26 E+02	2.99 E-09	1.66 E+00
^{106}Rh	5.76 E+02	1.62 E-10	5.51 E+00	^{144m}Pr	2.74 E+00	1.51 E-11	9.20 E-04
^{107}Pd	7.68 E+00	1.49 E+01	4.22 E-04	^{147}Pm	2.42 E+05	2.61 E-01	8.91 E+01
^{110}Ag	8.61 E-05	2.06 E-17	6.45 E-10	^{148}Pm	0.00	0.00	0.00
^{110m}Ag	6.47 E-03	1.36 E-09	1.08 E-04	^{148m}Pm	0.00	0.00	0.00
^{113m}Cd	1.78 E+03	8.21 E-03	1.96 E+00	^{151}Sm	8.69 E+04	3.30 E+00	1.02 E+01
^{115m}Cd	0.00	0.00	0.00	^{152}Eu	4.87 E+02	2.82 E-03	2.20 E+00
^{113m}In	9.28 E-08	5.55 E-18	2.14 E-10	^{154}Eu	5.62 E+04	2.08 E-01	5.04 E+02
^{113}Sn	9.28 E-08	9.24 E-15	1.54 E-11	^{155}Eu	1.15 E+04	2.47 E-02	8.32 E+00
^{119m}Sn	7.28 E-02	1.62 E-08	3.76 E-05	^{153}Gd	4.97 E-05	1.41 E-11	4.48 E-08
^{121m}Sn	3.98 E+01	6.73 E-04	4.18 E-02	^{160}Tb	2.03 E-15	1.80 E-22	1.62 E-17
Fission and activation product totals					1.35 E+07	3.53 E+02	6.79 E+04
Actinides							
^{234}U	4.08 E+02	6.53 E+01	1.15 E+01	^{241}Pu	3.02 E+06	2.93 E+01	9.36 E+01
^{235}U	1.60 E+01	7.40 E+03	4.34 E-01	^{242}Pu	2.42 E+01	6.34 E+00	7.03 E-01
^{236}U	6.11 E+01	9.44 E+02	1.63 E+00	^{241}Am	1.67 E+05	4.87 E+01	5.48 E+03
^{238}U	3.16 E+02	9.40 E+05	7.85 E+00	^{242}Am	8.16 E+01	1.01 E-07	6.80 E-01
^{237}Np	2.70 E+01	3.83 E+01	7.79 E-01	^{242m}Am	8.20 E+01	8.44 E-03	1.25 E-01
^{238}Pu	5.12 E+04	2.99 E+00	1.67 E+03	^{243}Am	4.89 E+01	2.45 E-01	1.54 E+00
^{239}Pu	9.93 E+04	1.60 E+03	3.06 E+03	^{242}Cm	6.77 E+01	2.05 E-05	2.45 E+00
^{240}Pu	5.52 E+04	2.42 E+02	1.72 E+03	^{244}Cm	5.81 E+02	7.18 E-03	2.00 E+01
Actinide totals					3.73 E+06	9.51 E+05	1.30 E+04

Note: 02/12/96 run for K West Basin N Reactor fuels, results decayed to 12/31/97. Total mass 9.531 E+02 t uranium; total activity 2.80 E+07 Ci, total heat generation 8.09 E+04 W (2.76 E+05 Btu/h).

The MCOs will perform the above-listed safety-class functions at the CVDF, to be located in the 100 K Area, and at the CSB and HCS Annex, to be located in the 200 East Area. The following discussions address the NPH loadings at both of these locations on the Hanford Site.

2.2.1 Tornado and Wind Loadings

According to the DOE requirements and guidance provided in DOE Order 5480.28 and DOE Standard 1020-94, the Hanford Site does not have a design basis tornado. However, to implement NRC nuclear safety equivalency as identified in WHC-SD-SNF-DB-003, *Spent Nuclear Fuel Project Path Forward, Additional NRC Requirements* (Garvin 1996), a design basis tornado must be identified and included in the design for the CVDF, CSB, and HCS Annex. Tornado protection for the MCO will be provided by the facilities in which it resides. Tornado protection for the MCO while it is located in the K Basins is not required.

2.2.1.1 Forces on Structures. While the MCO is located within the CVDF, CSB, and HCS Annex, it will not experience an extreme wind or tornado wind loading. Therefore, there is no need to convert such loadings to forces on the MCO.

2.2.1.2 Tornado-Generated Missiles. Protecting the MCO from tornado-generated missiles is facility specific. The following options may be applied:

- Provide a structure or barrier that does not allow for missile penetration that would put the MCO at risk
- Show by analysis that none of the credible or NRC postulated missiles will penetrate the MCO or the shipping cask-MCO combination
- Show that the risk of a significant radiological release caused by missile impact is acceptably low (acceptance criteria for $<1.0 \times 10^{-6}$ events/yr using conservative methods with a close acceptance criterion of 50 mSv (5 rem) (Tallman 1996a, 1996b).

For the first and second options, the load combinations must be in accordance with NUREG-0800, *Standard Review Plan*, Section 3.3.2, "Tornado Loading" (NRC 1981).

2.2.2 Design Basis Flood

Within the CVDF, CSB, and HCS Annex, the MCO will always be protected against the design basis runoff flood level for the probable maximum precipitation (PMP). This will be accomplished through facility design and by providing sufficient runoff capacity. The MCO will be protected from the river probable maximum flood (PMF) by locating the CVDF, CSB, and HCS Annex above the PMF level. Specific performance category 3 values for the PMP and PMF are provided for the CSB in WHC-SD-SNF-DB-009, *Canister Storage Building Natural Phenomena Hazards* (Tallman 1996a), and for the CVDF in WHC-SD-SNF-DB-010, *Cold Vacuum Drying System Natural Phenomena Hazards* (Tallman 1996b). These performance category 3 NPH values shall be applied to

the safety-class MCO and to those SSCs that function to protect the MCO. The PMP and PMF requirements for the CSB also apply to the HCS Annex. With this protection provided for the MCO by the facilities, there is no need to perform analyses of the loading that the PMP or PMF might have on an MCO. The flood protection provided by each facility is described in the facility-specific safety analysis report (SAR).

2.2.3 Seismic-System Analyses

At the CSB, the design ground acceleration for the design basis earthquake is 0.35 *g*. Although this will be amplified by the position of the MCOs within the facility, the DBA drop accelerations bound any imposed earthquake accelerations from the K Basins, CSB, CVDF, and HCS.

2.2.4 Snow and Ice Loadings

In the CVDF, CSB, and HCS Annex, the MCO will always be protected against snow and ice loadings by facility designs that ensure that neither will make contact with the MCO. As such, snow and ice will not stress the MCO either by temperature transients or extremes or by dead weight loading. During transport, the cask lid will protect the MCO.

2.2.5 Combined Load Criteria

The confinement/containment features of the MCOs are designed and fabricated to meet the intent of the load combination criteria in the Boiler and Pressure Vessel Code (ASME 1995a), Section III, Subsection NB.

2.2.6 Baseline Load Criteria

This section describes the criteria selected to provide the baseline loadings, including temperatures, which when met will ensure the mechanical and structural integrity of the MCO. The loadings and criteria are those specified by WHC-S-0426, *Performance Specification for Spent Nuclear Fuel Project, Multi-Canister Overpack* (WHC 1996c), or unique to particular applications.

The purpose of the MCO is to confine, contain, and maintain SNF in a critically safe array. Use of the criticality control exclusion void is discussed in Chapters 3.0 and 6.0.

2.2.6.1 Performance Criteria Loadings. The MCO consists of a shell, a shield plug, a baseplate with lower radial support plates, a center insert criticality or basket support tube, baskets designed to hold particular specified fuels, process tubes, and incidental process equipment. These components, as an assembly, are subjected to the following performance criteria loadings.

- The MCO shall maintain fuel elements or fragments thereof in a critically safe array throughout its 40-year design life and during and after being subjected to DBAs.

- The MCO shall relieve internal pressure in excess of 1.0 MPa gauge (150 lb/in^2 gauge). This criterion is enabled through use of a rupture disk.

- MCO handling features and equipment shall be capable of holding the maximum fully loaded weight of the component in question. In the case of the total MCO package, this includes the heaviest loaded fuel arrangement (Section 3.2), plus water, plus a margin for a stuck assembly, bringing the total handling load to 10,900 kg (24,000 lb). The features and equipment must exhibit the safety factors required by ANSI N14.6-1986, *For Radioactive Materials — Special Lifting Devices for Shipping Containers Weighing 10,000 Pounds (4500 kg) or More* (ANSI 1986). This standard requires that any handling or lift feature required to perform noncritical lifts shall be capable of demonstrating a safety factor of three on material yield and of five on material ultimate strength.

- The MCO shall be capable of performing its function when exposed to atmospheric temperatures ranging from -33 °C to 46 °C (-27 °F to 115 °F) and relative humidity ranging from 5% to 100%.

2.2.6.2 Design Loadings. The following loadings apply to the design of the MCO.

- The thermal source term internal to the MCO from the confined SNF is an average of 396 W and a maximum of 835 W plus allowable margin.

- The radioactive source term for worst-case shielding and dose consequences consists of 270 Mark IV fuel elements of 0.95% ^{235}U irradiated to 16% ^{240}Pu. Activity for these fuels is found in WHC-SD-SNF-TI-009 (Willis 1995). Radiation effects have been considered for polymers.

- The internal design pressure is 1.0 MPa gauge (150 lb/in^2 gauge).

- The maximum design temperature is 375 °C (700 °F) and the maximum operating temperature is 350 °C (660 °F). For design features requiring temperatures at the various MCO life cycle stages, the following are appropriate:

  - K Basin loading, 6 °C to 38 °C (43 °F to 100 °F)

  - Cold vacuum drying, 10 °C to 75 °C (50 °F to 167 °F)

  - Transportation, -17 °C to 75 °C (2 °F to 167 °F)

  - Hot conditioning, up to 375 °C (700 °F) as the maximum design temperature, 350 °C (660 °F) as the maximum operating temperature

  - Fuel staging and storage, up to 205 °C (400 °F).

- The design thermal transient is 100 °C (122 °F) per hour from 20 °C to 350 °C (68 °F to 662 °F) for a maximum of five cycles.

- The fuel design temperature within the MCO is 300 °C (570 °F).

- The design temperature differential between any portions of the MCO containment boundary materials, i.e., the shell and shield plug, is 100 °C (180 °F).

- In addition to the design load limits, certain fuel and MCO shell limitations are associated with facility management.

  - During MHM handling, staging, and storage the CSB, temperatures are allowed to go to 132 °C (270 °F). The facility may limit temperatures further if they choose. The fuel temperature is limited to 205 °C (400 °F) during normal steady-state conditions.

  - During HCS custody and HCS operations at the CSB, the MCO shell temperature is allowed to go to 350 °C (662 °F). There is an absolute cutoff at 375 °C (707 °F) for the highest allowed temperature on any portion of the MCO shell with no exceptions. The facility may limit the temperatures further. The fuel temperature inside the MCO is limited to 300 °C (572 °C).

2.2.6.3 Design Basis Accident Loadings. The following DBA loadings are required to be safely applied. They must meet the Service Level D requirements of the Boiler and Pressure Vessel Code (ASME 1995a), Section III, Subsection NB, for safety-class items or lower class items required to prevent failure of the safety-class items.

- The MCO shall withstand a DBA fire on the outside of the cask. This fire will reach a temperature of 800 °C (1,475 °F) with an emissivity coefficient of 0.9 for a period of 30 minutes. The fire will raise the MCO shell temperature to 122 °C (220 °F) for 180 minutes after the fire.

- While at the CSB and HCS Annex the MCO shall maintain confinement, containment, and subcriticality during a design basis earthquake having a zero period, 5% damped, horizontal ground acceleration of 0.35 *g*. Response spectra for other damping values are provided in WHC-SD-W236A-TI-002, *Probabilistic Seismic Hazard Analysis, DOE Hanford Site, Washington* (Geomatrix 1996).

- While at the CVDF, the MCO shall maintain confinement, containment, and subcriticality during a design basis earthquake having a zero period, 5% damped, horizontal ground acceleration of 0.26 *g*. Response spectra for other damping values are provided in WHC-SD-W236A-TI-002 (Geomatrix 1996).

- The MCO shall survive accelerations created by the following DBA drops while maintaining confinement, containment, and subcriticality (the temperature range for the drops is 25 °C to 200 °C [75 °F to

390 °F] and the pressure range is 0 Pa to 1.0 MPa gauge [0 to 150 lb/in^2 gauge]):

  - A 0.6-m (2-ft) vertical drop of the loaded and sealed unconstrained MCO onto flat reinforced concrete

  - A drop while loaded and confined to the sealed transportation cask in the worst orientation (the acceleration load has been tentatively set at 100 *g* pending outcome of the cask drop calculations)

  - A drop into the cask for drop heights not to exceed 4 m (13 ft) (the acceleration load again should be near 100 *g*)

  - A vertical drop of the unconstrained MCO into a CSB tube with and without another MCO already within the tube (the tubes will contain impact absorbers to reduce the impact acceleration on the MCO's internals to 50 *g* when the MCO's acceleration is limited to 35 *g*); protection for the impacted surfaces as well as the internals of the MCOs must be in place (WHC-S-0426, Section 3.3.2.2 [WHC 1996c], requires the use of impact absorbers between the upper and lower MCOs to satisfy this requirement)

  - A drop into HCS furnace with load applied to CSB bottom impact absorber in bottom of furnace

- A loaded basket subject to criticality controls required in WHC-SD-SNF-CSER-005 (Schwinkendorf 1996), such as the Mark IA, must not exceed stress levels higher than the applicable service level requirements allowed in the Boiler and Pressure Vessel Code (ASME 1995a), Subsection NG; any exceptions to this will be noted and defined; handling loads for both loaded and unloaded baskets will meet the design criteria for noncritical loads defined in ANSI N14.6-1986 (ANSI 1986).

2.3 SAFETY PROTECTION SYSTEMS

2.3.1 General

The activities associated with the MCO and its contents have been reviewed from initial loading of the MCO through long-term storage. The following sections discuss the protection afforded the MCO throughout its life cycle. The various forms of protection range from the physical structures housing the MCO to pressure relief devices both internal and external to the MCO to instrumentation associated with the processing facilities.

2.3.2 Protection by Confinement Barriers and Systems

Within the shipping cask, CVDF, CSB, and HCS Annex, an MCO is not the sole barrier against radiological release. This is different from most

facilities licensed under 10 CFR 72. In those facilities, the cask (the MCO equivalent but with integral shielding) is the only radionuclide barrier beyond the fuel cladding.

For the SNF Project, radionuclide releases from an MCO are analyzed by considering facility-specific mitigation features, siting considerations affecting atmospheric dispersion, and the location of the onsite and offsite receptors. Credible oxygen ingress and vent paths are by design limited to those discussed in Section 2.2. As a radionuclide barrier, the MCO must not fail under any credible condition. However, maintaining this feature has the following facility-specific considerations.

- Within the CSB, impact absorbers must be provided in the storage tubes as required to prevent failure of a dropped MCO (see Section 2.2.6.3).

- Within the CSB and HCS Annex, safety-class features must be provided to prevent the MHM from shearing an MCO by moving while the MCO is in an intermediate position in a tube (WHC 1996a). Maintaining the MCO in a thermally safe situation for prevention of fuel fire is also a safety-class function.

- In the CSB the structural integrity of the tube system, inclusive of the upper floor penetration and lower base plate support, is taken credit for as a safety-class item to prevent common mode failure of the MCOs and to maintain configuration for criticality prevention.

The following are MCO-specific features designed to achieve the lowest practical level of radioactive release from an MCO to the facility during normal and off-normal conditions.

- The MCO vent is provided with an internal bank of four HEPA filters. As these filters cannot be tested after MCO assembly, no credit is taken for their presence in accident analyses. However, the filters should remain effective during the staging period.

- The MCO is designed to remain intact for all credible events (see Chapter 11.0).

- When required, the MCO is provided with a rupture disk designed to relieve at a preset pressure up to 1.0 MPa (150 lb/in^2). With this protection, should the MCO overpressurize (caused, for example, by hydrogen generation together with an inoperative pressure relief device), the radionuclide release will be limited by relief through the rupture disk passage.

  During shipment from the K Basins to the CVDF, the MCO may be vented. During shipment to the CSB, the vent is inactive and the MCO is sealed. The vent is covered during processing in the CVDF and during processing in the HCS Annex. After conditioning in the HCS Annex, the pressure relief device and the rupture disk are covered and remain covered during CSB interim storage.

The means by which the MCO is protected against off-normal operations and external loadings are facility-specific considerations and are addressed in each facility's SAR (WHC 1996a, WHC 1996g). Each facility will be responsible for providing operators and equipment to address such considerations.

2.3.3 Protection by Equipment and Instrumentation Selection

2.3.3.1 Pressure Relief Equipment. When required, the MCO is provided with a rupture disk to relieve internal pressures in excess of the normal operating pressure (Goldmann 1996). This rupture disk shall meet the following design criteria (WHC 1996c).

- The rupture disk must relieve MCO internal pressures greater than 1.0 MPa gauge (150 lb/in^2 gauge).
- The rupture disk must perform the above functions in the design temperature range of 10 °C to 200 °C (50 °F to 392 °F).
- The rupture disk must perform the above functions after being subject to the DBAs.
- The rupture disk must perform the above functions in a humid environment (up to 100% humidity for short-term only) and a corrosive atmosphere.
- The rupture disk must perform the above functions without preventive maintenance.
- The rupture disk must be designed for contact assembly and replacement, if necessary, using appropriate handling equipment as required for working on the MCO. Design consideration shall be given to DOE Order 6430.1A.
- The exposed surfaces shall be such as to facilitate their decontamination.

2.3.3.2 High-Efficiency Particulate Air Filter. The MCO is provided with an internal bank of four HEPA filters. The function of the HEPA filters is to provide the filter for flow through the penetration, connection, and pathways to vent the gas in the MCO on a periodic or continuous basis through the pressure relief device (Goldmann 1996).

2.3.3.3 Instrumentation. The MCO is not provided with any instrumentation. Process systems requiring pressure indication will attach necessary instrumentation to the process ports of the shield plug. If necessary, for the function being performed, the systems also provide temperature, flow, and constituent measurements. Measurement of the MCO environment for operational and safety purposes shall be conducted and recorded by the systems connected to the process ports. The following functions will be monitored in succession:

- Water, drain, and gas purge system at the K Basins
- Water, drain, vacuum drying, and gas purge systems at the CVDF

2.4 DECOMMISSIONING CONSIDERATIONS

The intent of the SNF program is to ultimately ship the MCOs to a federal repository for disposal. There will be no need to decommission the MCO itself and there should be very little decontamination required for the MCO. In the event that decontamination processes are required, the extent of the process and the procedures to be followed will all be regulated by the specific facility in which the decontamination is to take place. However, decontamination and decommissioning efforts are beyond the project scope.

This page intentionally left blank.

3.0 STRUCTURAL EVALUATION

3.1 STRUCTURAL DESIGN

3.1.1 Multicanister Overpack

The MCO Performance Specification (WHC 1996c) was written to meet the intent of the Boiler and Pressure Vessel Code (ASME 1995a). The code requires information from which service loadings can be identified if the specification calls for computations to demonstrate compliance with specified service limits (ASME 1995a, Section III, NCA-2142.2). The Performance Specification (WHC 1996c) states that the MCO is to be designed to the intent of the Boiler and Pressure Vessel Code, Section III, Subsection NB.

The design loadings for pressure, temperature, and mechanical loads as noted in the Performance Specification (WHC 1996c) must meet the stress intensity limits for the stress categories noted in Design Condition Figure NB-3221-1 of the Boiler and Pressure Vessel Code (ASME 1995a) and summarized in Table 3-1. In addition, the limits for design loadings shall meet the requirements of the appropriate subsections of Section NCA-2142.4 (ASME 1995a), which are also summarized in the table.

Table 3-1. Stress Intensity Limits Under Normal and Accident Conditions.

Limits	P_m	P_L	P_b	P_L+P_b	$P_L+P_b+P_e+Q$	V	P_{comp}	P_{coll}
Design	S_m	$1.5xS_m$	∞xS_m	∞xS_m	--	$0.6xS_m$	S_m	--
Level A	--->	--->	--->	--->	$3xS_m$	$0.6xS_m$	--	--
Level D	$<2.4xS_m$ or $0.7S_u$	$1.5xP_m$ limit	--	$1.5xP_m$ limit	Appendix F of ASME Section III	$0.42xS_u$	$1.5xS_m$	$0.9xS_y$

Note: Design values are from ASME, 1995a, Boiler and Pressure Vessel Code, Section III, paragraphs NB-3211 and 3221, American Society of Mechanical Engineers, New York, New York; Level A (normal conditions) service limits are from ASME (1995a), Section III, paragraph NB-3222; Level D (accident conditions) service limits are from ASME (1995a), Section III, paragraph NB-3225 and Appendix F.

Q = secondary membrane plus bending stress.
P_b = primary bending stress intensity.
P_{comp} = maximum compressive stress.
P_{coll} = static or equivalent static loads as compared to collapse limits.
P_e = secondary expansion stress resulting from constraint of free end displacement.
P_l = primary local membrane stress intensity.
P_m = primary membrane stress intensity.
S_m = code stress intensity base allowable.
S_u = material ultimate strength.
S_y = material yield strength.
V = average primary shear stress.

The design specification may designate service limits as defined in Table 3-1. The Performance Specification (WHC 1996c) does not specifically designate these service limits, but the following limits are to be followed.

- Level A (normal conditions) service limits are sets of limits that must be satisfied for all normal service loadings to which the component or support may be subjected in the performance of its specified service function.

- Level D (accident conditions) service limits are those sets of limits that must be satisfied for all accident loadings identified. These loadings are typically off-normal drop or fire-induced conditions. These sets of limits permit gross deformations with some consequent loss of dimensional stability and damage requiring repair and may require removal of the component from service. For level D limits, the rules contained in Appendix F of the Boiler and Pressure Vessel Code (ASME 1995a) may be used in evaluating the level D service loadings, independent of all other design and service loadings.

The components used or immediately affected by lifting of components shall meet the requirements of ANSI N14.6-1986 (ANSI 1986), as specified for noncritical lifts. The design of the mechanical closure was evaluated in accordance with the Boiler and Pressure Vessel Code, Section III, Subsection NB (ASME 1995a). Results of the evaluation are contained in SCS-W-96-1606, *ASME Section III, Subsection NB, Analysis of the Multi-Canister Overpack Assembly with the Mechanical Closure Ring* (Shrivastava 1996).

3.1.2 Fuel Baskets

The MCO fuel baskets are categorized into two major types: intact fuel element baskets and scrap fuel (fragment) baskets. Fuel baskets must maintain criticality control for the higher enriched (Mark IA) fuel. These basic requirements lead to four different basket types.

- Type 1 will hold 48 Mark IA (higher enriched) intact-fuel elements and must have a criticality control exclusion void built into the basket.

- Type 2 will hold 54 Mark IV intact-fuel elements but does not need the exclusion void.

- Type 3 will hold Mark IA (higher enriched) scrap fuel (fragments) and must have a criticality control exclusion void built into the basket.

- Type 4 will hold Mark IV scrap fuel (fragments) but does not need the exclusion void.

Single pass reactor (SPR) fuel will be loaded into Mark IA scrap baskets. Fuel baskets were designed to maximize payload, minimize movement of fuel during transport, and maintain criticality control within the limits specified in Section 3.3.2.3 of WHC-S-0426 (WHC 1996c). The design should take into consideration the ease of loading fuel into the baskets, the ease of loading baskets into the MCO shell, and the gas circulation for conditioning processes.

The fuel baskets for criticality control shall be designed to the intent of the Boiler and Pressure Vessel Code (ASME 1995a), Section III, Subsection NG, as guided by NUREG/CR 3854 (NRC 1984), which classifies all container components used to control criticality during the transport of fissile materials as part of a second safety group called criticality. As such, all container components of that description and holding contents of any category (based on type and quantity of radioactive material being transported) are to be designed to the intent of the Boiler and Pressure Vessel Code (ASME 1995a), Section III, Subsection NG, with deviations from the code noted and described. All basket configurations will be designed to the conditions specified with deviations from these controls noted in the following paragraphs.

The design temperature for normal conditions will be 200 °C (400 °F) while within the MCO and 6 °C to 38 °C (43 °F to 100 °F) while being loaded with fuel and placed into the MCO. The design pressure is 1.0 MPa gauge (150 lb/in^2 gauge) around the baskets while within the MCO. The Mark IA basket designs, when exposed to normal operating loads, shall meet the requirements of service level A in the Boiler and Pressure Vessel Code (ASME 1995a), Section III, Subsection NG. In addition, both the loaded and the unloaded baskets shall meet, as required for handling, the requirement of demonstrating a safety factor of three on material yield strength, or a safety factor of five on material ultimate strength, whichever is most critical. The effects of operating temperature on material strengths will be taken into account.

The fuel baskets shall maintain the criticality control features defined for the accident conditions listed in Section 3.3.2.2 of WHC-S-0426 (WHC 1996c), while maintaining the limits imposed by the Boiler and Pressure Vessel Code (ASME 1995a), Section III, Subsection NG, service level D. These criticality control features are defined in WHC-SD-SNF-CSER-005 (Schwinkendorf 1996). Permanent deformation is allowed in all portions of the baskets not necessary to criticality control and process operations. The following features are considered necessary to criticality control and process operations.

- The Mark IA basket's criticality tube, when assembled in the MCO, may not shift more than 5.0 cm (2 in.) radially from the centerline.
- The Mark IA basket's criticality tube, when assembled in the MCO, may not be crushed or permanently distorted.

3.2 STRUCTURAL ANALYSES

3.2.1 Multicanister Overpack Buckling

Buckling calculations have been performed to show breach of the MCO will not occur at drop loadings that could be produced by operations or accidents postulated for the SNF Project. The basic assumption made for this analysis is that buckling or shell instability will occur before tearing or failure of the shell wall can occur. The results of these analyses show that yielding of the MCO shell, considered to be the start of linear buckling, does not occur

until a value is reached well above 100 *g*, the approximate maximum expected loading on the MCO. Total instability of the MCO shell when encapsulated by the transportation cask occurs at loadings greater than 500 *g*. The calculation discussions and analyses are provided in Appendix A.

Buckling of the MCO shell was evaluated in accordance with two theories based on either linear or nonlinear elasticity concepts. Linear shell theories adequately predict stresses for shells exhibiting small elastic deformations. The analysis in Appendix A provided a lower bound estimate of the vertical static load factor that may be applied to the MCO shield plug and shell combined weights to produce incipient instability of the shell. It is shown that incipient buckling (yielding) occurs at 206 *g* when the MCO is unpressurized.

Nonlinear large deflection theory was used to evaluate the potential for breach of the MCO shell because of accident conditions while inside the shipping and handling cask. In this case the shell's lateral deformations are controlled in the outward direction by the shipping cask wall and in the inward direction by the SNF baskets. It is shown that no breach will occur even if the vertical static load factor exceeds 700 *g* (Appendix A).

3.2.2 Multicanister Overpack Storage Basket Analysis

Structural analyses were performed for the SNF storage basket mock-up designs shown in Figures 1-5 through 1-8. These preliminary analyses, performed in accordance with the Performance Specification (WHC 1996c), investigated the handling of the loaded baskets and their usage in the MCO. The calculation discussions and analyses are provided in Appendix B.

The following specific areas were addressed:

- The ability of the basket center pipe to resist buckling and lateral deformation during separate vertical and lateral accelerations in order to meet the requirements imposed by criticality considerations and to prevent interference with the long process tube
- The ability of the basket baseplates to support the fuel elements and transfer the resulting loading to the support rods and the center pipe
- The ability of the MCO bottom cap and sidewall to resist perforation by fractured fuel elements during an accidental drop.

For vertical accelerations the center pipes were analyzed as pin-ended columns assuming a tight fit between baskets. These static analyses considered all the baskets were accelerated uniformly. The baseplate of the bottom basket provided support to the lower end of the column and the upper end of the center pipe was captured and supported by the MCO lid.This is an essential feature of the lid design along with its ability to provide vertical restraint for the six outer support rods. It is shown in Appendix B that the Mark IA center pipe meets criticality requirements and is capable of sustaining a vertical acceleration of 35 *g*'s stipulated in the Performance Specification (WHC 1996c). Since this is well above normal handling loads of

three factors to material yield strength and five factors to material ultimate strength, the design is judged adequate. The Mark IV center support tube is capable of sustaining a vertical acceleration of more than 10 *g*. During an accident condition, when higher vertical accelerations may be experienced, the Mark IV basket baseplates are designed to separate from the center support tube. This feature permits consolidation of the fuel while relieving the center pipe of excessive loading. Both scrap basket designs have six intermediate webs extending between the center pipe and the outer shell. These webs stabilize the outer shell and permit it to sustain vertical accelerations that are at least equal to those of the storage baskets.

For lateral accelerations the center pipes are supported by each of the basket baseplates as well as the lid. For the postulated lateral loading, the structural deformation of both the Mark IA and Mark IV center pipes is acceptable (see Appendix B). Note that only structural deformations are given, the effect of tolerances between assemblies and with the lid have not been investigated. The resulting stresses in the center pipes of both baskets are also well within the accident (level D) allowable of the Boiler and Pressure Vessel Code (ASME 1995a).

Because of their complex geometry, the 7.6-cm- (3-in.-) thick perforated baseplates of the storage baskets were analyzed with finite-element models. These analyses show the baseplates are structurally adequate for normal handling conditions and for accident accelerations in excess of those occurring at the time of designed separation from the Mark IV center pipe and in excess of 35 *g* for the Mark IA center pipe.

An evaluation of the potential for a fuel element perforating the bottom or sidewall of the MCO was also performed (Appendix B). While the maximum drop height of an unprotected MCO is 0.6 m (2 ft), it can be dropped 9 m (30 ft) when contained in the transportation and handling cask. For these scoping calculations a missile with the diameter of a fuel element was assumed to drop 9 m (30 ft). It was found that for this missile to just perforate the bottom cap would require the mass of nearly one-quarter of all the fuel in the MCO to be stuck to it and acting with it. It was also found that it requires a fractured fuel element, with a nearly knife-sharp edge, falling 9 m (30 ft) to just perforate the sidewall. Both these scenarios are considered extremely unlikely given the composite construction of the fuel elements.

Since the MCO and its storage baskets, as well as the cask and transportation system, are in the preliminary design stage, these calculation results should be viewed as preliminary and scoping in nature. Calculations will be reviewed after completion of the final design.

3.2.3 Multicanister Overpack Drop and Related Analyses

The requirements of the MCO Performance Specification (WHC 1996c) stipulate that the MCO shall withstand impacts from accidental drop and maintain fuel confinement, containment, and subcriticality. These drops are postulated to be bounded by the following design accident scenarios.

- A 0.6-m (2-ft) vertical drop of the loaded and sealed unconstrained MCO onto flat reinforced concrete

- A 100 *g* (approximate) impact as felt by the MCO in its worst-case orientation when dropped while loaded and constrained in the sealed transportation cask (i.e., the cask is configured to prevent MCO escape; the 100 *g* requirement is not absolute but a guideline value for design)

- A vertical drop of an unconstrained MCO into a CSB storage tube where the storage tube contains impact absorbers that limit the impact forces delivered to the MCOs (the impact forces are limited to 35 *g* on the MCO and 50 *g* on the MCO's contents).

Additional analyses were conducted to verify the above limitations were met when the MCO was dropped into the cask and that the MCO would survive when loaded. Analyses also were conducted to determine the pneumatic resistance to increased drop velocity when dropped back into the cask. These analyses show that the velocity at impact with the present "necked" diametral clearance of 0.6 cm (0.25 in.) is halved from that of a free drop.

The drop accident analyses provide the accelerations that are used to produce stress analyses for showing conformance to the allowable criteria. The MCO confinement is produced to the intent of the Boiler and Pressure Vessel Code (ASME 1995a), Subsection NB, which a criterion document. Parsons is performing stress analyses that will demonstrate compliance with the intent of Subsection NB.

The analyses and documentation for the drop scenarios are provided in Appendix C and include the drops for the cask itself, as the MCO is directly coupled in most cases and the analyses are easier to understand if they are all kept together. The results of the analyses show that the MCO successfully survives all of the postulated and design basis drops. This allows the lift of the MCO and/or cask to be classified as a noncritical lift according to ASME NOG-1-1995, *Rules for Construction of Overhead and Gantry Cranes (Top-Running Bridge, Multiple Girder)* (ASME 1995b), or ANSI N14.6-1986 (ANSI 1986). The analyses for dropping an MCO directly on top of another MCO in a CSB storage tube are provided in Appendix D.

3.2.4 Multicanister Overpack Mechanical Closure

The lower MCO in a CSB storage tube is subject to an overhead strike by another MCO that is being lowered into the storage tube above it. Impact absorbers are provided at the base of the CSB storage tube and in the space between the two MCOs. The goal for the mechanical closure is to survive an impact of about 35 *g* from an overhead strike by the heaviest MCO. An upper MCO dropping onto a lower MCO with this amount of force, without benefit of the upper impact absorber, will cause the mechanical seal to be compressed during the drop; but based on discussions with the seal manufacturer, the MCO mechanical closure is expected to maintain the MCO's seal. Separate analyses were conducted for the overhead strike on the locking and lifting ring and for the overhead strike on the shield plug body (see Appendix D). Analytical evaluations are continuing into the drop scenarios at the CSB storage tubes using the upper impact absorber between the two MCOs. The case of an overhead strike with no resulting deformation in the seal area would preserve the ability to disassemble the MCO in the same way it was assembled.

At the 35 *g* level, the heaviest MCO falling onto a lower MCO without benefit of the upper impact absorber damages the faces that bear on the compression limiter of the Helicoflex seal on the lower MCO. Options exist to seal a leaking MCO after such a drop. The MCO is recoverable after such a strike as the seal face deformation at the compression limiter is currently on the order of 0.76 mm (0.030 in.) on the shield plug portion face using 137.9 Mpa (20,000 lb/in^2) yield. On the production MCOs, higher yield materials are anticipated for use. The threads of the MCO neck and of the locking and lifting ring would survive sufficiently to provide adequate load path to lift the MCO from the CSB storage tube. If needed, the mechanical closure MCO might be resealed either by tightening the eight jack bolts in the locking and lifting rings or by installing the welded cover cap, which adds approximately 8.6 cm (3.38 in.) to the MCO's length. In the case of the cover cap installation, the resulting completed mechanical closure assembly robustness is essentially the same as the welded closure assembly.

3.3 WEIGHTS AND CENTERS OF GRAVITY

The SNF from the K Basins is placed into baskets that are loaded into the MCO. Five baskets loaded with Mark IV fuel assemblies, which are approximately 66 cm (26.1 in.) long, or six baskets loaded with Mark IA fuel assemblies, which are approximately 53 cm (20.9 in.) long, can be stacked within the MCO. The smaller SPR fuel assemblies will be loaded into scrap baskets and placed into MCOs. Also, fuel fragments greater than 0.6 cm (0.25 in.) in cross section will be loaded into the MCO using "scrap baskets." The plan is that no more than one scrap basket, together with intact fuel baskets, will be loaded in any MCO. However, WHC-SD-SNF-CSER-005 (Schwinkendorf 1996) allows up to two scrap baskets, one at each end of the MCO. Although two scrap baskets are acceptable from a criticality perspective, the limit of 300 kg (660 lb) of particulate in an MCO precludes actual use of more than one scrap basket. In addition, no scrap basket can be loaded to a weight exceeding that of a maximum weight normal fuel basket. Table 3-2 shows the weights and the center of gravity locations for these individual baskets, both empty and loaded with fuel assemblies. It also shows this information for various configurations of the MCO.

3.4 MECHANICAL PROPERTIES OF MATERIALS

3.4.1 Materials Discussion

The MCO Performance Specification (WHC 1996c), Subsection 3.3.4, states that the MCO shall be designed for fabrication from type 304L stainless steel. This means that those parts welded and necessary to maintain confinement and containment should be designed for fabrication from 304L stainless steel while some internal components might be better designed for fabrication from carbon steel. The use of the mechanical closure has resulted in the shield plug being made from carbon steel. A listing of the material properties for one candidate carbon steel is shown in Table 3-3 as well as the material properties for stainless steel. All materials listed in Table 3-3 satisfy the specification requirement that they be ASME/ASTM-certified materials.

Table 3-2. Summary of Weights and Center of Gravity Locations.

Item	Condition	Weight[a] (lb)	Center of gravity (in.)
Mark IA basket[b]	Empty	247	7.9
Mark IA basket[b,c]	Loaded - 48 fuel assemblies	2,153	10.5
Mark IV basket[b]	Empty	147	5.6
Mark IV basket[b,c]	Loaded - 54 fuel assemblies	3,137	13.1
MCO[d,e]	Empty Without upper shield plug Dry	1,900	70.2
MCO[d,e]	Empty With upper shield plug Dry	3,257	104.6
MCO[d,e]	Six loaded Mark IA baskets Without upper shield plug Filled with water	16,275	70.8
MCO[d,e]	Six loaded Mark IA baskets With upper shield plug Filled with water	17,487	76.8
MCO[d,e]	Six loaded Mark IA baskets With upper shield plug Dry	16,175	77.0
MCO[d,e]	Five loaded Mark IV baskets Without upper shield plug Filled with water	18,945	72.2
MCO[d,e]	Five loaded Mark IV baskets With upper shield plug Filled with water	20,157	77.4
MCO[d,e]	Five loaded Mark IV baskets With upper shield plug Dry	18,942	77.6

Note: The centers of gravity are located in the geometric center of the item, vertically above its bottom the given distance.

[a]The listed weights will change with final iterations on the fuel baskets. The final weights will be corrected as designs are finalized. The summed total weights will stay within allowable pick load limitations.

[b]Preliminary data obtained from Drawing SK-1-80208, Rev. 0, K-Basin SNF Storage Basket Mock-Up Mark IA & Mark IV, not dated; Drawing SK-1-80110, Rev. 0, K-Basin SNF Storage Basket Mock-Up, not dated; Drawing SK-2-300377, Rev. 0, MCO Prototype SNF Reracк Basket Grapple Adapter, dated March 22, 1996.

[c]Preliminary data obtained from S. M. Short, 1995, Spent Nuclear Fuel Project Technical Databook, WHC-SD-SNF-TI-015, Rev. 0, Westinghouse Hanford Company, Richland, Washington.

[d]Parsons Infrastructure and Technology, Inc., Interoffice Correspondence IOC-1196, W. E. Schenewerk to R. Bastar, March 3, 1996.

[e]Drawing SK-2-300378, Rev. 0, MCO Prototype Shell Bottom Machined Forging, dated March 19, 1996.

MCO = multicanister overpack.

Table 3-3. Mechanical Material Properties of the Multicanister Overpack.

ASTM spec/ component	Type or grade	Temperature °F (°C)	Yield S_y[a] kip/in^2 (MPa)	Ult. S_u[b] kip/in^2 (MPa)	S_m[c] kip/in^2 (MPa)	Modulus[d] 10^6 lb/in^2 (10^6 MPa)	Coefficient of expansion[e] 10^{-6} in/in/°F (10^{-6} cm/cm/°C)
SA-312 (MCO shell)	TP304L	70 (21.1) 100 (37.8) 200 (93.3) 300 (148.9) 392 (200) 752 (400)	25.0 (172.4) 25.0 (172.4) 21.3 (146.9) 19.1 (131.7)	70.0 (482.6) 70.0 (482.6) 66.2 (456.4) 60.9 (419.9)	16.7 (115.1) 16.7 (115.1) 16.7 (115.1) 16.7 (115.1)	28.3 (0.195) ---- 27.6 (0.190) 27.0 (0.186)	8.46 (15.23) 8.55 (15.39) 8.79 (15.82) 9.00 (16.20)
SA-182 (MCO shield plug, flanges, and bottom forging)	304L	70 (21.1) 100 (37.8) 200 (93.3) 300 (148.9) 392 (200) 752 (400)	25.0 (172.4) 25.0 (172.4) 21.3 (146.9) 19.1 (131.7) 17.6 14.7	65.0 (448.2) 65.0 (448.2) 61.5 (424.0) 56.5 (389.6) 58.7 70.0	16.7 (115.1)[f] 16.7 (115.1)[f] 16.7 (115.1)[f] 16.7 (115.1)[f] 15.9 13.3	28.3 (0.195) ---- 27.6 (0.190) 27.0 (0.186)	8.46 (15.23) 8.55 (15.39) 8.79 (15.82) 9.00 (16.20)
SA-193 (MCO flange bolts)	B7	70 (21.1) 100 (37.8) 200 (93.3) 300 (148.9) 392 (200) 752 (400)	105.0 (723.9) 105.0 (723.9) 98.0 (675.7) 94.1 (648.8)	125 (861.8)[a]	35.0 (241.3) 35.0 (241.3) 32.6 (224.8) 31.4 (216.5)	29.7 (0.205) ---- 29.0 (0.200) 28.5 (0.196)	5.60 (10.08) 5.73 (10.31) 6.09 (10.96) 6.43 (11.57)

References:
[a]Boiler and Pressure Vessel Code (ASME 1995a), Section II, Part D, Table Y-1.
[b]Boiler and Pressure Vessel Code (ASME 1995a), Section II, Part D, Table U.
[c]Boiler and Pressure Vessel Code (ASME 1995a), Section II, Part D, Table 2A.
[d]Boiler and Pressure Vessel Code (ASME 1995a), Section II, Part D, Table TM-1.
[e]Boiler and Pressure Vessel Code (ASME 1995a), Section II, Part D, Table TE-1.
[f]For the shield plug, since its thickness is greater than 12.7 cm (5.0 in.), S_m is 16.6 kip/in^2 (114.5 MPa).

ASTM = American Society for Testing and Materials.
MCO = multicanister overpack.
S_m = code stress intensity base allowable.
S_u = material ultimate strength.
S_y = material yield strength.

3.4.2 Hydrogen Effects on Mechanical Properties

Hydrogen gas is a principal contributor to the internal pressure in the MCO. The allowable gas amounts defined in WHC-SD-SNF-OCD-001, *Spent Nuclear Fuel Conditioning Product Criteria* (Miska 1996), show the sum of the total water and hydrogen plus the contingency put an upper limit on the hydrogen pressure of 0.85 MPa absolute (124 lb/in^2 absolute) at a temperature of 200 °C (392 °F). An extensive compilation of the effects of hydrogen on the mechanical properties of 304L stainless steel is provided in DP-1643, *Hydrogen Compatibility Handbook for Stainless Steels* (Caskey 1983). An evaluation of hydrogen effects on the shield plug materials will be performed. Much of the experimental information was obtained for a pressure of 69 MPa (10,000 lb/in^2), either as an external environment during the test or as a pressure for charging hydrogen internally into the steel at elevated temperatures. Experimental results for this high pressure conservatively bound effects for the MCO. Only in the case of tensile ductility are sufficient data available to determine values for the MCO pressure. A summary of information from DP-1643 (Caskey 1983), with parenthetical reference to specific figures or pages of that document follows.

- Ductility. The most commonly used index of hydrogen damage in stainless steels has been the change in reduction-of-area as measured for a fractured tensile specimen. The reduction-of-area is a measure of plasticity calculated from the original cross-sectional area (A_o) and the final cross-sectional area at the fracture (A_f).

  $$RA = 100\ (A_o - A_f)/A_o$$

  Another measure of ductility that is used extensively in DP-1643 (Caskey 1983) is plastic strain to failure (E_f).

  $$E_f = \ln\ (A_o/A_f).$$

  High hydrogen pressure can reduce reduction-of-area from a starting value of about 80% to a value of about 22% at a temperature of about -53 °C (-63 °F), which corresponds to a minimum in reduction-of-area. However, for a hydrogen pressure of about 1 MPa (145 lb/in^2), the reduction-of-area would only be reduced to about 64% at about 22 °C (72 °F). This level of reduction-of-area is typically more than adequate to ensure ductile structural behavior in engineering components. At a service temperature of 200 °C (392 °F), the reduction-of-area value would be even higher than 64% (Caskey 1983, Figures 12 and 13, pages 81, 83, 86).

- Yield Strength. High-pressure hydrogen produces small increases of about 10% to 15% in the yield strength of 304L stainless steel (Caskey 1983, pages 24, 31, 81, 82, 83).

- Tensile Strength. High-pressure hydrogen typically produces small decreases of about 10% to 15% in the tensile strength (Caskey 1983, pages 31, 81, 82). These small reductions do not influence design allowable stress intensity because this parameter is governed by yield strength for conditions applicable to MCO storage.

- Notch Strength. Stainless steels like 304L are typically strengthened by notches in the absence of hydrogen. High-pressure hydrogen produces a reduction of less than 20% in the notch strength (Caskey 1983, pages 47, 88, 89).

- Elastic/Plastic Fracture Toughness. High-pressure hydrogen produces reduction in the J-integral at maximum load of about 30%, and in the tearing modulus of about 20% (Caskey 1983, pages 84, 85). These changes are much too small to be of practical engineering significance for the MCO.

- Static Crack Growth. Slow crack growth under static loads did not occur in fracture mechanics tests of thin specimens of 304L stainless steel. Crack growth did occur in notched specimens loaded to 85% of the notch tensile strength (Caskey 1983, pages 50, 51, 52).

- Impact Energy. Impact tests of a dynamic tear test specimen showed only a small decrease in absorbed energy for tests in hydrogen at room temperature. Even at -196 °C (-321 °F), absorbed energy values did not indicate brittle fracture.

- Stress State. Burst testing of disks produces a biaxial stress state in the test specimen. Tests using hydrogen as the pressurizing gas show little change in burst pressure relative for helium tests for solution-annealed 304 stainless steel, but a reduction of about 45% in burst pressure for samples that were sensitized or welded (Caskey 1983, page 46).

The information above shows no significant loss in strength, ductility, or resistance to crack propagation that would adversely affect the design, analysis, or structural performance of the MCO.

3.5 GENERAL STANDARDS FOR MULTICANISTER OVERPACKS

3.5.1 Chemical and Galvanic Reactions

This assessment of chemical and galvanic reactions between the MCO and its environments is divided into three subsections that correspond to the three stages or time periods of operation. The first stage occurs when the MCO is submerged in the K Basins or later when it still contains liquid water. The second stage covers the MCO during the process of water removal and cold vacuum drying. The third stage begins after the removal of liquid water and extends through staging, hot conditioning, and interim storage.

Assessments of chemical reactions with the environments internal and external to the MCO are predicated on effective control of cleanness during fabrication, handling, and storage of MCO components before and during use. Standards such as ASTM A 380-94, "Standard Practice for Cleaning and Descaling Stainless Steel Parts, Equipment, and Systems" (ASTM 1996a), and ASME NQA-1, *Quality Assurance Requirements for Nuclear Facility Applications* (ASME 1994), are followed for cleanness control.

MCOs are fabricated using welded construction without post-welding heat treatment. As a consequence, residual stresses in and adjacent to the welds may reach yield strength levels. The MCO could be susceptible to stress corrosion cracking near the welds in the presence of aggressive environments. The selection of low carbon stainless steel was made to minimize the potential for stress corrosion cracking. The following paragraphs provide additional support as to why stress corrosion cracking is not anticipated to be a problem with the MCO.

3.5.1.1 Multicanister Overpack Containing Liquid Water. The time period during which an MCO is immersed in or is filled with liquid water is less than 2 days. This period is far too short for significant corrosion in the benign environments discussed below.

The 304L stainless steel material selected for the MCO spontaneously develops a passive oxide film in air. A properly fabricated and cleaned MCO therefore has a passive layer that protects against corrosion as it goes into service. For submerged service, the steel needs oxygen for the repair of damage to the film. This passivity is typically retained in natural waters, whether hot or cold, even those with relatively high pollution levels (Butler and Ison 1966). According to WHC-S-0453, *Fabrication Specification for the Multi-Canister Overpack* (WHC 1996b), the conductivity of water in the K Basins ranges from 1 μS/cm to 5 μS/cm, which is only slightly higher than that of good quality distilled water, but significantly lower than that of excellent quality raw water (ASTM 1996b). The passive layer ensures a very low rate of uniform corrosion that precludes any damage to the MCO, even for a time period of many years. Common sources of corrosion resistance information do not list typical values for the very low uniform corrosion rate associated with passivity. WHC-SD-W236A-TRP-001, *Multi-Function Waste Tank Facility Corrosion Test Report (Phase 1)* (Carlos 1993), reports one example of such a corrosion rate in 304L stainless steel at 97 °C (207 °F) in water containing small amounts of anions (i.e., 7 x 10^{-3} mol/L chloride, 3 x 10^{-3} mol/L fluoride, 1 x 10^{-3} mol/L nitrite, and 1 x 10^{-2} mol/L nitrate) at pH levels of 5 and 8. The maximum corrosion rate measured by weight loss (specimens were stripped of corrosion product layer) in a 120-day test was 5 x 10^{-4} mm/y (2 x 10^{-5} in/yr). At this corrosion rate, the predicted corrosion in 75 years would be 0.038 mm (1.5 x 10^{-3} in.). A design corrosion allowance is not required at this level of corrosion.

The MCO is susceptible to localized corrosion processes (e.g., pitting, crevice corrosion, or stress corrosion cracking if certain aggressive species are present in the water. The most important aggressive species for stainless steels is the chloride ion. Chloride ion content in the K Basins is below the detection limit (WHC 1996b), which is 0.083 p/M by weight. This level is well below that needed for protection against attack in fully submerged service. The fluoride ion also is typically of concern for localized corrosion. The fluoride ion content of K Basin water is 0.248 p/M (WHC 1996b). High-quality water typically used for mixing cleaning solutions, rinsing, and flushing of nuclear components would contain less than 1 p/M fluoride ion (ASME 1994). Therefore, the fluoride ion should not cause localized corrosion during the water-containing stage. Elevated temperature water containing dissolved oxygen can cause stress corrosion cracking of sensitized stainless steel (Sedricks 1992). However, the relatively low temperature of the water in the MCO and the use of 304L stainless steel to avoid sensitization (i.e., reduced

corrosion resistance due to carbide precipitation at grain boundaries, which typically does not occur below ~500 °C) preclude this type of stress corrosion cracking.

Polychlorinated biphenyls (PCBs) were identified in sludge samples from the K East Basin. The levels of PCBs were low, but their detection raises a concern for thermal or radiolytic decomposition that might contaminate the water in the MCO with chlorine and thereby produce corrosion damage. The corrosion rate of 316 stainless steel in water saturated with chlorine at room temperature was determined to be 0.008 mm/yr (ASM 1987, pp 1170-1174), a value that would be acceptable for the short duration of submerged service. A specific corrosion rate for 304L stainless steel was not available; however, it is not expected to be significantly different than that for 316 stainless steel. In addition, PCBs decompose slowly and levels are very low, so PCBs in the K East Basin do not present a corrosion threat. Additionally, PCBs are not expected to be contained in the MCOs because the fuel is cleaned before loading into the MCO.

Iodine is a fission product generated in the irradiation of N Reactor fuel; each MCO will contain about 180 g (0.4 lb) of iodine (Willis 1995). The iodine in light-water-reactor oxide fuel is tied up by the fission product cesium as cesium iodide (Kohli 1982). This compound can vaporize in oxide fuel and move to the fuel–cladding gap by vapor transport along pellet-to-pellet interfaces. This behavior is unlikely in N Reactor fuel, which has no fuel pellets or fuel–cladding gap. Iodine (or CsI) could be released to the water as the uranium fuel corrodes. The following estimate of the quantity of iodine that might be released assumes the iodine would be distributed rather uniformly in the fuel. An upper bound to the iodine release to the water is calculated assuming that the cladding does not exist, that the total uranium surface of the original fuel is exposed to corrosion for 48 hours, and that the corrosion rate of uranium in water is 0.57×10^{-3} g/cm^2/h (ASM 1987, p 814). The resulting estimate of maximum iodine content in the 500 L (130 gal) of water in the MCO was 0.7 p/M. The corrosion literature does not identify iodine or iodide ion as an aggressive species for stainless steel. However, the low level calculated above would be acceptable even for the aggressive chloride ion. Therefore, the conservative calculation shows iodine contamination is not a corrosion concern.

Cesium is also a fission product in N Reactor fuel and each MCO will contain about 1.2 kg (2.6 lb) of cesium (Willis 1995). Experience at the K Basins show that cesium is the major source of radioactivity in basin water. Using the same corrosion rate, surface area, and time for uranium corrosion as applied above for iodine, an estimate of maximum cesium content in the MCO water after 48 hours of corrosion is about 4 p/M. There is no evidence in the corrosion literature or in K Basin operational experience with fuel canisters that cesium in the water is detrimental to the corrosion resistance of stainless steel.

Other fission products are present in N Reactor fuel in very small quantities (Willis 1995). Even if these elements are dissolved in the water, they are not recognized as enhancing corrosion of stainless steel.

Only four possibilities for dissimilar metal contact exist in the MCO. The Zircaloy-2 fuel cladding will contact the MCO stainless steel baskets.

Both the cladding and the stainless steel exhibit passive oxide layers on their surfaces. The alloys exhibit similar galvanic corrosion potentials in seawater (ASM 1987, p 717-718). There should therefore be no accelerated galvanic corrosion for this alloy combination. It is possible that uranium fuel also will be in contact with the stainless steel baskets in a few locations. Since the uranium is actively corroding with a nonprotective oxide layer, this galvanic couple will not lead to accelerated corrosion of the stainless steel baskets. Also, it is possible that the carbon steel shield plug will come in contact with the stainless steel shell. Very little corroding is expected from this interface. The final interface is that of silver and carbon steel. There is expected to be insufficient water available to pose a concern for the seal area.

3.5.1.2 Multicanister Overpack during Removal of Liquid Water. Less than 48 hours is needed to remove liquid water from the MCO and establish a low water vapor pressure inside it (WHC 1996b). This period is too short for significant corrosion in the benign environment.

The vacuum drying operation includes monitoring of pressure increases near the end of the process to ensure that acceptable water vapor partial pressure has been established. The water vapor pressure (< 0.5 torr) prevents condensation inside the MCO. The single wet/dry cycle precludes significant build up of aggressive species such as chloride ion to levels that would cause localized corrosion. Once the liquid water is removed and condensation is precluded, liquid corrosion processes cease.

Water is also removed from the annulus between the shipping cask and the MCO. Any remaining moisture in the annulus will not produce corrosion damage on the exterior of the MCO during the short time required for shipment to the CSB and removal from the shipping cask.

3.5.1.3 Multicanister Overpack after Removal of Liquid Water. The passive film on 304L stainless steel that protects against liquid corrosion also protects against gaseous oxidation by impurities (e.g., oxygen or water vapor) in the inert gas environment established in the MCO (Adams 1983). Oxidation of stainless steel only becomes obvious at temperatures above about 400 °C (ASM 1987, pp 351-353). The higher partial pressures of gases such as hydrogen, water vapor, and oxygen that may exist before hot conditioning present no threat of significant gaseous reactions with the MCO. The heating that occurs after cold vacuum drying enhances the protection against condensation of water vapor inside the MCO.

Hydrogen generated by reactions of the uranium fuel with water vapor or by radiolysis of bound water in the MCO will not reduce the chromium oxide passive layer on the stainless steel, although it may reduce the iron oxide that may co-exist in mixed oxide layers (Adams 1983). Effects of gaseous hydrogen on the mechanical properties of 304L stainless steel are discussed in Section 3.4.2.

Thermal or radiolytic decomposition of PCBs after water removal could produce chlorine gas inside the MCO. For the maximum PCB level of 220 p/M by weight detected in the sludge, and a maximum corrosion product content in an MCO of 300 kg (after cold vacuum drying and hot conditioning) (Miska 1996), the maximum chlorine partial pressure in the MCO (assuming the PCB to be 100%

chlorine) is about 0.3 kPa (2 torr). Dry chlorine is compatible with stainless steels at normal pressures, but chlorine gas saturated with water vapor at ambient temperature is extremely corrosive to these alloys (Brown et al. 1947). Since the chlorine content from radiolysis would increase gradually, and water vapor pressure will be very low after hot conditioning, there is little likelihood of corrosion damage.

Fuel corrosion and the thermal environment could lead to release of iodine gas into the MCO. If the total 180 g (0.4 lb) of iodine contained in the fuel in an MCO were released, the iodine partial pressure would be 3.5 kPa (26 torr) at atmospheric temperature. In actuality, only a small fraction of the iodine would be expected to be released. Assuming the iodine partial pressure to be about the same as that for chlorine, the fact that iodine is less aggressive means that corrosion damage is very unlikely.

With the liquid removed from the MCO, galvanic corrosion is no longer possible. However, direct contact between the fuel and baskets could lead to liquid metal embrittlement of the stainless steel (Old 1980) by fission products. Cesium and tin are the low melting point (i.e., <205 °C) fission products generated in the greatest amounts. Liquid cesium would be expected to be fully compatible with stainless steel based on the demonstrated compatibility for sister elements sodium and lithium. Tin is present in amounts of about 0.1 g per fuel element (Willis 1995), so the amount present in a contact area is far too small to cause significant damage to an MCO basket. If eutectic liquid could form because localized fuel reactions produced small regions of very high temperature, attack on stainless steel could be severe. Estimates of temperatures required for liquid eutectic formations obtained from binary phase diagrams are 725 °C (1,336 °F) for iron-uranium, 950 °C (1,742 °F) for iron-zirconium, and 1,135 °C (2,075 °F) for uranium-zirconium (ASM 1986).

The environment at the exterior of the MCO will contain both water vapor and oxygen (either as air or as an impurity in inert gas). The passive oxide layer on the stainless steel will prevent significant reaction with these gases. The internal heat generation in the MCO acts to prevent moisture condensation on the exterior of the MCO. The following engineered and administrative features protect against accidental intrusion of water into the storage tubes at the CSB:

- A dry roof that does not collect water
- Absence of sprinklers for fire protection
- Prohibition against washing the deck
- O-ring seals in the storage tube shield plug with positive gas pressure in the tube.

3.5.2 Positive Closure

The MCO is loaded, shipped, handled, and stored in the vertical position. The MCO is closed with a shield plug that is inserted into the expanded neck of the MCO. The shield plug assembly weighs approximately 600 kg (1,350 lb)

and is retained in the MCO neck after the MCO is loaded. The mechanical closure is set into the expanded neck of the MCO, which is threaded on the inside. The neck of the MCO is all 304L stainless steel and has a 1.3-cm-(0.5-in.-) wide ledge in which the mechanical seal can seat. The Helicoflex seal, with an Inconel[1] helical wire and silver-plated stainless steel jacket, has an integral compression limiter that is approximately 0.64 cm (0.25 in.) wide. The actual seal is stainless steel with silver plating. The mechanical seal is secured to the sealing surface on the bottom of the shield plug with small machine screws. The plug portion of the mechanical closure uses carbon steel that is plated if necessary to meet corrosion requirements and has a corresponding ledge to capture the mechanical seal. The plug is held in place by a carbon steel, threaded, locking and lifting ring that threads into the MCO's expanded neck and pushes on the plug once the eight jack bolts are torqued to 560 ft·lbf each. The plug and locking and lifting ring may be plated with nickel or other suitable material to reduce corrosion potential.

Galling of the threads between the collar and the locking and lifting ring is minimized by choosing materials that are sufficiently different in properties that reduce the potential of galling between the metal threads. The threaded neck on the MCO is made of 304L stainless steel, which is relatively soft. The locking and lifting ring will be made of a low-alloy carbon steel similar to 4142, which was used successfully on the prototype that was machined from a forged blank. Hardening of the threads of the ring is also possible as is the use of acceptable low-gassing lubricant during assembly to further reduce the potential for galling.

Recovery from a galling situation with locked-up ring-to-MCO-neck threads would be similar to opening up a welded MCO in that the top end of the MCO surrounding the locking and lifting threads would have to be cut away, the shield plug assembly removed, and the fuel removed from the MCO shell. Removal of the shield plug would require rigging and a hoist to lift the shield plug from the neck of the MCO.

Connections to the inside of the MCO are accomplished through the ports on the top of the shield plug. The ports of the MCO are connected to the pressure relief device, the low-flow HEPA filter, and the long and short process tubes via the process connection. Access to these ports is made by removing a port cover that exposes the device. Tools are required to remove the sealed port cover. Once access is gained to these devices, additional tools are required to remove the in-place pressure relief device or low-flow HEPA filter, or to open the process connections. The passageways leading from these devices into the interior of the MCO make double turns to prevent a direct path for nonattenuated radiation from the interior SNF to the exterior of the MCO.

3.5.3 Lifting Devices

The lifting tools are still in the design process as of this writing.

---

[1]Inconel is a trademark of Inco Alloys International.

3.6 FUEL RODS

At no time in the retrieval, packaging, transportation, or conditioning process is the fuel cladding relied upon for confinement of radionuclides. Fuel movements in the fuel segregation campaign, and more recently during the fuel characterization work, have shown that even the most visibly damaged fuel can be moved and handled. For criticality purposes, it is assumed that the cladding remains mixed with the fuel.

3.7 SUPPLEMENTAL DATA

3.7.1 Computer Code Description

The SNF primary containment and confinement boundary structure, the MCO, was analyzed for structural strength and dynamic characteristics using finite-element codes described in the following paragraphs. The computer codes are those commonly used in the nuclear industry and particularly at the Hanford Site. The codes have all been validated and inputs verified for quality answers by the user groups onsite.

For dynamic solutions, in particular the cask-MCO drop scenarios, the K Basin transportation cask, MCO, and baskets were analyzed and modeled with a second generation, nonlinear, finite-element program called ABAQUS. ABAQUS uses finite-element formulation for the stress and strain domain and finite-difference formulations for the dynamic time domain. There are two versions of ABAQUS: ABAQUS/Standard, the implicit formulation, is best for static nonlinear solutions; and ABAQUS/Explicit is best for dynamic problems. In particular, ABAQUS/Explicit 5.4 was used for this analysis effort. ABAQUS/Explicit 5.4 uses a lumped-mass formulation with explicit central difference integration for the time domain solution of displacements, velocities, and accelerations. Each degree of freedom is idealized as an independent lumped mass with an initial position and velocity. External forces are applied to generate accelerations. Employing very small time steps (typically 0.5 microsecond), new positions and velocities are calculated, then finite-element reaction forces are calculated for each individual element and contact surface conditions are checked. The new updated forces produce new accelerations and the process repeats. ABAQUS also allows nonlinear modeling of the materials and material failure. The nonlinear material properties are defined versus strain. The ABAQUS finite-element formulation uses numerical integration to construct element stiffness matrices that relate internal element reaction forces produced by element boundary displacements. The repeated numerical integration allows the material properties to be updated based on the strain history at each element integration point through the element volume.

ANSYS is a finite-element program that has acceptance as a linear elastic design tool for mechanical and civil engineers. It is known for its early development and use as a robust pre- and postprocessor. ANSYS is being expanded to nonlinear analysis, but it is still viewed as a standard for linear elastic structural analysis in the nuclear industry. ANSYS was used extensively in the structural static analysis of the MCO and its components. The code has the ability to develop stresses related to thermal growths and

restraints in structures. In particular, the code was used to assess the specification requirement of 100 Celsius degrees (180 Fahrenheit degrees) difference between the shield plug (coolest) and the shell (hottest) on heatup and then in cooldown.

IMAGES-3D is a code well known for its user-friendliness and common use as design analysis tool. The trait of user-friendliness makes it popular as a preliminary sizing tool, but it also is used for linear static analysis and for simple dynamic solutions. The program is a three-dimensional, general purpose, finite-element analysis program for use on IBM[1] personal computers or compatible microcomputers. IMAGES-3D performs three types of analyses: static, modal, and dynamic.

[1]IBM is a trademark of International Business Machines, Incorporated.

4.0 THERMAL EVALUATION

The thermal-hydraulic aspects of the MCO and its payloads that are important to safety are presented in this chapter. Also presented are the basis for the design criteria and results of the thermal-hydraulic analyses for the normal conditions of transport, vacuum drying, staging, hot conditioning, and interim storage. Response to off-normal events and accident conditions, such as equipment failure and fire accidents, is addressed within the individual SARs for the facilities or the transportation cask.

4.1 DISCUSSION

The thermal evaluation addresses four distinct thermal conditions within the MCO; wet, vacuum, dry, and hot conditioning. Wet thermal conditions exist during loading at the K Basins, transport between the K Basins and the CVDF, and initial processing at the CVDF. Under wet conditions, the MCO is filled with water to a height approximately 10.2 cm (4 in.) below the MCO shield plug. The remaining void space within the MCO is filled with helium gas at the time of loading to yield an initial pressure of 122 kPa (17.7 lb/in^2 absolute). The pressure boundary under wet conditions is the transportation cask. The MCO itself is unsealed, and therefore unpressurized, whenever wet thermal conditions exist.

A combination of wet, vacuum, and dry thermal conditions exists during the various steps of the cold vacuum drying process. A maximum vacuum of 0.4 kPa (3 torr) exists in the MCO during the drying process. The MCO is backfilled with helium gas to a target pressure of 122 kPa (17.7 lb/in^2 absolute) after completion of cold vacuum drying and before transport to the CSB.

Dry thermal conditions exist following completion of the cold vacuum drying process, during transport between the CVDF and the CSB, and during staging and long-term interim storage in the CSB. Following cold vacuum drying and before hot conditioning, the water content consists primarily of chemically bound water. Under dry thermal conditions, the void space within the MCO is filled with either helium, argon, or nitrogen gas, depending on where in the processing cycle the MCO is.

Hot conditioning of the SNF payload is designed to remove the chemically bound water and decompose a portion of the uranium hydride. A variety of process purge gases is used to accomplish the hot conditioning. The final process step backfills the MCO with helium gas to a target pressure of 138 kPa (20 lb/in^2 absolute) at 50 °C (122 °F).

Table 4-1 presents a summary of the pertinent thermal features associated with the transportation of the MCO between the K Basins, CVDF, and CSB.

Table 4-1. Thermal Aspects of Wet and Dry Transfer of K Basin Spent Nuclear Fuel.

Design parameter	Wet transfer	Dry transfer
Water volume in MCO[a]	0.528 m^3 (18.64 ft^3)	0 m^3 (0 ft^3)
Gas volume in MCO	0.027 m^3 (0.96 ft^3)	0.56 m^3 (19.6 ft^3)
Initial MCO gas backfill	Helium at 122 kPa (17.7 lb/in^2 absolute)	Helium at 122 kPa (17.7 lb/in^2 absolute)
Allowed MCO leakage rate[b]	Open to cask	10 E-4 std cm^3/s, air
Water volume in cask	0.107 m^3 (3.79 ft^3)	0 m^3 (0 ft^3)
Gas volume in cask	0.015 m^3 (0.54 ft^3)	0.122 m^3 (4.33 ft^3)
Initial cask gas backfill	Helium at 122 kPa (17.7 lb/in^2 absolute)	Helium at 122 kPa (17.7 lb/in^2 absolute)
Allowed cask leakage rate[c]	10 E-7 std cm^3/s, air	10 E-7 std cm^3/s, air
Nominal transfer time[d]	8 hours	14 hours
Fire accident scenario (cask exposure)	6 minutes at 800 °C (1,475 °F)	6 minutes at 800 °C (1,475 °F)

Notes:
[a]Water volume refers to liquid, free volume. Chemically bound water and water absorbed in sludge, cracks, and crevices is not included.
[b]Leakage rate is verified at time of fabrication.
[c]Leakage rate is verified at fabrication and annually thereafter.
[d]Transfer time is defined as from time of closure at the shipping site to the time of venting at the receiving site.

MCO = multicanister overpack.

4.1.1 General Thermal Design Approach

The safety analysis of the thermal-hydraulic performance for the MCO assembly and its payload under the various SNF Project process flow steps is based on a combination of bounding assumptions for heat generation, conservative heat transfer conductances, and the application of administrative rules (technical safety requirements) governing the loading of the MCO, the allowable time to accomplish individual process steps, process performance criteria that must be met before certain process steps can be completed, and specific recovery steps to be undertaken should off-normal conditions arise. The combination of these elements will ensure that the MCO assembly is maintained in a safe, stable, and secure operating condition. A safe, stable, and secure operating condition is defined as either (1) an energy balanced, steady-state condition in which the energy gains to the system equal the energy losses from the system and the system is within its temperature and pressure limits or (2) a transient operating condition in which energy gains

may temporarily exceed the losses, but where administrative controls or safety-class systems are implemented to ensure the system is placed into a stable steady-state condition before exceeding the system temperature and pressure limits.

4.1.2 Thermal Design Features

The MCO is designed to safely contain a variety of SNF in five or six baskets. Chapter 1.0 of this report presents a description and design drawings of the MCO and its fuel baskets, while Chapter 2.0 provides a description of the spent fuel to be placed within the MCO, the general design criteria, and the design loads. An MCO is a 61-cm- (24-in.-) outer-diameter stainless steel pipe approximately 406 cm (160 in.) long with a bottom endcap forging and upper shield plug. The bottom endcap forging of the MCO is designed to position the lower fuel basket just above the bottom of the MCO. This position promotes draining and creates a lower plenum to aid the distribution of process flows evenly across the bottom of the lower basket. The shield plug serves as the access point for various system penetrations and process connections. All penetrations through the shield plug are 2.54 cm (1.0 in.) in diameter or less and are labyrinthed to minimize radiation streaming. The MCO shell and bottom forging are fabricated primarily of type 304L stainless steel. The shield plug is made of carbon steel and it will be mechanically sealed.

The SNF assemblies are placed within stainless steel fuel baskets, which are then loaded into the MCO. Because of height differences between the fuel assembly types, either five Mark IV fuel baskets or six Mark IA fuel baskets can be stacked axially within the MCO. Each fuel basket type is provided in an intact fuel and a scrap fuel configuration. The MCO is designed to support internal forced flows for purging and inerting of the free volume with either helium, nitrogen, or argon. The MCO and its internal basket arrangement are designed to dissipate the heat from the SNF assemblies passively through a combination of conductive and radiative heat transfer without internal convective flows. Figure 4-1 presents a schematic cross-sectional view of the MCO and the internal MCO components with the Mark IV fuel baskets.

A center pipe on each basket is designed to contain a grapple adapter for stacking the fuel basket within the MCO. The grapple is designed with a center penetration large enough to allow insertion of the center process tube when the upper shield plug is installed. The process tube, bottom strainer, and locator cones have the same configurations for all basket types. When undergoing processing, gas flows from external sources, through a connection to a fitting at the top of the MCO shield plug, and into the MCO via the center process tube. The gas flow exits the process tube at the bottom of the MCO, passes radially outward through the bottom strainer, and then flows up through the baseplate of the scrap or fuel baskets or is bypassed between the outer edge of the baskets and the MCO wall. Some of the gas exiting the process tube can flow back up through the annular space between the center hole in the baskets and the process tube. The center pipes used for the intact fuel and scrap baskets are designed to intersect and seal with each other. This not only provides additional support, but also prevents the flow that bypasses around the locator cones from mixing with the gas flow inside the baskets at each level.

Figure 4-1. Cross-Sectional View and Configuration of the Multicanister Overpack.

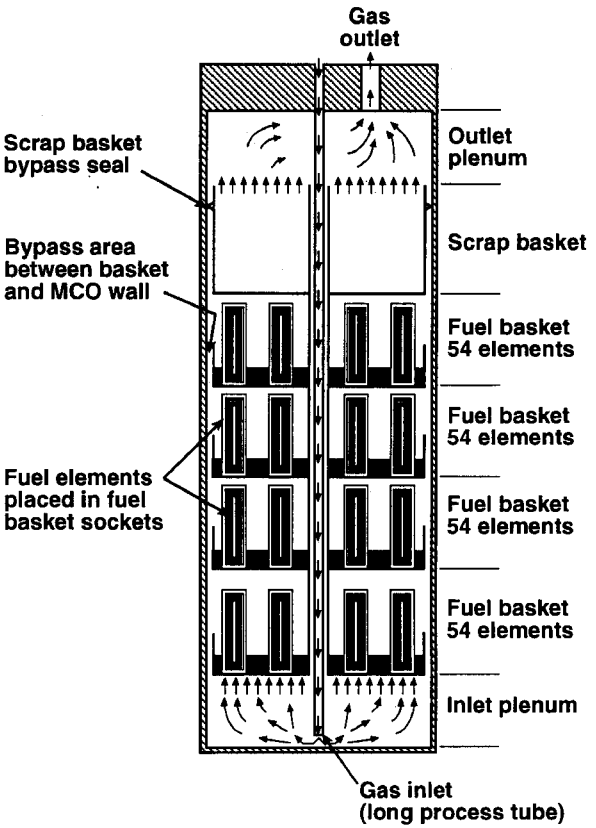

The intact fuel basket is designed to vertically support fuel assemblies in individual sockets bored into the 7.6-cm- (3-in.-) thick "socket" baseplate. A 27.9-cm- (11-in.-) high perforated outer skirt provides additional lateral support and confinement for smaller sections of fuel assembly. Only those portions of a combined fuel assembly (i.e., an outer and an inner element) that will fit in the basket's baseplate socket will be loaded into an intact fuel basket. Solo outer or inner elements either will be combined to make up a fuel assembly (for criticality reasons) or will be placed in the scrap basket. Those portions of the fuel assemblies that are greater than 0.6 cm (0.25 in.) in size, but are less than approximately 20 cm (8 in.) in length, or are too broken up to stand upright in the intact fuel basket, or will not fit in the baseplate socket because of swelling caused by damage or corrosion also will be placed in the scrap basket.

Portions of the SNF 0.6 cm (0.25 in.) in size or smaller will not be intentionally loaded into an MCO; instead, they will be handled in a separate operation. It is assumed that pieces smaller than 0.6 cm (0.25 in.) in size may be loaded unintentionally or created as a result of loading into the basket. The basket heights will be gauged before shield plug insertion to ensure that the presence of small pieces is not affecting the assembly of the MCO.

The design of the fuel basket for Mark IA fuel is shown in Figure 4-2. The basket consists of a center support tube, a 7.6-cm- (3-in.-) thick socket baseplate, a 27.9-cm- (11-in.-) high perforated outer skirt, and six 0.95-cm (0.375-in.) support rods. The fuel elements are vertically retained in the sockets by a 0.6-cm- (0.25-in.-) wide bar welded across the bottom of each socket. The socket diameters are large enough to allow processing gas to flow either up through the interior of the fuel elements or around the outside. The outer skirt is perforated, which allows mixing of the gas that flows around the outside ring of fuel elements with the bypass flow between the baseplate and the MCO wall. The fuel baskets are stacked one on top of another. Each fuel basket is supported by six support rods that fit into predrilled recesses in the bottom of the fuel basket above it. Approximately 3.8 cm (1.5 in.) of clearance exists between the top of the fuel assemblies and the lower surface of the basket above. Before entering the next basket above, some mixing or redistribution of the processing gas flows that traverse the fuel elements can occur with the gas flows that bypass the basket along its outer edge. The scrap baskets are designed with a solid skirt and a sheet metal seal on their outer edge to minimize the amount of gas flow that is bypassed. The design of the scrap baskets is discussed further below. Because of its higher initial enrichment, the Mark IA fuel is limited to 48 fuel assemblies per basket; the use of a large diameter center pipe physically excludes an innermost circle of six fuel assemblies.

The fuel basket socket design for Mark IV fuel is shown in Figure 4-3. Mark IV fuel assemblies have a lower initial enrichment, thus allowing 54 Mark IV fuel assemblies to be loaded per fuel basket. The center pipe on the Mark IV basket is smaller than that on the Mark IA basket. The other design features of the Mark IV fuel basket are similar to those discussed for the Mark IA basket.

Figure 4-2. Socket Design for Mark IA Fuel Basket.

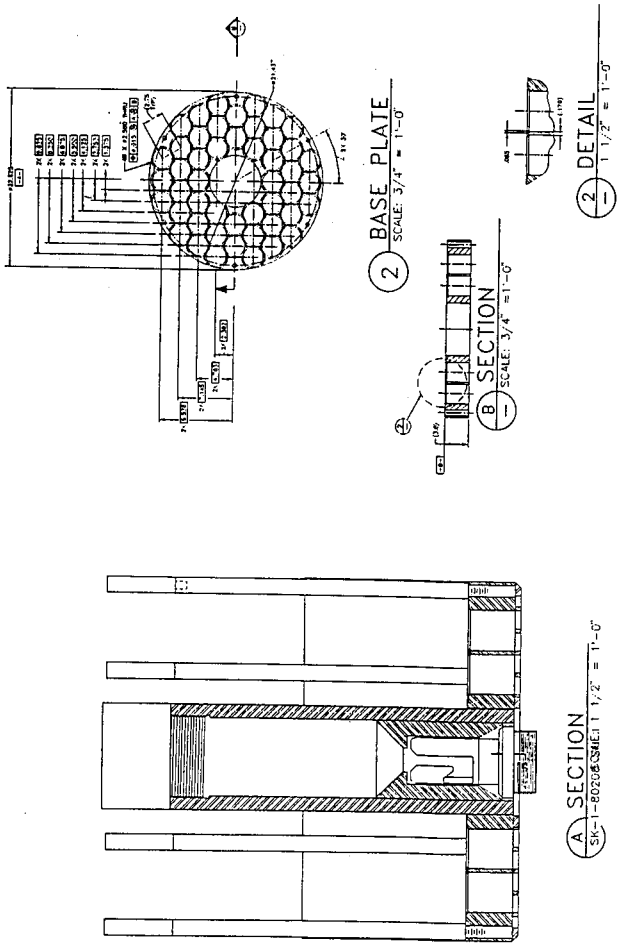

Figure 4-3. Scrap and Mark IV Fuel Assembly Baskets (Perforated Baseplate and Socket Design).

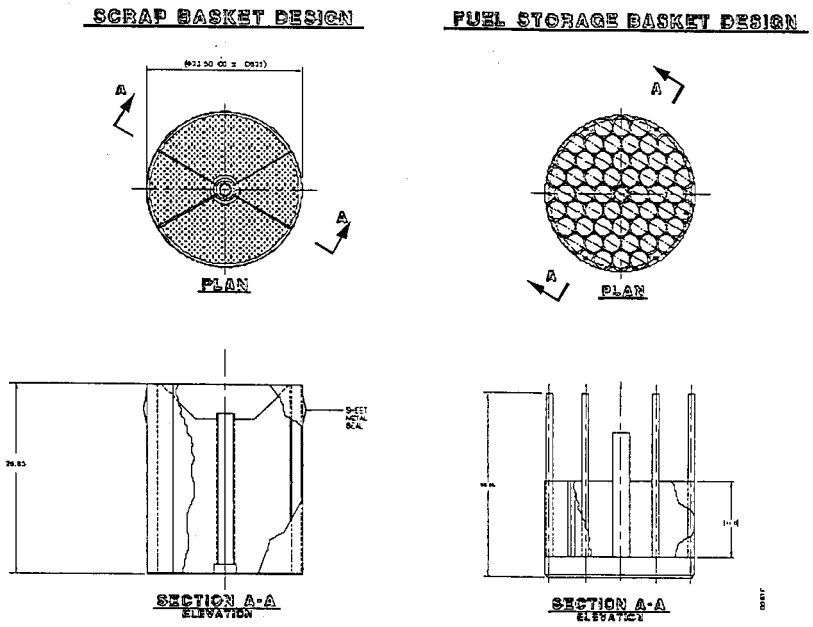

The basic scrap basket design is presented in Figure 4-3. As discussed above, the scrap baskets are designed to contain partial fuel elements and debris larger than 0.6 cm (0.25 in.) in diameter. As a consequence, the scrap basket baseplate is designed with numerous 0.6 cm (0.25 in.) holes that allow the passage of process gas but also contain the scrap material. The scrap basket baseplate has been intentionally designed with a relatively large pressure drop to prevent flow channeling from occurring because of an uneven or partial loading of scrap. Because of the relatively high pressure losses associated with the scrap basket baseplate, a full height outer skirt with peripheral flow restrictors is used. The solid skirt and flow restrictors are intended to minimize the amount of process flow bypassing the scrap baskets. The flow restrictors are fabricated of thin sheets of stainless steel tack welded to the outer diameter of the basket skirt.

4.2 SUMMARY OF THERMAL PROPERTIES OF MATERIALS

The thermodynamic properties for density, specific heat, thermal conductivity, viscosity, and emissivity for the various materials occurring in the MCO, the fuel baskets, and the SNF payload are summarized in Appendix E. Thermal properties are provided for materials that constitute a significant heat transfer path or that are important for the determination of temperatures for temperature sensitive materials. Properties for minor components such as fittings and seal materials are not provided. Where possible, the thermal properties are based on material presented in WHC-SD-SNF-TI-015 (Short 1995). References for additional material properties not obtained from WHC-SD-SNF-TI-015 (Short 1995) are presented in Appendix E.

The MCO shell, fuel baskets, process tube, canister collar, and canister cover are fabricated of type 304/304L austenitic stainless steel. The body of the MCO shield plug, its access port cover plates, and the locking and lifting ring are fabricated of mild carbon steel. Miscellaneous components such as the HEPA filter, rupture disk, and internal screen are fabricated of 304/304L stainless steel. The HEPA filter and shield plug access port covers are sealed using a Grafoil ring gasket. The main seal between the shield plug and the canister collar uses a Helicoflex seal.

The Mark IV and Mark IA fuel assemblies are fabricated of uranium metal with a Zircaloy-2 cladding. While the fuel assemblies will be cleaned prior to placement in the fuel baskets, residual uranium oxides may remain adhered to the surfaces of the assemblies, lodged under defects in the cladding, or plugged in the interior gaps of the fuel assemblies. WHC-SD-SNF-TI-028, *Spent Nuclear Fuel Project Gas Generation from N-Fuel in Multi-Canister Overpacks*, (Cooper 1996b), includes an estimate that up to 9% of this corrosion product consists of uranium hydride. Section 4.2.1.3 provides an estimate of the total amount and distribution of the corrosion product in an MCO.

Depending on the operation, the void spaces within the MCO are filled with water, water vapor, air, nitrogen, dilute oxygen, helium, or argon. As a result of radiolysis and chemical reactions involving the uranium metal and uranium hydride, a variable amount of hydrogen gas may be generated and mixed with the other fluids or gases filling the void spaces. The presence of

hydrogen and its concentration will be a function of the operation in question, the makeup of the payload within the MCO, and the amount of moisture available to drive the reaction.

The exact geometry and makeup of the material contained within the scrap basket is an unknown. The uncertain makeup and structure of the material to be loaded in a scrap basket requires that the thermal properties for the scrap be derived. The approach used is to treat the scrap as a homogeneous, porous medium. For porous media, the effective thermal conductivity (k_e) and the effective heat capacity (ρC_p) can be estimated based on the thermal properties for the solid portion and the fluid or gas filling the void volumes, and via the porosity of the porous medium. The solid portion assumes the properties associated with uranium metal. The fluid or gas properties for water, air, helium, nitrogen, or argon are assumed, depending upon the operation under consideration.

The effective thermal conductivity for the porous medium was calculated using Hadley's correlation, as shown by Equation 1 and documented in Table 3.1 of *Principles of Heat Transfer in Porous Media* (Kaviany 1995).

$$\frac{k_e}{k_f} = (1-\alpha_o)\left[\frac{P f_o + (k_s/k_f)(1-P f_o)}{1-P(1-f_o)+(k_s/k_f)P(1-f_o)}\right] + \alpha_o\left[\frac{2(1-P)(k_s/k_f)^2+(1+2P)(k_s/k_f)}{(2+P)(k_s/k_f)+1-P}\right] \quad (1)$$

where

f_o = $0.8+(0.1)P$
P = porosity
k_s = solid phase conductivity
k_f = conductivity of the fluid phase

and

$$\log\alpha_o = -1.084 - 6.778(P-0.298), \quad 0.298 \le P \le 0.580$$

$$\log\alpha_o = 0.405 - 3.154(P-0.0827), \quad 0.0827 \le P \le 0.298$$

$$\log\alpha_o = -4.898P, \quad 0 \le P \le 0.0827 .$$

This relationship provides the ratio between the effective conductivity (k_e) and the conductivity of the fluid (k_f) filling the void volume within the scrap as a function of the porosity of the medium and the thermal conductivity of the solid and fluid phases (uranium fuel and water, air, helium, and other gases) present. According to Table 3.2 of Kaviany (1995), the porosity of a porous medium comprised of particles with a uniform size will range from 0.26 to 0.476. As an alternative calculation, the porosity of the Mark IV scrap basket is computed based on the basket containing the equivalent of 54 intact fuel assemblies evenly packed over the volume of the basket. Given

that the total volume of a Mark IV fuel assembly is approximately 1,470 cm^3 (90 in^3) and that the total volume in the scrap basket is approximately 165,600 cm^3 (10,100 in^3), the porosity (P) of the scrap basket is computed as follows:

$$P = (\text{basket void volume}) \div (\text{total volume of the basket})$$
$$= (165{,}600\ cm^3 - 54 \text{ assemblies} \cdot 1{,}470\ cm^3) \div (165{,}600\ cm^3)$$
$$= 0.52.$$

Because the effective thermal conductivity within the sludge basket decreases with increasing porosity, the use of porosity values of 0.476 to 0.52 is conservative. Based on this porosity and the density of uranium, the mean density of the scrap basket with helium gas backfill is approximately 9.043 kg/cm^3 (0.326 lbm/in^3). A water-filled scrap basket has a mean density approximately 6% higher.

Based on the presentation given in Kaviany (1995), this correlation provides the best fit to the available test data for the range of parameters associated with the current analyses. Figure 4-4 presents a comparison of the effective thermal conductivity versus temperature based on Hadley's correlation for a uranium metal matrix with helium, nitrogen, or argon purge gases for porosities of 0.259 and 0.476. As seen, the effective thermal conductivities for a scrap basket with a uranium metal matrix are decreased significantly from the values associated with the thermal conductivity of the uranium metal. Uranium metal has a thermal conductivity ranging from approximately 26.8 J/m-s-K at 100 K to 39.1 J/m-s-K at 1,040 K. Minimum effective thermal conductivities are obtained with increased porosities and with either nitrogen or argon as the void volume gas. Maximum effective thermal conductivities are obtained with decreased porosities and with helium as the void volume gas.

The effective heat capacity of the porous entity is determined by the following equation.

$$[\rho C_p]_{eff} = \rho_f C_{p_f} P + (1-P)(\rho_s) C_{p_s} \qquad (2)$$

where

ρ_f = density of the fluid
Cp_f = specific heat of the fluid
ρ_s = density of the solid
Cp_s = specific heat of the solid
P = porosity of the porous media.

4.2.1 Thermal Source Term

The heat dissipation from the SNF payload arises from two sources: radiolytic decay and the heat of chemical reaction. The following sections define each of these source terms and their bases.

Figure 4-4. Effective Thermal Conductivity of Uranium Metal Matrix for Various Purge Gases and Porosities.

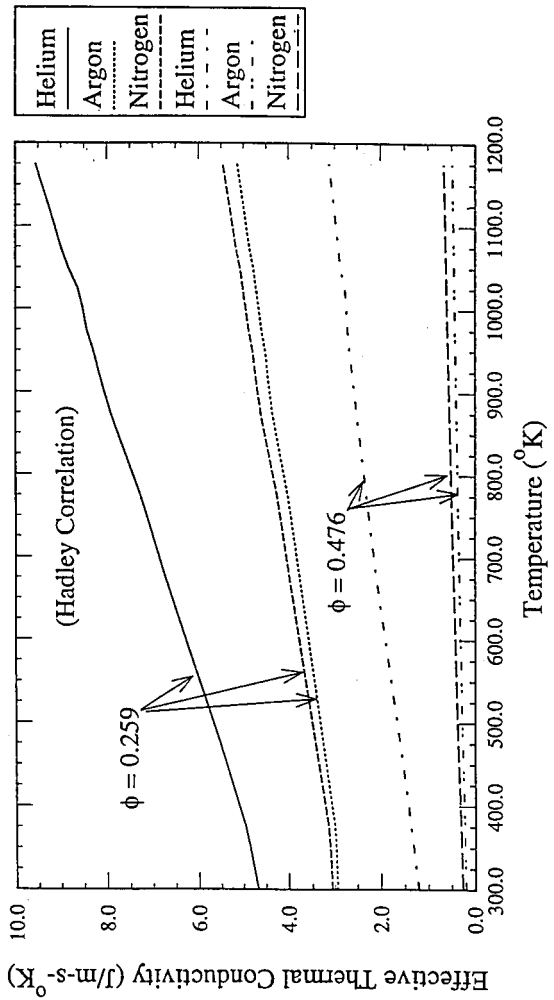

4.2.1.1 Radiolytic Decay Heat Source Term. The radiolytic decay heat source term is based on the estimated MCO inventory (Cowan 1995) for the various MCO loadings. Table 4-2 presents the radiolytic decay heat for the nominal (average) and worst-case (maximum) MCO. The minimum decay heat is expected to be on the order of one-third of the nominal value, or 0.489 W per SNF assembly. However, a value of zero watts should be assumed for the purposes of computing the minimum temperatures.

Table 4-2. Radiolytic Heat Source Term.

Payload	Average of 390 MCOs	Maximum MCO with 270 Mark IV assemblies	Maximum MCO with 288 Mark IA assemblies	SPR fuel, 1 MCO
Total decay heat	396 W	835 W	630 W	329 W
Decay heat per fuel assembly	1.467 W (assuming 270 Mark IV assemblies)	3.093 W	2.188 W	--

MCO = multicanister overpack.
SPR = single pass reactor.

These values for radiolytic decay heat are consistent with an earlier estimate (Willis 1995) that indicated values of 3.375, 1.58, and 0.53 W for the maximum, nominal, and minimum decay heat per SNF assembly, respectively.

4.2.1.2 Chemical Reaction Heat Source Term. The heat of chemical reaction arises when the exposed uranium surfaces of the damaged SNF fuel assemblies, scrap, and sludge react with the environment within the MCO. At the temperature levels seen during transport, this reaction consists primarily of the oxidation of uranium with moist air (oxygenated water reactions), oxygen-free water, dry air, or inert gases with an oxygen content. A secondary, but not significant, source of heat and hydrogen gas results from the decomposition of the uranium hydrite contained in any sludge loaded with the fuel. The relatively low temperature level and time to transport combine to limit the contributions from this source. The reactions with the hydrates are not included because the temperature levels seen during transportation will not support significant reaction with these compounds (Fryer et al. 1996).

The reactions of uranium in air or in a water/water vapor environment are represented by

$$U + O_2 \Rightarrow UO_2 + 259.3 \text{ kcal/mole of U} \quad (3)$$

and

$$U + 2H_2O \Rightarrow UO_2 + 2H_2 + 143.7 \text{ kcal/mole of U.} \quad (4)$$

It is estimated in WHC-SD-SNF-TI-028 (Cooper 1996b) that 9% of the corrosion product consists of uranium hydride. The hydride in the corrosion product

attached to the uranium metal is accounted for as part of the uranium reaction rates given in Equations (6) through (15) below. However, the hydride contained in the sludge is not accounted for and can provide a significant hydrogen gas source. The rate of reaction between uranium hydride and water is given by Equation (15) and represented by

$$2UH_3 + 4H_2O \Rightarrow 2UO_2 + 7H_2 + 287.4 \text{ kcal/mole of U.} \quad (5)$$

The rate at which the indicated uranium-water or uranium-oxygen reactions occur is a function of the temperature of the uranium, the partial pressure of water (if present), and the surface area involved. The relationships for the chemical reaction rates are taken from the recommendations made in WHC-SD-SNF-TI-033, *Spent Nuclear Fuel Project Estimate of Volatile Fission Products Release from Multi-Canister Overpacks* (Cooper 1996a), for the corrosion of N Reactor fuel. The relationships consist of Arrhenius Rate Law-type equations developed by Pearce (1989) and Ritchie (1981, 1986) for the reaction rate of unirradiated uranium in various environments and temperature ranges. The recommended equations are as follows:

- For dry air (<10-15 vppm H_2O)

  $T < 597$ K, $\text{Log } K = 8.9464 - 4638.2/T$ (6)

  $T > 597$ K, $\text{Log } K = 28.381 - 7\text{Log}(T) - 4638.2/T$ (7)

- For moist air

  $T < 373$ K, 11-75% RH, $\text{Log } K = 13.6780 - 5290.9/T$ (8)

  $T < 373$ K, 100% RH, $\text{Log } K = 8.333 - 3730/T$ (9)

  $373 \text{ K} < T < 463$ K, <100% RH, $\text{Log } K = 10.566 - 4990/T + 0.3\text{Log}(P)$ (10)

  $T > 463$ K, <100% RH, $\text{Log } K = 6.1931 - 2963/T + 0.3\text{Log}(P)$ (11)

- For oxygen-free water vapor

  $T < 373$ K, $\text{Log } K = 7.364 - 3016/T$ (12)

  $373 \text{ K} < T < 523$ K, $\text{Log } K = 4.33 - 2144/T + 0.5\text{Log}(P)$ (13)

  $523 \text{ K} < T < 735$ K, $\text{Log } K = -22.915417 + 30066.5/T - 9.119078 \times 10^6/T$ (14)

  $735 \text{ K} < T < 923$ K, $\text{Log } K = -23.905197 + 42718.8/T - 1.787581 \times 10^7/T^2$ (15)

where K is the predicted weight gain from the reaction in $mg/cm^2/h$ (i.e., milligrams of oxygen per cubic centimeter per hour), P is the partial pressure of the water vapor in kPa, and T is the temperature in degrees Kelvin.

The reaction rate of uranium hydrite, as provided in WHC-SD-SNF-TI-028 (Cooper 1996b), is as follows:

$$K = (10^{(5.69034 - 2644.11/T)} \times 1000/241) \times 0.09 \times \text{Exp}[10^{(5.69034 - 2644.11/T)} \times \Delta t] \quad (16)$$

where K is the number of gram moles of hydrite that react per hour per kilogram of sludge, T is the temperature in degrees Kelvin, 241 is the molecular weight of UH_3, and Δt is the time in hours since the MCO was loaded.

4.2.1.3 Surface Area Estimate. The chemical corrosion of the uranium metal occurs at the solid surface and not within the solid volume. As such, an estimate of the exposed surface area is needed. The amount of uranium metal with surfaces exposed to the MCO environment will vary from shipment to shipment depending upon the amount and extent of damaged fuel loaded in each MCO, the presence or absence of a scrap basket, and the amount and composition of sludge contained in any shipment.

An estimate of the amount and distribution of exposed surface area is presented in WHC-SD-SNF-TI-026, *Spent Nuclear Fuel Project Surface Area Estimates for N-Reactor Fuel in the K East Basin* (Cooper and Johnson 1996). Based on chemical and visual observations of the storage pools, Cooper and Johnson (1996) recommend as a worst-case scenario an MCO that contains 66,000 cm^2 (10,230 in^2) of exposed surface area in the form of fuel assemblies with split cladding. The damaged fuel assemblies are assumed to be equally divided over four intact fuel baskets. In addition to the fuel with split cladding, the worst-case MCO contains a single scrap basket holding portions of fuel assemblies with the equivalent of 54,000 cm^2 (8,370 in^2) of exposed surface area. The total apparent corroding area in the worst-case MCO is 120,000 cm^2 (18,600 in^2).

Since the reaction rate relationships provided above were developed for unirradiated uranium samples, an adjustment to the apparent exposed surface area is required to account for the increased surface area and reactivity of the N Reactor fuel caused by combination of corrosion and irradiation. This adjusted surface area, termed a "reactivity product factor," is obtained by multiplying the apparent surface area by 10 as recommended in Cooper (1996c). Thus , the reactivity product factor to be used with the reaction rate equations for the worst-cast MCO is 1,200,000 cm^2 (186,000 in^2). Laboratory characterization and additional storage pool survey work are being performed to validate these assumptions.

Since the majority of the fuel assemblies stored in the K Basins storage pools are undamaged, the average or nominal shipment will contain significantly less corroded or damaged fuel than that predicted for the worst-case scenario. WHC-SD-SNF-TI-026 (Cooper and Johnson 1996) includes an estimate that the surface area of the exposed uranium metal in the average MCO containing K East fuel will be slightly less than 3,000 cm^2 (465 in^2), or 30,000 cm^2 (4,650 in^2) with inclusion of the area adjustment factor.

The chemical reaction equations, Equations 3, 4, and 5, together with the reaction rate equations, Equations 6 through 15, and the total exposed surface area estimates are used to predict the surface heat flux on each fuel assembly or scrap section and the rate of hydrogen gas generation. Pressure calculations are based on a total void volume of 0.0425 m^3 (1.50 ft^3) during transport from the K Basins to the CVDF and of 0.555 m^3 (19.60 ft^3) during transport from the CVDF to the CSB facility. The pressurization calculations include the absorption of hydrogen gas in the water. See Appendix E for additional details.

Table 4-3 presents a summary of the chemical reaction source term assumed for the worst-case and nominal MCO fuel loadings in this analysis.

Table 4-3. Chemical Reaction Heat Source Term.

Payload	Scrap baskets			Intact fuel baskets		
	#	Reactivity product factor	Sludge	#	Reactivity product factor*	Sludge*
Worst case	1	540,000 cm^2	54.4 kg	4	660,000 cm^2	87.6 kg
Nominal	0	--	--	5	30,000 cm^2	6.75 kg

*The reactivity product factor divided equally among intact fuel baskets for worst-case multicanister overpack and lumped in center fuel basket for nominal multicanister overpack. Sludge divided equally among fuel baskets.

4.3 SPECIFICATIONS FOR MULTICANISTER OVERPACK COMPONENTS

The specifications for MCO components are documented in WHC-S-0426 (WHC 1996c) and summarized below.

The materials utilized in the MCO design that are considered temperature sensitive are the Helicoflex seal used between the MCO shield plug and the MCO vessel wall, the composite gaskets if used for the port access covers, and the rupture disk and its seal. The Helicoflex metallic seal (P/N H-304868) is composed of a close-wound Inconel helical spring surrounded by a type 300 stainless steel inner lining and a 0.051-cm- (0.020-in.-) thick silver outer lining. According to the manufacturer, the seal has a maximum design temperature rating of 370 °C (698 °F) at a pressure of 1.0 MPa (150 lb/in^2 gauge).

The MCO rupture disk is specified as a 25.4-mm (1-in.) diameter Continental Disc Corporation rupture disk, model 0196-042 (P/N CD30760). The disk is fabricated from type 316L stainless steel and has a rupture pressure rating of 1,034 kPa (150 lb/in^2 gauge) at 190 °C (375 °F).

The remaining materials used in the fabrication of the MCO have significantly higher temperature capabilities. The type 304/304L stainless steel has a melting temperature above 1,400 °C (2,550 °F) and a maximum service temperature rating of 427 °C (800 °F) in accordance with Section III, Subsection NB, of the ASME Boiler and Pressure Vessel Code (ASME 1995a). The carbon steel used for the MCO shield plug has a melting point above 1,400 °C (2,550 °F) and a maximum normal service temperature of 371 °C (700 °F) in accordance with Subsection NB, Section III of the ASME Boiler and Pressure Vessel Code (ASME 1995a).

Although the uranium metal in the spent nuclear fuel assemblies has a melting temperature of 1,090 °C (1,994 °F), the eutectics between uranium and iron occur at 725 °C (1,337 °F). The Zircaloy-2 cladding has a melting temperature above 1,800 °C (3,272 °F). The zirconium–beryllium end caps have

a melting temperature of 980 °C (1,800 °F). The maximum service temperature limit for the uranium metal depends on the MCO process under consideration, the amount of exposed surface area, and the amount of water retained in the MCO to drive the chemical reaction rate. Process controls are to be implemented to ensure that temperature excursions do not occur in the metal.

4.4 THERMAL EVALUATION FOR NORMAL CONDITIONS

The SNF Project was established to expedite the removal, stabilization, and storage of SNF and sludge from the K Basins at the DOE's Hanford Site. Figure 4-5 illustrates the SNF Project process steps from the retrieval of the fuel at the K Basins through fuel staging and interim storage in the CSB. The thermal-hydraulic evaluations performed for the SNF Project process flow steps to date include WHC-SD-WM-ER-525, *Thermal Hydraulic Feasibility Assessment for the Spent Nuclear Fuel Project* (Heard et al. 1996a), WHC-SD-SNF-ER-012, *Thermal Hydraulic Feasibility Assessment of the Hot Conditioning System Process* (Heard et al. 1996b), and WHC-SD-SNF-ER-014, *MCO Pressurization Analysis of Spent Nuclear Fuel Transportation and Storage* (Fryer et al. 1996).

This section summarizes the thermal models developed to evaluate the thermal-hydraulic performance of the SNF Project process flow steps and the results for the normal conditions under each of these steps. The impact of off-normal or accident conditions, such as equipment failure or fire, and specific details of the thermal models are addressed in the individual facility SARs. The thermal models are used to investigate the range of environmental and process conditions expected and to determine the process controls required to obtain a safe, stable, and secure operating condition. A safe, stable, and secure operating condition is defined as either (1) an energy balanced, steady-state condition where the energy gains to the system equal the energy losses from the system and the system is within its temperature and pressure limits or (2) a transient operating condition where energy gains may temporarily exceed the losses, but where administrative controls are implemented to ensure the system is placed into a stable steady-state condition before exceeding the system temperature and pressure limits.

Table 4-4 lists the load combinations considered for wet and dry transportation. The difference between the worst-case and probable maximum normal conditions of transport (NCT) for the hot ambient case is the assumed starting temperature for the SNF and cask. The difference between the probable minimum NCT and the worst case is that the probable minimum condition assumes nominal fuel loading and heat dissipation while the worst-case NCT for the cold ambient condition assumes a zero heat load. This latter load combination leads to the analytically trivial result under steady-state conditions of a uniform -33 °C (-27 °F) temperature.

The SNF, MCO, and cask temperatures are expected to be on the order of 10 °C (50 °F) at the time of loading at the K Basins and following cold vacuum drying. To allow for process variations or additional heatup, such as that resulting from operational delays, a nominal value of 15 °C (59 °F) is assumed for the purposes of this report. In addition, an initial temperature of 25 °C (77 °F) is also considered for the worst-case NCT hot ambient load combination.

Figure 4-5. Process Flow for the Spent Nuclear Fuel Project.

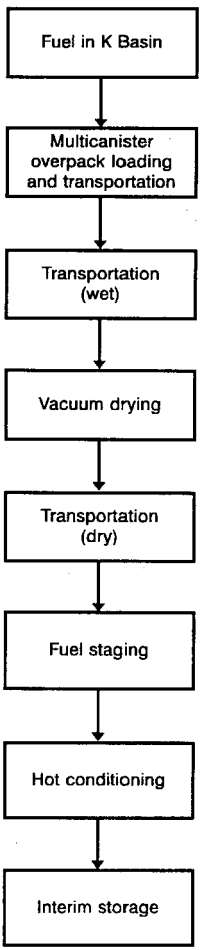

CVD4-5.CH3
12-16-96

Table 4-4. Load Combinations For Normal Conditions of Transport.

Normal transport load combinations		Applicable conditions							
		Initial spent nuclear fuel temperature			Insolation		Fuel loading		
		25 °C	15 °C	10 °C	Maximum*	Zero	Maximum	Nominal	Zero
Hot ambient*	Worst case	X			X		X		
46 °C (115 °F)	Probable maximum		X		X		X		
	Nominal		X		X			X	
Cold ambient	Probable minimum			X		X		X	
-33 °C (-27 °F)	Worst case			X		X			X

*Diurnal cycle for ambient temperature and insolation in accordance with J. G. Fadeff, 1992, Environmental Conditions for On-Site Hazardous Materials Packages, WHC-SD-TP-RPT-004, Rev. 0, Westinghouse Hanford Company, Richland, Washington.

4.4.1 Thermal Models

A number of one-, two-, and three-dimensional, lumped-parameter, finite-element, and subchannel thermal models of the MCO and its payload have been developed. The thermal models are used to investigate the thermal-hydraulic performance of MCOs, together with the payload of intact assemblies and scrap fuel, under transport, cold vacuum drying, staging, hot conditioning, and interim storage conditions. The models vary in the level of temperature resolution provided within the MCO, the complexity of the heat transfer modes modeled, and the presence or absence of algorithms for modeling the chemical reaction heat, water retention, and vacuum drying. They vary also in their steady-state and transient modeling capabilities. The models developed are based on either the HUB[1] engineering spreadsheet program, the FIDAP[2] computer program, the COBRA-TF computer program, or the SINDA/FLUINT computer program. While some of the process steps have been evaluated by using more than one thermal model, the results presented here are selected from the model considered the most current and representative of the process under consideration. The other models serve to provide code-to-code validation of the results obtained.

For the purposes of simulation, the MCO is assumed to contain a total of five storage baskets loaded axially end-to-end. While the thermal models have been used to analyze a variety of loading configurations, the design basis loadings for safety purposes are defined in Section 4.2.1.3. The material thermal properties assumed for the models are summarized in Appendix E.

[1]HUB is a registered trademark of J. Marvin, Incorporated.

[2]FIDAP is a registered trademark of Fluid Dynamics, Incorporated.

Table 4-5 presents the N Reactor fuel dimensions, while Figures 4-6 and 4-7 present cross-sectional and isometric views of a Mark IV fuel assembly.

Table 4-5. N Reactor Fuel Dimensions.

Fuel type	Mark IA	Mark IV
Overall nominal dimensions (inches)		
Outer element OD	2.404	2.425
Outer element ID	1.767	1.701
Inner element OD	1.246	1.279
Inner element ID	0.440	0.479
Cladding thickness (mils)		
Outer element, outer cladding	25	25
Outer element, inner cladding	25	20
Inner element, outer cladding	40	30
Inner element, inner cladding	25	20
Nominal maximum length (inches)		
Outer element	20.88	26.10
Inner element	20.82	26.04
Assumed end cap thickness (inches)		
Outer element	0.200	0.200
Inner element	0.200	0.200

ID = inner diameter.
OD = outer diameter.

Comparisons between the Mark IA and Mark IV temperature results demonstrated that the thermal results for the Mark IA fuel assemblies are encompassed by those seen for the Mark IV assemblies. This occurs because of the Mark IV fuel basket's inherently higher thermal resistance, which is due to the additional inner ring of fuel assemblies present in the Mark IV fuel basket. Because of criticality concerns associated with the Mark IA fuel, a 15.2-cm (6-in.) Schedule 40 pipe centered within each Mark IA fuel basket provides a mechanical mechanism to prevent the loading of more than 48 Mark IA fuel assemblies in each basket.

Figure 4-6. Cross-Sectional View of Mark IV Fuel Assembly.

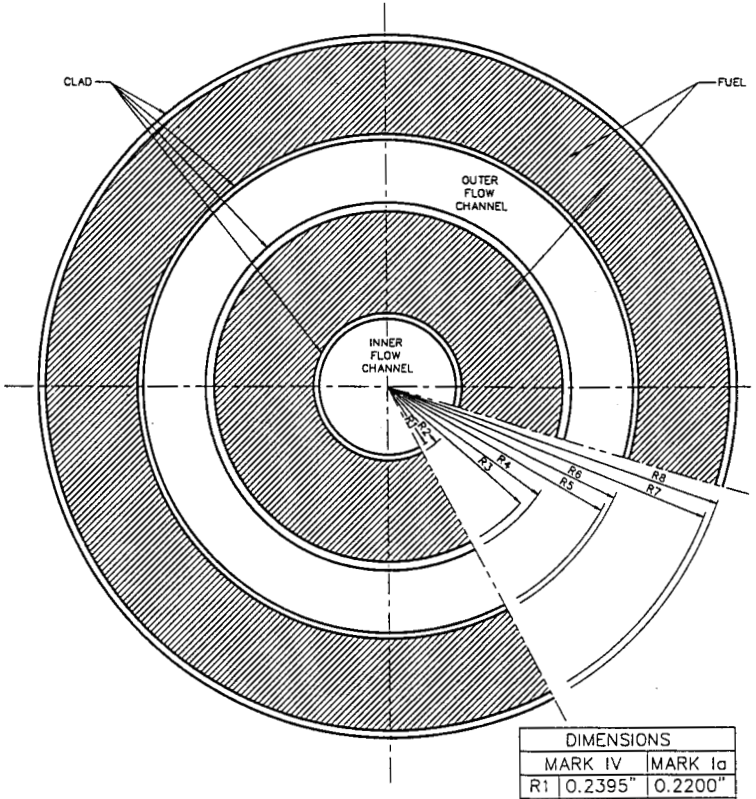

DIMENSIONS		
	MARK IV	MARK Ia
R1	0.2395"	0.2200"
R2	0.2595"	0.2450"
R3	0.6095"	0.5830"
R4	0.6395"	0.6230"
R5	0.8505"	0.8835"
R6	0.8705"	0.9085"
R7	1.1875"	1.1770"
R8	1.2125"	1.2020"

D0610101 (12-13-95)

Figure 4-7. Isometric View of Mark IV Fuel Assembly.

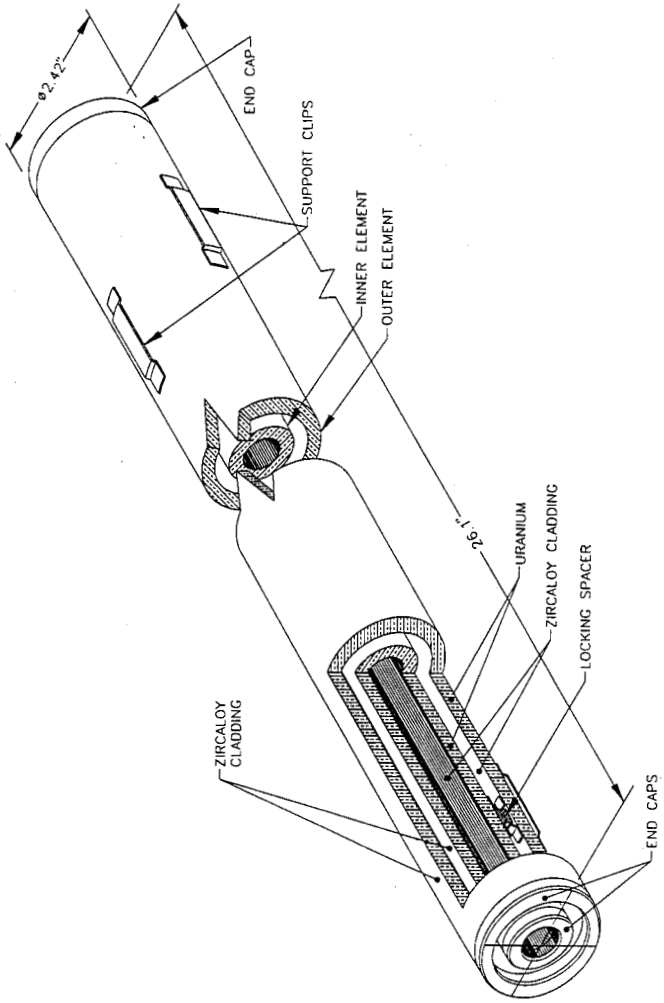

The primary system dimensions assumed for the analyses are as follows.

- The overall axial lengths of the Mark IV fuel elements range from 44.2 cm (17.4 in.) to a maximum of 66.3 cm (26.1 in.).
- The overall axial lengths of the Mark IA fuel elements range from 36.3 cm (14.3 in.) to a maximum of 53.1 cm (20.9 in.).
- The MCO's outer diameter is assumed to be 61 cm (24 in.) with a wall thickness of 1.27 cm (0.50 in.).
- A 1.51-cm (0.595-in.) diametrical gap is assumed between the MCO's outer diameter and the transportation cask's inner diameter.
- The transportation cask's outer diameter is assumed to be approximately 102 cm (40 in.) with a wall thickness of approximately 18.6 cm (7.3 in.).
- For the models involving the CSB storage tube, a 7.6-cm (3-in.) diametrical gap is assumed between the MCO's outer diameter and the storage tube's inner diameter.
- The storage tube is assumed to be 71 cm (28 in.) in diameter with a 1.27 cm (0.50 in.) wall thickness.

4.4.2 Thermal Model Descriptions

4.4.2.1 HUB. HUB is an integrated, spreadsheet format, computational notebook program. Equations can be written into the document or embedded in tables and graphs and computationally linked throughout a document. Equations for the heat transfer from the fuel to the environment through the MCO and tube or cask walls are entered into the HUB program, along with the chemical and decay heat generation rates, convective heat transfer coefficients, and the thermal properties of the materials, to obtain the solution for the temperatures of each surface.

The HUB computer program is used to provide one-dimensional, steady-state and transient representation of a single fuel basket within the MCO, with the MCO in the transportation cask, and within a CSB storage tube. Figure 4-8 illustrates the lumped mass approach used by HUB to simulate the heat transfer between the fuel assemblies and the MCO wall. This modeling approach assumes that the fuel region can be modeled as alternating rings of fuel and fill gas gaps, conserving the total surface area of the fuel and the fuel volume. The volume of fill gas in the gaps also is conserved and is equal to the volume of fill gas surrounding the actual fuel assemblies. The annular fuel rings of the model are shown superimposed on the actual fuel arrangement. The MCO wall and the cask or storage tube walls are also modeled as cylinders. Heat transfer between each of the fuel ring surfaces and between the outer fuel ring and the MCO wall is simulated as radiant heat transfer when the MCO is at a vacuum and by conduction, convection, and radiation when a fill gas (i.e., helium, air, or argon) is present.

Figure 4-8. One-Dimensional Ring Model.

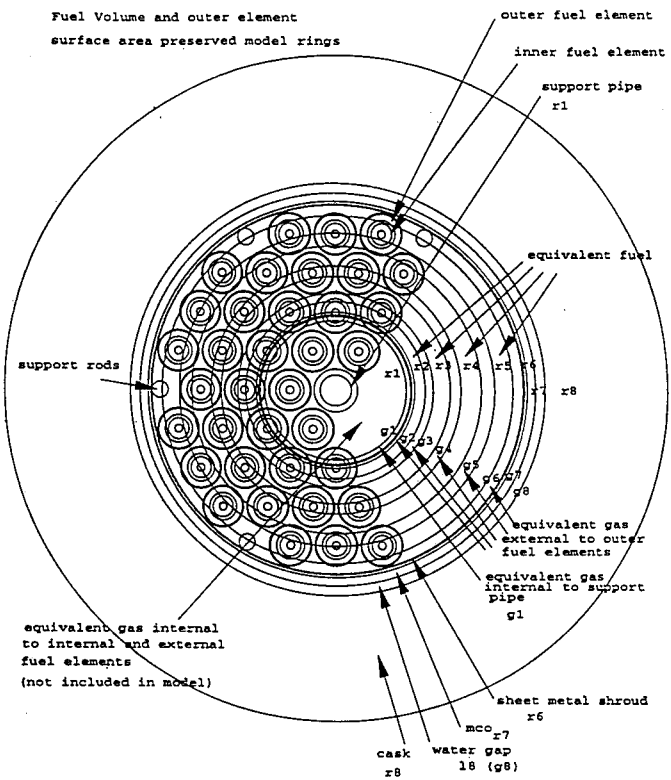

The analytical solution performs an energy balance across the outer surface of the transportation cask or storage tube to obtain a converged temperature solution for the outermost surface, wherein the energy losses from convective and radiative heat transfer equal the energy gains from the incident solar heat flux, chemical reactions, and nuclear decay heat. The resulting surface temperatures are then used as a boundary condition to derive the temperature drop across the transportation cask or storage tube based on applying Fourier's Law to an infinitely long cylinder with a known inner and outer diameter. Successive energy balances and applications of Fourier's Law across each of the gaps and solid components results in a series of coupled equations. Equations for the heat transfer from the fuel to the environment through the MCO and tube or cask walls are entered into HUB, along with the chemical and decay heat generation rates, convective heat transfer coefficients, and the thermal properties of the materials. HUB solves these equations analytically to determine the successive temperature drops and corresponding surface temperatures for each of the cylindrical elements.

4.4.2.2 FIDAP. FIDAP (Fluid Dynamic Analysis Package) is a commercially available, general purpose, computer package that uses finite element methods to simulate many classes of single- or multiphase compressible or incompressible flows, including heat transfer and mass transport of chemical species in both nonreacting and reacting flows as discussed below. The simulation can be either steady-state or transient and can model flows in complex arbitrary geometries that are axisymmetric, two-dimensional, or three-dimensional. Mixed coordinate or moving or rotating systems are supported. The program modules provide all aspects of the model generation and automatic meshing or paving, problem setup, view factor calculations, solution, and postprocessing of a flow and/or thermal analysis.

FIDAP supports reactions based on both chemical kinetic-controlled models, such as the Arrhenius Rate Law, in which the reaction rate is determined from chemical kinetic considerations, and mixing-controlled reactions in which the mixing action of a turbulent velocity field determines the rate of reaction. Both mass fraction and molar concentration forms for the reaction models are supported. Simple one-step, competing, controlling, and multistep chemical models also are supported.

FIDAP has been validated and verified for use at Hanford (Heard 1994). The corresponding HUB and COBRA-TF models have been compared against the FIDAP results.

The FIDAP results presented herein address the performance of the MCO concept under the hot conditioning process (see Figure 4-9). Two detailed three-dimensional FIDAP models of a single fuel basket and a single scrap basket tier within an MCO within the HCS were constructed from Figures 4-10 and 4-11. The resulting nodalization patterns for the fuel and scrap basket tier models are shown in Figures 4-12 and 4-13.

Figure 4-9. Mark IV Geometry for Multicanister Overpack Sector Model Within the Hot Conditioning System.

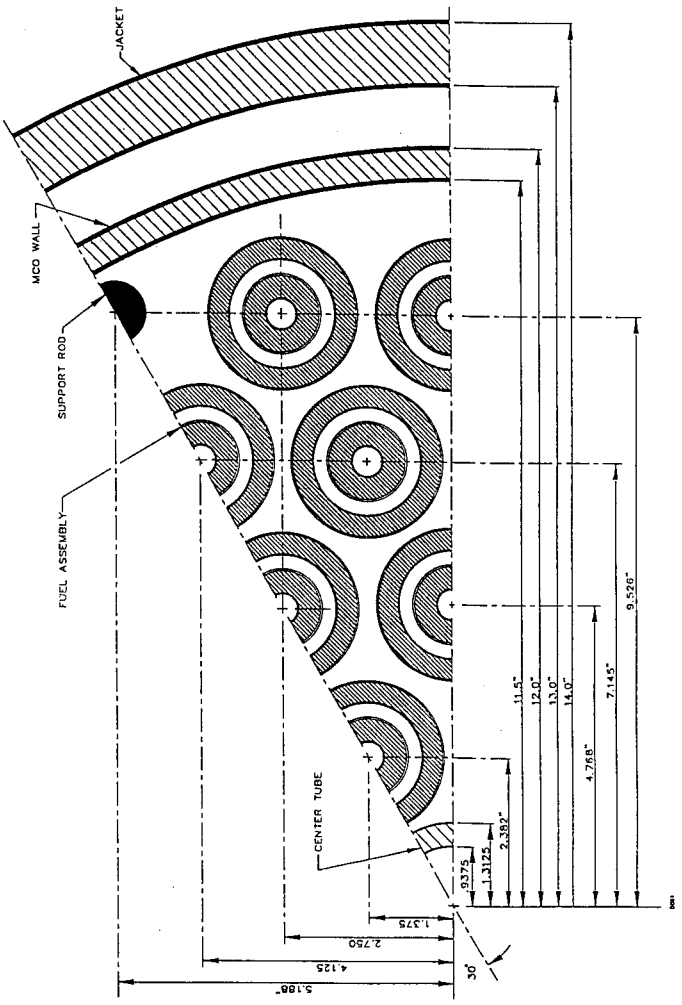

Figure 4-10. Mark IV Fuel Geometry and Configuration for a Single-Tier Model of a Fuel Basket.

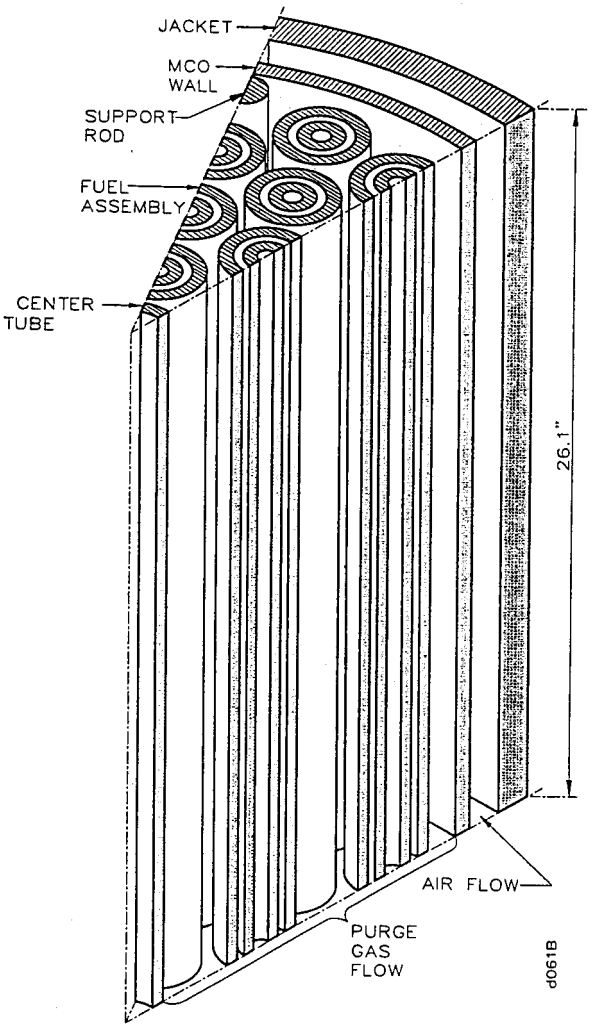

Figure 4-11. Scrap Basket Geometry and Configuration for a Single-Tier Porous Media Model of a Scrap Fuel Basket.

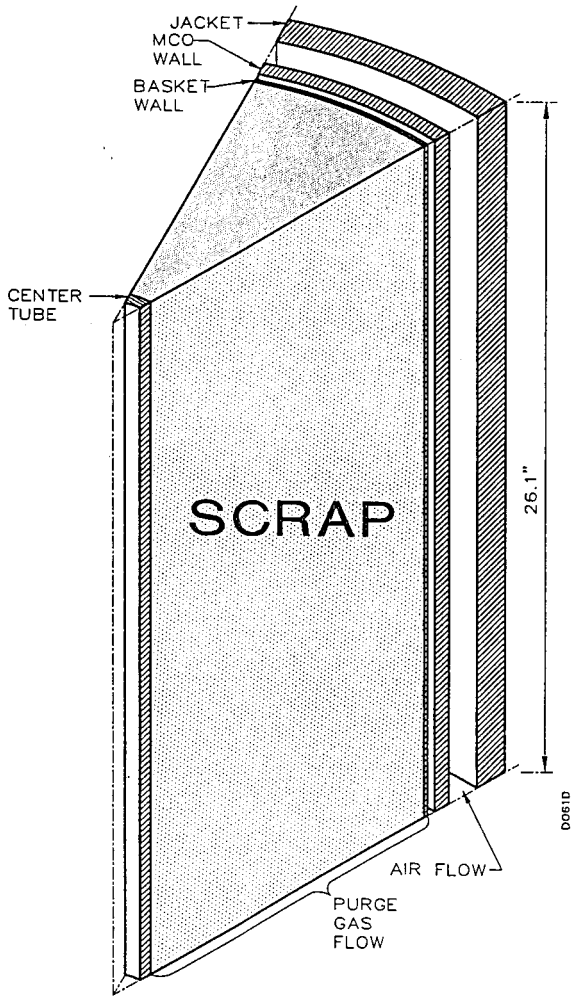

Figure 4-12. Nodalization Pattern for the Single-Tier Model of a Fuel Basket and Multicanister Overpack Within a Storage Tube.

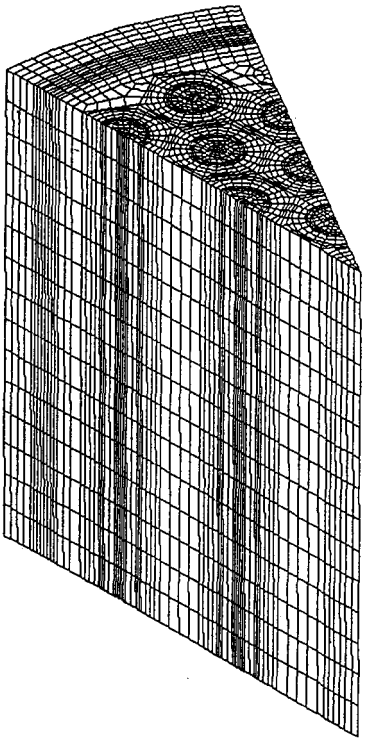

Figure 4-13. Nodalization Pattern for the Single-Tier Model of a Scrap Basket and Multicanister Overpack Within a Storage Tube.

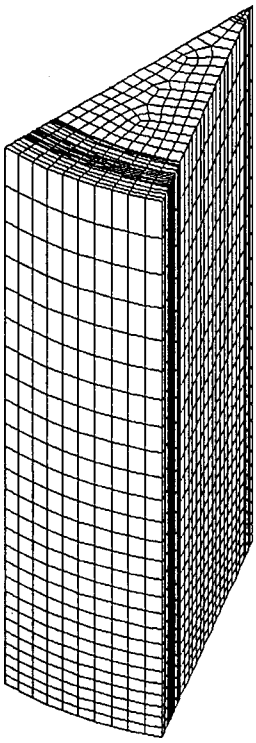

Each of the following three-dimensional thermal-hydraulic models was developed to investigate the range of temperatures and heatup rates for the scrap and the fuel baskets during the HCS process:

- A three-dimensional, 30° sector model of a single fuel basket or tier containing the equivalent of 54 Mark IV fuel assemblies within an MCO positioned within the HCS
- A three-dimensional, 30° sector model of a fully loaded single scrap basket or tier within an MCO positioned within the HCS.

Computer limitations prevented the development of a full-length, detailed, finite-element, three-dimensional model of an MCO. All three modes of heat transfer (i.e., conductive, convective, and radiative) are incorporated by means of specialized surface or continuum elements and are available for use.

The calculation of radiative heat transfer is automated within FIDAP. View-factor calculations performed by FIDAP include the effect of full or partially obstructing surfaces. The view factors are calculated on an individual element basis for all elements comprising radiative surfaces. A gray-body approach without participating media is assumed for each of the radiating surfaces within the model. The outer surface of the system is assumed to be radiating to a user-determined black-body temperature.

For the correct treatment of thermal radiation within three-dimensional domains, the radiating surfaces must be fully enclosed. For the small gaps associated with the basket skirt-MCO inner dimension and the MCO outer dimension-jacket inner dimension, this enclosure is provided by the two radiation surfaces, the two reflective surfaces associated with the lines of symmetry, and the upper and lower planes associated with the inlet and outlet flow boundaries. The first four surfaces are automatically handled within FIDAP. However, for "windows" and "openings" (e.g., an inlet or outlet flow boundary), a reference temperature for calculating the radiative heat transfer must be supplied as a boundary condition by the user.

For the inlet flow boundary, this is fairly simple. A uniform inlet temperature and flow distribution can be assumed. The outlet temperature, especially with chemical reactions, is more difficult to estimate, thus requiring an iterative approach where T_{REF} is updated based on the mean outlet temperature from the previous run. This treatment usually requires a single iteration to obtain agreement within five degrees of the mixed mean outlet temperature and the assumed T_{REF}. A slight conservatism is imposed such that T_{REF} is always slightly greater than the mixed mean temperature.

Convective heat transfer coefficients can be applied separately to each of the interior surfaces. Both forced and natural convection are handled.

4.4.2.3 COBRA-TF. The COBRA-TF computer code was developed by the Pacific Northwest Laboratory for the NRC to perform analyses of thermal-hydraulic transients in various components of light water reactors. COBRA-TF is a three-dimensional, finite difference model for two-phase, multi-species fluid flow and heat transfer. The code was originally developed for simulating single- or two-phase flows within a variety of geometries associated with reactor components. The basic code is therefore suitable for modeling fluid

flow and heat transfer within the MCO. Additional modifications were made to the code to accommodate geometry and processes unique to the MCO passivation operation. These include an addition to the radiation subchannel model to include the geometry of the fuel storage baskets, a revised heat transfer model for rubble in the scrap baskets, and the addition of the specific hydride and oxidation reactions for uranium.

A three-dimensional integrated thermal-hydraulic model of the MCO internals was constructed using the COBRA-TF simulation code. The integrated COBRA-TF model considered both momentum (flows) and energy (temperature). The model was prepared in order to verify proposed design and operating conditions for the hot conditioning and passivation process. Details of the model are described below.

For purposes of design evaluation, the MCO was assumed to contain a total of five storage baskets loaded axially end-to-end. Of the five baskets, two were assumed to contain scrap, one placed at the top of the MCO and the other at the bottom. The remaining three fuel storage baskets at the center of the MCO were assumed to contain intact Mark IV fuel elements. Depth of the rubblized fuel in the scrap baskets was taken to be 63.5 cm (25 in.); the fuel storage baskets contained 54 fuel elements each. The assumed MCO axial configuration is shown on Figure 4-14. The MCO configuration and dimensions were obtained from drawing SK-2-300379. Basket dimensions and details were obtained for the Mark IV fuel basket from drawing SK-1-80209 and for the scrap baskets from drawing SK-1-80210.

The COBRA-TF model divides the MCO into seven vertical sections. Starting at the bottom of the MCO, these include an inlet plenum, a bottom rubble basket, three fuel baskets, a top rubble basket, and an outlet plenum (see Figure 4-14). Because of symmetry about the MCO centerline, only a 30° sector of the MCO is modeled explicitly. Each section is divided into a number of vertical and lateral flow channels that are defined by the section geometry. Figure 4-15 illustrates the vertical flow channels assigned to a fuel basket containing Mark IV fuel assemblies. The lateral flow channels for this same sector are shown in Figure 4-16. Note that lateral flow between those channels internal to the fuel elements and those external to the fuel elements can occur only in the region between the top of the fuel elements and the bottom of the next basket. The vertical channels within each axial section are divided into the same series of axial lengths as shown in Figure 4-14.

For the analysis of HCS operations, a purge gas is introduced into the process tube at the center of the inlet plenum at a specified rate. The purge gas is then allowed to flow downward through the process tube into the lower plenum and finally upward through and around the baskets within the MCO. The purge gas exits via the outlet plenum through the short process tube in the MCO shield plug. Flow distribution within the MCO is calculated based on the friction and momentum loss between nodes. Friction loss is calculated by the code based on the wetted surface areas and the fluid Reynolds number. Momentum loss between nodes is calculated based on loss coefficients input to the code. The loss coefficients are based on empirical correlations for the various types of geometry.

Figure 4-14. Axial Model of Multicanister Overpack Containing Three Fuel and Two Scrap Baskets.

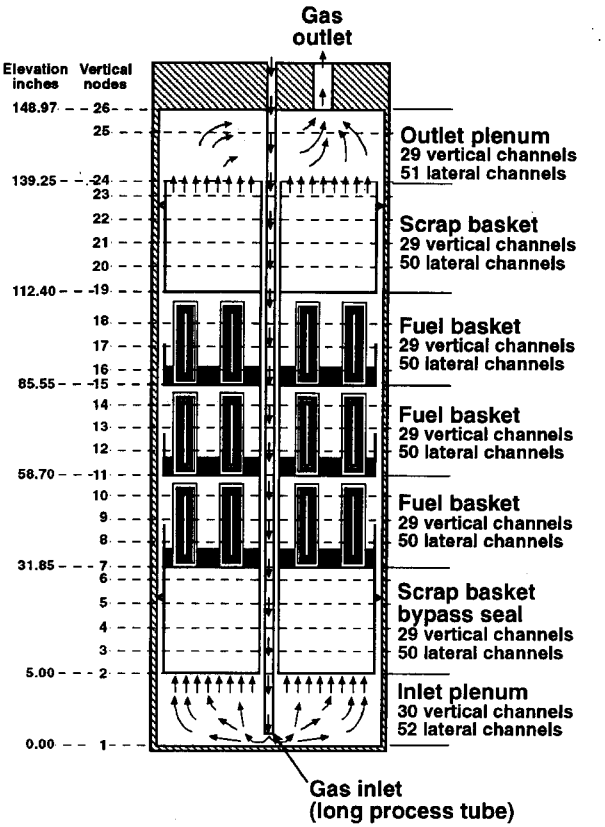

Figure 4-15. Horizontal Flow Subchannels for Fuel Basket.

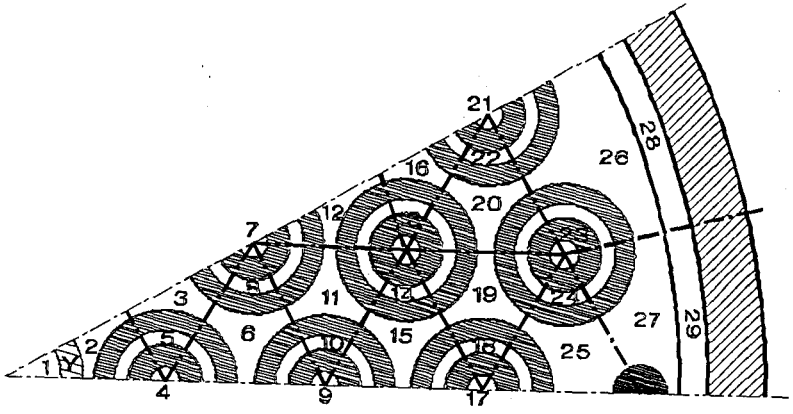

Figure 4-16. Lateral Flow Subchannels for Fuel Basket.

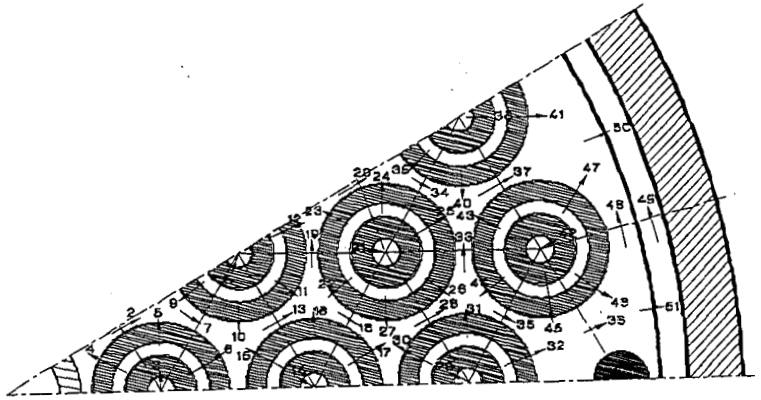

The inlet plenum is treated as a free volume with pressure loss for the lateral flow through the inlet strainer and along the MCO baseplate and the spacer bars. The inlet plenum also provides connection to the vertical flow channels through the scrap basket, between the scrap basket and MCO wall, and between the process tube and the storage basket center pipe.

The scrap basket is treated as a porous media rubble bed and represents a modification to COBRA-TF. Pressure loss across the rubble bed is calculated using an empirical correlation (Idelchik 1994) that is a function of the height of the bed, the mean particle size, the bed porosity, and the fluid temperature rise across the bed. The current calculations assume that the rubblized fuel in the scrap basket has a mean diameter of 1.90 cm (0.75 in.), a porosity of 0.46, and a bed height of 63.5 cm (25 in.) (similar to a basket of hard coal). The hydraulic model for the scrap basket also includes loss coefficients for the perforated bottom plate and for an assumed flexible flow resistor between the outside wall of the scrap basket and the inside wall of the MCO.

The design of the fuel storage baskets allows the purge gas entering a basket from below to flow directly through the interior channels of each fuel element. The design also includes two paths that bypass flow around the outside of the fuel elements. The first path is next to the fuel elements and is produced by the clearance between the outside diameter of each fuel element and the inside diameter of the baseplate socket. The second bypass channel is around the outside surface of the storage basket through the clearance between the basket and inside wall of the MCO. This passage could potentially prevent oxygen in the purge gas from reacting with the uranium metal on the surface of the fuel elements during the passivation process. However, because the outside skirt on the basket is perforated and only partial height (28 cm [11 in.]), the bypass flow can mix with the gas flowing past the outside surface of the fuel elements and potentially with the interior gas flows in the space between the top of the fuel elements and bottom of the next storage basket. Fluid friction losses for flow through and around the fuel storage baskets is calculated within COBRA-TF based on the input geometry and the fluid Reynolds number. Momentum losses are calculated based on loss coefficients input to the code. The loss coefficients are based on empirical correlations for the various types of geometry (Idelchik 1994).

The integrated COBRA-TF model includes three energy sources. The first heat source is nuclear decay heat. The second heat source is chemical and related to the rate of fuel oxidation (Cooper 1996c). The third heat source is that supplied to or removed from the MCO by operation of the hot passivation station. This third source is treated as a temperature boundary condition to the model.

The radiolytic decay heat used in the analyses conservatively assumes a total of 929 W for an MCO containing 270 Mark IV fuel elements (0.0446 W/in^3 of fuel) versus the 835 W presented in Table 4-2. For the model of intact fuel elements, this value is volume weighted over the inner and outer fuel annuli. For the scrap basket model this value is applied to the nonporous volume of the scrap. With a porosity of 0.46, the resulting decay heat input to the scrap basket is very similar to that of a 54-element fuel storage basket. Chemical energy from the reaction between uranium metal and oxygen also is included in the analyses. The reaction rate relationship used is

based on a modified form of the Ritchie reaction rate relationship based on oxygen concentration (Heard et al. 1996b).

Heat transfer between the fuel, the purge gas, and the inside walls of the surrounding MCO is calculated within the code as a combination of conduction, convection, and thermal radiation. Heat transfer coefficients for convective flows are calculated by the code as a function of the local Reynolds number, wetted perimeter of the flow passages, and thermodynamic properties of the purge gas. In the limit, as flow goes to zero, the convective heat transfer becomes simple heat conduction. Convective heat transfer within the scrap basket rubble bed is calculated in a manner similar to that for the intact fuel elements except that the heat transfer area is determined from the fuel volume and an estimated surface-to-volume ratio associated with the assumed porosity of the rubble.

Radiant heat transfer is determined between surface nodes at the same axial location. Radiation in the axial direction is neglected because of geometry effects (axial view factors are generally small) and because axial temperature gradients are generally small. The radiating surfaces within the model are assumed to be gray and the intervening gas transparent. Emissivity is input for each surface as a function of the material type. Surface view factors are calculated by the code based on subchannel templates (geometry surrounding a particular flow channel). Additional templates were added to the code to accommodate the socket-type fuel storage baskets. Radiation heat transfer was not explicitly applied to the rubble bed itself because the correlations for material conductivity implicitly include the effects of radiation. Radiation heat transfer between the outside surface of the scrap basket and inside wall of the MCO was included however.

4.4.2.4 SINDA/FLUINT. The SINDA/FLUINT heat transfer code (SINDA 1995) is used to evaluate the thermal performance of the MCO assembly in the transportation cask. SINDA is a finite difference, lumped parameter code developed under the sponsorship of the NASA Johnson Space Center. The SINDA code has been evaluated and validated for simulating the thermal response of transportation packages (Glass 1988) and has been used for the analysis of several transportation packages for nuclear material, including the recently licensed Radioisotope Thermoelectric Generator Transportation System (Ferrell 1995) for DOE.

The SINDA code (SINDA 1995) provides the capability to simulate steady-state and transient temperatures using temperature-dependent material properties and heat transfer via conduction, convection, and radiation. Complex algorithms may be programmed into the solution process for such purposes as computing convective heat transfer coefficients as a function of the local geometry, gas thermal properties, and temperatures or to compute the chemical reaction heat as a function of the local temperature and pressure conditions.

A major feature of the SINDA/FLUINT code (SINDA 1995) is its ability to use submodels to represent common geometry sections of the cask, fuel baskets, and other components, and then, by thermally connecting the individual submodels, to form a complete model of the cask and MCO assembly. This approach not only simplifies the modeling but reduces the verification process

by minimizing the amount of original coding required to provide a complete thermal representation of the system.

The radiation heat transfer between the various surfaces is computed assuming the standard gray-body relationship. The surface emissivities assumed are listed in Appendix E. The view factors for complex geometries within the MCO were computed using the VIEW program (Emery 1991) while view factors for simple geometries were computed using standard relationships or via the string method (Kreith 1973).

Five thermal submodels were used to analyze the performance of the entire MCO cask and the MCO assembly.

- The bottom end region of the MCO cask and MCO assembly
- The typical axial midsection of the MCO cask
- A 3-dimensional model of the closure lid end region of the MCO cask and MCO shield plug
- A 3-dimensional model of the Mark IV intact fuel basket within the MCO assembly
- A scrap basket within the MCO assembly.

The dimensional data and material specifications used in the thermal model of the cask were taken from Transnuclear, Inc. Drawing 3035-3, Rev. 1, dated June 24, 1996. The MCO assembly and MCO shield plug dimensions and material specifications were obtained from Drawing SK-2-300461, dated September 18, 1996. Similar information for the Mark IV and Mark IA intact fuel baskets and scrap baskets were obtained from Drawings H-2-827589 to H-2-827592, dated October 24, 1996.

Figure 4-17 illustrates the layout of the various thermal submodels used to evaluate the thermal performance of the MCO cask and MCO assembly. This layout, showing the MCO arrangement with the Mark IV fuel, consists of five identical submodels (i.e., submodels BSKT1, BSKT2, BSKT3, BSKT4, and BSKT5), together with submodels for the lid and end regions of the cask and MCO. As an alternative, four intact fuel baskets and one scrap basket were modeled within the MCO cavity.

As seen from the figure, the END submodel encompasses the lower 23.8 cm (9.38 in.) of the cask and end plug of the MCO shell. Above the END submodel are five submodels of the MCO fuel baskets and the associated section of the cask wall. Each of these submodels span the 68.2-cm (26.85-in.) length of the fuel baskets. Above the last fuel basket is a thermal submodel of the MCO shield plug, the void space below the shield plug, and a 27.2-cm (10.69-in.) section of the cask wall. The LID submodel encompasses the upper 40.1-cm (15.79 in.) section of the cask wall. Additional details of the thermal model of the transportation cask will be provided in the safety analysis report for packaging.

Figure 4-17. Overview of SINDA Thermal Submodels Layout.

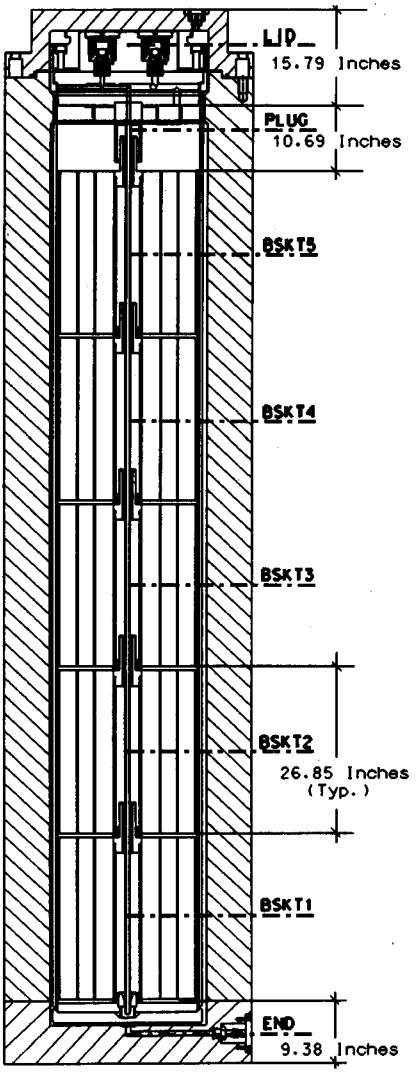

Heat transfer through and from the typical midbody section of the cask wall is simulated using an axisymmetric representation of the cask. An axisymmetric model is appropriate given that the cask thickness and the relatively small variation in heat flux from the MCO in the circumferential direction results in a minimal variation of cask wall temperatures in the circumferential direction. Modeling of the MCO assembly used a three dimensional approach because of the variation in heat flux and the relatively low thermal mass offered by the MCO shell and fuel baskets. The MCO shell is divided into three axial sections over the axial length of the fuel basket and into 30° segments in the circumferential direction.

Taken together, the submodels provide an axisymmetric thermal model of the MCO cask shell and a three-dimensional thermal model of the cask lid and of the MCO assembly. Heat transfer between the cask's inner surface and the MCO is assumed to be via straight conduction (i.e., Nu = 1) through either a water or helium gas medium, as appropriate for the transportation mode under consideration. The presence of hydrogen gas is conservatively ignored for this analysis (the thermal conductivity of hydrogen is 20% to 30% greater than helium). Gray-body radiation interchange across the gap is also included for those sections with a helium backfill. Heat transfer from the outer surface of the cask is via convection and radiation to the ambient environment. The presence of the transport trailer is ignored for the purposes of this analysis. This assumption maximizes the heat input into the cask during both the NCT and hypothetical accident conditions analysis.

The basic thermal submodel of the fuel baskets and the fuel elements represents a 90° segment of a single level. The plan view of the Mark IV fuel basket assembly shown in Figure 4-18 illustrates the placement of the thermal nodes used to model the baseplate of the Mark IV fuel basket and the lower 6.6 cm (2.6 in.) section of each fuel assembly that fits within the sockets of the fuel basket baseplate. Within the 90° segment, 11 complete fuel assemblies and 5 partial fuel assemblies are represented. Symmetry conditions are assumed at the model boundaries. The enlarged view of a representative fuel assembly within the basket illustrates the placement of the thermal nodes used to simulate each fuel assembly and the surrounding basket structure.

Thermal resolution within each full fuel assembly is provided through the use of 24 thermal nodes, 12 for each element, over four axial segments within the fuel elements. Each axial segment is represented by three nodes in the circumferential direction. The lowest axial segment (shown in Figure 4-18) is 6.6 cm (2.6 in.) high. The three other axial segments not shown are 27.94 cm (11 in.), 23.88 cm (9.4 in.), and 7.62 cm (3 in.) high, respectively. Heat transfer from the inner to the outer element is treated as conduction and radiation (for dry transport) across the 0.53-cm (0.21-in.) gap separating the elements. Convection from the outer surface of the outer element is assumed. While the presence of hydrogen gas is conservatively ignored (the thermal conductivity of hydrogen is 20% to 30% higher than that for helium), the beneficial effect on convective heat transfer caused by the density increase of the fill gas is included.

Figure 4-18. SINDA Thermal Model of Intact Fuel Basket and Lower Fuel Element Section.

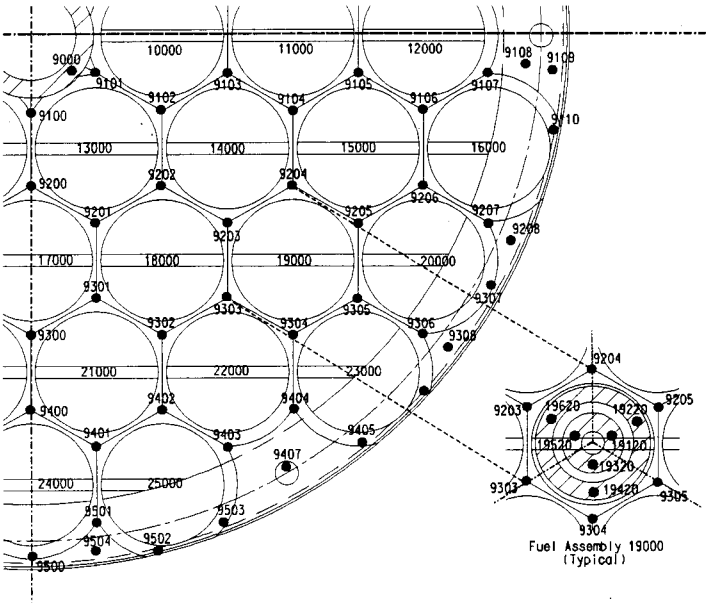

The Mark IV scrap basket is modeled as a homogeneous, porous medium using 20 thermal nodes to provide a two-dimensional, axisymmetric representation of the heat generation and temperatures within the scrap bed. An additional 14 thermal nodes provide a two-dimensional, axisymmetric thermal representation of the scrap basket's side walls, base, and center tube.

In addition to computing temperatures, the thermal model computed the transient pressure rise within the MCO and cask. The calculation included the pressure rise effects from four sources: (1) the ideal gas expansion with changes in temperature, (2) the pressure rise caused by hydrogen gas generation from chemical reactions, (3) the expansion of the water, and (4) the amount of hydrogen dissolved in the water volume for the wet transfer phase. The void volumes and initial backfill pressures assumed are listed in Table 4-1. The pressure rise caused by hydrogen gas generation is computed using the chemical reaction and gas generation rates listed in Section 4.2, while the amount of hydrogen dissolved in the water during the wet transport phase is determined using Henry's law, the volume of the water, and the partial pressure of hydrogen gas.

4.4.3 Maximum and Minimum Temperatures

4.4.3.1 Wet Transfer of MCO. The wet transfer of the MCO and transportation cask between the K Basins and the CVDF is evaluated using the SINDA/FLUINT thermal model and a transient simulation of the transfer process. The thermal evaluation is based on assumptions listed in Tables 4-1, 4-2, 4-3 and 4-4. The nominal, probable maximum, and worst-case NCT loadings for hot ambient conditions are evaluated using a transient simulation of the transport process with a diurnal cycle for ambient temperature and insolation based on the Hanford peak summer day. To ensure that the cask is exposed to the highest heat flux portion of the diurnal cycle during the projected transportation time frame, an 8:00 a.m. start time is assumed for the simulated transportation process.

The minimum expected temperature is also evaluated using a transient simulation based on the nominal case fuel loading with a steady-state ambient air temperature of -33 °C (-27 °F) and no solar radiation. The analytically trivial case of no decay or chemical reaction heat together with the minimum ambient conditions of -33 °C (-27 °F) and no solar radiation is also considered to ensure material compliance with worst-case minimum temperatures.

The results of the thermal evaluations of the maximum temperatures expected under normal conditions of wet transport are illustrated in Figures 4-19 through 4-22. All of the temperatures are within the allowable limits of the associated component. In addition, the surface temperature of the cask remains below 85 °C (185 °F) as required for exclusive use packages by Title 10, *Code of Federal Regulations*, Part 71, "Packaging and Transportation of Radioactive Material," Section 71.43(g).

Figures 4-19 and 4-20 illustrate the transient response of the MCO and cask over a 24-hour period for the same payload configuration but with different assumed starting temperatures for the payload, MCO, and cask. The effect of the sinusoidal diurnal cycle for ambient air temperature and insolation are apparent in the figures. The cask lid closure seal temperature

Figure 4-19. Wet Transfer Transient with Probable Maximum Multicanister Overpack.

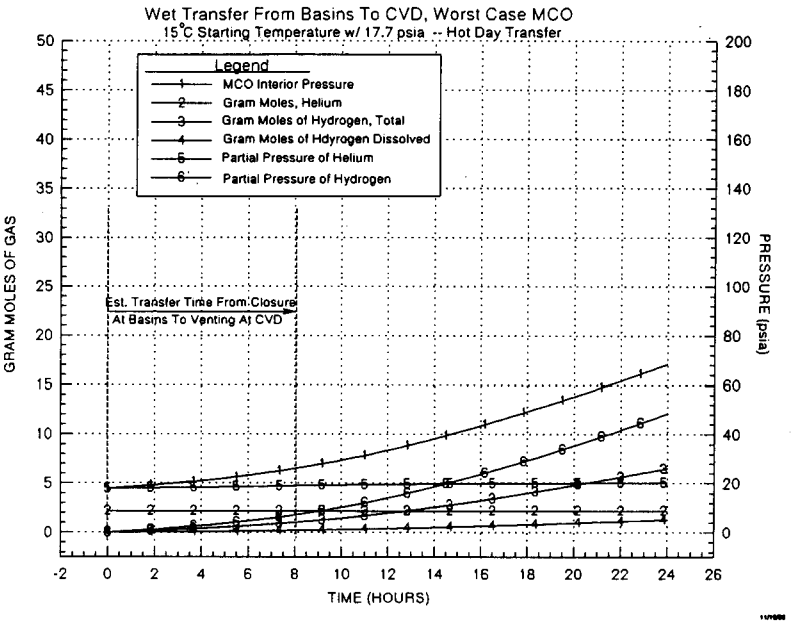

Figure 4-20. Wet Transfer Transient with Worst-Case Multicanister Overpack.

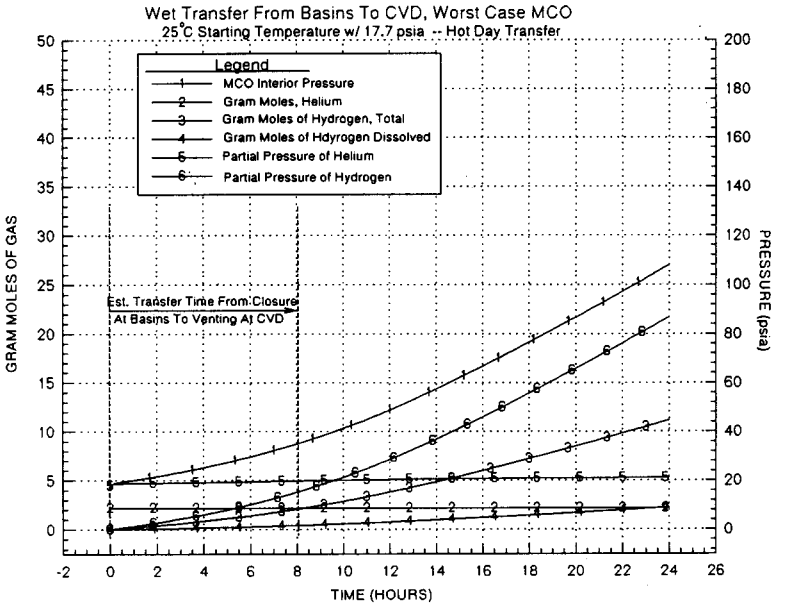

Figure 4-21. Off-Normal Wet Transfer Transient, Probable Maximum Multicanister Overpack.

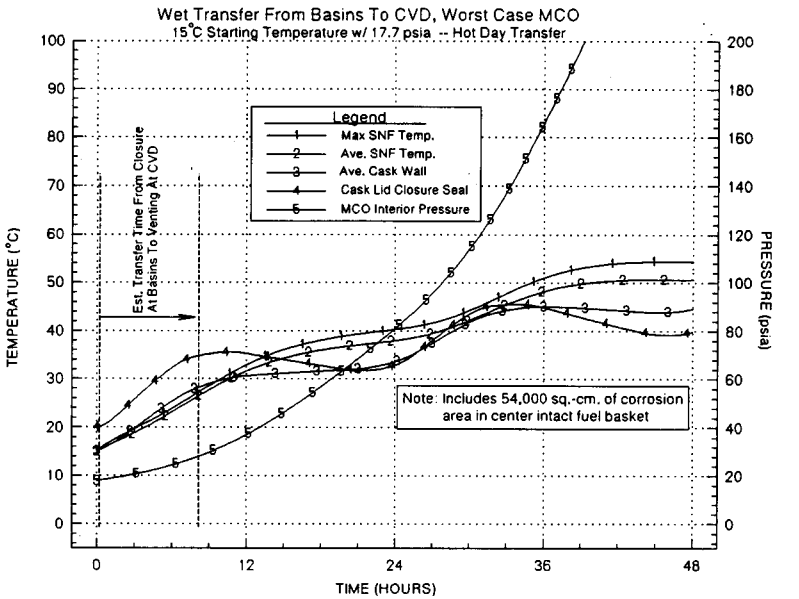

Figure 4-22. Wet Transfer Transient with Nominal Multicanister Overpack.

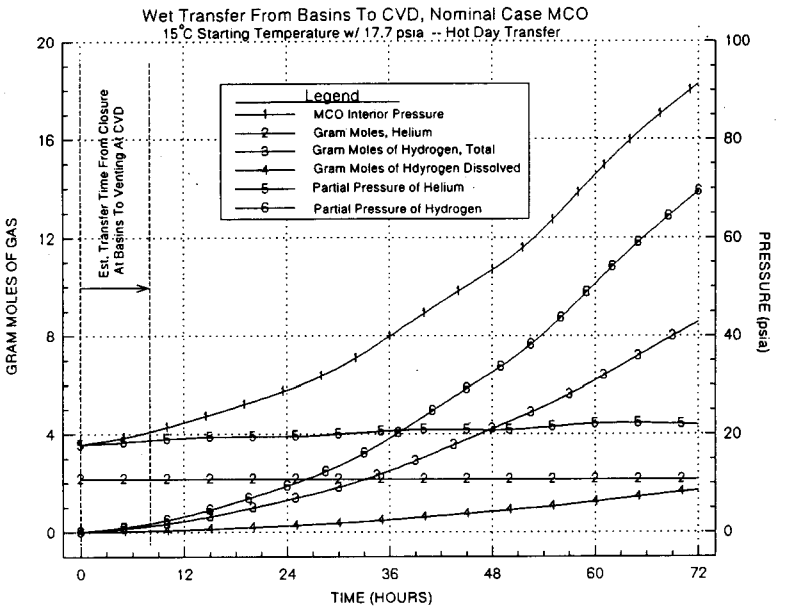

begins at 20 °C (68 °F) since the lid is assumed to be at room temperature before being placed on the cask. Starting the transport with a 25 °C (77 °F) SNF temperature results in a 21% increase in cask pressure after 8 hours and a 62% increase after 24 hours over that seen with a 15 °C (59 °F) SNF temperature. However, in both cases the expected cask pressure after 24 hours remains below the 1.0 MPa (150 lb/in^2 gauge) pressure limitation on the cask.

While the transfer from the K Basins to the CVDF will require less than 8 hours under normal conditions and less than 24 hours during most off-normal events, a major failure in the transportation system while en route could require up to 48 hours to remedy. To assess the thermal effects related to an extended transportation delay, a 48-hour transport transient is evaluated using the probable maximum case NCT load combination. For conservatism, an additional 54,000 cm^2 (8,370 in^2) of corrosion area is added to the center fuel basket. The results for this extreme load combination encompass the effect of transporting two scrap baskets and also address the sensitivity of transient results to the differences in the thermal resistance posed by intact fuel baskets versus scrap baskets.

As seen from Figure 4-21, the 48-hour transient is successfully completed without a thermal excursion in the SNF payload. However, the cask pressure is predicted to exceed its 1.0 MPa (150 lb/in^2 gauge) pressure limitation after 35 hours. Therefore, under this extreme load combination, it will be necessary to relieve the cask pressure to remain within safety limits if the time to accomplish the transfer is more than four times that expected for nominal transfer. The recovery mode available for this off-normal transport scenario during the wet transfer phase is to open the cask vent port. Circulating a source of cool or chilled water in the cask-MCO annulus to cool the MCO and reduce the chemical reaction rate is not recommended since the continued generation of hydrogen gas will pose operational and safety problems with a closed loop cooling system.

While Figures 4-19 through 4-21 address the bounding transport combinations as required for safety analysis purposes, the majority of the shipments between the K Basins and the CVDF are expected to be within the defined nominal NCT load combination. Figure 4-22 illustrates the transient thermal response expected for this load combination. As seen from the figure, no temperature excursions or excessive pressures will occur within the cask during a time frame that is nine times that nominally expected to accomplish the transfer.

Table 4-6 presents the minimum temperatures for the probable minimum NCT load combination, as defined in Table 4-4. All temperatures are within the thermal capabilities of the associated component. In addition to this analytically derived minimum condition, the worst-case minimum temperature of -33 °C (-27 °F) based on assuming steady-state conditions, no solar radiation, and no radiolytic or chemical reaction heat, is also within the thermal capabilities of all materials used in the MCO and cask. Obviously, a water-filled cask with little or no heat load cannot be left exposed to freezing temperatures without risking damage.

Table 4-6. Multicanister Overpack Cask and Multicanister Overpack Assembly Minimum Temperatures for Normal Wet and Dry Transport Conditions.

Location and condition	Probable minimum temperatures[a] °C (°F)	
	Wet transfer[b]	Dry transfer[b]
Spent nuclear fuel, maximum	12 (53)	23 (74)
Spent nuclear fuel, average	9 (49)	16 (61)
Rubble basket fuel, maximum	11 (52)	18 (65)
MCO sidewall, average	6 (43)	4 (40)
MCO sidewall, maximum	7 (44)	6 (42)
MCO shield plug, average	4 (39)	-2 (28)
MCO shield plug, seals	3 (38)	-3 (27)
Cask sidewall, average	2 (36)	-3 (26)
Cask sidewall, maximum	3 (38)	-3 (27)
Seal port, lid end	-9 (16)	-14 (6)
Seal port, bottom end	-3 (27)	-8 (17)
Closure lid seals, maximum	-3 (26)	-8 (17)

[a] Temperatures shown are for the end of the normal transport time of 8 hours for wet transfer and 14 hours for dry transfer. Assumes the nominal MCO fuel loading, a starting temperature for cask and contents of 10 °C (50 °F), and fixed -33 °C (-27 °F) ambient temperature with no solar radiation.
[b] Worst-case minimum temperatures are -33 °C (-27 °F).

The maximum internal pressures, as shown in Figures 4-19 through 4-22, are predicted to remain within the allowable limit of 1.0 MPa (150 lb/in^2 gauge) for the cask during the time frame allotted for normal transport, plus that for the typical off-normal event recovery time period. A venting of the cask interior to the atmosphere will be required for the worst-case off-normal event, but no thermal excursion will occur.

Based on the above data and with the application of administrative rules governing transport time, acceptable cask-MCO temperatures before transport, and relief of cask pressures for off-normal transport time frames, the MCO system will be safe to transport under the range of payload configurations and environmental conditions examined.

4.4.3.2 Vacuum Drying. The thermal safety aspects related to the vacuum drying process are evaluated using the simplified COBRA-TF thermal model described above. The evaluation examines the transient thermal response of the SNF fuel assemblies and scrap basket following draining of the MCO but before full dryout of the fuel and sludge. The analysis addresses the case in which the MCO is held under near vacuum conditions while the drying occurs, as well as the procedure in which the MCO is purged with helium. The following general assumptions also are made for this analysis.

- The scrap basket is assumed to have the same heat transfer characteristics as an intact fuel basket in order to conservatively cover the case of large pieces of fuel being placed upright in the scrap basket.

- The sludge is assumed to be distributed on the scrap and fuel baskets as shown in Table 4-3. The sludge is assumed to contain 10% water in hydrate form, or 14.2 kg (31.3 lb) of water for a total sludge content of 142 kg (313 lb). Free surface water is assumed to have been removed under the assumption that time to remove the hydrate water determines whether a temperature excursion will or will not occur. If an excursion occurs, then the presence of any remaining free water will serve to result in higher SNF temperatures, depending on the amount of water. If an excursion does not occur before the removal of the hydrate water, the free water will have been removed as well.

- The model assumes that the hydrates decompose and the resultant water vapor reacts with the exposed uranium surfaces to which the sludge is attached according to the rate equations given in Section 4.2.1.2 for oxygen-free uranium-water reactions.

- Lower bounding values for the emissivity of the fuel (0.4) and the stainless steel surfaces of the MCO (0.2) are assumed for the case in which the MCO is filled with helium. An emissivity of 0.7 for the fuel and 0.3 for the stainless steel surfaces are assumed for vacuum conditions.

Figures 4-23 through 4-26 illustrate the predicted thermal response for the worst-case and nominal MCO load configurations under vacuum and helium backfill conditions. The results presented in Figure 4-23 indicate that a temperature excursion could occur in the fuel for vacuum conditions and the worst-case MCO loading after approximately 10 hours of vacuum drying. If significant amounts of water are still present at this stage of the drying process, exceeding design limits is possible and would be addressed by the safety features incorporated with the CVDF equipment.

The calculation of the vacuum drying process with the nominal MCO load configuration is presented in Figure 4-24. The results indicate that no thermal excursions will occur over the 30 hours of operation simulated. Further, the temperature trends indicate that safe and stable conditions are being established within the MCO. Similar results are seen in Figures 4-25 and 4-26 for the worst-case and nominal MCO load configurations with a helium backfill.

Safety features available to control fuel temperatures during the cold vacuum drying process include reducing the MCO wall temperature using the active heating and cooling system, purging the MCO cavity with helium, and monitoring pressure rise and species content to assess the level of chemical reactions within the MCO. Additional evaluations are underway to establish the process parameters that will ensure that temperature excursions will not occur for the range of payload configurations and environmental conditions expected for the MCO.

Figure 4-23. Worst-Case Multicanister Overpack Heatup for Cold Vacuum Drying, Multicanister Overpack under Vacuum, 50 °C at Multicanister Overpack Wall.

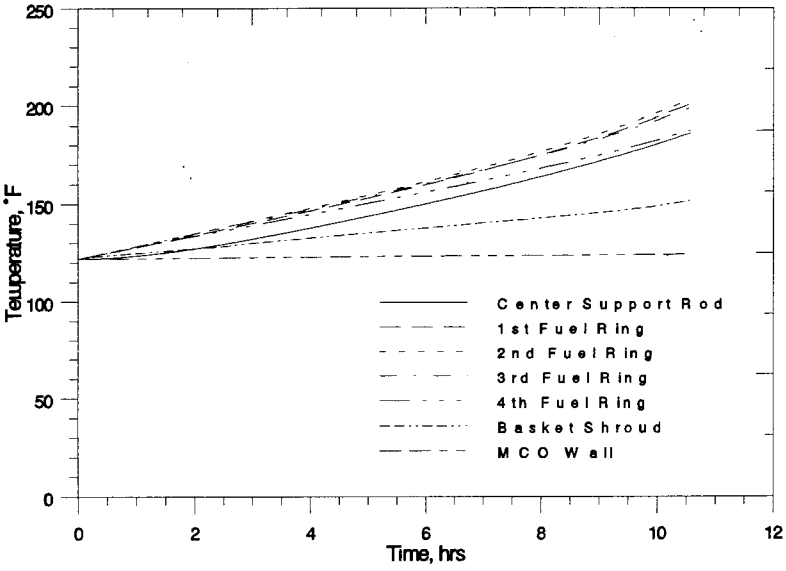

Figure 4-24. Nominal Case Multicanister Overpack Heatup for Cold Vacuum Drying, Multicanister Overpack under Vacuum, 50 °C at Multicanister Overpack Wall.

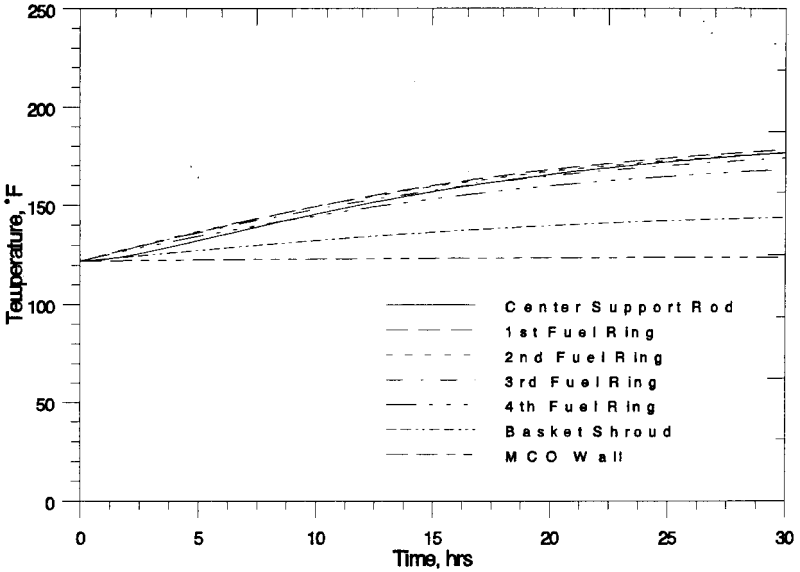

Figure 4-25. Worst-Case Multicanister Overpack Heatup for Cold Vacuum Drying, Multicanister Overpack with Helium Backfill, 50 °C at Multicanister Overpack Wall.

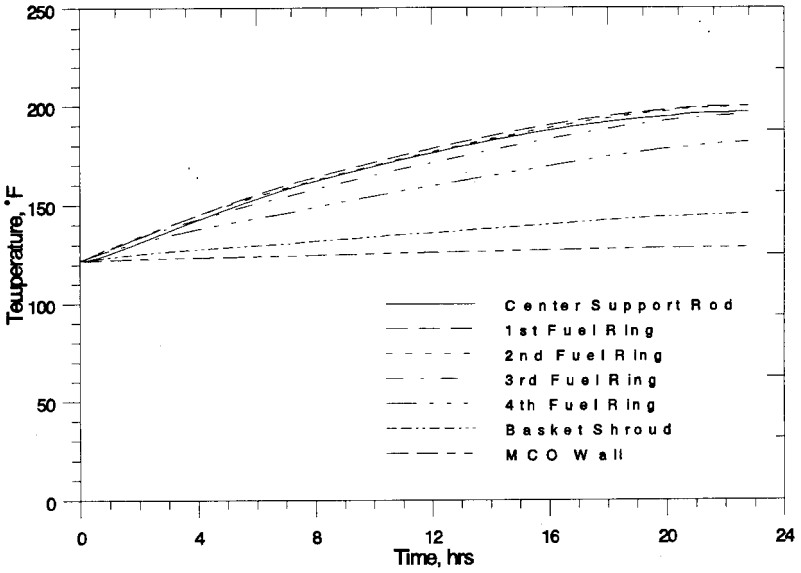

Figure 4-26. Nominal Multicanister Overpack Heatup for Cold Vacuum Drying, Multicanister Overpack with Helium Backfill, 50 °C at Multicanister Overpack Wall.

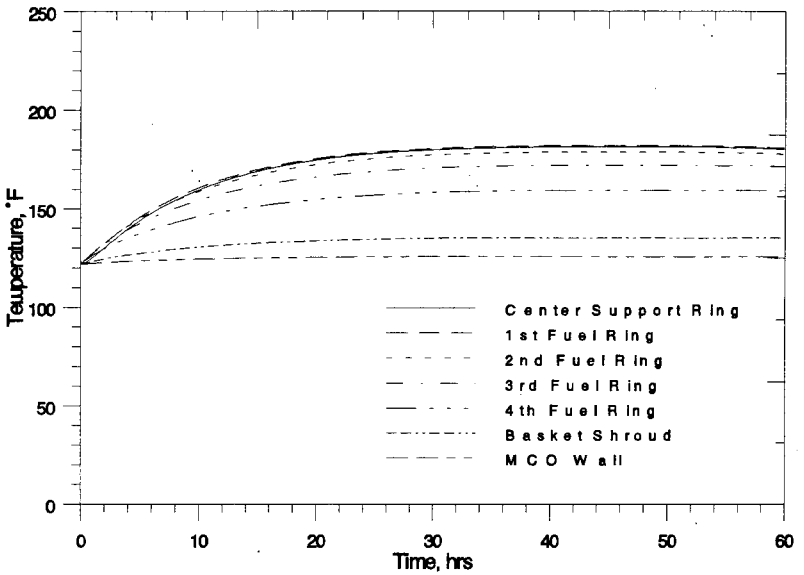

Based on the above data, the safety basis for the nominal MCO configuration is demonstrated. Further analysis is underway to establish the safety basis for cold vacuum drying under all conditions.

4.4.3.3 Dry Transfer of Multicanister Overpack. The dry transfer of the MCO and transportation cask between the CVDF and the CSB is evaluated using the SINDA/FLUINT thermal model and a transient simulation of the transfer process. As with the wet transfer process, the thermal evaluation is based on the assumptions listed in Tables 4-1, 4-2, 4-3, and 4-4. The nominal, probable maximum, and worst-case NCT loadings for hot ambient conditions are evaluated using a transient simulation of the transport process with a diurnal cycle for ambient temperature and insolation based on the Hanford peak summer day. To ensure that the cask is exposed to the highest heat flux portion of the diurnal cycle during the projected transportation time frame, an 8:00 a.m. start time is again assumed.

The minimum expected temperature is evaluated using a transient analysis, the nominal case fuel loading, a steady-state ambient temperature of -33 °C (-27 °F) and no solar radiation, and a nominal transport time of 14 hours. The analytically trivial case of no decay or chemical reaction heat together with the minimum ambient conditions of -33 °C (-27 °F) and no solar radiation also is considered to ensure material compliance with worst-case minimum temperatures.

The results of the thermal evaluations for normal conditions of dry transport are presented in Figures 4-27 through 4-30. All of the temperatures are within the allowable limits of the associated component. In addition, the surface temperature of the cask remains below 85 °C (185 °F) as required by 10 CFR 71, Section 71.43(g), "General Standards for all Packages," for exclusive use packages.

Figures 4-27 and 4-28 illustrate the transient results over a 24-hour period for the same payload configuration but with different assumed starting temperatures for the payload, MCO, and cask. Although the MCO is nominally dry following cold vacuum drying, the chemical reaction rates are computed assuming a 100% relative humidity within the MCO. The sinusoidal effect of the diurnal cycle for the ambient air temperature and insolation can be seen in the results for the cask wall and closure lid seal.

Over the 24-hour period simulated by these analyses, the difference in MCO pressurization between starting the transport with a 25 °C (77 °F) SNF temperature versus a 15 °C (59 °F) SNF temperature is not as great as is seen for the wet transfer leg. This is because a drained MCO presents a larger volume in which to absorb the hydrogen gas that is generated, even at the higher SNF temperatures that occur in dry transfer. As a result, the difference in MCO pressure is only 83 kPa (12 lb/in^2) greater after 24 hours for the higher SNF starting temperature. In either case, the expected MCO and cask pressures after 24 hours remain well below the 1.0 MPa (150 lb/in^2 gauge) pressure limitation.

Figure 4-27. Dry Transfer Transient with Probable Maximum Multicanister Overpack.

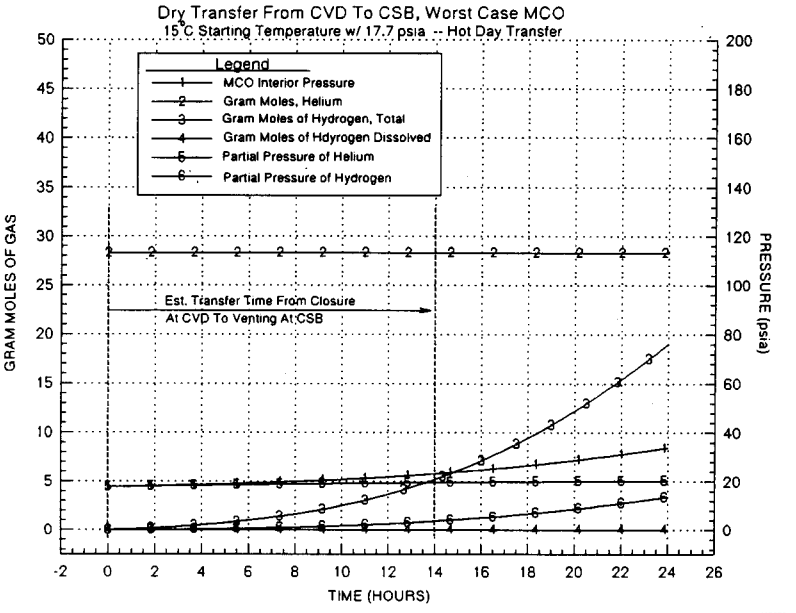

Figure 4-28. Dry Transfer Transient with Worst-Case Multicanister Overpack.

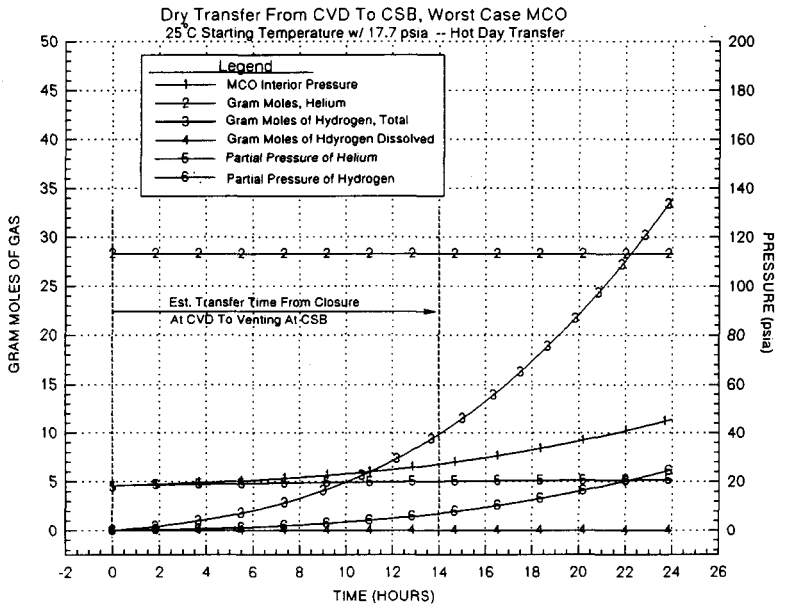

Figure 4-29. Off-Normal Dry Transfer Transient with Probable Maximum Multicanister Overpack.

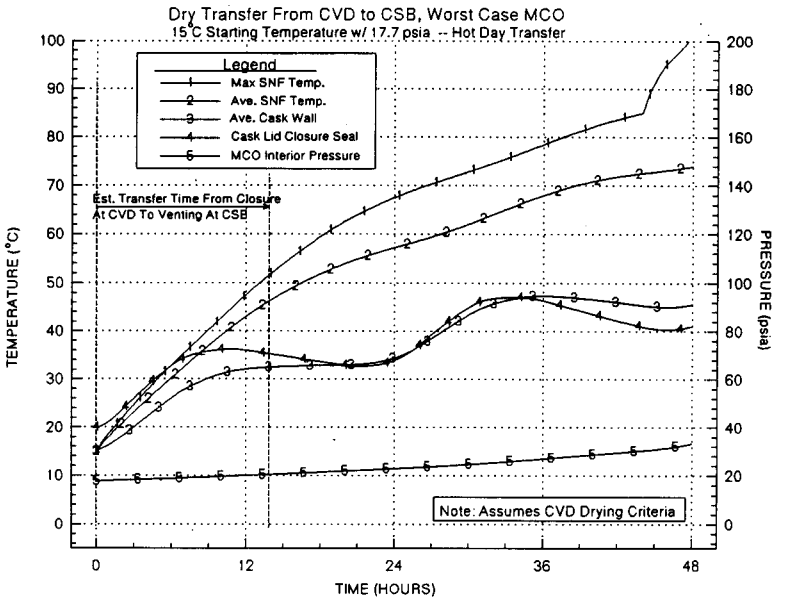

Figure 4-30. Dry Transfer Transient with Nominal Multicanister Overpack.

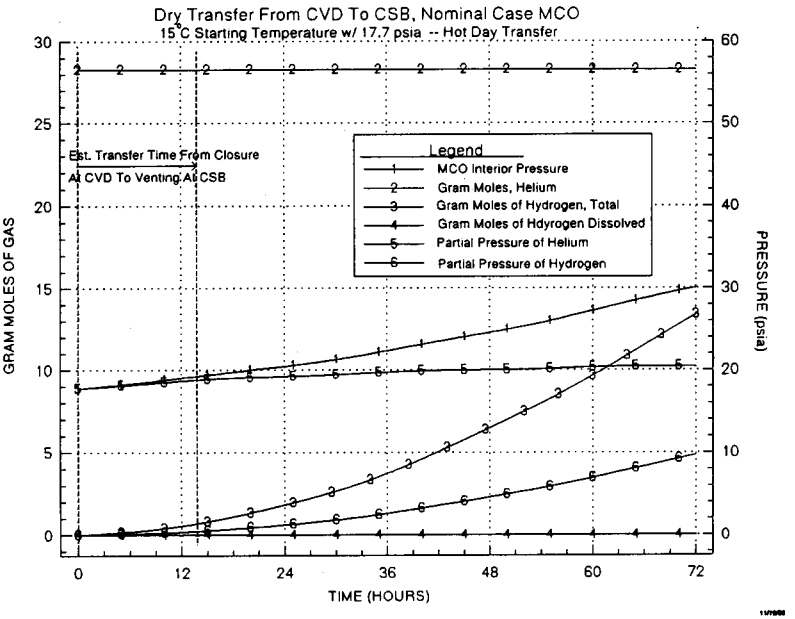

While the transfer from CVDF to CSB is expected to require less than 14 hours under normal conditions and less than 24 hours under most off-normal events, a major failure in the transportation system while en route could require up to 48 hours to remedy. To assess the thermal effects related to an extended transport delay, a 48 hour transport transient is evaluated using the probable maximum case NCT load combination. The results are presented in Figure 4-29 for two assumptions on the amount of moisture available to drive the chemical reaction. The first assumption is that an unlimited amount of moisture is available within the MCO following cold vacuum drying and this moisture is available at a partial pressure associated with the average fuel temperature. Under this assumption, illustrated in the lower plot, the transient analysis indicates a temperature excursion within the fuel will occur after approximately 35 hours.

The second assumption, illustrated in the upper plot, is that the cold vacuum drying process has removed sufficient moisture from the fuel, scrap, and sludge content within the MCO such that the chemical reaction rate is only 5% of that which an unlimited amount of moisture would support. This assumption is maintained until any portion of the fuel exceeds 85 °C (185 °F), at which time the reaction rate is returned to its full value as predicted by the chemical reaction rate equations for the given temperature and partial pressure conditions. Based on the amount of corrosion area assumed for this analysis and a 75 °C (167 °F) average fuel temperature, the assumed 5% limitation equals a monitored pressure rise limitation of 1.4 kPa (0.2 lb/in^2) per hour or less at the CVDF. Under this criterion, those MCOs exhibiting pressure rises in excess of this rate would be required to remain under the cold vacuum drying process before being allowed to be transported.

The transient results, assuming the CVDF drying criterion is applied, demonstrates that a safe transport window of more than 48 hours exists for dry transfer of the worst-case MCO loading. Although the peak SNF temperature takes a sudden rise once it exceeds the 85 °C (185 °F) setpoint for the criterion, the transition is not expected to be a step function because the next higher release point for the hydrates is 100 °C (212 °F) or higher.

While Figures 4-27 to 4-29 address the bounding conditions assumed, the majority of the shipments are expected to fit within the nominal NCT load combination. Figure 4-30 illustrates the transient thermal response expected for this load combination with a 3-day transport time frame. The results demonstrate that, despite the extended transport time assumed and the assumption of unlimited water availability, no temperature excursions or excessive pressures will occur within the MCO or cask.

Table 4-6 presents the minimum temperatures for the probable minimum NCT load combination, as defined in Table 4-4. All temperatures are within the thermal capabilities of the associated component. In addition, the worst-case minimum temperature of -33 °C (-27 °F), which is reached assuming steady-state conditions, no solar radiation, and no radiolytic or chemical reaction heat, also is within the thermal capabilities of all materials used in the MCO and cask.

The maximum internal pressures expected for the normal NCT dry transfer process, shown in Figures 4-27 through 4-30, remain well within the pressure limitations of the both the MCO and the cask.

Based on the above data and with the application of administrative rules governing transport time, acceptable cask-MCO temperatures before transport, and the application of a drying criterion for the cold vacuum drying process, the MCO system will be safe to transport under all payload configurations and environmental conditions examined.

4.4.3.4 Fuel Staging. The thermal safety aspects related to the staging of the MCOs at the CSB before hot conditioning is evaluated using the simplified COBRA-TF thermal model. The evaluation examines the transient thermal response of the SNF fuel assemblies and scrap basket following placement in the storage tube at the CSB. The analysis assumes the worst-case summer day temperatures and a storage vault that is full. The following general assumptions also are made for this analysis.

- The scrap basket is assumed to have the same heat transfer characteristics as an intact fuel basket in order to conservatively cover the case of large pieces of fuel being placed upright in the scrap basket.

- The quantity of sludge in the scrap and fuel baskets is shown in Table 4-3. The bounding case assumes a 10% water in hydrate form, or 14.2 kg (31.3 lb) of water given the assumed total sludge content of 142 kg (313 lb). The nominal case assumes a 4.3% water in hydrate form, or 0.29 kg (0.64 lb) of water given a total sludge content of 6.7 kg (14.8 lb).

- The model assumes that the hydrates decompose and the resultant water vapor reacts with the exposed uranium surfaces to which the sludge is attach according to the rate equations given in Section 4.2.1.2 for oxygen-free uranium-water reactions.

- Lower bounding values for the emissivity of the fuel (0.4) and the stainless steel surfaces of the MCO (0.2) are assumed. These values play a secondary role for the case in which the MCO is filled with helium.

Figures 4-31 and 4-32 illustrate the predicted thermal response for an MCO with the bounding and nominal, respectively, amount of hydrate water in the sludge. The results indicate that a temperature excursion will occur in either case; however, the amount of water available limits the peak fuel temperature to values that are within design limits. This conclusion is tentative for the bounding water content case since the hydrate decomposition model used does not allow for water migration from the fuel element bearing the sludge to occur. If a hot element can scavenge water vapor from the other fuel baskets, it is possible that the peak fuel temperatures will be higher than those predicted. This potential increase in temperature, expected to be slight, is currently being evaluated.

As seen from Figure 4-33, there is enough water in the bounding sludge case to cause the MCO to overpressurize during staging. This possibility is addressed by the use of a pressure relief valve. Based on a 0.64-cm (0.25-in.) throat area and worst-case gas generation rates, the valve would need to open once per minute for one second to relieve the pressure buildup. The nominal sludge case (Figure 4-34) does not contain sufficient water to cause the MCO to overpressurize.

Figure 4-31. Temperature Response for Staging at the Canister Storage Building, Nominal Case Multicanister Overpack, Bounding Sludge.

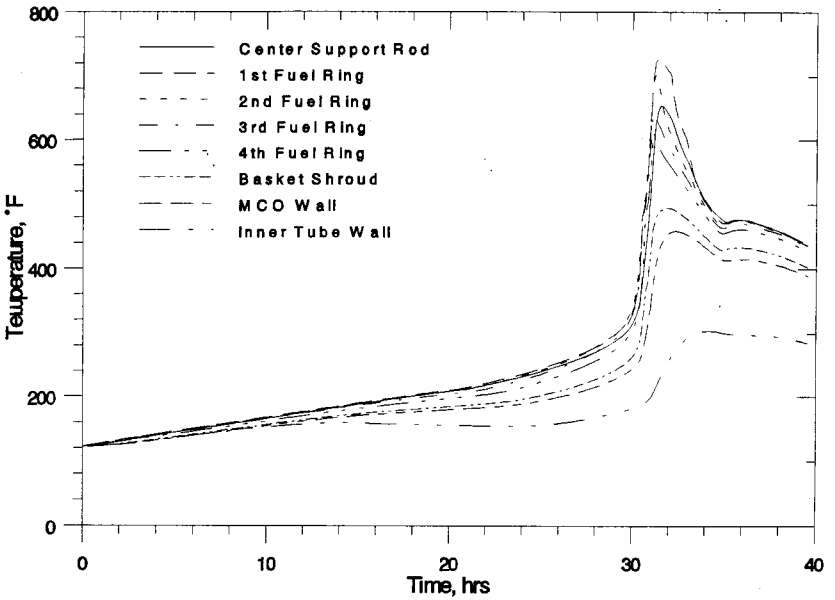

Figure 4-32. Temperature Response for Staging at the Canister Storage Building, Nominal Multicanister Overpack and Sludge.

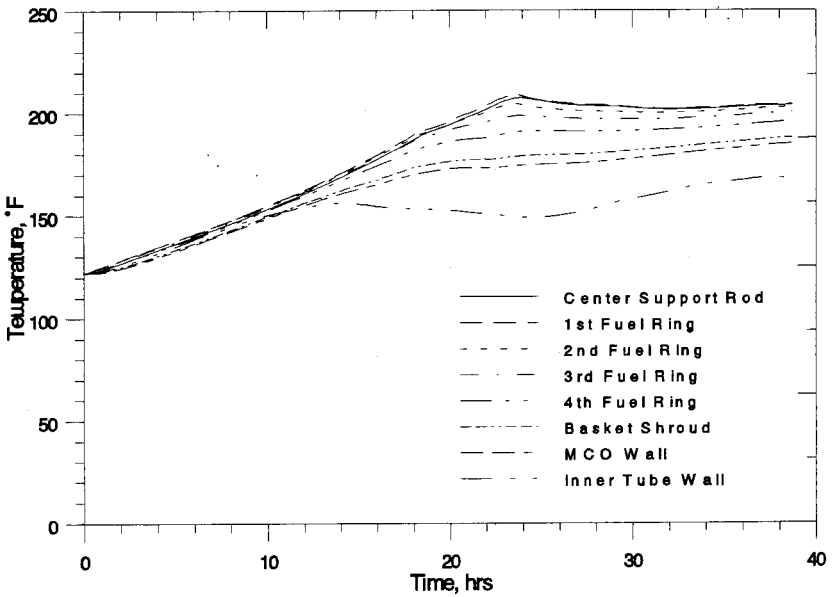

Figure 4-33. Pressure Response for Staging at the Canister Storage Building, Nominal Multicanister Overpack, Bounding Sludge.

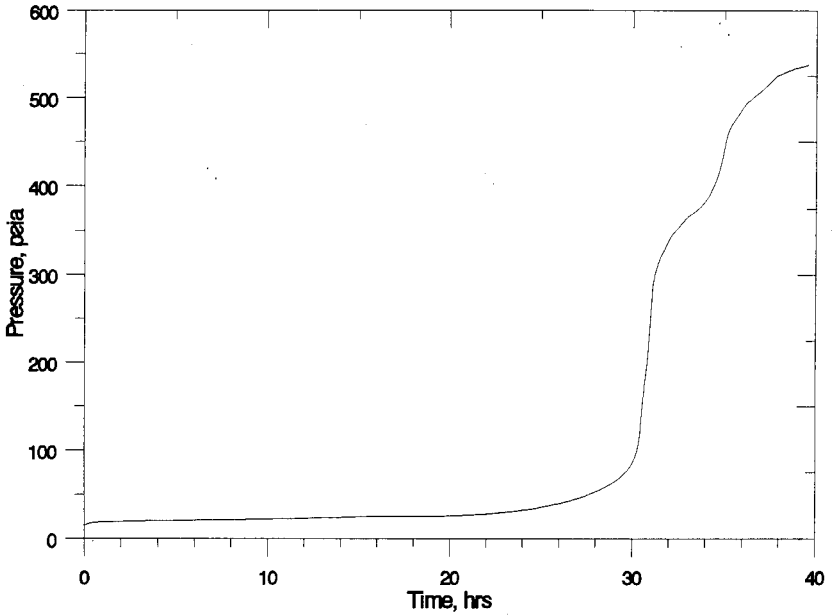

Figure 4-34. Pressure Response for Staging at the Canister Storage Building, Nominal Multicanister Overpack and Sludge.

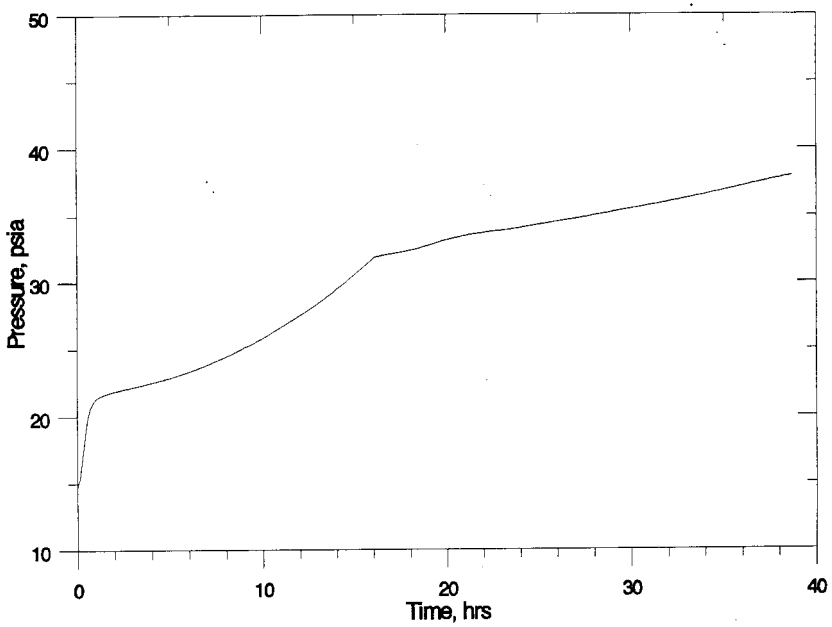

The worst-case MCO load configuration, as defined in Table 4-3, was not evaluated. However, its results are expected to be comparable to the bounding sludge case presented in Figure 4-31 because the water content will limit the fuel temperature rise. The primary difference will be in the shorter time required to consume the available water.

Based on the above data, the safety basis for the MCO under staging conditions and the nominal MCO loading configuration have been established. Further efforts underway to refine the estimate of the hydrates remaining in the MCO after cold vacuum drying are expected to establish a basis significantly less than the 10% maximum currently assumed. The lower hydrate content and a revised hydrate decomposition model are then expected to demonstrate the safety basis for fuel staging for the full range of conditions examined.

4.4.3.5 Hot Conditioning. A series of analyses (Heard et al. 1996b) have been completed investigating the thermal-hydraulic performance and feasibility of the HCS process. A series of one-, two-, and three-dimensional models, as discussed in Section 4.4.1, were used to perform the analyses. This analyses included chemical reactions, internal flow distributions, combined thermal-hydraulic effects, and mass transport. The subject analyses focused on quantifying the internal flow distributions within the MCO, establishing the governing energy production and removal capabilities during the HCS process steps, and performing process simulations for the various purge gases under consideration. The HCS process is discussed in the following paragraph.

After short-term staging within the CSB, the MCO, containing up to 288 fuel assemblies, is transferred by the MHM to the HCS Annex where the MCO is connected to the HCS. Hot conditioning consists of heating the MCO and fuel to approximately 300 °C (approximately 575 °F), which will remove the chemically bound water and decompose a portion of the uranium hydride producing uranium metal and hydrogen. The hydrogen is assumed to be released from the fuel and removed from the system or allowed to chemically react within the MCO with residual amounts of oxygen to produce water vapor, which would react with the uranium metal producing uranium oxide and more hydrogen gas until either the uranium hydride, the residual water vapor, or oxygen is depleted. A passivation step is then planned in order to reduce the overall chemical reactivity of the small particles of uranium metal created by the decomposition of uranium hydride. The passivation step consists of cooling the MCO to approximately 150 °C (300 °F) and adding a controlled amount of oxygen to the MCO to oxidize a large fraction of the remaining highly reactive exposed uranium metal particles or surfaces.

Recent analyses (Heard et al. 1996b) that simulated the HCS process indicate that a helium purge with 2% oxygen could, under certain conditions, lead to temperature excursions because the rate at which the damaged fuel will react with the oxygen strongly depends on the fuel temperature. Additional analysis and design iteration are underway to determine process parameters under which the passivation step can be performed that would ensure that the temperature excursions would not occur or, as an alternative, to determine whether the passivation process can be eliminated altogether without creating a long-term safety hazard should an inadvertent and sudden ingress of oxygen occur. Thus, further analysis is required to verify the safety basis for the

full hot conditioning process. However, the process parameters will be required to stay within the boundaries established in the MCO safety analysis.

4.4.3.6 Interim Storage. At the point at which the MCO is placed into interim storage, the loosely bound water will have been removed. Therefore, no rapid chemical reactions will occur. While long-term reactions with the tightly bound hydrated or chemisorbed water that is released by radiolysis will occur, the rate will be slow enough to maintain equilibrium temperatures. Therefore, the maximum temperatures during interim storage are encompassed by those for staging after the water has been consumed. See Figure 4-31. Overpressurization will not occur if the water content following hot conditioning is 2.5 kg (5.5 lb) or less.

Current evaluation of the hydrate decomposition under the CVDF and HCS processes, together with further characterization of the K Basin fuel and sludge, are expected to provide the safety basis for the maximum water content under interim storage. As an alternative, the MCO closure cap will be filled with a rupture disk to preclude overpressurization.

4.4.4 Minimum Temperatures

The minimum temperature for an MCO during any of the SNF Project process steps can be no less than the minimum ambient temperature of -33°C (-27°F) (Fadeff 1992). This minimum is based on steady-state operations and no decay or chemical corrosion heat. Such conditions will exist only for empty MCOs before their use. The operational minimum temperature will occur during transportation between facilities. Table 4-6 presents the minimum expected temperatures for the probable minimum NCT load combination, as defined in Table 4-4. In either case, the temperatures are within the thermal capabilities of the associated component.

4.4.5 Maximum Internal Pressures

The maximum pressurization during the wet and dry transportation are presented in Sections 4.4.3.1 and 4.4.3.3. The results demonstrate that the MCO pressure will remain within the 1.1 MPa (165 lb/in^2 absolute) pressure limitation for all normal conditions of transport.

Section 4.4.3.4 indicates that overpressurization (internal pressure > 1.1 MPa (165 lb/in^2 absolute) can occur within 30 hours of being placed in staging at the CSB if sufficient water and/or damaged fuel exists within the MCO. The analysis shows that the planned placement of a relief valve on the MCO pressure boundary will control the internal pressure to less than or equal to 1.0 MPa (150 lb/in^2 absolute) during staging.

The MCO will not overpressurize following hot conditioning if there is less than 2.5 kg (5.5 lb_m) of water remaining in the MCO. Verification of this level of water retention is currently underway through analysis and physical characterization.

This page intentionally left blank.

5.0 SHIELDING EVALUATION

5.1 SHIELDING DESIGN DESCRIPTION

The MCO is designed to ensure a high degree of integrity for the confinement of radioactive materials, not necessarily to provide a high level of shielding. However, various shields surround the MCO from its initial loading stage, through various mechanical processes, to its eventual residence in a long-term storage building. Process-dependent shielding is provided by water in the load-out pit; by the cask during transportation and drying; by tubes, tube plugs, operating deck, and handling equipment in the CSB during staging and storage; and by conditioning cell assemblies during the hot conditioning process. Therefore, dose rates immediately above the top plug of an MCO, where process operations occur beyond the protection of any extra facility shielding materials, are considered the most relevant for this topical report.

5.2 RADIATION SOURCE DEFINITION

The source term used for these evaluations represents a worst-case source loading for shielding analysis. Nominal shipments are bounded by this evaluation. The source consists of 6.34 MTU of Mark IV fuel irradiated to 16% ^{240}Pu as given in Section 2.2.6.2. A detailed discussion of the process used to obtain worst-case photon source terms and worst-case neutron source terms for Mark IA and Mark IV fuel is given in WHC-SD-SNF-TI-009 (Willis 1995). The direct contribution of the beta source to the dose outside the cask will be prevented because of the attenuation provided by the self-shielding of the fuel elements, as well as by the steel shielding of the cask, cask lid, and MCO plug. Bremsstrahlung photons within the source region are included in the calculation of the photon source.

5.2.1 Gamma Source

The photon source spectra were calculated using ORIGEN2 (Wittekind 1994b) and the shielding source term given in Willis (1995). Table 5-1 lists the photon source per MCO. The total photon strength is 6.45×10^{15} photons/s/MCO.

For dose rates above the cask, only the top 10 cm (4 in.) of the top tier were included as source for calculational efficiency. A comparison of dose rates at the bottom of the MCO plug indicates that the top 10 cm (4 in.) of source contribute about 96% of the total photon dose. All results using only the top 10 cm (4 in.) of source will be scaled by this factor (multiplication by 1.04).

Table 5-1. Photon Source Term for the Multicanister Overpack.

Energy (MeV)	Mark IV fuel 16.0 % ^{240}Pu (photons/s/MCO)
1.50 E-02	1.75 E+15
2.50 E-02	3.87 E+14
3.75 E-02	4.20 E+14
5.75 E-02	3.46 E+14
8.50 E-02	1.95 E+14
1.25 E-01	1.47 E+14
2.25 E-01	1.66 E+14
3.75 E-01	8.64 E+13
6.62 E-01*	2.81 E+15
8.50 E-01	1.04 E+14
1.25 E+00	4.33 E+13
1.75 E+00	1.29 E+12
2.25 E+00	9.42 E+10
2.75 E+00	4.67 E+09
3.50 E+00	6.04 E+08
5.00 E+00	3.71 E+05
7.00 E+00	4.23 E+04
1.10 E+01	4.84 E+03
Total	6.45 E+15

*Changed from 0.575 MeV to 0.662 Mev to accurately reflect Ba^{137m} gamma ray.

MCO = multicanister overpack.

5.2.2 Neutron Source

The neutron source term was calculated using ORIGEN2 (Wittekind 1994b) and the shielding source term given in the Shielding Design Bases provided in WHC-SD-SNF-TI-009 (Willis 1995). The source includes both spontaneous fission and (α,n) reactions as summarized in Table 5-2. The (α,n) contribution was calculated assuming an oxide fuel. Since N Reactor fuel is not an oxide fuel (Willis 1995), the (α,n) contribution conservatively bounds oxidation of any trace elements or impurities. With 6.34 MTU per MCO this results in a total neutron source strength of 1.090×10^7 neutrons/s/MCO.

Table 5-2. Neutron Source Term for the Multicanister Overpack.

Source component source	Source strength (neutrons/s/MCO)
(α,n)	3.578 E+06
Spontaneous fission	7.317 E+06
Total	1.090 E+07

MCO = multicanister overpack.

There is only a small difference between the energy shape of the spontaneous fission spectra of the different isotopes. The watt spectrum used is

$$f(E) = C \exp(-E/.906) \sinh([3.848E]^{0.5})$$

where E is the neutron energy in MeV, and C is a normalization constant so that the integral over f(E) is unity. The fission spectrum for ^{244}Cm, which has an average neutron energy of 2.15 MeV (Breismeister 1993), is given in Table 5-3. The energy distribution of the (α,n) neutrons is given in Table 5-4; the average neutron energy of this distribution is 2.01 MeV (Jobs and Liskien 1990).

5.3 SHIELDING MODEL SPECIFICATION

5.3.1 Configuration of the Shielding and Source

Although this discussion addresses only the immediate vicinity on top of the shield plug, the cask and cask lid are included in the model. This is to prevent a potential overestimation of dose rates, especially at large distances away from the top surface where particle scattering from the surrounding air could reach to the dose point if the cask were not included.

Table 5-3. Energy Distribution of Neutrons from Fission Events. (2 sheets)

Upper energy (MeV)	Cumulative probability	Probability of bin
0.00	0.00000	0.00000
0.10	0.01194	0.01194
0.20	0.03167	0.01972
0.30	0.05590	0.02424
0.40	0.08316	0.02726
0.50	0.11250	0.02934
0.60	0.14326	0.03076
0.70	0.17493	0.03167
0.80	0.20711	0.03218
0.90	0.23950	0.03238
1.00	0.27182	0.03232
1.20	0.33550	0.06368
1.40	0.39690	0.06140
1.60	0.45523	0.05832
1.80	0.50997	0.05475
2.00	0.56087	0.05090
2.20	0.60782	0.04695
2.40	0.65083	0.04301
2.60	0.69001	0.03917
2.80	0.72550	0.03549
3.00	0.75752	0.03202
3.20	0.78628	0.02876
3.40	0.81202	0.02574
3.60	0.83499	0.02297
3.80	0.85542	0.02043
4.00	0.87353	0.01812
4.20	0.88956	0.01603
4.40	0.90371	0.01415
4.60	0.91616	0.01246

Table 5-3. Energy Distribution of Neutrons from Fission Events. (2 sheets)

Upper energy (MeV)	Cumulative probability	Probability of bin
4.80	0.92711	0.01095
5.00	0.93671	0.00960
5.50	0.95578	0.01907
6.00	0.96931	0.01354
6.50	0.97884	0.00953
7.00	0.98550	0.00665
7.50	0.99011	0.00461
8.00	0.99329	0.00318
9.00	0.99695	0.00366
10.00	0.99863	0.00169
11.00	0.99940	0.00076
12.00	0.99974	0.00034
13.00	0.99989	0.00015
14.00	0.99995	0.00007
15.00	0.99998	0.00003

Table 5-4. Energy Distribution of Neutrons from (α,n) Events. (2 sheets)

Upper energy (MeV)	Cumulative probability	Probability of bin
0.00	0.00000	0.00000
0.10	0.01059	0.01059
0.20	0.02243	0.01184
0.30	0.03396	0.01153
0.40	0.04766	0.01371
0.50	0.06636	0.01869
0.60	0.08738	0.02103
0.70	0.11044	0.02305
0.80	0.13567	0.02523
0.90	0.15981	0.02414
1.00	0.17975	0.01994
1.10	0.20062	0.02087
1.20	0.22321	0.02259
1.30	0.24860	0.02539
1.40	0.27601	0.02741
1.50	0.30405	0.02804
1.60	0.33349	0.02944
1.70	0.36542	0.03193
1.80	0.40093	0.03551
1.90	0.43785	0.03692
2.00	0.47664	0.03879
2.10	0.51558	0.03894
2.20	0.55623	0.04065
2.30	0.59751	0.04128
2.40	0.63707	0.03956
2.50	0.67492	0.03785
2.60	0.71137	0.03645
2.70	0.74611	0.03474
2.80	0.77819	0.03209

Table 5-4. Energy Distribution of Neutrons from (α,n) Events. (2 sheets)

Upper energy (MeV)	Cumulative probability	Probability of bin
2.90	0.80935	0.03115
3.00	0.83863	0.02928
3.10	0.86449	0.02586
3.20	0.88879	0.02430
3.30	0.90966	0.02087
3.40	0.92664	0.01698
3.50	0.94097	0.01433
3.60	0.95327	0.01231
3.70	0.96324	0.00997
3.80	0.97181	0.00857
3.90	0.97928	0.00748
4.00	0.98536	0.00607
4.10	0.99081	0.00545
4.20	0.99439	0.00358
4.30	0.99720	0.00280
4.40	0.99891	0.00171
4.50	1.00000	0.00109

The MCO characteristics have been described in detail in Section 1.2.1 of this report. The shielding model is specified as follows.

- The cask, cask lid, and MCO are made from stainless steel.
- The MCO shield plug is made from carbon steel. However, the model treated the shield plug as stainless steel. The two are roughly equivalent for shielding purposes.
- The inside diameter of the MCO is 58.42 cm (23 in.), and the inside height is 376 cm (148 in.) to the bottom of the MCO plug.
- The MCO plug is 30.48 cm (12 in.) thick, and the cask lid is 7.62 cm (3 in.) thick, for a total top shield axial thickness of 38.1 cm (15 in.).
- The MCO sidewall is 1.27 cm (0.5 in.) thick, and the cask sidewall is 19.5 cm (7.69 in.), for a total thickness of 20.8 cm (8.19 in.). (Actual cask sidewall thickness has been changed to 7.31 in. Any decrease in shielding was compensated for by operational improvements to reduce annual dose.)
- The bottom of the MCO is 4.47 cm (1.76 in.) thick, and the bottom of the cask is 13.7 cm (5.38 in.) thick, for a total bottom shield thickness of 21.3 cm (8.38 in.).

There are two types of lids on top of an MCO shield plug. The first is the drying lid, which is a component with a hole in the center. This lid is used to retain the MCO in a cask during the cold vacuum drying process and to allow water to be circulated in the cask-MCO annulus. The hole in the lid is used to gain access to the MCO processing ports. See Figure 5-1 (note that this figure shows the axial stabilizer for the basket; the guard plate is not shown). The second type of lid is the solid lid (no large holes in the center) used during transfer operations. Only the drying lid is discussed here.

The design of the shield plug vent port penetrations has not reached a conclusion yet. The extent of drilling, the direction of junctions, and the actual plug thickness have not been finalized. The current calculational model has been made according to the assembly sections drawing (Figure 5-1) from one of the MCO vendors. Although the design is not yet final, it is suitable for calculational use at this time. A cylindrical cavity at the center near the top surface of the plug is a grapple. The extensions of the HEPA filter vent, the pressure relief rupture disk, and the long drain port intersect at about 25 cm (10 in.) below the surface of the plug at the center and slant to the edge of the MCO. The short drain port near the side is connected to a multibend duct that slants to the center at the bottom of the plug. A SABRINA three-dimensional plot of the MCNP model for the penetrations is shown in Figure 5-2.

Figure 5-1. Preliminary Assembly Sections Drawing of the Shield Plug Port Penetrations.

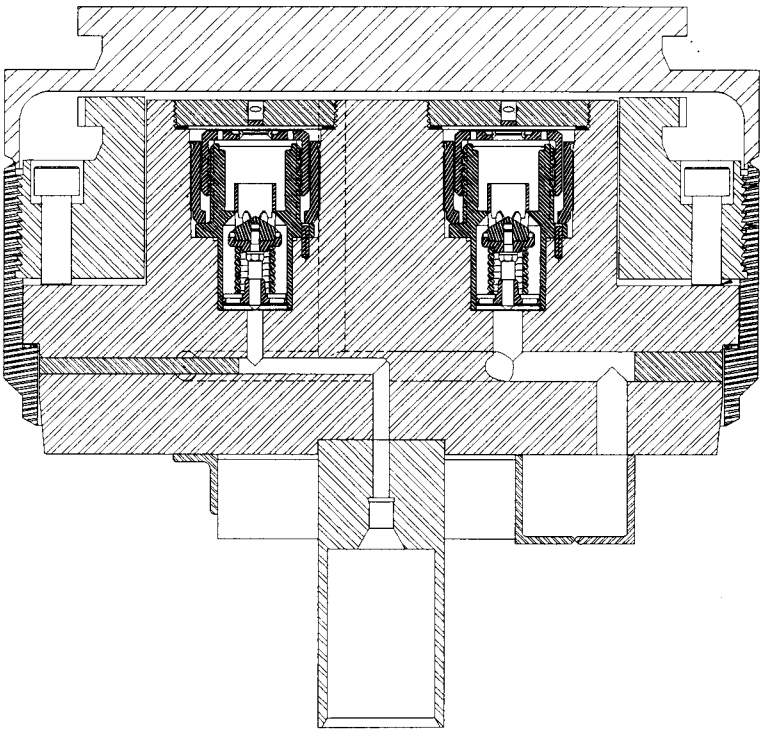

Figure 5-2. Three-Dimensional Plot of the Penetrations Through the Shield.

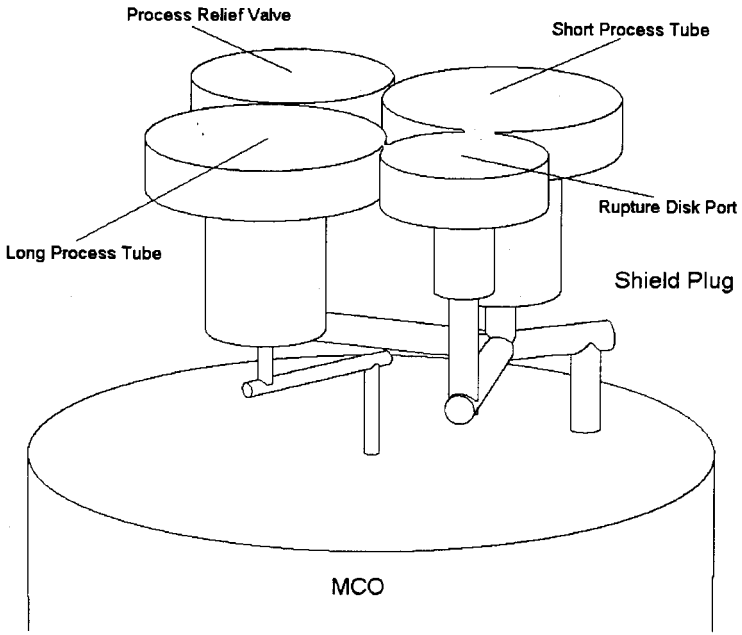

The source geometry consists of five baskets placed one on top of the other inside the MCO. The baskets were modeled as 70.5 cm (27.8 in.) tall, with each basket containing 54 Mark IV series E fuel assemblies. The total length of each assembly is 66.3 cm (26.1 in.) including end caps (Willis 1995). Rather than modeling the end caps, the source was extended to include the full 66.3-cm (26.1-in.) length, thus introducing a small additional amount of conservatism.

5.3.2 Material Properties

Shielding consists of the transport cask, cask lid, MCO, and MCO plug. The transport cask and lid are made from 304 stainless steel. The MCO plug is made from 304L stainless steel or carbon steel. However, the shielding properties of 304 and 304L stainless steel do not differ significantly at the same density. Table 5-5 summarizes the material properties. The shielding attenuation properties are obtained from the data library for the MCNP computer code (Breismeister 1993).

Table 5-5. Materials and Densities Used for Shielding.

Material	Density (g/cc)	Remarks
304/304L stainless steel	8.0	Used in the cask, cask lid, MCO, and MCO plug
Carbon steel*		Possible use in shield plug assembly
Air	0.00123	Provides scattering media for neutrons; photon models neglected attenuation and scattering in air out to 6 m
Uranium	18.77	Fuel elements modeled as ^{238}U with 0.947% ^{235}U; also, assembly end caps conservatively replaced by uranium (source)
Zirconium	6.55	Fuel cladding

*Note: Carbon steel is roughly equivalent to 304 stainless steel.

MCO = multicanister overpack.

5.4 SHIELDING ANALYSES

5.4.1 Computer Programs

The Monte Carlo computer code, MCNP (Breismeister 1993; Carter 1996), was used to perform the dose rate calculations. MCNP has powerful geometry routines and uses an ENDF/B database for cross sections. The MCNP quality assurance documentation for use at the Hanford Site is given in WHC-SD-MP-SWD-30001, *Certification of MCNP Version 4A for WHC Computer Platforms* (Carter 1996).

5.4.2 Flux-to-Dose-Rate Conversion

Table 5-6 lists the flux-to-dose-rate conversion factors used to calculate the gamma ray dose rates. These conversion factors are from ANSI/ANS-6.1.1-1991, *Neutron and Gamma-Ray Fluence-to-Dose Factors* (ANSI/ANS 1991), and conservatively assume the radiation exposure is from an anterior-posterior exposure. Table 5-7 lists the flux-to-dose-rate conversion factors used to calculate the neutron dose rates. These conversion factors are from *Spent Nuclear Fuel Project Canister Storage Building — Neutron Quality Factors* (Phillips and Jacobs 1996).

5.4.3 Dose Rates

A conservative MCO photon source term for the dose rate calculation consists of a fully loaded MCO with 6.34 MTU for Mark IV fuel. The neutron dose on the top of the MCO through the shield plug and 7.62-cm (3-in.) thick cask lid was 0.85 mrem, and the dose without the cask lid at the top of the MCO was 0.15 mrem at 1 m. Therefore neutron dose rates for the current model are considered negligible.

Tables 5-8 and 5-9 give dose rates for the MCO with the lid off and with the lid on. Dose rates that are essentially unchanged in going from lid off to lid on are not repeated in Table 5-9. Figure 5-3 shows dose rate locations corresponding to the entries on Tables 5-8 and 5-9.

Distances above the top of the cask are measured with respect to the top of the lid (9.5 cm [3.75 in.] above the top of the MCO plug) to allow for more direct comparison between lid-off and lid-on dose rates. The lid of the cask in this model provides no shielding within the center 43 cm (17-in.) diameter. Dose rates to the side and bottom of the cask and above ports E1 and E2 are virtually unchanged between the lid-on and lid-off cases. It can be seen that the lid-on dose rate at contact is larger than that of the lid-off case. This is due to the fact that the doughnut-shaped lid attenuates photons that would otherwise escape at a slant and potentially reach the dose rate location by intermediate scattering in air.

Table 5-6. Photon Dose Conversion Factors.

Energy (MeV)	Fluence to dose 1 E-12 Sv-cm^2	Flux to dose rate (mrem/h)/(p/cm^2/s)
1.00 E-02	0.0620	2.232 E-5
1.50 E-02	0.1570	5.625 E-5
2.00 E-02	0.2380	8.568 E-5
3.00 E-02	0.3290	1.184 E-4
4.00 E-02	0.3650	1.314 E-4
5.00 E-02	0.3840	1.382 E-4
6.00 E-02	0.4000	1.440 E-4
8.00 E-02	0.4510	1.624 E-4
1.00 E-01	0.5330	1.919 E-4
1.50 E-01	0.7770	2.797 E-4
2.00 E-01	1.0300	3.708 E-4
3.00 E-01	1.5600	5.616 E-4
4.00 E-01	2.0600	7.416 E-4
5.00 E-01	2.5400	9.144 E-4
6.00 E-01	2.9900	1.076 E-3
8.00 E-01	3.8300	1.379 E-3
1.00 E+00	4.6000	1.656 E-3
1.50 E+00	6.2400	2.246 E-3
2.00 E+00	7.6600	2.758 E-3
3.00 E+00	10.2000	3.672 E-3
4.00 E+00	12.5000	4.500 E-3
5.00 E+00	14.7000	5.292 E-3
6.00 E+00	16.7000	6.012 E-3
8.00 E+00	20.8000	7.488 E-3
1.00 E+01	24.7000	8.892 E-3
1.20 E+01	28.9000	1.040 E-2

Note: These conversion factors are from ANSI/ANS-6.1.1-1991, Neutron and Gamma-Ray Fluence-to-Dose Factors, American Nuclear Society, La Grange Park, Illinois.

Table 5-7. Neutron Flux to Dose Rate Conversion Factors.

Energy (MeV)	Fluence to dose 1 E-12 Sv-cm^2	Flux to dose rate (mrem/h)/(n/cm^2/s)
2.50 E-08	10.2	3.68 E-3
1.00 E-07	10.2	3.68 E-3
1.00 E-06	12.4	4.46 E-3
1.00 E-05	12.4	4.46 E-3
1.00 E-04	12.0	4.31 E-3
1.00 E-03	10.2	3.68 E-3
1.00 E-02	9.92	3.57 E-3
1.00 E-01	60.3	2.17 E-2
5.00 E-01	257	9.26 E-2
1.00 E+00	367	1.32 E-1
5.00 E+00	433	1.56 E-1
7.00 E+00	408	1.47 E-1
1.00 E+01	408	1.47 E-1
1.40 E+01	578	2.08 E-1

Note: These conversion factors are from J. D. Phillips, Sr., and E. R. Jacobs, 1996, Spent Nuclear Fuel Project Canister Storage Building – Neutron Quality Factors.

Table 5-8. Photon Dose Rates for a Multicanister Overpack with the Lid Off.

Location	Contact* (mrem/h)	At 1 m (mrem/h)	At 2 m (mrem/h)	At 6 m (mrem/h)
Top	31 (0.04)	8.4 (0.06)	3.5 (0.08)	0.56 (0.10)
Port E1	50 (0.07)	7.7 (0.10)	3.1 (0.11)	0.55 (0.19)
Port E2	100 (0.10)	8.2 (0.12)	2.9 (0.10)	0.59 (0.30)

Note: Numbers inside the parentheses are the relative (multiply by 100 to obtain percent) statistical uncertainties for one standard deviation.

*Although the lid is not in place, dose rate locations above the cask are given with respect to top of lid (9.5 cm [3.75 in.] above top of MCO plug) to allow for comparison to the lid on cask. The contact dose rates represent a radial average to the inside diameter (43 cm [17 in.]) of the casket lid.

Table 5-9. Photon Dose Rates for a Multicanister Overpack with the Lid On.

Location	Contact (mrem/h)	At 1 m (mrem/h)	At 2 m (mrem/h)	At 6 m (mrem/h)
Top	34 (0.04)	7.4 (0.10)	2.4 (0.13)	0.27 (0.20)

Note: Numbers inside the parentheses are the relative (multiply by 100 to obtain percent) statistical uncertainties for one standard deviation.

Figure 5-3. Dose Rate Locations.

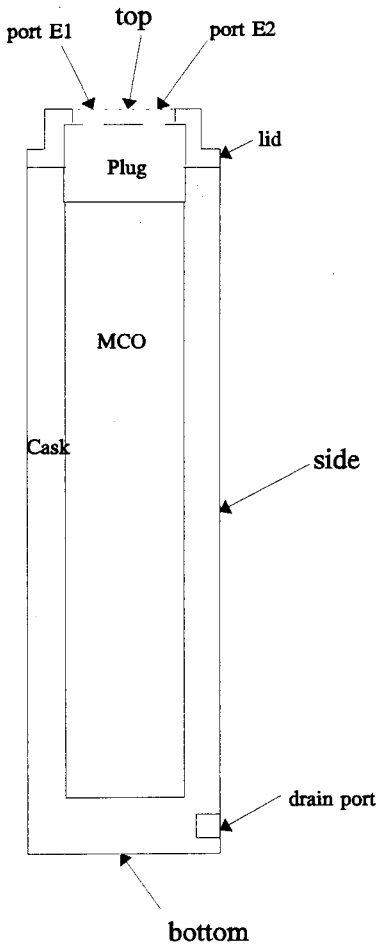

6.0 CRITICALITY EVALUATION

This chapter identifies, describes, discusses, and analyzes the criticality safety physics used for design of the MCO and its components and systems that are important to safety.

6.1 DISCUSSION AND RESULTS

The MCO is required to meet criticality criteria that are consistent with commercial reactor fuel handling (Garvin 1996). Therefore, the k_{eff} (a measure of reactivity) of the MCOs during transport to or processing in the CVDF and CSB must be less than 0.95 under both normal conditions and credible off-normal conditions. Analysis in this chapter shows the k_{eff} of the contents of the cask-MCO package under normal conditions to be below this limit by a substantial degree. Dry cask-MCO packages have a k_{eff} less than 0.4. Packages flooded with water and loaded with intact N Reactor fuel assemblies have a k_{eff} less than 0.90. Dry MCOs stacked two per tube in a 10 tube by 22 tube array have a k_{eff} less than 0.4 for any density of water between the tubes and a k_{eff} less than 0.9 for flooded tubes and vault space.

The MCO container, holding dry fuel, cannot be made critical under any conditions. The only criticality concern is with water moderation internal to the MCO. MCOs containing either Mark IV or Mark IA fuel are below a k_{eff} of 0.90 for flooded intact fuel loadings. MCOs containing scrap in the top and bottom tiers with intact fuel in the other tiers have a k_{eff} that is less than 0.90. If a scrap basket is misplaced from the top to the second from the bottom, so two scrap baskets occupy the bottom two tiers, the k_{eff} increases to only about 0.91. A Mark IV basket loaded with scrap is more limiting because of the absence of any safety-class structure that excludes scrap from the center of the fuel basket; the Mark IA scrap basket has such a structure.

Fuel types are to be segregated by enrichment. Mixing Mark IV and Mark IA fuel assemblies, components, or scrap together in the same MCO is not allowed. Because Mark IV material is less reactive than Mark IA material, Mark IV assemblies or 0.95 wt% ^{235}U scrap may be loaded into baskets designed for Mark IA fuel. No assemblies, components, or scrap with fissionable material greater than 0.95 wt% ^{235}U may be loaded into fuel baskets that do not contain the 16.8-cm- (6.6-in-) diameter, stainless steel schedule 80 pipe insert.

The inside diameter of the MCO provides geometry control and in combination with additional constraints and limits, such as the central insert pipe in the Mark IA baskets, control of fuel type or enrichment in MCO loading, and limiting the number and placement of scrap baskets, ensures k_{eff} is less than 0.95 for normal conditions and credible accidents. For accidents, two independent, concurrent, and highly unlikely incidents must occur before k_{eff} is allowed to exceed 0.95. This is the double contingency principle of criticality safety.

The 100 *g* drop is the limiting accident condition. This accident condition is represented by completely rubblizing the intact fuel and cladding. The top and bottom baskets contain scrap, and the other baskets

contain rubble. The baskets are assumed to lose their structural attachment and fall on top of one another forming a column of baskets separated by the stainless steel baseplates of the fuel baskets. The analysis models the resulting material under fully moderated and reflected conditions. A conservative packing fraction of 0.4 is used for the analysis. (Packing fractions for gravel beds range from 0.4 to 0.45.) A final packing fraction of 0.4 from fuel crushing is based on a hexagonal lattice of fuel at a center-to-center spacing of 7.1 cm (2.8 in.) (the Mark IV lattice packing fraction is 0.443, and the Mark IA lattice packing fraction is 0.392). This assumes that the vertical impact that crushes the fuel does not significantly decrease bulk density. This is considered to be conservative because higher density would further reduce the moderation, which would further reduce k_{eff}. In this limiting accident condition, the k_{eff} for the MCO is less than 0.94 for both fuel types. Even for the case of Mark IA baskets with thin, central stainless steel inserts that are displaced off-center by 2 in., the results are less than 0.92.

If the 100 *g* drop accident occurs during transport of the MCO container from the K Basins to the CVDF, a time when the MCO is fully water flooded, the MCO could exceed the $k_{eff} < 0.95$ criterion for a transient phase during the rebound. This requires both optimal sizing and spacing of the fuel rubble that results in optimal self-shielding and moderation. The drop accident must both agglomerate the smaller fuel fragments that result from the impact and disperse these agglomerates into optimal spacing during the same rebound. This scenario is considered incredible. The calculated k_{eff} for this scenario does not exceed 0.98. The end state satisfies the $k_{eff} < 0.95$ criterion once gravity has compacted the rubble down to a packing fraction of 0.40, a condition that results in significant undermoderation.

6.2 SPENT FUEL LOADING

6.2.1 N Reactor Fuel Description

The fuel dimensions pertinent to the criticality analysis and to criticality prevention are given in Table 6-1. This table lists the enrichments for the fresh (unirradiated) fuel before it was loaded in the N Reactor.

Analyses on the effects of burnup and fission product decay show that the fresh N Reactor fuel is more reactive (higher infinite criticality factor k_{inf}) than the spent fuel in spite of the presence of plutonium products in the spent fuel (Schwinkendorf 1996). Reduced uranium enrichment and the presence of fission products compensate for any increase in k_{inf} because of the plutonium content in the spent fuel. Analysis of the effect on k_{eff} of decay of fission products over a long period of time (e.g., 100 years or more) is described in WHC-SD-SNF-CSER-005 (Schwinkendorf 1996) and provides justification for use of the fresh fuel characteristics in the analyses presented in this chapter. As such, all the criticality analyses discussed in this chapter are conservatively performed for the fresh N Reactor fuel.

Table 6-1. Description of N Reactor Fresh Fuel Elements.

	Mark IV				Mark IA		
Pre-irradiation enrichment of ^{235}U	0.947% enriched				1.25-0.947% enriched		
Type-length code1*	E	S	A	C	M	T	F
Length (cm)	66.3	62.5	58.9	44.2	53.1	49.8	37.8
Element diameter (cm)							
1. Outer of outer	6.15				6.10		
2. Inner of outer	4.32				4.50		
3. Outer of inner	3.25				3.18		
4. Inner of inner	1.22				1.11		
Cladding mass (kg)							
1. Outer element	1.09	1.04	0.99	0.79	0.88	0.83	0.66
2. Inner element	0.55	0.52	0.50	0.40	0.54	0.51	0.04
Mass of uranium in outer (kg)							
1. (0.947% ^{235}U)	16.0	15.0	14.1	10.5			
2. (1.25% ^{235}U)					11.1	10.4	7.85
Mass of uranium in inner (kg) 0.947% ^{235}U	7.48	7.03	6.62	4.94	5.49	5.12	3.90
Weighted average of uranium in element (kg)	22.7				16.3		
Ratio of Zircaloy-2 to uranium (kg/MTU)	70.0	70.8	71.6	77.1	85.5	86.3	90.4
Weighted average (kg/MTU)	70.3				85.7		
% of total elements	63				37		
% of length type of each fuel	78	10	7	5	87	10	3
Displacement volume (l/MTU)	67				67		

*Letter code differentiates the different lengths of the Mark IV or Mark IA fuel elements (i.e., a type "E" element is 66.3 cm [26.1 in.] long).

MTU ≈ metric tons of uranium.

As shown in Table 6-1, there are two types of fuel assemblies, Mark IA and Mark IV, with different lengths and uranium enrichments. Each fuel assembly consists of two hollow, coaxial, cylindrical uranium metal elements separated by spacers. Each of the elements is clad with Zircaloy (i.e., Zircaloy-clad tube-in-tube metallic uranium geometry). The Mark IA fuel assembly has two different uranium enrichments: the inner element with an enrichment of 0.947% (0.95%) ^{235}U and the outer element with an enrichment of 1.25% ^{235}U. The weighted average enrichment of a Mark IA assembly is 1.15% ^{235}U. The Mark IV assembly has only one enrichment, 0.95% ^{235}U. Some fresh Mark IV fuel assemblies contain natural uranium (0.71% ^{235}U), but those assemblies are treated as 0.95% ^{235}U fuel in the analyses presented in this chapter. The Mark IA fuel has a higher k_{inf} and, correspondingly, has more potential for criticality than the Mark IV fuel in an optimum lattice arrangement.

The Mark IA fuel assemblies and scrap are stored in the K West Basin only. Mark IV fuel assemblies and scrap are in both K West and K East Basins. It is suspected that removal from existing canisters, cleaning, and repacking of seemingly intact fuel assemblies in the K Basins could generate an additional amount of scrap fuel.

Operations procedures at the K Basins will segregate fuel by enrichment and load it in the designated baskets. This will prevent inadvertent mixing of higher and lower enrichment fuel in the same type of basket (e.g., the Mark IA fuel scrap will be loaded in the baskets designed for Mark IA scrap and not in the Mark IV scrap baskets). However, to account for uncertainties in sorting fuel assemblies or scrap by enrichment, bounding analyses have been performed as reported in this chapter.

Both K West and K East Basins contain SPR fuel, which is not shown in Table 6-1. The SPR fuel was fabricated with aluminum cladding. This fuel was not used in the N Reactor. All SPR fuel will be collocated in the K West Basin before packaging into the MCOs. It constitutes only about 0.1% of the total fuel inventory, the equivalent of one MCO load, approximately. The enrichment of the SPR fresh fuel varies from highly depleted to a maximum of 1.25% enriched ^{235}U (Willis 1995). The 1.25% enriched fuel is estimated to be less than 5% of the total SPR fuel inventory.

It is planned that the SPR fuel will be loaded in the MCO such that the results of the criticality analysis performed for Mark IA and Mark IV fuels apply to and envelop the accident conditions involving the SPR fuel. The analyses specific to the SPR fuel reported in this chapter will be used to develop a strategy for safe loading of the SPR fuel.

6.2.2 Multicanister Overpack Fuel Basket Description

The design parameters for the fuel baskets are shown schematically in Figures 6-1 and 6-2 for fuel assemblies and for fuel scrap, respectively. Sketches of the MCO and the MCO storage tube are shown in Figure 6-3.

Figure 6-1. Fuel Assemblies Storage Basket.

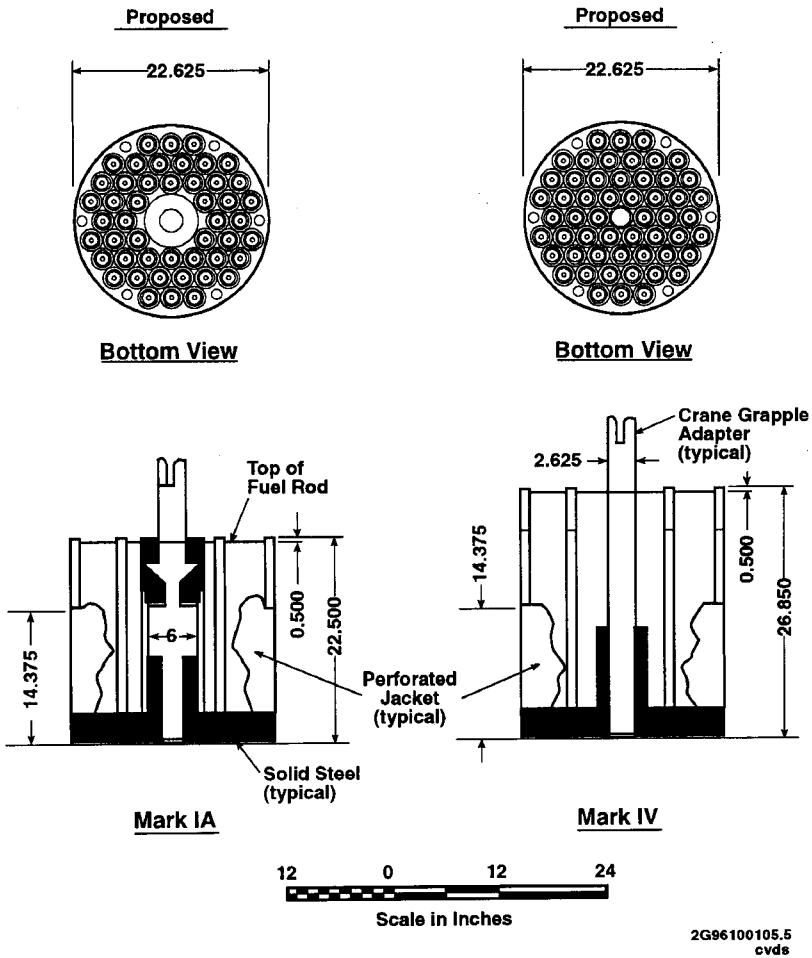

Figure 6-2. Fuel Scrap Storage Basket.

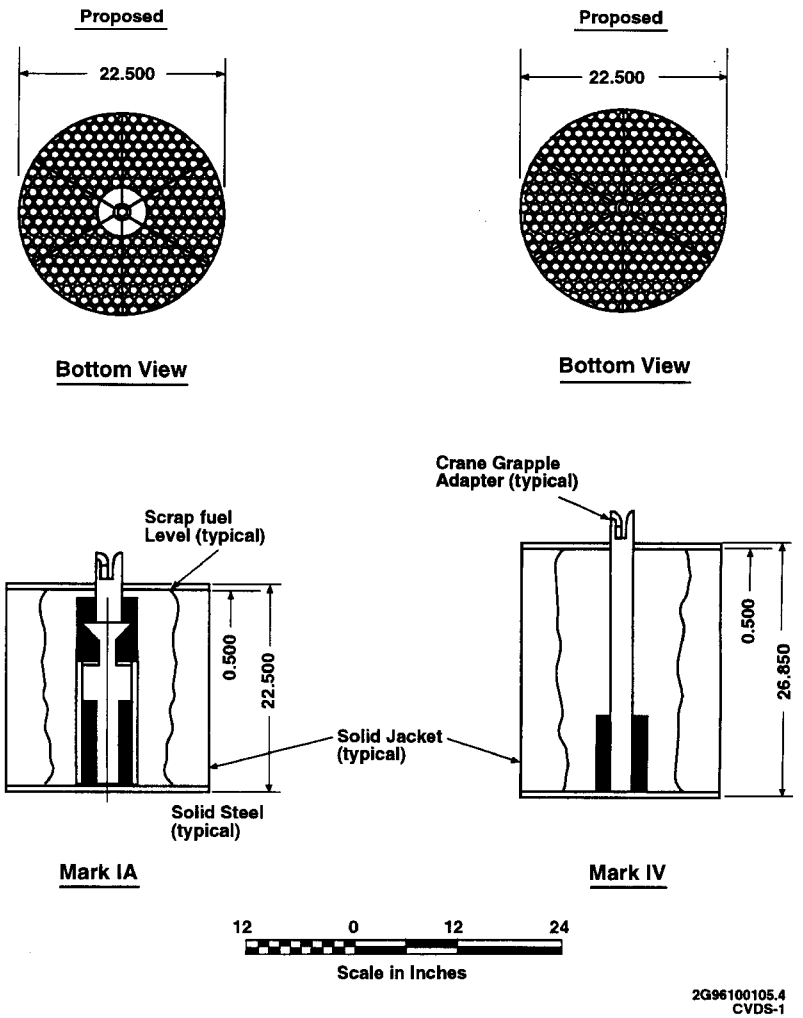

Figure 6-3. Multicanister Overpack and Storage Tube.

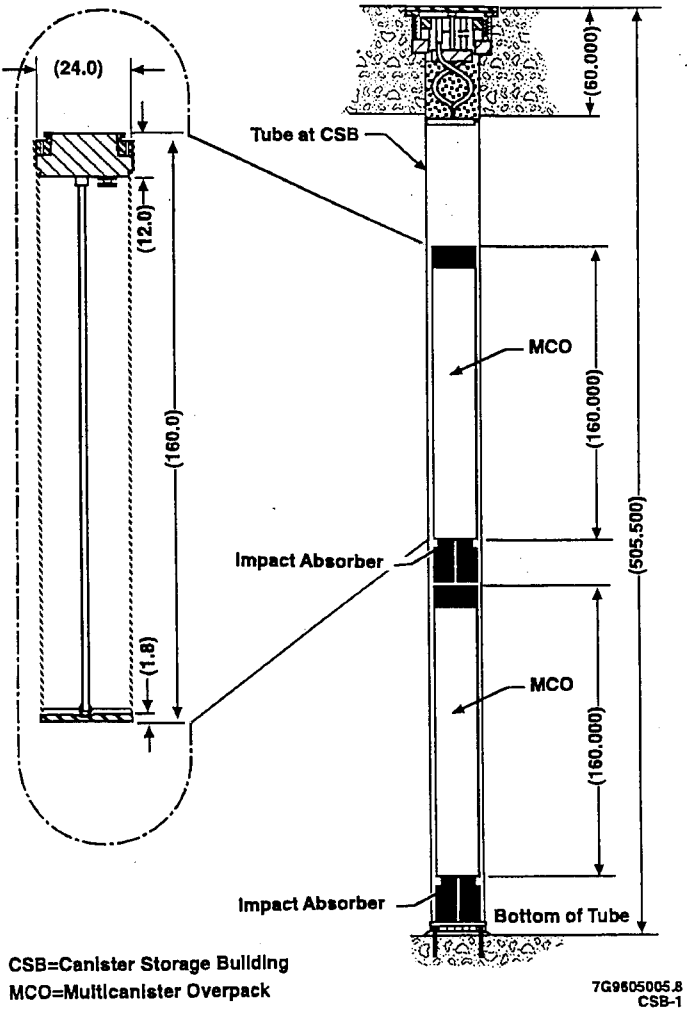

If placed in an optimum geometry, the Mark IA fuel will not meet the criticality criterion, $K_{eff} \leq 0.95$. Therefore, the fuel baskets for the Mark IA fuel were specially designed with a standard 16.8-cm- (6.6-in.-) diameter pipe insert installed along the central line of the fuel basket, as shown in Figures 6-1 and 6-2. Also, the Mark IA fuel baskets are shorter, which reduces the amount of Mark IA scrap that can be loaded in each basket. But, most importantly, the centrally located hollow cylindrical insert creates neutron leakage to reduce the criticality potential for the Mark IA fuel in the MCO.

The fuel baskets are designed for the largest fuel assemblies of Mark IV and Mark IA design. The Mark IV fuel basket is designed to hold 54 Mark IV fuel assemblies, and the Mark IA basket is designed to hold 48 Mark IA fuel assemblies. An MCO is designed to hold five baskets containing Mark IV fuel assemblies and scrap, or six baskets containing Mark IA fuel assemblies and scrap. As shown in Table 6-1, the Mark IA fuel assemblies are shorter than the Mark IV assemblies, except for Mark IV fuel type C. This limits the amount of fuel per Mark IA basket while permitting six baskets of Mark IA fuel per MCO. The fuel elements, when loaded in the baskets, form a tight lattice with minimal separation between neighboring fuel elements. The lattice has a hexagonal center-to-center pitch of about 7.1 cm (2.8 in.) compared with outside diameters of about 6.1 cm (2.4 in.) for the fuel assemblies, as shown in Table 6-1.

Broken pieces of the fuel assemblies will be treated as scrap and packed separately in baskets specifically designed for loading scrap into the MCOs, as depicted in Figure 6-2. The Mark IA fuel scrap basket has a centrally located, hollow cylindrical insert, similar in design to that for the basket for Mark IA fuel assemblies.

6.2.3 Multicanister Overpack Loading

The authorized contents for the MCO transportation cask are one MCO filled with 270 Mark IV fuel elements or 288 Mark IA fuel elements from the N Reactor or the equivalent in SPR fuel elements.

The fissionable material is N Reactor Mark IV and Mark IA fuel assemblies and scrap material from the same fuel. Based on the weights for the longest intact fuel assemblies, the maximum loading for a basket of Mark IV assemblies is about 1,269 kg (2,798 lb). For five basket tiers, this results in 6,345 kg (13,991 lb) total Mark IV fuel per MCO. For the six basket tiers of Mark IA assemblies, the masses are 796 kg (1,756 lb) per basket and 4,776 kg (10,531 lb) per MCO. These data, for baskets of the longest assemblies, were assumed as the limiting loadings for criticality safety evaluations.

The designated scrap baskets may be loaded with fuel scrap or segments of fuel assembly components, with or without cladding. Such scrap material comprises a considerable fraction of the material stored in the K Basins. The volume of loaded scrap is limited to the basket height, 67.3 cm (26.5 in.) for Mark IV baskets and 53.3 cm (21 in.) for Mark IA baskets. If scrap has a higher packing fraction than intact fuel assemblies, a scrap basket could contain more uranium mass than a basket of whole elements.

The total fuel mass limit given in Chapter 12.0, "Technical Controls and Limits," is larger than the limiting mass loading used in the criticality safety evaluations. The larger limit is derived from considerations such as handling, heat generation, and free volume, not from criticality considerations. Criticality considerations do not impose restrictions on mass loading of a fuel basket or MCO.

6.3 DESCRIPTION OF CALCULATIONAL MODEL

The MCO is 406 cm (160 in.) long with a 61-cm (24-in.) outside diameter and a 1.3-cm (0.5-in.) wall thickness. A total of five Mark IV baskets or six Mark IA baskets are loaded in an MCO. The dimensions of the baskets are such that the combined active height of the fuel or fuel scrap inside the MCO is approximately the same, irrespective of the type of fuel. Each MCO is modeled with two scrap baskets, one at the top and the other at the bottom. Whole assemblies are modeled with the inner and outer metal annuli intact and with all the zirconium cladding in place.

The normal condition is modeled with each type of spent fuel contained in the baskets designated for that type of fuel (see Figures 6-1 and 6-2) and the baskets, in turn, stacked in an MCO. The Mark IA basket holds 48 Mark IA fuel assemblies and has a central pipe insert (16.8-cm [6.6-in.] outside diameter) specifically designed for criticality control. The Mark IA fuel scrap basket has a similar central insert (15.2-cm- [6-in.-] diameter). MCOs holding Mark IA fuel (maximum length 53.0 cm [20.88 in.]) can be loaded with six baskets. Figure 6-4 shows the cask arrangement for a loading of whole Mark IA fuel assemblies.

The Mark IV basket holds 54 Mark IV fuel assemblies and does not have the centrally located pipe insert for criticality control. MCOs holding Mark IV fuel can be loaded with five baskets. The Mark IV fuel assemblies were produced in different lengths, from 43.2 cm to 66.3 cm (17 in. to 26.1 in.). For the calculational model, the axial extent of the fuel's annular cylinders was 26.1 in. per basket. Figure 6-5 shows the cask arrangement for a loading of whole Mark IV fuel assemblies.

Because of their higher enrichment, Mark IA assemblies are not allowed in Mark IV baskets. However, the lower enrichment Mark IV assemblies that are short enough to fit in Mark IA baskets would be acceptable; they would decrease the basket's reactivity. Both Mark IA and Mark IV baskets have a centrally located, 6.6-cm- (2.6-in.-) outside diameter tube for installation of the long process tube for vacuum drying the fuel in the MCO.

The design of the MCO and the fuel baskets is in the process of being finalized. The effects of any design change on criticality safety will be analyzed, as required.

One MCO is handled at a time in all operations except staging and storage in a CSB storage tube. Two MCOs are stacked per tube in the CSB during the staging mode preceding hot conditioning as well as during long-term interim storage. The MCOs may be sealed after hot conditioning for long-term interim storage.

Figure 6-4. Loading Arrangement for Mark IA Fuel in Multicanister Overpack.

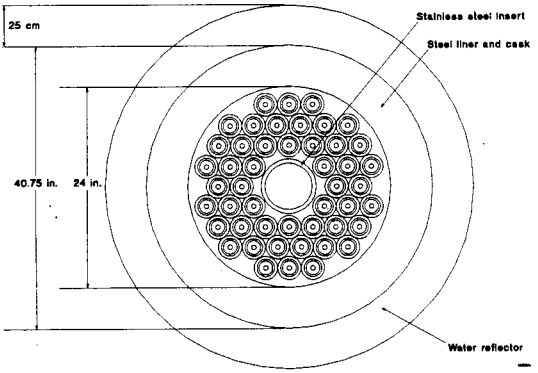

Figure 6-5. Loading Arrangement for Mark IV Fuel in Multicanister Overpack.

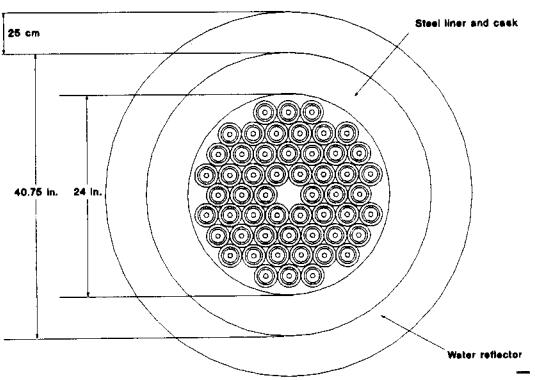

From criticality considerations, the normal condition is the "dry" condition inside and outside the MCOs while they are in storage, received in the shipping cask, or moved to and from the HCS Annex at the CSB, except for some moisture content before the MCO has gone through the hot conditioning process. Water content in the fuel was conservatively modeled at a level above its credible limit.

Various configurations of the MCOs and the storage tubes define boundary conditions as input into the criticality analyses (shown in Figures 6-6, 6-7, and 6-8). At the operating deck of the CSB, the MCOs are handled as a single unit located inside the MHM. Figure 6-6 (model A) depicts an MCO inside the MHM, which has 25-cm- (10-in.-) thick steel walls in a bell-shaped configuration. The operating deck's concrete floor functions as a neutron reflector and thermalization boundary at the bottom. This model bounds the cask-MCO configuration, which has steel walls 20 cm (8 in.) thick. Collocation of two or more MCOs at the operating deck is prevented by design and operating procedures. As such, all criticality scenarios at the operating deck are analyzed for a single MCO.

The MCO storage tubes in the CSB vault are arranged in a hexagonal matrix, shown in Figure 6-7 as model B. The storage tubes form a 10 (north-south) by 22 (east-west) array with two MCOs per tube. The tube's center-to-center distance is 1.42 m (4 ft, 8 in.) in the east-west direction and 1.37 m (4 ft, 6 in.) in the north-south direction.

The exterior vault walls are 1.4 m (4.5 ft) thick, the partition walls between vaults are 0.9 m (3 ft) thick, the vault basemat is 1.7 m (5.5 ft) thick, and the operating deck is 1.2 m (4.0 ft) thick. The vault walls, basemat, and operating deck are constructed of reinforced high-density concrete. Concrete at a thickness of 0.3 m (1 ft) is asymptotically as effective as an unlimited thickness of the concrete structure for neutron reflection and thermalization properties. As such, the concrete structures are assumed to be 0.3 m (1 ft) thick in the analyses reported in this chapter.

Figure 6-7 (model B) displays a 10 by 22 by 2 finite array with an effective 0.3-m- (1-ft-) thick concrete reflector boundary in all directions. This model is used to evaluate the neutronic interactive effects of fuel in neighboring tubes and of the surrounding concrete under normal (dry) conditions and under abnormal conditions when the spaces between the tubes and the MCOs are filled with varying densities of water, from very-low-density dispersed water (zero to 0.1 g/cm^3) to a fully flooded condition (1.0 g/cm^3). As the density of water is increased above the 0.1 g/cm^3 range, the tube-to-tube neutron interaction decreases and the tubes are decoupled rapidly. Based on the results of the analysis, it is assumed that the water-filled MCO-tube arrangement functions like an infinite lattice where a boundary of neutron flux symmetry is defined around each tube location. Neutron leakage is zero across this boundary, or the neutrons generated in an MCO-tube cell are fully reflected back into the cell. This infinite array configuration is depicted in Figure 6-8 as model C.

Figure 6-6. Model A, Multicanister Overpack in the Multicanister Overpack Handling Machine.

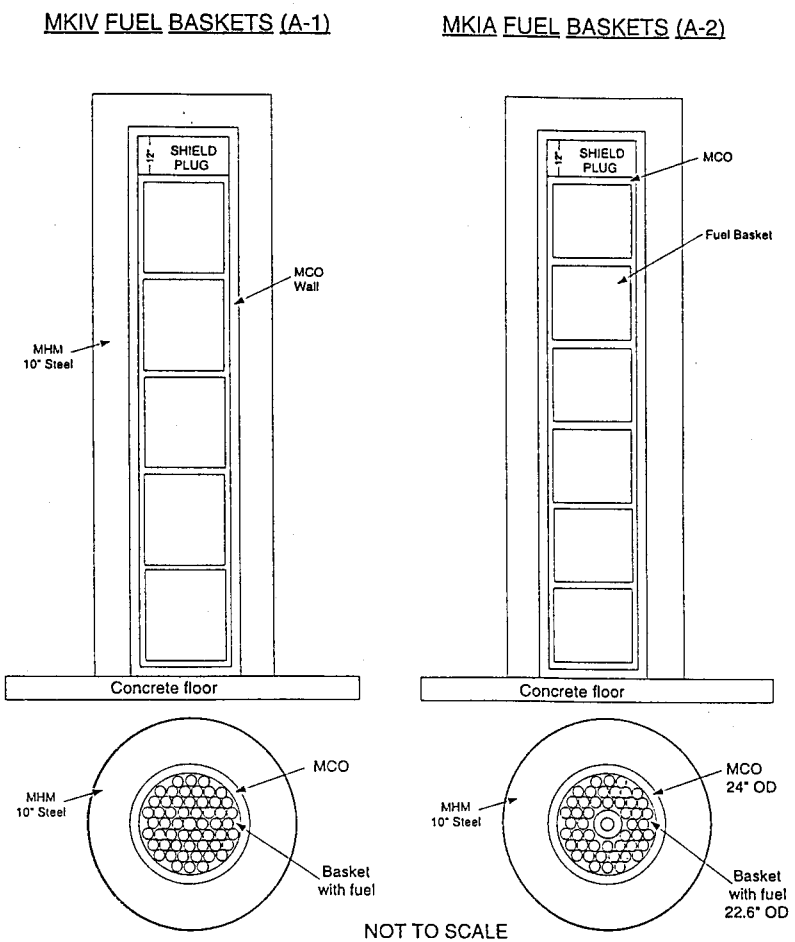

Figure 6-7. Model B, Multicanister Overpacks in Vault Tubes (Finite Array).

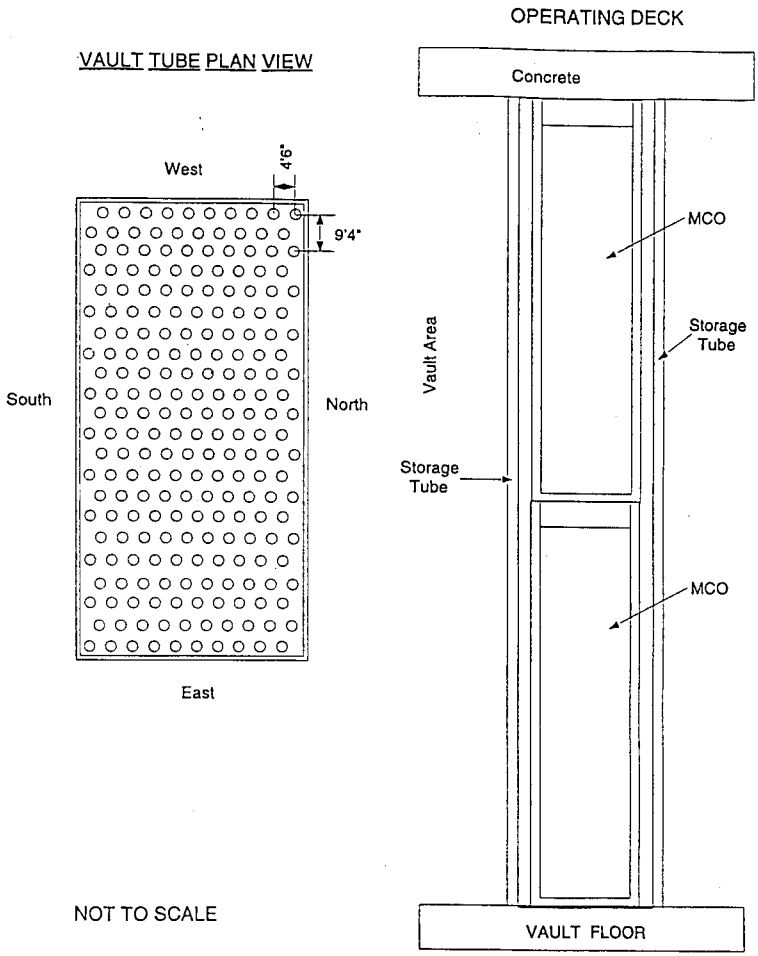

Figure 6-8. Model C, Multicanister Overpacks in Vault Tubes (Infinite Lattice Cell) and Model D, One Multicanister Overpack Encased in Concrete.

MODEL "C"

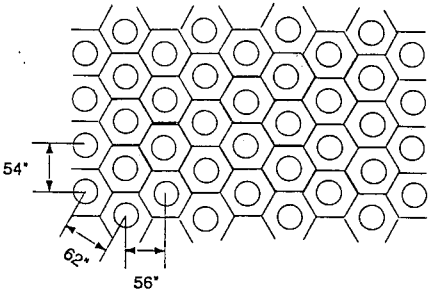

MODEL "D"

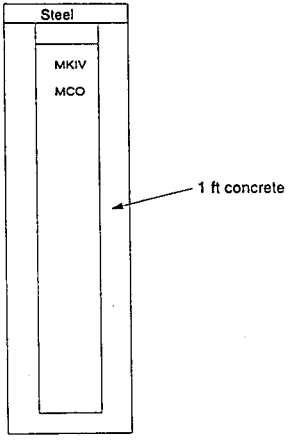

NOT TO SCALE

Figure 6-8 also depicts model D, in which an MCO is encased in concrete. Model D is used to evaluate the effects of concrete around a single MCO to simulate a configuration of operating deck concrete when an MCO is lowered into the storage tubes or a postulated accident scenario of an MCO falling from the MHM onto the operating area.

Modeling fuel elements or fuel scrap inside the MCO and the effect of interspersed moderation are discussed in Section 6.7.

Material densities and weight fractions are provided in Table 6-2 for constituent nuclides of all materials used in the calculational models for the normal and accident analyses provided in this section. Fissionable isotopes are considered at their most credible reactivity. Masses for materials in all regions are consistent with atomic number densities and volumes occupied.

The analysis tools used in the preparation of this document are the WIMS-E (Gubbins et al. 1982) and GOLF (Schwinkendorf 1994) codes, used for parametric studies and the calculation of ideal geometry critical dimensions, and the MCNP code (Breismeister 1993), used for modeling of three-dimensional geometries in detail. The WIMS-E lattice transport code (Gubbins et al. 1982) was used to generate infinite neutron multiplication factors, k_∞, for lattices and two-group cross sections for use by GOLF (Schwinkendorf 1994), which was used to calculate finite radial dimensions for both cylinders and hemispheres. Section 6.6 presents the validation of the criticality computer codes used to demonstrate the acceptability of the MCO reactivity.

The MCNP code (Breismeister 1993) was used to obtain the results discussed in the following sections. The MCNP N Reactor fuel bias, discussed in Section 6.6.3, was determined to be -5 mk (Wittekind 1993). To allow for this bias in the code, results in these sections should be compared with a limiting value of 0.945 for k_{eff}.

6.4 CRITICALITY CALCULATION RESULTS FOR NORMAL CONDITIONS

The calculational or experimental methods and results used to determine the nuclear reactivity for the maximum fuel loading intended to be contained in the cask are discussed in this section.

6.4.1 Loading with Intact Assemblies Only

6.4.1.1 Dry Multicanister Overpack Loadings of Intact Assemblies. Table 6-3 contains the MCNP results for casks containing MCO baskets loaded only with intact Mark IA or Mark IV fuel assemblies. The upper section of the table contains data for dry loadings; these results clearly show that criticality is not a concern for dry MCO containers. The k_{eff} for an infinite square array of dry Mark IA MCOs is only 0.3008 ± 0.0015, or 0.3038 at the upper 95% confidence level. The k_{eff} values for dry MCOs loaded with intact Mark IV fuel assemblies are about 10% higher. This is because there are more fuel assemblies per basket and each fuel assembly has more uranium metal.

Table 6-2. Material Densities and Weight Fractions Used in Calculations.

Material	No.	Density (g/cm^3)	Isotope	Wt fraction
Mark IV inner elements	m1	18.58	92235.50c 92238.50c	0.009471 0.990529
Zircaloy cladding	m2	6.55	40000.50c	1.000
Stainless steel	m3	8.03 g/cc	6000.50c 25055.50c 14000.50c 24000.50c 28000.50c 26000.55c	0.0004 0.0200 0.0100 0.1900 0.0925 0.6871
Water	m4	1.000	1001.50c 8016.50c	0.1119 0.8881
Carbon steel	m5	8.03	6000.50c 25055.50c 14000.50c 24000.50c 28000.50c 26000.55c 5010.50c 5011.55c	0.000396 0.0198 0.0099 0.1881 0.091575 0.680229 0.00199 0.00801
Mark IV outer elements	m6	18.58	92235.50c 92238.50c	0.009471 0.990529
Mark IA scrap	m7	18.82	92235.50c 92238.50c	0.011494 0.988506
1.25 wt% ^{235}U scrap	m8	18.82	92235.50c 92238.50c	0.012491 0.987509
CSB concrete	m9	2.26	1001.50c 8016.50c 11023.50c 12000.50c 13027.50c 14000.50c 15031.50c 16032.50c 36084.50c 20000.50c 22000.50c 26000.55c	0.0031 0.4407 0.0182 0.0376 0.0607 0.2157 0.0009 0.0009 0.0066 0.1306 0.0049 0.0788

CSB = Canister Storage Building.

Table 6-3. Analysis Results for Intact Fuel in Multicanister Overpacks in Shipping Casks.

File ID	Fuel type[a]	Payload cluster		Interior water	MCO array details (single units have 25.0 cm H_2O reflector)	Calculation results[b]		
		No. of baskets	Assemblies per basket			k_{eff}	Std. dev.	95% CI k_{eff}
plan_b83	Mark IA	6	48	All dry	Two touching	0.3028	0.0016	0.3059
plan_104	Mark IA	6	48	All dry	Infinite array square lattice	0.3008	0.0015	0.3038
plan_b90	Mark IV	5	54	All dry	Two touching	0.3293	0.0016	0.3324
plan_103	Mark IV	5	54	All dry	Infinite array square lattice	0.3341	0.0016	0.3374
plan_b81	Mark IA	6	48	Flooded	Single MCO	0.8483	0.0032	0.8546
plan_b82	Mark IA	6	48	Flooded	Two touching	0.8515	0.0028	0.8571
plan_b88	Mark IV	5	54	Flooded	Single MCO	0.8778	0.0028	0.8834
plan_b89	Mark IV	5	54	Flooded	Two touching	0.8794	0.0031	0.8855

[a]Mark IV type neglects tie rod at center, which excludes center assembly in array. Mark IA has a 6-in. diameter steel insert, excluding assemblies from seven central positions.
[b]The limiting value for k_{eff} should be considered 0.945 to allow for a code bias of -5 mk (see Section 6.6.3).

CI = confidence interval.
MCO = multicanister overpack.

6.4.1.2 Flooded Multicanister Overpack Loadings of Intact Assemblies. When the MCOs loaded with intact fuel assemblies are fully flooded, the k_{eff} is higher, but well within the safety limit value of 0.95. The lower part of Table 6-3 gives the calculated results for cases in which the MCO is flooded inside. For a single cask holding six baskets of intact Mark IA fuel, fully flooded with water, the k_{eff} is 0.855 at the upper 95% confidence level. Putting a second identically loaded cask next to this raises the k_{eff} only about 0.4%, illustrating the significant effect of the cask shielding for diminishing interactions between the casks in an array.

Similar trends are noted for flooded casks of whole Mark IV fuel assemblies. Even though a Mark IV fuel assembly is less reactive than a Mark IA assembly, more Mark IV fuel assemblies will be loaded into each basket. This results in a value for k_{eff} that is 3% to 4% higher than for Mark IA fuel but still below 0.90. The MCOs loaded with Mark IV fuel will therefore tend to be more limiting from a criticality viewpoint. When fully flooded, MCOs loaded with intact Mark IV fuel assemblies also yield a k_{eff} well below the safety limit of 0.95. For the side-by-side casks case, the k_{eff} is 0.886 at the upper 95% confidence level.

These data for the flooded casks of whole fuel assemblies prove conformance with the criticality safety requirements under normal conditions, including the transport phase.

6.4.2 Loading with Intact Assemblies and Scrap

Calculation of k_{eff} values for MCO cask loadings that include baskets of scrap (scrap and intact fuel may be mixed in a scrap basket) is highly subjective, as it requires assumptions about the nature of the scrap. These assumptions include average piece size and volumetric distribution. The degree of moderation and the effective shielding of ^{238}U resonances, and thus reactivity, are highly sensitive to these parameters. The approach adopted for this analysis has been to evaluate the k_{eff} values for the most reactive possible scrap configurations; this implies precise values for piece diameters and optimized separations of the scrap pieces. Based upon the results for these hypothetical, worst-case scrap configurations, it then can be inferred that any realistic scrap loadings will be subcritical and within the safety margin requirements.

6.4.2.1 Flooded Multicanister Overpack Loadings that Include Mark IA Scrap. The MCNP cases reported in Table 6-4 model casks loaded with MCOs that contain baskets of Mark IA scrap and intact or rubblized Mark IA assemblies. Because the flooded scrap configuration can be more reactive, the k_{eff} values are larger than for loadings of intact assemblies only. The results in Table 6-4 show that two 1.25 wt% ^{235}U scrap baskets can be included in an MCO loaded with Mark IA fuel when the baskets are placed at the top and bottom. Acceptable values for k_{eff} are found for the contingencies of one misplaced scrap basket in a flooded MCO and for a drop accident with a flooded MCO.

Table 6-4. Analysis Results for Mark IA Fuel and Scrap in Flooded Multicanister Overpacks in Casks.

File ID	Basket contents by tier number (from top)						Other details	Fuel OD (in.)	Calculation results*		
	Tier 1	Tier 2	Tier 3	Tier 4	Tier 5	Tier 6			k_{eff}	Std. Dev.	95% CI k_{eff}
CASE1A	1.25 wt% ^{235}U scrap	48 Mark IA	48 Mark IA	48 Mark IA	48 Mark IA	1.25 wt% ^{235}U scrap	Dry MCO	23.00	0.3808	0.0019	0.3846
CASE1	1.25 wt% ^{235}U scrap	48 Mark IA	48 Mark IA	48 Mark IA	48 Mark IA	1.25 wt% ^{235}U scrap	Wet MCO	23.00	0.8721	0.0030	0.8780
CASE5	48 Mark IA	48 Mark IA	48 Mark IA	48 Mark IA	1.25 wt% ^{235}U scrap	1.25 wt% ^{235}U scrap	Misloaded, wet MCO	23.00	0.9016	0.0030	0.9076
CASE3	1.25 wt% ^{235}U scrap	1.15 wt% ^{235}U rubble	1.15 wt% ^{235}U rubble	1.15 wt% ^{235}U rubble	1.15 wt% ^{235}U rubble	1.25 wt% ^{235}U scrap	Drop model normal insert	23.25	0.9104	0.0027	0.9157
CASE3A	1.25 wt% ^{235}U scrap	1.15 wt% ^{235}U rubble	1.15 wt% ^{235}U rubble	1.15 wt% ^{235}U rubble	1.15 wt% ^{235}U rubble	1.25 wt% ^{235}U scrap	Drop model thick insert	23.25	0.9319	0.0029	0.9378
plan_b74	48 Mark IA	48 Mark IA	48 Mark IA	1.25 wt% ^{235}U scrap	48 Mark IA	48 Mark IA	Misloaded, wet MCO	24.00	0.9393	0.0026	0.9445
plan_b73	48 Mark IA	48 Mark IA	1.25 wt% ^{235}U scrap	1.25 wt% ^{235}U scrap	48 Mark IA	48 Mark IA	Misloaded, wet MCO	24.00	0.9587	0.0031	0.9649

*The limiting value for k_{eff} should be considered 0.945 to allow for a code bias of -5 mk (see Section 6.6.3).

CI = confidence interval.
MCO = multicanister overpack.
OD = outer diameter.

CASE1A in Table 6-4 shows that for a normally loaded, dry MCO in a cask, the k_{eff} is small, less than 0.4. The dry case includes 3 kg of water as residual water left in the MCO after drying. Its density in the MCO is 0.005 g/cm^3. When this fuel loading (four baskets of Mark IA intact assemblies and a top and a bottom basket of 1.25 wt% ^{235}U scrap) is flooded, as in CASE1 (Figure 6-9), the k_{eff} increases to almost 0.9. The dry case is representative of the MCO with significant reflection after being dried in the HCS Annex at the CSB. The flooded case models the MCO in a cask before processing in the CVDF. These results show that the normally loaded MCO, when isolated from other units by the cask or distance, is acceptably subcritical over the range from fully flooded to dried.

CASE5 (Table 6-4 and Figure 6-10) shows that even if the second scrap basket is loaded in the most reactive location, next to the other scrap basket, the k_{eff} is less than 0.91. Cases plan_b74 and plan_b73 are less refined models of the loaded and flooded MCO in the cask. Plan_b74 shows that if a single scrap basket is placed in the center of the stack, the value for k_{eff} is acceptable. Plan_b73 shows that if two scrap baskets are placed in the center positions, the value for k_{eff} is above the acceptable limit of 0.95, although subcritical. If the cause of misloading the two scrap baskets in this case meets the requirements of the double contingency principle, no further action is required. Design acceptance is dependent on meeting the requirements of double contingency.

Dropping a cask-MCO is assumed to rubblize the intact fuel in the central MCO baskets, drop the baskets into a stack separated by 0.375-in. plates, and to offset the 6-in. central pipe insert 2 in. off center, allowing rubble and scrap closer to the center line of the MCO. The scrap and baskets with fuel rubble are assumed to expand to the inside diameter of the MCO, 23.25 in. The MCO is engineered to limit the radial expansion to this value. The fragments of the fuel rubble are assumed to combine in optimum particle sizes modeled as rods. However, the rubble particles at this time are assumed to remain at the location in which they were crushed and not be momentarily suspended by rebound.

CASE3 (Table 6-4 and Figure 6-11) represents a single MCO containing six Mark IA baskets. The four central baskets contain Mark IA fuel reduced completely to rubble with an enrichment equal to 1.15 wt% ^{235}U, and the remaining two baskets (top and bottom) contain Mark IA scrap with an enrichment of 1.25 wt% ^{235}U. The stainless steel insert is assumed to be displaced a distance of 2 in. from the center line of the MCO by the force of the impact. CASE3A (Figure 6-12) represents the same conditions described in CASE3 (Figure 6-11), except that the thin-walled stainless steel insert is replaced with a thicker-walled insert. The MCO is fully flooded and fully reflected by the steel of the cask and water surrounding the cask.

CASE3 and CASE3A (Table 6-4 and Figures 6-11 and 6-12) show that for a flooded MCO that is dropped, the value for k_{eff} is less than 0.94 regardless of which of the two central inserts is in place. The k_{eff} at the upper 95% confidence level for the normal, thin 6-in. pipe insert is only 0.9157. For the drop accident (one contingency), the MCO loaded normally with Mark IA fuel and scrap is within allowable limits.

Figure 6-9. Analysis Input Models CASE1 and CASE2: Axial Geometry.

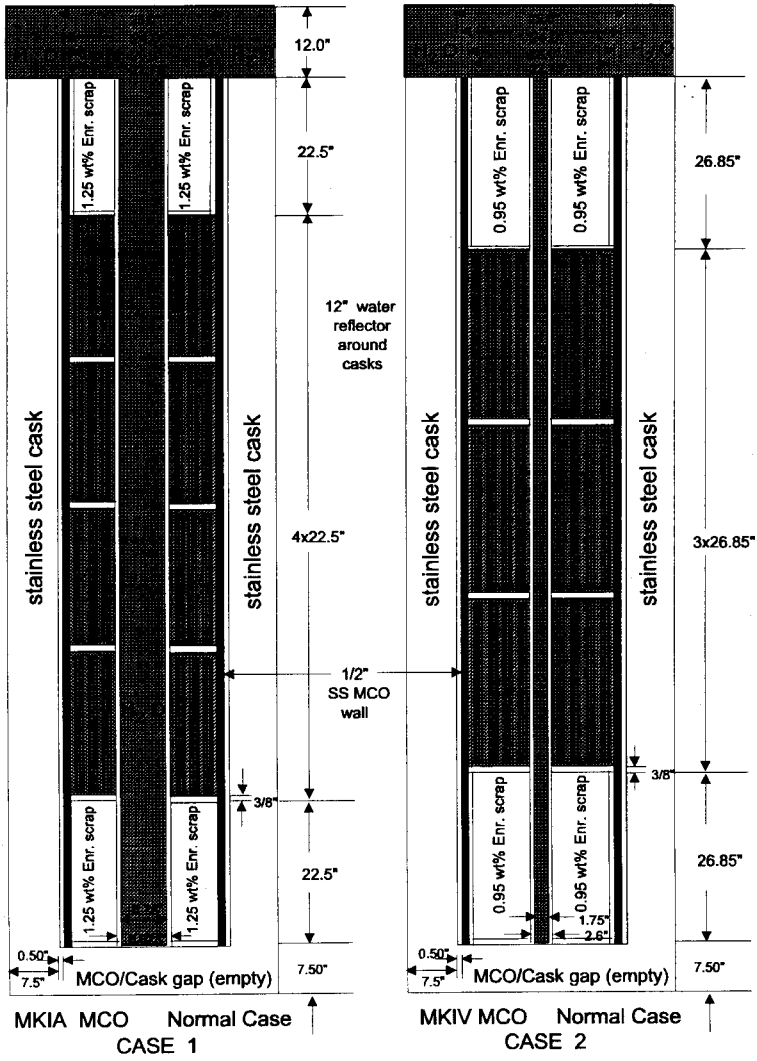

Figure 6-10. Analysis Input Models CASE5 and CASE6: Axial Geometry.

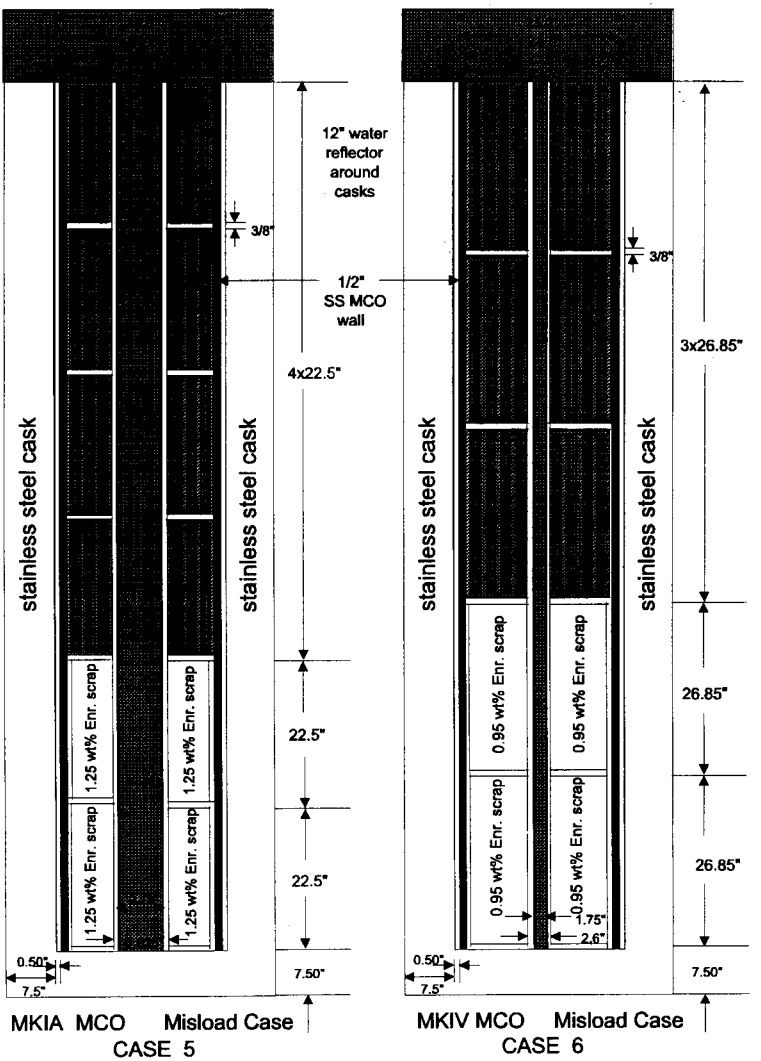

Figure 6-11. Analysis Input Model CASE3: Axial Geometry.

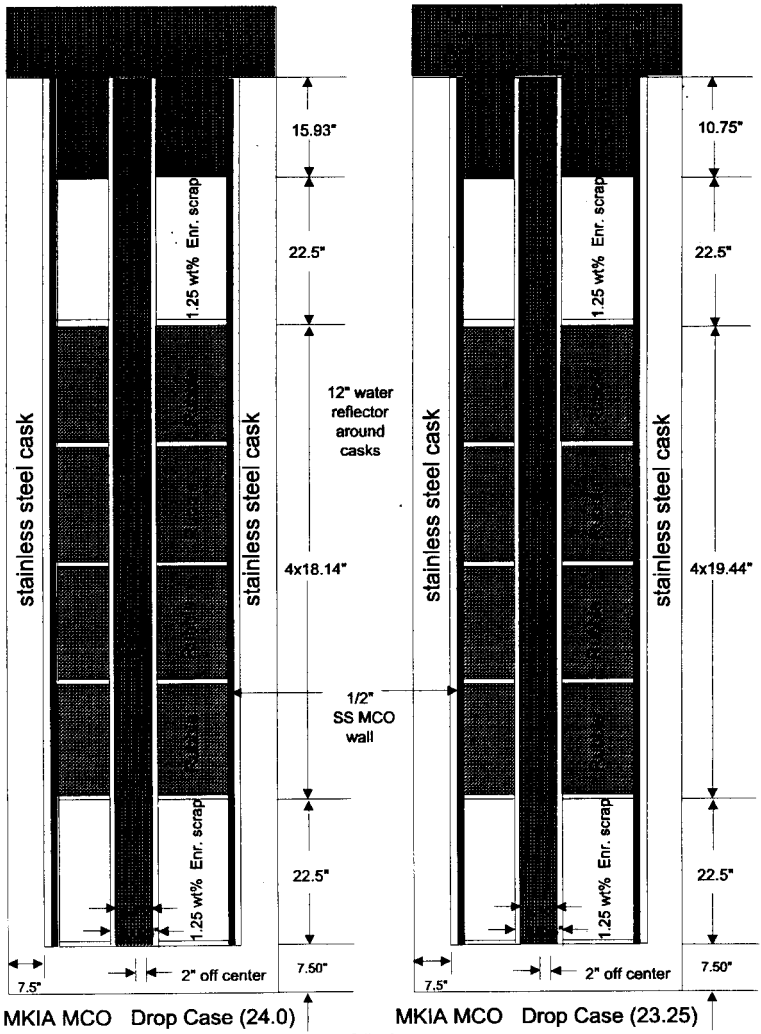

Figure 6-12. Analysis Input Model CASE3A: Axial Geometry.

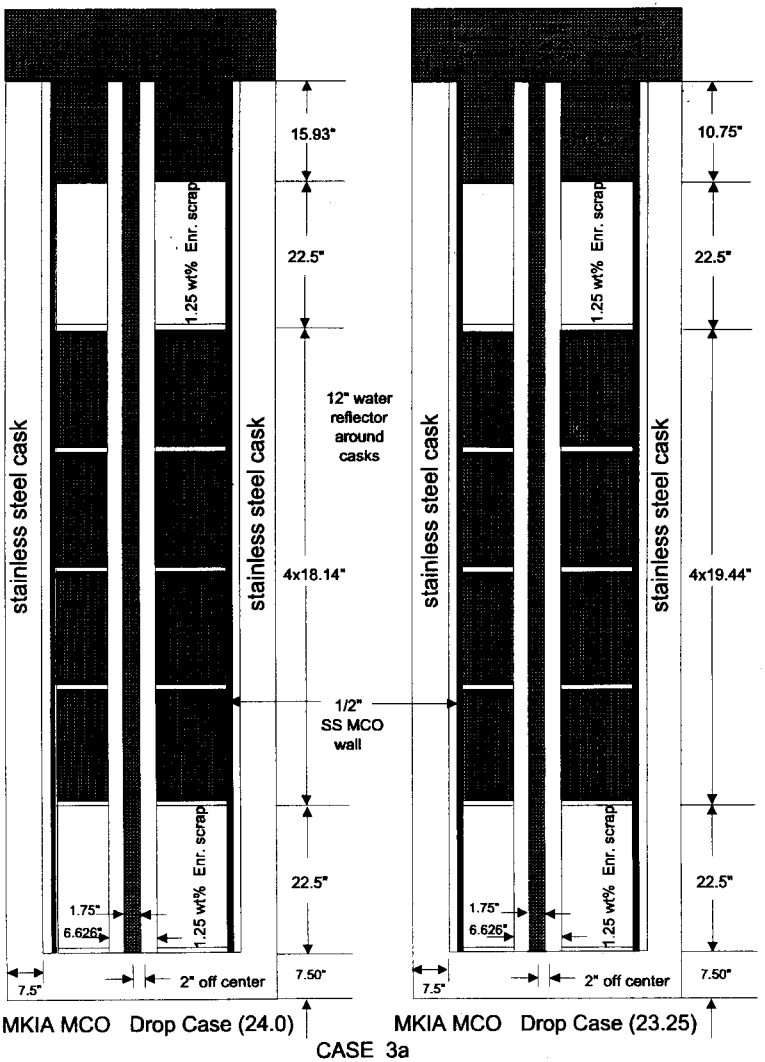

The calculations in Table 6-4 used a rubble packing fraction equal to 0.40 and had the cladding remaining with the fuel. This model is not optimally moderated for maximum reactivity, but a packing fraction of 0.40 is reasonably conservative for a rubble bed.

6.4.2.2 Flooded Multicanister Overpack Loadings that Include Mark IV Scrap. The MCNP cases reported in Table 6-5 model casks loaded with MCOs that contain baskets of Mark IV scrap and intact or rubblized Mark IV assemblies. Because the flooded scrap configuration can be more reactive, the k_{eff} values are larger than those cases in Table 6-3. The results in Table 6-5 show that two 0.95 wt% ^{235}U scrap baskets can be included in an MCO loaded with Mark IV fuel when the scrap baskets are placed at the top and bottom. Acceptable values for k_{eff} are found for the contingencies of one misplaced scrap basket in a flooded MCO and for a drop accident with a flooded MCO.

CASE2A in Table 6-5 shows that for a normally loaded, dry MCO in a cask, the k_{eff} is small, less than 0.4. The dry case includes 3 kg of water as residual water left in the MCO after drying. Its density in the MCO is 0.005 g/cm^3. When this fuel loading (three baskets of Mark IV intact assemblies and a top and a bottom basket of 0.95 wt% ^{235}U scrap) is flooded, as in CASE2 (Figure 6-9), the k_{eff} increases to almost 0.9. The dry case is representative of the MCO with significant reflection after being dried in the HCS Annex at the CSB. The flooded case models the MCO in a cask before processing in the CVDF. These results show that the normally loaded MCO, when isolated from other units by the cask or distance, is acceptably subcritical over the range from fully flooded to dried.

Case plan_108 (Table 6-5) models all five baskets filled with Mark IV inner elements in a close-packed hexagonal array. The MCO is flooded and fully reflected. This result shows that intact fuel is more reactive than close-packed inner elements.

CASE6 (Table 6-5 and Figure 6-10) shows that even if the second scrap basket is loaded in the most reactive location, next to the other scrap basket, the k_{eff} is less than 0.91. CASE2B shows the reactivity of a misplaced basket of Mark IV fuel scrap in the central location. The k_{eff} is less than 0.91. Case plan_133, a less refined model of the loaded and flooded MCO in the cask, shows that if two scrap baskets are placed in central positions, the k_{eff} value is acceptable. This exceeds the requirements of the double contingency principle since each misplaced basket is a contingency and the double contingency principle does not require subcriticality for two contingencies.

Dropping the cask-MCO is assumed to rubblize the intact fuel in the MCO and to drop the baskets into a stack separated by 0.375-in. plates. The scrap and rubble baskets are assumed to expand to the inside diameter of the MCO (23.23 in.). The MCO is engineered to limit the radial expansion to this value. The fragments of the fuel rubble are assumed to combine in optimum particle sizes modeled as rods. However, the rubble particles at this time are assumed to remain at the location in which they were crushed and not be momentarily suspended by rebound. CASE4 (Figure 6-13) shows that for a flooded MCO that is dropped, the k_{eff} is less than 0.94. For the drop accident (one contingency), the MCO loaded normally with Mark IA fuel and scrap is within allowable limits.

Table 6-5. Analysis Results for Mark IV Fuel and Scrap in Flooded Multicanister Overpacks in Casks.

File ID	Basket contents by tier number[a]					Other details (fuel assemblies, scrap as unburned 0.95% ^{235}U)	Fuel OD (in.)	Calculation results[b]		
	Tier 1	Tier 2	Tier 3	Tier 4	Tier 5			k_{eff}	Std. dev.	95% CI k_{eff}
plan_108	Mark IV inner element	Mark IV inner element	Mark IV inner element	Mark IV inner element	Mark IV inner element	All baskets fully packed with clad Mark IV inner elements	24.00	0.6762	0.0024	0.6809
CASE2A	0.95 wt% ^{235}U scrap	54 Mark IV	54 Mark IV	54 Mark IV	0.95 wt% ^{235}U scrap	Dry MCO	23.00	0.3866	0.0022	0.3910
CASE2	0.95 wt% ^{235}U scrap	54 Mark IV	54 Mark IV	54 Mark IV	0.95 wt% ^{235}U scrap	Wet MCO	23.00	0.8824	0.0022	0.8869
CASE2B	0.95 wt% ^{235}U scrap	54 Mark IV	0.95 wt% ^{235}U scrap	54 Mark IV	0.95 wt% ^{235}U scrap	Wet MCO, one misplaced scrap basket in middle position	23.00	0.8955	0.0029	0.9014
CASE6	54 Mark IV	54 Mark IV	54 Mark IV	0.95 wt% ^{235}U scrap	0.95 wt% ^{235}U scrap	Two scrap baskets next to each other near the bottom, wet MCO	23.00	0.9007	0.0025	0.9058
CASE4	0.95 wt% ^{235}U scrap	0.95 wt% ^{235}U rubble	0.95 wt% ^{235}U rubble	0.95 wt% ^{235}U rubble	0.95 wt% ^{235}U scrap	Drop model	23.25	0.9341	0.0028	0.9398
plan_133	54 Mark IV	54 Mark IV	0.95 wt% ^{235}U scrap	0.95 wt% ^{235}U scrap	54 Mark IV	Misloaded, wet MCO	24.00	0.9493	0.0016	0.9525

[a] Tiers number from the top to the bottom of the MCO.
[b] The limiting value for k_{eff} should be considered 0.945 to allow for a code bias of -5 mk (see Section 6.6.3).

CI = confidence interval.
MCO = multicanister overpack.
OD = outer diameter.

Figure 6-13. Analysis Input Model CASE4: Axial Geometry.

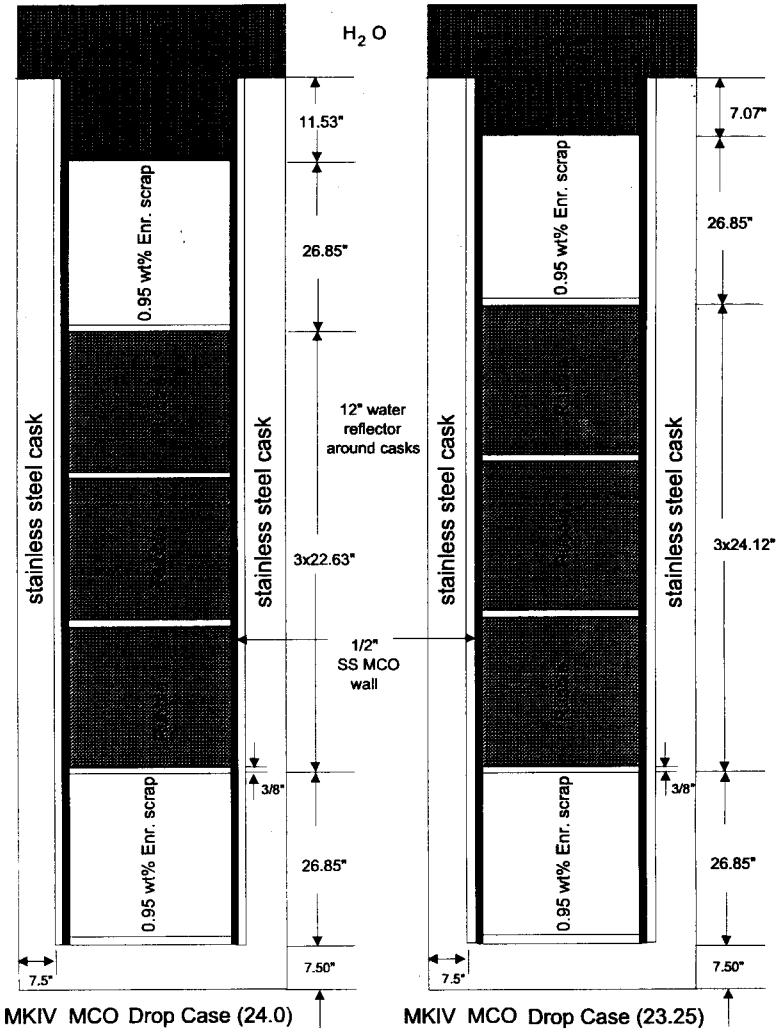

The calculations in Table 6-5 used a rubble packing fraction equal to 0.40 and had the cladding remaining with the fuel. This model is not optimally moderated for maximum reactivity, but a packing fraction of 0.40 is reasonably conservative for a rubble bed. The MCO was fully flooded and fully reflected by the steel of the cask and water surrounding the cask.

6.4.3 Canister Storage Building

The vault to be used in the CSB contains an array of storage tubes, 10 by 22, with concrete on four sides, the top, and the basemat below. Two MCOs are placed in each storage tube in a vertical column. The operations floor at the top of the tubes is 1.2-m- (4-ft-) thick concrete. Each tube is a penetration in the operating floor that extends down to the vault floor. A 30-cm (12-in.) impact limiter is located at the bottom of each tube and between the two MCOs in a tube. The vault walls are closest along the 22-tube side, but over 3 m (10 ft) distant on the 10-tube side.

The MCNP results in Table 6-6 are for normally loaded MCOs inside tubes at the CSB and inside the MHM. The fuel is contained in the 23-in.-diameter baskets. MCOs with Mark IV fuel are modeled with three central baskets of 54 fuel assemblies each and scrap in the top and bottom baskets. MCOs with Mark IA fuel are modeled with four central baskets of 48 intact fuel assemblies each and scrap in the top and bottom baskets. For Cases ocl.1 and ocl.2, the concrete walls are modeled only 27 and 28 in. from the center line of the CSB storage tube at the edge of the 10 by 22 unit array. The four cases in Table 6-6 give the k_{eff} for normal, dry MCOs containing air with water vapor at 0.0051 g/cm^3 (3 kg of water per MCO), which is a conservative estimate of twice the expected residual water in the fuel after hot conditioning. The space between the MCO and CSB storage tube and the space between storage tubes is modeled with a water density of vapor (0.0012 g/cm^3). At that density the intertube moderating effect of water vapor has fallen below the maximum and is equivalent to zero water for having humidity in the air between the tubes.

The MCOs are raised and lowered through the concrete floor and moved to and from the HCS Annex using the MHM. An MCO in the HCS is modeled surrounded by a 1-ft-thick cylinder of concrete at a radial distance of 1 ft. When an MCO is removed from or inserted into a storage tube, it is closely surrounded for 4 ft along its length by the operating deck slab. An MCO closely reflected by thick concrete will be analyzed in Section 6.5. However, the greatest reflection during its movement in the CSB is when the MCO is in the MHM closely reflected by 10 in. of stainless steel. A single MCO is modeled with stainless steel directly around and above, with thick concrete below.

Case ocl.4 (Table 6-6) has dry Mark IA fuel in the center baskets and scrap in the top and bottom baskets. The k_{eff}, 0.3041, plus two standard deviations (σ = 0.0017) is 0.3075. Case ocl.5 (Table 6-6) has dry Mark IV fuel in the center baskets and scrap in the top and bottom baskets. The k_{eff}, 0.3280, plus two standard deviations (σ = 0.0015) is 0.3311. For the two types of fuel in a normal arrangement with maximum reflection for normal CSB activities, the upper 95% confidence level k_{eff} is less than 0.35. This result shows that when the MCO is moved, under normal conditions and in normal work areas, there is a significant reactivity margin for criticality safety.

Table 6-6. Analysis Results for Normally Loaded Multicanister Overpacks Inside the Canister Storage Building and Multicanister Overpack Handling Machine.

File ID	Fuel type	Payload cluster		Water density (g/cm^3)		Calculation results[a]		
		Number of baskets	Assemblies per basket	MCO interior	Between storage tubes and outside MCOs	k_{eff}	Std. dev.	95% CI k_{eff}
ocl.1	Mark IA[b]	1 top 4 middle 1 bottom	1.25 wt% ^{235}U scrap 48 Mark IA 1.25 wt% ^{235}U scrap	0.0051	0.0012 (vapor)	0.3789	0.0005	0.3799
ocl.2	Mark IV[b]	1 top 3 middle 1 bottom	0.95 wt% ^{235}U scrap 54 Mark IV 0.95 wt% ^{235}U scrap	0.0051	0.0012 (vapor)	0.3719	0.0006	0.3731
ocl.4	Mark IA[c]	1 top 4 middle 1 bottom	1.25 wt% ^{235}U scrap 48 Mark IA 1.25 wt% ^{235}U scrap	0.0051	N/A	0.3041	0.0017	0.3075
ocl.5	Mark IV[c]	1 top 3 middle 1 bottom	0.95 wt% ^{235}U scrap 54 Mark IV 0.95 wt% ^{235}U scrap	0.0051	N/A	0.3280	0.0015	0.3311

[a] The limiting value for k_{eff} should be considered 0.945 to allow for a code bias of -5 mk (see Section 6.6.3).
[b] Model using 10 x 22 x 2 array of MCOs in CSB storage tubes with concrete walls, floors and walls. Fuel density corresponds to the actual 10 x 22 x 2 hexagonal array of CSB.
[c] MCO stored in MHM. Modeled as having 10 in. of steel on top and side, and a 2-ft-thick concrete floor below.

CI = confidence interval.
MCO = multicanister overpack.
N/A = not applicable.

The thick steel shielding in the MHM and the concrete in the HCS isolate the MCO neutronically, so interaction with external fissile material is not a consideration. Also, extracting an MCO through the CSB operating deck would decrease its reactivity by distance and isolation because of the deck and MHM.

The MCNP results in Table 6-7 present the normal array reactivity. Intact Mark IV fuel is modeled in all five baskets of the MCO with 54 fuel elements per basket or in the three central baskets with scrap in the top and bottom baskets. MCOs with Mark IA fuel are modeled with four central baskets of 48 intact fuel assemblies each and scrap in the top and bottom baskets. The four cases in Table 6-7 give the k_{eff} for normal, dry cases. The air inside the MCO is modeled as water vapor at 0.0012 g/cm^3 or at a conservative estimate of twice the expected residual 3 kg of water per MCO water in the fuel after hot drying (0.0051 g/cm^3 of water [3 kg of water per MCO]). The space between the MCO and CSB storage tube and the space between storage tubes is modeled with a water density of vapor (0.0012 g/cm^3). At that density the intertube moderating effect of water vapor has fallen below the maximum and is equivalent to zero water for having humidity in the air between the tubes.

Case plan_149 (Table 6-7) has all intact, dry, Mark IV fuel in a 24-in.-diameter basket. The other cases have intact fuel in the center baskets and scrap in the top and bottom baskets, with a basket diameter of 23 in. Cases csb04 and csb03 (Table 6-7) model the 10 by 22 array of storage tubes using the two fuel enrichments and concrete walls, basemat, and operating deck, which is at the level of the top of the storage tubes. The operating deck is modeled as 4 ft thick and the walls and floors 1 ft thick. These two cases model conservatively the moisture expected in the MCOs and the humidity that could be in the space around the tubes. For these two normally loaded cases, the k_{eff} is less than 0.4. The normally loaded CSB vault is safely subcritical and well within the allowable reactivity limit. These results demonstrate conclusively that for normal conditions, the reactivity of dry MCOs in the CSB storage tubes is very low.

Case ocl.3 (Table 6-7) models an infinite array of storage tubes with the same vertical fuel and reflector arrangement as case ocl.2 (Table 6-6). As expected, the k_{eff} for an infinite array is larger, although not by a significant amount, than the 10 by 22 array surrounded by walls of concrete.

6.4.4 Cold Vacuum Drying Facility

The CVDF, shown in Figure 6-14, has five processing bays, four active and one spare, that each house a transfer cask trailer containing a single cask-MCO. The transfer cask has a shielded central region and a removable lid; each cask contains a single MCO.

The transfer cask trailer is received at the CVDF with the MCO flooded and the shielded region containing the MCO dry and covered. After the trailer is secured in a CVDF processing bay, the lid of the cask is removed and water is piped through a process line into the transfer cask annulus completely surrounding the MCO with water. The water in the cask annulus outside the MCO will be heated, if needed, to facilitate vacuum drying. A process suction line is connected to the MCO and the water inside the MCO is pumped out.

Table 6-7. Analysis Results for Normally Loaded Multicanister Overpacks in the Canister Storage Building.

File ID	Fuel type	Payload cluster		Water density (g/cm^3)		Calculation results[a]		
		Number of baskets	Assemblies per basket	MCO interior	Between storage tubes and outside MCOs	k_{eff}	Std. dev.	95% CI k_{eff}
plan_149	Mark IV[b]	5	54	0.0012	0.0012 (vapor)	0.3841	0.0020	0.3880
csb04	Mark IA[c]	1 top 4 middle 1 bottom	1.25 wt% ^{235}U scrap 48 Mark IA 1.25 wt% ^{235}U scrap	0.0051	0.0012 (vapor)	0.3789	0.0008	0.3804
csb03	Mark IV[c]	1 top 3 middle 1 bottom	0.95 wt% ^{235}U scrap 54 Mark IV 0.95 wt% ^{235}U scrap	0.0051	0.0012 (vapor)	0.3729	0.0007	0.3744
ocl.3	Mark IV[d]	1 top 3 middle 1 bottom	0.95 wt% ^{235}U scrap 54 Mark IV 0.95 wt% ^{235}U scrap	0.0051	0.0012 (vapor)	0.3997	0.0018	0.4033

[a] The limiting value for k_{eff} should be considered 0.945 to allow for a code bias of -5 mk (see Section 6.6.3).
[b] Mark IV type neglects the tie rod at center, which excludes the center assembly in the array. MCOs are in a 10 x 22 lattice with two MCOs placed within each storage tube. One-foot-thick concrete walls are modeled on four sides and the floor, but not the top.
[c] Model of actual 10 x 22 x 2 hexagonal array of MCOs in CSB storage tubes with concrete walls, floor, and walls.
[d] Modeled as an infinite array of CSB storage tubes with two MCOs and concrete above and below.

CI = confidence interval.
MCO = multicanister overpack.

Figure 6-14. Typical Processing Bay at the Cold Vacuum Drying Facility.

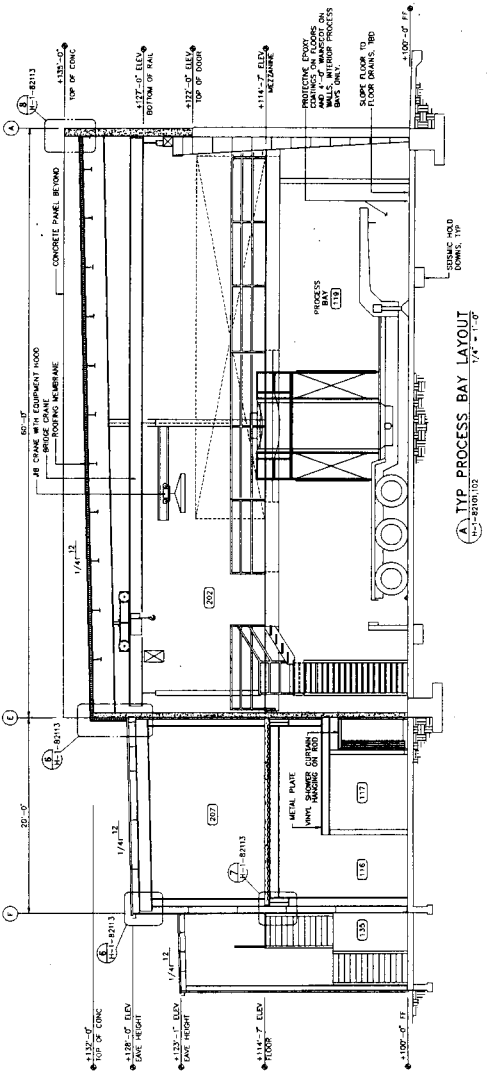

The waste water from the MCO is pumped to a 1,135-L (300-gal) tank in the radioactive liquid waste system. Water from the 1,135-L (300-gal) tank is filtered and transferred to the 18,900-L (5,000-gal) storage tank. After the bulk water is removed, the MCO is further vacuum dried.

The results of MCNP computer calculations provided in Table 6-8 show the reactivities of normally loaded MCOs. An MCO containing Mark IV fuel is loaded with five baskets, the central three baskets each loaded with 54 intact Mark IV fuel elements and the baskets on the top and bottom loaded with scrap pieces from Mark IV fuel. An MCO containing Mark IA fuel is loaded with six baskets, the central four baskets each loaded with 48 intact Mark IA fuel elements and the baskets on the top and bottom loaded with scrap pieces from Mark IA fuel. The Mark IA fuel in the scrap baskets is assumed to have an enrichment of 1.25 wt.% ^{235}U. Each MCO is isolated neutronically by the cask shielding region from other MCOs and fissionable material outside the transfer cask. The MCO and the cask's outer annulus are assumed to be flooded, which is the most reactive and limiting situation. Cases 1 and 2 in Table 6-8 represent the Mark IA and Mark IV MCOs with the MCO and cask annulus flooded and the lids in place on the transfer cask. Cases 3, 4, 5, 6, 7, and 8 represent variations of Mark IA and Mark IV fuel with the MCO either dry or wet and the cask annulus either dry or wet. The 95% confidence level reactivities do not exceed 0.90 for any of these cases. All of these reactivities are well below the criticality safety limit.

6.4.5 Sensitivity Studies

A number of design variable uncertainties (i.e., an assortment of fuel assembly lengths, unresolved cask dimensions, and degrees of fuel corrosion) affect the MCO reactivity. Base case calculations were performed with conservative assumptions (e.g., the longest lengths for Mark IV and Mark IA fuel assemblies, extremes of unresolved design dimensions, and optimum or full moderator densities). The following cases show the relationship of MCO reactivity to several examples of design variable uncertainties.

6.4.5.1 Fuel Length. The Mark IA and Mark IV fuel assemblies were manufactured in discrete lengths. The longest Mark IA fuel assembly is 53.0 cm (20.88 in.) and the longest Mark IV fuel assembly is 66.3 cm (26.1 in.). The reactivities of flooded MCOs loaded using these fuel lengths are listed in Table 6-8. Cases 1 and 2 in Table 6-9 are flooded MCOs loaded with Mark IA fuel assemblies that are 49.8 cm and 37.8 cm long in the four central baskets. Cases 3, 4, and 5 in Table 6-9 are flooded MCOs loaded with Mark IV fuel assemblies that are 62.5 cm, 58.9 cm, and 44.2 cm long in the three central baskets. The mean and 95% confidence level reactivities of these cases show a modest sensitivity to the fuel length variations. The maximum k_{eff} for an MCO loaded with 49.8-cm Mark IA assemblies was approximately 4 mk above the longest-length fuel assemblies. Mark IV fuel reactivity decreased for all lengths shorter than 66.3 cm, with a maximum decrease of about 7 mk for the fuel length corresponding to 58.9 cm.

Table 6-8. Analysis Results for Normal Multicanister Overpack Shipping Casks in the Cold Vacuum Drying Facility.

Case ID	File ID	Fuel type	MCO water density	Cask annulus density	Number of scrap baskets	Comments	Calculation results*		
							k_{eff}	Standard deviation	95% CI k_{eff}
1	ocvd1.1	Mark IA	1.0	1.0	2	Flooded MCO, annulus	0.8826	0.0031	0.8888
2	ocvd1.2	Mark IV	1.0	1.0	2	Flooded MCO, annulus	0.8894	0.0023	0.8940
3	ocvd1.3	Mark IA	0.0051	1.0	2	Dry MCO, flooded annulus	0.3768	0.0017	0.3801
4	ocvd1.4	Mark IV	0.0051	1.0	2	Dry MCO, flooded annulus	0.3877	0.0018	0.3912
5	ocvd1.5	Mark IA	1.0	0.0012	2	Flooded MCO, dry annulus	0.9017	0.0028	0.9072
6	ocvd1.6	Mark IV	1.0	0.0012	2	Flooded MCO, dry annulus	0.9000	0.0025	0.9049
7	ocvd1.7	Mark IA	0.0051	0.0012	2	Dry MCO, annulus	0.2995	0.0011	0.3017
8	ocvd1.8	Mark IV	0.0051	0.0012	2	Dry MCO, annulus	0.3216	0.0016	0.3248

*The limiting value for k_{eff} should be considered 0.945 to allow for a code bias of -5 mk (see Section 6.6.3).

CI = confidence interval.
MCO = multicanister overpack.

Table 6-9. Analysis Results for Multicanister Overpack Shipping Cask Sensitivity Studies. (2 sheets)

Case ID	File ID	Fuel type	MCO water density	Cask annulus density	Number of scrap baskets	Comments	Calculation results*		
							k_{eff}	Standard deviation	95% CI k_{eff}
1	ocvd4.1	Mark IA	1.0	1.0	2	4 baskets of 49.8 cm fuel	0.8877	0.0036	0.8949
2	ocvd4.2	Mark IA	1.0	1.0	2	4 baskets of 37.8 cm fuel	0.8808	0.0031	0.8869
3	ocvd4.3	Mark IV	1.0	1.0	2	3 baskets of 62.5 cm fuel	0.8837	0.0024	0.8885
4	ocvd4.4	Mark IV	1.0	1.0	2	3 baskets of 58.9 cm fuel	0.8817	0.0034	0.8884
5	ocvd4.5	Mark IV	1.0	1.0	2	3 baskets of 44.2 cm fuel	0.8852	0.0028	0.8908
6	ocvd4.11	Mark IV	1.0	1.0	2	3 baskets of intact fuel mass reduced by 10%	0.8891	0.0028	0.8947
7	ocvd4.12	Mark IV	1.0	1.0	2	3 baskets of intact fuel mass reduced by 20%	0.8883	0.0032	0.8947
8	ocvd4.13	Mark IV	1.0	1.0	2	3 baskets of intact fuel mass reduced by 30%	0.8808	0.0029	0.8866
9	ocvd4.14	Mark IV	1.0	1.0	2	3 baskets of intact fuel mass increased by 100 kg UO_2	0.8680	0.0025	0.8730
10	ocvd4.15	Mark IV	1.0	1.0	2	3 baskets of intact fuel mass increased by 200 kg UO_2	0.8552	0.0023	0.8597

Table 6-9. Analysis Results for Multicanister Overpack Shipping Cask Sensitivity Studies. (2 sheets)

Case ID	File ID	Fuel type	MCO water density	Cask annulus density	Number of scrap baskets	Comments	Calculation results*		
							k_{eff}	Standard deviation	95% CI k_{eff}
11	ocvd4.16	Mark IV	1.0	1.0	2	3 baskets of intact fuel mass increased by 300 kg UO_2	0.8463	0.0028	0.8519
12	ocvd4.17	Mark IV	1.0	1.0	2	0.5 in. decrease of cask annulus region	0.8991	0.0028	0.9047
13	ocvd4.18	Mark IV	1.0	1.0	2	0.5 in. increase of cask annulus region	0.8829	0.0028	0.8885
14	ocvd4.19	Mark IV	1.0	1.0	2	1.0 in. increase of cask annulus region	0.8793	0.0030	0.8853
15	ocvd4.20	Mark IV	1.0	1.0	2	1.5 in. increase of cask annulus region	0.8776	0.0036	0.8848
16	ocvd4.21	Mark IV	1.0	1.0	2	2.0 in. increase of cask annulus region	0.8707	0.0031	0.8770

*The limiting value for k_{eff} should be considered 0.945 to allow for a code bias of -5 mk (see Section 6.6.3).

CI = confidence interval.
MCO = multicanister overpack.

6.4.5.2 Fuel Mass. The next two sets of sensitivity cases involve counteracting situations of realistic fuel mass being lost by corrosion before loading and of fuel mass being added in the lower baskets by corrosion particles of uranium oxide dropping from upper baskets. The second set of cases investigates the reactivity effect of fuel mass redistribution that was modeled as a conservative uniform mass increase in the MCO central intact fuel baskets.

Fuel mass will be lost from damaged fuel because of corrosion and because of cleaning of the fuel in the K Basins before the fuel is loaded into the MCOs. The effect on reactivity of this fuel mass loss is shown in Cases 6, 7, and 8 (Table 6-9), in which a uniform loss of mass in an MCO containing Mark IV fuel was modeled as a density reduction of 10%, 20%, and 30%, respectively. The mean and 95% confidence level reactivities of these cases show a slight and uncertain effect on reactivity for uniform mass loss at and below 20%. The results show a definite decrease of about 9 mk in reactivity corresponding to a decrease of 30% fuel density.

Fuel mass in each of the three intact fuel baskets was assumed to be increased by uranium oxide dropped from corroded Mark IV fuel and Mark IV fuel scrap in the upper baskets. The increased mass was assumed to be redistributed in the interstitial regions between fuel assemblies and in the coolant channels of the fuel assemblies. The effects on reactivity of this fuel mass increase are shown in Cases 9, 10, and 11 (Table 6-9), in which a uniform mass of 100 kg, 200 kg, and 300 kg of UO_2 was modeled as being distributed in the central three fuel baskets. The mean and 95% confidence level reactivities of these cases show a progressive decrease with increasing UO_2 mass when compared to Case 2 for the Mark IV MCO in Table 6-8.

6.4.5.3 Thickness of Cask Annulus Water. The effect of cask annulus water thickness on reactivity also was investigated. The reactivities determined are shown in Cases 12 through 16 in Table 6-9 for a Mark IV MCO. Case 12 assumed no cask annulus gap, and Cases 13 through 16 assumed progressive increments of 0.5 in. above the base case thickness of 0.5 in. These cases show that the reactivity progressively decreases with increasing cask annulus thickness.

6.4.5.4 Interspersed Moderator Density. Several calculations have been performed to address interspersed moderator density within the MCO. Both fully flooded and dry cases have been evaluated, as well as intermediate water densities that span the range from fully flooded to dry conditions (see Section 6.7.2). Explicit calculations treating partially water-filled MCOs have been performed. These cases, shown in Figure 6-15, indicate a slight k_{eff} peak greater than the fully flooded case. The increase in k_{eff} at the peak (above the fully flooded case) is only on the order of the 2σ error in the MCNP results, but the trend appears smooth. The "zero" water level corresponds to the axial mid-plane of the MCO, and arises from the coordinate system used in the MCNP input model. The lowest water level shown in Figure 6-15 corresponds to the lower scrap basket being half-flooded; the dry case is so unreactive (k_{eff} < 0.40) that the vertical scale becomes expanded to the point where the shape in the remaining curve becomes difficult to see.

Figure 6-15. k_{eff} Versus Water Level Internal to a Mark IV Loaded Multicanister Overpack.

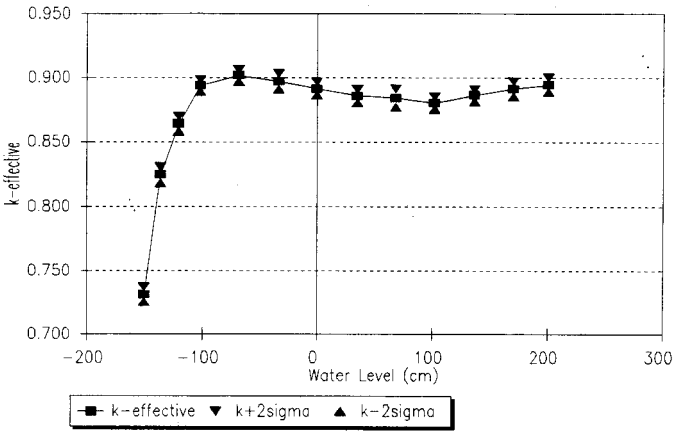

6.4.5.5 Plutonium Buildup on Scrap. Optimal scrap is treated as unexposed fuel pieces, with no plutonium buildup. One concern has been that plutonium buildup on the exterior surface of fuel elements might preferentially corrode off the element and contribute to more highly reactive scrap pieces in basin sludge. This question has been addressed for decladding waste streams sent to the Hanford Site Tank Farms (Rogers et al. 1996, Schwinkendorf 1996). While enhanced plutonium buildup near the outer surface of nuclear fuel (not just Hanford Site reactor fuel) is well known, the peaking factor (which may be defined as the plutonium concentration at the surface divided by the fuel average plutonium concentration) is not much greater than a factor of two. Enhanced ^{235}U depletion also occurs at the fuel surface. Criticality is affected by both the ^{239}Pu buildup and the ^{235}U depletion. However, fuel corrosion tends to progress axially from damaged ends and not radially inward. Additional parametric studies may be pursued in the future, but this is not expected to be a significant factor.

6.4.5.6 Lattice Spacing. The MCO analyses use a center-to-center hexagonal spacing of 2.8 in. for fuel assemblies. The spacing is established by rings on the bottom of the fuel baskets. Previous analyses have shown that the optimal spacing of N Reactor fuel in water is around 3.1 in. Using a larger spacing would make loading the MCO containers easier, but it also would increase the reactivity of the lattice, because the original design was undermoderated.

The effect of fuel assembly spacing was analyzed using MCNP calculations for the geometric arrangement shown in Figure 6-16, but with lattice spacing increased to 2.9 and 3.0 in. The 3.0-in. spacing is difficult to pack into the MCO because the outermost 12 assemblies impact the inner wall of the MCO. If these outermost 12 assemblies are removed, a spacing of 3.1 in. is possible. This fuel arrangement is shown in Figure 6-16.

Figure 6-16. Reduced Loading for Mark IA Fuel in Multicanister Overpack (12 Assemblies Removed).

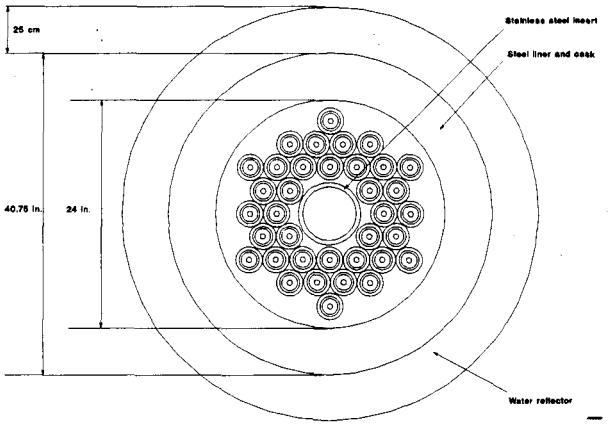

Figure 6-17 shows MCNP results for the effect on k_{eff} of lattice spacing and the removal of 12 fuel assemblies. The removal of 12 elements reduces the reactivity and does not present a potential problem if the baskets are not fully loaded. The nominal basket diameter is equal to 22.6 in., and the diameter for a drop accident fuel basket is 23.25 in. The maximum lattice spacing for a 22.6-in. diameter basket is 2.86 in. Dividing an additional quarter inch among six lattice elements on all dimensions would give a maximum hexagonal spacing of less than 2.9 in. With the spacing of the bottoms of the fuel at 2.8 in. and the unrestrained tops at 2.9 in., the average spacing would be 2.85 in. The increase in k_{eff} for the half-inch increase in lattice spacing is less than 0.004, as shown in Figure 6-17. This effect of increased fuel element spacing at the unrestrained tops of the intact fuel elements is small and will be neglected. Since decreasing the lattice spacing decreases the k_{eff}, ring spacing on the fuel bottom plates of less than 2.8-in. is conservatively covered by this analysis. The actual lattice spacing of 2.77 in. is conservatively approximated by 2.8 in.

Figure 6-17. k_{eff} Versus Lattice Spacing - Mark IA Fuel Assemblies.

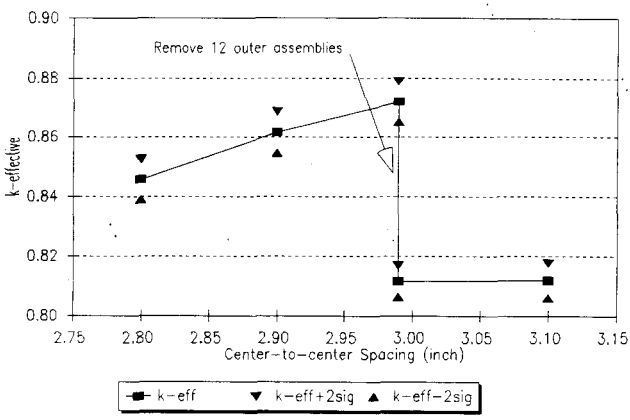

6.4.5.7 Partial Fuel Loading. The effect of removing certain fuel assemblies, leaving "holes" in the loading pattern, also was analyzed. The lattice is slightly undermoderated, so there was concern that a partial loading might result in a higher k_{eff} as the fuel was loaded into the MCO. Figure 6-18 shows the decrease in k_{eff} as the number of fuel assemblies drops from 48 to 42. These results show that even though the fully loaded lattice is slightly undermoderated, partial fuel loading will still be less reactive than the fully loaded case because there is less fissile material in a finite system. The k_{eff} is affected more by total fissile material than by the spacing. When loading fuel, adding parts of elements should be less reactive than whole elements. Loading outer elements first, or parts of a fuel element, would be bounded by the total mass of fissile material in whole elements. Figure 6-17 shows that as fuel assemblies are removed, the k_{eff} will decrease.

6.4.5.8 Loading Mark IA Outer Elements Only. This section demonstrates the reactivity effect of partially filled baskets that will occur during the retrieval process. When loading the MCO fuel baskets with intact fuel assemblies, the plan is to first load each basket with outer elements, and then insert inner elements into the outer elements. This is a variation on what was analyzed in the previous section, where six whole assemblies were removed from the loading pattern. Because the lattice is slightly undermoderated at a pitch of 2.8 in., removal of some fuel was thought to potentially increase reactivity. Removing all inner elements removes fuel more uniformly than extracting whole assemblies. Mark IA outer elements become optimal (have minimal critical mass) at a spacing of 2.9 to 3.0 in. center-to-center in a hexagonal lattice. This is less than the optimal 3.1-in. lattice spacing for intact assemblies. If the fuel baskets are loaded with only Mark IA outer elements, the lattice is somewhat closer to optimal

Figure 6-18. Partial Loading of Fuel - Mark IA Fuel Assemblies.

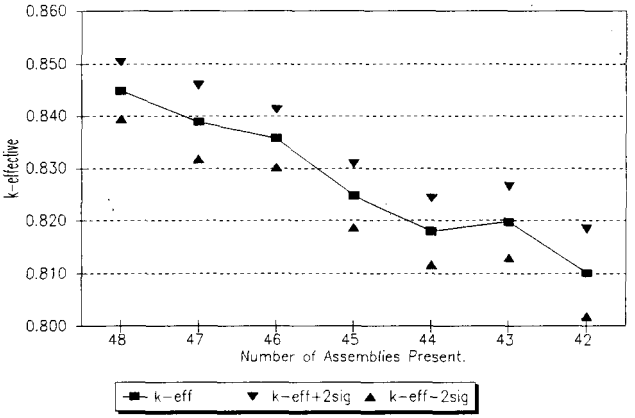

spacing. The Mark IA base case was redone with all Mark IA inner elements removed, and the result was a k_{eff} of 0.8804 ± 0.0031 (0.8866 at the upper 95% confidence level). Comparing this with the nominal value, k_{eff} equals 0.8826 ± 0.0031 (0.8888 at the upper 95% confidence level) leads to the conclusion that removing fissile material from a finite system with significant radial leakage overrides the infinite lattice effects and the k_{eff} actually decreases.

6.4.5.9 Fuel Temperature. The effect of temperature on reactivity was evaluated for both Mark IV and Mark IA fuel assemblies. The WIMS-E lattice code (Gubbins et al. 1982) was used to calculate the lattice k_∞ and Doppler coefficient for both Mark IV and Mark IA fuel as a function of temperature. The Doppler coefficient may be approximated between two discrete temperatures using the following relationship:

$$\alpha(T) \equiv \left.\frac{\partial \rho}{\partial T}\right|_r \approx \left.\frac{\Delta \rho}{\Delta T}\right|_r = \frac{10^5 \left(k_\infty(T+\Delta T) - k_\infty(T-\Delta T)\right)}{k_\infty(T+\Delta T)\, k_\infty(T-\Delta T)\, (2\Delta T)} \text{ pcm/K.}$$

The 10^5 multiplier in the above equation converts the raw reactivity, $\Delta\rho$, into units of pcm, or percent milli-k. Figure 6-19 illustrates the lattice k_∞ and Doppler coefficients as functions of temperature for both of these fuel types. As expected, both N Reactor fuel types have negative Doppler coefficients because of their large ^{238}U contents. Mark IV fuel exhibits a slightly more negative Doppler coefficient than Mark IA fuel because the ^{238}U

content is greater. At room temperature (MCNP calculations reported in this chapter were performed at 300 K), the Doppler coefficients are approximately equal to -3 pcm/K. As temperature increases, the Doppler coefficients become less pronounced. The somewhat erratic behavior of the Doppler coefficients is caused by finite code convergence; differentiation amplifies any nonuniformity in the k_∞ results. Estimating the change in k_{eff} for an MCNP calculation at a different temperature can be accomplished by reference to Figure 6-I9. At room temperature (300 K), the Doppler coefficient for Mark IV fuel is shown in Figure 6-19 to be -3 pcm/K. For a temperature of 10 °C (283 K), this represents a reduction of 17 °C from 300 K. The estimated change in k_{eff} would be an increase of approximately 50 pcm, or 0.5 mk, which is trivial compared to the 1σ error in typical MCNP results.

Figure 6-19. Lattice k_∞ and Doppler Coefficients for N Reactor Fuel Assemblies.

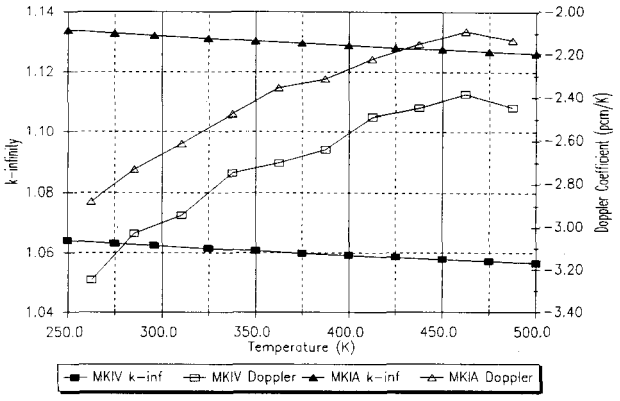

6.4.5.10 Dimensional Tolerance. The effect of dimensional tolerance on reactivity was analyzed parametrically by a series of calculations using the WIMS-E code (Gubbins et al. 1982). Table 6-10 contains the radial dimension specifications for Mark IV and Mark IA fuel types (Jack 1988). Table 6-11 shows the variation in lattice k_∞ as the radial fuel dimensions are varied. Either minimum or maximum dimensions were selected to arrive at either minimum or maximum uranium fuel region thicknesses. In all cases, the fuel assemblies were placed in an infinite water lattice at optimal spacing. The sensitivity of reactivity to radial dimension tolerances is shown to be less than 1 mk.

Table 6-10. Radial Dimension Specifications for N Reactor Mark IV and Mark IA Fuel Assemblies.

	Mark IA (in.)	Mark IV (in.)
Outer element:		
Outer diameter	2.391 - 2.416	2.410 - 2.435
Inner diameter	1.754 - 1.779	1.691 - 1.716
Inner element:		
Outer diameter	1.237 - 1.256	1.267 - 1.286
Inner diameter	0.431 - 0.450	0.473 - 0.492

Table 6-11. Sensitivity of Lattice k_∞ to Radial Dimension Tolerances.

	Mark IA	Mark IV
Minimum uranium thickness	1.131423	1.062878
Nominal uranium thickness	1.132133	1.062349
Maximum uranium thickness	1.132055	1.061646

6.4.5.11 Enrichment Tolerance. The effect of enrichment tolerance on reactivity was analyzed parametrically by a series of calculations using the WIMS-E code (Gubbins et al. 1982). The enrichment tolerance for N Reactor fuel was equal to 0.006 wt% ^{235}U (Gant and Zilar 1977). Table 6-12 shows the variation in lattice k_∞ as the fuel enrichment was either increased or decreased by 0.006 wt% ^{235}U. In all cases, the fuel assemblies are placed in an infinite water lattice at optimal spacing. The sensitivity of reactivity to enrichment tolerance has been shown to be approximately ±2 mk for a ±0.006 wt% ^{235}U enrichment variation.

Table 6-12. Sensitivity of Lattice k_∞ to Enrichment Tolerances.

	Mark IA	Mark IV
Minimum uranium enrichment	1.130463	1.060261
Nominal uranium enrichment	1.132133	1.062349
Maximum uranium enrichment	1.133780	1.064408

6.4.5.12 Packing Fraction. The packing fraction is the volume fraction of fuel in the unit lattice. An optimal packing fraction was used for scrap with both size and spacing varied to maximize reactivity. This packing fraction varies according to enrichment but is equal to 0.320 for Mark IV scrap and 0.294 for Mark IA scrap. Curves showing optimal reactivity are presented in Section 6.7. A value of 0.40 was used to represent rubble formed from crushed fuel from the drop accident. This packing fraction is adequately conservative. It is close to the lattice packing fractions of 0.443 for intact Mark IV fuels and 0.392 for intact Mark IA fuels. A more realistic packing fraction representing rubble will be larger than this assumed value and will decrease the MCO reactivity. For Mark IV rubble, the lattice k_∞ is reduced from 1.08978 for the optimal configuration (scrap) to 1.07757 (for a packing fraction of 0.40). For Mark IA rubble, the lattice k_∞ is reduced from 1.15472 for the optimal configuration (scrap) to 1.13399 (for a packing fraction factor of 0.40). Still more reactivity loss would be experienced for higher packing fractions, as this would drive the system to be even more undermoderated.

6.5 CONTINGENCY ANALYSIS

6.5.1 Summary and Conclusions

This section of the analysis describes the contingency conditions of the MCO in the K Basins, the CSB, and CVDF. The MCOs under contingency conditions in these facilities are analyzed, and the resulting neutron multiplication factors are compared to the allowable limit. The comparison shows that the design of the MCO is constrained in order to meet the multiplication safety limit of 0.95.

The most significant accident condition is the 100 *g* cask drop. It could rubblize the fuel elements and increase the reactivity of those baskets. For basket diameters of 23.25 in. and a maximum rubble packing factor of 0.40, and including the steel of the basket in the baseplate, the MCO design meets the criticality safety limits. If baskets collapse into a stack, the resulting upper tolerance limit values are close to allowable limits. The basket integrity in the drop accident is still under review. If baskets can collapse, further analysis using more realistic characterization will need to show conclusively that basket collapse is acceptable.

Mark IA fuel (1.25 wt% ^{235}U enrichment) baskets have a central spacer to exclude fuel from the higher reactivity space. The drop accident could offset that spacer. The analysis shows that the spacer design is to allow only a 2-in. offset in the drop accident. At that offset, the upper tolerance for the multiplication value is within acceptable limits.

An MCO was analyzed for misloading one canister of Mark IA fuel instead of the lower enrichment Mark IV fuel. For both intact fuel elements and scrap, the results were within allowable limits for MCOs alone, in a cask, or in the CSB.

For dry MCOs in the CSB, the reactivity is low. Only adding water can increase the reactivity. Analysis of adding water and even misloading an MCO

with one contingency of higher enrichment fuel does not exceed allowable limits. The passage of an MCO from the MHM to the storage tube was analyzed. For each material as reflector, the MCO was within limits for dry and flooded conditions.

The analysis shows that for a third scrap basket in the flooded MCO in its cask at the CVDF, the upper tolerance values are within allowable limits. Adding a third scrap basket is considered to be the worst contingency expected for the CVDF.

6.5.2 Multicanister Overpack Drop

For the 100 *g* drop accident, the fuel assemblies are changed to rubblized fuel. Cladding is assumed to remain in place metallurgically bonded to the uranium scrap. Calculations have shown that the maximum reactivity remains about the same with or without cladding; just the rod size and spacing changes. The total uranium is conserved from before the drop. Under these constraints, a rod diameter is used to maximize the reactivity of the rubble model. For 0.95 wt%, 1.15 wt%, and 1.25 wt% enriched uranium metal, the size and spacing optimize in such a way that the water-to-uranium volume ratio is higher than would typically be expected in a packed debris bed; the optimal packing fraction for scrap rods is on the order of 30% to 35%. The model uses a conservative packing fraction of 0.40. Experience with random, packed beds indicates that a packing fraction of 64% is more typical for irregularly shaped pieces (Berryman 1983); using the more typical packing fraction drives the lattice far below critical because of undermoderation.

MCNP calculations were performed that considered neutron absorption provided by structural materials. These included the perforated stainless steel baseplates, stainless steel baskets, and the central steel pipes in the fuel baskets. After impact, the basket material was modeled as part of the baseplate. The pipe was modeled as-is. The stainless steel basket material and perforated baseplates were conservatively modeled as solid 0.38-in. plates between the fuel in the baskets. The inside diameter of the fuel was assumed to increase to 23.25 in. because the MCO restrains further radial expansion of rubblized fuel.

MCNP results for a flooded MCO loaded with scrap are contained in Table 6-13. In calculation plan b77, all of the rubble is assumed to be 1.15 wt% ^{235}U enriched rods. The nominal k_{eff} is greater than the 0.945 allowable limit. The assumptions for this result are that the scrap is optimally sized and spaced rods without cladding material present.

Calculation plan 140 includes the cladding material in the optimized lattice. This calculation is below the 0.945 criterion at the upper 95% confidence level. This is representative of the k_{eff} of the MCO during a transient phase — the MCO is in free fall after impacting and before everything has come to rest. Credit may not be taken during this phase for gravity compaction of the debris, and the debris pieces may be free to arrange themselves into optimal spacing.

Table 6-13. Analysis Results for Flooded Multicanister Overpack Shipping Casks Loaded with Scrap.

Case ID	Fuel type[a]	Cladding	Packing factor	Basket spacing[b] (in.)	Other	Calculation results[c]		
						k_{eff}	Std. dev.	95% CI k_{eff}
plan_b77	Mark IA	No	0.2962	0.375	Optimal sized and spaced rod fills basket	0.9485	0.0027	0.9538
plan_140	Mark IA	Yes	0.3011	0.375	48 Mark IA fuel mass	0.9355	0.0031	0.9417
plan_141	Mark IA	Yes	0.4	5.54	48 Mark IA fuel mass	0.8366	0.0025	0.8415
plan_154	Mark IA	Yes	0.4	0.375	48 Mark IA fuel mass	0.9049	0.0026	0.9100
plan_b93	Mark IV	No	0.3541	0.375	54 Mark IV fuel mass	0.9661	0.0028	0.9717
plan_142	Mark IV	Yes	0.3541	0.375	54 Mark IV fuel mass	0.9536	0.0025	0.9587
plan_143	Mark IV	Yes	0.4	3.37	54 Mark IV fuel mass	0.9159	0.0032	0.9223
plan_153	Mark IV	Yes	0.4	0.375	54 Mark IV fuel mass	0.9404	0.0031	0.9466
plan_155[d]	Mark IV	Yes	0.4	0.375	54 Mark IV fuel mass	0.9400	0.0012	0.9424

[a] Mark IV type neglects tie rod at center, which excludes center assembly in array. Mark IA has a 6-in.-diameter steel insert, excluding assemblies from seven central positions.
[b] Spacing between top of scrap or rubble and the bottom of scrap or rubble in the basket above.
[c] The limiting value for k_{eff} should be considered 0.945 to allow for a code bias of -5 mk (see Section 6.6.3).
[d] Same as plan_153, but four times the number of neutron histories were used to reduce the Monte Carlo statistical error.

CI = confidence interval.
MCO = multicanister overpack.

Calculation plan_141 assumes a more realistic packing fraction of 0.40, and that total uranium is conserved from fully loaded fuel baskets. The debris height is only 40 cm in each fuel basket, leaving standing water above this level. There is no debris assumed inside the 6-in. steel insert. This is representative of the k_{eff} of the MCO after everything has come to rest, and the debris has compacted and displaced water from the debris matrix, so an undermoderated system exists. Case plan_141 is much lower than Case plan_140, not only because of reduced moderation at the lattice level but because a 5.54-in. separation, filled with water (and the stainless steel baseplates), is assumed between the settled rubble in each basket. This layering of rubble and water provides significant neutronic isolation.

If the accident is severe enough, the axial positioning of the fuel baskets cannot be ensured. Case plan_154 assumes that all the fuel baskets have fallen down on each other, removing the water separation between the rubble-filled baskets. The k_{eff} is equal to 0.9100 at the upper 95% confidence level, still below the allowable limit of 0.945.

These analyses were repeated for MCOs containing Mark IV fuel. The bottom half of Table 6-13 presents the results. In calculation plan_b93, all of the scrap is assumed to be 0.95 wt% ^{235}U enriched rods. With all of the five baskets loaded with optimally spaced scrap, the nominal k_{eff} exceeds the 0.945 safety limit. The calculation assumes optimally sized and spaced rods with no credit taken for cladding material. When the cladding material is added in and the rod size is optimized for the total uranium in a full load of 54 assemblies, as in calculation plan_142, the value for k_{eff} drops to 0.95361 ± 0.0025 (0.9587 at the upper 95% confidence level). This is representative of the k_{eff} of the MCO during a transient phase — the MCO is in free fall after impacting and before everything has come to rest. Credit may not be taken during this phase for gravity compaction of the debris, and the debris pieces may arrange themselves into optimal spacing.

Calculation plan_143 assumes a more realistic packing fraction of 0.40, and the k_{eff} is reduced to 0.9159 ± 0.0032. The magnitude of the reduction in k_{eff} is less than for the Mark IA material because there is only about half as much water isolation between rubble layers. If the fuel baskets now slide down vertically so that there is no water between compacted fuel baskets (calculation plan_153), the k_{eff} increases to 0.9404 ± 0.0031, or 0.9466 at the upper 95% confidence level. This result is just slightly above the 0.945 safety limit. After recalculation using four times as many neutron histories, the statistical error decreased. The new result was a k_{eff} of 0.93995 ± 0.00122, or a k_{eff} of 0.9424 at the upper 95% confidence level, which does meet the 0.945 limit.

Figure 6-20 shows the calculated k_{eff} of an MCO loaded with Mark IA rubble, as a function of the central 6-in. pipe insert shifting offcenter. As the insert shifts offcenter, rubble is assumed to fill in the void, thus allowing the scrap to move to a region of the fuel basket of maximum neutron importance (i.e., the center). This figure is for a rubble diameter of 24 in. The calculated k_{eff} exceeds 0.945 at the upper 95% confidence level when the offset exceeds about 1.5 in. The MCO design will limit the rubble to a 23.25-in. diameter. CASE3 and CASE3A presented in Table 6-4 for the normal 6-in. pipe central insert and a thicker insert, with a 2-in. offset, were found to have values for k_{eff} of 0.916 and 0.938. The two cases also included

1.25 wt% ^{235}U scrap in the top and bottom baskets rather than 1.15 wt% ^{235}U rubble in these baskets. The results show that the design of the insert must restrain the Mark IA fuel material from the center region with an allowable offset from the center line of 2 in. or less for the drop accident. The thick insert will raise the reactivity, but not unacceptably.

Figure 6-20. k_{eff} Versus Insert Offset, All 1.15 wt% ^{235}U Rubble.

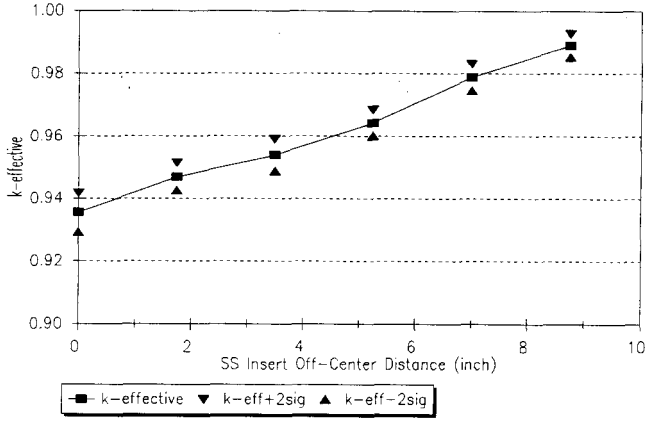

6.5.3 Mark IA Fuel and Scrap Loaded into Mark IV Baskets

This section and Table 6-14 present the effects of misloading MCOs with fuel and scrap. Each MCO analyzed contained five Mark IV baskets fully flooded and fully reflected by the cask steel and surrounding water. For the CSB, this represents the contingencies of flooding and multiple misloadings; for the CVDF, this represents multiple misloading contingencies. Because the Mark IV baskets have a small central tie rod and do not have the central 15.2-cm (6-in.) stainless steel insert pipe, they are capable of holding 54 fuel assemblies, six more than the Mark IA baskets. The normal loading of Mark IV MCOs is three central baskets containing intact Mark IV fuel and top and bottom baskets containing Mark IV scrap with an enrichment of 0.95 wt% ^{235}U. One or more of these baskets is misloaded for each case in Table 6-14. The MCO is in a cask that also is flooded between the MCO and the cask wall.

CASE7A in Table 6-14 (Figure 6-21) is for a single, flooded MCO containing a normal load of Mark IV fuel, except that one central Mark IV basket is filled with intact Mark IA fuel. The MCO is fully reflected by the steel of the cask and water surrounding it. The resulting k_{eff} is less than 0.9. Loading all three central baskets with Mark IA intact fuel results in a k_{eff} that is only slightly larger and still less than 0.9, which is less than the allowable value. The last three cases show the degree to which misloading

Table 6-14. Analysis Results for Mark IA Fuel and Scrap Misloaded in Flooded Multicanister Overpacks in Casks.

File ID	Basket contents by tier number[a]					Other details (fuel assemblies, scrap as unburned 0.95 wt% ^{235}U)	Fuel OD (in.)	Calculation results[b]		
	Tier 1	Tier 2	Tier 3	Tier 4	Tier 5			k_{eff}	Std. dev.	95% CI k_{eff}
CASE7A	0.95 wt% ^{235}U scrap	54 Mark IV	54 Mark IA	54 Mark IV	0.95 wt% ^{235}U scrap	Flooded MCO and cask, 1 fuel misloading	23.00	0.8872	0.0025	0.8922
CASE7B	0.95 wt% ^{235}U scrap	54 Mark IA	54 Mark IA	54 Mark IA	0.95 wt% ^{235}U scrap	Flooded MCO and cask, 3 fuel misloadings	23.00	0.8928	0.0031	0.8990
CASE7C	0.95 wt% ^{235}U scrap	54 Mark IV	54 Mark IV	54 Mark IV	1.25 wt% ^{235}U scrap	Flooded MCO and cask, 1 scrap misloading	23.00	0.9664	0.0030	0.9724
CASE7D	1.25 wt% ^{235}U scrap	54 Mark IV	54 Mark IV	54 Mark IV	1.25 wt% ^{235}U scrap	Flooded MCO and cask, 2 scrap misloadings	23.00	0.9804	0.0029	0.9863
CASE7	1.25 wt% ^{235}U scrap	54 Mark IA	54 Mark IA	54 Mark IA	1.25 wt% ^{235}U scrap	Flooded MCO and cask, all baskets misloaded	23.00	0.9744	0.0034	0.9812

[a] Tiers are numbered from the top of the MCO.
[b] The limiting value for k_{eff} should be considered 0.945 to allow for a code bias of -5 mk (see Section 6.6.3).

CI = confidence interval.
MCO = multicanister overpack.
OD = outer dimension.

Figure 6-21. Analysis Input Models CASE7 and CASE7A: Axial Geometry.

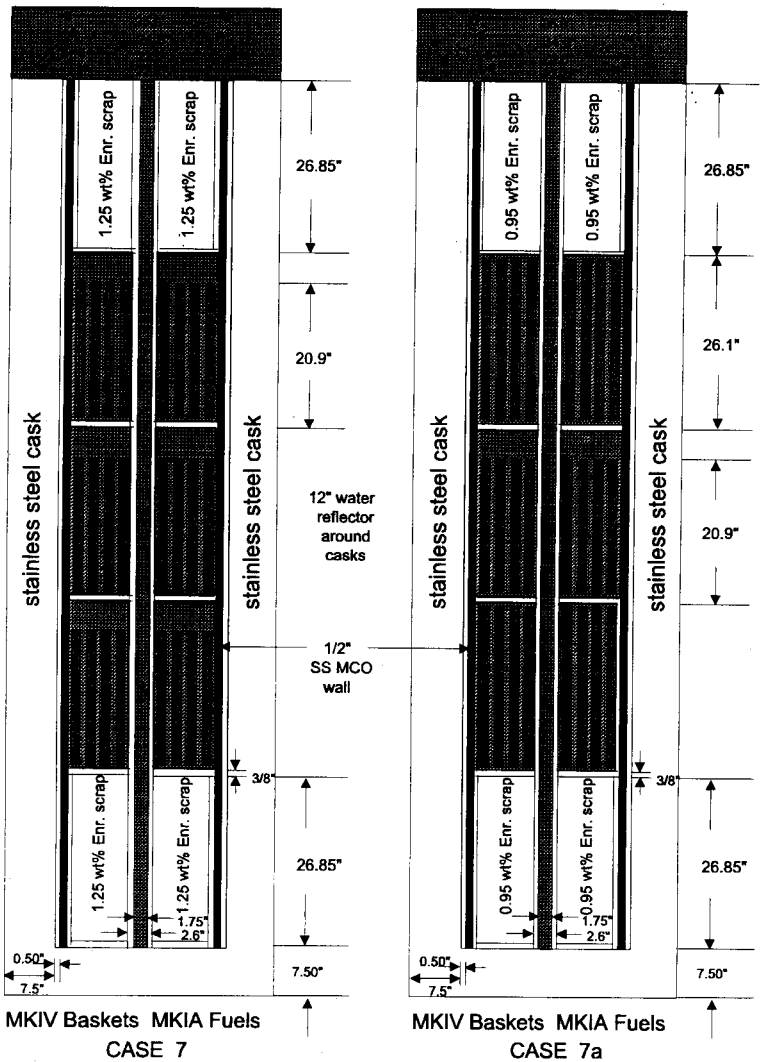

scrap in the top and/or bottom basket, and fully misloading all baskets with Mark IA fuel, raises the k_{eff} above the allowables. However, only 14 of the 54 or 48 fuel assemblies in a basket are loaded from a single K Basin canister. Selecting and loading a single Mark IA canister instead of a Mark IV canister is a contingency.

Only the K West Basin is allowed to have fuel enriched to greater than 0.95 wt% ^{235}U. The K West Basin does not have a significant amount of sludge on the basin floor, nor does the sludge contain a significant amount of fissile material. So the misloaded fuel or scrap must come from a misloaded or mislabeled canister. Because the canister was originally filled with whole fuel assemblies, the maximum enrichment would be 1.15 wt% ^{235}U. In spite of this, scrap is defined for this criticality analysis as optimally sized and spaced rods of the highest enrichment found in a particular type of fuel. Scrap originating from Mark IA fuel is therefore modeled as 1.25 wt% ^{235}U rods. A single contingency was analyzed in which one fuel canister containing Mark IA scrap, with the mass equivalent of 14 fuel assemblies, was misidentified and handled as though it were 0.95 wt% ^{235}U scrap. The mass equivalent of 14 assemblies of 1.25 wt% ^{235}U rods was inserted into one of the Mark IV scrap baskets in an otherwise normally loaded Mark IV MCO. The k_{eff} at the upper 95% confidence level was 0.925, which is well below the allowable limit of 0.945. Thus for a single contingency, the flooded MCO in a cask meets the double contingency principle. CASE7 (Figure 6-21) shows that for a completely flooded and misloaded MCO with Mark IA fuel and scrap in all Mark IV baskets in a cask, the system exceeds the allowable safety limit, but this case also exceeds the restraint of the double contingency principle for multiple contingencies.

Figure 6-22 shows the k_{eff} for flooded MCOs loaded with Mark IV fuel in the CSB array of storage tubes for a range of water densities between tubes. The curve rises only marginally, to a maximum of 0.93 at a water density of 0.002 g/cm^3. This figure shows that an infinite array of fully flooded MCOs loaded with Mark IV fuel in the CSB array will be within allowable limits for all values of interspersed moderation between the storage tubes.

6.5.4 Canister Storage Building

Table 6-6 has shown that the storage of dry MCOs in the CSB is significantly subcritical. The only occurrence that could raise the reactivity to a level of concern is to flood the MCOs. Putting an optimally dense water mist between the tubes could further optimize the system. The CSB has excluded a sprinkler system and has no other piped-in water, except limited piping for cooling the HCS. During staging and interim storage, the MCOs are to be sealed. The storage tube plugs utilize dual elastomeric O-ring seals. Flooding the MCOs is not considered credible. However, a still wet MCO may be delivered to the CSB. The effect of flooding on reactivity is calculated to show that even this event is within allowable limits. The reactivity of moving an MCO in the MHM and in and out of the storage tubes through the concrete floor is calculated. The effect of having a misloaded MCO also is investigated.

Figure 6-22. Interspersed Moderation for Flooded Mark IV Multicanister Overpacks in the Canister Storage Building.

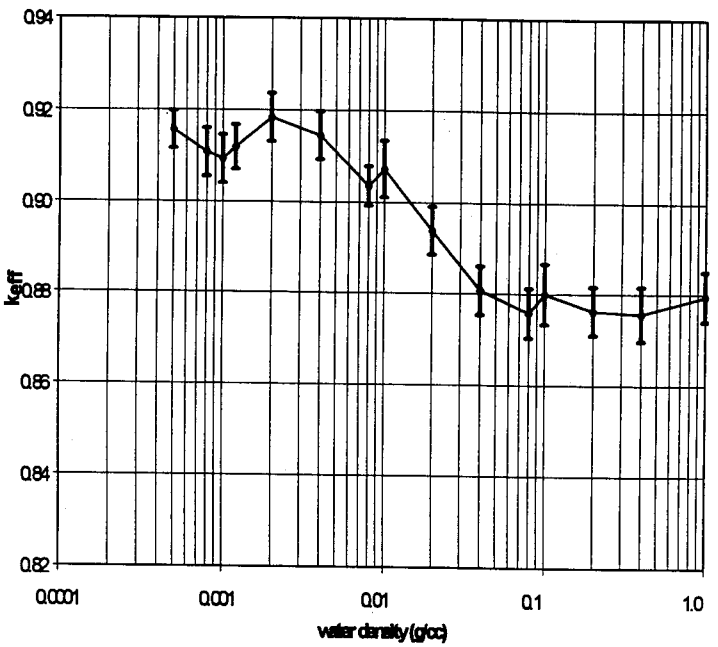

6.5.4.1 Multicanister Overpack in the Multicanister Overpack Handling Machine. The MHM is modeled as a stainless steel cylinder with 10-in.-thick walls. The MCO is drawn up into it from the cask delivered to the CSB. The MCNP cases oc1.4 and oc1.5 in Table 6-6 analyzed the configuration of the tight-fitting MHM around and above the MCO with concrete for the operating floor below the normally configured MCOs loaded with the two types of fuel. The upper 95% confidence interval values are 0.307 and 0.331, respectively, for Mark IA and Mark IV fuel. This is a normal operation reactivity for dry fuel. It is possible that an MCO could be delivered to the CSB without having been dried. Case oc4.1 in Table 6-15 analyzes the MHM model with Mark IV fuel and the MCO flooded. The upper 95% confidence interval is 0.907 for the contingency of a flooded MCO in the MHM; the reactivity is well within acceptable limits.

6.5.4.2 Multicanister Overpack in Transit through the Concrete Operating Deck. The next operation at the CSB is to lower an MCO, which has been removed from the transport cask, into a storage tube through the concrete operating deck, modeled as 4-ft thick. This operation also would be carried out when removing an MCO from a storage tube to move it to the HCS and when returning it to a storage tube. MCOs are about 406-cm (160 in.) long, so part of the MCO could be in the MHM, passing through the deck, and in the storage tube. The problem is modeled by determining the MCO's reactivity for each reflective material independently. The reactivity effect of the MHM was assessed in Section 6.5.4.1 and the reactivity effect of being in a storage tube will be assessed below. The reactivity of an MCO normally loaded with Mark IV fuel and scrap, while closely surrounded by concrete and with stainless steel on the top (Table 6-15, Case oc1.7b), is 0.375 (high 95% confidence interval value). This is the normally low reactivity for a dry MCO. The value increases to 0.895 when the MCO is flooded, as shown in Table 6-15, Case oc4.2. This case is slightly less than for the MHM result, where the side and top reflection was 10 in. of stainless steel. The result of the one contingency of the MCO being flooded during movement in the CSB is that the reactivity is within the allowable of 0.945.

6.5.4.3 Vault Flooding. In Table 6-7, the reactivity of a fully loaded vault modeled as an infinite rectangular array was 0.403 (Case oc1.3) for MCOs normally loaded with Mark IV fuel and scrap. The lack of water lines in the CSB, and the fact that the only access to the vault space between the storage tubes is the two stacks that allow natural convection circulation to cool the space, precludes water entry into the vault space between the tubes. However, to show the conservative nature of the CSB, the contingency of water flooding the vault is analyzed using the infinite array model. The results are shown in Table 6-16. Progressively filling the vault to a quarter full (the bottom MCO is half submerged), and to half full (the bottom MCO is completely submerged), lowers the upper 95% confidence level value to 0.380 and 0.374, as shown in Cases oc2.1 and oc2.2, respectively. Case oc2.8 has an even lower value of 0.339 for the vault fully flooded (both MCOs submerged). The greater the flooding of the vault, the greater the neutronic isolation of each storage tube. The progressive flooding of a vault decreases the overall reactivity of the array.

Table 6-15. Analysis Results for Multicanister Overpack Lowered Through the Canister Storage Building Operating Deck.

File ID	Fuel type	Payload cluster		Water density (g/cm^3)		Calculation results[a]		
		Number of baskets	Assemblies per basket	MCO interior	Between storage tubes and outside MCOs	k_{eff}	Std. dev.	95% CI k_{eff}
oc1.7b	Mark IV[b]	1 top 3 middle 1 bottom	0.95 wt% ^{235}U scrap 54 Mark IV 1.25 wt% ^{235}U scrap	0.0051	N/A	0.3708	0.0022	0.3751
oc4.1	Mark IV[c]	1 top 3 middle 1 bottom	0.95 wt% ^{235}U scrap 54 Mark IV 0.95 wt% ^{235}U scrap	1.00	N/A	0.9016	0.0015	0.3311
oc4.2	Mark IV[b]	1 top 3 middle 1 bottom	0.95 wt% ^{235}U scrap 54 Mark IV 0.95 wt% ^{235}U scrap	0.0051	N/A	0.8892	0.0030	0.8952

[a] The limiting value for k_{eff} should be considered 0.945 to allow for a code bias of -5 mk (see Section 6.6.3).
[b] MCO being lowered through concrete floor. Concrete reflection on the side and bottom, steel reflection on top.
[c] MCO stored in MHM. Modeled as having 10 in. of steel on top and sides, and a 2-ft-thick concrete floor below.

CI = confidence interval.
MCO = multicanister overpack.

Table 6-16. Analysis Results for Canister Storage Building Vault Flooding.

File ID	Fuel type	Payload cluster		Water density (g/cm^3)		Calculation results[a]		
		Number of baskets	Assemblies per basket	MCO interior	Between storage tubes and outside MCOs	k_{eff}	Std. dev.	95% CI k_{eff}
oc2.1	Mark IV[b]	1 top 3 middle 1 bottom	0.95 wt% ^{235}U scrap 54 Mark IV 0.95 wt% ^{235}U scrap	0.0051	1.00 (Vault flooded to one-quarter height)	0.3764	0.0016	0.3797
oc2.2	Mark IV[b]	1 top 3 middle 1 bottom	0.95 wt% ^{235}U scrap 54 Mark IV 0.95 wt% ^{235}U scrap	0.0051	1.00 (Vault flooded to half height)	0.3711	0.0014	0.3740
oc2.8	Mark IV[b]	1 top 3 middle 1 bottom	0.95 wt% ^{235}U scrap 54 Mark IV 0.95 wt% ^{235}U scrap	0.0051	1.00 (Vault flooded to full height)	0.3348	0.0020	0.3388
ocsb05	Mark IV[c]	1 top 3 middle 1 bottom	0.95 wt% ^{235}U scrap 54 Mark IV 0.95 wt% ^{235}U scrap	0.0051	0.008 (Vapor)	0.3874	0.0008	0.3889

[a]The limiting value for k_{eff} should be considered 0.945 to allow for a code bias of -5 mk (see Section 6.6.3).
[b]Infinite square array.
[c]Modeled using 10 x 22 x 2 array of MCOs in CSB storage tubes with concrete walls, floors and walls. Fuel density corresponds to the actual 10 x 22 x 2 hexagonal array of CSB.

CI = confidence interval.
MCO = multicanister overpack.

A more effective way to increase the reactivity of an array of undermoderated elements is to insert water as a vapor or mist between the array elements. The infinite horizontal array model of CSB storage tubes containing two normally loaded MCOs was run with water densities from 0.0005 to 1.0 g/cm^3 between the tubes. The MCOs were normally loaded with three central baskets of intact Mark IV fuel assemblies and top and bottom baskets loaded with Mark IV scrap. Figure 6-23 plots this data for internally dry MCOs, and Figure 6-22 plots this data for internally flooded MCOs. The peak in reactivity occurs at 0.008 g/cm^3 for internally dry MCOs. Case ocsb05 (Table 6-16) shows the results of the 10 by 22 by 2 hexagonal array model of normally loaded Mark IV fuel in the MCOs with 0.008 g/cm^3 of intertube moisture. The upper 95% confidence interval value is 0.389. This is about 0.03 less than the conservative infinite array model value. Thus, the actual reactivity for the dry MCO in the CSB storage tube is highly subcritical.

The storage tubes are designed to be cooled by the natural circulation of outside air through the vault space, from one stack to a stack of different height. The relative humidity of ambient air is about 10^{-5}, and fog has a water content of about 10^{-8} g/cm^3. A water content of 0.008 g/cm^3 is saturated steam at a temperature well above 100 °C (212 °F). Air with 50% relative humidity at a temperature just below 100 °C (212 °F) has about 2.3×10^{-4} g/cm^3 water. To have 0.008 g/cm^3 of water in the vault space is an off-normal condition that assumes the air circulation is blocked, water is added, and the MCOs have time to heat the air and water well above 100 °C (212 °F). For dry MCOs, this water content will be used as a conservative assumption in calculations. Figure 6-23 shows that at the lower water densities of normal operations, the reactivity of the storage vault will be lower by about 0.02.

Figure 6-23 also shows that for water densities greater than 0.008 g/cm^3 in the vault, the reactivity drops to that for a single fully water-reflected MCO. This section also showed that for water flooding of the vault space, the reactivity was below 0.44. For this degree of subcriticality, even at optimum intertube water density, no restriction on fire fighting would be necessary to restrict water from the vault for criticality control. Although it should be noted that neither fire fighters nor water used in firefighting in other parts of the facility would have access to the vault space except though the operating decks.

6.5.4.4 Flooding the CSB Storage Tube. Analysis results in Table 6-17 show that flooding the 3.8-cm (1.5-in.) gap between the MCO and storage tube has no significant effect on the reactivity of dry MCOs in the CSB storage tubes. Comparing Cases ocl.3 and ocl.3b, for hot steam in the gap, with oc2.11 and oc2.11b, for full density water in the gap, shows all high 95% confidence interval values are between 0.40 and 0.42. Each pair of cases uses 0.0012 g/cm^3 and 0.008 g/cm^3 of water in the intertube space. Case oc2.14b uses 0.008 g/cm^3 intertube water density with the gap filled with half density water and also shows 95% confidence interval values in the 0.40 to 0.42 range. These cases modeled Mark IV fuel. Mark IA fuel is used in Cases oc2.10a and oc2.10ba with full density water in the gap and the values are less, about 0.315. These results indicate that for dry MCOs, the possibility of flooding storage tubes in fire suppression is not a criticality concern.

Figure 6-23. Interspersed Moderation for Dry Mark IV Multicanister Overpacks in the Canister Storage Building.

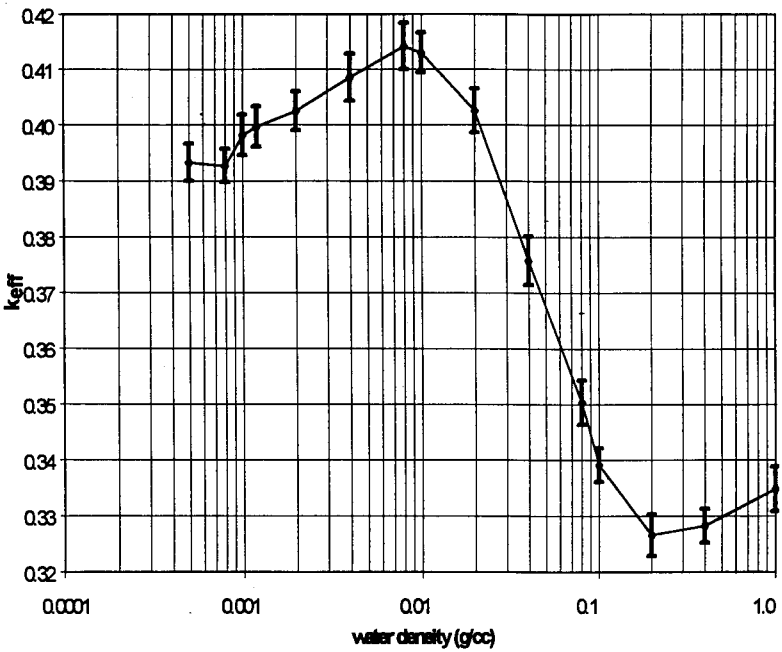

Table 6-17. Analysis Results for Canister Storage Building Storage Tube Flooding.

File ID	Fuel type	Payload cluster		Water density (g/cm^3)		Calculation results[a]		
		Number of baskets	Assemblies per basket	MCO interior	Between storage tubes and outside MCOs	k_{eff}	Std. dev.	95% CI k_{eff}
oc1.3	Mark IV[b]	1 top 3 middle 1 bottom	0.95 wt% ^{235}U scrap 54 Mark IV 0.95 wt% ^{235}U scrap	0.0051	0.0012 (vapor)	0.3841	0.0020	0.3880
oc1.3b	Mark IV[b]	1 top 3 middle 1 bottom	0.95 wt% ^{235}U scrap 54 Mark IV 0.95 wt% ^{235}U scrap	0.0051	0.008 (vapor)	0.4114	0.0020	0.4154
oc2.11	Mark IV[b]	1 top 3 middle 1 bottom	0.95 wt% ^{235}U scrap 54 Mark IV 0.95 wt% ^{235}U scrap	0.0051	0.0012 (vapor) between storage tubes 1.0 outside MCOs	0.4069	0.0018	0.4105
oc2.11b	Mark IV[b]	1 top 3 middle 1 bottom	0.95 wt% ^{235}U scrap 54 Mark IV 0.95 wt% ^{235}U scrap	0.0051	0.008 (vapor) between storage tubes 1.0 outside MCOs	0.4042	0.0026	0.4093
oc2.14b	Mark IV[b]	1 top 3 middle 1 bottom	0.95 wt% ^{235}U scrap 54 Mark IV 0.95 wt% ^{235}U scrap	0.0051	0.008 (vapor) between storage tubes 0.5 outside MCOs	0.4109	0.0020	0.4150
oc2.10a	Mark IA[b]	1 top 4 middle 1 bottom	1.25 wt% ^{235}U scrap 48 Mark IV 1.25 wt% ^{235}U scrap	0.0051	0.0012 (vapor) between storage tubes 0.5 outside MCOs	0.4021	0.0024	0.4069
oc2.10ba	Mark IA[b]	1 top 4 middle 1 bottom	1.25 wt% ^{235}U scrap 48 Mark IV 1.25 wt% ^{235}U scrap	0.0051	0.008 (vapor) between storage tubes 0.5 outside MCOs	0.4008	0.0024	0.4056

[a] The limiting value for k_{eff} should be considered 0.945 to allow for a code bias of -5 mk (see Section 6.6.3).
[b] Infinite square array.

CI = confidence interval.
MCO = multicanister overpack.

It should be noted that flooding a storage tube is considered a contingency. The floor plug is double sealed, and water and water lines are excluded from the vault operating floor and area. Some unusual occurrence would have to happen to bring water onto the operating floor and breech the floor plug seals to the storage tubes.

6.5.4.5 Flooded Multicanister Overpacks. The possibility exists that an MCO could be delivered to the CSB that had not been dried. A single wet MCO is considered a contingency. Analysis results in Table 6-18 show that the entire array of MCOs in the CSB could be wet and the facility would still be within acceptable limits. The model uses an infinite array of normally loaded MCOs with the internal nonmetal spaces filled with full density water. The first two cases, oc2.12 and oc2.12b, have 0.008 g/cm^3 water in the storage tube and intertube water densities of 0.0012 g/cm^3 and 0.008 g/cm^3, respectively. The MCNP results are 0.917 and 0.907. When full density water is put in the storage tubes, cases oc2.13 and oc2.13b with 0.0012 g/cm^3 and 0.008 g/cm^3 of water in the intertube space, the results are lower, 0.884 and 0.890. These results show that for flooded storage tubes and MCOs that are normally loaded with Mark IV intact fuel in the center three baskets and with Mark IV scrap in the top and bottom baskets, the reactivity is below the allowable limit of 0.945, with a margin of over 0.03 for multiple contingencies (i.e., all MCOs flooded with and without all storage tubes flooded). Again, fire fighting does not have to be restricted because flooding the MCOs and storage tubes does not raise the reactivity of the CSB storage vault above allowable limits.

The entries in Table 6-19 all have flooded MCOs and storage tubes. The model for the first two entries, plan_151 and plan_150, uses a fuel diameter of 24 in., the MCO inside diameter, and the model for the next two entries, csb1 and csb2, uses 23 in., the basket diameter. The first two entries have intact fuel and the last two have intact fuel in the center baskets and scrap in the top and bottom baskets. All are normally loaded and have the single contingency of flooding. In three of these cases, the vault space also is flooded. In all cases, the values for k_{eff} and the 95% confidence intervals are below 0.92. For these conditions, the contingency of flooding raises the reactivity, but not above allowable limits. The last three cases, csb3, oc3.5, and oc3.6, present the results of more than two contingencies and are included for understanding the consequences of gross misloading.

6.5.4.6 Multicanister Overpacks with Misloaded Fuel. Several MCNP calculations have shown that the CSB is significantly subcritical even for loading Mark IA fuel and scrap in all the Mark IV baskets in all MCOs stored in the CSB, as long as the MCOs are not flooded. The model has a 23.0-in. fuel diameter, 1.25 wt% ^{235}U scrap in the top and bottom Mark IV baskets, 54 Mark IA intact fuel assemblies in each of the three center Mark IV baskets, and two MCOs vertically in an infinite array of CSB tubes. With all tubes and intertube spaces dry, the k_{eff}, standard deviation, and upper 95% confidence values are 0.3787, 0.0017, and 0.3821, respectively. If full density water is added between the CSB tubes and inside the CSB tubes outside the MCOs (interior of MCOs dry), the values decrease from loss of interaction to 0.3688, 0.0021, and 0.3731. Figure 6-23 shows the upper 95% confidence level for the range 1.0 to 0.0005 g/cm^3 of water between the CSB tubes with the MCOs' interiors dry. The maximum value is less than 0.42 at an intertube density of 0.008 g/cm^3 of water. Even for flooding the CSB vaults, a misloaded MCO is significantly less reactive than the allowed limits as long

Table 6-18. Analysis Results for Multicanister Overpack Internal Flooding.

File ID	Fuel type	Payload cluster		Water density (g/cm^3)		Calculation results[a]		
		Number of baskets	Assemblies per basket	MCO interior	Between storage tubes and outside MCOs	k_{eff}	Std. dev.	95% CI k_{eff}
oc2.12	Mark IV[b]	1 top 3 middle 1 bottom	0.95 wt% ^{235}U scrap 54 Mark IV 0.95 wt% ^{235}U scrap	1.0	0.0012	0.9119	0.0025	0.9168
oc2.12b	Mark IV[b]	1 top 3 middle 1 bottom	0.95 wt% ^{235}U scrap 54 Mark IV 0.95 wt% ^{235}U scrap	1.0	0.008	0.9016	0.0027	0.9069
oc2.13	Mark IV[b]	1 top 3 middle 1 bottom	0.95 wt% ^{235}U scrap 54 Mark IV 0.95 wt% ^{235}U scrap	1.0	0.0012 between storage tubes 1.0 outside MCOs	0.8782	0.0029	0.8840
oc2.13b	Mark IV[b]	1 top 3 middle 1 bottom	0.95 wt% ^{235}U scrap 54 Mark IV 0.95 wt% ^{235}U scrap	1.0	0.008 between storage tubes 1.0 outside MCOs	0.8849	0.0026	0.8902

[a] The limiting value for k_{eff} should be considered 0.945 to allow for a code bias of -5 mk (see Section 6.6.3).
[b] Infinite square array.

CI = confidence interval.
MCO = multicanister overpack.

Table 6-19. Analysis Results for Normally Loaded Multicanister Overpacks Flooded in the Canister Storage Building.

File ID	Fuel type[a]	Payload cluster		Water density (g/cm^3)		Calculation results[b]		
		Number of baskets	Assemblies per basket	MCO interior	Between storage tubes	k_{eff}	Std. dev.	95% CI k_{eff}
plan_151	Mark IV	5	54 Mark IV	1.0	0.10 (heavy mist)	0.8645	0.0033	0.8711
plan_150	Mark IV	5	54 Mark IV	1.0	1.0 (full density)	0.8638	0.0035	0.8708
csb1	Mark IV	1 top 3 middle 1 bottom	0.95 wt% ^{235}U scrap 54 Mark IV 0.95 wt% ^{235}U scrap	1.0	1.0 (full density)	0.8716	0.0023	0.8762
csb3	Mark IA	1 top 4 middle 1 bottom	1.25 wt% ^{235}U scrap 48 Mark IA 1.25 wt% ^{235}U scrap	1.0	1.0 (full density)	0.8196	0.0020	0.8250
oc3.5	Mark IV	1 top 3 middle 1 bottom	0.95 wt% ^{235}U scrap 54 Mark IV 54 Mark IA 54 Mark IV 0.95 wt% ^{235}U scrap	0.0051	.008 (mist)	0.4085	.0021	0.4128
oc3.6	Mark IV	1 top 3 middle 1 bottom	0.95 wt% ^{235}U scrap 54 Mark IV 54 Mark IA 54 Mark IV 0.95 wt% ^{235}U scrap	1.0	.008 (mist)	0.9108	.0031	0.9170

[a] Mark IV type has tie rod at center, excludes center assembly in array, but is much smaller than the Mark IA type with a 6-in.-diameter steel insert that excludes seven central assemblies. MCOs in a 10 x 22 square lattice with two MCOs at each storage tube. One-foot-thick concrete walls are modeled on four sides and the floor.

[b] The limiting value for k_{eff} should be considered 0.945 to allow for a code bias of -5 mk (see Section 6.6.3).

CI = confidence interval.
MCO = multicanister overpack.

as the MCO's interior is dry. This is true even for the multiple contingencies (i.e., completely misloading each MCO in the CSB). Figure 6-23 shows the results for an infinite array of MCOs, but here the MCO is flooded. Multiple contingencies, flooding all MCOs, is subcritical. The design of the CSB exceeds the requirements of the double contingency principle.

Calculations have been done for a case of loading one K Basin canister of Mark IA fuel into a Mark IV scrap basket, and for a case of loading one Mark IV scrap basket in place of an intact fuel basket. One contingency is to load an MCO with one too many scrap baskets of the correctly enriched material. Scrap baskets are modeled as optimally spaced and moderated material and are more reactive than baskets of intact fuel. The third scrap basket is modeled next to the top scrap basket in the bottom MCO in a storage tube. This puts three scrap baskets as close to one another as possible with a single contingency. The results of the analysis are shown in Table 6-20. The upper 95% confidence interval value is 0.417 for case oc3.1b, which uses an intertube optimal water density of 0.008 g/cm^3. The value is lower, 0.397, for case oc3.1, which uses an intertube water density of 0.0012 g/cm^3. For a second contingency, the MCO being flooded, the upper 95% confidence interval jumps to 0.930, as shown for case oc3.2. This result shows that for multiple contingencies, the reactivity is still below allowable limits. The analysis is conservative in that all tubes in the array have an extra scrap basket and the array is modeled as an infinite array.

Another contingency is for a canister of Mark IA fuel to be misplaced and mislabeled as Mark IV fuel in K Basins. This one canister is loaded into a Mark IV basket, so a basket intended for 0.95 wt% ^{235}U enriched scrap is loaded with the equivalent of 14 assemblies of 1.25 wt% ^{235}U enriched scrap, and the rest of the basket is loaded with 0.95 wt% ^{235}U Mark IV scrap. Scrap baskets are more reactive than intact fuel baskets, so this case would cover other cases of a canister of Mark IA fuel in Mark IV baskets. The upper 95% confidence interval value is 0.4165 for case oc3.3b, which uses an intertube optimal water density of 0.008 g/cm^3. The value is lower, 0.401, for case oc3.3, which uses an intertube water density of 0.0012 g/cm^3. For a second contingency, the MCO being flooded, the high 95% confidence interval jumps to 0.925, as shown in case oc3.4, which has an intertube water density of 0.0012 g/cm^3. This result shows that for multiple contingencies, the reactivity is still below allowable limits. The analysis is conservative in that all tubes in the array have an extra scrap basket and the array is modeled as an infinite array.

Figure 6-22 shows that the effect of water density between CSB storage tubes raises the k_{eff} only 0.02 at most over a range of 1.0 to 0.0005 g/cm^3. Only the change caused by intertube water density is applied in this graph. The addition of water does not pose a hazard to storage or movement of a normally loaded MCO in the CSB.

6.5.5 Cold Vacuum Drying Facility

Contingency case reactivities for misloaded fuel in the flooded MCO and transfer cask are shown in Table 6-21. Cases 1 through 4 are situations in which the limit of two scrap baskets per MCO is assumed to be inadvertently exceeded by the loading of a third scrap basket. In Cases 1 and 3, the

Table 6-20. Analysis Results for MCO Misloading. (3 sheets)

File ID	Fuel type	Payload cluster		Water density (g/cm^3)		Calculation results[a]		
		Number of baskets	Assemblies per basket	MCO interior	Between storage tubes and outside MCOs	k_{eff}	Std. dev.	95% CI k_{eff}
oc3.1b	Mark IV[b]	Top MCO 1 top 3 middle 1 bottom Bottom MCO 2 top 2 middle 1 bottom	Top MCO 0.95 wt% ^{235}U scrap 54 Mark IV 0.95 wt% ^{235}U scrap Bottom MCO 0.95 wt% ^{235}U scrap 54 Mark IV 0.95 wt% ^{235}U scrap	0.0051	0.008	0.4134	0.0018	0.4169
oc3.1	Mark IV[b]	Top MCO 1 top 3 middle 1 bottom Bottom MCO 2 top 2 middle 1 bottom	Top MCO 0.95 wt% ^{235}U scrap 54 Mark IV 0.95 wt% ^{235}U scrap Bottom MCO 0.95 wt% ^{235}U scrap 54 Mark IV 0.95 wt% ^{235}U scrap	0.0051	0.0012	0.3939	0.0015	0.3970
oc3.2	Mark IV[b]	Top MCO 1 top 3 middle 1 bottom Bottom MCO 2 top 2 middle 1 bottom	Top MCO 0.95 wt% ^{235}U scrap 54 Mark IV 0.95 wt% ^{235}U scrap Bottom MCO 0.95 wt% ^{235}U scrap 54 Mark IV 0.95 wt% ^{235}U scrap	1.0	0.0012	0.9248	0.0024	0.9296

Table 6-20. Analysis Results for MCO Misloading. (3 sheets)

File ID	Fuel type	Payload cluster		Water density (g/cm^3)		Calculation results[a]		
		Number of baskets	Assemblies per basket	MCO interior	Between storage tubes and outside MCOs	k_{eff}	Std. dev.	95% CI k_{eff}
oc3.3b	Mark IV[b]	Top MCO 1 top 3 middle 1 bottom Bottom MCO 1 top 3 middle 1 bottom	Top MCO 0.95 wt% ^{235}U scrap 54 Mark IV 0.95 wt% ^{235}U scrap Bottom MCO 0.95 wt% ^{235}U scrap mixed with 1 canister of 1.25 wt% ^{235}U scrap 54 Mark IV 0.95 wt% ^{235}U scrap	0.0051	0.008	0.4131	0.0017	0.4165
oc3.3	Mark IV[b]	Top MCO 1 top 3 middle 1 bottom Bottom MCO 1 top 3 middle 1 bottom	Top MCO 0.95 wt% ^{235}U scrap 54 Mark IV 0.95 wt% ^{235}U scrap Bottom MCO 0.95 wt% ^{235}U scrap mixed with 1 canister of 1.25 wt% ^{235}U scrap 54 Mark IV 0.95 wt% ^{235}U scrap	0.0051	0.0012	0.3973	0.0019	0.4011

Table 6-20. Analysis Results for MCO Misloading. (3 sheets)

File ID	Fuel type	Payload cluster		Water density (g/cm^3)		Calculation results[a]		
		Number of baskets	Assemblies per basket	MCO interior	Between storage tubes and outside MCOs	k_{eff}	Std. dev.	95% CI k_{eff}
oc3.4b	Mark IV[b]	Top MCO 1 top 3 middle 1 bottom Bottom MCO 1 top 3 middle 1 bottom	Top MCO 0.95 wt% ^{235}U scrap 54 Mark IV 0.95 wt% ^{235}U scrap Bottom MCO 0.95 wt% ^{235}U scrap mixed with 1 canister of 1.25 wt% ^{235}U scrap 54 Mark IV 0.95 wt% ^{235}U scrap	1.0	0.008	0.9207	0.0023	0.9254

[a] The limiting value for k_{eff} should be considered 0.945 to allow for a code bias of -5 mk (see Section 6.6.3).
[b] Infinite square array.

CI = confidence interval.
MCO = multicanister overpack.

Table 6-21. Analysis Results for Flooded Multicanister Overpack Shipping Cask with Misloaded Fuel in the Cold Vacuum Drying Facility.

Case ID	File ID	Fuel type	MCO water density	Cask annulus density	Number of scrap baskets	Misloaded scrap basket location	Comments	Calculation results*		
								k_{eff}	Std. dev.	95% CI k_{eff}
1	ocvd3.1	Mark IA	1.0	1.0	3	Near end	Scrap basket limit exceeded	0.9040	0.0028	0.9097
2	ocvd3.7	Mark IA	1.0	1.0	3	Near center	Scrap basket limit exceeded	0.8918	0.0035	0.8988
3	ocvd3.2	Mark IV	1.0	1.0	3	Near end	Scrap basket limit exceeded	0.9002	0.0022	0.9046
4	ocvd3.6	Mark IV	1.0	1.0	3	Near center	Scrap basket limit exceeded	0.8966	0.0028	0.9021

*The limiting value for k_{eff} should be considered 0.945 to allow for a code bias of -5 mk (see Section 6.6.3).

CI = confidence interval.
MCO = multicanister overpack.

misloaded scrap basket is in a position adjacent to an end scrap basket. In Cases 2 and 4, the misloaded scrap basket is in a position closest to the center of the MCO. For both Mark IA and Mark IV fuel, the reactivity is greatest when the misloaded scrap basket is adjacent to an end scrap basket. The upper 95% confidence level reactivity for misloaded scrap baskets adjacent to an end scrap basket is 0.910 for Mark IA fuel (case 1) and 0.905 for Mark IV fuel (case 3). These reactivities are below the criticality safety limit.

6.6 CRITICAL BENCHMARK EXPERIMENTS

This section provides justification and shows the validity of the calculational method and neutron cross-section values used in the analyses.

6.6.1 Code Descriptions

Benchmark experiments are primarily used to confirm two aspects of the neutron transport analysis tool:

- That the computer code has a sound treatment of the neutron transport
- That the nuclear cross section database used in the transport code is in agreement with the relevant integral experiments.

The MCNP computer code (Breismeister 1993) is used worldwide and has been extensively tested with its ENDF/B-V-based cross sections. The code development group at Los Alamos National Laboratory, where MCNP was developed, also has a set of 25 calculational benchmarks that extensively test various options within the code. These 25 benchmarks are used to confirm that new versions of the code give exactly the same answer as before and that executables for users at other sites give exactly the same answer. Hence, the 25 calculational benchmarks supplement additional calculations that are made on experimental benchmarks.

MCNP validation efforts specifically appropriate for low-enriched uranium metal systems have been made that have covered N Reactor fuel elements in water (Wittekind 1991, Wittekind 1992, Wittekind 1993) and low-enriched uranium solutions (Wittekind 1994a).

The WIMS-E code (Gubbins et al. 1982) was used in this analysis to illustrate trends while the detailed three-dimensional criticality calculations were performed using MCNP. WIMS-E also has been extensively validated against critical experimental data. Previous validation efforts have covered low-enriched uranium metal billets (Erickson 1992, Schwinkendorf 1985a, Schwinkendorf 1985b), Mark IA fuel assemblies and uranium metal rods (Schwinkendorf 1992a), and low-enriched uranium solutions (Schwinkendorf 1992b, Wittekind 1992).

6.6.2 Details of Benchmark Calculations

MCNP has been tested extensively, but the focus here is on a series of benchmark calculational comparisons (Whalen et al. 1991) to experiments that were made at Los Alamos National Laboratory. The first and second series of the comparisons in LA-12212, *MCNP: Neutron Benchmark Problems* (Whalen et al. 1991), were made to confirm agreement with experiments for fixed source calculations. The third series was for comparison to critical assemblies. These calculations included comparisons for fast neutron systems (Godiva and Jezebel assemblies), for low-enriched uranium systems, for graphite and water-reflected systems, and for interactive (array) units. The powerful geometry features in MCNP were used to model these systems in detail.

The uranium metal rods validation included critical experimental data from two sources. The first (Hellens and Honeck 1962) was for 1.0 wt% ^{235}U-enriched rods and included measured boron poison effects. The published results were in the form of bucklings, not critical masses or k_{eff}. In order to compare WIMS-E results to the published results, WIMS-E results were output as two-group lattice-averaged cross sections for each experiment, and an analytical formula was used to calculate buckling for each case. WIMS-E results compared very well with experimental results, both as a function of water-to-uranium volume ratio and as a function of amount of poison added. The second source (Kupinski and Toffer 1970) contained data over a range of rod outside diameters and ^{235}U enrichments (0.444-cm [0.175-in.] outside diameter to 7.62-cm [3.0-in.] outside diameter and 3.0 wt% ^{235}U to 4.89 wt% ^{235}U). These results were in the form of critical masses in spherical and cylindrical geometry. Validations also exist for the earlier WIMS-D version of the code in UNI-3486, *WIMS Critical Mass Validation for 1.95 wt% and 3.85 wt% Uranium Billets* (Schwinkendorf 1985a), which documents comparisons with annular uranium metal tubes over a range of enrichments from 0.947 wt% ^{235}U to 2.1 wt% ^{235}U.

6.6.3 MCNP Code

Agreement between MCNP and experiments for k_{eff} was within 1% for all of the critical systems referenced in LA-12212 (Whalen et al. 1991). The MCNP N Reactor fuel bias was determined to be -5 mk (Wittekind 1993). This means that MCNP would calculate k_{eff} about 5 mk less than experimental measurements. The MCNP low-enriched solution bias was determined to be -3 mk (Wittekind 1994a). This means that MCNP would calculate k_{eff} about 3 mk less than experimental measurements.

6.6.4 WIMS-E Code

WIMS-E (Gubbins et al. 1982) tends to follow critical experimental data more accurately than WIMS-D but is still conservative. Therefore, it has been the practice to neglect the imposition of a bias when using WIMS-E to calculate k_∞, buckling, or cross sections that are input to a diffusion theory code (to calculate idealized, finite dimensions). Inclusion of the bias would reduce the degree of conservatism in the result.

6.6.5 Results Of Rod And Cylinder Comparisons

Treating a random arrangement of scrap as a lattice of uranium rods in water has been recently questioned. The question is whether a regular lattice in cylindrical geometry will necessarily produce a bounding k_∞ for any arbitrarily shaped chunk of material. Will an explicit spherical lattice optimize to a higher k_∞. If it does, then how would one bound irregular lattice geometries? These questions were addressed with a series of MCNP calculations comparing a hexagonal rod lattice with a three-dimensional lattice based on spheres arranged in a face-centered-cubic geometry. The fissionable material assumed was uranium metal with an enrichment equal to 0.95 wt% ^{235}U. For both rods and spheres, a double parameter search was made to find the maximum k_∞ (as the spacing was varied), as a function of uranium chunk diameter. The results indicate that even though the maximum k_∞ may occur for slightly different diameters, the maximized value for k_∞ was essentially the same (well within the 1σ uncertainty in the calculation). The use of rod lattices to model scrap is therefore considered to be appropriate.

6.7 SUPPLEMENTAL DATA

6.7.1 WIMS-E Calculations for k-Infinity of Fuel Scrap Loads

Assuming uncontrolled geometry, broken fuel pieces may clump together in such a way as to achieve optimal heterogeneity for self-shielding. If these optimally sized fuel pieces become optimally spaced in water, maximum reactivity will result. Previous analysis has shown what the minimum critical masses are for various fuel assemblies, components, scrap, solutions, and uranium billets for a set of ideal geometries, such as sphere or slab (Schwinkendorf 1995). Fuel baskets loaded with scrap are assumed to have their entire volume filled with optimal rods.

The variation in maximum lattice k_∞ is shown in Figure 6-24 for 0.95 wt%, 1.15 wt%, and 1.25 wt% uranium metal rods in water. Each point plotted is the maximum value for each particular rod diameter (as the moderator-to-uranium ratio is varied). The maximum k_∞ is equal to 1.092 for 0.95 wt% ^{235}U enriched scrap.

If the rod optimization is redone with the cladding retained in the lattice, the optimal k_∞ is reduced somewhat, but not significantly. The zirconium cladding is not a strong neutron poison, but it does displace moderator. If the lattice is optimized with the cladding present, the optimal spacing shifts to a higher value, retaining an optimal water-to-uranium ratio. Figure 6-25 contains the results of this optimization. The maximum k_∞ for Mark IV scrap is now 1.0898, a reduction of only 3 mk from the older optimization.

Figure 6-24. Maximum k-infinity Versus Rod Outside Diameter, Uranium Metal Rods in Water.

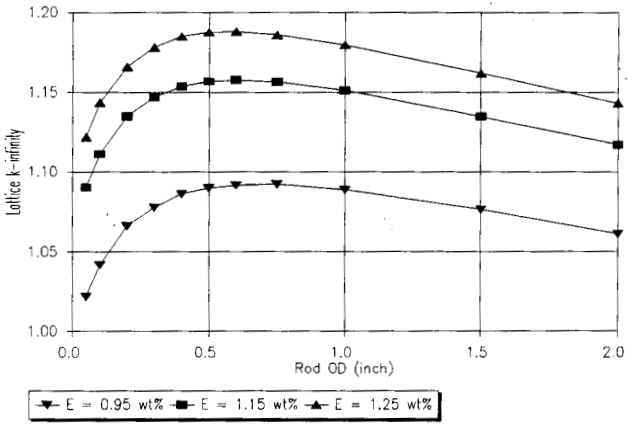

Figure 6-25. Maximum k-infinity Versus Rod Outside Diameter, Cladding Material Conserved.

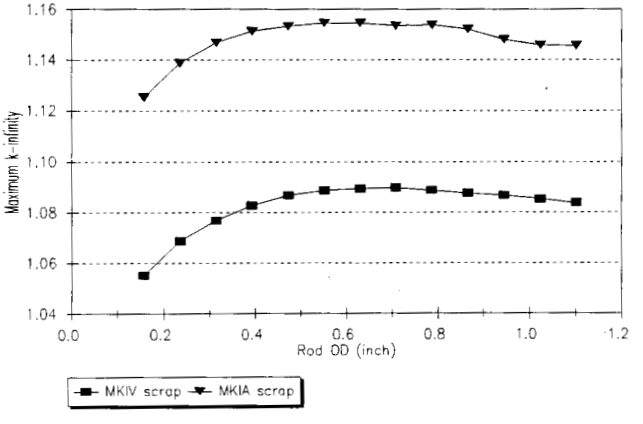

In order to understand the degree of conservatism inherent in treating broken fuel pieces as optimal scrap, additional calculations were performed in which the scrap material was assumed to consist of non-optimally sized uranium rods. These rods had a diameter equal to the radial thickness of a fuel assembly's outer element and preserved the cladding in direct proportion to the amount of cladding present in intact fuel. Only one typical rod diameter was varied, and k_∞ was calculated as the spacing is varied. Figure 6-26 presents these results. The thickness of the uranium in the Mark IV outer element is equal to 0.40275 cm, so this was the diameter of the Mark IV scrap assumed in Figure 6-26. The thickness of the uranium in the Mark IA outer element is 0.3467 cm, so this was the diameter of the Mark IA scrap rods. The maximum k_∞ for the Mark IV scrap (0.95 wt% ^{235}U enriched) in Figure 6-26 is 1.077. This is more representative of what broken debris may be and indicates how much conservatism is in the uranium metal optimal rod model (about 15 mk). It is not clear that broken pieces would not clump together in an uncontrolled geometry and thus behave neutronically as a larger piece of scrap. The optimal scrap model must therefore be used for nuclear criticality safety calculations.

Figure 6-26. k-infinity Versus Spacing Smaller, Non-optimally Sized Rods.

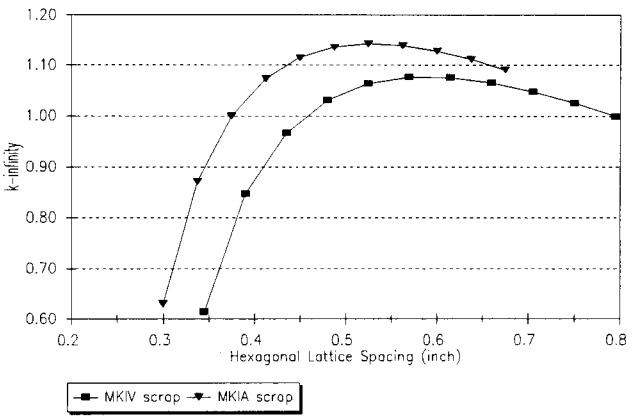

Additional conservatism exists in the assumption of zero fuel exposure. N Reactor fuel stored in the K Basins has documented exposure distributions for each key; these records are backed up by direct measurement performed during the fuel segregation campaign in the early 1980s. Credit could be taken for those keys known to have high burnup.

The moderator-to-uranium volume ratio that optimizes reactivity is probably higher than would exist in a randomly oriented bed of rubble (maximum k_∞ occurs for water-to-uranium ratios around two, which is equivalent to a fuel packing fraction of 0.33). Data exist that suggest that a more likely packing fraction for gravel is in the range 0.40 to 0.45. If this is true, WIMS-E lattice calculations indicate that the corresponding reduction in k_∞ may be on the order of 20 to 30 mk. If the constraint is made that the packing fraction is equal to 0.40, then it is possible to redo the rod optimization. For every rod diameter, the packing fraction of 0.40 determines what the spacing is. Figure 6-27 contains these results. The maximum k_∞ for 0.95 wt% ^{235}U scrap in Figure 6-27 is 1.078.

Figure 6-27. Maximum k-infinity Versus Rod Outside Diameter, Volumetric Packaging Fraction = 0.40.

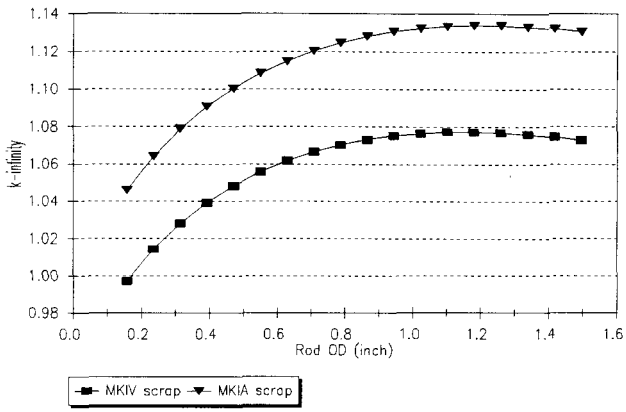

6.7.2 Interspersed Moderation

As water moderation is decreased inside the MCO, the k_{eff} of the system decreases rapidly, as shown in Figure 6-28. The k_{eff} is insensitive to changes in water density in between MCO containers. As the water between MCO containers is reduced (with water density held constant at 1.0 g/cm^3 inside the MCO), the k_{eff} does not change significantly, compared with the 95% confidence intervals of the results themselves. These results are shown in Figure 6-29.

Figure 6-28. Interspersed Moderation, Water Density Variation Inside Multicanister Overpack.

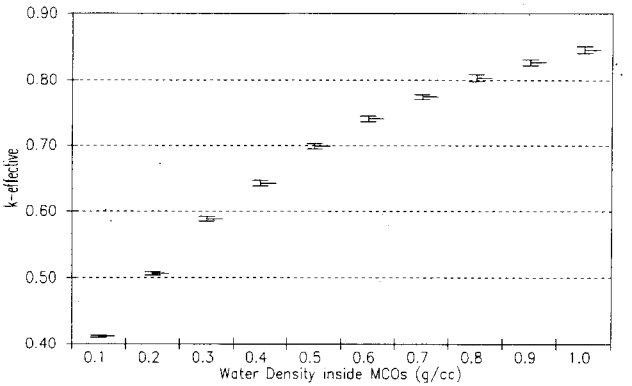

Figure 6-29. Interspersed Moderation, Water Density Variation Outside Multicanister Overpack.

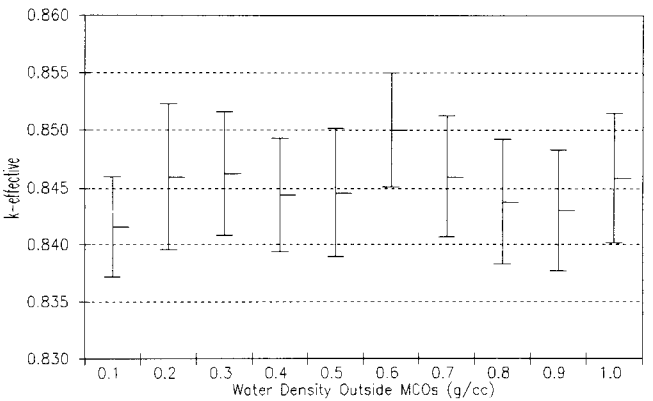

6.7.3 Rod Versus Spherical Geometry for Scrap or Rubble Model

This section shows that either spheres or cylinders can be used to find the maximum reactivity by optimizing the size and spacing of the shape selected. By inference, cylinders may be used to find the maximum reactivity for rubble or scrap. That is the applicability of treating a random arrangement of rubble, or scrap, as a pristine lattice of uranium rods in water. The question is whether a regular lattice in cylindrical geometry will necessarily produce a bounding k_∞ for any arbitrarily shaped chunk of material. The question that was actually checked is whether an explicit spherical lattice optimizes to a higher k_∞ than a cylindrical one. The comparison between an optimized array of spheres and cylinders was addressed with a series of MCNP calculations comparing a hexagonal pitch rod lattice with an explicit, three-dimensional, lattice unit based on spheres arranged in a face-centered-cubic geometry. The fissionable material assumed was uranium metal with an enrichment equal to 0.95 wt% ^{235}U. For both rods and spheres, a double parameter search was made to find the maximum k_∞ (as the spacing was varied) as a function of uranium chunk diameter. MCNP is not an ideal computer code for applications of this nature. Trends that must be smooth tend not to be because of the statistical nature of the code output. However, WIMS-E does not have a lattice module for spherical geometry.

Theoretically, the two most important parameters in a lattice cell problem are (1) the degree of self-shielding (how heterogeneous is the chunk?), and (2) the neutron spectrum (how well moderated is the system, or is the system overmoderated or undermoderated?). The degree of self-shielding in the lattice unit will determine how effectively neutrons are born from fission and then escape from the fuel in order to thermalize in the water. The ability of neutrons to thermalize in water, in the absence of ^{238}U resonance absorption, is very important for low-enriched uranium metal systems. Lattice calculations of k_∞ are greater for optimal heterogeneous systems because the thermalization of neutrons in the absence of strong absorbers (i.e., ^{238}U) increases the resonance escape probability, which is one of the factors in the four-factor formula for k_∞. The degree of self-shielding is quantified in neutron transport theory using the concept of the mean chord length. The mean chord length, <R>, can be thought of as the average distance a neutron travels through a heterogeneous chunk of material. A simple formula for calculating the mean chord length (Duderstadt and Hamilton 1976) is <R> = 4 x (volume/area). For either a spherical or rod lattice, this becomes

$$\langle R \rangle = \frac{4(\pi R^2 L)}{2\pi RL}$$
$$= 2R$$
$$= D \text{ for a cylinder of length } L.$$

$$\langle R \rangle = \frac{4\left[\frac{4}{3}\pi R^3\right]}{4\pi R^2}$$

$$= \frac{4}{3}R$$

$$= \frac{2}{3}D \text{ for a sphere.}$$

More refined methods exist for calculating an effective mean chord length for more tightly-packed lattices involve applying the Dancoff correction to adjust for rod shadowing effects (Bell and Glasstone 1979). Because the Dancoff correction becomes more important for more tightly packed lattices, it is less important for the optimal lattices of concern for finding maximum reactivity (spacing for optimal reactivity tends to be greater). However, this discussion is presented to show approximately how spheres and rods optimize to different diameters. These more sophisticated methods are already built into WIMS-E (Gubbins et al. 1982), the lattice code used to generate the results in this report.

If the degree of self-shielding is to be the same between the cylindrical and spherical lattices, the mean chord length must be the same. This occurs when the diameter of the cylinder is equal to two-thirds of the diameter of the equivalent sphere, or the sphere diameter is 1.5 times the diameter of the cylinder. Figure 6-30 presents the results of the MCNP calculations. Each MCNP k_{eff} shown in Figure 6-30 was a maximum value, out of 10 MCNP calculations that varied the spacing between either the rods or spheres. As expected, the shapes of the two curves are different, but the lattice k_∞ that the two curves maximized themselves to is essentially the same (well within the 2 σ error of the calculation). It is interesting to note that this maximum k_∞ is very close to the value that WIMS-E maximized to for uranium rods of the same enrichment (1.09226). The maximum k_∞ was 1.09082 ± 0.00265 for the cylindrical lattice, and 1.09189 ± 0.00247 for the spherical lattice. Finally, the sphere diameter that produces the maximum is about 1.5 times the diameter that produces a maximum for the rods, as predicted by theory.

The foregoing discussion was intended to solidly establish that whether random, irregularly shaped scrap or rubble is treated as rods or as spheres makes no difference in the calculated value of the maximum reactivity of the material.

By inference, it is now postulated that true irregularly shaped pieces, assuming that they are optimally sized and spaced, will not be more reactive than either the rod or sphere models. The rod and sphere comparison was in excellent agreement with certain transport theory predictions, and hence greater confidence may be put in the assumption that the primary factors that have significance in determining unit lattice reactivity are the mean (or effective) chord length and the degree of moderation. These factors are not sensitive to the spatial details of the lattice geometry. Therefore, treating scrap material using parametric calculational results obtained from a lattice calculation, such as WIMS-E, is assumed to be valid.

Figure 6-30. Maximum MCNP k-inf Versus Outside Diameter. Face-Centered-Cubic Spherical versus Hexagonal Rod Lattices.

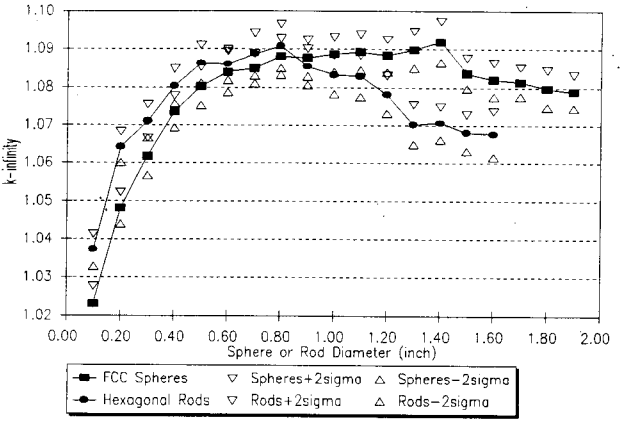

7.0 CONFINEMENT

The MCO represents the first confinement/containment boundary for the SNF during storage. The MCO provides confinement when it is vented and containment when it is sealed. The MCO is a single-boundary system that serves the following uses during its lifetime:

- The innermost SNF container as part of the transport shipping packaging
- The process vessel for the SNF during cold vacuum drying and hot conditioning of the SNF
- The container for the SNF during staging at the CSB
- The container for the SNF during interim storage at the CSB.

7.1 CONFINEMENT BOUNDARY

The confinement boundary for the MCO is composed of the MCO lower end cap, the MCO shell wall, and the MCO shield plug.

- The lower end of the MCO is a machined cap made of 304L stainless steel. A pocket at the bottom of the cap collects bulk water for removal from the MCO. The minimum thickness for the lower end cap is 1.3 cm (0.5 in.) where it is welded to the shell wall.
- The shell wall of the MCO is a 61-cm- (24-in.-) outside-diameter pipe section with a 1.3-cm- (0.5-in.-) thick wall section. The shell is made of 304L stainless steel. The shell wall and lower end of the MCO will be manufactured and leak tested before use at the Hanford Site.
- The shield plug assembly includes the plug body itself and the penetrations and devices necessary for interface to the process and safety equipment. The devices at the end of the penetrations from the interior of the MCO form a portion of the confinement boundary for the MCO.

The MCO confinement and pressure boundary is designed and manufactured to meet the intent of the standards in the Boiler and Pressure Vessel Code (ASME 1995a), Section III, Subsection NB, with some exceptions. The MCO design pressure is 1.0 MPa gauge (150 lb/in^2 gauge) at 200 °C (392 °F). The maximum temperature allowed after fuel is inserted into the MCO is 375 °C (700 °F). The operating maximum temperature during hot conditioning is limited to 350 °C (660 °F) for the MCO vessel proper, with the SNF payload design fuel dryout temperature being 300 °C (570 °F).

7.1.1 Confinement Penetrations

Penetrations into the MCO are bored through the shield plug to the interior of the MCO. The penetrations terminate on the outside of the shield plug as ports, with devices and fittings that allow the MCO to interface with process- and safety-related devices. Four devices are associated with the penetrations: two process tubes and two pressure relief devices. Fittings and covers that go over the devices offer additional confinement for the MCO.

The two process tubes are connected to ports on the external faces of the MCO. These process tubes are used to introduce fluids into and remove fluids from the MCO. The long process tube path has a nominal diameter of 1.3 cm (0.5 in.); the short process tube has a nominal diameter of 2.5 cm (1 in.). Both process tubes are protected by wire screens (2-mm mesh openings) on the interior of the MCO to prevent larger particles from being moved out of the MCO (Figure 1-9).

A bank of four HEPA filters inside the MCO filters exit gases during vacuum drying and hot conditioning. The HEPA filters, which are not testable after installation, are connected to a penetration in the MCO shield plug that leads to an external pressure relief device that activates well below the 1.0 MPa (150 lb/in^2) design pressure. These HEPA filters serve to minimize the potential for contamination spread if the MCO pressure relief device actuates during staging at the CSB. These filters also are sized to bleed off any gas buildup caused by possible radiolytic production of hydrogen and other gases inside the MCO.

The pressure relief path is a nominal 2.5-cm (1-in.) path via the short process tube with the rupture disk venting outside the MCO during overpressurization. This path has to have a flow-rate capacity that keeps the MCO pressure below the 1.0 MPa gauge (150 lb/in^2 gauge) limit.

7.1.2 Seals, Welds, and Closure

MCO confinement/containment is established by a combination of seals and welds. The shell wall pipe and MCO bottom are joined by welding, and the joint is inspected and examined before the MCO is loaded with fuel. The shield plug penetrations are sealed during transport and during processes through hot conditioning to keep the leakage rate of the penetrations to acceptable levels. Sometime after hot conditioning, a single cover is placed over the entire shield plug and welded to the MCO shell wall.

Two approaches to forming the closure of the shield plug to the MCO shell were considered. The first type of closure is a circumferential weld around a 304L stainless steel shield plug joining the shield plug to the MCO shell wall. Welding for this type of closure would be performed after the cask–MCO had been processed at the CVDF. Helium would be used to test the leak rate for this type of closure before the MCO was shipped from the CVDF to the CSB. The second type of closure, which has been selected for use by the SNF Project, is a mechanical closure where the shield plug is held in place by a threaded locking ring containing jack bolts. The locking ring would be placed into the MCO neck extension after the shield plug was inserted. Once assembled, the eight jack bolts in the locking ring would be tightened down

into the shield plug's back side to push the shield plug into the seal between the MCO shell and the shield plug. This type of closure would be made before the cask-MCO was transported to the CVDF. The seal is maintained during thermal transients and drop accidents by developing and maintaining sufficient preload through the seal. This type of seal system will be qualified early on during the prototypic testing program and by analysis, and as a result, each MCO may not need individual leakage rate determinations after loading is complete at the K Basins.

The cask is fully prepared to accommodate either a welded or mechanical closure as the MCO's outside dimensions and shape at the closure end are essentially the same in both cases. Cask operations has taken on the task of setting the shield plug into the MCO neck underwater in the load-out pit. Selection of the mechanical closure means that cask operations would also install the locking and lifting ring and tighten the eight jack bolts and perform the cursory leakage rate test with the MCO and cask out of the basin pool if needed. The mechanical closure has the advantage of relieving cask operations of the installation of the shield plug restraint and seal to the MCO shell that would be required for a welded shield plug.

At the CVDF selection of the mechanical closure relieves workers of the tasks of welding the shield plug into the neck of the MCO, determining the leakage rate of the weld, and dye penetrant testing. This is a savings of approximately 14 hours in each MCO's cycle time of 66 hours through the CVDF.

At the HCS, either the welded or mechanical closure involves seal welding of the MCO some time after the hot conditioning process has been completed and gas evolution inside the MCO is at acceptable levels. In the case of the mechanical closure, seal welding is accomplished by installing a cover cap with rupture disk over the entire end of the MCO and performing the weld with automatic welding equipment. In the case of the welded closure, seal welding is accomplished by welding four smaller covers over the ports in the shield plug.

7.2 REQUIREMENTS FOR NORMAL CONDITIONS OF STORAGE

The MCO confinement boundary is tested at various times and places to ensure the leakage rate requirements are met. The MCO shell and bottom end are leakage rate tested before the subassembly is loaded with fuel. The mechanical closure system will be qualified for suitability and only a cursory examination of the seal occurs at the K Basins after fuel loading and MCO closing are complete. It is not anticipated that the eight jack bolts in the mechanical closure will need retorquing while the MCO is in staging at the CSB. This is based on the tightness of the jack bolts after the prototypic MCO had gone through five thermal cycles and vibration testing. The bolts were tight after testing of the prototype was complete. Creep analysis of the nearby metals in affected areas and around the mechanical seal can be performed if needed. After staging and hot conditioning are complete and gas evolution rates inside the MCO are at acceptable levels, a cover cap is welded to the MCO shell over the top of the shield plug and locking and lifting ring. The cover cap weld is volumetrically examined by ultrasonic inspection equipment once the MCO is sealed and prepared for interim storage in the CSB storage tubes.

7.2.1 Release of Radioactive Material

During sealed interim storage in the CSB, the MCO has no penetrations that are open for sensing or venting. The atmosphere inside the MCO is not interacting with the atmosphere of the CSB storage tube. Release of particulate material into the CSB storage tube is not probable during sealed interim storage. The capability for pressure relief does, however, exist in a pressure relief device as well as a rupture disk.

7.2.2 Pressurization of Confinement Vessel

Before storage the MCO and SNF are conditioned. This process heats the MCO and SNF to 300 °C (575 °F) under vacuum and decomposes most of the compounds holding water and hydrogen. As a result, these pressurization-producing materials, needed to create pressure by radiolysis, are minimized. During storage, properly hot conditioned MCOs will not have excessive pressure buildup from radiolysis of materials inside the MCO. Any unexpected gas release from the MCO would go into the CSB storage tube, which is inside the CSB building proper.

7.3 CONFINEMENT REQUIREMENTS FOR HYPOTHETICAL ACCIDENT CONDITIONS

The MCO is usually stored in the CSB storage tube. This tube is fitted with a shield plug. The operating deck of the CSB is surrounded by the above-ground portion of the CSB's walls and by the roof. Thus, under long-term storage, confinement is provided by the MCO and by the storage tube. The CSB is designed to withstand the loads imposed by Hanford Site hazards (e.g., tornadoes, seismic events) as well as to mitigate or prevent accidents such as MCO drops into the storage tubes.

7.3.1 Fission Gas Products

Fission product generation and release during each step of the proposed process the MCO will be subjected to is discussed in WHC-SD-SNF-TI-033 (Cooper 1996a).

7.3.2 Release of Contents

The MCO is fitted with a pressure relief device. This device is designed to release at about 1.0 MPa gauge (150 lb/in^2 gauge). It has a throat of approximately 2.5 cm (1 in.) leading to the interior of the MCO. Because the MHM cannot accommodate a high flow rate release, the MCO will be fitted with an orifice plate after the pressure relief device to limit the release rate from the MCO into the MHM and CSB storage tubes. This lower release rate will allow CSB systems and the MHM to handle the release and prevent the spread of contamination. Also a lower release rate from the MCO will sweep less of the particulate inventory up in the release stream, leaving more of the particulate inside the MCO.

8.0 OPERATING PROCEDURES

The SNF Project is not yet to the point where specific handling procedures can be drafted and evaluated with any degree of accuracy. Therefore, the processes associated with shipping cask and MCO movement, from initial fuel loading in the K Basins through long-term storage in the CSB, are described here on a facility-specific basis. Much of the detail presented is subject to change. By including sufficient detail to enable the reader to understand the process as it currently exists and as it relates to each facility, the need for continued reference to the facility SARs may be precluded. As the facility-specific procedures are generated, they will be referenced in this section and, if appropriate, included as appendixes. The facility-specific information, once generated, will supersede the information presently contained in this section.

8.1 CURRENT K BASIN PROCESS DESCRIPTION

Current K Basin activities involve the safe storage and handling of fuel, sludge, radioactive debris, and contaminated debris. The following fuel storage and handling activities are performed:

- Inspecting fuel storage racks and canisters
- Operating fuel handling tools and equipment
- Moving fuel and IXC transfer casks
- Pumping sludge
- Removing debris.

All N Reactor fuel elements in the K Basins are stored in canisters. The canisters are stored in racks that provide a unique storage location for each canister and, more importantly, serve to keep the fuel in the canister in a critically safe configuration. Fuel handling tools and equipment are used to load fuel elements into canisters, seal and insert chemicals into the canisters, and move the canisters around in the basin. Casks are used for shipping fuel canisters and spent basin water treatment resins out of the basin. Fuel stored in unsealed canisters is the major source of sludge on the K East Basin floor. Sludge pumping equipment is used to clean the fuel storage pool floor and is presently used only in the K East Basin. Both basins have significant accumulations of sludge in the sand filter backwash pits. The sludge present in the pits accumulates from periodic backwashes of the sand filter, which is part of the basin skimmer system.

8.2 K BASIN FUEL REMOVAL PROCESS DESCRIPTION

Handling of the MCO begins at the CSB when a new, open, MCO shell is loaded into an empty transport cask. During transport to the K Basins, a protective cover prevents the interior and exterior of the MCO from being contaminated with foreign materials. At or prior to activities at the K Basins, the cask-MCO is unloaded from the conveyance, and the locking and lifting ring is test-threaded into the MCO neck to check fit-up and then

removed. This operation minimizes the potential for threading problems later in the load-out pit. The cask–MCO is then placed in the load-out pit and prepared for fuel loading.

The SNF Project provides the basis for modification of the K East and K West Reactors' fuel storage basins and facilities to enable the retrieval, cleaning, reracking, loading, and removal of the SNF, as well as removal of the sludge. The K West Basin's fuel removal operational readiness review includes all modifications and upgrades required to accommodate the necessary operations for SNF removal.

The K Basin Fuel Retrieval System will be used to retrieve fuel and package it in MCO baskets in preparation for loading into the MCO. Fuel will be retrieved from the basin in accordance with campaign letters that implement an overall plan for fuel removal. These campaign letters will provide the control necessary to ensure the proper fuel is removed in the proper sequences. The campaign letters also provide controls to keep the special nuclear material classification below a category 2 for each MCO.

Fuel will be moved, using the K Basin monorail cranes, from the basin storage locations to a storage area near the fuel retrieval equipment in the west bay of the basin. Gas pressure will be relieved and the canister caps will be removed from the sealed canisters before cleaning the fuel. Fuel canisters will be loaded into the Fuel Retrieval System's primary cleaning machine for cleaning and for loosening stuck fuel. Following cleaning, the canisters will be discarded and the fuel will be inspected, as necessary, to ensure it is acceptably clean. If necessary, fuel elements will be cleaned in a secondary cleaning station.

Fuel scrap will be loaded into MCO scrap baskets. Intact fuel elements will be loaded into MCO fuel assembly baskets. Operational controls will ensure the fuel is loaded into the correct MCO basket type and that the proper amount of fuel is loaded into the MCO baskets. Filled baskets will be moved to the MCO basket queue to await preparation for loading into the MCO. The MCO basket queue can hold 10 MCO baskets.

In the loading queue the MCO basket is prepared for placement into a new shipping cask–MCO. MCO baskets are moved manually from the loading queue to the modified south load-out pit in the basin. A loading funnel is put into the neck of the MCO to prevent damage to the MCO closure surfaces during the loading of the fuel baskets. This step may be performed before the cask–MCO is put into, and flooded in, the load-out pit. The MCO basket is inserted into a cask–MCO using a modified monorail and a new hoist. After the fuel level has been shown to be acceptable, the loading funnel is removed from the neck of the MCO.

The shield plug assemblies and the long process tubes are stored at a warehouse in the 100 K Area until the components are needed at a basin. A shield plug assembly is brought into the load-out pit area, and the shield plug assembly is prepared for installation while the MCO is underwater in the load-out pit. The shield plug is attached to the hoist rigging, and the long process tube is attached to the shield plug. Water-level equalization apparatus, which will be used to adjust the water level inside the MCO once the shield plug is in place, also is attached to the shield plug. The shield

plug is then swung out over the submerged MCO containing the SNF payload, and the long process tube is inserted into the top basket's axis. The shield plug assembly is slowly lowered down and into the MCO's neck. Once shield plug insertion is complete, the cask-MCO is raised up out of the water, the water level inside the MCO is adjusted to the proper level, and the water-level equalization apparatus is removed from the shield plug. Necessary decontamination steps will occur at this time.

The rest of the mechanical closure assembly, including the previously tested locking ring, is installed into the neck of the MCO and the jack bolts tightened. The mechanical closure system will be a qualified closure joint for the MCO. Under normal conditions, the mechanical closure also allows the MCO, once flooded, to be fairly easily downloaded into the basin pool. Downloading might be accomplished in the event of dropping the MCO into the cask, loading fuel for transfer to another basin, and failing the leakage rate test.

The cask-MCO is prepared for movement by the load-out area's crane. The K East and K West fuel transfer bay cranes are rated for 30 tons. They will be used to support the transfer of approximately 100 casks-MCOs, per basin, per year, for 2 years. The lifted loads will be at or near the rated capacity of the existing cranes. One of the strategies for improving safety and operability is providing improved load-out basin transfer area bridge cranes. The current bridge cranes were constructed in the 1950's. They are being modified to meet the requirements of the SNF mission using the developed SNF strategy. Planned modifications include an auxiliary hoist and radio remote control for hoist and travel movement.

The cranes position the cask-MCO assembly between the basin load-out pit areas and the transportation staging area. The cask-MCO assembly is placed in the immersion pail to minimize possible contamination. The immersion pail which fits around the cask-MCO, is sealed, and a positive pressure maintained across the basin water and cask boundary. The immersion pail attached to the cask-MCO is set on the floor of the south load-out pit during fuel basket loading. The cask-MCO fully loaded with SNF weighs approximately 30 tons.

A new lifting fixture is attached to the crane and the cask-MCO is moved from the load-out pit to the transportation trailer.

The basis for classification of each of the process elements is the safety evaluations that contain the hazards analysis. The hazards analysis looked at the process steps, potential hazards, causes, consequences, safety features (engineered and administrative), inventory at risk, consequence category, frequency category, and reviewers remarks.

Associated hazards and hazard classifications can be found in the K Basins modified SAR.

8.3 COLD VACUUM DRYING FACILITY

8.3.1 General Facility Description

The CVDF will receive loaded MCOs from the K Basins. The CVDF is a new, stand-alone, modular structure located in the Hanford Site 100 K Area. The site selected for the CVDF is to the southwest of Building 165 KW, the Power Control Building, and 105 KW, the Reactor Building. This site is close to all required utilities and within the inner security boundary. The new facility is located near the path the fuel transport truck will take leaving the 105 KW Reactor Building and is close to rail lines that may facilitate future removal of waste.

The CVDF contains five process bays (including one empty bay) within a single-story, pre-engineered metal frame and concrete panel building containing a second-level mezzanine. Attached to the process bays is a single-story, pre-engineered metal building that encloses administrative rooms and change rooms. The exterior skin of the building is a mixed use of precast concrete panels and insulated metal panels. The CVDF will be constructed in accordance with the *Uniform Building Code* (ICBO 1994) and DOE Order 6430.1A, with egress requirements conforming to NFPA 101, *Safety to Life from Fire in Buildings and Structures* (NFPA 1991). The recommended configuration of the CVDF requires a building footprint of approximately 1,300 m^2 (14,400 ft^2) for the process bays and support areas and 280 m^2 (3,000 ft^2) for administrative and change rooms.

Each process bay is designed as an enclosure for an MCO cask transporter without the tractor attached. Operational space necessary to meet the functional requirements of the CVDF is included. Process bay construction is designed to provide separation and confinement within each bay. The pre-engineered metal building system has a bay width of 9 m (30 ft) and a rigid steel frame system that has a nominal width of 18 m (60 ft). The height of the process bay is nominally 9.75 m (32 ft), which is dictated by the manned access required at the working level of the shipping cask, the crane access required to remove the cask lid, and the physical requirements for all the process equipment.

Each process bay provides ground space for the following items:

- A cask transporter, without the tractor attached (a safety-related confinement zone)
- Personnel circulation and functional space around the cask transporter
- Seismic restraint hold-down devices for the cask–MCO, if required
- Vacuum drying system equipment and pump assemblies
- Access to the working level of the cask and transporter

- Radiological control between the process bay and the access corridor (operators change clothing and are monitored for radiological contamination before being admitted to the access corridor)
- Bridge crane access for removal of the cask lid and maintenance on equipment
- Auxiliary services, including inert gas, and pneumatic and electrical power
- A cabinet for supplies.

Access to the working level of the cask is accomplished using a mezzanine level with space for the following items:

- Connections from the vacuum drying system to the cask-MCO
- Heating, ventilating, and air conditioning (HVAC) equipment and electrical panels
- Jib crane and slot hood assembly.

The process bay support area serves as a differential pressure zone between the controlled process bay and the uncontrolled circulation corridor. Functional requirements for each process bay support area include the following:

- Seating space for two allowing for dressing and undressing with special work permit clothing
- Storage for clean special work permit clothing
- Storage for dirty special work permit clothing
- Space for personnel contamination monitor equipment.

Access throughout the process portion of the building is accomplished using a corridor that is contiguous with the main change room for radiological control of access-egress between the administrative and process areas. Support rooms off the corridor include a decontamination room, swipe count room, process water tank room, miscellaneous materials storage room, and equipment storage room.

The administrative area controls personnel access into the CVDF process bay area and provides space for lunch-conference room, quality assurance functions, shift manager, health physics technician and radiation monitoring, control room, electrical-telecommunications room, fire riser room, change rooms and rest rooms, and access-egress control and personnel control monitoring of the process bays.

The HVAC system for the CVDF consists of one HVAC supply system for each process bay, one for the corridor area, and one for the administrative Area. Each supply system operates independently but interfaces with the building control system. The process bay HVAC system is a constant volume

recirculating system with two-stage HEPA filtration in the return air system. Each bay incorporates a local slot hood that continuously exhausts a portion of the air from the bay area. Air exhausted through slot hoods in each bay combines into a single system and is then filtered through a two-stage HEPA plenum. Partially redundant exhaust fans, running in parallel, direct the exhaust air to the stack. Each bay also has a general exhaust system that is used to maintain design pressures. This general exhaust combines with the corridor exhaust system.

The access corridor area HVAC system is a constant volume once-through system. Air is ducted to the access corridor and support rooms. Air supplied to the access corridor is transferred to the material storage room and change rooms. The change rooms will maintain a positive pressure with respect to the process bays. Air in the corridor support rooms, the controlled rooms in the administrative area, and the general exhaust from the process bays is exhausted to a separate two-stage HEPA plenum. A separate set of partially redundant exhaust fans, running in parallel, directs the exhaust air to the stack.

The administrative area is served by a packaged unit with chilled water cooling and electric heat. Air is recirculated through the administrative area, and an economizer is used to reduce energy costs. Air from the rest rooms and shower areas is exhausted to the outside.

The electrical system will provide power distribution, lighting, grounding, and lightning protection for the CVDF and its equipment and instruments as required. Normal power will be provided with a grounding system to ensure safety to personnel and equipment, to provide a connection to earth for transformer neutral, to provide a discharge path to ground for lightning and surge arresters, and to provide a reference point for electronic systems.

Normal power will be provided by extending an existing 13.8 kV primary circuit from existing poles adjacent to the site. Using fused cutouts and lightning arrestor, the existing overhead circuit will be converted to an underground circuit to supply the new building's pad-mounted transformer. All underground primary conduit will be concrete encased. Secondary power at 277/480 V will be routed into the building through underground conduits. Power will be distributed by a free-standing, metal-enclosed switchboard.

Uninterruptible power (one 50 kVA, 480 V to 208/120 V) complete with battery packs, battery disconnect switch and circuit breaker, maintenance bypass cabinet, and computer power center will be provided to ensure safety-related critical systems have continuous power supplied during and after a design-base accident.

8.3.2 Cold Vacuum Drying Facility Process Description

The sequence of actions that are required to occur in the CVDF between the time that an MCO is ready for shipping from the K Basins until the process bay is ready to receive another MCO can be summarized as follows.

1. Receiving Activities. The basin workers notify the CVDF control room that a shipment is ready. CVDF workers in the control room select a bay and notify the truck driver, who drives to the CVDF and positions the transporter in front of the bay door. The bay door is opened and an exhauster trunk attached to the truck's exhaust pipe so that diesel fumes do not enter the CVDF. The truck backs into the bay and locates the transporter.

2. Preparation Activities. Once the MCO has been accepted, the trailer is secured and the tractor is disconnected, and driven out of the facility.

3. Receiving Inspection and Acceptance Activities. Receiving inspection activities are performed to verify that the MCO is properly labeled so that special nuclear material accountability is maintained; to verify that there is no removable contamination on the exposed surfaces of the cask; and to assay the radiation field in the vicinity of the cask and MCO top where workers will be present. Decontamination and resurvey occur if contamination is found.

4. Process Setup Activities. After the cask–MCO assembly is secured and determined to be free of contamination, radiation monitoring instrumentation is attached to the transporter work platform and activated; water hoses are attached to the cask ports; the cask lid is removed and replaced with a cask process lid; an overhead boom is swung in that carries a local exhaust hood and the process connection spools; and the process hoses are attached to the MCO top ports.

5. Processing Activities. Process activities include heating the MCO to the drying temperature (the water is left in order to obtain effective heat transfer to the materials inside); draining the water from the MCO; executing a sequence of purge and evacuation cycles; verifying dryness by means of pressure rise test; backfilling with helium; helium leak checking; and ultimately, cooling the cask. All these operations are run from the control room.

6. Postprocessing Examination. After processing the MCO temperature is raised to 75 °C (167 °F), held at this temperature for 6 hours, and monitored for the gas generation rate. After a successful examination, the cask–MCO are cooled to 25 °C (77 °F). The postprocessing examination will encompass a 12-hour period (which envelopes the nominal CVDF to CSB transport window).

7. Postprocessing Activities. Postprocessing activities are the reverse of the preparation activities. The process hoses are disconnected; they are to be handled as contaminated items (ends are bagged). The boom is swung out of the way. The water in the annular space between the cask and the MCO is drained. The cask top is placed, sealed, and the annular space dried. Helium is injected into the annular space. Instruments are removed from the transporter. The tractor arrives and is connected to the transporter. The transporter is released and driven away.

8. Bay Restoration Activities. Cleanup work required to prepare the bay for the next MCO includes mopping the floor, changing filters, changing out and cleaning up contaminated spools, and calibrating equipment.

8.3.2.1 Vacuum-Gas Purge System. The function of the vacuum/gas purge system is to remove the bulk water from the MCO and to dry the SNF under vacuum using a cycle of evacuation and inert gas backfill and purge stages. There will be one vacuum-gas purge system for each of the process bays. The final product will be a dried MCO that has been backfilled with inert gas. The vacuum-gas purge system will be required to interface with the monitoring and control system to allow for computer control of the MCO during all stages of the drying operation.

8.3.2.2 Multicanister Overpack Temperature Control. The MCO-cask temperature control system maintains the MCO at the proper operating temperatures during all stages of the MCO drying process. This includes heating the MCO during vacuum drying, and cooling the MCO after vacuum drying. The temperature control system pumps water at various design temperatures through the annular space between the MCO and the cask at a rate of 75 L/min (20 gal/min) and a design pressure of 140 kPa (20 lb/in^2). During the vacuum drying phase of the operation, the temperature control system maintains a continuous operating temperature for a period of not more than 2 days per drying operation. After vacuum drying, the temperature control system cools the MCO and cask down to an acceptable temperature for shipping. The temperature control system interfaces with the monitoring and control system to allow for computer control of the MCO during all stages of the drying operation.

8.3.2.3 Liquid Handling System. The liquid handling system provides a local point of collection for the process liquids in each of the process bays. Liquids are pumped from the collection system in each bay to a 19,000-L (5,000-gal) central liquid holding tank. This liquid will be transported by tanker to another facility for final treatment and disposal. The liquid handling system interfaces with the monitoring and control system to allow for computer control during the drying process.

8.3.2.4 Monitoring and Control System. The monitoring and control system is designed as a fully-integrated control system that provides not only process control but data acquisition and management. The system uses digital signaling between a distributed network of programmable logic controllers and driver software, which can be handled by personal computer-sized hardware. Each local personal computer has a view screen with dynamic graphical display to show the change in the operating parameter. All personal computers allow total access to all systems so redundancy is achieved if a computer becomes inoperative. Access to the level of control can be programmed into the software of the control system so that only authorized personnel may operate the system. A television camera located in each process bay and outside viewing the truck area entry allows control room personnel to view the operation. A television screen is situated near each personal computer control station.

8.3.2.5 Solid Waste Disposal. Solid waste is generated during the course of normal operation within each of the process bays and the other areas of the facility. This waste includes, but is not limited to, HEPA filters, liquid

handling system filters, smears from various health physics technician surveys, decontamination rags, plastic hose end and boom covering bags, and rags and wipes from general process bay cleanup. These items, and other similar types of potentially contaminated solid waste, are placed into a designated drum in each bay. When drums are full they are monitored to determine waste class and placed in a temporary storage area in the facility. The drums are picked up by others for treatment and/or disposal.

8.4 CANISTER STORAGE BUILDING

The CSB is located in the 200 East Area of the Hanford site. The CSB is a hazard class 2 facility that consists of three equally sized below-grade concrete vaults, with total approximate dimensions of 55 m x 50 m x 15 m deep (180 ft x 165 ft x 48 ft deep), covered by a concrete operating deck. An above-grade steel operating area structure is located above the vaults. Support functions and equipment are housed in a smaller building at the north side of the operations building. The reference elevation of the facilities at the top of the operating deck is 216 m (709 ft) above mean sea level. The basemat is nominally 1.7 m (5 ft 6 in.) thick; its surface elevation is 203.2 m (666 ft, 9 in.). The distance from the surface of the basemat to the underside of the operating deck is 11.4 m (37 ft, 3 in.). The exterior walls and air inlet and outlet plenums are 1.4 m (4 ft, 6 in.) thick. Interior partition walls between vaults are 0.9 m (3 ft) thick.

Only heavy, thick concrete structures are below grade: the interior and exterior vault walls, the intake and exhaust plenums, and the basemat. The northernmost vault (vault 1) will be equipped with tubes to provide storage for MCOs. The MCO storage vault is cooled by natural convection through a dedicated inlet and exhaust air stack and plenum. Based on SAR assumptions, thermal analysis indicates that the maximum air temperature inside the vault is 56 °C (133 °F) coincident with a steady-state intake air temperature of 46 °C (115 °F). The storage tubes are supported from the basemat of the vault and are accessed through shield plugs in the operating deck. The safety classification of the CSB vault structure is covered on pages 3-7 and 3-8 of WHC-SD-HWV-PSE-001, *Hanford Waste Vitrification Plant Canister Storage Building Preliminary Safety Analysis Report Addendum* (WHC 1994), which designated all of the structures contained in the below-grade or vault package as safety class.

Fully isolating vault 1 from vaults 2 and 3 provides sufficient shielding to permit personnel to install storage tubes in vaults 2 and 3 at a future time while vault 1 is operating. The total activity is given as 310,798 Ci for one MCO. The source term is driven primarily by alpha emitters. Based on SAR assumptions, shielding analysis indicates that the dose rate at the base of the intake stack is less than 0.05 mrem/h, and in the adjoining below-grade vault, the dose rate is less than 0.4 mrem/h.

The MCO storage tubes are provided with stainless steel expansion bellows to permit unrestricted thermal growth of the storage tube, accommodate differential movement of the operating deck in relation to the basemat slab, and seal the operating area from the vault. Tube plugs provide shielding and are equipped with double elastomeric seals. The tube plugs are recessed into the deck and extend slightly below the deck level at elevation 214.5 m (704

ft). The weight of the tube plugs rests solely on the storage tubes. The tube plugs are provided with venting and reinerting connections and HEPA-filtered relief devices. Tube plugs have locks to prevent loss of confinement should an MCO rupture disk burst. Tube plug covers protect the tube plug connections and devices and are flush with the operating deck. The tube plug covers have vents for plug relief valves.

Tube base assemblies are affixed to the basemat and the storage tubes are inserted into the tube base assemblies. The tube base assemblies have provisions for convective cooling to ensure that the temperature at the basemat slab will not exceed the 66 °C (150 °F) concrete temperature limit. The basemat slab embeds serve as alignment and horizontal seismic restrain points for the storage tube base assemblies. As described in Section 3.4, "Accident Analysis," the hazard analyses determined that the below-grade portion of the CSB is safety class.

A 1.5-m- (5-ft-) thick, standard, reinforced concrete operating deck structure forms the at-grade portion of the CSB. The operating deck and other operations areas are enclosed in a steel building. The operating deck contains numerous through-thickness steel sleeves (floor embeds) that receive the storage tubes and floor plugs for both the MCO and the MCO overpack locations in vault 1 and that provide a location for the tube plug cover plates in vault 1 or embed cover plates in vaults 2 and 3. Vault 1 contains 220 storage tubes, each capable of staging or storing two MCOs, plus 6 additional storage tubes to accommodate MCO overpacks. Each storage tube will contain an impact absorber to mitigate the consequences of a dropped MCO. The storage tubes are safety class, and along with the impact absorbers, they are designed to withstand all credible DBAs (WHC 1996b). The impact absorber is designed to prevent the breach of the storage tube and the MCO.

MCOs are transported from the CVDF in shielded casks and received into the operating area at the northwest corner of the CSB. Upon arrival at the CSB, the cask containing the MCO is unloaded by a gantry-type receiving crane. The crane is used to transfer the casks from the truck to a below-grade service station at the north end of the operating area. In the service station the cask lid is removed and the MCO is prepared for storage.

The MCO is then prepared for staging and placed in the MHM. The MHM contains an on-board confinement system to mitigate against the effects of an accidental drop of an MCO during placement in a storage tube. Maintaining the inerted gas environment in the MCO during transport from the service station to the storage tube will be ensured by the inert gas system on the MHM. The MHM is designated safety significant for its confinement function. The MHM is designed to maintain the atmosphere around the MCO inerted and the pressure inside the MHM cask negative with respect to the operating area.

Initially the MCOs containing SNF are staged in an inerted condition in the storage tubes. The MCOs are sealed with a safety-class rupture disk and a non-safety class pressure relief device. The SNF contained in the MCO is prone to hydrogen gas generation from radiolysis of bound and free water and from metal oxidation reactions. The hydrogen concentration must be maintained below the lower explosive limit. Although the storage tube is inerted, it is expected that the tube plug seals will permit some slow exchange of storage tube atmosphere with the operating area. To ensure that the gas concentration

will be kept out of flammable range, the storage tubes are evacuated periodically and reinerted. These operations are performed on a routine basis depending on observed hydrogen generation rates during staging. Tube purge and vent carts are provided to facilitate these hydrogen-related storage tube operations. Equipment on the carts can detect airborne radioactivity and dangerous concentrations of hydrogen in a sampled tube. Upon determining that the tube atmosphere is acceptable, cart equipment evacuates the tube and exhausts it into the operating area through HEPA filters. The storage tube then is reinerted to a slightly positive pressure. Tube purge and vent carts are designated safety significant to maintain an inerted atmosphere around an MCO. They are designed to safety significant criteria to prevent the hydrogen concentration in the storage tubes from reaching the lower explosive limit.

If the pressure inside a tube rises above 60 kPa gauge (9 lb/in^2 gauge), the tubes begin to vent to the operating area through a relief valve and HEPA filter in the tube plugs. Excess hydrogen generation is one cause for a rise in pressure inside the tube. The tube plugs are designed to maintain acceptable leakage levels and to vent only when over pressure in the tube occurs. The storage tube and the concrete plug above the tube are safety class and have been designed to remain intact and functional when subjected to a design basis earthquake. The tube plugs are designated safety class to control the ingress of air or egress of inerting gases to acceptable levels.

The MHM transfers the MCOs from the tubes to the HCS and returns them to the CSB storage tubes for sealed storage. Eventually, the MCOs containing SNF will be processed in the HCS. Upon completion of hot conditioning, the MCOs will be sealed and will then be stored in the CSB.

8.5 HOT CONDITIONING SYSTEM

The HCS is housed in an annex to the CSB. The HCS removes residual chemically bound water and metal hydrides from the fuel in the MCOs. The process minimizes the potential for subsequent pressurization of the sealed MCOs by removing constituents that can change phase to a gaseous state under storage conditions.

Hot conditioning of the fuel inside the MCOs takes place in one of six ovens, each located in a process pit below the CSB Annex operating deck. The ovens are essentially thermos bottles heated by forced convection air flow provided by support skids on the operating deck. The MCO is placed inside the oven, being supported by the stepped collar on the MCO. An insulating cover is placed over the top of the MCO.

The process pit provides secondary confinement and the process pit covers serve as supplemental radiation shielding. The covers have been designed with an integral inner plug. The MHM removes the inner plug of the cover to place the MCO inside the process oven and then replaces the inner plug, mimicking the cycle that the MHM goes through when an MCO is placed in or retrieved from a CSB storage tube. This allows the MHM to move the MCO into the process furnace while maintaining secondary confinement of the MCO.

To allow access to the top of the MCO for process line hookup, a portable enclosure is placed over the process pit. The process pit cover with its

integral plug is then temporarily opened to allow access to the top of the MCO. During the period while the process pit covers are opened, secondary confinement includes the process enclosure. A remote manipulator inside the process enclosure is used to attach process lines to the MCO and to remove them, and to service equipment under the process trench cover.

A process equipment module associated with each oven contains the convective heating and cooling supply system. Heated (up to 350 °C [575 °F]) or cooled air is supplied to the process furnace. The process module also contains a vacuum pump, process gas recirculation blower, and inert gas purge system to facilitate process offgas handling. Process lines that connect the process equipment module and the oven run below floor level in a trench. The thick steel plate that covers the trench provides shielding from any potential particulate or condensed volatile radioactive materials in the lines. The process lines have a cold trap and metal HEPA filter contained within the process trench.

The oven is insulated by a vacuum jacket that is supported by a vacuum pump on the service modules. A service module contains an exhaust fan and air cleaning equipment for the air in the process pits and trenches. The exhausts pass through air cleaning equipment before being discharged from the facility through a stack.

The radiation exposure associated with making and breaking the MCO connections, and with changing the in-trench HEPA filters and cold trap, is such that supplemental shielding is required to keep the operator exposure ALARA. Furthermore, the connections are made a few feet below the floor level where manual reach is awkward. Therefore, the portable process enclosure is used for these operations. It provides shielding and contains a hoist and remotely operated manipulator. The hoist is used to handle the process pit cover and the manipulators are used to make and break the MCO connections. The MCO is designed to support remotely manipulated connections and valves. The enclosure is ventilated so that it provides secondary confinement while the MCO's top is exposed and while the MCO ports are serviced.

After hot conditioning has been completed, the final closure is made while the MCO is still in the oven. The new cover cap is welded to the MCO shell and is designed to mate with the MHM grapple. After the MCO has been backfilled with an inert cover gas and sealed, the MHM returns it to a CSB storage tube for dry interim storage until a suitable long-term repository can be established. Once conditioned, an MCO is not expected to need venting during long-term interim dry storage at the CSB.

9.0 ACCEPTANCE CRITERIA AND MAINTENANCE PROGRAM

9.1 ACCEPTANCE CRITERIA

9.1.1 Visual Inspections and Nondestructive Examination

The fabrication specification for the MCO (WHC 1996b) describes the examinations to be performed by the fabricator of the MCO. The final closure weld for the MCO is a field weld that will be completed and examined by Duke Engineering and Services Hanford, Incorporated, personnel. The fabrication specification requires the fabricator to submit a written manufacturing plan and schedule, and to submit written and approved examination procedures and reports for buyer approval. The drawings appended to the fabrication specification (WHC 1996b) identify the welds to be examined and the type of examinations to be performed, and the specification text identifies the acceptance criteria. These requirements are presented below.

Personnel performing nondestructive examinations shall be qualified in accordance with NB-5520 or NF-5520, as applicable, SNT-TC-1A, and ANSI N45.2.6. Only individuals qualified for nondestructive testing levels I, II, or III may perform nondestructive testing. Personnel qualified at level I shall not interpret the results of an examination or make a determination of the acceptability of an examined part. Examinations shall be performed in accordance with Section V, Articles 2, 6, 7, and 9 for radiographic, liquid penetrant, magnetic particle, and visual methods, respectively.

All welds made by the fabricator shall be visually examined in accordance with the requirements of NB-4424 and NF-4424 as required. These requirements specify that welds that fail to meet the requirements will be repaired as necessary and re-examined.

The weld joining the cylindrical shell of the MCO to the bottom forging is a full-penetration circumferential weld that is to be examined by radiography, with acceptance determined according to the criteria of NB-5320 of the Boiler and Pressure Vessel Code (ASME 1995a), and by liquid penetrant examination, with acceptance determined according to the criteria of NB-5350 (ASME 1995a). Defects in weld metal detected by these examinations will be repaired and the repair examined in accordance with NB-4450.

Welds in the fuel baskets and associated support structures shall conform to the requirements of NF-4000 for class 1 plate and shell-type supports. Some welds require liquid penetrant examination, with acceptance determined according to NF-5350. Defects in weld metal detected in these examinations shall be repaired and the repair examined in accordance with NF-4450.

The weld joining the cylindrical shell to the collar is a full-penetration circumferential weld. Examination shall be by radiography, with acceptance determined according to NB-5320 (ASME 1995a). Defects in weld metal detected in these examinations shall be repaired and the repair examined in accordance with NB-4450.

The MCO and shell assembly welds will be radiographically examined, and the mechanical closure assembly, except for the actual production Helicoflex seal, will be hydrostatically tested at the fabricator's plant. These main structural parts of the MCO assembly outside of the shield plug penetrations, ports, connectors, and port covers will have no known exceptions to the Boiler and Pressure Vessel Code (ASME 1995a), Subsection NB.

The cover cap portion of the MCO will have two exceptions to the Boiler and Pressure Vessel Code (ASME 1995a), Subsection NB: the seal weld likely will be volumetrically inspected by ultrasonic means rather than by radiography, and pressure testing likely will not be done.

9.1.1.1 Pressure Tests. The mechanical closure and shell assembly will be hydrostatically tested then helium leakage rate tested as an assembled unit at the fabricator's plant. While at the basin load-out pit, the assembled MCO, with the shield plug and locking and lifting ring installed, will have the eight jack bolts torqued down. As this will be a qualified assembly, the goal is to make only a cursory leakage rate determination at the K Basins. If this goal is not met, leakage rate testing will have to occur either at each basin or at the CVDF.

9.1.1.2 Leakage Rate Tests. After joining the bottom forging to the shell, the welded assembly shall be helium leakage rate tested in accordance with Section V, Article 10, Appendix V of the Boiler and Pressure Vessel Code (ASME 1995a) to meet the intent of ANSI N14.5-1987, *For Radioactive Materials — Leakage Tests on Packages for Shipment* (ANSI 1987). The leakage rate test shall be performed by installing a test head on the top end of the shell and using a pressure difference of 0.1 MPa (1 atm). The maximum acceptable leakage is 1×10^{-4} standard cm^3/s (6.1×10^{-6} in^3/s).

Leak testing of the MCO shield plug will be performed in stages. After installation of the shield plug connections (i.e., quick connectors, HEPA filter, and rupture disk), the quick connectors and rupture disk shall be helium leak tested in accordance with the Boiler and Pressure Vessel Code (ASME 1995a), Section V, Article 10, Appendix V. The leak test shall be performed by internally pressurizing the connections to a test pressure of 69 kPa to 103 kPa (10 to 15 lb/in^2). The maximum acceptable leakage is 1×10^{-4} standard cm^3/s (6.1×10^{-6} in^3/s) for the connectors and the rupture disk.

After installation of the ring joint gasket and bolted blind flange for each of the connections (except the rupture disk), the entire shield plug assembly shall be tested in accordance with the Boiler and Pressure Vessel Code (ASME 1995a), Section V, Article 10, Appendix V. The leak testing shall be performed by installing a test hood/box on the top end of the shield plug and subjecting the connections to a test pressure differential of 0.1 MPa (1 atm). The maximum allowable total leakage is 1×10^{-7} standard cm^3/s (6.1×10^{-9} in^3/s), if required.

The long and short process tube assemblies (i.e., pipe, fittings, strainer, and closure plate) shall be leak tested in accordance with Section V, Article 10, Appendix I, of the Boiler and Pressure Vessel Code (ASME 1995a) after installation in the shield plug. Pressure for this bubble test shall be 69 kPa to 103 kPa (10 to 15 lb/in^2). The acceptance standard is

that there shall be no continuous bubble formation. If the acceptance standard is not met, the leak shall be located and repaired, and the assembly shall be tested again to the same acceptance standard.

The MCO shall be leak tested in the fabrication shop after the shield plug has been inserted, the locking ring installed, and the jack bolts tightened. The assembled MCO is then tested by hydrostatic means.

9.1.2 Components

9.1.2.1 Valves and Rupture Disks. Rupture disks will be accepted based on the ND requirements (ASME 1995a).

Acceptance criteria for valves are yet to be determined.

9.1.2.2 Gaskets. Acceptance criteria for gaskets for the mechanical closure of the MCO have not yet been determined.

9.1.3 Shielding Integrity

The shield plug is the only MCO component that provides a specific shielding function. Tests or dose rate measurements to characterize performance of the shield plug are not required. The codes used for the shielding analysis are identified in Chapter 5.0.

9.1.4 Thermal Acceptance

Thermal test requirements have not yet been determined.

9.2 MAINTENANCE PROGRAM

9.2.1 Subsystem Maintenance

The MCO subsystems do not require maintenance.

9.2.2 Valves and Rupture Disks

Maintenance requirements of the plug valves are expected to be minimal. Removal of the plug from the shield plug body is not expected unless the valve is damaged during operations.

Rupture disks do not require maintenance. Replacement of rupture disks would likely occur if the disk were actuated in service.

This page intentionally left blank.

10.0 RADIATION PROTECTION

10.1 ENSURING THAT OCCUPATIONAL RADIATION EXPOSURES ARE AS LOW AS REASONABLY ACHIEVABLE

10.1.1 Policy Considerations

The MCO design, in combination with other equipment and facilities, incorporates features to provide radiological protection and control and to support the basic philosophy of reducing radiation exposure levels to ALARA values. The MCO design takes into consideration the planned inspections, handling, and repair of the MCO. Design of the MCO was performed in a manner consistent with HSRCM-1, the ALARA Program (WHC 1995), and 10 CFR 835 requirements.

10.1.2 Design Considerations

Careful consideration has been directed towards designing the MCO to ensure the best possible radiological control features are incorporated and that occupational radiation exposure from MCO operations will be ALARA. The MCO needs to effectively reduce radiation exposure levels and also to perform its intended purpose efficiently. The MCO design utilizes connections that provide for remote manipulator operation or connection via long-handled tools to minimize the time during which a worker's hands are in proximity to the MCO shield plug. Sealing the MCO mechanically results in personnel dose rates of 195.6 mrem·person per MCO at the K East Basin and 117.6 mrem·person per MCO at the K West Basin. These dose rates presume a 1 in 100 mechanical repair ratio. For a total campaign of 400 MCOs, split equally between the two basins, a total personnel dose of 62.6 rem·person is spread out over the 2-year period.

Radiation shielding features have been incorporated into the MCO design. The MCO shield plug shields workers against gamma rays and neutrons emanating from the inside the MCO. This shielding will achieve an average dose across the top of the shield plug of 0.3 mSv/h (30 mrem/h) on contact (within 5 cm [2 in.]) for the average MCO fuel material to be handled. This value includes radiation streaming between the MCO shield plug and the MCO shell and around penetrations. For the worst-case fuel to be handled in the MCO, the average dose across the top of the shield plug on contact (within 5 cm [2 in.]) will not exceed 1.0 mSv/h (100 mrem/h). By reducing the average intermittent radiation dose rate level to 0.3 mSv/h (30 mrem/h) for very brief "hands-on" operations, the extremity dose is minimized while maintaining a practical and efficient design requiring minimal maintenance. The MCO design also has been influenced strongly by the desire for low maintenance, which translates into less radiation exposure overall for plant operations.

The MCO design allows for the fuel to be downloaded back into the K Basins should the MCO be leaking, defective, or damaged. The MCO shell design includes a flat floor and a small liquid collection sump at the bottom, and features and devices to facilitate the loading and stacking of the baskets within its storage cavity.

10.1.3 Operational Considerations

The MCO design provides lifting devices for the MCO shell and shield plug so lifting equipment can be used for safe lifting and handling of the MCO components and loaded MCOs. Hands-off handling of MCOs with lifting devices will be a key feature in reducing overall radiation exposure.

Facility-specific operating procedures and training will have a primary focus on safety and radiation control (and ALARA). Controlling radiation exposure depends on the careful coordinating of handling operations and the minimizing of residence time in radiation dose fields. Management emphasis on radiation protection and ALARA in team-building situations such as procedures development and training will help reinforce the appropriate safety culture and ALARA awareness for MCO operations.

10.2 RADIATION PROTECTION DESIGN FEATURES

Design of the MCO also has been driven by the need for a high-integrity, high-reliability container. The sealed MCO will maintain a maximum total leak rate (all leak paths) of 1×10^{-4} standard cm^3/s (6.1×10^{-9} in^3/s) during operations to remove fuel from the K Basins (after sealing the MCO), and during transfer, transport, and interim fuel storage, as required. The fully assembled MCO will retain fuel elements and fuel fragments (greater than 2 mm).

The exposed surfaces of the MCO will be smooth to the greatest extent practicable to minimize imperfections and facilitate ease of decontamination. Corners and other features that could collect contamination have been minimized to decrease contamination potential and to facilitate decontamination. Also, the MCO pressure relief strategy incorporates an internal bank of four HEPA filters.

10.3 ESTIMATED ONSITE COLLECTIVE DOSE ASSESSMENT

Planned MCO operations on a facility-specific basis will be reviewed to determine potential onsite dose estimates associated with major functions such as storage, handling, maintenance, or inspections. Facility-specific operations will factor estimated dose rates into overall facility operations and radiation protection management. Detailed dose assessments will be performed outside the scope of this topical report to facilitate appropriate operational planning activities.

11.0 MULTICANISTER OVERPACK ACCIDENTS

The MCO is the primary container for SNF from packaging in the K Basins through long-term interim storage at the CSB. The MCO functions as a container during transportation of the SNF, as a process vessel during conditioning of the SNF, and as a storage container. Throughout its lifetime the MCO may be subjected to a variety of challenges from accident conditions. Except for a postulated release of the water drained from the MCO during cold vacuum drying, all accident scenarios culminating in radioactive releases to the environment involve a breach of MCO containment.

WHC-SD-TP-SARP-017 (WHC 1996d) describes and analyzes potential accidents affecting the cask-MCO package during transportation from the K Basins to the CVDF, and from there to the CSB. The Safety Analysis Report for Packaging (SARP) shows that the package will not lose its ability to contain the SNF material in the event of a vehicle accident or fire (WHC 1996d). It also quantifies the maximum transport time to ensure the package's internal pressure cannot rise to levels that will breach the package containment during transport.

Hazard analyses for the cold vacuum drying process, for receiving, staging and storage at the CSB, and for the hot conditioning process identified credible accident initiators and sequences (WHC 1996a, WHC 1996e, WHC 1996f). A binning process revealed categories of accidents from which bounding scenarios for each facility were chosen. Descriptions of the hazard analysis and bounding accident selection for each facility are in the facilities' safety analysis documents (WHC 1996a, WHC 1996e, WHC 1996f).

The hazards analyses identified classes of accidents that, in general, are common to more than one phase of the process. These classes are MCO overpressurization and rupture disk relief, mechanical challenges to the MCO boundary (crane drops and impacts from other objects), hydrogen deflagration or detonation, and rapid oxidation of the nuclear fuel.

It is necessary to leave full development of the accident scenarios, and evaluation of the potential for exposure of humans to hazardous releases, to the facilities' safety analyses. MCO initial conditions at the commencement of an accident vary with the process stage. Therefore, the sequence of physical phenomena driving the release is unique at each stage.

Estimates of radiological and toxicological consequences to onsite and public receptors depend in part on meteorological conditions that are specific to the location at which the release occurs. Therefore, no estimates of accident results are made here. Instead, the general accident types, and analyses and conclusions that may be useful for developing the facilities' accident analyses, are presented.

11.1 SAFETY PHILOSOPHY FOR THE MULTICANISTER OVERPACK

The MCO has the primary containment function for the SNF throughout the process cycle. Therefore, the SNF Project is committed to providing a robust vessel that will withstand all credible challenges to that function.

The design basis is that the MCO will be shown to survive all credible DBAs without a catastrophic failure. In this case, catastrophic failure is taken to mean any breach of the MCO besides relief device actuation or process line breaks. Therefore, scenarios that postulate catastrophic breach of the MCO are considered as beyond DBAs.

The containment function of the MCO has been designated safety class. Hazard analyses identified credible event sequences that could challenge the structural integrity of the MCO (WHC 1996a, WHC 1996e, WHC 1996f). The forces that could provide this challenge during an accident may be external or internal to the MCO. The following DBA scenarios involve external forces:

- For the CVDF
  - Tipping the shipping cask, with the MCO inside, from the trailer
  - Truck collision with the MCO-cask-trailer system
  - External pressurization
- For the CSB
  - Sideways movement of the MHM while an MCO is part way in or out of the tube
  - Drop from the MHM or receiving crane into the cask
  - Drop from the MHM to the bottom of the tube
  - Drop from the MHM onto an MCO already in the tube.

For each of these scenarios, analysis shows that the MCO will not fail when subjected to the forces involved or the need for measures to protect the MCO from these forces has been identified (WHC 1996a, WHC 1996e). For the latter case, effective protective measures will be included in the system design. SSCs designed to perform this protective function would also be designated safety class.

Internal forces that could challenge the MCO integrity beyond actuation of the pressure relief device are the pressure pulse from a hydrogen detonation and pressure rise from a runaway fuel oxidation reaction. Therefore, the path forward process is designed to prevent occurrence of the physical conditions that could allow either event to occur.

11.2 MULTICANISTER OVERPACK ACCIDENT SOURCE TERM

The objective of accident analysis is to demonstrate that facility design adequately protects people and the environment from uncontrolled release of hazardous materials. Once the spent fuel is packed in the MCO at the K Basins, the MCO provides primary containment for the material, so a release scenario must postulate breach of the MCO boundary.

The spent fuel and associated particulate material constitute the hazardous contents of the MCO. Particles of the product of uranium corrosion, as well as other components of canister sludge, will remain on fuel surfaces and in crevices even after the fuel is washed. Additional oxide will form as exposed uranium metal reacts with air or water during transportation and processing.

Prevention of an MCO catastrophic breach precludes uncontrolled release of the fuel to the environment. Therefore, the dominant contributor to the radiological and toxicological release is the portion of the MCO particulate inventory that can become airborne and leave the MCO with the MCO gases. The material at risk for release is therefore taken to be the estimated bounding particulate content of the MCO. An estimate of the maximum amount of particulate that could be in an MCO after packaging, transportation, cold vacuum drying, and hot conditioning is provided in WHC-SD-SNF-TI-023, *Bounding Particulate Contents of a Multicanister Overpack* (Pajunen and Cowan 1996). The analysis shows that no more than 300 kg (660 lb) of particulate would be associated with fuel in an MCO that is packed with four baskets of fuel assemblies and one basket of fuel scrap.

The accident analyses assume that the particulate material in the MCO has the physical properties of uranium oxide. Data from characterization of sludge taken from open canisters in the K East Basin and from closed canisters in the K West Basin will be used to validate whether this assumption is conservative.

The bounding source term used for the accident analysis was based on data for the fuel in the K East and K West Basins given in WHC-SD-SNF-TI-009 (Willis 1995). That document defines an inventory for safety analysis based on selecting high-burnup Mark IV fuel, the fuel type that results in the highest estimated dose to people exposed to the material, and then treating all the fuel in the basins as high-burnup fuel. Nuclear accountability records gave the basis for the quantity, exposure variation, and decay time variation of the stored fuel. The radionuclide inventory was estimated from these data.

The radioactive inventory assumed for the MCO is the inventory associated with 270 high-burnup Mark IV fuel assemblies. The MCO will contain finely divided particulate material associated with the fuel. As noted, this includes particulate left on fuel surfaces and in crevices after fuel washing and racking into the MCO, with expected increases in oxidation products following cold vacuum drying, staging, and hot conditioning. The current baseline for the maximum theoretical quantity (for safety basis) of particulate material in the MCO is 300 kg (660 lb) (Pajunen and Cowan 1996).

The particulate inventory of the MCO dominates the airborne release. It is expected to be similar in makeup, and radionuclide content, to the sludge found in the canisters in the K Basins. Because the canister corrosion products have not yet been characterized, the analyses assume that the available particulate material contains the same radionuclide content as the fuel.

The SNF is primarily uranium metal, which is known to have toxicological effects. Plutonium and other heavy metals are present in smaller quantities.

It is not expected that the toxicological consequences of the release of these substances would require mitigating features beyond those required by the radiological doses.

The dose per unit material inhaled is the value for the total committed effective dose equivalent. The relative contribution of each nuclide to the total composite dose was calculated using the GENII computer code (Napier et al. 1988). The committed effective dose equivalent for a 50-year dose commitment period was calculated using the code's worst-case solubilities library (Huang 1996). This is the most conservative dose conversion factor library used by GENII.

The major radiation exposure pathway for the identified accidents is inhalation of radioactive material. Although there could be dose contributions from the groundshine and submersion pathways, the dose from the other pathways contributes less than 1% of the total dose for the radionuclides of interest. Therefore, the dose from groundshine and submersion are not included in the radiological dose calculations.

Potential doses from the ingestion pathway are not considered because DOE, state, and federal emergency preparedness plans in place limit ingestion of contaminated food in the event of an accident. The primary determinant of exposure from the ingestion pathway is the effectiveness of public health measures (i.e., interdiction) rather than the severity of the accident itself. The ingestion pathway, if it occurs, is a relatively slow-to-develop pathway and is not considered an immediate threat to an exposed population in the same sense as the inhalation pathway.

Table 11-1 shows the results of the radiological analysis of the K Basins fuel and the corresponding committed effective dose equivalent per gram of respirable release. Only those isotopes contributing more than 0.1% to the inhalation dose are reported, except for the gases ^{3}H and ^{85}K. Those two isotopes are included because their release pathways and release fractions can be significantly different than the isotopes primarily bound in the solid matrix. Isotopes of plutonium, ^{241}Am, ^{244}Cm, and ^{90}Sr constitute 99.6% of the total inhalation dose. The relative contribution from the remaining nuclides is minor in comparison. The specific dose for the safety analysis inventory is 4.3×10^{3} Sv/g (4.3×10^{5} rem/g).

11.3 BOUNDING ACCIDENTS FOR THE MULTICANISTER OVERPACK

Preliminary hazards analyses for each of the SNF facilities and processes identified credible accidents that could result in release of radioactive or toxic material from the MCO. The preliminary hazard analyses revealed some classes of accidents involving the MCO that are common to more than one of the processes. These include MCO breach caused by structural challenges, MCO overpressure and rupture disk relief, runaway fuel corrosion reaction, and hydrogen deflagration or detonation in the MCO.

Table 11-1. Radiological Analysis of K Basins Fuel (Combined Basin Inventories Decayed to January 1, 1995).

Radionuclide	Activity (Ci/MTU)	Committed effective dose equivalent per unit intake Sv/g (rem/g)
^{3}H	3.57 E+01	3.3 E-05 (3.3 E-03)
^{85}Kr	5.39 E+02	3.0 E-05 (3.0 E-03)
^{90}Sr	7.84 E+03	1.6 E+01 (1.6 E+03)
^{90}Y	7.84 E+03	7.0 E-01 (7.0 E+01)
^{137}Cs	1.08 E+04	3.3 E+00 (3.3 E+02)
^{238}Pu	1.71 E+02	6.7 E+02 (6.7 E+04)
^{239}Pu	1.58 E+02	7.0 E+02 (7.0 E+04)
^{240}Pu	1.28 E+02	5.8 E+02 (5.8 E+04)
^{241}Pu	9.25 E+03	7.6 E+02 (7.6 E+04)
^{241}Am	3.58 E+02	1.6 E+03 (1.6 E+05)
^{244}Cm	5.36 E+00	1.4 E+01 (1.4 E+03)
Total		4.3 E+03 (4.3 E+05)

*1.0 Ci = 3.7×10^{10} Bq.

MTU = metric ton of uranium.

The preliminary hazard analysis process is a systematic examination of the planned activities involving the SNF as it moves through a facility. A multidisciplinary team examines each planned activity at a facility to identify and record potential off-normal or accident-initiating events. The process identifies potential consequences of the event, and suggests design features and administrative controls to prevent or mitigate the consequences. Qualitative estimates of the consequence severity and the frequency of the initiating event are recorded.

Grouping of the identified accidents provides a means for choosing scenarios whose consequences bound the rest. Detailed analysis of the accident progression, unmitigated by any active design features, estimates the bounding airborne release for radiological and toxicological consequences to collocated workers and to the public. These estimates become the basis for selecting facility design features to protect receptors from unacceptably high exposure to the released material. Design features identified to provide this protective function are designated safety class if their primary purpose is to protect the public or safety significant if they are needed for protection of the collocated worker.

The MCO is the primary confinement/containment vessel for the SNF and associated particulate corrosion products. Its additional function is to maintain the SNF in a subcritical geometry. Prevention of nuclear criticality is a safety-class function. Based on the assumption that an uncontrolled fire in the dry fuel could occur if the fuel were exposed to unlimited quantities of air, and that the consequences of such a fire would provide unacceptably high doses to the public, the project has committed to preclude conditions that would permit such exposure. A catastrophic failure of the MCO could allow unlimited air to reach the fuel. Therefore, the fuel containment function of the MCO is a safety-class function. The MCO is designated safety class for both these functions.

Other safety-class or safety-significant design features, such as limiting particulate release, are facility specific and are not discussed here. The following sections discuss classes of accidents that involve the MCO and are common to the various facilities. The accident initiator, initial conditions, and some physical parameters that affect the accident's progress may be different depending on where the accident occurs. However enough similarities exist to allow for a generic treatment of the accident analysis.

Where appropriate, estimated release quantities from the MCO are given. Ultimate calculation of dose consequences to receptors depends on passive facility features to mitigate the release to the environment and on the location of the maximum receptor with respect to the facility. Therefore the calculation of dose consequences, and comparison with acceptance criteria, are reserved for the safety documentation for the individual facilities.

11.3.1 Multicanister Overpack Mechanical Damage from Impacts

Accidents that challenge the structural integrity of the MCO through external impacts are of two types: MCO drops or falls and external objects hitting the MCO. Design criteria for the MCO require that it retain its ability to contain the fuel and maintain subcritical configuration of the contents for all normal, off-normal, and credible accident events. Therefore, for all credible drops, falls, or impacts from external objects, analysis must show that these two design functions of the MCO are maintained.

At various stages in the process, the MCO, with its load of SNF, will be hoisted and lowered with cranes and transported by truck from one facility to another. After loading at the K Basins, it will be lifted, in its shipping cask, onto a flatbed truck trailer and fastened in place. The MCO will remain in the cask, on the trailer, during transport to the CVDF, during cold vacuum drying, and during transport from the CVDF to the CSB.

When the transport arrives at the CSB, an overhead crane will hoist the cask with the MCO inside it from the trailer and lower it into the receiving pit. After servicing, the MHM will hoist the MCO out of the cask, carry it to its designated vault location, and lower it into a storage tube. After 2 to 5 years of staging, the MHM will again lift the MCO from the tube, transport it to the HCS Annex, and place it in the hot conditioning oven. After processing, the MHM will move the MCO back to its storage tube and place it for long-term interim storage.

The MCO could be dropped from the crane during any of the lifting operations. In addition, the effect of tipping the cask off the truck, or tipping the trailer with the cask attached to it during a transportation accident, must be addressed. Impacts from external objects that must be considered include MHM movement while the MCO is partially in a storage tube, drop of one MCO onto another already in a storage tube, impact from a design basis tornado missile, a transportation vehicle collision accident, and flying debris from other accidental occurrences, such as unsecured depressurizing gas storage bottles. Design analyses are required to show that the MCO will survive its containment/confinement and noncritical configuration functions when subjected to any of these challenges, or the facility design must include features to preclude the event.

11.3.1.1 Multicanister Overpack Drops. The MCO crane drop scenarios include the following:

- MCO inside the transportation cask
  - While placing the loaded MCO-cask on the transport trailer (MCO and cask filled with water, maximum center of mass drop 9 m (30 ft) to reinforced concrete.
  - While moving the MCO-cask from the transport trailer to the CSB receiving pit (maximum center of mass drop 9 m (30 ft) to receiving area floor)
  - While placing the MCO-cask in the receiving pit (maximum center of mass drop 9 m (30 ft) or less into receiving pit)
- MCO alone
  - While lifting the MCO from the cask in the receiving pit (maximum center of mass drop 6.6 m (21.5 ft) into the cask); speed at impact is regulated by hydrostatic effects)
  - While moving the MCO to its storage tube, or between its tube and the HCS Annex (maximum center of mass drop 2.4 m (8 ft) to the operating deck floor)
  - While inserting the MCO into, or removing it from, a storage tube with no other MCO already in place (maximum center of mass drop 13.5 m [44 ft] to the bottom of the tube)
  - While inserting the MCO into, or removing it from, a storage tube with the lower MCO already in place (maximum center of mass drop 9.5 m [31 ft] to the top of the lower MCO).

Design analyses in Appendixes A, B, C, and D show that the MCO containment and internal configuration functions will survive the bounding drop scenarios. The free fall into the tube, either to the tube bottom, or onto another MCO, was analyzed assuming an impact limiter was in place at the bottom of the tube.

11.3.2 Multicanister Overpack Pressurization

Internal processes in the MCO will generate gases and release them to the MCO atmosphere. Fuel corrosion reactions and nuclear decay processes are the primary sources of gas generation. Whenever there is not an open flow path for communication of the MCO's atmosphere with the atmosphere of its surroundings, there is a potential for pressure buildup in the MCO.

Water is the important component of the MCO's contents from the perspective of gas generation. Water is the oxidant for the fuel corrosion reactions in the absence of free oxygen. The primary product of these reactions is hydrogen gas. In addition, the nuclear radiation field dissociates water into hydrogen and oxygen gases.

Process design will minimize the potential for pressurizing the MCO to its design limit (1.0 MPa gauge [150 lb/in^2 gauge]) by minimizing the amount of water available to participate in fuel corrosion reactions and radiolytic processes. However, there is a large uncertainty in the ability to predict or measure the quantity of water that will be left in an MCO. Therefore, the MCO will have overpressure relief when it is not directly vented to its surroundings. Before the hot conditioning process is accomplished, a relief valve with an upstream filter will ensure that the internal pressure remains below the MCO design pressure. A rupture disk, set to break at 1.0 MPa gauge (150 lb/in^2 gauge), is the ultimate protection against MCO breach caused by overpressure. After hot conditioning, it is possible for the relief valve to be disabled, and then the rupture disk will provide the only pressure relief on the MCO.

Rupture disk relief caused by MCO internal pressurization is an accident condition that has been identified for the CVDF and the CSB. The bounding scenario is a blowdown from 1.0 MPa gauge (150 lb/in^2 gauge) to atmospheric pressure. During the blowdown, MCO gases containing entrained particulates will leave the MCO and can enter the surrounding environment.

The inventory at risk is the 300 kg (660 lb) safety bounding case of particulate material in the MCO available for release. A particulate release fraction for an MCO blowdown from 1.0 MPa gauge (150 lb/in^2 gauge) to atmospheric pressure was estimated. Resuspension rate parameters for fuel assembly baskets and a scrap basket in the MCO were estimated using calculated flow velocities through the fuel baskets and experimental data for particulate resuspension. Calculation of the mass flow from the MCO breach during the blowdown provided the basis for estimating flow velocities over the fuel surfaces and estimating the duration of the event.

An MCO will contain five or six baskets of SNF stacked one above the other. The baskets will have perforated plate bottoms to facilitate draining and gas flow during processing. Most of the baskets will contain whole fuel assemblies resting vertically on their ends. They are arranged in a matrix in the basket with spaces between them. There will be a maximum of 54 fuel assemblies in a fuel basket. Some baskets will hold broken fuel pieces, ranging in size from half a fuel element to 0.6-cm (0.25-in.) pieces. In these scrap baskets, the fuel pieces will be randomly distributed and are modeled as a bed of rubble. There will be, at most, one scrap basket in an MCO.

The standard equations for compressible flow and choked flow were employed in a simple computer simulation to calculate the flow behavior during the blowdown. The following key MCO assumptions were used in the analysis.

- The area of the MCO rupture disk orifice was taken to be 3.2×10^{-5} m^2, corresponding to a 0.25-in.-diameter hole. The flow loss coefficient for the opening was 1.27, to account for a sudden contraction, friction losses, abrupt turns, and a sudden expansion.
- The MCO gas was assumed to be hydrogen, and the MCO free volume was 1.0 m^3.
- The temperature of the MCO gas was taken to be 75 °C throughout the event.

The standard compressible flow equation (Daily and Harleman 1966) gives

$$W = \frac{A}{\sqrt{K}} \left[\gamma P \rho \left(\frac{2}{\gamma+1} \right)^{\frac{\gamma+1}{\gamma-1}} \right]^{0.5}$$

where

W = mass flow rate (kg/s)
A = flow area (3.2×10^{-5} m^2)
K = loss coefficient (1.27)
ρ = density of the gas (kg/m^3)
P = gas pressure (Pa)
γ = ratio of specific heats for a gas (1.4 for diatomic gases, 1.667 for monatomic gases).

During the blowdown, pressure and gas density change with time.

The maximum free stream velocity past the fuel was calculated from the mass flow rate.

$$V_{MAX} = \frac{W}{\rho A_f}$$

where

A_f = the flow area through a cross section of a fuel basket (0.14 m^2 [224 in^2]).

A_f was taken as the difference between the cross-sectional area of the MCO and the total cross-sectional areas of 54 fuel assemblies. This equation applies to the upper portion of fuel loaded in the uppermost position. The free stream velocity is zero at the bottom of the MCO and increases linearly along the height of the MCO.

The gas velocity through the interstices in the scrap basket was estimated by observing that the free stream flow would be further restricted by passing through the smaller cross-sectional area available in the scrap basket. Using a void fraction, e, of 0.5 for the scrap, and assuming the maximum free stream velocity from the fuel basket for the gas as it enters the scrap basket, the interstitial velocity in the scrap basket, V_i, is given by

$$V_i = \frac{V_{MAX}}{e}.$$

The maximum possible interstitial velocity corresponds to a scrap basket in the uppermost position in the MCO. The maximum free stream velocity in a fuel basket was found to be 0.16 m/s. MCO blowdown for this case was estimated based on the calculated blowdown period for a 500-L gas volume provided in WHC-SD-WM-CN-079, *MCO Blowdown Release Fraction* (Kummerer and Plys 1996). Using a ratio of the new volume (1,000 L) to the original volume (500 L), the blowdown was estimated to be approximately 110 seconds. For this analysis, a 10% uncertainty factor was applied and the particulate release was determined on the basis of a 120-second MCO blowdown period. WHC-SD-WM-CN-079 (Kummerer and Plys 1996) also shows MCO pressure, gas temperature, and gas velocity transients during blowdown.

Data from measurements of particle resuspension rates in low air flow over surfaces were examined to provide a resuspension parameter for the fuel surfaces and the scrap basket. Report SR-0980-5, *Experimental Studies of Resuspension and Weathering of Deposited Aerosol Particles* (Reynolds and Slinn 1979), measured resuspension of ZnS particles from a surface in horizontal flows between 2 and 8 m/s. The particle mean diameter was 3 μm, and the particulate mass concentration on the surface was 10^{-3} g/cm^2.

The relationship derived from the data gives the following

$$\Lambda = 7.4 \times 10^{-10}\, U_\infty^{3.08}$$

where

Λ = resuspension rate parameter (1/s)
U_∞ = free stream velocity (m/s).

The resuspension rate parameter, Λ, was calculated from measured experimental parameters and is defined as follows:

$$\Lambda = \frac{M}{\chi A_s t}$$

where

M = resuspended mass
A_s = surface area
χ = particulate mass concentration on the surface
t = time the surface is exposed to the airflow.

The maximum air velocity of interest in the MCO is well below the flows used in the experiments. Extrapolating the experimentally derived relationship for Λ to the calculated MCO flow velocities gives

$$\Lambda = 7.4 \times 10^{-10} \ (0.16)^{3.08}$$

$$= 2.6 \times 10^{-12}/s$$

where

Λ = the resuspension parameter.

Using the experimentally derived resuspension rates, the airborne release fraction can be estimated by multiplying the resuspension parameter by the duration time of the blowdown. It is conservatively assumed that $\Lambda = 10^{-6}/s$.

$$ARF = \Lambda t$$

$$= \frac{10^{-6}}{s} \times 120 \ s$$

$$= 1.2 \times 10^{-4}.$$

This approach represents a departure from the pressurized powder models presented in DOE-HDBK-3010-94, *Airborne Release Fractions/Rates and Respirable Fractions/Rates for Nonreactor Nuclear Facilities* (Mishima 1994). It is an attempt to provide a model that more closely represents the physical configuration of the MCO system while still providing adequate conservatism. Key uncertainties involved in the approach, and conservative assumptions used to address them, include the following.

- Uniformly distributed flow across the MCO cross section is assumed. Flow splits would be likely to cause higher flows at the periphery with lower velocities through the fuel baskets so that entrained particulate would be lower than assumed by the analysis. Additional conservatism is provided by increasing the assumed airborne release fraction to the lower limit of the experimental data taken at 2 m/s (6.5 ft/s) air velocity.

- The data are reasonable for a scrap basket with 6-cm- (0.25-in.-) diameter particles that resemble gravel. The resuspension parameter is likely to be much higher for a smooth surface. However, surfaces in the MCO bearing corrosion products are expected to be rough. Data from "Initial Correlation of Particle Resuspension Rates as a Function of Surface Roughness Height" (Sehmel and Simpson 1975) show that an increase of about 3 orders of magnitude could be expected

for smooth surfaces, but the low end of the data still corresponds to a velocity of 2 m/s or greater, so a value of 10^{-6}/s is taken to bound the case.

- At present, no quantitative assumption can be made about the expected particle mass concentration, χ, on the fuel surfaces. However, concentrations greater than the 10^{-3} g/cm experimental condition are anticipated. Greater values of χ would give lower values for Λ. Therefore, the experimental data are judged to bound the SNF from the standpoint of surface particle mass concentrations.

- The expected MCO particulate may display different suspension characteristics than the material used to generate the experimental data. As characterization data on fuel particulate become available, the conservatism of using these data will be confirmed.

The respirable fraction is conservatively taken to be 1.0 because the experimental data are based on particles largely in the respirable range. Additional conservatism is introduced into the calculation by neglecting redeposit of particles by impaction caused by turns and bends in the gas-particle flow path, particularly as the flow passes through the scrap basket.

With the maximum particulate loading of 300 kg (660 lb) per MCO on arrival at the CSB, the estimated inventory released is

$$(1.2 \times 10^{-4})(300 \text{ kg}) = 3.6 \times 10^{-2} \text{ kg}.$$

11.3.3 Hydrogen Deflagration/Detonation Internal to the Multicanister Overpack

Hydrogen combustion inside the MCO must be prevented to protect its safety-class functions for containment of fuel.

Hydrogen gas will be produced in the MCO primarily from the corrosion of uranium, radiolysis of water, and degradation of uranium hydride. The primary source of hydrogen in the MCO is water. Before and during cold vacuum drying, significant quantities of water are available in the MCO. The cold vacuum drying process is designed to minimize the quantity of water in the MCO before staging or storage in the CSB. However, there is a large uncertainty in the ability to predict or measure the quantity of water that will be left in the MCO. It also is difficult to predict the quantity of hydrogen in the form of metal hydrides that will be available for release.

It is assumed that whenever the MCO is not vented to its environment, significant quantities of hydrogen will accumulate in the MCO gas space. If oxygen is available to react with the hydrogen, an explosive mixture may result. Five volume percent oxygen in a mixture of hydrogen with other gases is considered the lower limit to support a sustained reaction. Energy sources as low as those produced by sparks from metal striking against metal, or static sparks, can ignite flammable hydrogen-oxygen mixtures. Therefore, it is assumed that ignition sources of sufficient energy exist in the MCO.

The high likelihood of hydrogen and ignition source presence in the MCO gas space leads to the conclusion that oxygen must be eliminated to prevent conditions for ignition. Therefore, the MCO will be purged and backfilled with inert gas, probably helium, during transport, staging and storage. In the CSB, the secondary confinement structures (storage tube and MHM) around the MCO will likewise be filled with inert gas. There are also plans to inert the HCS process enclosure, ovens, and trench.

The preliminary hazard analyses conducted for each facility (WHC 1996a, WHC 1996g) identified potential accident conditions that could allow air to enter an MCO containing a significant proportion of hydrogen. Analyses indicate that the internal geometry of the MCO may allow for transition to detonation if a detonable mixture exists in the MCO. Uncertainties in important parameters for estimating hydrogen generation rates make it difficult to ensure that the gas mixture will not be in the detonable range, so it is assumed that a detonation would occur if oxygen is present. Therefore, facility designs will incorporate systems to prevent oxygen ingress to the MCO when process conditions may have allowed hydrogen buildup.

Radiolysis of water will produce oxygen as well as hydrogen in the MCO. This radiolysis of water to produce oxygen and hydrogen is the only identified source of oxygen in a pressurized MCO. Irradiation of metal oxides and organic compounds which may be part of the fuel particulate has not been identified as a source of measurable oxygen. In an effort to define the key parameters contributing to the presence of oxygen in the MCO, as well as how the availability of this oxygen may be limited, an extensive study is being conducted. An unvented MCO in staging or storage in the CSB may accumulate oxygen as well as hydrogen, leading to a flammable or explosive mixture. If enough exposed fuel surface is available, the oxygen produced by radiolysis will react with the uranium, producing more hydrogen, but making the oxygen unavailable for further reaction ("gettering").

Oxygen consumption rates for uranium metal in dry air were reviewed. Significant uncertainties in the literature rate data exist. The data in WHC-SD-SNF-TI-020, *Spent Nuclear Fuel Project Recommended Reaction Rate Constants for Corrosion of N Reactor Fuel* (Cooper 1996c), show a wide scatter at the planned temperatures (70-100 °C) for CSB fuel storage. An alternative rate equation proposed in WHC-SD-SNF-ER-014 (Fryer et al. 1996) differs from that in WHC-SD-SNF-TI-020 (Cooper 1996c) by a factor of 10. Bounding evaluations of oxygen getter performance were based on WHC-SD-SNF-TI-020 (Cooper 1996c) as this correlation provides conservative estimates of reacting surface area requirements. A range of rate equations was used in a probabilistic assessment of getter requirements.

A rationale for establishing the minimum effective area of exposed metal fuel based on the amount of uranium reacted was developed. The minimum effective uranium surface area is based on the corrosion rate of uranium in water at basin conditions to oxidize 1 kg of uranium over the fuel storage lifetime. The minimum area, computed based on the oxygen free water rate equation in WHC-SD-SNF-TI-020 (Cooper 1996c), is 1,330 cm^2/kg of fuel oxide formed. For the bounding MCO, the minimum uranium metal area that can generate 145 kg of fuel particulate is 193,000 cm^2.

The temperature of uranium in the MCO is dependent upon the power level of the MCO and the CSB inlet air temperature. The reaction rate is very sensitive to temperature. The increased fuel temperatures for the maximum heat generation MCOs more than offset the increased radiolytic production of oxygen due to the higher source term. Additional analysis would be needed to better define the minimum acceptable temperatures for oxygen consumption as a function of the MCO heat load position in the CSB, and the seasonal variation. For maximum oxygen removal efficiency, increasing the MCO temperature at the CSB would be necessary. Substitution of argon as the inert gas to fill both the CSB tube and the MCO increases the MCO internal temperature but this effect may not be sufficient to increase oxygen consumption rates to meet the maximum oxygen generation rate at bounding conditions.

For "gettering" to be successful, the oxygen taken up into the uranium must be equal to the generation from radiolysis. This has been expressed as a simplified steady state equation and evaluated for a range of input conditions. A probabilistic model arrived at a probability of 0.996 that no detonable mixture would be observed in an MCO without adding uranium getter or providing facility features to enhance gettering. This probability is above the 10^{-6} level, which is considered to be necessary before the event can be considered incredible; the 0.996 probability of no flammable mixture in any given MCO indicates that fewer than two MCOs would be expected to required oxygen removal. The results of a very conservative point value analysis show that, depending on the backfill gas in the MCO, 0.75 to 2 years is required for radiolytic oxygen to build up to 5%. Several options exist that would preclude development of flammable mixtures. The gettering analysis shows that if the CSB vault air temperature is maintained above 40 °C, oxygen removal by reaction with the existing uranium surface of the fuel is sufficient to preclude the potential for having a flammable mixture. MCO storage temperature control would be required to bound all possible combinations of environmental conditions and conservative assumptions.

Development of an MCO monitoring scheme either during processing or storage would provide an alternative to storage temperature control. Through a detailed inspection program, the status of each MCO could be monitored to assure that no hydrogen combustion would occur. The inspection requirements could than be modified as MCO specific data are collected.

As a final alternative, analysis efforts could be continued. Although time consuming, there is confidence that given enough information regarding characterization, corrosion product mass, and water content, analyses would confirm the ability of the current design to preclude a flammable atmosphere. If a credible case relying on oxygen gettering cannot be established, the MCOs will require venting during staging and storage.

11.3.4 Fuel Ignition

Fuel ignition is defined as a rapidly accelerating fuel corrosion reaction. The reaction generates heat and the reaction rate increases with temperature. If the heat is not dissipated efficiently, surrounding areas of fuel react and the temperature rise accelerates. Spontaneous ignition of uranium fuels in air has been observed at processing facilities.

Both the oxygen and the water in air will react to oxidize uranium metal. The reaction with water is more energetic than that with oxygen. Therefore, the potential for fuel ignition is greater in moist air atmospheres.

In the CSB, the potential for fuel ignition will be precluded by limiting air ingress rates into the MCO in the case of a rupture disk or process line break. In the CSB, the initial condition for the accident scenario is dry inert gas in the MCO gas space. Preliminary analysis has shown that if the openings for ingress of air are limited to the equivalent of one or two 1.3-cm- (0.50-in.-) diameter holes, the reaction is oxidant limited and will not accelerate to ignition. This analysis needs to be verified with the current baseline MCO assumptions.

It is not as easy to preclude a fuel ignition event in the cold vacuum drying or hot conditioning facilities. Until the cold vacuum drying process is completed, the MCO atmosphere will contain significant amounts of water vapor. A process upset could allow the fuel temperature to rise in the presence of moisture, providing conditions for potential fuel ignition. During hot conditioning, air ingress into an MCO that is at process operating temperatures could initiate ignition. Detailed analyses of the potential for, and effects of, a fuel ignition event in the MCO will be covered in the safety documentation for those facilities because the initial conditions for the event are significantly different in each case. Mitigation of these events, if required, is the responsibility of the facilities.

11.3.5 Thermal Transients

A number of scenarios have been identified that could allow the MCO shell to exceed its design temperature or design rate of temperature change limits. These include, among others, a failure of temperature control during hot conditioning and a loss of vault convective cooling during staging or storage in the CSB. Exceeding the design temperature of the MCO does not, of itself, lead to an MCO breach and release of any of the MCO contents. The issue is whether a degraded MCO is likely to continue to perform its expected functions for its lifetime. The effects of exceeding the MCO design temperature and rate of temperature rise criteria on the MCO's ability to fulfill its containment function over its 40-year lifetime must be fully assessed. This assessment includes evaluating the response of the MCO systems relied upon to maintain confinement to the temperature transients postulated in accident scenarios at the facilities and during transport. The analysis is the basis for establishing criteria for continued MCO service after an off-normal or accidental temperature excursion. Additional detail is provided in Chapter 4.0.

This page intentionally left blank.

12.0 TECHNICAL CONTROLS AND LIMITS

12.1 INTRODUCTION

This chapter identifies the necessary and sufficient set of system limits that will form the basis for developing the limiting conditions for operation (LCO) and surveillance requirements needed to establish the safety envelope for MCO-related operations. MCO-specific operating controls, limits, and supporting bases will be developed from this information and from facility-specific analyses. Actual controls will be in the facility technical safety requirements.

Facility-specific LCOs and surveillance requirements will be established for MCOs in the SARs, operational documents, controlled manuals, and technical specifications for each SNF Project facility that will process and handle the MCO. Operating controls and limits, when established, will include analyses of the bases and descriptions of anticipated surveillance requirements. MCO operating controls and limits include, as appropriate, both technical and administrative matters that are important to safety (e.g., spent fuel loadings, operating variables, or components). In addition, operating controls and limits address the attainment of ALARA levels of releases and exposures.

12.2 SYSTEM LIMITS

System limits are those limits that are not directly surveillable but that are key to ensuring safe MCO performance. Each system limit will correspond to one or more LCOs, either in this report or in the facility-specific SARs.

12.2.1 Multicanister Overpack Temperature System Limits

The MCO temperature limits are based on three considerations: the fuel melt limit, the steel limit, and the sealed MCO pressurization limit. These limits are summarized in Table 12-1. The following discussion presents these limits and develops the bases for the limits.

Table 12-1. Multicanister Overpack Temperature System Limits.

Parameter	Applicability	Safety limit	Basis
Fuel	All times	725 °C (1,337 °F)	Lowest fuel structural material eutectic formation
MCO thermal limit	All times	375 °C (700 °F)	52 °C margin from ASME limit
MCO thermal limit	Sealed MCO	200 °C (392 °F)	System pressure-related limit

MCO = multicanister overpack.

Eutectics between uranium and iron and between zirconium and iron occur at 725 °C (1,337 °F) and 950 °C (1,740 °F), respectively. It is not necessary that uranium be molten to form these eutectics. In principle, the interdiffusion of iron and uranium can lead to liquid formation even when both pure metals remain solid. Whether the physical contact between uranium and iron in the MCO can be intimate enough to lead to eutectic formation is doubtful in an MCO. Nonetheless, since 725 °C (1,340 °F) is well beyond the temperatures the MCO is expected to experience, there is merit in using this lower temperature as a system limit to further protect the MCO from damage.

The maximum steel boundary temperature is 375 °C (700 °F). This is appropriate based on the MCO boundary, which is constructed of 304L stainless steel in accordance with the intent of the Boiler and Pressure Vessel Code, Section III, Subsection NB (ASME 1995a). Selection of 304L stainless steel effectively limits the maximum temperature to 427 °C (800 °F) since L grades exhibit low strength in higher temperature ranges. The 375 °C (700 °F) limit was chosen to add an additional margin to the code limit. The Boiler and Pressure Vessel Code (ASME 1995a) case N 47 extends the rules of Subsection NB (ASME 1995a) to temperatures above 427 °C (800 °F), but this case does not permit construction using 304L stainless steel.

The most restrictive temperature limit is 200 °C (392 °F) at the outer MCO pressure boundary when sealed and pressurized to 1.0 MPa gauge (150 lb/in^2 gauge).

12.2.2 Multicanister Overpack Pressure System Limits

The MCO pressure limits are based on the specific design selected and the capabilities of 304L stainless steel in this design. These limits are summarized in Table 12-2.

Table 12-2. Multicanister Overpack Pressure Limits.

Location or feature	Applicability	Limit	Basis
MCO pressure boundary	Temperature at or below 200 °C (392 °F)	1.0 MPa gauge (150 lb/in^2 gauge)	Design limit
MCO pressure boundary	Temperature above 200 °C (392 °F) and at or below 375 °C (700 °F)	0.5 MPa gauge (75 lb/in^2 gauge)	Design limit

Note: This table is derived for HCS process use with the MCO under exclusive process supervision by HCS personnel. HCS is the only system allowed to exceed the 132 °C (270 °F) skin/containment boundary temperature limit of the MCO.

HCS = Hot Conditioning System.
MCO = multicanister overpack.

12.3 LIMITING CONDITIONS FOR OPERATION

Table 12-3 identifies the LCOs and surveillance requirements that establish the safety envelope for the MCO.

12.4 DESIGN FEATURES

The following design features are of special importance to each of the physical barriers and to maintenance of safety margins in the MCO:

- The MCO pressure boundary, including penetrations, seals, and plugs
- The MCO baskets, including features required for criticality control and structural integrity during collisions or drop accidents
- The MCO plug shielding capability
- The MCO oxygen gettering capability.

Design limits include the MCO transient limits noted in Table 12-4.

The cycle limits and rate of change are carried forward from the performance specification. Following an analysis for cyclic operation and testing, justification for a different cyclic life may be available.

12.5 ADMINISTRATIVE CONTROLS

Administrative control incorporates the control of design changes, compliance with process parameters, and quality assurance controls.

- The use of the Engineering Change Notice process ensures MCO design configuration control and the evaluation of change impact on all operational phases.
- The use of technical procedures ensures that process parameters are controlled within defined limits and that specified environmental conditions are maintained.

Table 12-3. Multicanister Overpack Operating Controls and Limits. (2 sheets)

	Specification or limiting condition for operation	Applicability	Objective	Action	Surveillance requirement	Bases
Maximum fuel mass	≤6,825 kg (15,050 lb)	Determined upon loading the MCO before transfer from the K Basins	Avoid exceeding mass limits for cranes	If the total mass exceeds the limit, reload the basket to meet the limit.	Measure the mass of each tier's basketload of fuel before insertion in the MCO.	Total mass of the cask and MCO combination to be lifted by the crane must be less than the K Basins' 30-ton crane limit, as well as less than subsequent facilities' crane limits. This limit preserves the free volume of an MCO at 0.5 m^3 (134 gal), ensuring that the analyses of pressurization for an MCO are valid. This limit ensures the total decay heat for each MCO remains below the 835 W maximum (plus appropriate margin) assumed in analyses.
Initial pressure	Pressure limits to be established by TSRs for the cask transportation system, the CVDF, the CSB, and the HCS	Established as the as-left pressure each time an MCO is sealed or shipped to another subproject or facility	Avoid overpressurization	If this pressure is exceeded, vent the MCO and reestablish the initial condition	Monitor immediately before sealing or shipping.	MCO pressurization analyses rely upon knowing the initial conditions before sealing. Significant excess pressure could result in MCO pressure exceeding the design limits.
Oxygen concentration	As-left oxygen concentration when MCO is sealed is ≤4%, or lower limit to be established by TSRs for the CSB	Determined immediately before sealing	Preclude hydrogen deflagration during long-term storage	If the oxygen limit is not achieved, place the MCO in a safe condition by purging and reestablishing an acceptable concentration.	Measure before sealed closure.	Oxygen will be generated by radiolytic decomposition of surface water over the MCO storage lifetime. Hydrogen will be released by both chemical reaction and radiolysis. It is likely that all oxygen and most hydrogen created will react with the residual exposed uranium. This limit ensures that the oxygen concentration will not exceed the lower explosive limit, precluding a deflagration of the oxygen-hydrogen mixture. This precludes failure of the MCO from acute pressure loading.

Table 12-3. Multicanister Overpack Operating Controls and Limits. (2 sheets)

	Specification or limiting condition for operation	Applicability	Objective	Action	Surveillance requirement	Bases
Pressure relief	Pressure relief up to 1.0 MPa gauge (150 lb/in^2 gauge)	Process points where the MCO is sealed, at staging or interim storage at the CSB	Preclude high-pressure (>1.0 MPa [>150 lb/in^2]) venting and unacceptable release and dose consequences	Replace the MCO rupture disk and pressure relief valve if they are not verified as fabricated and/or operable by the vendor according to applicable SNF Project manufacturing specifications. If the cover flange is found to be in place when sealing of the MCO is required, remove the flange.	Verify that the rupture disks and pressure relief valves are manufactured and/or operable by the vendor according to applicable SNF Project manufacturing specifications upon receipt from the vendor. Verify that rupture disk and pressure relief valve are not disabled by a cover flange.	MCO release scenarios for design and sizing of safety systems are based on release at a maximum pressure of 1.0 MPa gauge (150 lb/in^2 gauge). Increase in the pressure results in more significant releases.
Fuel type	Mark IA fuel may not be placed in a Mark IV basket	Determined during fuel loading operations within the K Basins	Control criticality	If an inappropriate configuration is identified, do not load the fuel into the MCO.	Verify correct basket and fuel loading during fuel retrieval.	Critically safe geometry within the MCO is maintained within the MCO assembly by design. The MCO shell is critically safe for loading with Mark IV fuel and the basket design is critically safe for Mark IA fuel. Even though a critically safe geometry may be maintained with two scrap baskets loaded into the MCO, the limitation on total particulate material mandates that no more than a single scrap basket shall be placed in any MCO for either type fuel.

CSB = Canister Storage Building.
CVDF = Cold Vacuum Drying Facility.
HCS = Hot Conditioning System.
MCO = multicanister overpack.
SNF = spent nuclear fuel.
TSR = technical safety requirement.

Table 12-4. Multicanister Overpack Transient Limits.

Location	Applicability	Limit	Basis
MCO pressure boundary	Temperature up to 375 °C (700 °F) and pressure up to 0.5 MPa gauge (75 lb/in^2 gauge)	<20 cycles at 75 °C (165 °F) <5 cycles at 375 °C (700 °F)	Design limit
MCO pressure boundary	All thermal transients	Rate of change <100 °C (180 °F) per hour	Design limit

13.0 QUALITY ASSURANCE

Quality assurance requirements will be applied to all aspects of the MCO design, fabrication, inspection, testing, handling, shipping, storage, and documentation. These requirements shall form a part of procurements, letters of instructions, and statements of work used as guidance for subcontractors, vendors or suppliers, or other agencies performing activities affecting the quality of the MCO.

The MCO is the one element that is common to all phases of the SNF Project. The MCO is present from initial fuel loading through ultimate disposition. Therefore, the MCO is subject to those quality assurance requirements that are associated with each phase of the overall process. Specifically, the MCO must meet the quality assurance requirements associated with design, fabrication, K Basins activities, transportation, and each of the facilities in which the MCO will be processed or stored.

13.1 DESIGN

The design agent must execute quality assurance programs that provide the following assurances:

- Assure performance requirements and design criteria are established, documented, and clearly understood
- Assure studies, analyses, and design decisions are fully documented
- Assure design meets performance requirements and design criteria
- Assure design is complete, adequate, and properly documented
- Assure traceability to the requirements of the contract technical specification is maintained.

13.2 FABRICATION

The seller is required to have an acceptable quality assurance program that shall be in effect throughout the fabrication, assembly, and testing of the MCO. The seller's quality assurance program shall apply to all components except as discussed in Sections 13.2.1.3 and 13.2.1.4. This program shall meet the applicable requirements of 10 CFR 71, Subpart H, and of Title 10, *Code of Federal Regulations*, Part 830, "Nuclear Safety Management," Subpart A, and Section 830.120, "Quality Assurance Requirements" (10 CFR 830). The quality assurance program must be accepted by the buyer before procurement of materials and fabrication is begun.

The MCOs should be fabricated in accordance with a quality assurance program meeting the minimum requirements of NHF-S-0548 (currently a draft) and subject to review and approval. Each component of the MCO is determined to be safety class, safety significant, or general service (non-safety significant). The attributes of the component that must be checked also are determined.

Table 13-1 summarizes the various components, their functions, safety classification, and failure consequences.

Quality records shall be directly traceable to an item; therefore, unique identifiers, as well as purchase order numbers, are required for items and components. The fabrication data package should include as-builts, nonconformance reports, certified materials test reports, hydrostatic test reports, nondestructive examination reports, and qualification and certification reports. An approved shipping and handling plan or procedure should also be specified.

13.2.1 Procurement of Category A Materials

Category A materials shall be procured from a supplier or manufacturer whose quality assurance program has been surveyed and/or audited by the seller to ensure the program meets the applicable requirements of 10 CFR 71, Subpart H. Quality assurance programs meeting the requirements of the Boiler and Pressure Vessel Code (ASME 1995a), Section III, NCA-3800, or the applicable requirements of ASME NQA-1 (ASME 1994) are an acceptable basis for these surveys and audits.

13.2.2 Procurement of Category B Materials

The following four methods are acceptable for procuring category B materials.

1. Procure material from a supplier or manufacturer holding a current ASME Section III Quality System Certificate (Materials).

2. Procure material from a supplier or manufacturer that has been surveyed and audited in accordance with the requirements of 10 CFR 71, Subpart H.

3. Procure materials from any supplier or manufacturer and perform all the examinations and tests required by the material specification. The seller shall prepare and supply a certified material test report stating that the material meets all the requirements of the specification.

4. Procure material from an ISO-9000 certificate holder.

13.2.3 Procurement of Category C Materials

Category C materials shall be procured from any source. A certificate of conformance shall be provided for all materials and items.

13.2.4 Procurement of Category "Not Important To Safety" Materials

Materials "not important to safety" shall be procured from any source.

Table 13-1. Multicanister Overpack Component Safety Designation. (2 sheets)

System/component	Function	SSC designation	Failure consequences
Multicanister overpack components			
Shell	Contain and protect SNF	SC	Release of radioactive contents that could exceed offsite exposure limits; loss of double-contingency protection against nuclear criticality accident
Shield plug	Contain SNF, protect personnel	SC[a]	Release of radioactive contents that could exceed offsite exposure limits
Locking and lifting ring plus bolts	Maintain pressure on main seal, allow for lift of loaded MCO	SC[a]	Release of radioactive contents that could exceed offsite exposure limits
Cover cap	Seal MCO after hot conditioning	SC	Release of radioactive contents that could exceed offsite exposure limits
Mark IA baskets	Maintain Mark IA SNF elements and scrap in a critically safe configuration	SC	Loss of double-contingency protection against nuclear criticality accident
Mark IV baskets	Contain Mark IV SNF elements and scrap	GS	No release consequences
Primary rupture disk	Protect MCO pressure boundary	SC	Overpressurization of MCO resulting in an uncontrolled release that could exceed offsite exposure limits
Plug valves	Process ports to accommodate gas flows in support of MCO processing	SS[a]	Inability to process the MCO; release of radioactive materials into the environment that exceed exposure limits
Process internal filter	Maintain most radioactive solid materials within the MCO	SS[b]	Release of radioactive materials from the MCO; pressure buildup within the MCO; loss of defense-in-depth protection for release of radioactive materials
External HEPA filter	Allow MCO to be stored in a vented configuration at the surrounding atmospheric pressure	SS[a]	Release of radioactive contaminants into the storage tube; pressure buildup within the MCO; loss of defense-in-depth protection for release of radioactive materials
Long process tube	Remove bulk water, introduce gases during processing, and reflood, if necessary	SS[a]	Inability to remove water from MCO; inability to introduce gases to process MCO; prevent processing that puts the MCO into a safe configuration
Short process tube	Remove water before shipping to CVDF; connect to rupture disk as vent path, backup process exit	SC	Failure of rupture disk to relieve internal MCO pressure; inability to remove water before shipping to CVDF
2-mm process tube screens	Keep particles > 2 mm in diameter in the MCO	SS	Particles larger than 2 mm may leave the MCO
Port covers	Seal ports during handling, transport, and storage; protect appliance under port cover	SS[a]	Damage appliance under the cover; release of contents into environment; possibly prevent processing to put the MCO into a safe configuration

Table 13-1. Multicanister Overpack Component Safety Designation. (2 sheets)

System/component	Function	SSC designation	Failure consequences
Seal	Seal MCO shield plug to shell	SC	Release of contents into surroundings that could exceed exposure limits
Orifice plates	Regulate gas flow from the MCO	SS[a]	Unregulated rate of gas release from the MCO
Process relief valve	Allow gases to leave MCO at a pressure below safety-class pressure relief device setting	SS[a]	Pressure buildup within the MCO resulting in venting through rupture disk
Guard plate on shield plug	Protect internal MCO process filter, short process tube, and 2-mm screen	SS	Potential damage to filter, short process tube, and screen
Bottom impact limiters	Protect MCO during drop in CSB tube	SC	Loss of MCO contents
Intermediate impact limiters	Protect MCO during drop in CSB tube	SC	Loss of MCO contents
Basket grapple receptacle	Provide an interface between the baskets and the MCO loading system	SS	Drop of fuel basket resulting in spilled fuel within the basin

[a]Will be downgraded to general service after cover cap is installed.
[b]May have a safety-class designation for up to 1 year after MCO loading.

CVDF = Cold Vacuum Drying Facility.
GS = general service (i.e., non-safety significant).
HEPA = high-efficiency particulate air (filter).
MCO = multicanister overpack.
SC = safety class.
SNF = spent nuclear fuel.
SS = safety significant.
SSC = structure, system, and component.

13.3 QUALITY CONTROL

13.3.1 Examination Point Program

An examination point program shall be prepared and included in the seller's manufacturing plan and submitted for approval. This examination point program shall include a description of all examination points and hold points.

13.3.2 Subcontractor Quality Control Procedures

The seller's and the seller's subcontractor's quality control procedures shall include the use of fabrication travelers or other process control documents. Fabrication travelers shall reference or describe the procedures used in accomplishing the tasks, the examination, the test requirements, and any examination hold points. Fabrication travelers shall include hold and witness points for review by the buyer.

13.3.3 Dimension Control

All dimensions, as indicated on the referenced design drawings, shall be measured and documented in accordance with the seller's examination procedures.

13.3.4 Access to Facilities for Quality Control

The buyer and the owner, or the owner's authorized agent, shall have full access to the seller's or the seller's subcontractors' facilities for reviewing progress and determining acceptability of quality control activities.

13.3.5 Access to Facilities for Quality Assurance

The buyer and the owner, or the owner's authorized agent, shall have full access to the seller's or seller's subcontractors' facilities for auditing the implementation of the seller's quality assurance program and for performing quality control surveillance of the MCO. Any findings resulting from audit or surveillance of the seller's or subcontractors' facilities shall be addressed and promptly corrected to the buyer's, owner's, or the owner's authorized agent's satisfaction.

13.3.6 Nonconformance

Nonconformances with purchase documents, drawings, approved procedures, or material requirements dispositioned as "repair" or "use-as-is" shall be submitted to the buyer for review and approval prior to implementation. The accepted nonconformance disposition shall include a technical justification provided by the buyer.

13.4 QUALITY REQUIREMENTS FOR SHIPPING RELEASE

The MCO shall not be shipped until the following requirements are met.

- All tests and examinations have been performed.
- The MCO final documentation package is complete and approved by the buyer's quality representative.

The seller shall notify the buyer two weeks before his intended shipping date and allow the buyer sufficient time before shipment to review the documentation package. The documentation package shall be complete and final before it is submitted for review, including documentation of the final performance tests. The buyer reserves the right to witness repetition of any or all of the final performance tests, and the pressure test, after the MCO and its documentation packages have been completed.

13.4.1 Certificate of Compliance

With the final documentation package, the seller shall submit to the buyer, a certificate of compliance to this specification and the design drawings. As a minimum, the certificate shall include, but not be limited to the following information:

- Purchase order number
- Procurement specification and design drawing numbers, including any approved changes, and nonconformances applicable to the equipment
- A certificate by the person who is responsible for the seller's quality assurance function
- Provisions for the signature of the buyer's quality representative. The buyer's signature is to indicate an agreement that the equipment and its documentation are ready for shipment, it does not constitute acceptance by the buyer.

13.5 PROCESS AND STORAGE FACILITIES

For the specific facilities, the MCO will fall under the quality assurance program identified in the SAR for each facility. The commitment to NRC equivalency may impact these quality assurance programs and result in different criteria than are required in other phases of the SNF Project. The specifics of the quality assurance program to be followed and the applicability of various codes and standards may be found in the facility SARs.

13.6 TRANSPORTATION

The quality assurance requirements to be followed during all stages of transporting the MCO are contained in the SARP. Specific instruction regarding when the SARP requirements apply is contained in the SARP.

This page intentionally left blank.

14.0 REFERENCES

10 CFR 71, "Packaging and Transportation of Radioactive Material," *Code of Federal Regulations*, as amended.

10 CFR 72, "Licensing Requirements for the Independent Storage of Spent Nuclear Fuel and High-Level Radioactive Waste," *Code of Federal Regulations*, as amended.

10 CFR 830, "Nuclear Safety Management," *Code of Federal Regulations*, as amended.

10 CFR 835, "Occupational Radiation Protection," *Code of Federal Regulations*, as amended.

Adams, R. O., 1983, "A Review of Stainless Steel Surfaces," *Journal of Vacuum Science and Technology A*, Vol. 1, pp 12-18.

ANSI, 1986, *For Radioactive Materials — Special Lifting Devices for Shipping Containers Weighing 10,000 Pounds (4500 kg) or More*, ANSI N14.6-1986, American National Standards Institute, New York, New York.

ANSI, 1987, *For Radioactive Materials — Leakage Tests on Packages for Shipment*, ANSI N14.5-1987, American National Standards Institute, New York, New York.

ANSI/ASME, 1989, *Testing of Nuclear Air-Cleaning Systems*, ANSI/ASME N510-1989, American Society of Mechanical Engineers, New York, New York.

ANSI/ANS, 1991, *Neutron and Gamma-Ray Fluence-to-Dose Factors*, ANSI/ANS-6.1.1-1991, American Nuclear Society, La Grange Park, Illinois.

ASM, 1986, *Binary Alloy Phase Diagrams*, T. B. Massalski, Editor, Vol. 2, American Society for Metals, Metals Park, Ohio, pp 1121, 1129, 2151.

ASM, 1987, *Corrosion*, Metals Handbook, Ninth Edition, Vol. 13, American Society for Metals, Metals Park, Ohio.

ASME, 1994, *Quality Assurance Requirements for Nuclear Facility Applications*, ASME NQA-1, Part II, Subpart 2.1, American Society of Mechanical Engineers, New York, New York.

ASME, 1995a, *Boiler and Pressure Vessel Code*, American Society of Mechanical Engineers, New York, New York.

ASME, 1995b, *Rules for Construction of Overhead and Gantry Cranes (Top-Running Bridge, Multiple Girder)*, ASME NOG-1-1995, American Society of Mechanical Engineers, New York, New York.

ASTM, 1996a, "Standard Practice for Cleaning and Descaling Stainless Steel Parts, Equipment, and Systems," A 380-94, *1996 Annual Book of ASTM Standards*, Vol. 01.03, American Society for Testing and Materials, Philadelphia, Pennsylvania.

ASTM, 1996b, "Standard Test Methods of Corrosivity of Water in the Absence of Heat Transfer (Electrical Methods)," D 2776- , *1996 Annual Book of ASTM Standards*, Vol. 11.01, American Society for Testing and Materials, Philadelphia, Pennsylvania.

Bell, G. I., and S. Glasstone, 1979, *Nuclear Reactor Theory*, Robert E. Krieger Publishing Co., Inc., Huntington, New York, pp. 122 - 125.

Berryman, J. G., 1983, "Definition of Dense Random Packing," *Advances in the Mechanics and the Flow of Granular Materials*, edited by M. Shahinpoor, Trans-Tech, Clausthal, Germany.

Breismeister, J. F., Editor, 1993, *MCNP — A General Monte Carlo N-Particle Transport Code, Version 4A*, LA-12625, Los Alamos National Laboratory, Los Alamos, New Mexico.

Brown, M. H., W. B. DeLong, and J. R. Auld, 1947, "Corrosion by Chlorine and by Hydrogen Chloride at High Temperatures," *Industrial and Engineering Chemistry*, Vol. 39, pp 839-844.

Butler, G., and H. C. K. Ison, 1966, *Corrosion and its Prevention in Waters*, Reinhold Publishing Corporation, New York, New York.

Carlos, W. C., 1993, *Multi-Function Waste Tank Facility Corrosion Test Report (Phase 1)*, WHC-SD-W236A-TRP-001, Rev. 0, Westinghouse Hanford Company, Richland, Washington.

Carter, L. L., 1996, *Certification of MCNP Version 4A for WHC Computer Platforms*, WHC-SD-MP-SWD-30001, Rev. 8, Westinghouse Hanford Company, Richland, Washington.

Caskey, G. R., 1983, *Hydrogen Compatibility Handbook for Stainless Steels*, DP-1643, E. I. du Pont de Nemours & Company, Savannah River Laboratory, Aiken, South Carolina.

Cooper, T. D., 1996a, *Spent Nuclear Fuel Project Estimate of Volatile Fission Products Release From Multi-Canister Overpacks*, WHC-SD-SNF-TI-033, Rev. 0, Westinghouse Hanford Company, Richland, Washington.

Cooper, T. D., 1996b, *Spent Nuclear Fuel Project Gas Generation from N-Fuel in Multi-Canister Overpacks*, WHC-SD-SNF-TI-028, Rev. 0, Westinghouse Hanford Company, Richland, Washington.

Cooper, T. D., 1996c, *Spent Nuclear Fuel Project Recommended Reaction Rate Constants for Corrosion of N Reactor Fuel*, WHC-SD-SNF-TI-020, Rev. 0, Westinghouse Hanford Company, Richland, Washington.

Cooper, T. D., and A. B. Johnson, 1996, *Spent Nuclear Fuel Project Surface Area Estimates For N-Reactor Fuel in the K East Basin*, WHC-SD-SNF-TI-026, Rev. 1, Westinghouse Hanford Company, Richland, Washington.

Cowan, R. G., 1995, *Revised MCO Inventory* (Internal Memo RGC-95-001 to M. K. Mahaffey, December 1), Westinghouse Hanford Company, Richland, Washington.

Daily, J. W., and D. R. F. Harleman, 1966, *Fluid Dynamics*, Addison-Wesley Publishing Company, Reading, Massachusetts.

DOE Order 5480.11, 1988, *Radiation Protection for Occupational Workers*, U.S. Department of Energy, Washington, D.C.

DOE Order 5480.28, 1993, *Natural Phenomena Hazards Mitigation*, U.S. Department of Energy, Washington, D.C.

DOE Order 6430.1A, 1989, *General Design Criteria*, U.S. Department of Energy, Washington, D.C.

DOE-STD-1020-94, 1994, *Natural Phenomena Hazards Design and Evaluation Criteria for Department of Energy Facilities*, U.S. Department of Energy, Washington, D.C.

DOE-STD-1022-94, 1994, *Natural Phenomena Hazards Site Characteristics Criteria*, U.S. Department of Energy, Washington, D.C.

DOE-STD-1023-95, 1995, *Natural Phenomena Hazards Assessment Criteria*, U.S. Department of Energy, Washington, D.C.

Duderstadt, J. J., and L. J. Hamilton, 1976, *Nuclear Reactor Analysis*, John Wiley & Sons, Inc., New York, pp. 432 - 435.

Emery, A., 1991, *View--A Radiation Viewfactor Calculation Program*, Version 5.6.9, University of Washington, Seattle, Washington.

Erickson, D. G., 1992, *WIMS-E Critical Mass Validation for 1.95 wt% and 3.85 wt% Uranium Billets*, WHC-SD-NR-CSER-004, Rev. 0, Westinghouse Hanford Company, Richland, Washington.

Fadeff, J. G., 1992, *Environmental Conditions For On-Site Hazardous Materials Packages*, WHC-SD-TP-RPT-004, Rev. 0, Westinghouse Hanford Company, Richland, Washington.

Ferrell, P. C., 1996, *Radioisotope Thermoelectric Generator Transportation System Safety Analysis Report for Packaging*, WHC-SD-RTG-SARP-001, Rev. 0, Westinghouse Hanford Company, Richland, Washington.

Fryer, B. C., M. J. Thurgood, and D. M. Ogden, 1996, *MCO Pressurization Analysis of Spent Nuclear Fuel Transportation and Storage*, WHC-SD-SNF-ER-014, Rev. 0, Westinghouse Hanford Company, Richland, Washington.

Gant, R. G., and J. A. Zilar, 1977, *Specifications for Uranium Metal Billets for N Reactor Fuel Elements*, UNI-M-22, Rev. 1, United Nuclear Industries, Inc., Richland, Washington.

Garvin, L. J., 1996, *Spent Nuclear Fuel Project Path Forward, Additional NRC Requirements*, WHC-SD-SNF-DB-003, Rev. 1, Westinghouse Hanford Company, Richland, Washington.

Geomatrix, 1996, *Probabilistic Seismic Hazard Analysis, DOE Hanford Site, Washington*, WHC-SD-W236A-TI-002, Rev. 1, prepared by Geomatrix Consultants, Incorporated, for Westinghouse Hanford Company, Richland, Washington.

Glass, R. E., 1988, *Standard Thermal Problem Set for the Evaluation of Heat Transfer Codes Used in the Assessment of Transportation Packages*, SAND88-0380, Sandia National Laboratories, Albuquerque, New Mexico.

Goldmann, L. H., 1996, *Spent Nuclear Fuel Multi-Canister Overpack Technical Functions and Requirements*, WHC-SD-SNF-FRD-016, Rev. 0, Westinghouse Hanford Company, Richland, Washington.

Grumbly, T. P., 1995, *Concurrence with the K-Basins Spent Nuclear Fuel Project Policy on Nuclear Safety Requirements* (Memorandum EM-36-3.1.6.7 to Manager, U.S. Department of Energy, Richland Operations Office, July 20), U.S. Department of Energy, Washington, D.C.

Gubbins, M. E., M. J. Roth, and C. J. Taubman, 1982, *A General Introduction to the Use of the WIMS-E Modular Program*, AEEW-R 1329, Reactor Physics Division, AEE Winfrith, England.

Hansen, C. A., 1995, *Approval of Spent Nuclear Fuel (SNF) Path Forward Recommendation* (letter to President, Westinghouse Hanford Company, February 14), U.S. Department of Energy, Richland, Operations Office, Richland, Washington.

Heard, F. J., 1994, *FIDAP — Validation/Verification*, WHC-SD-WM-ER-302, Rev. 1, Westinghouse Hanford Company, Richland, Washington.

Heard, F. J., E. R. Cramer, T. R. Beaver, and M. J. Thurgood, 1996a, *Thermal Hydraulic Feasibility Assessment for the Spent Nuclear Fuel Project*, WHC-SD-WM-ER-525, Rev. 0, Westinghouse Hanford Company, Richland, Washington.

Heard, F. J., T. R. Beaver, and M. J. Thurgood, 1996b, *Thermal Hydraulic Feasibility Assessment of the Hot Conditioning System Process*, WHC-SD-SNF-ER-012, Rev. 0, Westinghouse Hanford Company, Richland, Washington.

Hellens, R. L., and H. C. Honeck, 1962, "A Summary and Preliminary Analysis of the BNL Slightly Enriched Uranium, Water Moderated Lattice Measurements," *Light Water Lattices*, Brookhaven National Laboratory, International Atomic Energy Agency, Vienna.

HSRCM-1, 1994, *Hanford Site Radiological Control Manual*, Rev. 2, Westinghouse Hanford Company, Richland, Washington.

Huang, C. H., 1996, *Unit Dose Calculation for the K Basins Safety Regulatory Assessment Feed Basis*, WHC-SD-WM-TI-742, Rev. 0, Westinghouse Hanford Company, Richland, Washington.

ICBO, 1994, *Uniform Building Code*, International Conference of Building Officials, Whittier, California.

Idelchik, I. E., 1994, *Handbook of Hydraulic Resistance*, Third Edition, CRC Press, Incorporated, Ann Arbor, Michigan.

Implementation Guide G-10 CFR 835/B2, Revision 2, "Occupational ALARA Program"

Jack, M. L., 1988, *NUSAR — N Reactor Updated Safety Analysis Report*, WHC-EP-0240, Vol. 3, Westinghouse Hanford Company, Richland, Washington.

Jobs, G. J. H., and H. Liskien, 1990, *Energy Spectra of Neutrons Produced by A-Particles in Thick Targets of Light Elements*, Ann. Nucl. Energy, Vol. 10, pp 541-552.

Kaviany, M., 1995, *Principles of Heat Transfer in Porous Media*, Springer-Verlag, New York, New York.

Kohli, R., 1982, "A Thermodynamic Assessment of the Behavior of Cesium and Rubidium in Reactor Fuel Elements," *Material Behavior and Physical Chemistry in Liquid Metal Systems*, H. U. Borgstedt, Editor, Plenum Press, New York, New York, pp 345-350.

Kreith, F., 1973, *Principles of Heat Transfer*, 3rd Edition, Harper & Row Publishers, New York, New York.

Kummerer, M., 1995, *Hazard Category Analysis for the Canister Storage Building*, WHC-SD-SNF-HC-007, Rev. 0, Westinghouse Hanford Company, Richland, Washington.

Kummerer, M., and M. Plys, 1996 *MCO Blowdown Release Fraction*, WHC-SD-WM-CN-079, Rev. 0, Westinghouse Hanford Company, Richland, Washington.

Kupinski, A. F., and H. Toffer, 1970, *Use of the HAMMER System for Evaluating Light-Water Moderated, Critical Assemblies*, DUN-7286, Douglas United Nuclear, Richland, Washington.

Mishima, J., 1994, *Airborne Release Fractions/Rates and Respirable Fractions/Rates for Nonreactor Nuclear Facilities*, DOE-HDBK-3010-94, U.S. Department of Energy, Washington, D.C.

Miska, C. R., 1996, *Spent Nuclear Fuel Conditioning Product Criteria*, WHC-SD-SNF-OCD-001, Rev. 0, Westinghouse Hanford Company, Richland, Washington.

Napier, B. A., R. A. Peloquin, J. V. Ramsdell, and D. L. Strenge, 1988, *GENII - The Hanford Environmental Radiation Dosimetry Software System*, Vol. 1, PNL-6584, Pacific Northwest Laboratory, Richland, Washington.

NFPA, 1991, *Safety to Life from Fire in Buildings and Structures*, NFPA 101, National Fire Protection Association, Quincy, Massachusetts.

NRC, 1978, *Information Relevant to Ensuring that Occupational Radiation Exposures at Nuclear Power Stations Will Be As Low As is Reasonably Achievable*, Regulatory Guide 8.8, Rev. 3, U.S. Nuclear Regulatory Commission, Washington, D.C.

NRC, 1981, *Standard Review Plan*, NUREG-0800, U.S. Nuclear Regulatory Commission, Washington, D.C.

NRC, 1984, *Fabrication Criteria for Shipping Containers*, NUREG/CR 3854, U.S. Nuclear Regulatory Commission, Washington, D.C.

NRC, 1989a, *Standard Format and Content for a Topical Safety Analysis Report for a Spent Fuel Dry Storage Cask*, Regulatory Guide 3.61, U.S. Nuclear Regulatory Commission, Washington, D.C.

NRC, 1989b, *Standard Format and Content for the Safety Analysis Report for an Independent Spent Fuel Storage Installation or Monitored Retrievable Storage Installation (Dry Storage)*, Regulatory Guide 3.48, Rev. 1, U.S. Nuclear Regulatory Commission, Washington, D.C.

NRC, 1996, *Standard Review Plan for Dry Cask Storage Systems*, NUREG-1536, for comment, U.S. Nuclear Regulatory Commission, Washington, D.C.

Old, C. F., 1980, "Liquid Metal Embrittlement of Nuclear Materials," *Journal of Nuclear Materials*, Vol. 92, pp 2-25.

Pajunen, A. L., and R. G. Cowan, 1996, *Bounding Particulate Contents of a Multicanister Overpack*, WHC-SD-SNF-TI-023, Rev. 1, Westinghouse Hanford Company, Richland, Washington.

Parsons Infrastructure and Technology, Inc., Interoffice Correspondence IOC-1196, W. E. Schenewerk to R. Bastar, March 3, 1996.

Pearce, R. J., 1989, *A Review of the Rates of Reaction of Unirradiated Uranium in Gaseous Atmospheres*, Report RD/B/6231/R89, Central Electricity Generating Board, Berkeley Nuclear Laboratories, Berkeley, England.

Phillips, J. D., Sr., and E. R. Jacobs, 1996, *Spent Nuclear Fuel Project Canister Storage Building - Neutron Quality Factors*.

Reynolds, B. W., and W. G. N. Slinn, 1979, *Experimental Studies of Resuspension and Weathering of Deposited Aerosol Particles*, Report SR-0980-5, Oregon State University, Corvallis, Oregon.

Ritchie, A. G., 1981, "A Review of the Rates of Reactions for Uranium in Oxygen and Water Vapor at Temperatures up to 300 °C," *Journal of Nuclear Materials*, 102, pp 170-182.

Rogers, C. A., K. N., Schwinkendorf, and H. Harris, 1996, *Criticality Parameters for Tank Waste Evaluation*, WHC-SD-SQA-CSA-507, Rev. 0, Westinghouse Hanford Company, Richland, Washington.

Schwinkendorf, K. N., 1985a, *Validation of the WIMS Code for Tubular Uranium Fuel Elements*, UNI-SA-142, UNC Nuclear Industries, Incorporated, Richland, Washington.

Schwinkendorf, K. N., 1985b, *WIMS Critical Mass Validation for 1.95 wt% and 3.85 wt% Uranium Billets*, UNI-3486, UNC Nuclear Industries, Incorporated, Richland, Washington.

Schwinkendorf, K. N., 1992a, *Criticality Safety Evaluation Report, 105-KE Basin Fuel Encapsulation*, WHC-SD-NR-CSER-007, Rev. 1, Westinghouse Hanford Company, Richland, Washington.

Schwinkendorf, K. N., 1992b, *Validation of WIMS-E for Prediction of Uranium, Plutonium Nitrate Solution Critical Masses*, WHC-IP-0840-FMEF, Westinghouse Hanford Company, Richland, Washington.

Schwinkendorf, K. N., 1994, *Software Certification Package for the GOLF Code*, WHC-SD-NR-SWD-024, Rev. 0, Westinghouse Hanford Company, Richland, Washington.

Schwinkendorf, K. N., 1995, *Criticality Safety Evaluation Report for 300 Area N Reactor Fuel Fabrication and Storage Facility*, WHC-SD-NR-CSER-010, Rev. 1, Westinghouse Hanford Company, Richland, Washington.

Schwinkendorf, K. N., 1996, *Criticality Safety Evaluation Report for Spent Nuclear Fuel Processing and Storage Facilities*, WHC-SD-SNF-CSER-005, Rev. 2, Westinghouse Hanford Company, Richland, Washington.

Sedricks, A. J., 1992, "Stress-Corrosion Cracking of Stainless Steels," *Stress Corrosion Cracking*, Russell H. Jones, Editor, ASM International, Metals Park, Ohio, pp 118-119.

Sehmel, G. A., and C. L. Simpson, 1975, "Initial Correlation of Particle Resuspension Rates as a Function of Surface Roughness Height," *Pacific Northwest Laboratory Annual Report for 1974 to the USAEC Division of Biomedical and Environmental Research*, BNWL-1950, Battelle Pacific Northwest Laboratories, Richland, Washington.

Sellers, E. D., 1996, *Hazard Category for the Spent Nuclear Fuel Project Canister Storage Building (CSB)* (Letter 95-SFD-250 to President, Westinghouse Hanford Company, January 10), U.S. Department of Energy, Richland Operations Office, Richland, Washington.

Short, S. M., 1995, *Spent Nuclear Fuel Project Technical Databook*, WHC-SD-SNF-TI-015, Rev. 0, Westinghouse Hanford Company, Richland, Washington.

Shrivastava, H. P., 1996, *ASME Section III, Subsection NB, Analysis of the Multi-Canister Overpack Assembly with the Mechanical Closure Ring*, SCS-W-96-1606, ICF Kaiser Hanford, Richland, Washington.

SINDA, 1995, *Systems Improved Numerical Differencing Analyzer and Fluid Integrator*, Version 3.1, prepared by Cullimore and Ring Technologies, Inc., Littleton, Colorado, for NASA, Johnson Spacecraft Center, Texas.

SK-1-80110, Rev. 0, *K-Basin SNF Storage Basket Mock-Up*, not dated.

SK-1-80208, 1996, *K-Basin SNF Storage Basket Mock-Up Mark IA and Mark IV*, Rev. 0, Company, City, State.

SK-1-80209, 1996, *K-Basin SNF Storage Scrap Basket Mock-Up Mark IV*, Rev. 0, Company, City, State.

SK-1-80210, 1996, *K-Basin SNF Storage Scrap Basket Mock-Up Mark IA*, Rev. 0, Company, City, State.

SK-2-300377, Rev. 0, *MCO Prototype SNF Rerack Basket Grapple Adapter*, dated March 22, 1996.

SK-2-300378, 1996, *MCO Prototype Shell Bottom Machined Forging*, Rev. 0.

Tallman, A. M., 1996a, *Canister Storage Building Natural Phenomena Hazards*, WHC-SD-SNF-DB-009, Rev. 4, Westinghouse Hanford Company, Richland, Washington.

Tallman, A. M., 1996b, *Cold Vacuum Drying System Natural Phenomena Hazards*, WHC-SD-SNF-DB-010, Rev. 1, Westinghouse Hanford Company, Richland, Washington.

Whalen, D. J., D. A. Cardon, J. L. Uhle, and J. S. Hendricks, 1991, *MCNP: Neutron Benchmark Problems*, LA-12212, Los Alamos National Laboratory, Los Alamos, New Mexico.

WHC, 1994, *Hanford Waste Vitrification Plant Canister Storage Building Preliminary Safety Analysis Report Addendum*, WHC-SD-HWV-PSE-001, Rev. 0A, Westinghouse Hanford Company, Richland, Washington.

WHC, 1995, *WHC Occupational ALARA Program*, WHC-IP-1043, Rev. 0, Westinghouse Hanford Company, Richland, Washington.

WHC, 1996a, *Canister Storage Building Safety Analysis Report - Phase 2: Safety Analysis Documentation Supporting Canister Storage Building Subsurface Construction and Fabrication of Tubes, Multicanister Overpack Handling Machine, and Receiving Crane*, WHC-SD-SNF-RPT-004, Rev. 2, Westinghouse Hanford Company, Richland, Washington.

WHC, 1996b, *Fabrication Specification for Multi-Canister Overpack*, WHC-S-0453, Rev. 0, Westinghouse Hanford Company, Richland, Washington.

WHC, 1996c, *Performance Specification for the Spent Nuclear Fuel Project, Multi-Canister Overpack*, WHC-S-0426, Rev. 1, Westinghouse Hanford Company, Richland, Washington.

WHC, 1996d, *Preliminary Safety Analysis Report for Packaging (Onsite) Multiple Canister Overpack Cask*, WHC-SD-TP-SARP-017, Rev. 0, DRAFT, Westinghouse Hanford Company, Richland, Washington.

WHC, 1996e, *Preliminary Safety Evaluation for the Spent Nuclear Fuel Project's Cold Vacuum Drying System*, WHC-SD-SNF-PSE-003, Rev. 0, Westinghouse Hanford Company, Richland, Washington.

WHC, 1996f, *Preliminary Safety Evaluation for the Spent Nuclear Fuel Project's Hot Conditioning System*, WHC-SD-SNF-PSE-004, Rev. 0, Westinghouse Hanford Company, Richland, Washington.

WHC, 1996g, *Safety Analysis Report for the Cold Vacuum Drying Facility, Phase 1, Supporting Civil/Structural Construction*, WHC-SD-SNF-SAR-002, Rev. 0, Westinghouse Hanford Company, Richland, Washington.

Willis, W. L., 1995, *105-K Basin Material Design Basis Feed Description for Spent Nuclear Fuel Project Facilities*, WHC-SD-SNF-TI-009, Rev. 0A, Westinghouse Hanford Company, Richland, Washington.

Wittekind, W. D., 1991, *N Reactor Spent Fuel Compacted Storage Criticality Calculations*, WHC-SD-NR-CSA-004, Westinghouse Hanford Company, Richland, Washington.

Wittekind, W. D., 1992, *K Basin Criticality Evaluation for Irradiated Fuel Canisters in Sludge*, WHC-SD-NR-CSER-001, Rev. 0, Westinghouse Hanford Company, Richland, Washington.

Wittekind, W. D., 1993, *Criticality Safety Evaluation K Basin Storage Rack Seismic Qualification*, WHC-SD-NR-CSER-009, Rev. 0, Westinghouse Hanford Company, Richland, Washington.

Wittekind, W. D., 1994a, *MCNP Calculations of K-Infinity for 100KE Basin Sludge Samples*, WHC-SD-NR-CSER-008, Rev. 1, Westinghouse Hanford Company, Richland, Washington.

Wittekind, W. D., 1994b, *Software Configuration Control Package for the ORIGEN2 Code*, WHC-SD-NR-SWD-023, Rev. 0, Westinghouse Hanford Company, Richland, Washington.

This page intentionally left blank.

APPENDIX A

MULTICANISTER OVERPACK BUCKLING

This page intentionally left blank.

ICF KAISER HANFORD

DESIGN ANALYSIS

Revision 0
Page No. 1 of 3

Client: Westinghouse Hanford K Basin SNF Project
Subject: MCO Elastic Buckling Evaluation

Date: 02/15/96
Orginator : L. L. Hyde
Checker : D. M. Chenault

ELASTIC BUCKLING OF THE MCO

Analyze the elastic buckling capability of the Multi-Canister Overpack (MCO) shell with and without internal pressure. Determine the vertical drop acceleration which this capability allows.

Reference: *Structural Analysis of Shells*, E. H. Baker, et. al., R. E. Krieger Publishing Company, Huntington, N. Y., 1981

In accordance with Section 10-3 of the Reference the elastic buckling stress of an initially straight moderately long cylinder, at 200°C is,

Modulus of Elasticity, $E := 26.6 \cdot 10^6 \cdot \frac{lb}{in^2}$

Material Yield Stress, $F_y := 17600 \cdot \frac{lb}{in^2}$

Material Poissons Ratio, $\mu := 0.3$

MCO Shell Thickness, $t := 0.5 \cdot in$

MCO Shell Mean Radius, $R := \frac{24 \cdot in - t}{2}$ $R = 11.75 \cdot in$

Buckling Stress Coefficient, $C_c := \frac{1}{\sqrt{3 \cdot (1 - \mu^2)}}$ $C_c = 0.605$

Buckling Correlation Factor, $\gamma := .73$ for, $\frac{R}{t} = 23.5$

Buckling Stress, $\sigma_e := \gamma \cdot C_c \cdot \frac{E \cdot t}{R}$

$\sigma_e = 500098 \cdot \frac{lb}{in^2}$ >> F_y

ICF KAISER HANFORD

DESIGN ANALYSIS

Client: Westinghouse Hanford K Basin SNF Project
Subject: MCO Elastic Buckling Evaluation

Date: 02/15/96
Orginator : L. L. Hyde
Checker : D. M. Chenault

ELASTIC BUCKLING OF THE MCO (cont'd)

If the MCO shell is treated as a simply supported cylinder 160 inches long, the Euler column elastic buckling stress is,

$$L := 160 \cdot in$$

$$\sigma_{Euler} := \frac{\pi^2}{2} \cdot E \cdot \left(\frac{R}{L}\right)^2 \qquad \sigma_{Euler} = 707925 \cdot \frac{lb}{in^2} \qquad >> \quad \sigma_e$$

Since R/t << 700 the influence of internal pressure is negligible on the above calculated elastic buckling stress but it does influence the effective compressive stress.

The allowable compressive stress in the MCO shell is limited to F_y when the internal pressure is zero and becomes F_{yp} when it has an internal pressure of 150 psi.

$$p := 150 \cdot \frac{lb}{in^2} \qquad F_y = 17600 \cdot \frac{lb}{in^2}$$

$$F_{yp} := F_y + \frac{p \cdot R}{2 \cdot t} \qquad F_{yp} = 19363 \cdot \frac{lb}{in^2}$$

Find the vertical acceleration of the MCO shield plug and shell weights which will produce yielding in the shell

Area of shell, $A_{sh} := \pi \cdot \left[\left(R + \frac{t}{2}\right)^2 - \left(R - \frac{t}{2}\right)^2\right]$ $A_{sh} = 36.91 \cdot in^2$

Density of 304L, $\delta_{ss} := 0.29 \cdot \frac{lb}{in^3}$

Length of shield plug, $l_p := 12 \cdot in$

Length of shell, $l_{sh} := 160 \cdot in - l_p$

ICF KAISER HANFORD

DESIGN ANALYSIS

Client: Westinghouse Hanford K Basin SNF Project
Subject: MCO Elastic Buckling Evaluation

Date: 02/15/96
Orginator : L. L. Hyde
Checker : D. M. Chenault

ELASTIC BUCKLING OF THE MCO (cont'd)

Weight of MCO shield plug, $W_{plug} := \pi \cdot \left(R + \frac{t}{2}\right)^2 \cdot l_p \cdot \delta_{ss}$ $W_{plug} = 1574 \cdot lb$

Weight of MCO shell, $W_{shell} := A_{sh} \cdot l_{sh} \cdot \delta_{ss}$ $W_{shell} = 1584 \cdot lb$

Allowable vertical accelleration when the internal pressure is zero,

$$a_{mco} := \frac{F_y \cdot A_{sh}}{W_{plug} + W_{shell}} \qquad a_{mco} = 206 \quad g$$

Allowable vertical accelleration when the internal pressure is 150 psi,

$$a_{mco} := \frac{F_{yp} \cdot A_{sh}}{W_{plug} + W_{shell}} \qquad a_{mco} = 226 \quad g$$

MCO DROP STATIC ANALYSIS

INTRODUCTION

This is a follow-up analysis to Bob Winkel's ANSYS analysis of the MCO drop for the purpose of evaluating the potential of a breach of the MCO while inside the shipping cask. In the analysis described below, a somewhat different approach is adopted for the following 4 cases:

1. The gap between baskets and MCO is 3/8 in and the internal pressure is zero.
2. The gap between baskets and MCO is 1/8 in and the internal pressure is zero.
3. The gap between baskets and MCO is 3/8 in and the internal pressure is 150 psi.
4. The gap between baskets and MCO is 1/8 in and the internal pressure is 150 psi.

ANALYSIS APPROACH

For each of the above 4 cases, ABAQUS 5.4 is used to analyze a 20-inch length of the MCO as an axisymmetric cylindrical shell subjected to a *uniform* axial load at the upper node to simulate the impact force from a possible drop. Nine integration points are used along the thickness of each of the 100 shell elements. The choice of using shell elements is justified by the small ratio of thickness (0.5 inch) to radius of curvature of the shell (11.75 inches at mid-thickness). Large deformations and plasticity effects are also considered. For all 4 test cases, a gap of 0.5 inch is assumed between the MCO and its containing cask. The baskets and the cask are assumed to provide rigid and frictionless surfaces. In order to improve convergence of this nonlinear contact problem, a uniform axial displacement is ramped from 0 to a maximum of 2 inches (corresponding to a maximum relative displacement of 14.5 inches between the top 12-inch plug and the bottom 3- inch base). It is assumed that there are no *initial imprefections.*

RESULTS

Figure 1 shows a deformed MCO configuration at the end of the load step (i.e. after the 2 inch top displacement is achieved) for case 1. The nodes 22 and 65 shown on this figure are the locations of the maximum principal plastic strains. Locations of maximum principal plastic strains (at the extreme outer and inner fibres) were identified by examination of the plastic strain summary at the end of the strain tables printed out on the *.dat ABAQUS output file. Figure 3 provides additional insight into the accumulation of plastic strains at these points where one observes node 22 undergoes plastic straining before node 65 until node 22 contacts the cask wall at which point the build up of plastic straining at this node virtually stops, and plastic straining continues at node 65 until it contacts the cask wall. It is also observed that this plastic strain component is practically the same at the inner and outer fibres. This "kinking" deformation mode propagates along the full length of the MCO. As a result, the MCO can tolerate forces in excess of 700g as shown in Figure 2.
The same conclusion can be drawn from the trends in Figures 4, 6, and 7 for cases 2, 3, and 4, respectively.

CONCLUSION

While monotonic hardening of the MCO is observed under perfectly axisymmetric conditions, with no breach under 700g, a more accurate and conservative analysis is recommended where a 3-D model is considered with an initially imperfect configuration and a concentrated load since buckling is essentially a 3-D nonsymmetrical phenomenon.

Questions can be addressed to Michel (Mike) Dib.

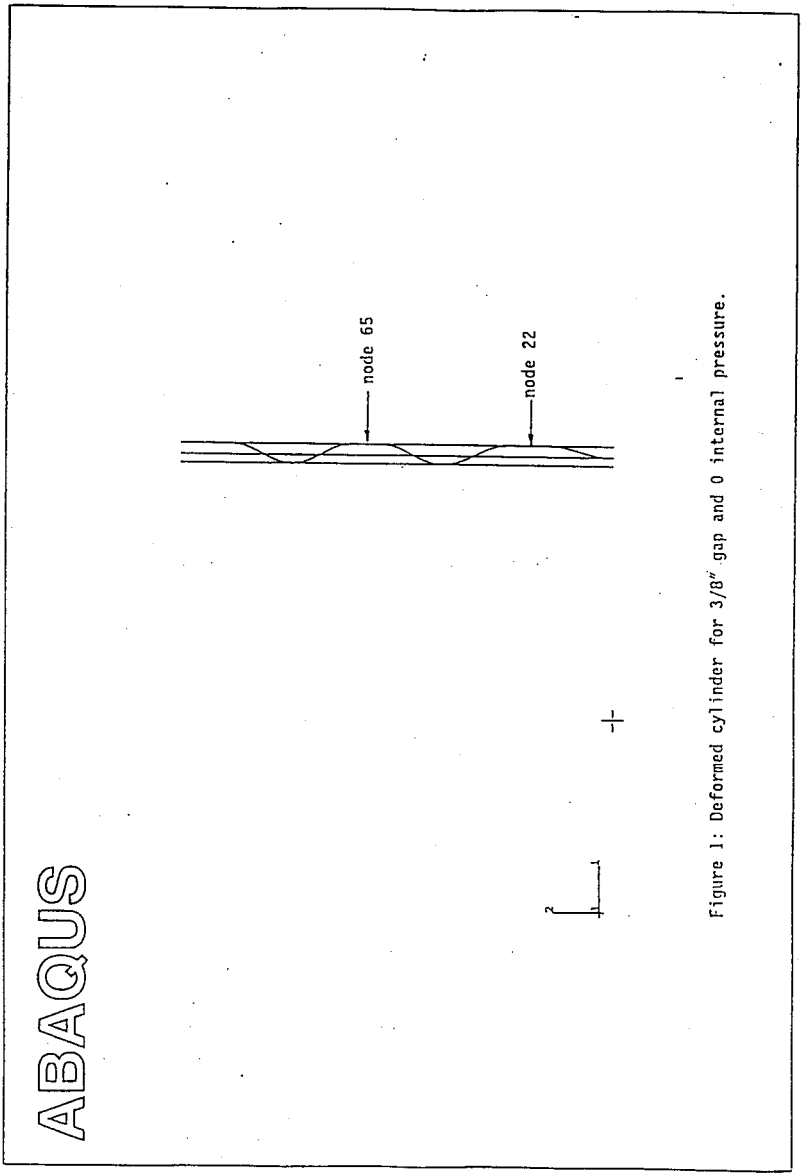

Figure 1: Deformed cylinder for 3/8" gap and 0 internal pressure.

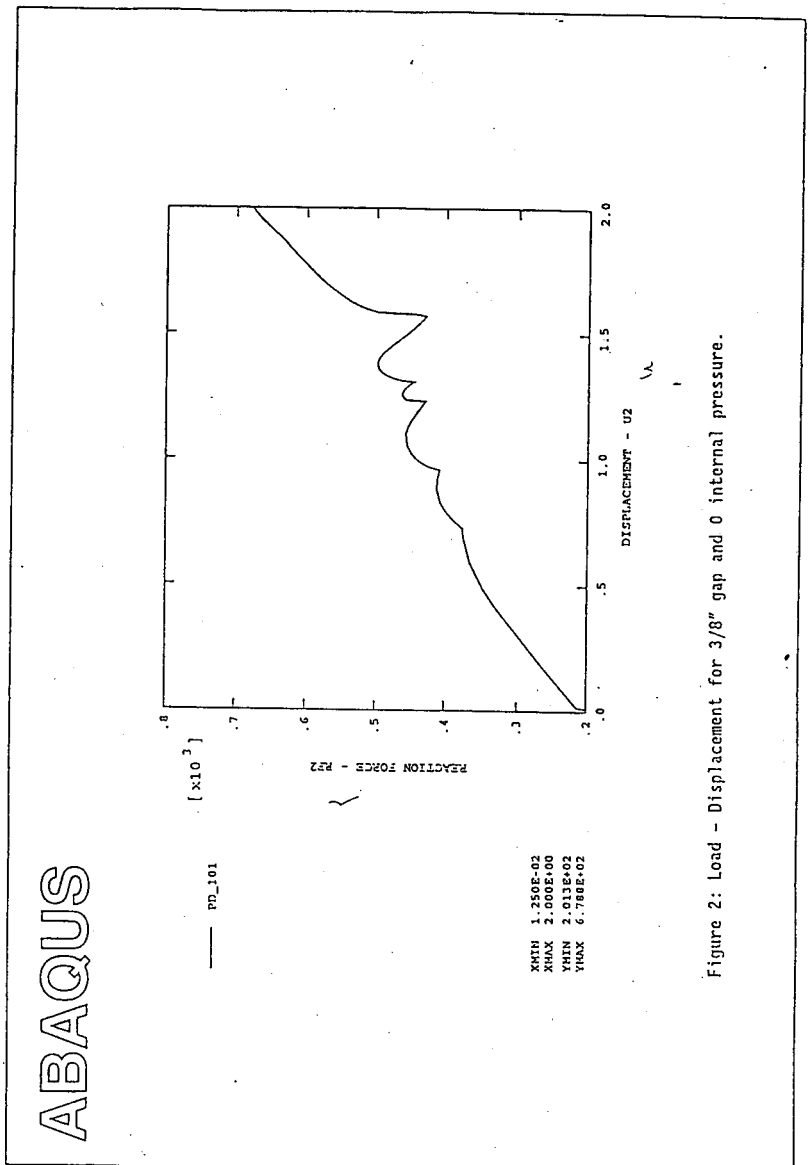

Figure 2: Load - Displacement for 3/8" gap and 0 internal pressure.

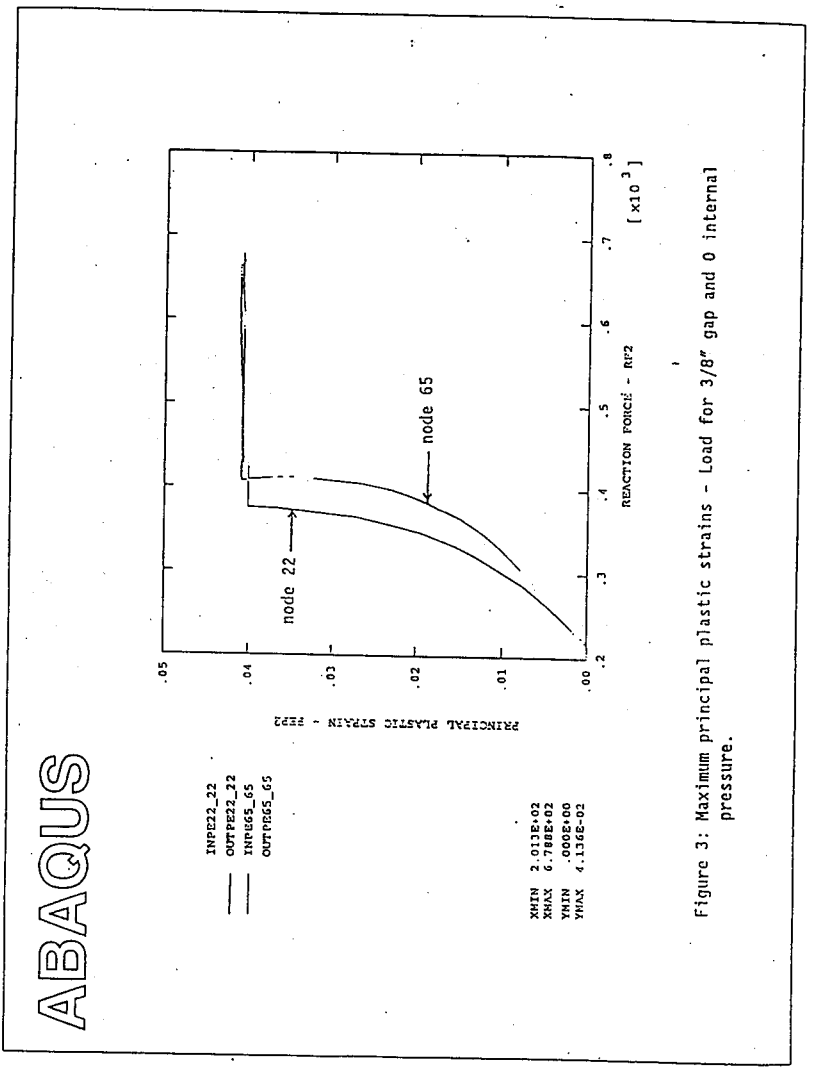

Figure 3: Maximum principal plastic strains - Load for 3/8" gap and 0 internal pressure.

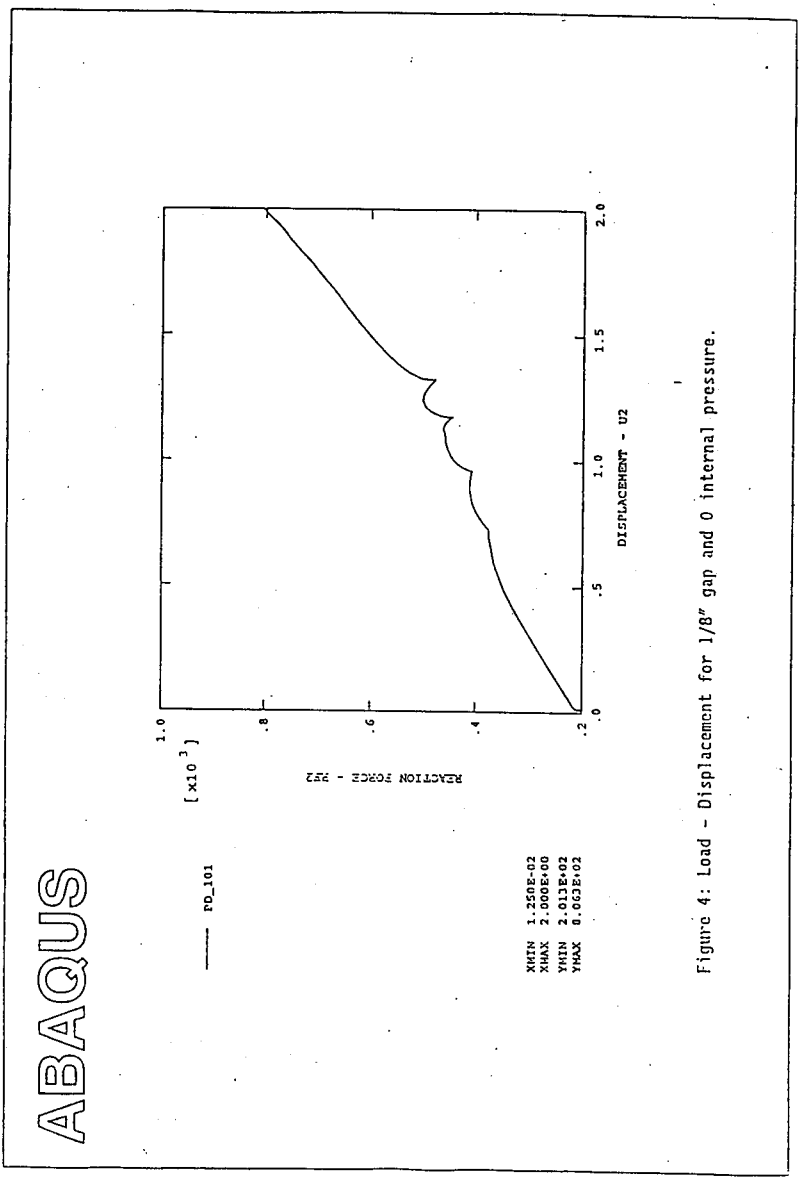

Figure 4: Load - Displacement for 1/8" gap and 0 internal pressure.

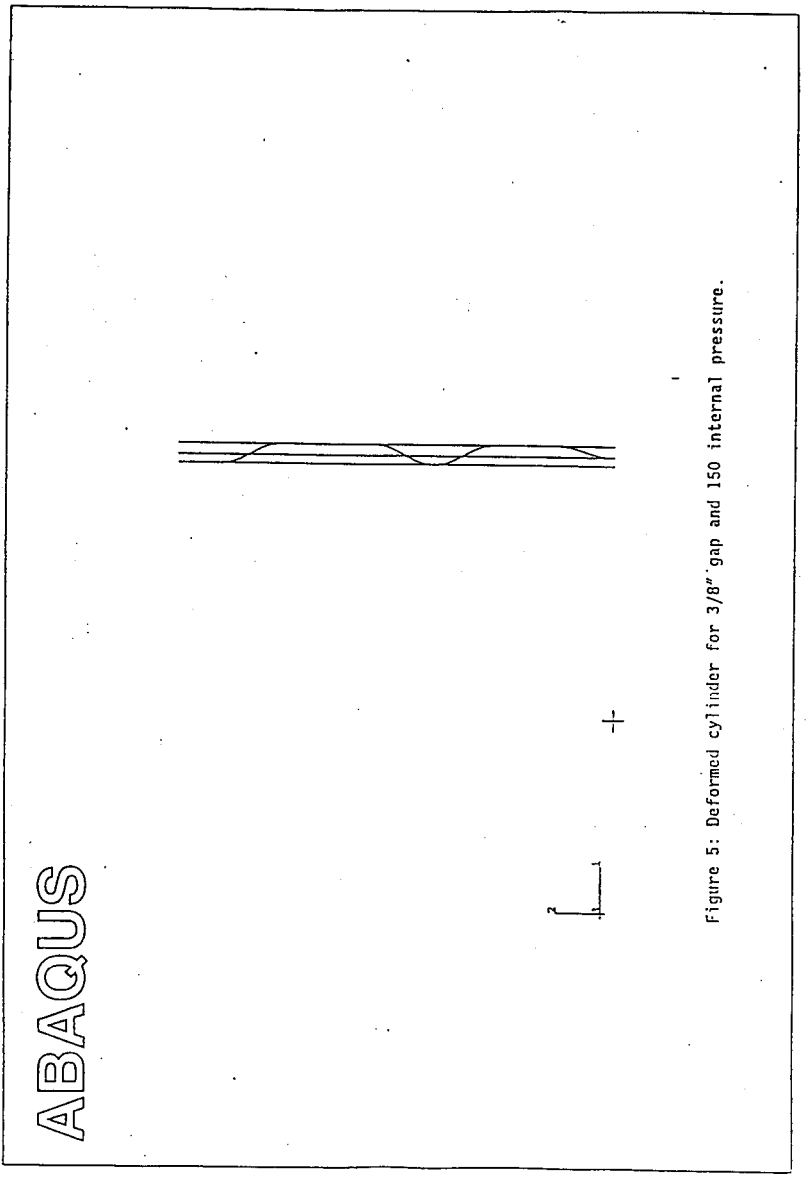

Figure 5: Deformed cylinder for 3/8" gap and 150 internal pressure.

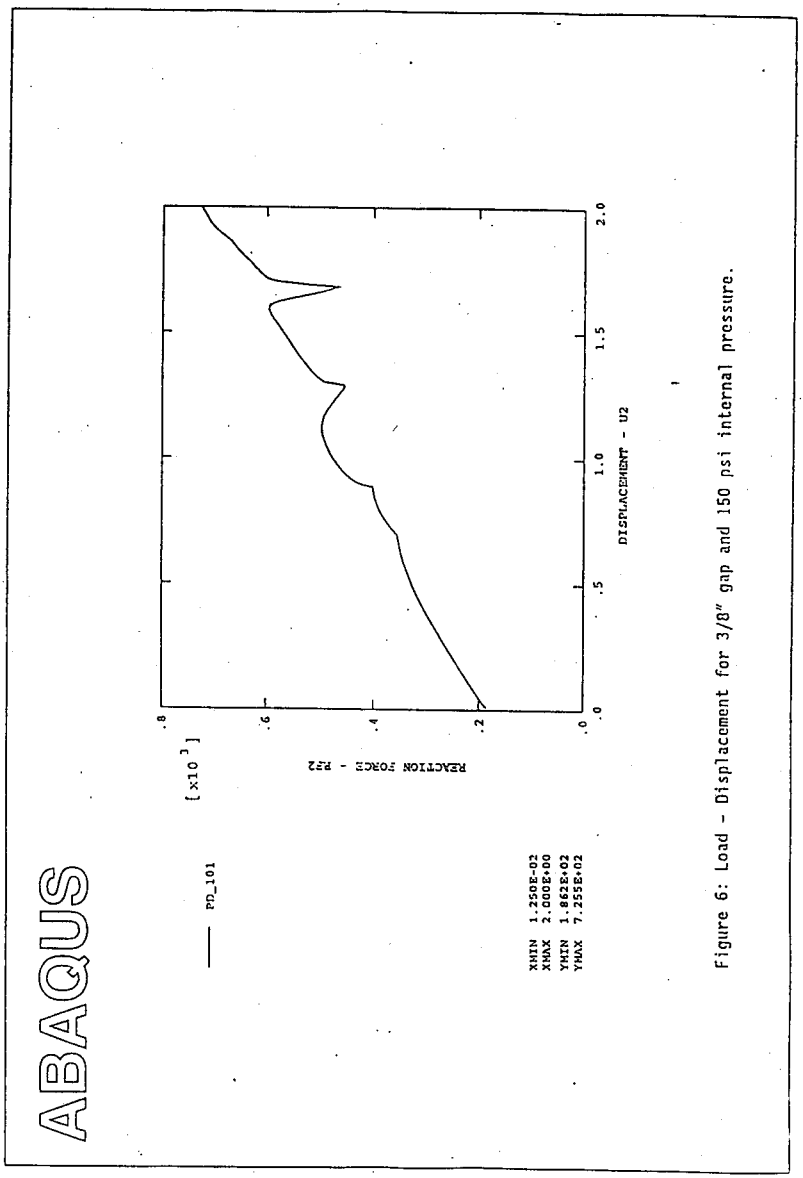

Figure 6: Load - Displacement for 3/8" gap and 150 psi internal pressure.

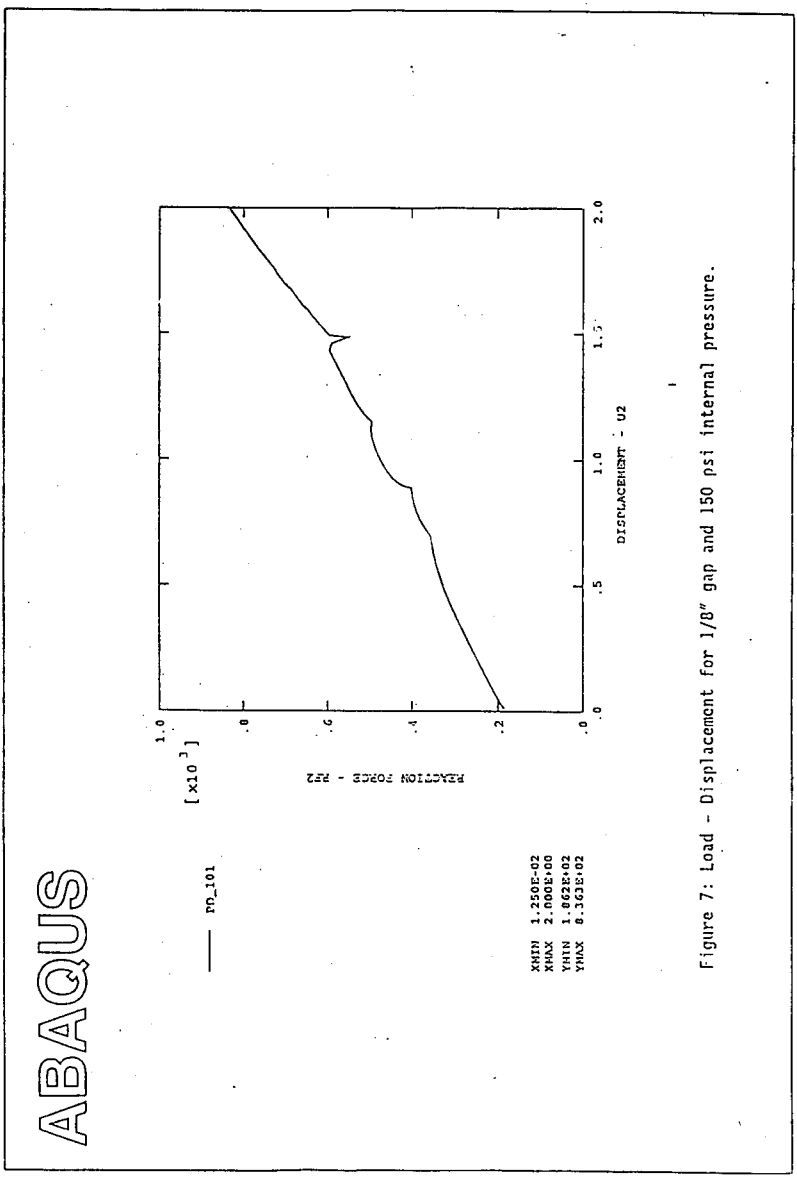

Figure 7: Load - Displacement for 1/8" gap and 150 psi internal pressure.

APPENDIX B

MULTICANISTER OVERPACK STORAGE BASKET ANALYSIS

This page intentionally left blank.

APPLICATION FOR PERMISSION TO USE COPYRIGHTED MATERIAL

To: Mr. Frederick Parker **Date:** January 7, 1997

Permission is requested to reproduce the following copyrighted material from:

Pages 13 and 58 of the old Kilsby-Roberts Tubing and Pipe Stock List Catalogue.

Title of work or project in which this material will be included:

Immediate application is for the information to be included in the appendices of a report for the Spent Nuclear Fuel Project. However, permission to use this information for any and all reports associated with the Spent Nuclear Fuel Project at the Hanford Site is requested.

Estimated publication date:

Initial publications should be completed by the end of 1999. A grant of permission to use the above described material would be interpreted to extend to any updates or revisions to Spent Nuclear Fuel Project documents.

Manager seeking permission:

Mr. L. J. Garvin III, Regulatory Programs, Spent Nuclear Fuel Project
Fluor Daniel Northwest

L. J. Garvin III — Date: 1/7/97

Application approved by:

Name: Mr. Frederick Parker Date: 1/10/97

Company Name and Address: Earl M. Jorgensen Company
3050 East Birch Street
Brea, CA 92821

Signatory's Position: V-Pres Marketing

Signature:

APPLICATION FOR PERMISSION TO USE COPYRIGHTED MATERIAL

To: Mr. Timothy Hardin Date: January 7, 1997

Permission is requested to reproduce the following copyrighted material from:

Analysis results output pages bearing the IMAGES 3-D copyright header.

Title of work or project in which this material will be included:

Immediate application is for analysis output results to be included in the appendices of a report for the Spent Nuclear Fuel Project. However, permission to use such output pages bearing the IMAGES 3-D copyright header for any and all reports associated with the Spent Nuclear Fuel Project at the Hanford Site is requested.

Estimated publication date:

Initial publications should be completed by the end of 1999. A grant of permission to use the above described material would be interpreted to extend to any updates or revisions to Spent Nuclear Fuel Project documents.

Manager seeking permission:

Mr. L. J. Garvin III, Regulatory Programs, Spent Nuclear Fuel Project
Fluor Daniel Northwest

L. J. Garvin III — Date: 1/7/97

Application approved by:

Name: TIMOTHY C. HARDIN Date: 01/08/97

Company Name and Address: ROBERT L. CLOUD & ASSOCIATES, INC.
2150 Shattuck Ave., Suite 500
Berkeley, CA 94704

Signatory's Position: Executive Vice President

Signature: Timothy C. Hardin

EVALUATION OF THE CENTER PIPE OF MARK 1A STORAGE AND SCRAP BASKETS

It is credible to postulate that the MCO can be dropped vertically and that the unit could then fall in a side slapdown manner. Thus, a vertical impact followed by a lateral impact is a possible design accident. It must be assured this condition does not violate the criticality control measures of the design which are: 1) the pipe is not crushed; and 2) the pipe does not shift laterally more than two inches.

The Cask/MCO drop analyses included in the MCO Topical Report show the following results:

1) Worst orientation 30 foot vertical drop of cask onto concrete with MCO inside
   - Drop on corner of cask lid
   - MCO modeled without internal baskets or fuel
   - Mass of baskets and fuel lumped on MCO shield plug
   - Resulting in MCO acceleration of 113 g

2) 13 foot vertical drop of MCO onto steel plate
   - Representing fall back into the cask
   - No air piston effect with the cask considered
   - 6 Mark 1A baskets, fully loaded with fuel, included in MCO model
   - Resulting in acceleration of MCO and bottom basket of 116 g
   - Resulting in accelerations of the next to bottom basket of 15 g, the upper basket of 17 g and the intermediate baskets of 25 g

It can be hypothesized that since the 13 foot drop of the MCO resulted in an acceleration of 116 g of the bottom basket and a much lower acceleration for the remaining baskets, the same action would occur if the baskets had been included in the 30 foot cask drop model. The loading from the bottom basket is reacted directly into the MCO bottom closure, while those of the upper 5 baskets are reacted by the six support rods (on the perimeter of the basket baseplate) and by the center pipe.

Prior to performing the accident condition drop analyses, 35 g (heaviest baskets) to 50 g (lightest baskets) were specified for the MCO internals. The loading from the bottom basket is reacted directly into the bottom of the MCO. However the center pipe of this basket, along with the six support rods, must react all of the loading from the five upper baskets. Since the drop condition analyses are showing the average vertical accelerations of these five baskets is less than the 35 g specified, evaluate the center pipe for 35 g.

A preliminary design incorporated a center pipe for both the Mark 1A storage and scrap baskets of 6 inch Schedule 120 pipe (6.625" OD x 0.562" wall) along with six 1" diameter support rods. Evaluate the capability of this design first and then investigate alternates.

EVALUATION OF THE CENTER PIPE OF MARK 1A STORAGE AND SCRAP BASKETS

Axial Buckling Analysis of the Center Pipe

Consider the center pipe to be a pinned end column as shown. It is assumed the baskets provide no lateral support. Find the allowable load of the column under an axial load and under a distributed axial load as shown.

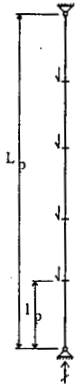

Reference: Drawings SK-1-80208 "*K-Basin SNF Storage Basket Mock-Up Mark 1A & Mark IV*", and SK-1-80210, "*K-Basin SNF Storage Scrap Basket Mock-Up Mark 1A*", (undated)

Center Pipe for Mark IA Basket--(6" Sch 120)

$l_p := 22.5 \cdot in$ $L_p := 143 \cdot in$ (from bottom of shield plug)

$OD := 6.625 \cdot in$

$t_{wall} := 0.562 \cdot in$

$A_p := \frac{\pi}{4} \cdot \left[OD^2 - \left(OD - 2 \cdot t_{wall} \right)^2 \right]$ $A_p = 10.7 \cdot in^2$

$I_p := \frac{\pi}{64} \cdot \left[OD^4 - \left(OD - 2 \cdot t_{wall} \right)^4 \right]$ $I_p = 49.61 \cdot in^4$

$r_p := \sqrt{\frac{I_p}{A_p}}$ $r_p = 2.15 \cdot in$

$E := 26.6 \cdot 10^6 \cdot \frac{lb}{in^2}$ at 400°F

The column end fixity coefficient for a concentrated axial load is, $c_a := 1$

and for a uniformly distributed load is, $c_d := 1.87$

The Euler concentrated buckling load is, $P_{crit} := c_a \cdot \frac{\pi^2 \cdot E \cdot A_p}{\left(\frac{L_p}{r_p} \right)^2}$ $P_{crit} = 636918 \cdot lb$

ICF KAISER HANFORD

DESIGN ANALYSIS

Revision 0
Page No. 3 of 50

Client: Westinghouse Hanford K Basin SNF Project
Subject: MCO Storage Baskets

Date: 09/13/96
Orginator : L. L. Hyde
Checker : D. M. Chenault

EVALUATION OF THE CENTER PIPE OF MARK 1A STORAGE AND SCRAP BASKETS

Axial Buckling Analysis of the Center Pipe

The Euler distributed buckling load is, $P_{crit} := c_d \cdot \frac{\pi^2 \cdot E \cdot A_p}{\left(\frac{L_p}{r_p}\right)^2}$ $P_{crit} = 1191037 \cdot lb$

The baskets are designed to the intent of the ASME B&PV Code, Subsection NB (NB-3133), and Appendix F (F-1331) which limits the maximum allowable compressive stress in cylinders and tublular products as follows:

Factor A is defined as, $A := \frac{0.125 \cdot t_{wall}}{0.5 \cdot OD}$

Factor B is defined as, $B := 8340 + 2720 \cdot \log(A \cdot 100)$ for 304L SS at 400°F when 0.10 > A > 0.01, B = 9780 maximum

$B = 9228$

The allowable stress is, $S_{allow} := 1.5 \cdot B \cdot \frac{lb}{in^2}$ $S_{allow} = 13842 \cdot \frac{lb}{in^2}$

The allowable compressive load is, $P_{crit} := A_p \cdot S_{allow}$ $P_{crit} = 148175 \cdot lb$ <<<===

In addition to the center pipe the baskets are supported by six (6) 1" diameter rods located symmetrically about the baseplate circumference. The rods are attached to the baseplate and cantilevered upward from it.

The length of the rods is, $l_r := l_p - 3.375 \cdot in$ $l_r = 19.125 \cdot in$

and the diameter, $d_r := 1.0 \cdot in$

The buckling load of the rod is, $c := \frac{1}{4}$ $I_r := \frac{\pi \cdot d_r^4}{64}$

$P_{crod} := c \cdot \frac{\pi^2 \cdot E \cdot I_r}{l_r^2}$ $P_{crod} = 8808 \cdot lb$

Three of the rods will carry the vertical load initially until their allowable load is exceeded then the remaining rods will start to pick up load until eventually all six react the load

$P_{rods} := 6 \cdot P_{crod}$ $P_{rods} = 52849 \cdot lb$

Each basket holds 48 Mark IA fuel elements which weigh 39.71 lbs each. The basket weighs approximately 150 lbs, so the total weight is, $W_{IA} := 2055 \cdot lb$

EVALUATION OF THE CENTER PIPE OF MARK 1A STORAGE AND SCRAP BASKETS

The Mark IA fuel baskets are stacked six high within the MCO as shown. Vertical loads resulting from vertical accelerations of each basket are reacted by the six 1" rods of the basket directly below. When the a basket loading exceeds the capability of these rods (P_{rods}) the center pipe takes the additional load. Assuming the baskets are accelerated uniformly find the maximum vertical acceleration (a) which they may experience without exceeding the structural capability of the center pipe (P_{crit}).

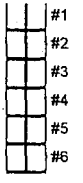

Let the load of each basket be the weight of the basket times the acceleration and the reaction be the capability of the six rods and the load in the center pipe. Then the load in the pipe from basket #1 for an acceleration of 'a' will be,

$a := 19.56$

$P_1 := W_{1A} \cdot a - P_{rods}$ $\quad P_1 = -12654 \cdot lb$

$P_1 := 0 \cdot lb$

similarly for the other baskets,

$P_2 := 2 \cdot (W_{1A} \cdot a) - P_{rods} - P_1$ $\quad P_2 = 27542 \cdot lb$

$P_3 := 3 \cdot (W_{1A} \cdot a) - P_{rods} - P_1 - P_2$ $\quad P_3 = 40196 \cdot lb$

$P_4 := 4 \cdot (W_{1A} \cdot a) - P_{rods} - P_1 - P_2 - P_3$ $\quad P_4 = 40196 \cdot lb$

$P_5 := 5 \cdot (W_{1A} \cdot a) - P_{rods} - P_1 - P_2 - P_3 - P_4$ $\quad P_5 = 40196 \cdot lb$

$P_{pipe} := P_1 + P_2 + P_3 + P_4 + P_5$

$P_{pipe} = 148130 \cdot lb$ $\quad \sim\sim P_{crit}$

This shows that the 6" Schedule 120 center pipe combined with six 1" diameter support rods incorporated into the preliminary design will support a vertical acceleration of 19.5 g before the allowable stress of the pipe is exceeded. Since this is less than 35 g investigate alternatives.

ICF KAISER HANFORD

DESIGN ANALYSIS

Revision 0
Page No. 5 of 50

Client: Westinghouse Hanford K Basin SNF Project
Subject: MCO Storage Baskets

Date: 09/13/96
Orginator : L. L. Hyde
Checker : D. M. Chenault

EVALUATION OF THE CENTER PIPE OF MARK 1A STORAGE AND SCRAP BASKETS

The minimum required wall thickness (t_{wall}) of a 6" nominal diameter center pipe to sustain an average vertical acceleration of the upper five baskets of 35 g is:

$a := 35$

$P_1 := W_{IA} \cdot a - P_{rods}$ $\quad P_1 = 19076 \cdot lb$

$P_2 := 2 \cdot (W_{IA} \cdot a) - P_{rods} - P_1$ $\quad P_2 = 71925 \cdot lb$

$P_3 := 3 \cdot (W_{IA} \cdot a) - P_{rods} - P_1 - P_2$ $\quad P_3 = 71925 \cdot lb$

$P_4 := 4 \cdot (W_{IA} \cdot a) - P_{rods} - P_1 - P_2 - P_3$ $\quad P_4 = 71925 \cdot lb$

$P_5 := 5 \cdot (W_{IA} \cdot a) - P_{rods} - P_1 - P_2 - P_3 - P_4$ $\quad P_5 = 71925 \cdot lb$

$P_{pipe} := P_1 + P_2 + P_3 + P_4 + P_5$ $\quad P_{pipe} = 306776 \cdot lb$

The minumum wall thickness required for a 6" nominal diameter pipe is:

Assume $B = B_{max} = 9780$ $\quad B := 9780$

$S_{allow} := 1.5 \cdot B \cdot \frac{lb}{in^2}$ $\quad A_p := \frac{P_{pipe}}{S_{allow}}$

$t_{wall} := \frac{1}{2} \cdot \left(OD - \sqrt{OD^2 - \frac{4}{\pi} \cdot A_p} \right)$ $\quad t_{wall} = 1.235 \cdot in$

Check value of B,

$A := \frac{0.125 \cdot t_{wall}}{0.5 \cdot OD}$ $\quad B := 8340 + 2720 \cdot \log(A \cdot 100)$ $\quad B = 10158$

Since $B > B_{max}$ the assumption used for B was correct

Thus, with six 1.00" diameter support rods, a 6.625" OD center pipe with a 1.235" wall is required. Since this appears excessively thick and it not a standard section investigate increasing the diameter of the support rods.

EVALUATION OF THE CENTER PIPE OF MARK 1A STORAGE AND SCRAP BASKETS

If the six support rods around the perimeter of the baseplate are changed from 1" to 1-3/8" diameter then the wall thickness of a 6" nominal diameter center pipe required to sustain an average vertical acceleration of 35 g of the five upper baskets is,

For, $d_r := 1.375 \cdot in$ the rod load is controlled by Code allowable stress instead of buckling,

$$P_{rod} := \frac{\pi}{4} \cdot d_r^2 \cdot S_{allow} \qquad P_{rod} = 21783 \cdot lb$$

and for the six rods, $P_{rods} := 6 \cdot P_{rod}$ or, $P_{rods} = 130700 \cdot lb$

$a := 35$

$P_1 := W_{IA} \cdot a - P_{rods}$ $P_1 = -58775 \cdot lb$ $P_1 := 0 \cdot lb$

$P_2 := 2 \cdot (W_{IA} \cdot a) - P_{rods} - P_1$ $P_2 = 13150 \cdot lb$

$P_3 := 3 \cdot (W_{IA} \cdot a) - P_{rods} - P_1 - P_2$ $P_3 = 71925 \cdot lb$

$P_4 := 4 \cdot (W_{IA} \cdot a) - P_{rods} - P_1 - P_2 - P_3$ $P_4 = 71925 \cdot lb$

$P_5 := 5 \cdot (W_{IA} \cdot a) - P_{rods} - P_1 - P_2 - P_3 - P_4$ $P_5 = 71925 \cdot lb$

$P_{pipe} := P_1 + P_2 + P_3 + P_4 + P_5$ $P_{pipe} = 228925 \cdot lb$

The minumum wall thickness of a 6" nominal diameter pipe required is:

Assume B is, $B := 9739$

$$S_{allow} := 1.5 \cdot B \cdot \frac{lb}{in^2} \qquad A_p := \frac{P_{pipe}}{S_{allow}}$$

$$t_{wall} := \frac{1}{2} \cdot \left(OD - \sqrt{OD^2 - \frac{4}{\pi} \cdot A_p} \right) \qquad t_{wall} = 0.866 \cdot in \quad <<==== $$

Check value of B,

$$A := \frac{0.125 \cdot t_{wall}}{0.5 \cdot OD} \qquad B := 8340 + 2720 \cdot \log(A \cdot 100) \qquad B = 9739$$

Since B equals the assumed value the calculated thickness is correct

Thus, with six 1-3/8" diameter support rods a 6.625" OD center pipe with a 0.866" wall is required to sustain 35 g and conform to the intent of the ASME Code. A 6" nominal diameter double extra strong (6"-Schedule XXS) pipe with a wall thickness of 0.864" is adequate.

EVALUATION OF THE CENTER PIPE OF MARK 1A STORAGE AND SCRAP BASKETS

SUMMARY

To sustain an average vertical acceleration of the upper 5 baskets of 35 g requires:

A. A 6.625" outside diameter center pipe with a 1.235" thick wall and six 1.00" diameter support rods, or

B. A 6.625" outside diameter center pipe with a 0.866" thick wall (6"-Scheule XXS) and six 1-3/8" diameter support rods.

ICF KAISER HANFORD

DESIGN ANALYSIS

Revision 0
Page No. 8 of 50

Client: Westinghouse Hanford K Basin SNF Project
Subject: MCO Storage Baskets

Date: 09/13/96
Orginator : L. L. Hyde
Checker : D. M. Chenault

EVALUATION OF THE CENTER PIPE OF MARK 1A STORAGE AND SCRAP BASKETS

Evaluate weld of center pipe to basket baseplate.

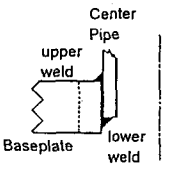

The diameter of the 6" nominal pipe is, $OD := 6.625 \cdot in$

The length of a single fillet weld is, $l_w := \pi \cdot OD$

The area of a single fillet weld is, $A_W = (0.707 \times t_w) \times l_W$
where t_w is the weld thickness

The shear stress in the weld is, $S_S = P / A_W$
where P is the load in the center pipe

The maximum load in the center pipe occurs at the bottom basket and is due to the upper five baskets. The load from the bottom basket is reacted directly into the bottom of the MCO. For a 6"-Schedule XXS pipe with 1-3/8" supports rods the load is (see page 6),

$$P := 228925 \cdot lb$$

The allowable shear stress for the weld, in accordance with Appendix F of the ASME Code, is 42% of the material ultimate stress (S_u). For 304L at 400^{0}F,

$$S_u := 58700 \cdot \frac{lb}{in^2}$$

The required thickness for a single fillet weld is,

$$t_w := \frac{1}{0.707} \cdot \frac{P}{l_w \cdot (0.42 \cdot S_u)} \qquad t_w = 0.631 \cdot in \quad <====$$

Note that this thickness may be distributed between the upper and lower single fillet welds as dictated by the design. For example, with a 3/16" upper weld the lower weld may be 1/2".

ICF KAISER HANFORD

DESIGN ANALYSIS

Client: Westinghouse Hanford K Basin SNF Project
Subject: MCO Storage Baskets

Date: 09/13/96
Orginator : L. L. Hyde
Checker : D. M. Chenault

EVALUATION OF THE CENTER PIPE OF MARK 1A STORAGE AND SCRAP BASKETS

Since the required fillet welds are large and could result in warping of the baseplate, investigate an alternate configuration for this attachment. The amount of welding can be reduced if the center pipe is fitted into "socket" in the baseplate, as shown.

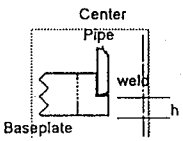

Determine the required height 'h' of the ledge in the baseplate which will resist the maximum load of the center pipe

$$h := \frac{P}{\pi \cdot OD \cdot (0.42 \cdot S_u)} \qquad h = 0.446 \cdot in$$

Since the baseplate is 3 inches thick, machine the socket 2 inches deep leaving h = 1". The weld must only transmit the load from the one baseplate into the pipe (71,925 lbs). A partial penetration butt weld half the center pipe wall thickness, as shown, will be adequate.

EVALUATION OF THE CENTER PIPE OF MARK 1A STORAGE AND SCRAP BASKETS

Evaluate the Outer Retaining Ring at the bottom of the basket baseplate

To provide the required load transfer between the ring and support rods of the next lower basket, without introducing eccentricities, the ring must be in full contact with the rod. Thus the ring must be 1.375" wide. Find the thickness required to support the maximum rod load of 21,783 lbs. as given on page 6.

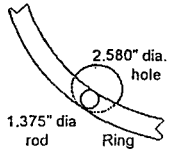

The worst case is the ring spanning one of the 2.580" diameter fuel element holes at the perimeter of the baseplate with the 1.375" support rod loading in the center of the span as shown

Consider the ring a simply supported beam with a span equal to the length of the chord it subscribes in the 2.580" diameter hole at the rings mid-depth

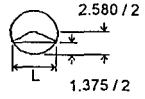

$$L := 2\cdot\sqrt{2\cdot\frac{1.375}{2}\cdot\frac{2.580}{2}-\left(\frac{1.375}{2}\right)^2}\cdot in \qquad L = 2.281\cdot in$$

Due to relative flexibility of the ring in bending compared to the support rod axial stiffness the rod load will peak at its outer edges so the loading configuration will be,

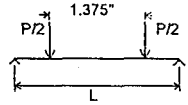

$P := 21783\cdot lb$

The maximum bending moment in the ring occurs at mid-span and is,

$$M := \frac{P}{2}\cdot\left(\frac{L}{2}-\frac{1.375}{2}\cdot in\right) \qquad M = 4936\cdot in\cdot lb$$

The allowable bending stress (F_b), for 304L, in accordance with the ASME Code, Appendix F, is 2.4 x 1.5 x S_m

$$S_m := 15900\cdot\frac{lb}{in^2} \quad \text{at } 400^0F \qquad F_b := 2.4\cdot 1.5\cdot S_m \qquad F_b = 57240\cdot\frac{lb}{in^2}$$

The required thickness of the ring then becomes,

$$t_{ring} := \sqrt{\frac{6\cdot M}{1.375\cdot in\cdot F_b}} \qquad t_{ring} = 0.613\cdot in \quad <=====$$

Fabricate the ring from 1-3/8" wide by 5/8" thick stock

EVALUATION OF THE CENTER PIPE OF MARK 1A STORAGE AND SCRAP BASKETS

Evaluate the Retaining Bars at the bottom of basket baseplate

The fuel elements are retained in the baseplates by bars which are welded to the bottom. Each bar spans several holes of the baseplate and it welded between each hole. It is conservative to analyze these as simply supported beams uniformly loaded by the weight of the fuel element.

Conservatively, assume the length of the span is the hole diameter plus 1/4",

$l_b := (2.580 + 0.25) \cdot in$

The weight of the Mark 1A fuel element is, $W_{1A} := 39.71 \cdot lb$

or for the required 35 g acceleration, $W_A := 35 \cdot W_{1A}$

The bending moment in the bar is, $M_b := \frac{1}{8} \cdot W_A \cdot l_b$

The bars are 1/4" wide. Find the required height of the bar,

$$h_{bar} := \sqrt{\frac{6 \cdot M_b}{\frac{1}{4} \cdot in \cdot F_b}}$$

$h_{bar} = 0.454 \cdot in$ <====

Fabricate the bars from 1/4" x 1/2" stock

Find the length of end welds (l_w) required, assuming 1/8" fillets

The allowable shear strength (S_s) is 42% of the ultimate tensile strength (S_u),

$S_u := 58700 \cdot \frac{lb}{in^2}$ at 400°F, thus, $S_s := 0.42 \cdot S_u$,or $S_s = 24654 \cdot \frac{lb}{in^2}$

$$l_w := \frac{\frac{1}{2} \cdot W_A}{\left(0.707 \cdot \frac{1}{8} \cdot in\right) \cdot S_s}$$

$l_w = 0.319 \cdot in$ <=====

Weld the bars with a single 1/8" fillet 3/8" long or double 1/8" fillets 3/16" long on each side of each hole, i.e., place two welds on the bar between holes, one adjacent to each hole. The weld of the bars to the rings should be the same size.

EVALUATION OF THE CENTER PIPE OF MARK 1A STORAGE AND SCRAP BASKETS

Evaluate the weld of the outer ring to the baseplate, assume 1/8" fillet weld

The bars are spaced 1.375" on the ring which has a 22.375" OD, thus the weld requirement is l_w per space.

The length of perimeter is, $Pr := \pi \cdot 22.375 \cdot in$ $Pr = 70.3 \cdot in$

The total length of weld required is, $l_{tw} := \frac{l_w}{1.375 \cdot in} \cdot Pr$ $l_{tw} = 16.3 \cdot in$

1" long 1/8" fillet welds spaced at 4" on the circumference are adequate

Evaluate the weld of the inner ring to the baseplate, assume 1/8" fillet weld

The inner ring, which has an OD of 8.187", interrupts five bars so must carry the loading from these

The length of the perimeter is, $Pri := \pi \cdot 8.187 \cdot in$ $Pri = 25.72 \cdot in$

The total length of weld required is, $l_{twi} := 2 \cdot (5 \cdot l_w)$ $l_{twi} = 3.2 \cdot in$

Six equally spaced 1" long 1/8" fillet welds are adequate

Client: Westinghouse Hanford K Basin SNF Project
Subject: MCO Storage Baskets

Date: 09/13/96
Orginator : L. L. Hyde
Checker : D. M. Chenault

Analyze the Mark IA Fuel Basket Center Pipe for Lateral Loading

The center pipe of the baskets supporting the Mark IA fuel has the requirement that it can not move laterally more than two inches, for purposes of criticality control, when subjected to a lateral acceleration of 50 g (lightest basket). During a lateral acceleration the pipe will be loaded by a portion of the fuel elements in the basket. This loading will induce a local deformation in the pipe as well an overall beam type bending deformation. To check this local deformation analyze a section of the pipe as a ring and, to check the overall deformation, analyze the pipe as a beam supported by the baseplates of the baskets.

Consider a section of the pipe as a ring with the weight of eight fuel elements in a 30° sector acting on the it. Apply a cosine distribution of this load on the pipe as shown.

Note: Use the pipe wall thickness determined for Alternate B since if it is adequate the larger thicknesses determined for Alternates A and C will be adequate also

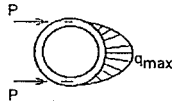

$OD_p := 6.625 \cdot in$ $t_{wall} := 0.864 \cdot in$

$R_p := \frac{1}{2} \cdot (OD_p - t_{wall})$

Weight of the Mark IA fuel element is, $W_f := 39.71 \cdot lb$

Applying the weight of eight fuel elements on a 30° sector gives q_{max} of,

$$q_{max} := \frac{8 \cdot W_f}{2 \cdot R_p \cdot \int_0^{\frac{\pi}{6}} \cos(\theta)^2 \, d\theta} \qquad q_{max} = 115 \cdot \frac{lb}{in}$$

Applying this same q_{max} over a 180° sector of the pipe as shown above will then result in a total load on the ring (pipe) of,

$$P := q_{max} \cdot R_p \cdot \int_0^{\frac{\pi}{2}} \cos(\theta)^2 \, d\theta \qquad 2 \cdot P = 522 \cdot lb$$

or, $\frac{2 \cdot P}{48 \cdot W_f} \cdot 100 = 27.4$ percent of the total basket load

ICF KAISER HANFORD

DESIGN ANALYSIS

Revision 0
Page No. 14 of 50

Client: Westinghouse Hanford K Basin SNF Project
Subject: MCO Storage Baskets

Date: 09/13/96
Orginator : L. L. Hyde
Checker : D. M. Chenault

Analyze the Mark IA Fuel Basket Center Pipe for Lateral Loading (cont'd)

Reference: *Rings and Arcuate Beams*, A. Blake, Aerojet General Corp., Product Engineering, January 7, 1963.

$\theta := 0, .05 \cdot \pi .. .5 \cdot \pi$ $\quad M_1(\theta) := P \cdot R_p \cdot (0.6366 \cdot \theta \cdot \sin(\theta) + 0.7958 \cdot \cos(\theta) - 0.9053)$

$\beta := .5 \cdot \pi, .55 \cdot \pi .. \pi$ $\quad M_2(\beta) := P \cdot R_p \cdot (0.1592 \cdot \cos(\beta) - .0947)$

θ deg	$M_1(\theta)$ in·lb
0	-82.3
9	-77.9
18	-65.1
27	-45.1
36	-19.8
45	8.2
54	36
63	59.9
72	76.2
81	81.2
90	71.1

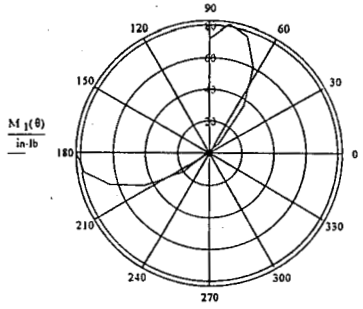

1.5708

β deg	$M_2(\beta)$ in·lb
90	-71.1
99	-89.9
108	-108.1
117	-125.4
126	-141.5
135	-155.7
144	-167.9
153	-177.7
162	-184.9
171	-189.3
180	-190.8

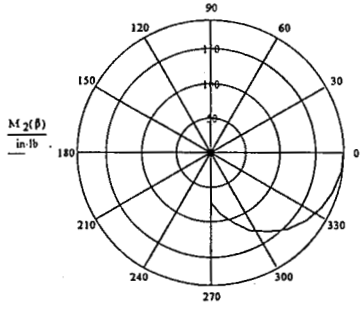

3.14159

Analyze the Mark IA Fuel Basket Center Pipe for Lateral Loading (cont'd)

Maximum Radial Displacement;

Unsupported length of pipe (max), $L_p := 23 \cdot in$

$E := 26.6 \cdot 10^6 \cdot \frac{lb}{in^2}$ @ 400°F $\qquad I_w := \frac{L_p \cdot t_{wall}^3}{12}$

$\theta := 0$

$u_1 := \frac{P \cdot R_p^3}{E \cdot I_w} \cdot \left[0.5570 \cdot \theta \cdot \sin(\theta) + \left(0.9382 - 0.1592 \cdot \theta^2\right) \cdot \cos(\theta) - 0.9053\right] \qquad u_1 = 6.237 \cdot 10^{-6} \cdot in$

$\beta := \pi$

$u_2 := \frac{P \cdot R_p^3}{E \cdot I_w} \cdot ((0.0796 \cdot \beta - 0.2500) \cdot \sin(\beta) + 0.0681 \cdot \cos(\beta) + 0.0947) \qquad u_2 = 5.043 \cdot 10^{-6} \cdot in$

Maximum bending stress in pipe wall, $\beta := \pi$

$f_b := \frac{6 \cdot M_2(\beta)}{L_p \cdot t_{wall}^2} \cdot 50 \qquad f_b = -3333 \cdot \frac{lb}{in^2}$

The allowable bending stress per ASME Section III Appendix F is 150% of 2.4 x S_m

$S_m := 15900 \cdot \frac{lb}{in^2}$ at 400°F,

$F_b := \frac{150}{100} \cdot (2.4 \cdot S_m) \qquad F_b = 57240 \cdot \frac{lb}{in^2}$

Analyze the Mark IA Fuel Basket Center Pipe for Lateral Loading (cont'd)

The overall beam bending deformation is,

$$I_b := \frac{\pi}{64}\cdot\left[OD_p^{\,4} - \left(OD_p - 2\cdot t_{wall}\right)^4\right]$$

$$u_b := \frac{5}{384}\cdot\frac{(2\cdot P)\cdot L_p^{\,3}}{E\cdot I_b} \qquad u_b = 4.684\cdot 10^{-5}\cdot in$$

The total lateral deformation of the center pipe when subjected to the maximum lateral acceleration is,

$$\left(u_1 + u_b\right)\cdot 50 = 0.003\cdot in \qquad <<< \text{ 2 inch limit of criteria}$$

The longitudinal bending stress in the pipe is,

$$f_b := \frac{\frac{1}{8}\cdot(2\cdot P)\cdot L_p\cdot\frac{OD_p}{2}}{I_b}\cdot 50 \qquad f_b = 3745\cdot\frac{lb}{in^2} \qquad <<< F_b$$

EVALUATION OF THE CENTER PIPE OF MARK 1A STORAGE AND SCRAP BASKETS

RECOMMENDATION

The preliminary design requires that the basket baseplates separate from the center pipe before the basket reaches its maximum vertical acceleration in order to limit the load in the center pipe to below the ASME Code allowable stress. While this is theoretically achievable, the criticality requirements imposed on the Mark 1A basket center pipes make it difficult to control this separation load in practice. (Note: This is not a concern for the Mark IV baskets which do not have any criticality requirements.) Additionally, for the postulated accident scenario of side slapdown subsequent to a vertical drop there exists uncertainty in predicting the configuration of the lateral support these separated baseplates provide the center pipe as well as the magnitude and distribution of the lateral loading on the center pipe. To address these concerns it is recommended the combination of the center pipe and the six support rods be designed to resist the maximum vertical acceleration prior to reaching their allowable stress. It is further recommended the design accommodate the 35g vertical acceleration invoked by the MCO Performance Specification.

To accomplish this it is recommended the center pipe wall thickness be increased to 0.864 inches (6"-Schedule XXS pipe) and the diameter of the six support rods to 1-3/8 inches. Additionally, the outer retaining ring, attached to the bottom of the baseplate, must be increased in size to 1-3/8" wide by 5/8" thick and the retaining bars must be 1/4" by 1/2". It is believed these changes will not affect any other geometry of the Mark 1A baskets with the exception of those items which interface with the center pipe internal diameter. And those items only require that their outer diameter by decreased by a like amount. This change will increase the MCO total weight. However, the maximum weight of the MCO fully loaded with Mark1A baskets will still be less than one loaded with Mark IV baskets.

CONCLUSION

These analyses show that the basket baseplates can be designed to remain in position with respect to their axial location on the center pipe. They also show that the structural deformation of the center pipe with respect to the MCO, due to lateral loading, is well within the required criticality displacement limit of two inches.

The Mark 1A loaded MCO will remain subcritical during the most severe accidental drop condition postulated by the Performance Specification.

ICF KAISER HANFORD

DESIGN ANALYSIS

Revision 0
Page No. 18 of 50

Client: Westinghouse Hanford K Basin SNF Project
Subject: MCO Storage Baskets

Date: 09/13/96
Orginator : L. L. Hyde
Checker : D. M. Chenault

Analyze the Mark IV Fuel Basket Center Pipe for Lateral Loading

The center pipe of the baskets supporting the Mark IV fuel has the requirement that it can not move so far laterally that it impinges upon the 1" diameter process tube when subjected to a lateral acceleration of 35 g (heaviest basket). During a lateral acceleration the pipe will be loaded by a portion of the fuel elements in the basket. This loading will induce a local deformation in the pipe as well an overall beam type bending deformation. To check this local deformation analyze a section of the pipe as ring and to check the overall deformation analyze the pipe as a beam supported by the baseplates of the baskets.

Consider a section of the pipe as a ring with the weight of nine fuel elements in a 30° sector acting on the it. Apply a cosine distribution of this load on the pipe as shown.

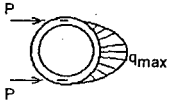

2.75" OD Tube with 0.5" wall

$OD_t := 2.75 \cdot in$ $t_{wall} := 0.5 \cdot in$

$R_t := \frac{1}{2} \cdot (OD_t - t_{wall})$

Weight of the Mark IV fuel element is, $W_f := 55.38 \cdot lb$

Applying the weight of nine fuel elements on a 30° sector gives q_{max} of,

$$q_{max} := \frac{9 \cdot W_f}{2 \cdot R_t \cdot \int_0^{\frac{\pi}{6}} \cos(\theta)^2 \, d\theta} \qquad q_{max} = 463.135 \cdot \frac{lb}{in}$$

Applying this same q_{max} over a 180° sector of the pipe as shown above will then result in a total load on the ring (pipe) of,

$$P := q_{max} \cdot R_t \cdot \int_0^{\frac{\pi}{2}} \cos(\theta)^2 \, d\theta \qquad 2 \cdot P = 818.427 \cdot lb$$

or, $\frac{2 \cdot P}{54 \cdot W_f} \cdot 100 = 27.4$ percent of the total basket load

ICF KAISER HANFORD

DESIGN ANALYSIS

Revision 0
Page No. 19 of 50

Client: Westinghouse Hanford K Basin SNF Project
Subject: MCO Storage Baskets

Date: 09/13/96
Orginator : L. L. Hyde
Checker : D. M. Chenault

Analyze the Mark IV Fuel Basket Center Pipe for Lateral Loading (cont'd)

Reference: *Rings and Arcuate Beams*, A. Blake, Aerojet General Corp., Product Engineering, January 7, 1963.

$\theta := 0, .05 \cdot \pi .. .5 \cdot \pi$ $\quad M_1(\theta) := P \cdot R_t \cdot (0.6366 \cdot \theta \cdot \sin(\theta) + 0.7958 \cdot \cos(\theta) - 0.9053)$

$\beta := .5 \cdot \pi, .55 \cdot \pi .. \pi$ $\quad M_2(\beta) := P \cdot R_t \cdot (0.1592 \cdot \cos(\beta) - .0947)$

θ deg	$M_1(\theta)$ in·lb
0	- 50.41
9	- 47.719
18	- 39.89
27	- 27.642
36	- 12.143
45	5.045
54	22.031
63	36.678
72	46.698
81	49.757
90	43.582

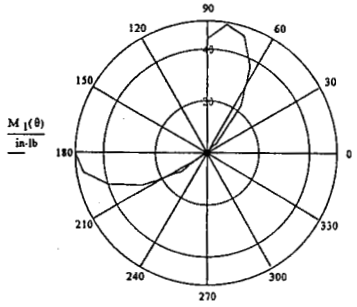

1.5708

β deg	$M_2(\beta)$ in·lb
90	- 43.597
99	- 55.062
108	- 66.244
117	- 76.87
126	- 86.675
135	- 95.42
144	- 102.89
153	- 108.899
162	- 113.3
171	- 115.984
180	- 116.887

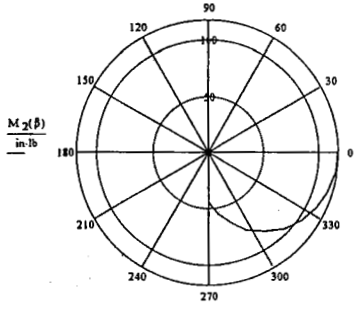

3.14159

Analyze the Mark IV Fuel Basket Center Pipe for Lateral Loading (cont'd)

Maximum Radial Displacement;

Length of pipe on each basket, $L_t := (26.85 - 3.375)\cdot in$

$E := 26.6\cdot 10^6 \cdot \frac{lb}{in^2}$ @ 400°F $\qquad I_w := \frac{L_t \cdot t_{wall}^3}{12}$

$\theta := 0$

$u_1 := \frac{P\cdot R_t^3}{E\cdot I_w}\cdot\left[0.5570\cdot\theta\cdot\sin(\theta) + \left(0.9382 - 0.1592\cdot\theta^2\right)\cdot\cos(\theta) - 0.9053\right] \qquad u_1 = 2.947\cdot 10^{-6}\cdot in$

$\beta := \pi$

$u_2 := \frac{P\cdot R_t^3}{E\cdot I_w}\cdot((0.0796\cdot\beta - 0.2500)\cdot\sin(\beta) + 0.0681\cdot\cos(\beta) + 0.0947) \qquad u_2 = 2.383\cdot 10^{-6}\cdot in$

Maximum bending stress in pipe wall, $\beta := \pi$

$f_b := \frac{6\cdot M_2(\beta)}{L_t\cdot t_{wall}^2}\cdot 35 \qquad f_b = -4183\cdot\frac{lb}{in^2}$

The allowable bending stress is 150% of 2.4 x Sm,

$S_m := 15900\cdot\frac{lb}{in^2}$ at 400°F

$F_b := \frac{150}{100}\cdot(2.4\cdot S_m) \qquad F_b = 57240\cdot\frac{lb}{in^2}$

The overall beam bending deformation is,

$I_b := \frac{\pi}{64}\cdot\left[OD_t^4 - \left(OD_t - 2\cdot t_{wall}\right)^4\right]$

$u_b := \frac{5}{384}\cdot\frac{(2\cdot P)\cdot L_t^3}{E\cdot I_b} \qquad u_b = 0.002\cdot in$

ICF KAISER HANFORD

DESIGN ANALYSIS

Revision 0
Page No. 21 of 50

Client: Westinghouse Hanford K Basin SNF Project
Subject: MCO Storage Baskets

Date: 09/13/96
Orginator : L. L. Hyde
Checker : D. M. Chenault

Analyze the Mark IV Fuel Basket Center Pipe for Lateral Loading (cont'd)

The total lateral deformation of the center pipe when subjected to the maximum lateral acceleration is,

$$\left(u_1 + u_b\right)\cdot 35 = 0.077\cdot in \quad << \quad \frac{\left(OD_t - 2\cdot t_{wall}\right) - 1\cdot in}{2} = 0.375\cdot in$$

The longitudinal bending stress in the pipe is,

$$f_b := \frac{\frac{1}{8}\cdot(2\cdot P)\cdot L_t\cdot\frac{OD_t}{2}}{I_b}\cdot 35 \qquad f_b = 49244\cdot\frac{lb}{in^2} \quad < F_b$$

Axial Buckling Analysis of Mark IV Basket Center Pipe

Center Pipe for Mark IV Fuel--(2.75" OD x 0.5" wall)

The Mark IV fuel baskets, which are 28.65 in. high, are stacked five high in the MCO.

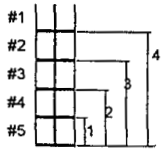

$l_p := 28.65 \cdot in$ where l_p is the height of each basket. Then $l_1 = 28.65"$, $l_2 = 57.30"$, $l_3 = 85.85"$, and $l_4 = 114.60"$.

$OD := 2.75 \cdot in$

$t_{wall} := 0.5 \cdot in$

$$A_t := \frac{\pi}{4} \cdot \left[OD^2 - \left(OD - 2 \cdot t_{wall} \right)^2 \right] \qquad A_t = 3.53 \cdot in^2$$

$$I_t := \frac{\pi}{64} \cdot \left[OD^4 - \left(OD - 2 \cdot t_{wall} \right)^4 \right] \qquad I_t = 2.35 \cdot in^4$$

$$r_t := \sqrt{\frac{I_t}{A_t}} \qquad r_t = 0.81 \cdot in$$

The Euler concentrated buckling load for the center pipe of one basket is,

$$P_{crit} := c_a \cdot \frac{\pi^2 \cdot E \cdot A_t}{\left(\frac{l_p}{r_t} \right)^2} \qquad P_{crit} = 750660 \cdot lb$$

This structure does not have to meet any criticality requirements so for this accident scenario the maximum compressive load in the pipe will be limited by the material yield stress,

$F_y := 17600 \cdot \frac{lb}{in^2}$ at 400°F

$P_{crit} := A_t \cdot F_y \qquad P_{crit} = 62204 \cdot lb$

Axial Buckling Analysis of Mark IV Basket Center Pipe (cont'd)

Center Pipe for Mark IV Fuel--(2.75" OD x 0.5" wall)

The pipe load is limited by F_y when the unsupported length is less than,

$$L_p := r_t \cdot \sqrt{\frac{c_a \cdot \pi^2 \cdot E \cdot A_t}{P_{crit}}} \qquad L_p = 99.5 \cdot in$$

when the unsupported length is greater than this the Euler load controls. Thus, the pipe can span more than the height of three baskets before it becomes buckling critical.

In addition to the center pipe the baskets are supported by six (6) 1-1/4" diameter rods located symmetrically about the baseplate circumference. The rods are attached to the baseplate and cantilevered upward from it.

The length of the rods is, $l_r := l_p - 3.375 \cdot in \qquad l_r = 25.275 \cdot in$

The buckling load of the rod is, $A_r := \frac{\pi \cdot 1.25^2}{4} \cdot in^2 \quad I_r := \frac{\pi \cdot 1.25^4}{64} \cdot in^4 \quad r_r := \sqrt{\frac{I_r}{A_r}}$

$c := \frac{1}{4}$

$$P_{crod} := c \cdot \frac{\pi^2 \cdot E \cdot A_r}{\left(\frac{l_r}{r_r}\right)^2} \qquad P_{crod} = 12313 \cdot lb$$

Three of the rods will carry the vertical load initially until they begin to buckle when the remaining rods will start to pick up load until eventually all six react the load

$$P_{rods} := 6 \cdot P_{crod} \qquad P_{rods} = 73875 \cdot lb$$

Each basket holds 54 Mark IV fuel elements which weigh 55.38 lbs each. The basket weighs approximately 150 lbs, so the total weight is,

$$W_{IV} := 3140 \cdot lb$$

Axial Buckling Analysis of Mark IV Basket Center Pipe (cont'd)

Center Pipe for Mark IV Fuel–(cont'd)

Use the same methodolgy as for the Mark IA fuel baskets. Vertical loads resulting from vertical accelerations of each basket are reacted by the six 1-1/4" rods of the basket directly below. When the a basket loading exceeds the buckling capability of these rods the center pipe takes the additional load. Assuming the baskets are accelerated uniformly find the maximum vertical acceleration which they may experience without exceeding the structural capability of the center pipe.

Let the load of each basket be the weight of the basket (W_{IV}) times the acceleration (a) and the reaction be the buckling load of the six rods (P_{rods}) and the load in the center pipe (P_n).

$a := 10.83$

$P_1 := W_{IV} \cdot a - P_{rods}$ $\quad P_1 = -39869 \cdot lb$

$P_1 := 0 \cdot lb$

$P_2 := 2 \cdot (W_{IV} \cdot a) - P_{rods} - P_1$ $\quad P_2 = -5863 \cdot lb$

$P_2 := 0 \cdot lb$

$P_3 := 3 \cdot (W_{IV} \cdot a) - P_{rods} - P_1 - P_2$ $\quad P_3 = 28143 \cdot lb$

$P_4 := 4 \cdot (W_{IV} \cdot a) - P_{rods} - P_1 - P_2 - P_3$ $\quad P_4 = 34006 \cdot lb$

$P_{tube} := P_1 + P_2 + P_3 + P_4$

$P_{tube} = 62149 \cdot lb$ $\quad \sim\sim P_{crit}$

This shows that a 2.75" OD x 0.5" wall tube will not buckle but it will achieve its yield load if the baskets are uniformly accelerated vertically at 10.83g. Which is greater than the normal handling loads of 3g/5g. This acceleration level is based on 1-1/4" diameter support rods.

Attachment of Mark IV Basket Baseplates to the Center Pipe

Center Pipe for Mark IV Fuel

$OD := 2.75 \cdot in$ outside diameter of pipe

$\pi \cdot OD = 8.64 \cdot in$ perimeter of pipe

In accordance with the MCO Performance Specification the attachment of the baseplates should limit the load in the center pipe to 75% of its buckling load so the atttachment of the Mark IV baseplates to the center pipe must support a load of 75% of 28,143 lbs.

$$P_w := 0.75 \cdot 28143 \cdot lb$$

The ultimate shear strength (S_s) of fillet welds is 42% of the material ultimate tensile strength (S_u). For 304L at 400°F,

$$S_u := 58700 \cdot \frac{lb}{in^2}$$

$$S_s := S_u \cdot \frac{42}{100} \qquad S_s = 24654 \cdot \frac{lb}{in^2}$$

The length of 3/16" fillet weld required is,

$$l_w := \frac{P_w}{S_s \cdot \left[0.707 \cdot \left(\frac{3}{16} \cdot in\right)\right]} \qquad l_w = 6.46 \cdot in$$

A 3/16" fillet skip weld around the perimeter which is 6-1/2" in total length is adequate.

Analyze Retaining Bars at Bottom of Mark IV Basket Baseplates

The fuel elements are retained in the basket baseplates by 1/4" x 3/8" bars which are welded to the bottom. These bars terminate at rings around the inside and outside diameters of the baseplate. Reference is made to Items 2, 11, and 12 of drawing SK-1-80208.

The analysis of the Center Pipe showed the baseplates of the Mark IV fuel baskets should only support 8.1 g (75% x 10.83g) in order to control the loading of the center pipe. To be conservative with these results analyze the fuel element retaining bars for 15g.

Each bar span several holes in the baseplate. They are welded to the baseplate with 1/8" fillet welds 1/4" long on each of the hole. It is conservative to analyze these as simply supported beams uniformly loaded by the weight of the fuel element.

The hole diameter is 2.58", so use a beam length to the center of the welds of,

$$l_b := (2.58 + 0.25)\cdot in$$

The weight of a Mark IV fuel element is, $W_{IV} := 55.38\cdot lb$

The bending moment in the bar is, $M_b := \frac{1}{8}\cdot W_{IV}\cdot l_b$

The allowable bending stress is 150% of 2.4 x Sm,

$$S_m := 15900\cdot\frac{lb}{in^2} \text{ at } 400^oF$$

$$F_b := \frac{150}{100}\cdot(2.4\cdot S_m) \qquad F_b = 57240\cdot\frac{lb}{in^2}$$

The actual bending stress in the bar is,

$$\sigma_b := \frac{6\cdot M_b}{\frac{1}{4}\cdot\left(\frac{3}{8}\right)^2\cdot in^3}\cdot 15 \qquad \sigma_b = 50152\cdot\frac{lb}{in^2} < F_b$$

Analyze Retaining Bars at Bottom of Mark IV Basket Baseplates (cont'd)

The allowable shear stress (S_s) is 42% of the material ultimate tensile stress (S_u). For 304L at 400°F,

$$S_u := 58700 \cdot \frac{lb}{in^2}$$

$$S_s := S_u \cdot \frac{42}{100} \qquad S_s = 24654 \cdot \frac{lb}{in^2}$$

The stress in the end welds is,

$$\sigma_w := \frac{\frac{1}{2} \cdot W_{IV}}{\left(0.707 \cdot \frac{1}{8}\right) \cdot 0.25 \cdot in^2} \cdot 15 \qquad \sigma_w = 18799 \cdot \frac{lb}{in^2} < S_s$$

Analysis of the Mark 1A and Mark IV Storage Basket Baseplates

Summary

The following elastic finite element (ANSYS) static analysis considered both the Mark IV fuel baseplate (Plate 1) and the Mark IA fuel baseplate (Plate 2). These baseplates are constructed of 3" thick 304L stainless steel plate which is drilled through to accept the fuel elements. The analysis also considered various support boundary conditions. Load Case 1 represents a tight fit of the baseplate to its center pipe in which the pipe provides radial support to the plate at it center hole. This is the most realistic condition for center support. Load Cases 2 and 3 provided only vertical support at the center pipe. Load Case 4 represents the baseplate supported by the six rods around its periphery. In addition a solid plate was used as a check. All results shown are for a 1g vertical down load of the baseplate fully loaded with fuel elements.

The allowable stress intensity is 23,850 psi (1.5 x 15,900) for normal conditions (Level A) and 57,240 psi (1.5 x 2.4 x 15,900) for accident conditions (Level D) at 400^{0}F. As expected the stresses in the Mark IV baseplate are the highest, concentrating in the thin ligaments near the center pipe. When supported by the rods (Load Case 4) only, which the tolerancing requires, the stresses allow nearly 17g vertical acceleration to the normal (Level A) allowable. This is well above the 3g/5g handling requirements. When the vertical accelerations exceed the buckling allowable of the rods the center pipe picks up the load (Load Case 1). It is seen the resulting stresses allow about 15g to obtain the accident (Level D) allowable. Load Case 1 for the Mark 1A baseplate shows the accident (Level D) allowable is not reached until over 36g vertical acceleration.

Conclusion

The baseplates are structurally adequate for the expected vertical accelerations. Since the bending stresses, which are shown to peak very locally in the ligaments of the baseplates, resulted from a static elastic analysis there is considerable potential for plastic deformation and redistribution of stresses. A more rigorous analysis would also confirm the baseplates are structurally adequate.

ICF KAISER HANFORD

DESIGN ANALYSIS

Revision 0
Page No 29 of 50

Client : Westinghouse Hanford K Basin SNF Project
Subject : MCO Storage Basket

Date : 9/12/96
Orginator: H.Shrivastava
Checker : L L Hyde

Analysis of the Mark 1A and Mark IV Storage Basket Baseplates (cont'd)

INTRODUCTION

For the dry storage of spent nuclear fuel currently stored in the K-Basin, two different designs of rerack basket are being considered. One of the two designs has a base plate with fifty four 2.583-in. diameter holes. Under these holes, bars will be welded to hold 54 Mark IV fuel assemblies in place. This plate also has a 2 5/8-in. diameter hole which provides space for a dip tube to run down the center of the Multi-Canister Overpack (MCO). The second design of the base plate will hold 48 Mark 1A fuel assemblies. The holes which hold the fuel assemblies in place have 2.58-in. diameter and the center hole for the dip tube is of 6 5/8-in. diameter. The diameter and thickness of the base plates are 22 5/8-in. and 3-in.; respectively for both designs.

This calculation is performed to evaluate the maximum stress intensity in the plates resulting from 1*g* vertical loading.

BASEPLATE MODEL

The holes for the fuel assemblies are symmetric in each 1/6th segment of the plate. As only the vertical loading needs to be considered, a 1/6th model is sufficient to analyze the plate. The ANSYS finite-element program, version 5.2 is used to generate the model and analyze the plate for the gravity loading. Figures 1 and 2 show the finite-element models of the two plates. Figure 3 shows a similar model of a solid plate which has a 2 5/8-in. diameter center hole. This model is analyzed to provide a comparison of stress intensities for a solid plate and a perforated plate.

Both the perforated plate and solid plate models use SOLID45 element of the ANSYS program. The perforated plates are meshed with tetrahedron elements as brick elements cannot be utilized because the holes make the plate geometry too complex for brick elements. The solid plate, however, is meshed with brick elements which are more suitable than the tetrahedrons for structural analyses.

Symmetry kinematic boundary conditions are imposed at $\theta = 0°$ and 60°. At the center hole, different boundary conditions are applied in three different analyses. These are described later with the load cases.

ICF KAISER HANFORD

DESIGN ANALYSIS

Revision 0

Page No 30 of 50

Client : Westinghouse Hanford K Basin SNF Project
Subject : MCO Storage Basket

Date : 9/13/96
Orginator: H.Shrivastava
Checker : L L Hyde

Analysis of the Mark 1A and Mark IV Storage Basket Baseplates (cont'd)

INPUT DATA

Plate outside radius = 11.3125 in.

Plate 1 (Mark IV) inside radius = 1.3125 in.

Plate 2 (Mark 1A) inside radius = 3.3125 in.

Plate Thickness = 3 in.

Material density = 0.283 lbf/in^3, Plate Material: SS 304L

Elastic Modulus = 28.3 x 10^6 lbf/in^2

Poisson's Ratio = 0.3

For plate 1, the weight of each Mark IV fuel assembly is 55.38 lbf which is distributed on 24 nodes around the hole circumference, i.e. the force at each node is 2.31 lbf. Similarly, for plate 2, the weight of each Mark 1A fuel assembly (39.71 lbf) is distributed on 24 nodes. Force on each node is 1.655 lbf.

The material density in case of the solid plate is adjusted to account for the total fuel assembly weight of 2,990 lbf. The resulting density is 2.008 lbf/in^3.

LOAD CASES

For both plates, the following load cases have been analyzed:

Load Case 1: The nodes at inner radius are radially restrained. Also, the bottom nodes at that location are vertically restrained. The solid plate is analyzed only for this case.

Load Case 2: The nodes at inner radius are only vertically restrained.

Load Case 3: Only the bottom nodes at the inner radius are vertically restrained as in case of Load Case 1. However, nodes are not restrained in the radial direction.

ICF KAISER HANFORD

DESIGN ANALYSIS

Revision 0

Page No 31 of 50

Client : Westinghouse Hanford K Basin SNF Project
Subject : MCO Storage Basket

Date : 9/13/96
Orginator: H.Shrivastava
Checker : L L Hyde

Analysis of the Mark 1A and Mark IV Storage Basket Baseplates (cont'd)

Load Case 4: This case is analyzed for plate 1 (Mark IV) only. The nodes at the inner surface are free. However, a node near $\theta = 0°$ and a node near $\theta = 60°$ near the outer radius are vertically restrained.

Figures 4, 5, and 6 show the three plate models with applied forces and the nodal displacement boundary conditions.

RESULTS

The results are tabulated below:

Load Case	Stress Intensity, lbf/in$_2$		
	Plate 1,Mark IV	Plate 2,Mark 1A	Solid Pl.
1	3,879	1,578	1,638
2	5,454	2,413	n/a
3	6,134	2,636	n/a
4	1,426	n/a	n/a

Figures 7-10 show the stress intensity contours for plate 1 (Mark IV) for various boundary conditions. Similarly, Figures 11-13 have stress intensity plots for plate 2 (Mark 1A). Solid plate stress intensity contours are plotted in Figure 14.

ICF KAISER HANFORD

DESIGN ANALYSIS

Revision 0
Page No 32 of 50

Client : Westinghouse Hanford K Basin SNF Project
Subject : MCO Storage Basket

Date : 9/13/96
Orginator: H.Shrivastava
Checker : L L Hyde

Analysis of the Mark 1A and Mark IV Storage Basket Baseplates (cont'd)

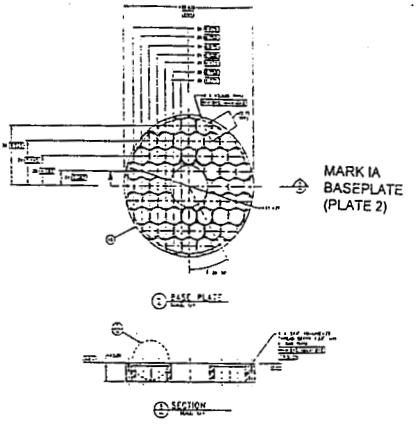

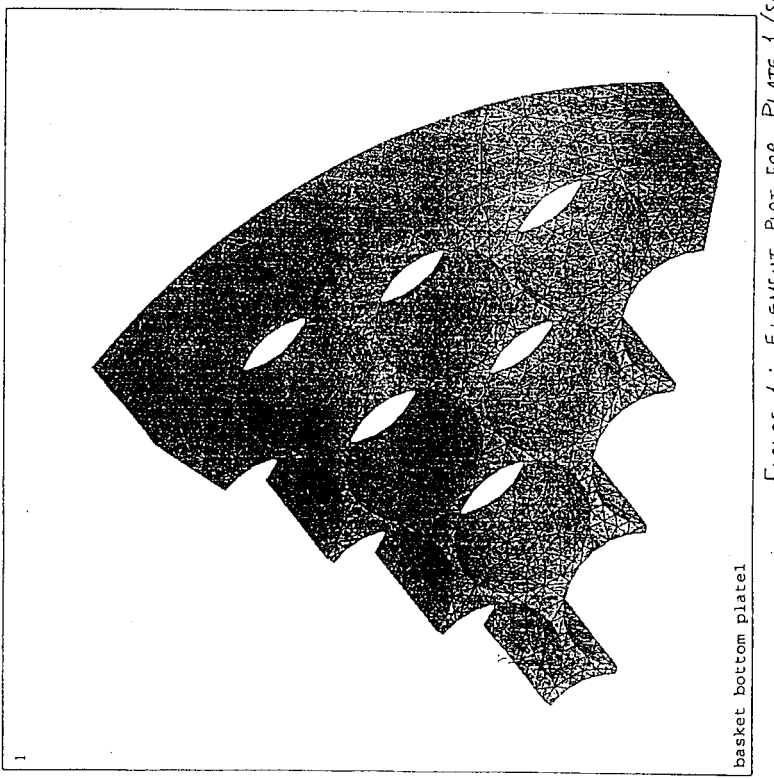

FIGURE 1: ELEMENT PLOT FOR PLATE 1 (SMALLER INNER RADIUS)

FIGURE 2: ELEMENT PLOT FOR PLATE 2

FIGURE 3: ELEMENT PLOT FOR SOLID PLATE

FIGURE 4: BOUNDARY CONDITIONS FOR PLATE 1

Page 9

PAGE 37 OF 50

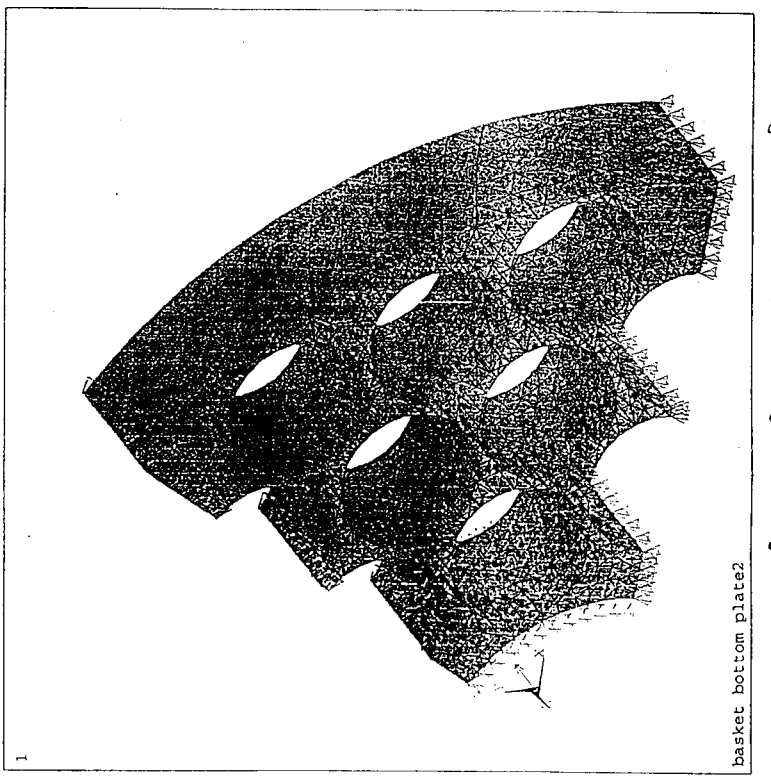

FIGURE 5: BOUNDARY CONDITIONS FOR PLATE 2

FIGURE 6: BOUNDARY CONDITIONS FOR SOLID PLATE

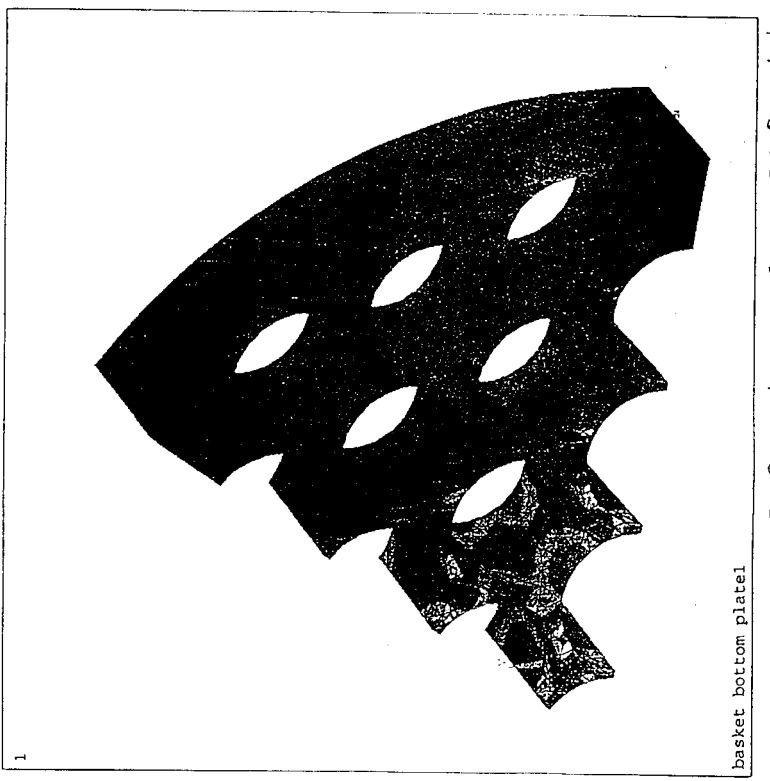

FIGURE 7: STRESS INTENSITY CONTOURS FOR PLATE 1, LOAD CASE 1

Page 12

PAGE 40 OF 50

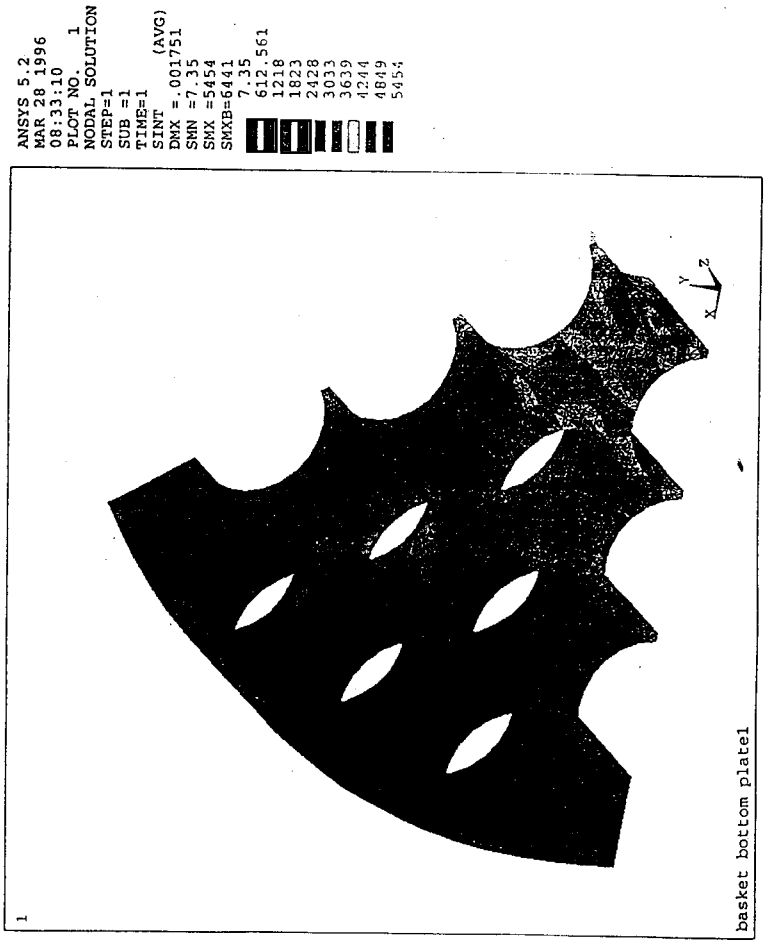

FIGURE 8: STRESS INTENSITY CONTOURS FOR PLATE 1, LOAD CASE 2

Page 13

PAGE 41 OF 50

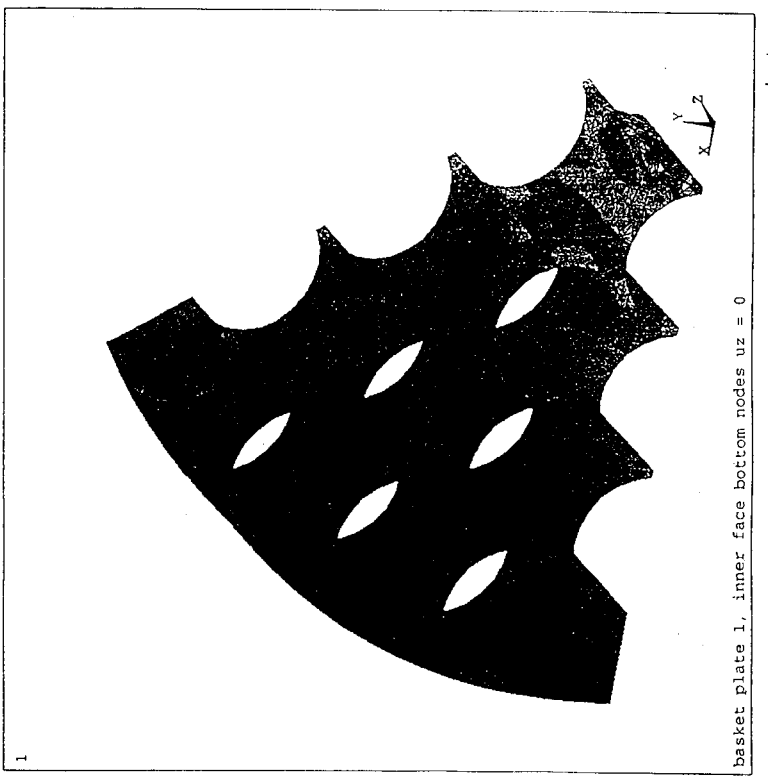

FIGURE 9: STRESS INTENSITY CONTOURS FOR PLATE 1, LOAD CASE 3

Page 14

PAGE 42 OF 50

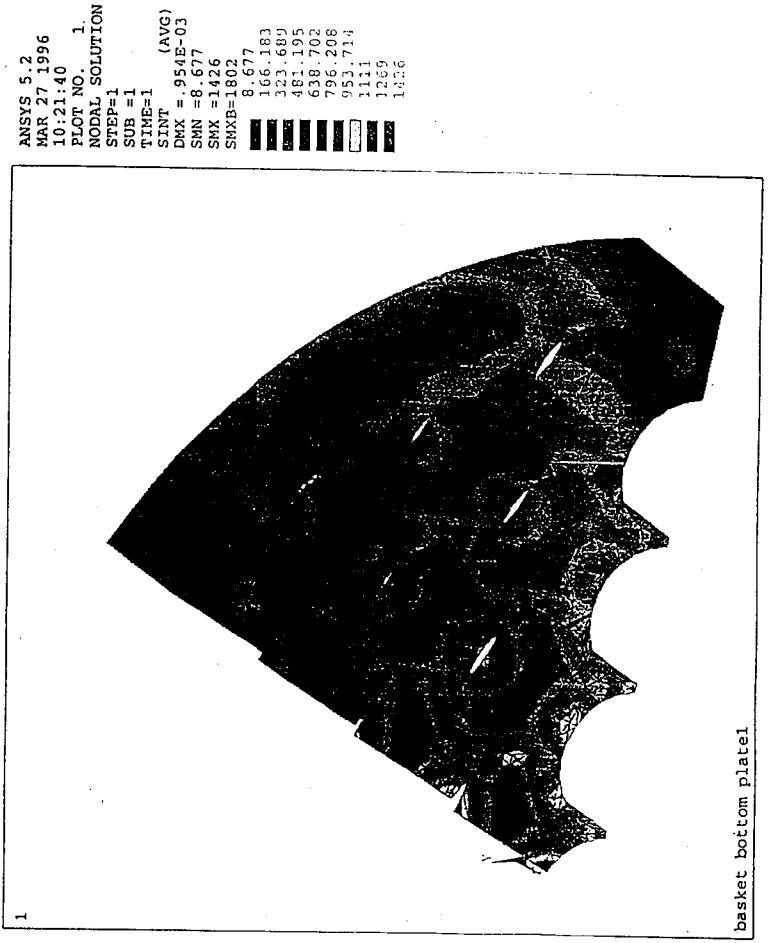

FIGURE 10 : STRESS INTENSITY CONTOURS FOR PLATE 1, LOAD CASE 4

Page 15

PLATE 43 OF 50

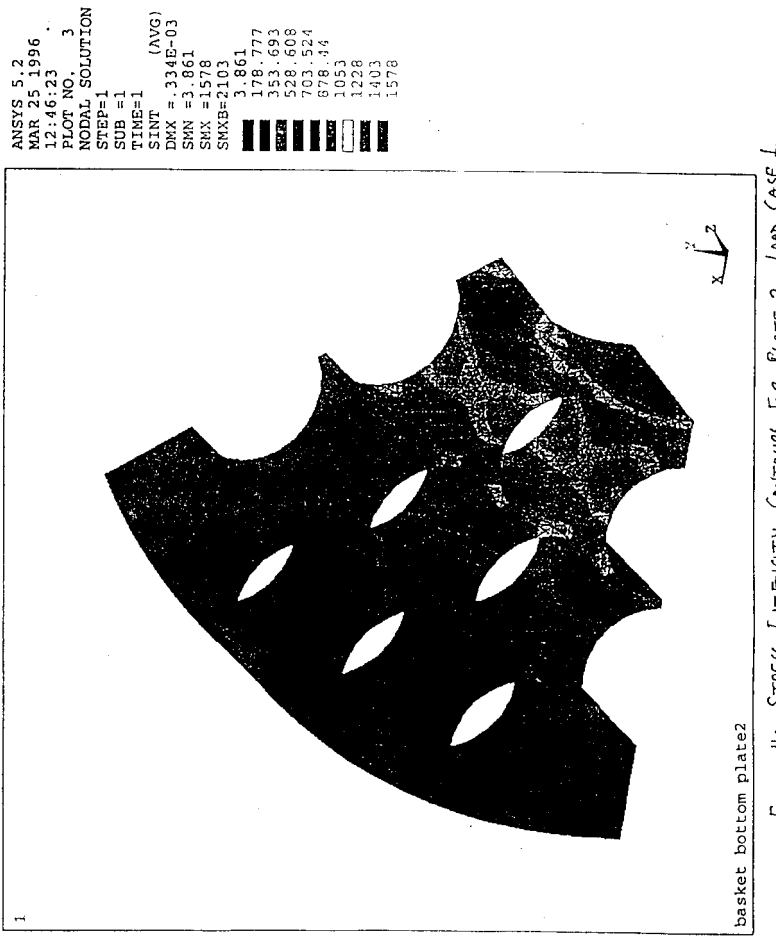

FIGURE 11: STRESS INTENSITY CONTOURS FOR PLATE 2, LOAD CASE 1.

Page 16

PAGE 44 OF 50

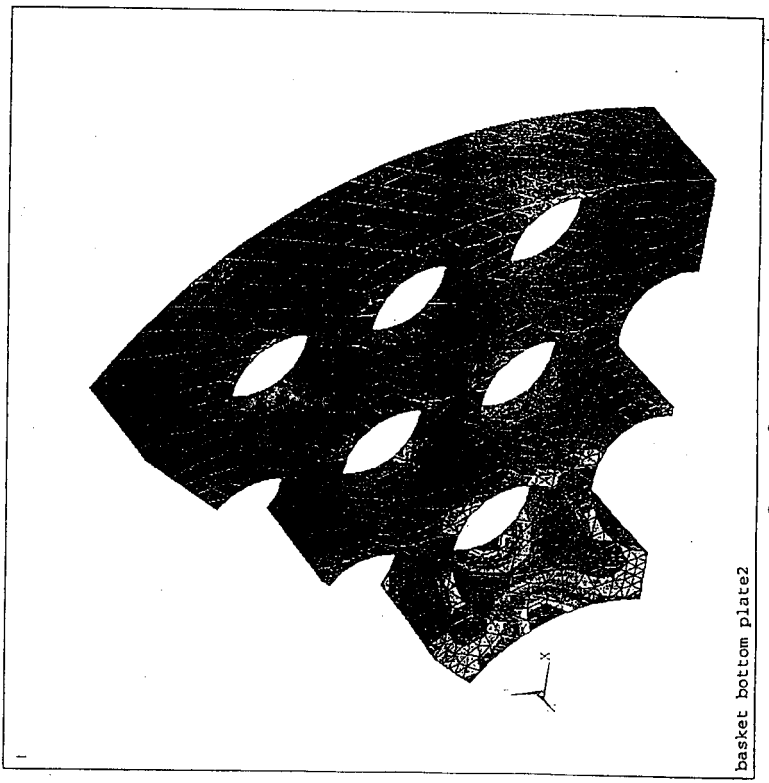

FIGURE 12: STRESS INTENSITY CONTOURS FOR PLATE 2, LOAD CASE 2

FIGURE 13 : STRESS INTENSITY CONTOURS FOR PLATE 2, LOAD CASE 3

Page 18

PAGE 46 OF 50

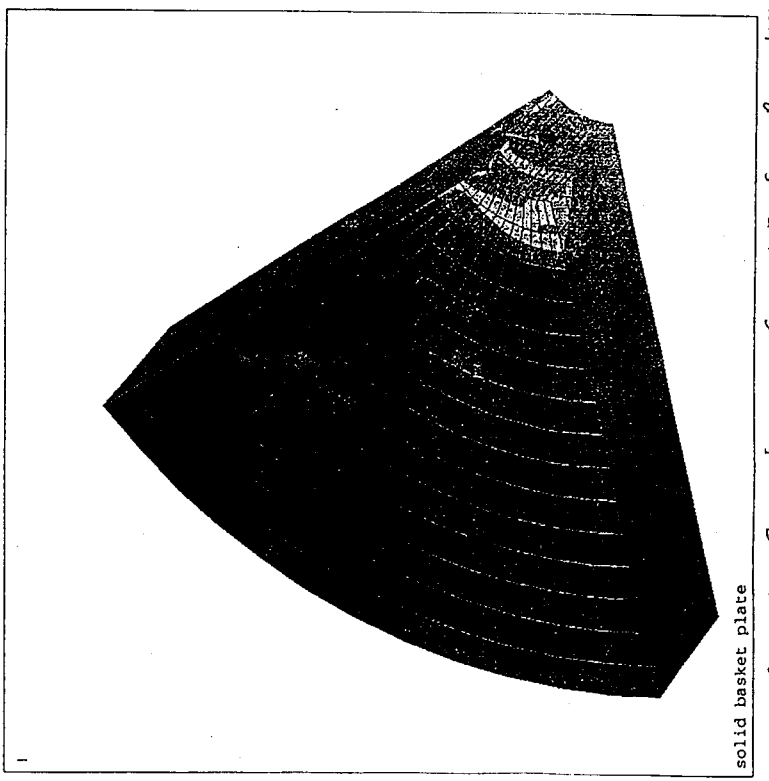

FIGURE 14: STRESS INTENSITY CONTOURS FOR SOLID PLATE, LOAD CASE 1

Will a fuel element perforate the bottom of the MCO during an accidental drop?

References: 1) *Design of Structures for Missile Impact*, BC-TOP-9A, Rev.2, Bechtel Power Corporation, San Francisco, CA. September 1974.
2) *SNFP Technical Databook*, WHC-SD-SNF-TI-015, Rev. 0 Westinghouse Hanford Company, Richland, WA.

There are two major types of fuel elements the Mark IV and the Mark IA. The MK IV fuel elements are heavier and more are loaded per MCO basket so it presents the maximum load case even though there are only 5 baskets per MCO while there are 6 baskets with MK IA fuel. The SK-1-80110, Rev. 0 drawing shows 54 MK IV fuel elements per basket.

Weight of MK IV fuel element per Reference 2: $W_e := 55.38\ lb$

Weight of fully loaded basket: $W_b := 54 \cdot W_e$

Diameter of MK IV fuel element per Reference 2: $D := 2.4\ in$

The maximum drop height of the unprotected MCO is two feet. However, during transportation it may be dropped 30 feet in the cask. Conservatively assume this scenario is equivalent to a missile (fuel element) being dropped onto a steel plate (bottom of the MCO). Find the thickness of plate (T) required to prevent perforation in accordance with the methodology of Reference 1.

Drop height: $H := 30\ ft$

$$T = \frac{(1/2 \times M_{eff} \times V_s^2)^{2/3}}{672 \times D}$$

where, $M_{eff} = W_{eff} / g$ and, $V_s = (2 \times g \times H)^{1/2}$

thus, $$T = \frac{(W_{eff} \times H)^{2/3}}{672 \times D}$$

or, $$W_{eff} = \frac{(672 \times D \times T)^{3/2}}{H}$$

ICF KAISER HANFORD

DESIGN ANALYSIS

Revision 0
Page No. 48 of 50

Client: Westinghouse Hanford K Basin SNF Project
Subject: MCO

Date: 09/13/96
Orginator : L. L. Hyde
Checker : D. M. Chenault

Will a fuel element perforate the bottom of the MCO? (cont'd)

Assume a percentage of the weight (p_w) of the fuel in the four baskets above the bottom basket act with one fuel element in the bottom basket and this fuel element must be prevented from perforating the bottom of the MCO. Consider a range of thicknesses for the bottom of the MCO and find the effective weight of the missile (W_{eff}) and the percentage of the total fuel weight (p_w) at incipient perforation.

let, $T := 0.5, 0.75 .. 3$ in

$$W_{eff}(T) := \frac{(672 \cdot D \cdot T)^{\frac{3}{2}}}{H} \text{ lb}$$

$$p_w(T) := \frac{W_{eff}(T) - W_e}{4 \cdot W_b} \cdot 100 \text{ percent}$$

$$n_{rods}(T) := (4 \cdot 54) \cdot \frac{p_w(T)}{100} + 1$$

T = thickness of bottom of MCO, inches
W_{eff} = weight of a 2.4 inch diameter missile which, when dropped 30 feet, will just perforate the bottom of an MCO of thickness (T), pounds
p_w = the percentage of the fuel weight in the four baskets above the bottom basket which are included in W_{eff}, percent
n_{rods} = the number of fuel rods whose combined weight is W_{eff}. Note: the total number of rods in the upper four baskets is (4 x 54 = 216)

T	$W_{eff}(T)$	$p_w(T)$	$n_{rods}(T)$	
0.5	763	5.9	14	
0.75	1402	11.3	25	
1	2159	17.6	39	
1.25	3017	24.8	54	<<==== Minimum thickness of current design
1.5	3966	32.7	72	
1.75	4998	41.3	90	
2	6107	50.6	110	
2.25	7287	60.5	132	
2.5	8534	70.9	154	
2.75	9846	81.8	178	
3	11218	93.3	203	

ICF KAISER HANFORD

DESIGN ANALYSIS

Calc. No.
Revision
Page No.

Client Westinghouse Hanford Company	WO/Job No. E50471/LE016/F7L7A1	
Subject Results Dropped MCO Loaded in Center Region with Mass Load Bottom MCO	Date July 10, 1996	By Carleton J. Moore
	Checked	By Larry L. Hyde
Location 100 K, K-Basins	Revised	By

Dropped MCO Bottom Contact Pressure at 0.003 second.

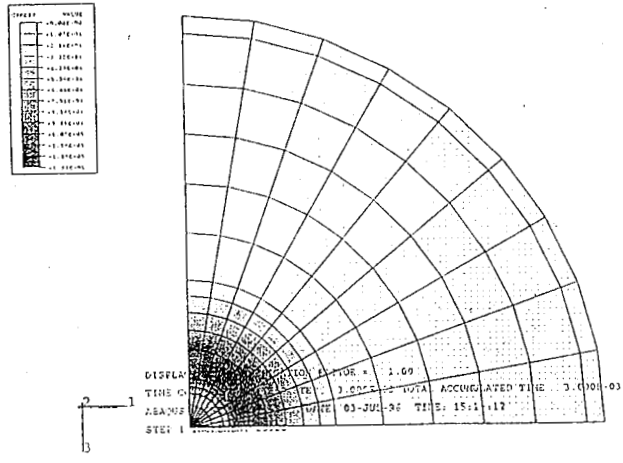

Figure 5-21

40

ICF KAISER HANFORD

DESIGN ANALYSIS

Calc. No.
Revision
Page No.

Client Westinghouse Hanford Company	WO/Job No. E50471/LE016/F7L7A1	
Subject Results Dropped MCO Loaded in Center Region with Mass	Date July 10, 1996	By Carleton J. Moore
Load Bottom MCO	Checked	By Larry L. Hyde
Location 100 K, K-Basins	Revised	By

Dropped MCO Bottom Contact Pressure at 0.006 second.

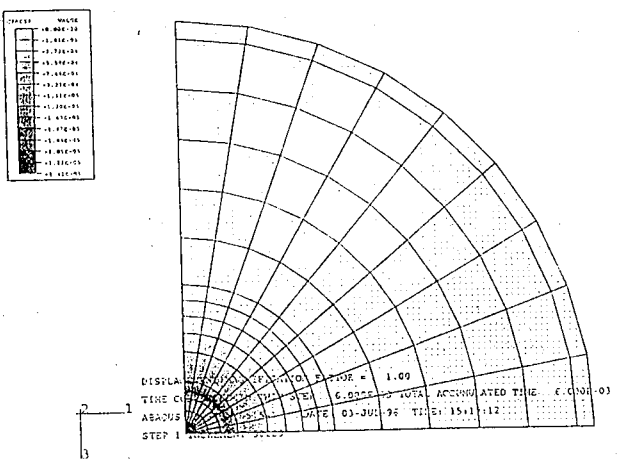

Figure 5-22

ICF KAISER HANFORD

DESIGN ANALYSIS

Calc. No.
Revision
Page No.

Client Westinghouse Hanford Company	WO/Job No. E50471/LE016/F7L7A1		
Subject Results Dropped MCO Landed in Center Region with Mass	Date July 10, 1996	By	Carleton J. Moore
Land Bottom MCO	Checked	By	Larry L. Hyde
Location 100 K, K-Basins	Revised	By	

Dropped MCO Bottom Contact Pressure at 0.033 second.

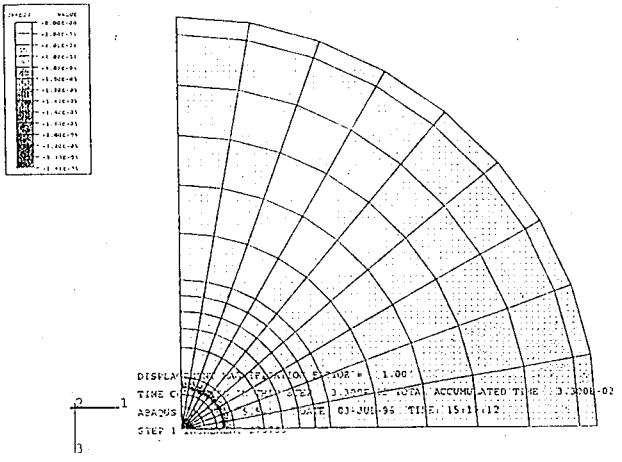

Figure 5-23

ICF KAISER HANFORD

DESIGN ANALYSIS

Calc. No.
Revision
Page No.

Client Westinghouse Hanford Company	WO/Job No. E50471/LE016/F7L7A1	
Subject Results Dropped MCO Loaded in Center Region with Mass Load Bottom MCO	Date July 10, 1996	By Carleton J. Moore
	Checked	By Larry L. Hyde
Location 100 K, K-Basins	Revised	By

Dropped MCO Bottom Contact Pressure at 0.048 second.

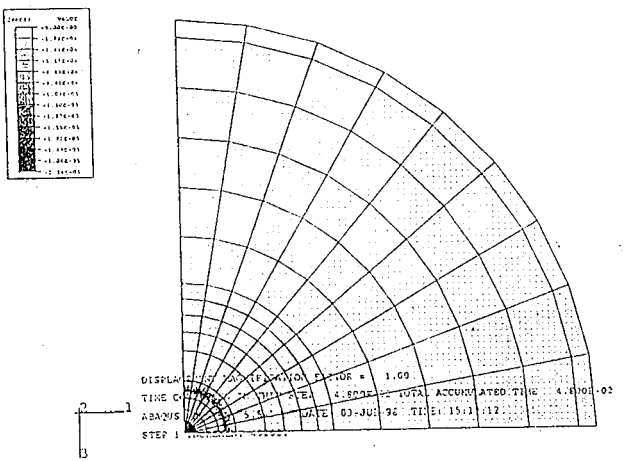

Figure 5-24

5.2 Dropped MCO Mass Loaded Full Diameter with Mass Loaded Bottom MCO

The basket and fuel mass in the dropped MCO is simulated with lump masses connected at the bottom across the full diameter corresponding an assumed shear failure of the basket bottoms. The basket and fuel mass in the bottom MCO is simulated with lumped masses on the inside bottom of the shield plug corresponding to the inertia load transmitted through the basket column.

Figure 5-25 shows the displacement (inch) versus time (second) of the bottom of the dropped MCO, the impacted shield plug, and the impact limiter. In Figure 5-25 the maximum deflection can be seen to be at 0.048 second. Figure 5-26 shows the velocity (in/sec) versus time (second) of the bottom of the dropped MCO, the impacted shield plug, and the impact limiter. Figure 5-27 shows the graphical calculation of deceleration g level. In Figure 5-27, after the initial contact the MCO's and top of the impact limiter can be seen to decelerate at approximately 14.8 g. Figure 5-28 shows additional acceleration dynamics superimposed on the calculated average deceleration.

Figure 5-29 shows the deflected shape of the MCO to MCO contact at 0.048 second. In Figure 5-29 the center region of the bottom of the dropped MCO can be seen to not be as significantly deformed as was for the case studied in Section 5.1, Figure 5-9. Also, in Figure 5-29 the bottom of the shield plug can be seen to be deformed by the inertia forces produced by the lumped masses modeling the fuel and basket load transfer to the top of the impacted MCO.

Figure 5-30 shows a von Mises stress contour at 0.006 second. Figure 5-31 shows the vertical stress contour at 0.006 second. The maximum tension stress is at the center bottom of the impacted shield plug. Figure 5-32 shows the radial stress contour for the solid elements at 0.006 second. Figure 5-33 gives the shear stress in the plane of the figure. Figure 5-34 shows the circumferential stress for the solid elements at 0.006 second.

Figure 5-35 shows the vertical plastic strain at 0.006 second. Figure 5-36 gives the equivalent plastic strain at 0.006 second.

Figure 5-37 shows the von Mises stress contour at 0.048 second. Figure 5-38 shows the vertical stress contour at 0.048 second. Figure 5-39 shows the radial stress of the solid elements at 0.048 second. Figure 5-40 shows the shear stress in the plane of the figure. Figure 5-41 shows the circumferential stress of the solid elements.

The stresses in Figures 5-30 through 5-41 show high stresses in the bottom of the impacted shield plug. This region is subject to high local loads imposed by the assumed load path for the concentrated lumped masses (mass modeling of baskets and fuel). The high stress region is confined in a manner that prevents failure but allows plastic deformation. In these plots the stresses at the lifting ring and MCO cylinder do not have a high stress history.

Figure 5-42 shows the vertical plastic strain at 0.048 second. Figure 5-43 shows the equivalent plastic strain at 0.048 second. Again the high plastic strains on the bottom center of the impacted shield plug imply a past stress history significantly exceeding yield.

Figure 5-44 shows a shaded contour plot of the contact pressure across the bottom of the dropped MCO at 0.003 second. Figure 5-45 shows the contact pressure contour at 0.009 second. Figure 5-46 shows the contact pressure contour at 0.015 second. Figure 5-47 shows the contact pressure contour at 0.018 second. Figure 5-48 shows the contact pressure contour at 0.020 second. Figure 5-49 shows the contact pressure contour at 0.033 second. Figure 5-50 shows the contact pressure contour at 0.048 second.

Figures 5-44 through 5-50 were selected to provide the maximum contact pressures. The dynamics of the impact event are such that the contact pressures between these maximums can be significantly less. In fact during the initial impact the bottom

ICF KAISER HANFORD

DESIGN ANALYSIS

Calc. No.
Revision
Page No.

Client Westinghouse Hanford Company	WO/Job No. E50471/LE016/F7L7A1	
Subject Results Dropped MCO Mass Loaded Full Diameter With Mass Loaded Bottom MCO	Date July 15, 1995	By Carleton J. Moore
	Checked	By Larry L. Hyde
Location 100K, K-Basins	Revised	By

of the dropped MCO is bouncing against the top of the static MCO (pressure can and do go to zero during this bouncing). Also the maximum contact pressures can be seen to be high compared to the normal static capability of the materials. Again the dynamics are such that both inertia forces and elastic forces balance the contact pressures. But plastic deformation of the impacted shield plug can only be relieved by inserting a shock absorber between the two MCO's.

ICF KAISER HANFORD

DESIGN ANALYSIS

Calc. No.
Revision
Page No.

Client Westinghouse Hanford Company	WO/Job No. E50471/LE016/F7L7A1	
Subject Results Dropped MCO Mass Loaded Full Diameter With Mass Loaded Bottom MCO	Date July 15, 1995	By Carleton J. Moore
	Checked	By Larry L. Hyde
Location 100K, K-Basins	Revised	By

Displacement Versus Time of the Bottom of Dropped MCO, the Impacted Shield Plug, and the Impact Limiter.

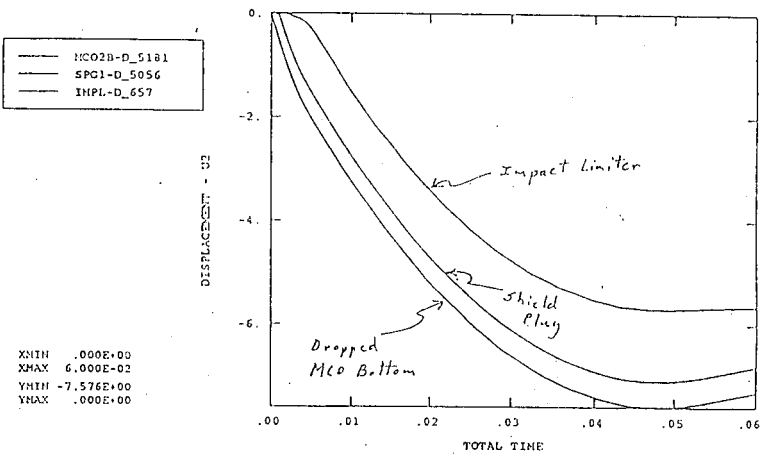

Figure 5-25

ICF KAISER HANFORD

DESIGN ANALYSIS

Calc. No.
Revision
Page No.

Client Westinghouse Hanford Company	WO/Job No. E5047I/LE016/F7L7A1	
Subject Results Dropped MCO Mass Loaded Full Diameter With Mass Loaded Bottom MCO	Date July 15, 1995	By Carleton J. Moore
	Checked	By Larry L. Hyde
Location 100K, K-Basins	Revised	By

Velocity Versus Time of the Bottom of Dropped MCO, the Impacted Shield Plug, and the Impact Limiter.

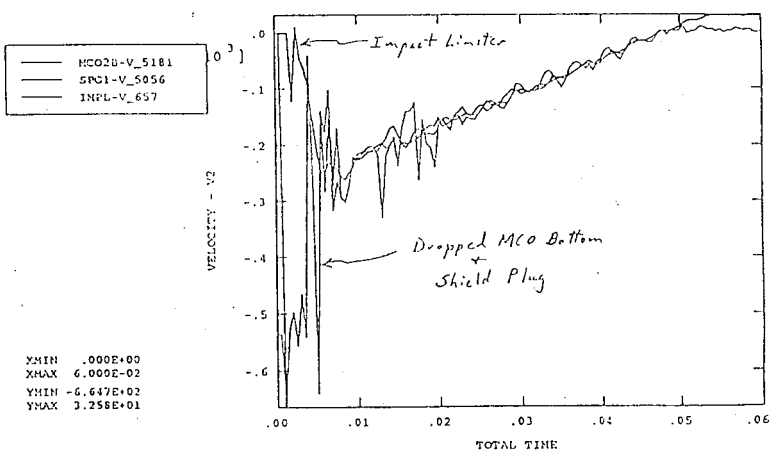

Figure 5-26

ICF KAISER HANFORD

DESIGN ANALYSIS

Calc. No. _____
Revision _____
Page No. _____

Client Westinghouse Hanford Company	WO/Job No. ES0471/LE016/F7L7A1		
Subject Results Dropped MCO Mass Loaded Full Diameter With Mass Loaded Bottom MCO	Date July 15, 1995	By	Carleton J. Moore
	Checked	By	Larry L. Hyde
Location 100K, K-Basins	Revised	By	

Graphical Calculation of Average Deceleration.

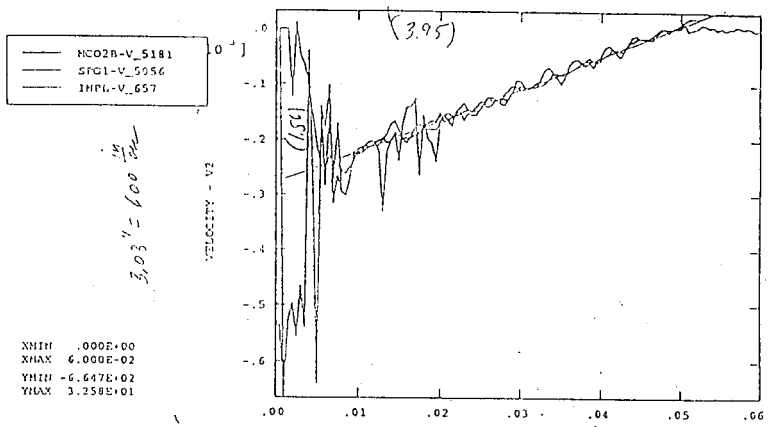

$\frac{dV}{dt} = \frac{308.9 \frac{in}{sec}}{.054 sec} = 5,720 \frac{in}{sec^2}$

$4.35^{-1} = .06 sec$

$\Rightarrow 14.8\ g$

Figure 5-27

ICF KAISER HANFORD

DESIGN ANALYSIS

Calc. No.
Revision
Page No.

Client Westinghouse Hanford Company	WO/Job No. E50471/LE016/F7L7A1	
Subject Results Dropped MCO Mass Loaded Full Diameter With Mass Loaded Bottom MCO	Date July 15, 1995	By Carleton J. Moore
	Checked	By Larry L. Hyde
Location 100K, K-Basins	Revised	By

Combined Acceleration Dynamics.

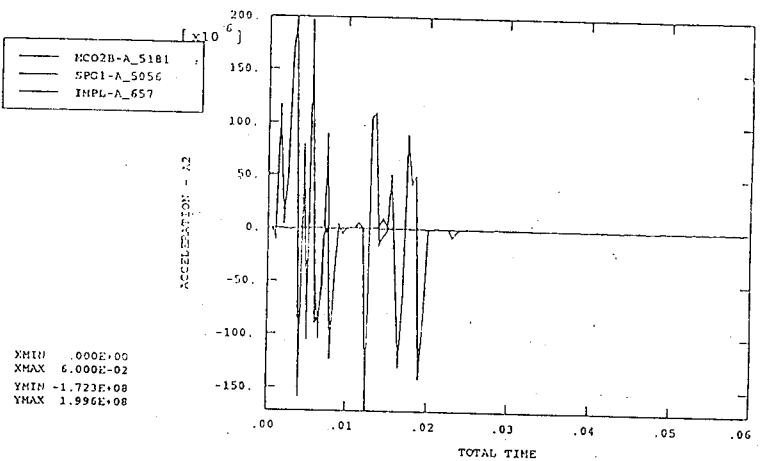

Figure 5-28

ICF KAISER HANFORD

DESIGN ANALYSIS

Calc. No.
Revision
Page No.

Client Westinghouse Hanford Company	WO/Job No. E50471/LE016/F7L7A1	
Subject Results Dropped MCO Mass Loaded Full Diameter With Mass Loaded Bottom MCO	Date July 15, 1995	By Carleton J. Moore
	Checked	By Larry L. Hyde
Location 100K, K-Basins	Revised	By

Deflected Shape at 0.048 Second.

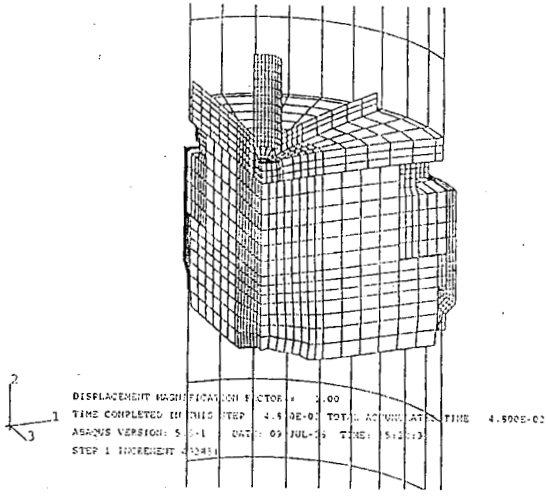

Figure 5-29

ICF KAISER HANFORD

DESIGN ANALYSIS

Calc. No.
Revision
Page No.

Client Westinghouse Hanford Company	WO/Job No. E50471/LE016/F7L7A1	
Subject Results Dropped MCO Mass Loaded Full Diameter With Mass Loaded Bottom MCO	Date July 15, 1995	By Carleton J. Moore
	Checked	By Larry L. Hyde
Location 100K, K-Basins	Revised	By

Von Mises Stress Contour at 0.006 Second.

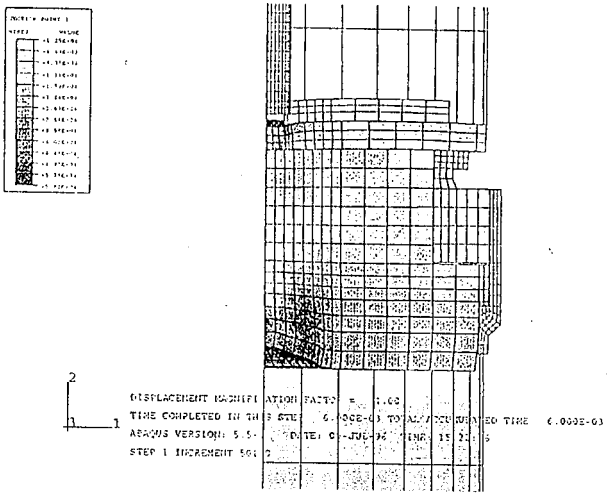

Figure 5-30

ICF KAISER HANFORD

DESIGN ANALYSIS

Calc. No.
Revision
Page No.

Client Westinghouse Hanford Company	WO/Job No. E50471/LE016/F7L7A1	
Subject Results Dropped MCO Mass Loaded Full Diameter With Mass Loaded Bottom MCO	Date Jul. 15, 1995	By Carleton J. Moore
	Checked	By Larry L. Hyde
Location 100K, K-Basins	Revised	By

Vertical Stress Contour at 0.006 Second.

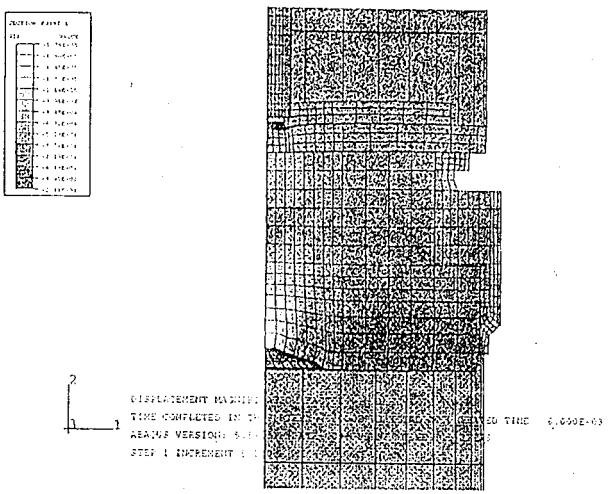

Figure 5-31

ICF KAISER HANFORD

DESIGN ANALYSIS

Calc. No.
Revision
Page No.

Client Westinghouse Hanford Company	WO/Job No. E5047H/LE016/F7L7A1	
Subject Results Dropped MCO Mass Loaded Full Diameter With Mass Loaded Bottom MCO	Date July 15, 1995	By Carleton J. Moore
	Checked	By Larry L. Hyde
Location 100K, K-Basins	Revised	By

Radial Stress Contour at 0.006 Second.

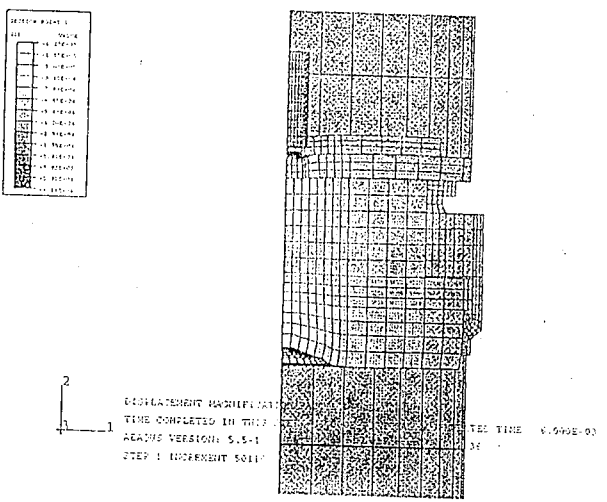

Figure 5-32

ICF KAISER HANFORD

DESIGN ANALYSIS

Calc. No.
Revision
Page No.

Client Westinghouse Hanford Company	WO/Job No. E50471/LE016/F7L7A1	
Subject Results Dropped MCO Mass Loaded Full Diameter With Mass Loaded Bottom MCO	Date July 15, 1995	By Carleton J. Moore
	Checked	By Larry L. Hyde
Location 100K, K-Basins	Revised	By

Shear Stress Contour at 0.006 Second.

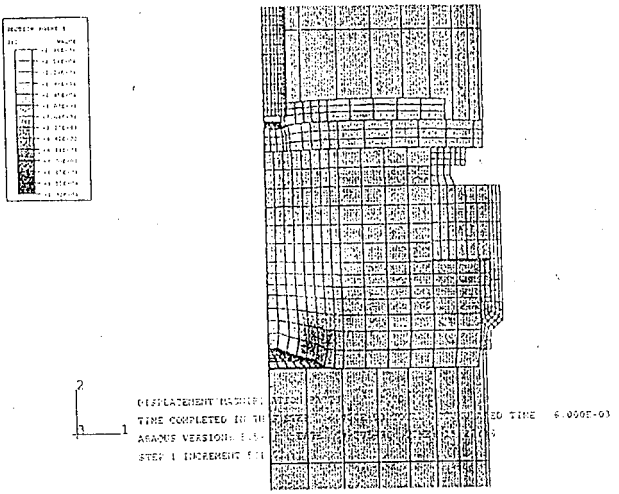

Figure 5-33

ICF KAISER HANFORD

DESIGN ANALYSIS

Calc. No.
Revision
Page No.

Client Westinghouse Hanford Company	WO/Job No. E50471/LE016/F7L7A1	
Subject Results Dropped MCO Mass Loaded Full Diameter With Mass Loaded Bottom MCO	Date July 15, 1995	By Carleton J. Moore
	Checked	By Larry L. Hyde
Location 100K, K-Basins	Revised	By

Circumferential Stress Contour at 0.006 Second.

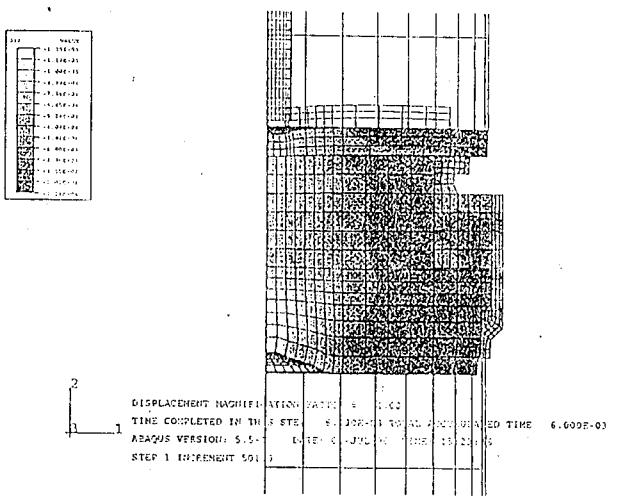

Figure 5-34

ICF KAISER HANFORD

DESIGN ANALYSIS

Calc. No.
Revision
Page No.

Client Westinghouse Hanford Company	WO Job No. E50471/LE016/F7L7A1	
Subject Results Dropped MCO Mass Loaded Full Diameter With Mass Loaded Bottom MCO	Date July 15, 1995	By Carleton J. Moore
	Checked	By Larry L. Hyde
Location 100K, K-Basins	Revised	By

Vertical Plastic Strain at 0.006 Second

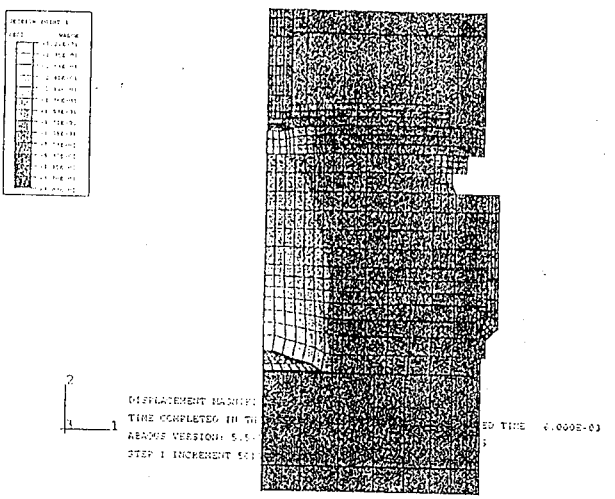

Figure 5-35

ICF KAISER HANFORD

DESIGN ANALYSIS

Calc. No.
Revision
Page No.

Client Westinghouse Hanford Company
WO/Job No. E50471/LE016/F7L7A1

Subject Results Dropped MCO Mass Loaded Full Diameter With Mass Loaded Bottom MCO
Date July 15, 1995 By Carleton J. Moore
Checked By Larry L. Hyde

Location 100K, K-Basins
Revised By

Equivatent Plastic Strain at 0.006 Second.

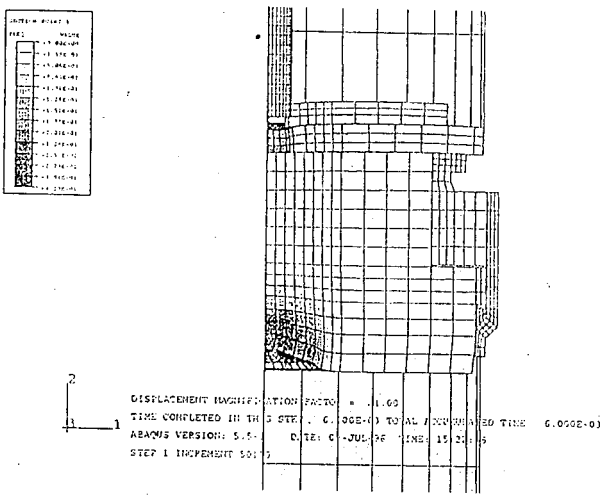

Figure 5-36

JCF KAISER HANFORD

DESIGN ANALYSIS

Calc. No.
Revision
Page No.

Client Westinghouse Hanford Company — WO/Job No. E50471/LE016/F7L7A1

Subject Results Dropped MCO Mass Loaded Full Diameter With Mass Loaded Bottom MCO — Date July 15, 1995 — By Carleton J. Moore

Location 100K, K-Basins — Checked — By Larry L. Hyde

Revised — By

Von Mises Stress Contour at 0.048 Second.

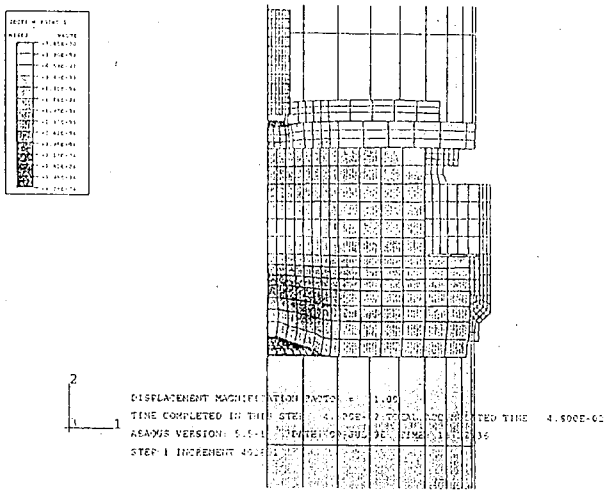

Figure 5-37

ICF KAISER HANFORD

DESIGN ANALYSIS

Calc. No.
Revision
Page No.

Client Westinghouse Hanford Company	WO/Job No. E50471/LE016/F7L7A1	
Subject Results Dropped MCO Mass Loaded Full Diameter With Mass Loaded Bottom MCO	Date July 15, 1995	By Carleton J. Moore
	Checked	By Larry L. Hyde
Location 100K, K-Basins	Revised	By

Vertical Stress Contour at 0.048 Second.

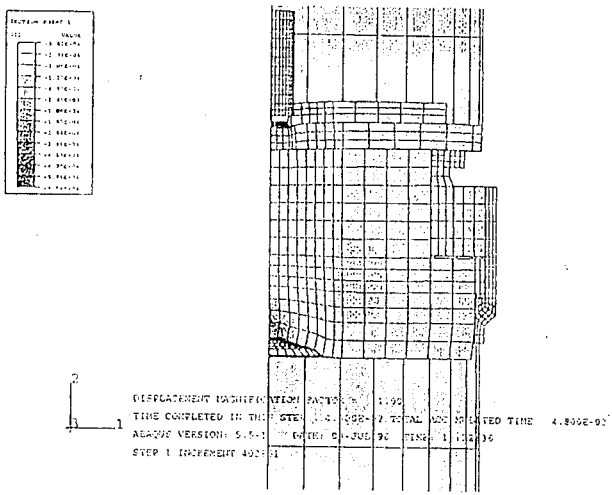

Figure 5-38

ICF KAISER HANFORD

DESIGN ANALYSIS

Calc. No.
Revision
Page No.

Client Westinghouse Hanford Company	WO/Job No. E50471/LE016/F7L7A1	
Subject Results Dropped MCO Mass Loaded Full Diameter With Mass Loaded Bottom MCO	Date July 15, 1995	By Carleton J. Moore
	Checked	By Larry L. Hyde
Location 100K, K-Basins	Revised	By

Radial Stress Contour at 0.048 Second.

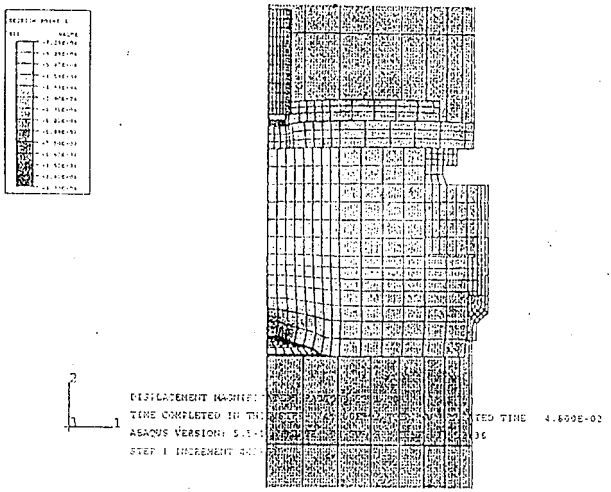

Figure 5-39

ICF KAISER HANFORD

DESIGN ANALYSIS

Calc. No.
Revision
Page No.

Client Westinghouse Hanford Company	WO/Job No. E50471/LE016/F7L7A1		
Subject Results Dropped MCO Mass Loaded Full Diameter With Mass Loaded Bottom MCO	Date July 15, 1995	By	Carleton J. Moore
	Checked	By	Larry L. Hyde
Location 100K, K-Basins	Revised	By	

Shear Stress Contour at 0.048 Second.

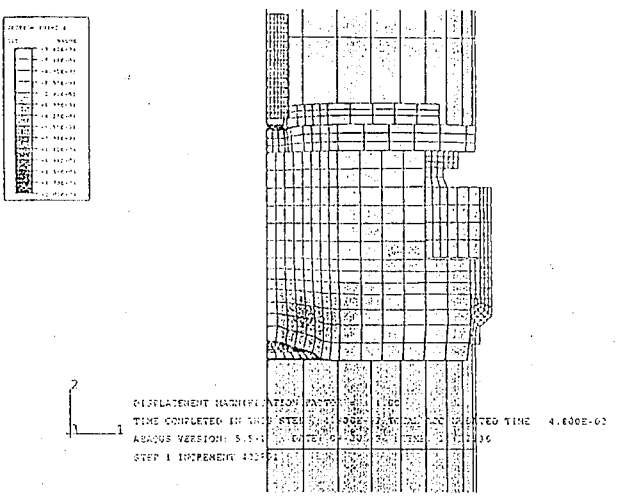

Figure 5-40

ICF KAISER HANFORD

DESIGN ANALYSIS

Calc. No.
Revision
Page No.

Client Westinghouse Hanford Company	WO/Job No. E50471/LE016/F7L7A1		
Subject Results Dropped MCO Mass Loaded Full Diameter With Mass Loaded Bottom MCO	Date July 15, 1995	By	Carleton J. Moore
	Checked	By	Larry L. Hyde
Location 100K, K-Basins	Revised	By	

Circumferential Stress Contour at 0.0-18 Second.

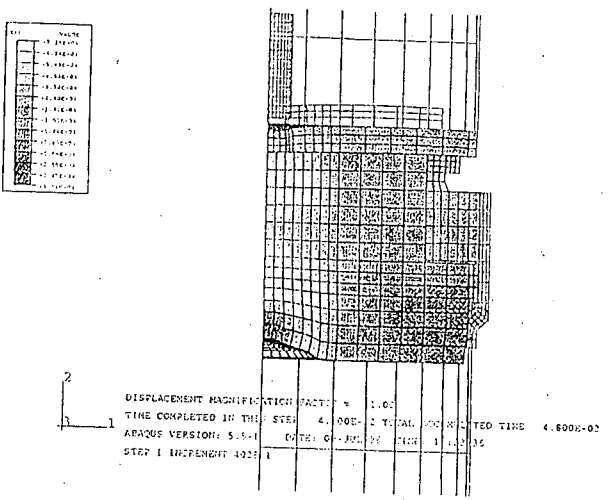

Figure 5-41

ICF KAISER HANFORD

DESIGN ANALYSIS

Calc. No.
Revision
Page No.

Client Westinghouse Hanford Company	WO Job No. E50171/LE016/F7L7A1	
Subject Results Dropped MCO Mass Loaded Full Diameter With Mass Loaded Bottom MCO	Date July 15, 1995	By Carleton J. Moore
	Checked	By Larry L. Hyde
Location 100K, K-Basins	Revised	By

Vertical Plastic Strain at 0.0138 Second.

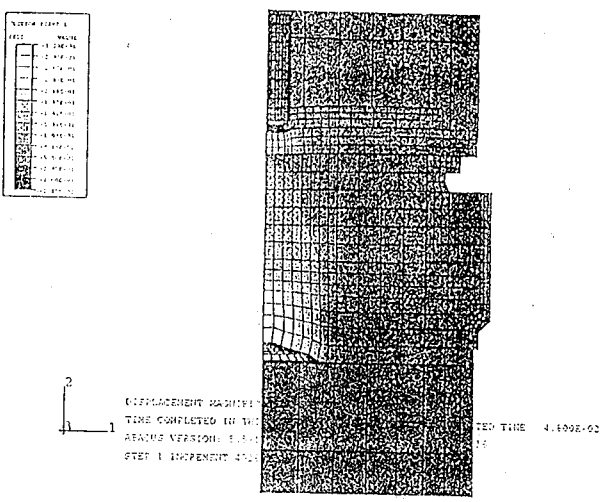

Figure 5-42

ICF KAISER HANFORD

DESIGN ANALYSIS

Calc. No.
Revision
Page No.

Client Westinghouse Hanford Company	WO/Job No. E50471/LE016/F7L7A1		
Subject Results Dropped MCO Mass Loaded Full Diameter With Mass Loaded Bottom MCO	Date July 15, 1995	By	Carleton J. Moore
	Checked	By	Larry L. Hyde
Location 100K, K-Basins	Revised	By	

Equivatent Plastic Strain at 0.048 Second.

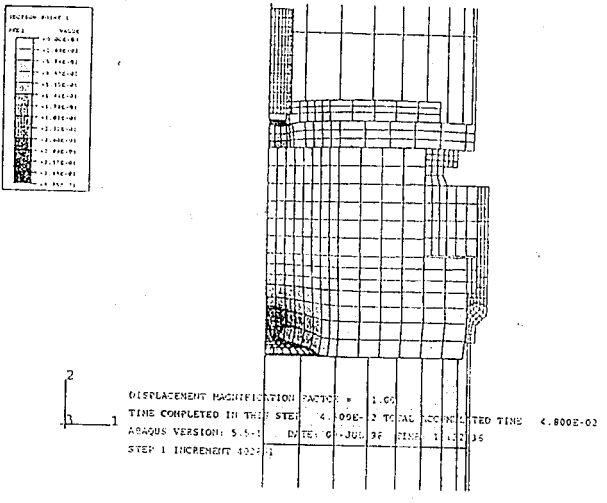

Figure 5-43

ICF KAISER HANFORD

DESIGN ANALYSIS

Calc. No.
Revision
Page No.

Client Westinghouse Hanford Company	WO/Job No. E50471/LE016/F7L7A1		
Subject Results Dropped MCO Mass Loaded Full Diameter With Mass Loaded Bottom MCO	Date July 15, 1996	By	Carleton J. Moore
	Checked	By	Larry L. Hyde
Location 100K, K-Basins	Revised	By	

Dropped MCO Bottom Contact Pressure at 0.003 Second.

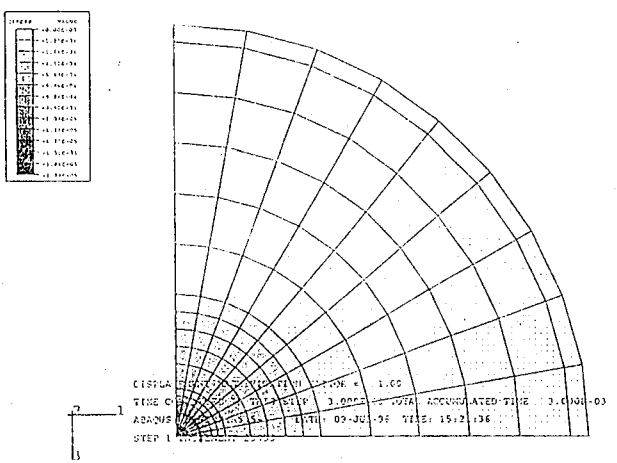

Figure 5-44

ICF KAISER HANFORD

DESIGN ANALYSIS

Calc. No.
Revision
Page No.

Client Westinghouse Hanford Company | WO/Job No. E50471/LE016/F7L7A1

Subject Results Dropped MCO Mass Loaded Full Diameter With Mass Loaded Bottom MCO | Date July 15, 1995 By Carleton J. Moore | Checked By Larry L. Hyde

Location 100K, K-Basins | Revised By

Dropped MCO Bottom Contact Pressure at 0.009 Second.

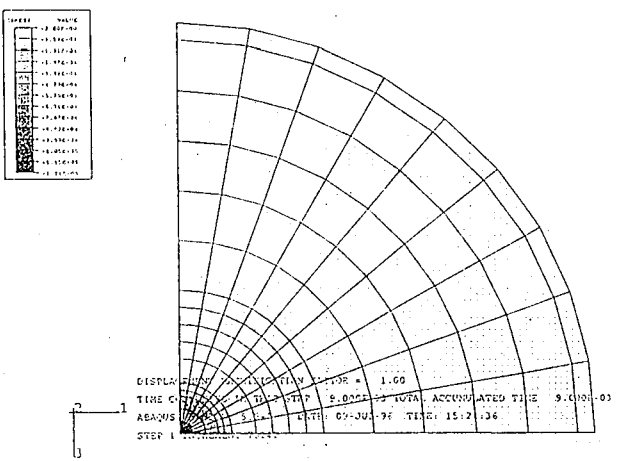

Figure 5-45

ICF KAISER HANFORD

DESIGN ANALYSIS

Calc. No.
Revision
Page No.

Client Westinghouse Hanford Company	WO/Job No. E50471/LE016/F7L7A1		
Subject Results Dropped MCO Mass Loaded Full Diameter With Mass Loaded Bottom MCO	Date July 15, 1995	By	Carleton J. Moore
	Checked	By	Larry L. Hyde
Location 100K, K-Basins	Revised	By	

Dropped MCO Bottom Contact Pressure at 0.015 Second.

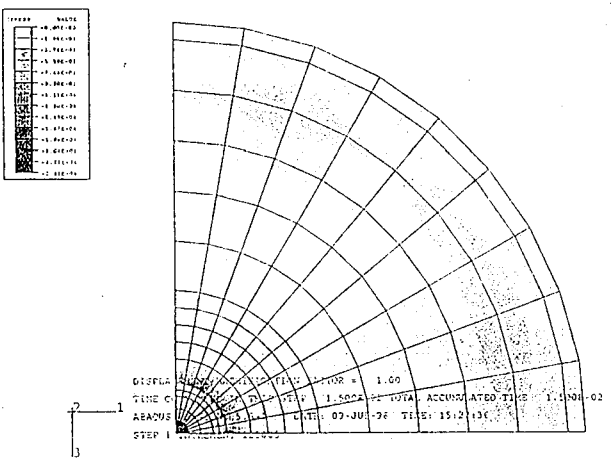

Figure 5-46

68

ICF KAISER HANFORD

DESIGN ANALYSIS

Calc. No.
Revision
Page No.

Client Westinghouse Hanford Company	WO/Job No. ES0471/LE016/F7L7A1		
Subject Results Dropped MCO Mass Loaded Full Diameter With Mass Loaded Bottom MCO	Date July 15, 1995	By	Carleton J. Moore
	Checked	By	Larry L. Hyde
Location 100K, K-Basins	Revised	By	

Dropped MCO Bottom Contact Pressure at 0.018 Second.

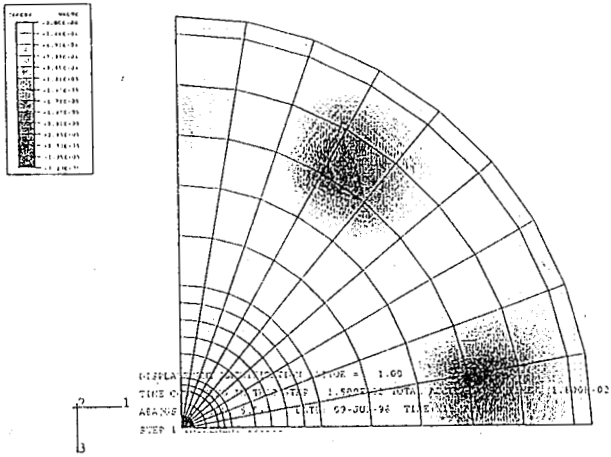

Figure 5-47

ICF KAISER HANFORD

DESIGN ANALYSIS

Calc. No.
Revision
Page No.

Client Westinghouse Hanford Company	WO/Job No. E50471/LE016/F7L7A1	
Subject Results Dropped MCO Mass Loaded Full Diameter With Mass Loaded Bottom MCO	Date July 15, 1995	By Carleton J. Moore
	Checked	By Larry L. Hyde
Location 100K, K-Basins	Revised	By

Dropped MCO Bottom Contact Pressure at 0.02 Second

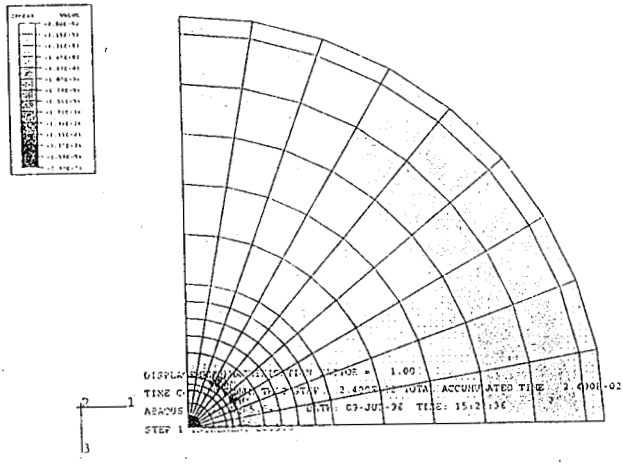

Figure 5-48

ICF KAISER HANFORD

DESIGN ANALYSIS

Calc. No.
Revision
Page No.

Client Westinghouse Hanford Company	WO/Job No. ES0171/LE016/F7L7A1		
Subject Results Dropped MCO Mass Loaded Full Diameter With Mass Loaded Bottom MCO	Date July 15, 1995	By	Carleton J. Moore
	Checked	By	Larry L. Hyde
Location 100K, K-Basins	Revised	By	

Dropped MCO Bottom Contact Pressure at 0.033 Second.

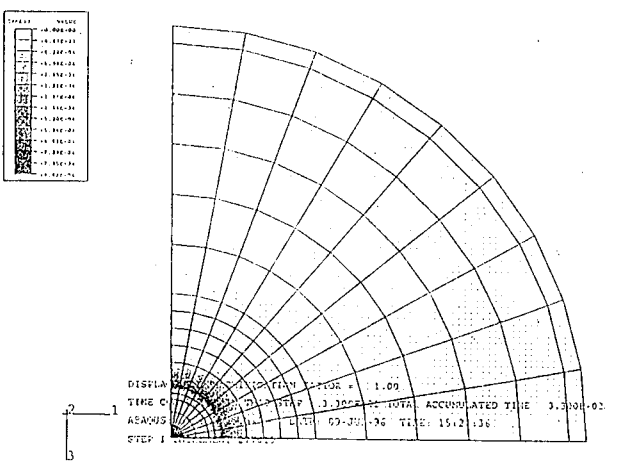

Figure 5-49

ICF KAISER HANFORD

DESIGN ANALYSIS

Calc. No.
Revision
Page No.

Client Westinghouse Hanford Company	WO/Job No. E50471/LE016/F7L7A1	
Subject Results Dropped MCO Mass Loaded Full Diameter With Mass Loaded Bottom MCO	Date July 15, 1995	By Carleton J. Moore
	Checked	By Larry L. Hyde
Location 100K, K-Basins	Revised	By

Dropped MCO Bottom Contact Pressure at 0.048 Second.

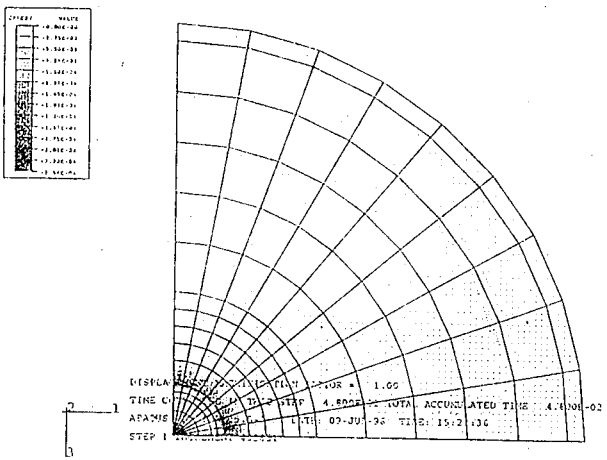

Figure 5-50

72

ICF KAISER HANFORD

DESIGN ANALYSIS

Calc. No.
Revision
Page No.

Client Westinghouse Hanford Company	WO/Job No. E50471/LE016/F7L7A1		
Subject Results, Dropped MCO Mass Load in Center Region with Empty Bottom MCO	Date July 24, 1996	By	Carleton J. Moore
	Checked	By	Larry L. Hyde
Location 100K, K-Basins	Revised	By	

5.3 Dropped MCO Mass Loaded in Center Region with Empty Bottom MCO

The basket and fuel mass in the dropped MCO is simulated with lump masses connected at the bottom in the center region corresponding to the inertia load path being transmitted through the basket column. The basket and fuel mass in the bottom MCO is not simulated (empty MCO). This analysis case models the impact before the basket and fuel mass in the impacted MCO contacts the inside bottom of the shield plug.

Figure 5-51 shows the displacement (inch) versus time (second) of the bottom of the dropped MCO, the impacted shield plug, and the impact limiter. In Figure 5-51 the maximum deflection of can be seen to be at 0.045 second. Figure 5-52 shows the velocity (in/sec) versus time (second) of the bottom of the dropped MCO, the impacted shield plug, and the impact limiter. Figure 5-53 shows the graphical calculation of deceleration g level. In Figure 5-53, after the initial contact the MCO's and top of the impact limiter can be seen to decelerate at approximately 28.6 g. Figure 5-54 shows additional acceleration dynamics superimposed on the calculated average deceleration.

Figure 5-55 shows the deflected shape of the MCO to MCO contact at 0.048 second. In Figure 5-55 the center region of the bottom of the dropped MCO can be seen to not be as significantly deformed as was for the case studied in Section 5.1, Figure 5-9. Also, in Figure 5-55 the bottom of the shield plug remains undeformed.

Figure 5-56 shows a von Mises stress contour at 0.006 second. Figure 5-57 shows the vertical stress contour at 0.006 second. The maximum tension stress is at the center bottom of the impacted shield plug. Figure 5-58 shows the radial stress contour for the solid elements at 0.006 second. Figure 5-59 gives the shear stress in the plane of the figure. Figure 5-60 shows the circumferential stress for the solid elements at 0.006 second.

ICF KAISER HANFORD

DESIGN ANALYSIS

Calc. No.
Revision
Page No.

Client Westinghouse Hanford Company	WO/Job No. E50471/LE016/F7L7A1		
Subject Results, Dropped MCO Mass Load in Center Region with Empty Bottom MCO	Date July 24, 1996	By	Carleton J. Moore
	Checked	By	Larry L. Hyde
Location 100K, K-Basins	Revised	By	

Figure 5-61 shows the vertical plastic strain at 0.006 second. Figure 5-62 gives the equivalent plastic strain at 0.006 second.

Figure 5-63 shows the von Mises stress contour at 0.045 second. Figure 5-64 shows the vertical stress contour at 0.045 second. Figure 5-65 shows the radial stress of the solid elements at 0.045 second. Figure 5-66 shows the shear stress in the plane of the figure. Figure 5-67 shows the circumferential stress of the solid elements.

The stresses in Figures 5-56 through 5-67 show low stresses at the lifting ring and MCO cylinder positions.

Figure 5-68 shows the vertical plastic strain at 0.045 second. Figure 5-69 shows the equivalent plastic strain at 0.045 second.

Figure 5-70 shows a shaded contour plot of the contact pressure across the bottom of the dropped MCO at 0.006 second. Figure 5-71 shows the contact pressure contour at 0.027 second. Figure 5-72 shows the contact pressure contour at 0.036 second. Figure 5-73 shows the contact pressure contour at 0.039 second. Figure 5-74 shows the contact pressure contour at 0.042 second. Figure 5-75 shows the contact pressure contour at 0.045 second.

Figures 5-70 through 5-75 were selected to provide the maximum contact pressures. The dynamics of the impact event are such that the contact pressures between these maximums can be significantly less. In fact during the initial impact the bottom of the dropped MCO is bouncing against the top of the static MCO (pressure can and do go to zero during this bouncing). Also the maximum contact pressures can be seen to be high compared to the normal static capability of the materials. Again the dynamics are such that both inertia forces and elastic forces balance the contact pressures. But plastic deformation of the impacted shield plug can only be relieved by inserting a shock absorber between the two MCO's.

ICF KAISER HANFORD

DESIGN ANALYSIS

Calc. No.
Revision
Page No.

Client Westinghouse Hanford Company	WO/Job No. E50471/LE016/F7L7A1	
Subject Results, Dropped MCO Mass Load in Center Region with Empty Bottom MCO	Date July 24, 1996	By Carleton J. Moore
	Checked	By Larry L. Hyde
Location 100K, K-Basins	Revised	By

Displacement Versus Time of the Bottom Of Dropped MCO, the Impacted Shield Plug, and the Impact Limiter.

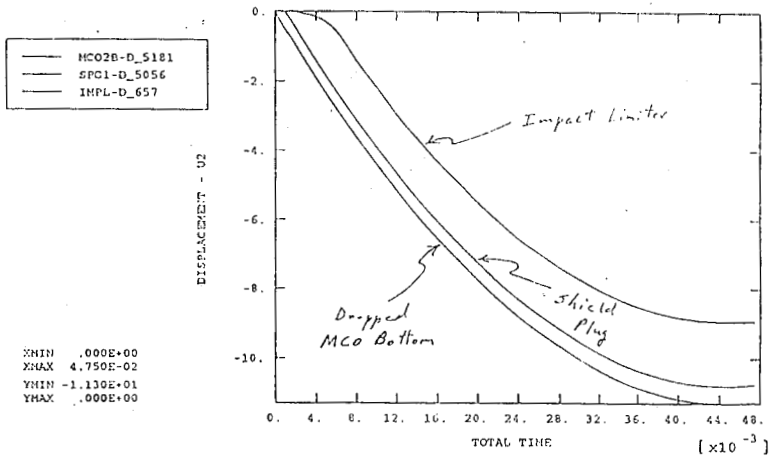

Figure 5-51

ICF KAISER HANFORD

DESIGN ANALYSIS

Calc. No.
Revision
Page No.

Client Westinghouse Hanford Company	WO/Job No. E50471/LE016/F7L7A1	
Subject Results, Dropped MCO Mass Load in Center Region with Empty Bottom MCO	Date July 24, 1996	By Carleton J. Moore
	Checked	By Larry L. Hyde
Location 100K, K-Basins	Revised	By

Velocity Versus Time of the Bottom Of Dropped MCO, the Impacted Shield Plug, and the Impact Limiter.

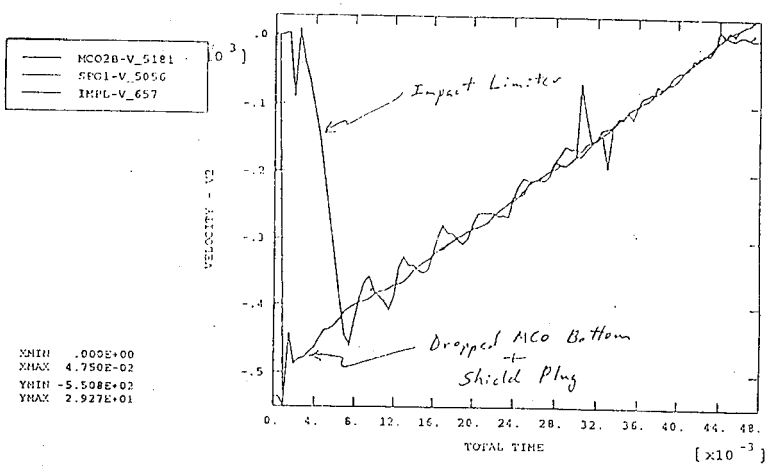

Figure 5-52

ICF KAISER HANFORD

DESIGN ANALYSIS

Calc. No.
Revision
Page No.

Client Westinghouse Hanford Company	WO/Job No. E50471/LE016/F7L7A1		
Subject Results, Dropped MCO Mass Load in Center Region with Empty Bottom MCO	Date July 24, 1996	By	Carleton J. Moore
	Checked	By	Larry L. Hyde
Location 100K, K-Basins	Revised	By	

Graphical Calculation of Average Deceleration.

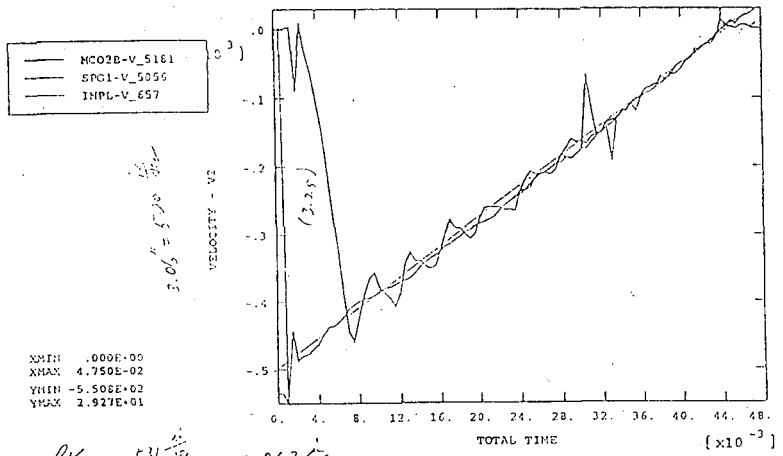

$\frac{dv}{dt} = \frac{531 \frac{in}{sec}}{.048 sec} = 11,063 \frac{in}{sec^2}$

$1.35'' = .046 cm$

$\Rightarrow 28.6\ g$

Figure 5-53

ICF KAISER HANFORD

DESIGN ANALYSIS

Calc. No.
Revision
Page No.

Client Westinghouse Hanford Company	WO/Job No. E50471/LE016/F7L7A1	
Subject Results, Dropped MCO Mass Load in Center Region with Empty Bottom MCO	Date July 24, 1996	By Carleton J. Moore
	Checked	By Larry L. Hyde
Location 100K, K-Basins	Revised	By

Combined Acceleration Dynamics

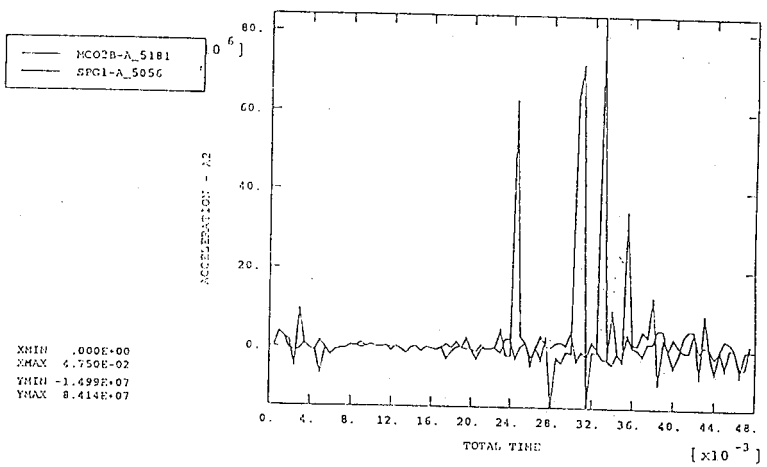

Figure 5-54

ICF KAISER HANFORD

DESIGN ANALYSIS

Calc. No.
Revision
Page No.

Client Westinghouse Hanford Company	WO/Job No. E50471/LE016/F7L7A1	
Subject Results, Dropped MCO Mass Load in Center Region with Empty Bottom MCO	Date July 24, 1996	By Carleton J. Moore
	Checked	By Larry L. Hyde
Location 100K, K-Basins	Revised	By

Deflected Shape at 0.045 Second.

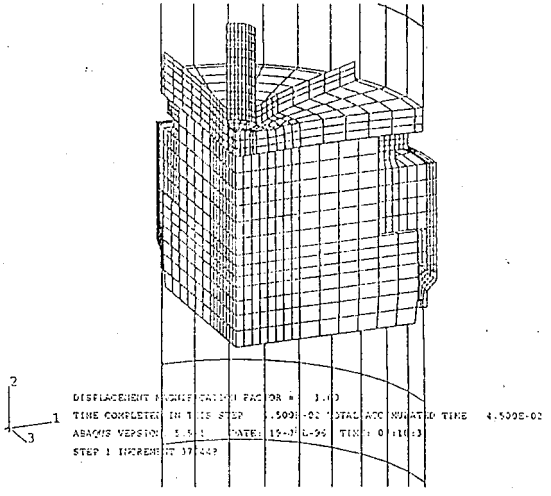

Figure 5-55

ICF KAISER HANFORD

DESIGN ANALYSIS

Calc. No.
Revision
Page No.

Client Westinghouse Hanford Company	WO/Job No. E5047I/LE016/F7L7A1	
Subject Results, Dropped MCO Mass Load in Center Region with Empty Bottom MCO	Date July 24, 1996	By Carleton J. Moore
	Checked	By Larry L. Hyde
Location 100K, K-Basins	Revised	By

Von Mises Stress Contour at 0.006 Second.

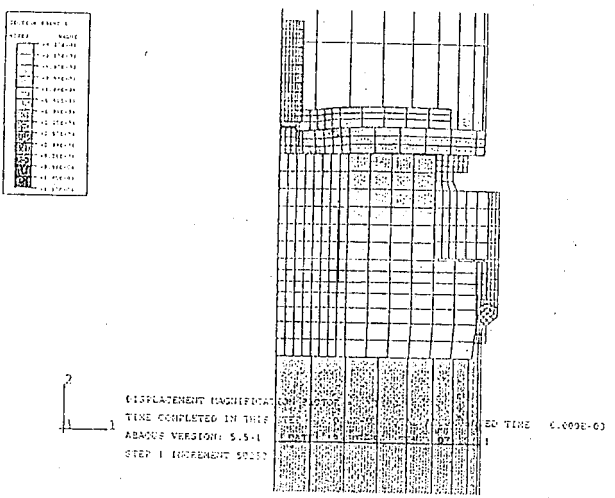

Figure 5-56

ICF KAISER HANFORD

DESIGN ANALYSIS

Calc. No.
Revision
Page No.

Client Westinghouse Hanford Company	WO/Job No. E5047I/LE016/F7L7A1	
Subject Results, Dropped MCO Mass Load in Center Region with Empty Bottom MCO	Date July 24, 1996	By Carleton J. Moore
	Checked	By Larry L. Hyde
Location 100K, K-Basins	Revised	By

Vertical Stress Contour at 0.006 Second.

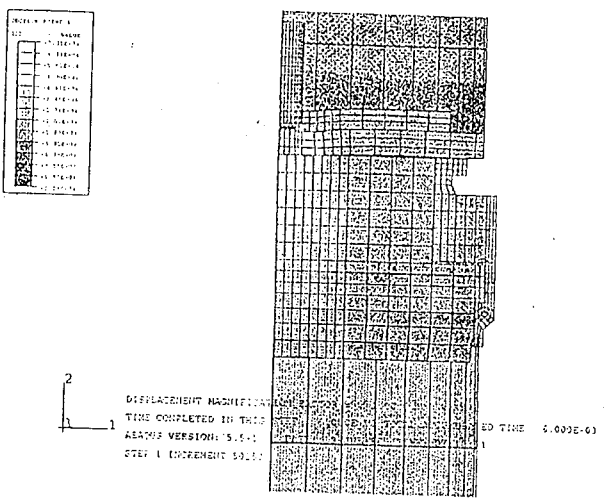

Figure 5-57

ICF KAISER HANFORD

DESIGN ANALYSIS

Calc. No.
Revision
Page No.

Client Westinghouse Hanford Company	WO Job No. E50471/LE016/F7L7A1		
Subject Results, Dropped MCO Mass Load in Center Region with Empty Bottom MCO	Date July 24, 1996	By	Carleton J. Moore
	Checked	By	Larry L. Hyde
Location 100K, K-Basins	Revised	By	

Radial Stress Contour at 0.006 Second

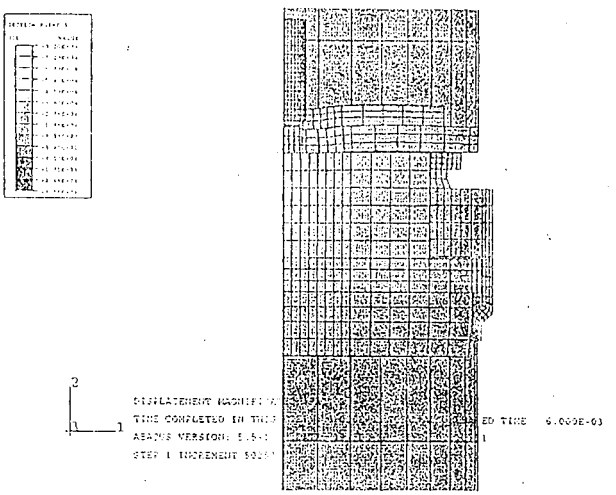

Figure 5-58

ICF KAISER HANFORD

DESIGN ANALYSIS

Calc. No.
Revision
Page No.

Client Westinghouse Hanford Company	WO Job No. E50471/LE016/F7L7A1	
Subject Results, Dropped MCO Mass Load in Center Region with Empty Bottom MCO	Date July 24, 1996	By Carleton J. Moore
	Checked	By Larry L. Hyde
Location 100K, K-Basins	Revised	By

Shear Stress Contour at 0.006 Second.

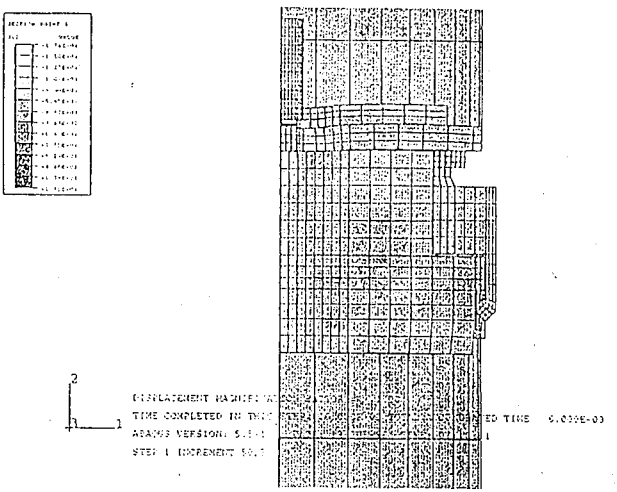

Figure 5-59

ICF KAISER HANFORD

DESIGN ANALYSIS

Calc. No.
Revision
Page No.

Client Westinghouse Hanford Company	WO/Job No. E50471/LE016/F7L7A1		
Subject Results, Dropped MCO Mass Load in Center Region with Empty Bottom MCO	Date July 24, 1996	By	Carleton J. Moore
	Checked	By	Larry L. Hyde
Location 100K, K-Basins	Revised	By	

Circumferential Stress Contour at 0.006 Second.

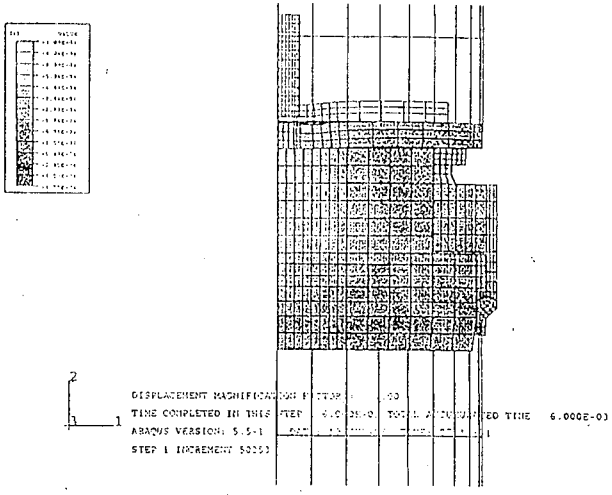

Figure 5-60

ICF KAISER HANFORD

DESIGN ANALYSIS

Calc. No.
Revision
Page No.

Client Westinghouse Hanford Company	WO Tsk No. ES0471/LE016/F7L7A1		
Subject Results, Dropped MCO Mass Load in Center Region with Empty Bottom MCO	Date Jul. 23, 1996	By	Carleton J. Moore
	Checked	By	Larry L. Hyde
Location 100K K-Basins	Revised	By	

Vertical Plastic Strain at 0.006 Second

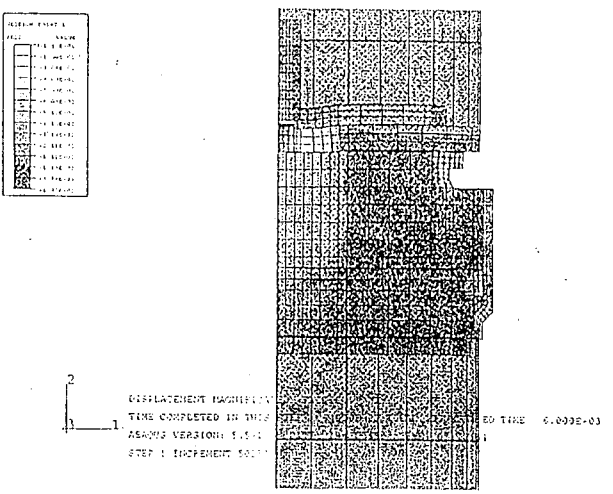

Figure 5-61

ICF KAISER HANFORD

DESIGN ANALYSIS

Calc. No.
Revision
Page No.

Client Westinghouse Hanford Company	WO/Job No. E504171/L6016/F7L7A1		
Subject Results, Dropped MCO Mass Load in Center Region with Empty Bottom MCO	Date July 24, 1996	By	Carleton J. Moore
	Checked	By	Larry L. Hyde
Location 100K, K-Basins	Revised	By	

Equivalent Plastic Strain at 0.006 Second.

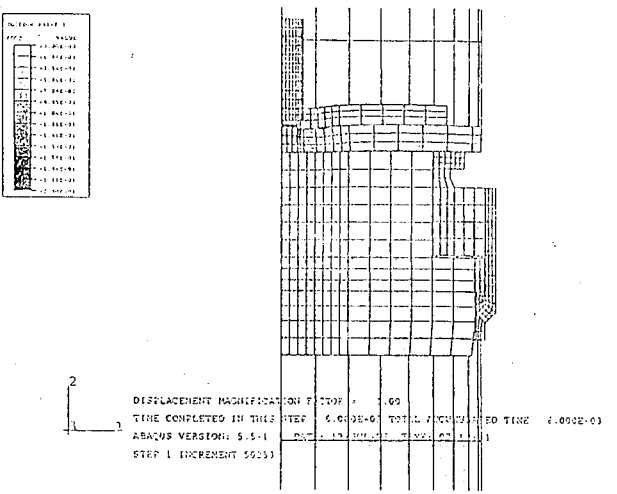

Figure 5-62

ICF KAISER HANFORD

DESIGN ANALYSIS

Calc. No.
Revision
Page No.

Client Westinghouse Hanford Company	WO/Job No. E50471/LE016/F7L7A1	
Subject Results, Dropped MCO Mass Load in Center Region with Empty Bottom MCO	Date July 24, 1996	By Carleton J. Moore
	Checked	By Larry L. Hyde
Location 100K, K-Basins	Revised	By

Von Mises Stress Contour at 0.045 Second.

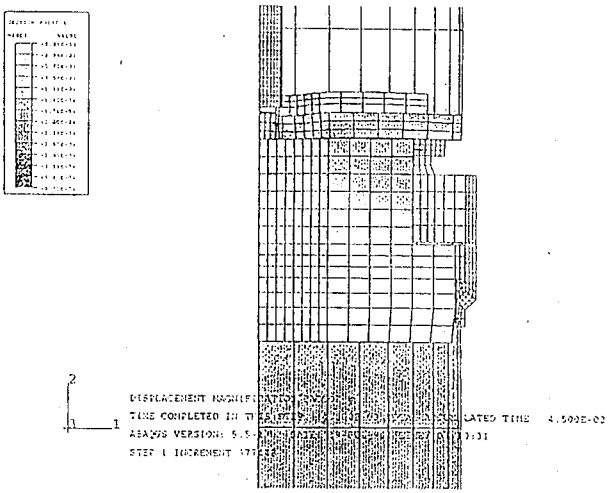

Figure 5-63

ICF KAISER HANFORD

DESIGN ANALYSIS

Calc. No.
Revision
Page No.

Client Westinghouse Hanford Company	WO/Job No. E50471/LE016/F7L7A1	
Subject Results, Dropped MCO Mass Load in Center Region with Empty Bottom MCO	Date July 24, 1996	By Carleton J. Moore
	Checked	By Larry L. Hyrle
Location 100K, K-Basins	Revised	By

Vertical Stress Contour at 0.045 Second.

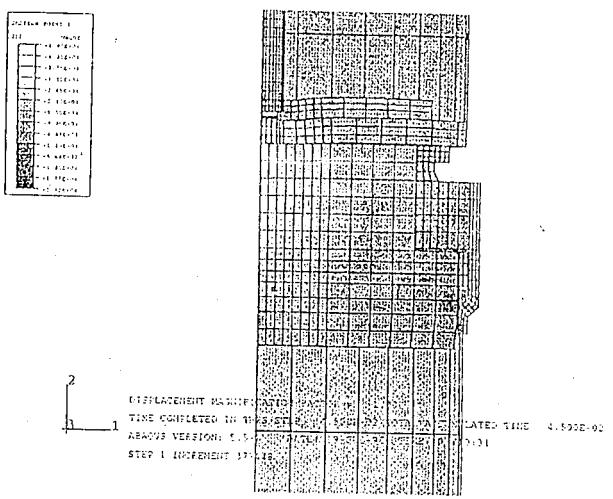

Figure 5-64

ICF KAISER HANFORD

DESIGN ANALYSIS

Calc. No.
Revision
Page No.

Client Westinghouse Hanford Company	WO/Job No. E50471/LE016/F7L7A1	
Subject Results, Dropped MCO Mass Load in Center Region with Empty Bottom MCO	Date July 24, 1996	By Carleton J. Moore
	Checked	By Larry L. Hyde
Location 100K, K-Basins	Revised	By

Radial Stress Contour at 0.045 Second.

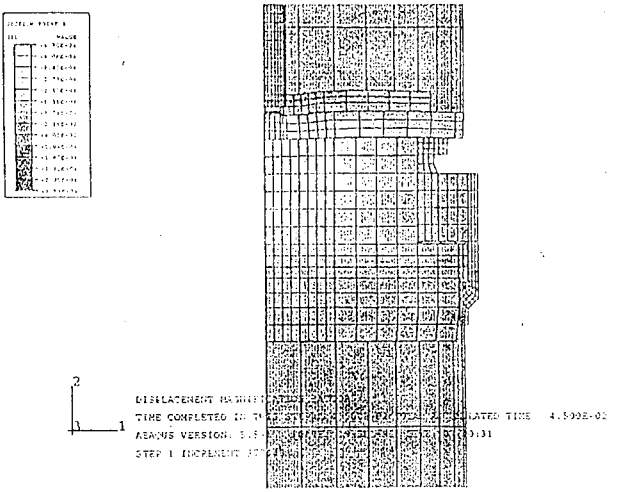

Figure 5-65

ICF KAISER HANFORD

DESIGN ANALYSIS

Calc. No.
Revision
Page No.

Client Westinghouse Hanford Company	W.O./Job No. E50471/LE016/F7L7A1	
Subject Results, Dropped MCO Mass Load in Center Region with Empty Bottom MCO	Date July 24, 1996	By Carleton J. Moore
	Checked	By Larry L. Hyde
Location 100K, K-Basins	Revised	By

Shear Stress Contour at 0.015 Second.

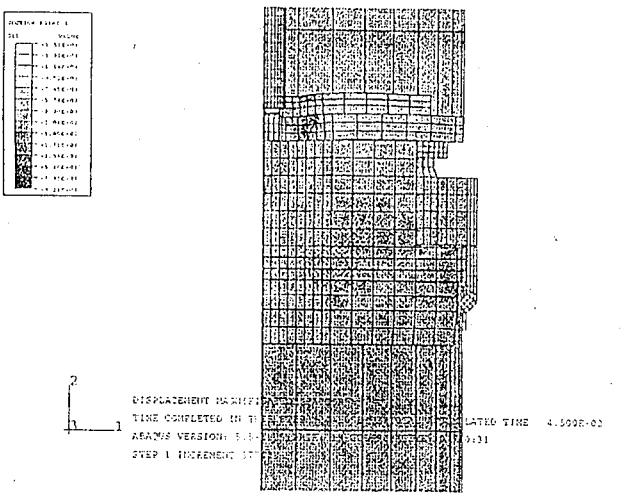

Figure 5-66

ICF KAISER HANFORD

DESIGN ANALYSIS

Calc. No.
Revision
Page No.

Client Westinghouse Hanford Company	WO/Job No. E50471/LE016/F7L7A1	
Subject Results, Dropped MCO Mass Load in Center Region with Empty Bottom MCO	Date July 24, 1996	By Carleton J. Moore
	Checked	By Larry L. Hyde
Location 100K, K-Basins	Revised	By

Circumferential Stress Contour at 0.045 Second.

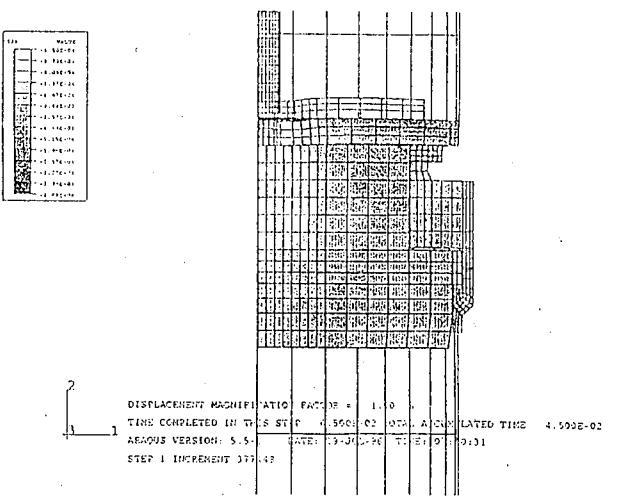

Figure 5-67

ICF KAISER HANFORD

DESIGN ANALYSIS

Calc. No.
Revision
Page No.

Client Westinghouse Hanford Company	WO/Job No. E5047I/LE016/F7L7A1		
Subject Results, Dropped MCO Mass Load in Center Region with Empty Bottom MCO	Date July 24, 1996	By	Carleton J. Moore
	Checked	By	Larry L. Hyde
Location 100K, K-Basins	Revised	By	

Vertical Plastic Strain Contour at 0.045 Second.

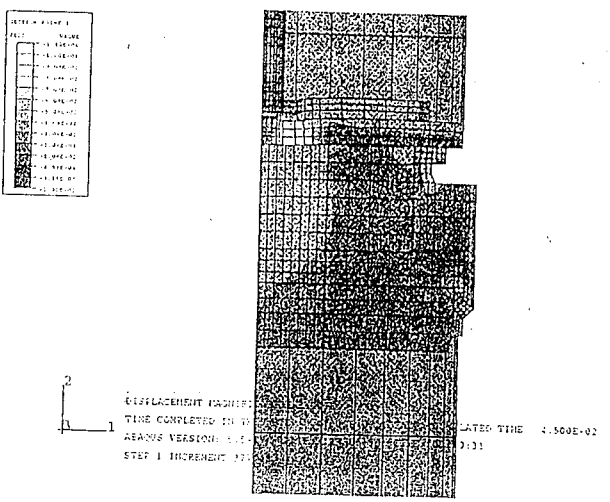

Figure 5-68

ICF KAISER HANFORD

DESIGN ANALYSIS

Calc. No.
Revision
Page No.

Client Westinghouse Hanford Company	WO/Job No. E50471/LE016/F7L7A1	
Subject Results, Dropped MCO Mass Load in Center Region with Empty Bottom MCO	Date July 24, 1996	By Carleton J. Moore
	Checked	By Larry L. Hyde
Location 100K, K-Basins	Revised	By

Equivalent Plastic Strain Contour at 0.045 Second.

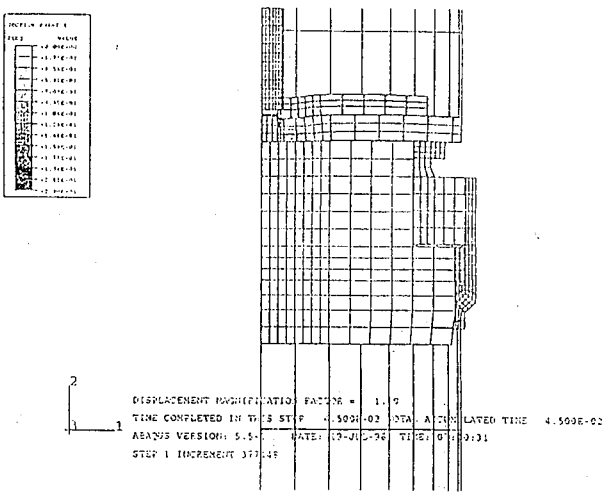

Figure 5-69

ICF KAISER HANFORD

DESIGN ANALYSIS

Calc. No.
Revision
Page No.

Client Westinghouse Hanford Company	WO/Job No. E50471/LE016/F7L7A1		
Subject Results, Dropped MCO Mass Load in Center Region with Empty Bottom MCO	Date July 24, 1996	By	Carleton J. Moore
	Checked	By	Larry L. Hyde
Location 100K, K-Basins	Revised	By	

Dropped MCO Bottom Contact Pressure at 0.006 Second.

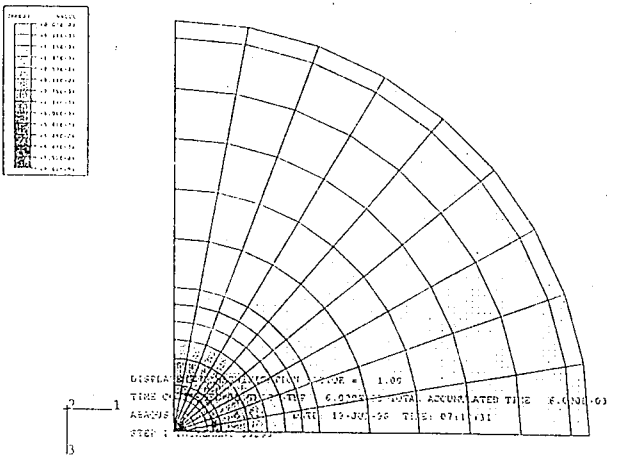

Figure 5-70

ICF KAISER HANFORD

DESIGN ANALYSIS

Calc. No.
Revision
Page No.

Client Westinghouse Hanford Company	WO/Job No. E50471/LE016/F7L7A1	
Subject Results, Dropped MCO Mass Load in Center Region with Empty Bottom MCO	Date July 24, 1996	By Carleton J. Moore
	Checked	By Larry L. Hyde
Location 100K, K-Basins	Revised	By

Dropped MCO Bottom Contact Pressure at 0.027 Second.

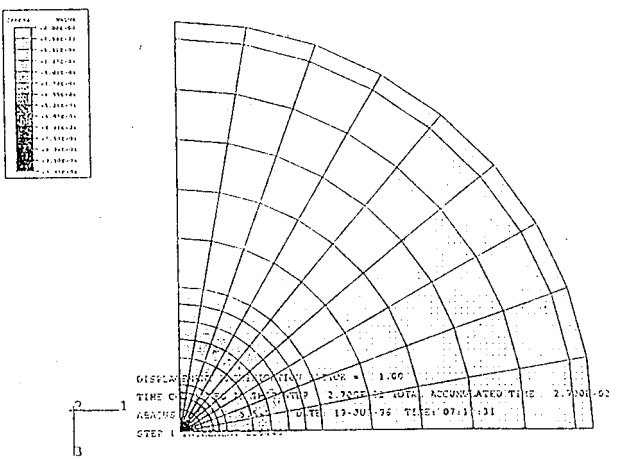

Figure 5-71

ICF KAISER HANFORD

DESIGN ANALYSIS

Calc. No.
Revision
Page No.

Client Westinghouse Hanford Company	WO/Job No. E50471/LE016/F7L7A1		
Subject Results, Dropped MCO Mass Load in Center Region with Empty Bottom MCO	Date July 24, 1996	By	Carleton J. Moore
	Checked	By	Larry L. Hyde
Location 100K, K-Basins	Revised	By	

Dropped MCO Bottom Contact Pressure at 0.036 Second.

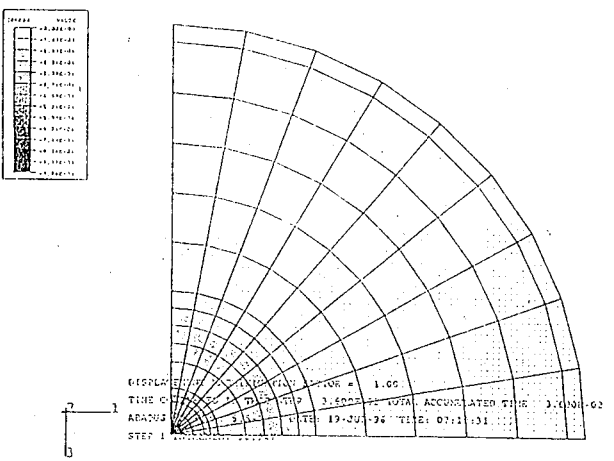

Figure 5-72

ICF KAISER HANFORD

DESIGN ANALYSIS

Calc. No.
Revision
Page No.

Client Westinghouse Hanford Company — WO/Job No. E50171/LE016/F7L7A1

Subject Results, Dropped MCO Mass Load in Center Region with Empty Bottom MCO — Date July 24, 1996 — By Carleton J. Moore

Checked — By Larry L. Hyde

Location 100K, K-Basins — Revised — By

Dropped MCO Bottom Contact Pressure at 0.039 Second.

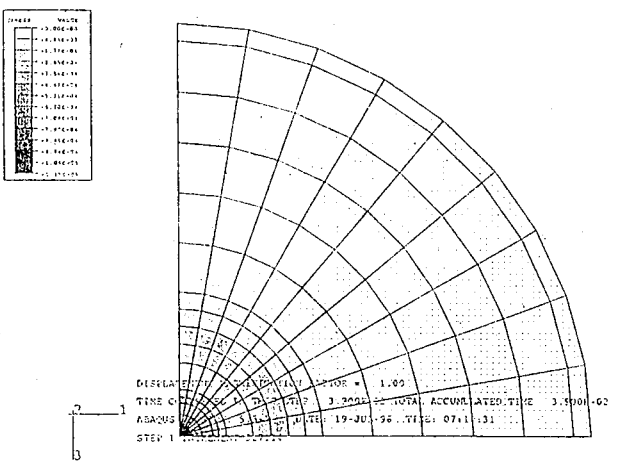

Figure 5-73

ICF KAISER HANFORD

DESIGN ANALYSIS

Calc. No.
Revision
Page No.

Client Westinghouse Hanford Company	WO/Job No. E50471/LE016/F7L7A1	
Subject Results, Dropped MCO Mass Load in Center Region with Empty Bottom MCO	Date July 24, 1996	By Carleton J. Moore
	Checked	By Larry L. Hyde
Location 100K, K-Basins	Revised	By

Dropped MCO Bottom Contact Pressure at 0.042 Second.

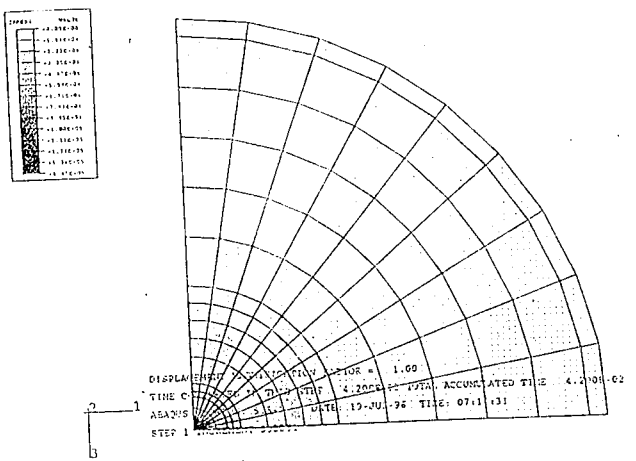

Figure 5-74

ICF KAISER HANFORD

DESIGN ANALYSIS

Calc. No.
Revision
Page No.

Client Westinghouse Hanford Company	WO/Job No. E50471/LE016/F7L7A1		
Subject Results, Dropped MCO Mass Load in Center Region with Empty Bottom MCO	Date July 24, 1996	By	Carleton J. Moore
	Checked	By	Larry L. Hyde
Location 100K, K-Basins	Revised	By	

Dropped MCO Bottom Contact Pressure at 0.045 Second.

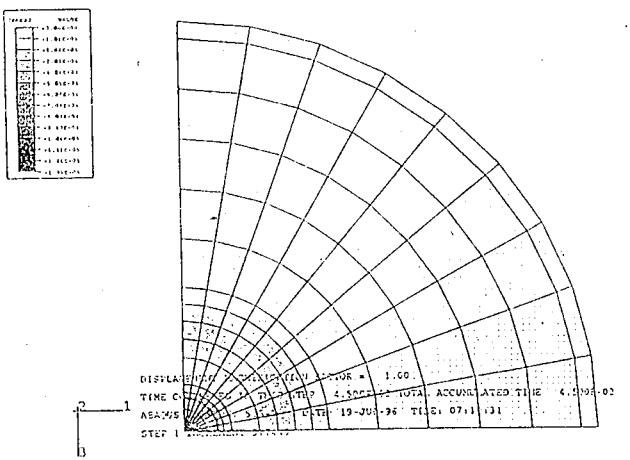

Figure 5-75

ICF KAISER HANFORD

DESIGN ANALYSIS

Calc. No.
Revision
Page No.

Client Westinghouse Hanford Company	WO/Job No. E50471/LE016/F7L7A1	
Subject Evaluation of the Lifting Ring MCO to MCO Impact Thread Stresses	Date August 5, 1996	By Carleton J. Moore
	Checked	By Larry L. Hyde
Location 100K, K-Basins	Revised	By

6.0 Evaluation of the Mechanical Closure Lifting Ring Thread Stresses

The MCO to MCO 31 foot impact analyses do not model the thread between the lifting ring and the MCO cylinder wall. But the threads can be checked by employing the stresses between the lifting ring and the MCO cylinder wall with an appropriate stress intensity factor.

The appropriate stress intensity factor can be obtained from R. E. Peterson's book " Stress Concentration Design Factors", published by John Wiley & Sons, Inc., New York, 1953. The threaded lifting ring can be considered to be a large bolt with the threaded MCO cylinder wall a large nut. A conservative stress intensity factor can be selected from the bolt and nut three-dimensional photoelastic test results.

With regard to failure in the threads at the nut face, various bolt and nut combinations were investigated by means of three-dimensional photoelastic tests. For standard bolts and nuts a stress intensity factor of 3.85 was obtained.

The vertical stresses corresponding to bolt and nut axial load forces were reviewed at the tread locations for the three documented impact cases of Sections 5.1, 5.2, and 5.3. The review required the zooming into the proper region and then resetting the stress legend scale to provide detail in the thread region.

The load case from Section 5.2 had the largest vertical stresses at the position of thread interface between the lifting ring and the MCO cylinder. The average compressive stress was under 4,000 lbf/in^2. The maximum impulsive compressive stress was under 12,000 lbf/in^2. Even with application of the stress intensity factor of 3.85 the material does not fail.

The shear stresses at the thread interface between the lifting ring and the MCO cylinder were found to be a maximum of 3,000 psi. Even if a intensity factor of 4 is applied for the thread detail the material will not fail.

ICF KAISER HANFORD

DESIGN ANALYSIS

Calc. No.
Revision
Page No.

Client Westinghouse Hanford Company	WO/Job No. E50471/LE016/F7L7A1		
Subject Evaluation of Shield Plug Seal Ledge Shoulder	Date August 8, 1996	By	Carleton J. Moore
	Checked	By	Larry L. Hyde
Location 100K, K-Basins	Revised	By	

7.0 Evaluation of the Shield Plug Seal Ledge Shoulder

The bottom of the shield plug has a quarter inch square shoulder around the circumference at the seal location. The plastic deformation of this shoulder was evaluated for the three documented impact cases of Sections 5.1, 5.2, and 5.3. The review required zooming into the proper region and resetting the strain legend scale to provide detail in the shoulder region. Also the deflections at each set were monitored for the nodes defining the shoulder.

The maximum compression on the shoulder was 0.030 inch for the impact case documented in Section 5.3. The maximum compression of the analysis of Section 5.3 corresponds to a strain level that varies from 10 to 13%. The impact analyses documented in Section 5.1 and 5.2 had a maximum compression of the shoulder of 0.012 inch.

Thus during an 31 foot MCO to MCO drop and impact the impacted shield plug seal would compress a maximum of 0.030 inch.

The plastic compression could be decreased by making the square 0.25 steel shoulder of higher yield or hardened material. But it would also be necessary to harden the both surfaces on the bottom of the shield plug and the top of the seal ledge to control the seal compression.

ICF KAISER HANFORD

DESIGN ANALYSIS

Calc. No.
Revision
Page No.

Client Westinghouse Hanford Company	WO/Job No. E50471/LE016/F7L7A1	
Subject Evaluation of Compression Preload Bolts for The MCO to MCO Impact	Date August 15, 1996	By Carleton J. Moore
	Checked	By Larry L. Hyde
Location 100K, K-Basins	Revised	By

8.0 Evaluation of the 8 Compression Preload Bolts

The axial loads during the three impact simulations were evaluated. The finite element quarter model simulation included compression preload bolts modeled with ideal beam elements connected directly to the lifting ring brick element solid mesh. The symmetry of the meshes that have been used on this project are such that it simulated twelve bolts. Although there has been some discussion of increasing the number of compression preload bolts, at this time the design is really only 8 bolts. The bolts interface with the shield plug through contact nodes on the bolt ends and a contact surface on the shield plug shoulder.

A maximum compressive force per bolt of 26,400 lbf was found in searching through the saved restart files (restart written every 0.003 second of simulation). This number must be factored up for 8 bolts giving a maximum bolt force of 39,600 lbf. This maximum force was from the simulation documented in Section 5.2.

An evaluation of the thread stresses was made using the reference, "Machine Design Theory and Practice", by Deutschman, Michels, and Wilson, page 809. The mechanical closure MCO design drawings show the bolts to be 1" 8UNC with 2.5 inches of mated threads.

The bolt thread maximum shear stress in the lifting ring was calculated to be 10,000 psi. The maximum bolt thread shear stress was 12,000 psi. The maximum thread bearing stress was calculated to be 8,900 psi.

Again the forces were in compression at the maximum for a very short time. The numbers can change some with a variation in bolt and tapped hole tolerances, but these stress levels are not close to material failure. Also, these impact simulations are accident conditions not design operational load conditions.

APPENDIX E

MATERIAL PROPERTIES USED FOR THERMAL-HYDRAULIC ANALYSES

This page intentionally left blank.

Density of Uranium at Room Temperature

Uranium Alloy No.	Minimum Density		Average Density	
	(g/cc)	(lb/in^3)	(g/cc)	(lb/in^3)
501	18.88	0.682	18.96	0.685
601	18.77	0.678	18.82	0.680
301	18.82	0.680		
503	18.80	0.679		
801	18.76	0.678		

Theoretical Density of Uranium

Phase	Temperature (°C)	Density (g/cm³)
α	25	19.070
	662	18.369
β	662	18.17
	675	18.15
	700	18.13
	725	18.11
	750	18.09
	772	18.07
γ	772	17.94
	800	17.91
	850	17.85
	900	17.79
	950	17.73
	1000	17.67
	1050	17.62
	1100	17.56

Thermal Conductivity of Uranium

Phase	Temperature (°C)	Thermal Conductivity[a] (W/m-°K)
α	27	27
	100	27
	200	29
	300	31
	400	33
	500	35
	600	38
	650	39
	666	39.1
β	666	39.1
	700	40
	750	41
	776	41.6
γ	776	41.6
	800	42.3
	850	43.4
	900	44.6

[a]Thermal conductivity is sensitive to purity and structure. The values in this table probably may vary by ± 20%.

Specific Heat, Enthalpy, and Entropy of Uranium

Phase	Temperature (°C)	Specific Heat (J/kg-°K)	Enthalpy (J/kg)	Entropy (J/kg-°K)
α	27	116.9	2.706×10^4	211.9
	127	124.3	3.873×10^4	245.1
	227	133.7	5.160×10^4	274.3
	327	144.6	6.549×10^4	299.8
	427	157.4	8.057×10^4	323.2
	527	173.4	9.704×10^4	345.4
	627	195.3	1.154×10^5	367.1
	668	206.3	1.242×10^5	376.8
β	668	178.4	1.361×10^5	389.4
	727	178.4	1.466×10^5	400.1
	774	178.4	1.550×10^5	408.5
γ	774	160.8	1.749×10^5	427.5
	827	160.8	1.834×10^5	435.3
	927	161.7	1.995×10^5	446.2
	1027	161.7	2.155×10^5	459.2
	1102	161.7	2.285×10^5	471.1

Emissivity (the ratio of radiant energy actually transferred to that transferred from a blackbody) for uranium is as follows:

Thermal Emissivity of Uranium

Form of Uranium	Emissivity
Unoxidized Uranium Metal	0.54
Molten Uranium	0.34
Oxide Coated Uranium Metal	0.30

Uranium Allotropic Transformation Temperatures

Phase Change	Average Temperature	
	°C	°F
$\alpha \rightarrow \beta$	662-666	1225-1231
$\beta \rightarrow \gamma$	770-776	1418-1429
$\gamma \rightarrow$ Liquid	1130-1033	2066-1891
Boiling Point	3700-4200	6692-7592

Enthalpy, or Heat Content, for Uranium Transformations

Phase Change	Enthalpy	
	(g-cal/g)	(Btu/lb)
$\propto \rightarrow \beta$	2.83	5.10
$\beta \rightarrow \gamma$	4.75	8.55
$\gamma \rightarrow$ Liquid (melting)	19.7	35.5
Liquid $\rightarrow$ gas (vaporization)	448	806

Zircaloy Alloy Concentrations

Alloying Element	Weight % of Alloy Element	
	Zr-2	Zr-4
Tin	1.20-1.70	1.20-1.70
Iron	0.07-0.20	0.18-0.24
Chromium	0.05-0.15	0.07-0.13
Nickel	0.03-0.08	0.007 Max.
Total Fe+Cr+Ni	0.18-0.38	0.28-0.37

Reported Densities of Zirconium and Zircaloys

Temperature			Density			
			Zirconium		Zr-2 and Zr-4	
Phase	°C	°F	(g/cc)	(lb/in^3)	(g/cc)	(lb/in^3)
∝	20	68	6.51	0.235	6.55	0.237
	862	1584	6.39	0.231		
β	862	1584	6.44	0.233		

Theoretical Density of Zirconium and Zircaloys

Phase	Temperature (°C)	Zirconium (g/cm^3)	Zr-2 and Zr-4 (g/cm^3)
α	25	6.51	6.55
	50	6.507	6.547
	100	6.501	6.541
	200	6.488	6.528
	300	6.474	6.513
	400	6.458	6.498
	500	6.442	6.481
	600	6.424	6.464
	862	6.39	
β	862	6.44	

Thermal Conductivity of Zr-2

Temperature (°C)	Thermal Conductivity (W/m-°K)
100	13.39
200	14.50
300	15.60
400	17.01
500	18.41
600	19.90
700	21.50
800	23.10

The specific heat of Zr-2 is approximated by the following linear equations:

Specific Heat of Zr-2

Temperature Range of Applicability (°F)	Specific Heat Equation (BTU/lb-°F)
32 - 1171	$0.06805 + (2.3872 \times 10^{-5})T$
1171 - 1495	$0.08589 + (2.3872 \times 10^{-5})T$
1782 - 1922	$0.08548 + (2.3872 \times 10^{-5})T$

To convert the value for specific heat from U.S. units to S.I. units (J/kg-°C), multiply the result from the specific heat equation by 4,186.8.

Zr-2 and Zr-4 Allotropic Transformation Temperatures

Phase Change	Average Temperature	
	°C	°F
Heating:		
$\beta \rightarrow \alpha + \beta$	815-830	1499-1526
$\alpha + \beta \rightarrow \beta$	975-995	1787-1823
Cooling:		
$\beta \rightarrow \alpha + \beta$	960-930	1760-1706
$\alpha + \beta \rightarrow \beta$	785-770	1445-1418
β Liquid	~1849	~3360

Enthalpy for zirconium transformations is as follows:

Enthalpy or Heat Content of Zr-4

Phase Change	Enthalpy	
	(g-cal/g)	(Btu/lb)
$\alpha \rightarrow \beta$	10.08	18.15
$\beta \rightarrow$ Liquid melting	60.30	108.50
Liquid $\rightarrow$ gas (vaporization)	1558	2805

Emissivity (the ratio of radiant energy actually transferred to that transferred from a blackbody) for zirconium and Zr-2 is as follows:

Thermal Emissivity of Zirconium and Zr-2

Material Type	Temperature Range (°C)	Emissivity
Zirconium	820-840	0.436
	1020-1540	0.426
Zr-2	1200-1750	0.43-0.46

Estimated Density of 304L Stainless Steel

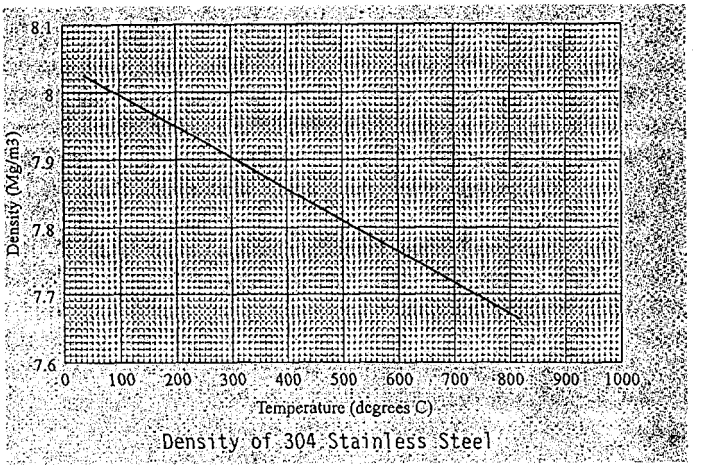

Go to: *[SNF Home]... [TDB Home]... [Change History]... [SNF Bibliography]... [User Comment]... [Help]*

Technical Databook Administrator: Marcy Gore

Last modified on Tuesday, September 12, 1995 16:15:42

The density of 304 Stainless Steel is approximated from the following polynomial equation:

$$\rho = 5.025447 \times 10^{2} - (1.603769 \times 10^{-2})T \qquad [lb/ft^3]$$

where

$T \equiv$ temperature (°F)

To convert the value for density from U.S. units to S.I. units (Mg/m^3), multiply "ρ" by 1.601846×10^{-2}.

Limitations of Use of Equation

The use of this equation is limited to the temperature range 100-1500°F (38-816°C).

Estimated Thermal Conductivity of 304L Stainless Steel

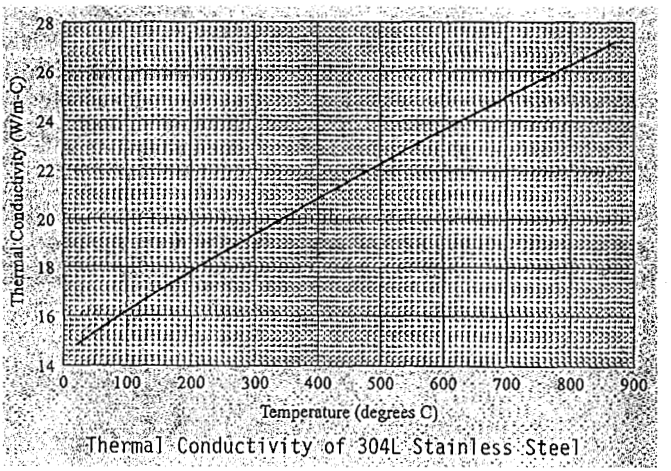

Go to: *[SNF Home]... [TDB Home]... [Change History]... [SNF Bibliography]... [User Comment]... [Help]*

Technical Databook Administrator: Marcy Gore

Last modified on Tuesday, September 12, 1995 16:16:38

The thermal conductivity of 304L Stainless Steel is approximated from the following polynomial equation:

$$k = 8.168027 + (5.845912 \times 10^{-3})T - (1.095476 \times 10^{-6})T^2 + (2.469959 \times 10^{-10})T^3 \quad [BTU/hr\text{-}ft\text{-}^\circ F]$$

where

$T \equiv$ temperature ($^\circ F$)

To convert the value for thermal conductivity from U.S. units to S.I. units (W/m-°C), multiply "k" by 1.729577.

Material Properties of 304 Stainless Steel

Temperature		Thermal Conductivity		Specific Heat	
(°F)	(°C)	(BTU/sec-inch-°F)	(W/m-°K)	(Btu/lbm-°F)	(J/kg-°K)
32	0	0.000179	13.38	0.120	502
70	21	0.000198	14.80	0.109	456
100	38	0.000202	15.10	0.111	464
200	93	0.000215	16.07	0.116	485
400	204	0.000239	17.86	0.125	523
600	316	0.000262	19.58	0.130	544
800	427	0.000284	21.23	0.135	565
1200	649	0.000325	24.29	0.040	586
1400	760	0.000344	25.71	0.145	607
1500	816	0.000354	26.46	0.149	623
1600	871	0.000364	27.20	0.151	632

Estimated Specific Heat of 304L Stainless Steel

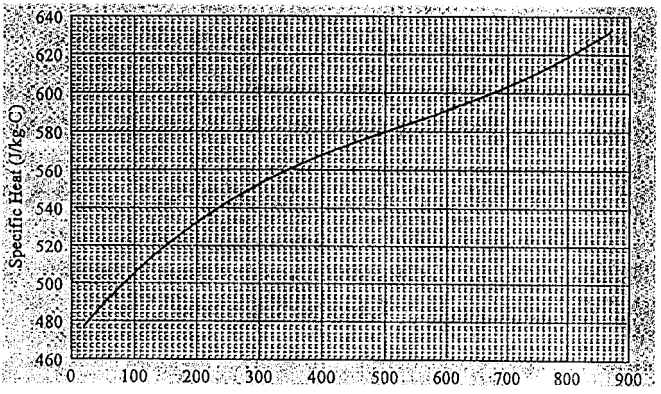

The specific heat of 304L Stainless Steel is approximated from the following polynomial equation:

$$c = 1.102380\times10^{-1} + (5.750184\times10^{-5})T - (4.189060\times10^{-8})T^2 + (1.369815\times10^{-11})T^3 \quad [BTU/lb\text{-}°F]$$

where

$T \equiv$ temperature (°F)

To convert the value for specific heat from U.S. units to S.I. units (J/kg-°C), multiply "c" by 4.186800×10^3.

Estimated Thermal Emissivity of Type 300 Stainless Steels

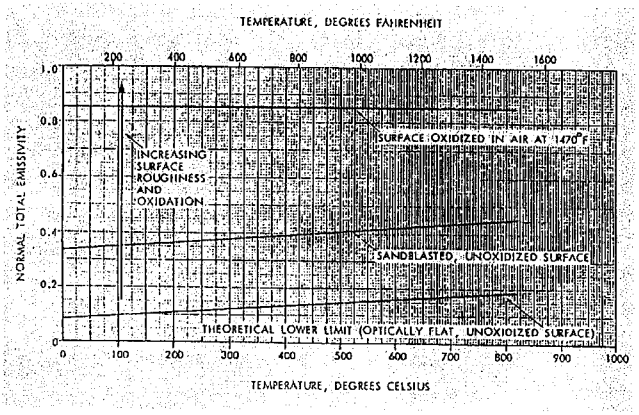

Go to: *[SNF Home]... [TDB Home]... [Change History]... [SNF Bibliography]... [User Comment]... [Help]*

Technical Databook Administrator: Marcy Gore

Last modified on Tuesday, September 12, 1995 16:25:28

Density of Air

The density of air is approximated by the following equation:

$\rho = 38.6438/(T+460)$ [lb/ft^3]

where

T = temperature (°F)

To convert the value for density from U.S. units to S.I. units (Mg/m^3), multiply "ρ" by 1.601846×10^{-2}.

Specific Heat of Air

Temperature		Specific Heat		Temperature		Specific Heat	
(°K)	(°R)	(Btu/lb-°R)	(J/kg-°K)	(°K)	(°R)	(Btu/lb-°R)	(J/kg-°K)
255	460	0.2402	1,005.67	544	980	0.2481	1,038.75
266	480	0.2402	1,005.67	555	1,000	0.2487	1,041.26
277	500	0.2402	1,005.67	566	1,020	0.2493	1,043.77
289	520	0.2403	1,006.09	577	1,040	0.2499	1,046.28
300	540	0.2403	1,006.09	589	1,060	0.2505	1,048.79
311	560	0.2405	1,006.93	600	1,080	0.2511	1,051.31
322	580	0.2406	1,007.34	611	1,100	0.2517	1,053.82
333	600	0.2408	1,008.18	622	1,120	0.2523	1,056.33
344	620	0.2409	1,008.60	633	1,140	0.253	1,059.26
355	640	0.2412	1,009.86	644	1,160	0.2536	1,061.77
366	660	0.2414	1,010.69	655	1,180	0.2542	1,064.28
377	680	0.2417	1,011.95	666	1,200	0.2549	1,067.22
389	700	0.2419	1,012.79	677	1,220	0.2555	1,069.73
400	720	0.2422	1,014.04	689	1,240	0.2561	1,072.24
411	740	0.2426	1,015.72	700	1,260	0.2568	1,075.17
422	760	0.2429	1,016.97	711	1,280	0.2574	1,077.68
433	780	0.2433	1,018.65	722	1,300	0.2580	1,080.19
444	800	0.2437	1,020.32	733	1,320	0.2587	1,083.13
455	820	0.2441	1,022.00	744	1,340	0.2593	1,085.64
466	840	0.2445	1,023.67	755	1,360	0.2600	1,088.57
477	860	0.2450	1,025.77	766	1,380	0.2606	1,091.08
489	880	0.2455	1,027.86	777	1,400	0.2612	1,093.59
500	900	0.2460	1,029.95	789	1,420	0.2618	1,096.10
511	920	0.2465	1,032.05	800	1,440	0.2625	1,099.04
522	940	0.247	1,034.14	811	1,460	0.2631	1,101.55
533	960	0.2476	1,036.65	866	1,560	0.2660	1,113.69

Thermal Conductivity of Air

Temperature		Thermal Conductivity		Temperature		Thermal Conductivity	
(°K)	(°R)	(W/m-°K)	(Btu/hr-ft-°R)	(°K)	(°R)	(W/m-°K)	(Btu/hr-ft-°R)
90	162	0.00830	0.004799	460	828	0.03697	0.02138
100	180	0.00922	0.005331	470	846	0.03761	0.02175
110	198	0.01015	0.005868	480	864	0.03825	0.02212
120	216	0.01106	0.006395	490	882	0.03880	0.02243
130	234	0.01197	0.006921	500	900	0.03951	0.02284
140	252	0.01287	0.007441	510	918	0.04020	0.02324
150	270	0.01375	0.007950	520	936	0.04080	0.02359
160	288	0.01463	0.008459	530	954	0.04140	0.02394
170	306	0.01550	0.008962	540	972	0.04200	0.02428
180	324	0.01637	0.009465	550	990	0.04260	0.02463
190	342	0.01723	0.009962	560	1,008	0.04320	0.02498
200	360	0.01810	0.01047	570	1,026	0.04380	0.02532
210	378	0.01895	0.01096	580	1,044	0.04440	0.02567
220	396	0.01980	0.01145	590	1,062	0.04500	0.02602
230	414	0.02063	0.01193	600	1,080	0.04560	0.02636
240	432	0.02145	0.01240	610	1,098	0.04620	0.02671
250	450	0.02226	0.01287	620	1,116	0.04680	0.02706
260	468	0.02305	0.01333	630	1,134	0.04730	0.02735
270	486	0.02384	0.01378	640	1,152	0.04790	0.02769
280	504	0.02461	0.01423	650	1,170	0.04840	0.02798
290	522	0.02538	0.01467	660	1,188	0.04900	0.02833
300	540	0.02614	0.01511	670	1,206	0.04960	0.02868
310	558	0.02687	0.01554	680	1,224	0.05010	0.02897
320	576	0.02759	0.01595	690	1,242	0.05070	0.02931
330	594	0.02830	0.01636	700	1,260	0.05130	0.02966
340	612	0.02900	0.01677	710	1,278	0.05180	0.02995
350	630	0.02970	0.01717	720	1,296	0.05240	0.03030
360	648	0.03039	0.01757	730	1,314	0.05300	0.03064
370	666	0.03107	0.01796	740	1,332	0.05350	0.03093
380	684	0.03173	0.01835	750	1,350	0.05410	0.03128
390	702	0.03239	0.01873	760	1,368	0.05460	0.03157
400	720	0.03305	0.01911	770	1,386	0.05520	0.03192
410	738	0.03371	0.01949	780	1,404	0.05580	0.03226
420	756	0.03437	0.01987	790	1,422	0.05630	0.03255
430	774	0.03503	0.02025	800	1,440	0.05690	0.03290
440	792	0.03568	0.02063	810	1,458	0.05750	0.03325
450	810	0.03633	0.02101	820	1,476	0.05800	0.03353

Thermal Conductivity of Air (contd)

Temperature		Thermal Conductivity	
(°K)	(°R)	(W/m-°K)	(Btu/hr-ft-°R)
830	1,494	0.05860	0.03388
840	1,512	0.05920	0.03423
850	1,530	0.0597	0.03452
860	1,548	0.0603	0.03486
870	1,566	0.0608	0.03515
880	1,584	0.0614	0.03550
890	1,602	0.0619	0.03579
900	1,620	0.0625	0.03614
910	1,638	0.0630	0.03643
920	1,656	0.0635	0.03671
930	1,674	0.0639	0.03695
940	1,692	0.0644	0.03723
950	1,710	0.0649	0.03752
960	1,728	0.0654	0.03781
970	1,746	0.0658	0.03804
980	1,764	0.0663	0.03833
990	1,782	0.0668	0.03862
1,000	1,800	0.0672	0.03885
1,010	1,818	0.0677	0.03914
1,020	1,836	0.0682	0.03943
1,030	1,854	0.0686	0.03966
1,040	1,872	0.0691	0.03995
1,050	1,890	0.0695	0.04018
1,060	1,908	0.0699	0.04041
1,070	1,926	0.0704	0.04070
1,080	1,944	0.0708	0.04093
1,090	1,962	0.0713	0.04122
1,100	1,980	0.0717	0.04146
1,110	1,998	0.0721	0.04169
1,120	2,016	0.0726	0.04198
1,130	2,034	0.0730	0.04221
1,140	2,052	0.0734	0.04244
1,150	2,070	0.0738	0.04267
1,160	2,088	0.0743	0.04296
1,170	2,106	0.0747	0.04319
1,180	2,124	0.0751	0.04342
1,190	2,142	0.0755	0.04365
1,200	2,160	0.0759	0.04388
1,210	2,178	0.0763	0.04411
1,220	2,196	0.0767	0.04435
1,230	2,214	0.0771	0.04458
1,240	2,232	0.0775	0.04481
1,250	2,250	0.0779	0.04504
1,260	2,268	0.0782	0.04521
1,270	2,286	0.0786	0.04544
1,280	2,304	0.0790	0.04568
1,290	2,322	0.0784	0.04533
1,300	2,340	0.0797	0.04608
1,310	2,358	0.0801	0.04631
1,320	2,376	0.0805	0.04654
1,330	2,394	0.0809	0.04677
1,340	2,412	0.0813	0.04701
1,350	2,430	0.0816	0.04718
1,360	2,448	0.0820	0.04741
1,370	2,466	0.0824	0.04764
1,380	2,484	0.0827	0.04782
1,390	2,502	0.0831	0.04805
1,400	2,520	0.0835	0.04828
1,410	2,538	0.0838	0.04845
1,420	2,556	0.0842	0.04868
1,430	2,574	0.0846	0.04891
1,440	2,592	0.0849	0.04909
1,450	2,610	0.0853	0.04932
1,460	2,628	0.0856	0.04949
1,470	2,646	0.0860	0.04972
1,480	2,664	0.0863	0.04990
1,490	2,682	0.0867	0.05013
1,500	2,700	0.0870	0.05030

Data Quality

The estimated accuracy on this data is as follows:

90 to 400°K = 1%
400 to 1500°K = 5%

Dynamic Viscosity (Absolute) of Air

Temperature		Viscosity		Temperature		Viscosity	
(°K)	(°R)	(10^{-6} Pa-s)	(10^{-7} lb-s/ft^2)	(°K)	(°R)	(10^{-6} Pa-s)	(10^{-7} lb-s/ft^2)
80	144	5.52	1.152	450	810	24.93	5.203
90	162	6.35	1.325	460	828	25.32	5.284
100	180	7.06	1.473	470	846	25.70	5.363
110	198	7.75	1.617	480	864	26.07	5.441
120	216	8.43	1.759	490	882	26.45	5.520
130	234	9.09	1.897	500	900	26.82	5.597
140	252	9.74	2.033	510	918	27.18	5.672
150	270	10.38	2.166	520	936	27.54	5.747
160	288	11.00	2.296	530	954	27.90	5.823
170	306	11.61	2.423	540	972	28.25	5.896
180	324	12.20	2.546	550	990	28.60	5.969
190	342	12.79	2.669	560	1,008	28.95	6.042
200	360	13.36	2.788	570	1,026	29.29	6.113
210	378	13.92	2.905	580	1,044	29.69	6.196
220	396	14.47	3.020	590	1,062	29.97	6.255
230	414	15.01	3.133	600	1,080	30.30	6.323
240	432	15.54	3.243	610	1,098	30.63	6.392
250	450	16.06	3.352	620	1,116	30.96	6.461
260	468	16.57	3.458	630	1,134	31.28	6.528
270	486	17.07	3.562	640	1,152	31.61	6.597
280	504	17.57	3.667	650	1,170	31.93	6.664
290	522	18.05	3.767	660	1,188	32.24	6.728
300	540	18.53	3.867	670	1,206	32.56	6.795
310	558	19.00	3.965	680	1,224	32.87	6.860
320	576	19.46	4.061	690	1,242	33.18	6.924
330	594	19.92	4.157	700	1,260	33.49	6.989
340	612	20.37	4.251	710	1,278	33.79	7.052
350	630	20.81	4.343	720	1,296	34.09	7.114
360	648	21.25	4.435	730	1,314	34.39	7.177
370	666	21.68	4.525	740	1,332	34.69	7.240
380	684	22.11	4.614	750	1,350	34.98	7.300
390	702	22.52	4.700	760	1,368	35.28	7.363
400	720	22.94	4.787	770	1,386	35.57	7.423
410	738	23.35	4.873	780	1,404	35.86	7.484
420	756	23.75	4.957	790	1,422	36.16	7.546
430	774	24.15	5.040	800	1,440	36.43	7.603
440	792	24.54	5.121	810	1,458	36.72	7.663

Dynamic Viscosity (Absolute) of Air (contd)

Temperature		Viscosity	
(°K)	(°R)	(10^{-6} Pa-s)	(10^{-7} lb-s/ft^2)
820	1,476	36.99	7.720
830	1,494	37.27	7.778
840	1,512	37.55	7.836
850	1,530	37.83	7.895
860	1,548	38.10	7.951
870	1,566	38.37	8.008
880	1,584	38.64	8.064
890	1,602	38.91	8.120
900	1,620	39.18	8.177
910	1,638	39.45	8.233
920	1,656	39.71	8.287
930	1,674	39.97	8.342
940	1,692	40.23	8.396
950	1,710	40.49	8.450
960	1,728	40.75	8.504
970	1,746	41.00	8.556
980	1,764	41.26	8.611
990	1,782	41.52	8.665
1,000	1,800	41.77	8.717
1,050	1,890	43.0	8.974
1,100	1,980	44.2	9.224
1,150	2,070	45.4	9.475
1,200	2,160	46.5	9.704
1,250	2,250	47.7	9.955
1,300	2,340	48.8	10.184
1,350	2,430	49.9	10.414
1,400	2,520	50.9	10.623
1,450	2,610	51.9	10.831
1,500	2,700	53.0	11.061
1,550	2,790	54.0	11.270
1,600	2,880	54.9	11.457
1,650	2,970	55.9	11.666
1,700	3,060	56.9	11.875
1,750	3,150	57.8	12.063
1,800	3,240	58.7	12.250
1,850	3,330	59.6	12.438
1,900	3,420	60.5	12.626
1,950	3,510	61.4	12.814
2,000	3,600	62.3	13.002

Data Quality

The estimated accuracy on this data is 2% over the entire temperature range.

Specific Heat of Helium at 1 Atm

Temperature (°K)	Specific Heat (J/kg-°K)
173	5,188
273	5,188
298	5,188
322	5,188
373	5,188
473	5,188
773	5,188
1,473	5,188

Thermal Conductivity of Helium at 1 Atm

Temperature		Thermal Conductivity	
(°K)	(°R)	(W/m-°K)	(Btu/hr-ft-°R)
100	180	0.073	0.0422
110	198	0.0776	0.0449
120	216	0.0819	0.0474
130	234	0.0863	0.0499
140	252	0.0907	0.0524
150	270	0.095	0.0549
160	288	0.0992	0.0574
170	306	0.1033	0.0597
180	324	0.1072	0.062
190	342	0.1112	0.0643
200	360	0.1151	0.0665
210	378	0.119	0.0688
220	396	0.1228	0.0710
230	414	0.1266	0.0732
240	432	0.1304	0.0754
250	450	0.1338	0.0774
260	468	0.1372	0.0793
270	486	0.1405	0.0812
280	504	0.1437	0.0831
290	522	0.1468	0.0849
300	540	0.1499	0.0867
310	558	0.1530	0.0885
320	576	0.1560	0.0902
330	594	0.1590	0.0919
340	612	0.1619	0.0936
350	630	0.1649	0.0953
360	648	0.1678	0.097
370	666	0.1708	0.0988
380	684	0.1737	0.1004
390	702	0.1766	0.1021
400	720	0.1795	0.1038
410	738	0.1824	0.1055
420	756	0.1853	0.1071
430	774	0.1882	0.1088
440	792	0.1914	0.1107
450	810	0.1947	0.1126
460	828	0.1980	0.1145
470	846	0.2013	0.1164
480	864	0.2046	0.1183
490	882	0.2080	0.1203
500	900	0.2114	0.1222
510	918	0.215	0.1243
520	936	0.218	0.126
530	954	0.222	0.1284

Temperature		Thermal Conductivity	
(°K)	(°R)	(W/m-°K)	(Btu/hr-ft-°R)
540	972	0.225	0.1301
550	990	0.229	0.1324
560	1,008	0.233	0.1347
570	1,026	0.236	0.1364
580	1,044	0.240	0.1388
590	1,062	0.243	0.1405
600	1,080	0.247	0.1428
610	1,098	0.251	0.1451
620	1,116	0.254	0.1469
630	1,134	0.258	0.1492
640	1,152	0.261	0.1509
650	1,170	0.264	0.1526
660	1,188	0.267	0.1544
670	1,206	0.269	0.1555
680	1,224	0.272	0.1573
690	1,242	0.275	0.159
700	1,260	0.278	0.1607
710	1,278	0.281	0.1625
720	1,296	0.254	0.1642
730	1,314	0.287	0.1659
740	1,332	0.29	0.1676
750	1,350	0.292	0.1688
760	1,368	0.295	0.1706
770	1,386	0.298	0.1723
780	1,404	0.301	0.174
790	1,422	0.304	0.1758
800	1,440	0.307	0.1775
810	1,458	0.309	0.1787
820	1,476	0.312	0.1804
830	1,494	0.315	0.1821
840	1,512	0.318	0.1839
850	1,530	0.321	0.186
860	1,548	0.323	0.187
870	1,566	0.326	0.188
880	1,584	0.329	0.19
890	1,602	0.332	0.192
900	1,620	0.335	0.194
910	1,638	0.337	0.195
920	1,656	0.34	0.197
930	1,674	0.343	0.198
940	1,692	0.346	0.2
950	1,710	0.349	0.202
960	1,728	0.352	0.204
970	1,746	0.354	0.205

Thermal Conductivity of Helium at 1 Atm (contd)

Temperature		Thermal Conductivity		Temperature		Thermal Conductivity	
(°K)	(°R)	(W/m-°K)	(Btu/hr-ft-°R)	(°K)	(°R)	(W/m-°K)	(Btu/hr-ft-°R)
980	1,764	0.357	0.206	1,800	3,240	0.57	0.33
990	1,782	0.36	0.208	1,900	3,420	0.596	0.345
1,000	1,800	0.363	0.21	2,000	3,600	0.62	0.358
1,100	1,980	0.389	0.225	2,500	4,500	0.739	0.427
1,200	2,160	0.416	0.24	3,000	5,400	0.851	0.492
1,300	2,340	0.443	0.256	3,500	6,300	0.958	0.554
1,400	2,520	0.469	0.271	4,000	7,200	1.064	0.615
1,500	2,700	0.494	0.286	4,500	8,100	1.169	0.676
1,600	2,880	0.521	0.301	5,000	9,000	1.271	0.735
1,700	3,060	0.545	0.315				

Data Quality

The estimated accuracy on this data is as follows:

100 to 340°K = 5%
340 to 1900°K = 10%
1900 to 5000°K = 25%

Dynamic Viscosity (Absolute) of Helium

Temperature		Viscosity		Temperature		Viscosity	
(°K)	(°R)	(10^{-6} Pa-s)	(10^{-6} lb_f-s/ft^2)	(°K)	(°R)	(10^{-6} Pa-s)	(10^{-6} lb_f-s/ft^2)
100	180	9.63	0.2011	600	1,080	31.99	0.6681
120	216	10.75	0.2245	620	1,116	32.71	0.6832
140	252	11.81	0.2467	640	1,152	33.42	0.6980
160	288	12.87	0.2688	660	1,188	34.11	0.7124
180	324	13.93	0.2909	680	1,224	34.81	0.7270
200	360	14.97	0.3127	700	1,260	35.49	0.7412
220	396	16.00	0.3342	720	1,296	36.18	0.7556
240	432	17	0.3350	740	1,332	36.85	0.7696
260	468	17.99	0.3757	760	1,368	37.52	0.7836
280	504	18.95	0.3958	780	1,404	38.19	0.7976
300	540	19.89	0.4154	800	1,440	38.84	0.8112
320	576	20.81	0.4347	850	1,530	40.44	0.8446
340	612	21.70	0.4532	900	1,620	42.01	0.8774
360	648	22.58	0.4716	1,000	1,800	45.04	0.9407
380	684	23.44	0.4896	1,100	1,980	48.0	1.0025
400	720	24.28	0.5071	1,200	2,160	50.8	1.0610
420	756	25.10	0.5242	1,300	2,340	53.5	1.1174
440	792	25.92	0.5414	1,400	2,520	56.1	1.1717
460	828	26.71	0.5578	1,500	2,700	58.6	1.2239
480	864	27.50	0.5743	1,600	2,880	61.0	2.2740
500	900	28.27	0.5904	1,700	3,060	63.4	1.3241
520	936	29.03	0.6063	1,800	3,240	65.7	1.3722
540	972	29.78	0.6220	2,000	3,600	70.0	1.4620
560	1,008	30.53	0.6376	2,200	3,960	74.2	1.5497
580	1,044	31.27	0.6531	2,400	4,320	78.3	1.6353

Data Quality

The estimated accuracy on this data is as follows:

100 to 300°K = 3%
300 to 2400°K = 1%

Specific Heat of Nitrogen at 1 Atm

Temperature		Specific Heat	
(°K)	(°R)	(J/kg-°K)	(Btu/lb - °R)
255	459	1,040	0.2484
300	539	1,040	0.2485
350	629	1,041	0.2487
400	719	1,045	0.2495
450	809	1,050	0.2507
500	899	1,057	0.2524
550	989	1,065	0.2544
600	1,079	1,075	0.2568
650	1,169	1,086	0.2593
700	1,259	1,098	0.2622
750	1,349	1,110	0.2652
800	1,439	1,122	0.2680
850	1,529	1,134	0.2710
900	1,619	1,146	0.2737
950	1,709	1,157	0.2764
1,000	1,799	1,168	0.2790
1,050	1,889	1,178	0.2814
1,100	1,979	1,187	0.2836
1,150	2,069	1,196	0.2857
1,200	2,159	1,205	0.2877
1,250	2,249	1,213	0.2896
1,300	2,339	1,220	0.2913
1,350	2,429	1,227	0.2931
1,366	2,459	1,229	0.2935

Data Quality

The estimated accuracy on this data is 0.6%.

Thermal Conductivity of Nitrogen at 1 Atm

Temperature		Thermal Conductivity		Temperature		Thermal Conductivity	
(°K)	(°R)	(W/m-°K)	(Btu/hr-ft-°R)	(°K)	(°R)	(W/m-°K)	(Btu/hr-ft-°R)
80	144	0.00762	0.00441	500	900	0.03864	0.02234
90	162	0.00852	0.00493	520	936	0.0398	0.02301
100	180	0.00941	0.00544	540	972	0.0408	0.02359
110	198	0.0103	0.00596	560	1,008	0.042	0.02428
120	216	0.01119	0.00647	580	1,044	0.0431	0.02492
130	234	0.01208	0.00698	600	1,080	0.0441	0.02550
140	252	0.01296	0.00749	620	1,116	0.0452	0.02613
150	270	0.01385	0.00801	640	1,152	0.0462	0.02671
160	288	0.01474	0.00852	660	1,188	0.0472	0.02729
170	306	0.01562	0.00903	680	1,224	0.0483	0.02793
180	324	0.01651	0.00955	700	1,260	0.0493	0.0285
190	342	0.01739	0.01005	720	1,296	0.0503	0.0291
200	360	0.01826	0.01062	740	1,332	0.0513	0.0297
210	378	0.01908	0.01103	760	1,368	0.0522	0.0302
220	396	0.01989	0.0115	780	1,404	0.0531	0.0307
230	414	0.02067	0.01195	800	1,440	0.0541	0.0313
240	432	0.02145	0.0124	820	1,476	0.0551	0.0318
250	450	0.02222	0.01285	840	1,512	0.0559	0.0323
260	468	0.02298	0.01329	860	1,548	0.0569	0.0329
270	486	0.02374	0.01373	880	1,584	0.0578	0.0334
280	504	0.02449	0.01416	900	1,620	0.0587	0.0339
290	522	0.02524	0.01459	920	1,656	0.0596	0.0345
300	540	0.02589	0.01497	940	1,692	0.0605	0.035
310	558	0.02761	0.01544	960	1,728	0.0613	0.0354
320	576	0.02741	0.01585	980	1,764	0.0622	0.036
330	594	0.02808	0.01624	1,000	1,800	0.0631	0.0365
340	612	0.02874	0.01662	1,050	1,890	0.0651	0.0376
350	630	0.02939	0.01699	1,100	1,980	0.0672	0.0388
360	648	0.03002	0.01736	1,150	2,070	0.0693	0.0401
370	666	0.03065	0.01772	1,200	2,160	0.0713	0.0412
380	684	0.03127	0.01808	1,250	2,250	0.0733	0.424
390	702	0.03189	0.01844	1,300	2,340	0.0754	0.0436
400	720	0.03252	0.0188	1,350	2,430	0.0775	0.0448
420	756	0.03376	0.01952	1,400	2,520	0.0797	0.0461
440	792	0.03501	0.02024	1,450	2,610	0.0819	0.0474
460	828	0.03626	0.02096	1,500	2,700	0.0842	0.0487
480	864	0.03749	0.02168	1,600	2,880	0.0893	0.0516

Thermal Conductivity of Nitrogen at 1 Atm (contd)

Temperature		Thermal Conductivity		Temperature		Thermal Conductivity	
(°K)	(°R)	(W/m-°K)	(Btu/hr-ft-°R)	(°K)	(°R)	(W/m-°K)	(Btu/hr-ft-°R)
1,700	3,060	0.0950	0.0549	2,700	4,860	0.1494	0.0864
1,800	3,240	0.1013	0.0586	2,800	5,040	0.1542	0.0892
1,900	3,420	0.108	0.0624	2,900	5,220	0.1590	0.0919
2,000	3,600	0.1146	0.0662	3,000	5,400	0.1640	0.0948
2,100	3,780	0.1207	0.0698	3,100	5,580	0.1691	0.0978
2,200	3,960	0.1263	0.0730	3,200	5,760	0.1743	0.1008
2,300	4,140	0.1314	0.0760	3,300	5,940	0.1795	0.1038
2,400	4,320	0.1361	0.0787	3,400	6,120	0.1853	0.1071
2,500	4,500	0.1406	0.0813	3,500	6,300	0.1915	0.1107
2,600	4,680	0.1449	0.0838				

Data Quality

The estimated accuracy on this data is as follows:

80 to 350°K = 2%
350 to 1200°K = 5%
1200 to 3500°K = 10%

Dynamic Viscosity (Absolute) of Nitrogen

Temperature		Viscosity		Temperature		Viscosity	
(°K)	(°R)	(10^{-6} Pa-s)	(10^{-6} lb_f-s/ft²)	(°K)	(°R)	(10^{-6} Pa-s)	(10^{-6} lb_f-s/ft²)
80	144	5.59	0.1167	600	1,080	29.27	0.6113
100	180	6.87	0.1435	620	1,116	29.91	0.6247
120	216	8.15	0.1702	640	1,152	30.54	0.6378
140	252	9.4	0.1963	660	1,188	31.15	0.6506
160	288	10.59	0.2212	680	1,224	31.76	0.6633
180	324	11.75	0.2454	700	1,260	32.35	0.6756
200	360	12.86	0.2686	750	1,350	33.8	0.7059
220	396	13.93	0.2909	800	1,440	35.2	0.7352
240	432	14.96	0.3124	850	1,530	36.55	0.7634
260	468	15.96	0.3333	900	1,620	37.86	0.7907
280	504	16.92	0.3534	950	1,710	39.12	0.817
300	540	17.86	0.3730	1,000	1,800	40.36	0.8429
320	576	18.77	0.3920	1,050	1,890	41.6	0.8688
340	612	19.65	0.4104	1,100	1,980	42.7	0.8918
360	648	20.5	0.4282	1,150	2,070	43.9	0.9169
380	684	21.33	0.4455	1,200	2,160	45.0	0.9398
400	720	22.14	0.4624	1,250	2,250	46.1	0.9628
420	756	22.93	0.4789	1,300	2,340	47.1	0.9837
440	792	23.7	0.4950	1,350	2,430	48.2	1.0067
460	828	24.0	0.5012	1,400	2,520	49.2	1.0276
480	864	25.18	0.5259	1,500	2,700	51.2	1.0693
500	900	25.9	0.5409	1,600	2,880	53.1	1.1090
520	936	26.6	0.5556	1,700	3,060	54.9	1.1466
540	972	27.29	0.5700	1,800	3,240	56.7	1.1842
560	1,008	27.96	0.5840	1,900	3,420	58.5	1.2218
580	1,044	28.63	0.5979	2,000	3,600	60.1	1.2552
				2,200	3,960	63.4	1.3241

Data Quality

The estimated accuracy on this data is 2%.

Specific Heat of Argon at 1 Atm

Temperature		Specific Heat	
(°K)	(°R)	(J/kg-°K)	(Btu/lb - °R)
99	179	542.9	0.1297
150	269	527.3	0.1260
200	359	523.6	0.1251
250	449	522.2	0.1247
300	539	521.5	0.1246
350	629	521.2	0.1245
400	719	521.0	0.1244
450	809	520.9	0.1244
500	899	520.8	0.1244
550	989	520.7	0.1244
600	1,079	520.6	0.1243
650	1,169	520.6	0.1243
700	1,259	520.5	0.1243
750	1,349	520.5	0.1243
800	1,439	520.5	0.1243
850	1,529	520.5	0.1243
900	1,619	520.5	0.1243
950	1,709	520.5	0.1243
1,000	1,799	520.5	0.1243
1,050	1,889	520.5	0.1243
1,100	1,979	520.5	0.1243
1,150	2,069	520.5	0.1243
1,200	2,159	520.5	0.1243
1,250	2,249	520.4	0.1243
1,300	2,339	520.4	0.1243
1,350	2,429	520.4	0.1243
1,366	2,459	520.4	0.1243

Thermal Conductivity of Argon at 1 Atm

Temperature		Thermal Conductivity	
(°K)	(°R)	(W/m-°K)	(Btu/hr-ft-°R)
100	180	0.00652	0.00377
110	198	0.00716	0.00414
120	216	0.00779	0.00450
130	234	0.00839	0.00485
140	252	0.00898	0.00519
150	270	0.00957	0.00553
160	288	0.01016	0.00587
170	306	0.01074	0.00621
180	324	0.01131	0.00654
190	342	0.01188	0.00687
200	360	0.01244	0.00719
210	378	0.013	0.00752
220	396	0.01355	0.00783
230	414	0.01409	0.00815
240	432	0.01462	0.00845
250	450	0.01515	0.00876
260	468	0.01567	0.00906
270	486	0.01619	0.00936
280	504	0.01671	0.00966
290	522	0.01722	0.00996
300	540	0.01772	0.01024
310	558	0.01822	0.01053
320	576	0.01871	0.01082
330	594	0.01919	0.01110
340	612	0.01966	0.01137
350	630	0.02013	0.01164
360	648	0.02059	0.0119
370	666	0.02103	0.01216
380	684	0.02147	0.01241
390	702	0.0219	0.01266
400	720	0.02233	0.01291
420	756	0.02318	0.01340
440	792	0.02400	0.01388
460	828	0.02481	0.01434
480	864	0.02559	0.01480
500	900	0.02638	0.01525
520	936	0.0272	0.01573
540	972	0.0280	0.01619

Temperature		Thermal Conductivity	
(°K)	(°R)	(W/m-°K)	(Btu/hr-ft-°R)
560	1,008	0.0287	0.01659
580	1,044	0.0294	0.01700
600	1,080	0.0301	0.0174
620	1,116	0.0308	0.0178
640	1,152	0.0315	0.0182
660	1,188	0.0322	0.0186
680	1,224	0.0329	0.0190
700	1,260	0.0336	0.0194
720	1,296	0.0343	0.0198
740	1,332	0.0349	0.0202
760	1,368	0.0356	0.0206
780	1,404	0.0362	0.0209
800	1,440	0.0369	0.0213
820	1,476	0.0375	0.0217
840	1,512	0.0381	0.0220
860	1,548	0.0387	0.0224
880	1,584	0.0393	0.0227
900	1,620	0.0398	0.0230
920	1,656	0.0404	0.0234
940	1,692	0.0410	0.0237
960	1,728	0.0416	0.024
980	1,764	0.0421	0.0243
1,000	1,800	0.0427	0.0247
1,050	1,890	0.0441	0.0255
1,100	1,980	0.0454	0.0262
1,150	2,070	0.0468	0.0271
1,200	2,160	0.0481	0.0278
1,250	2,250	0.0495	0.0286
1,300	2,340	0.0508	0.0294
1,350	2,430	0.0521	0.0301
1,400	2,520	0.0535	0.0309
1,450	2,610	0.0548	0.0317
1,500	2,700	0.0561	0.0324
1,600	2,880	0.0588	0.0340
1,700	3,060	0.0615	0.0356
1,800	3,240	0.0641	0.0371
1,900	3,420	0.0667	0.0386
2,000	3,600	0.0692	0.0400

Data Quality

The estimated accuracy on this data is as follows:

100 to 340°K = 1%
340 to 740°K = 5%
740 to 2000°K = 10%

Dynamic Viscosity (Absolute) of Argon

Temperature		Viscosity		Temperature		Viscosity	
(°K)	(°R)	(10^{-6} Pa-s)	(10^{-6} lb_f-s/ft^2)	(°K)	(°R)	(10^{-6} Pa-s)	(10^{-6} lb_f-s/ft^2)
60	108	5.34	0.1115	500	900	33.6	0.7028
80	144	6.83	0.1426	550	990	36.0	0.7519
100	180	8.34	0.1742	600	1,080	38.3	0.7999
120	216	9.91	0.2070	650	1,170	40.4	0.8438
140	252	11.49	0.2400	700	1,260	42.5	0.8876
160	288	13.04	0.2723	750	1,350	44.5	0.9294
180	324	14.55	0.3039	800	1,440	46.4	0.9691
200	360	16.01	0.3344	850	1,530	48.3	1.0088
220	396	17.44	0.3642	900	1,620	50.1	1.0464
240	432	18.82	0.3931	950	1,710	51.8	1.0819
260	468	20.16	0.4210	1,000	1,800	53.5	1.1174
280	504	21.45	0.4480	1,100	1,980	56.8	1.1863
300	540	22.72	0.4745	1,200	2,160	59.9	1.251
320	576	23.94	0.5000	1,300	2,340	62.8	1.3116
340	612	25.13	0.5248	1,400	2,520	65.6	1.3701
360	648	26.29	0.5491	1,500	2,700	68.4	1.4286
380	684	27.42	0.5727	1,600	2,880	71.0	1.4829
400	720	28.52	0.5956	1,700	3,060	73.5	1.5351
420	756	29.59	0.6180	1,800	3,240	76.0	1.5873
440	792	30.64	0.6399	1,900	3,420	78.4	1.6374
460	828	31.67	0.6614	2,000	3,600	80.7	1.6855
480	864	32.67	0.6823	2,200	3,960	85.1	1.7773

Data Quality

The estimated accuracy on this data is 2% over the entire temperature range.

Thermal Conductivity of Hydrogen

Temperature		Thermal Conductivity	
(°K)	(°R)	(W/m-°K)	(Btu/hr-ft-°R)
100	180	0.0676	0.03908
110	198	0.0738	0.04267
120	216	0.0801	0.04631
130	234	0.0864	0.04995
140	252	0.0926	0.05354
150	270	0.0986	0.05701
160	288	0.1046	0.06048
170	306	0.1105	0.06389
180	324	0.1164	0.06730
190	342	0.1222	0.07065
200	360	0.1280	0.07401
210	378	0.1338	0.07738
220	396	0.1395	0.08066
230	414	0.1451	0.08389
240	432	0.1506	0.08707
250	450	0.1560	0.09020
260	468	0.1613	0.09326
270	486	0.1665	0.09627
280	504	0.1717	0.09927
290	522	0.1767	0.10216
300	540	0.1815	0.10494
310	558	0.1863	0.10771
320	576	0.1910	0.11043
330	594	0.1954	0.11298
340	612	0.1994	0.11529
350	630	0.2033	0.11754
360	648	0.2069	0.11962
370	666	0.2106	0.12176
380	684	0.2142	0.12385
390	702	0.2177	0.12587
400	720	0.2212	0.12789
410	738	0.2248	0.12997
420	756	0.2283	0.13200
430	774	0.2318	0.13402

Temperature		Thermal Conductivity	
(°K)	(°R)	(W/m-°K)	(Btu/hr-ft-°R)
440	792	0.2354	0.13610
450	810	0.2389	0.13813
460	828	0.2424	0.14015
470	846	0.2459	0.14217
480	864	0.2494	0.14420
490	882	0.2529	0.14622
500	900	0.2564	0.14824
510	918	0.2600	0.15033
520	936	0.2640	0.15264
530	954	0.2670	0.15437
540	972	0.2700	0.15611
550	990	0.2740	0.15842
560	1,008	0.2770	0.16015
570	1,026	0.2800	0.16189
580	1,044	0.2840	0.16420
590	1,062	0.2880	0.16651
600	1,080	0.2910	0.16825
610	1,098	0.2950	0.17056
620	1,116	0.2980	0.17230
630	1,134	0.3010	0.17403
640	1,152	0.3060	0.17692
650	1,170	0.3080	0.17808
660	1,188	0.3120	0.18039
670	1,206	0.3150	0.18213
680	1,224	0.3190	0.18444
690	1,242	0.3220	0.18617
700	1,260	0.3250	0.18791
710	1,278	0.3290	0.19022
720	1,296	0.3320	0.19195
730	1,314	0.3360	0.19427
740	1,332	0.3390	0.19600
750	1,350	0.3430	0.19831
760	1,368	0.3460	0.20005
770	1,386	0.3500	0.20236

Thermal Conductivity of Hydrogen (contd)

Temperature		Thermal Conductivity		Temperature		Thermal Conductivity	
(°K)	(°R)	(W/m-°K)	(Btu/hr-ft-°R)	(°K)	(°R)	(W/m-°K)	(Btu/hr-ft-°R)
780	1,404	0.3530	0.20410	1,170	2,106	0.4850	0.28042
790	1,422	0.3560	0.20583	1,180	2,124	0.4880	0.28215
800	1,440	0.3600	0.20814	1,190	2,142	0.4920	0.28446
810	1,458	0.3630	0.20988	1,200	2,160	0.4950	0.28620
820	1,476	0.3670	0.21219	1,210	2,178	0.4980	0.28793
830	1,494	0.3700	0.21393	1,220	2,196	0.5020	0.29024
840	1,512	0.3740	0.21624	1,230	2,214	0.5050	0.29198
850	1,530	0.3770	0.21797	1,240	2,232	0.5080	0.29371
860	1,548	0.3800	0.21971	1,250	2,250	0.5120	0.29603
870	1,566	0.3840	0.22202	1,260	2,268	0.5150	0.29776
880	1,584	0.3870	0.22375	1,270	2,286	0.5180	0.29950
890	1,602	0.3910	0.22607	1,280	2,304	0.5210	0.30123
900	1,620	0.3940	0.22780	1,290	2,322	0.5250	0.30354
910	1,638	0.3970	0.22954	1,300	2,340	0.5280	0.30528
920	1,656	0.4010	0.23185	1,310	2,358	0.5310	0.30701
930	1,674	0.4040	0.23358	1,320	2,376	0.5350	0.30932
940	1,692	0.4080	0.23590	1,330	2,394	0.5380	0.31106
950	1,710	0.4110	0.23763	1,340	2,412	0.5410	0.31279
960	1,728	0.4140	0.23936	1,350	2,430	0.5450	0.31511
970	1,746	0.4180	0.24168	1,360	2,448	0.5490	0.31742
980	1,764	0.4210	0.24341	1,370	2,466	0.5520	0.31915
990	1,782	0.4250	0.24572	1,380	2,484	0.5550	0.32089
1,000	1,800	0.4280	0.24746	1,390	2,502	0.5590	0.32320
1,010	1,818	0.4310	0.24919	1,400	2,520	0.5620	0.32493
1,020	1,836	0.4350	0.25151	1,410	2,538	0.5650	0.32667
1,030	1,854	0.4380	0.25324	1,420	2,556	0.5690	0.32898
1,040	1,872	0.4420	0.25555	1,430	2,574	0.5720	0.33072
1,050	1,890	0.4450	0.25729	1,440	2,592	0.5760	0.33303
1,060	1,908	0.4480	0.25902	1,450	2,610	0.5790	0.33476
1,070	1,926	0.4520	0.26134	1,460	2,628	0.5820	0.33650
1,080	1,944	0.4550	0.26307	1,470	2,646	0.5860	0.33881
1,090	1,962	0.4590	0.26538	1,480	2,664	0.5900	0.34112
1,100	1,980	0.4620	0.26712	1,490	2,682	0.5930	0.34286
1,110	1,998	0.4650	0.26885	1,500	2,700	0.5970	0.34517
1,120	2,016	0.4690	0.27116	1,510	2,718	0.6000	0.34691
1,130	2,034	0.4720	0.27290	1,520	2,736	0.6040	0.34922
1,140	2,052	0.4750	0.27463	1,530	2,754	0.6070	0.35095
1,150	2,070	0.4780	0.27637	1,540	2,772	0.6110	0.35327
1,160	2,088	0.4820	0.27868	1,550	2,790	0.6140	0.35500

Thermal Conductivity of Hydrogen (contd)

Temperature		Thermal Conductivity	
(°K)	(°R)	(W/m-°K)	(Btu/hr-ft-°R)
1,560	2,808	0.6180	0.35731
1,570	2,826	0.6210	0.35905
1,580	2,844	0.6250	0.36136
1,590	2,862	0.6280	0.36309
1,600	2,880	0.6320	0.36541
1,610	2,898	0.6360	0.36772
1,620	2,916	0.6400	0.37003
1,630	2,934	0.6430	0.37177
1,640	2,952	0.6470	0.37408
1,650	2,970	0.6510	0.37639
1,660	2,988	0.6540	0.37813
1,670	3,006	0.6580	0.38044
1,680	3,024	0.6620	0.38275
1,690	3,042	0.6660	0.38507
1,700	3,060	0.6690	0.38680
1,710	3,078	0.6730	0.38911
1,720	3,096	0.6770	0.39143
1,730	3,114	0.6810	0.39374
1,740	3,132	0.6850	0.39605
1,750	3,150	0.6890	0.39836
1,760	3,168	0.6930	0.40068
1,770	3,186	0.6970	0.40299
1,780	3,204	0.7000	0.40472
1,790	3,222	0.7040	0.40704
1,800	3,240	0.7060	0.40819
1,810	3,258	0.7130	0.41224
1,820	3,276	0.7170	0.41455
1,830	3,294	0.7210	0.41686
1,840	3,312	0.7250	0.41918
1,850	3,330	0.7290	0.42149
1,860	3,348	0.7330	0.42380
1,870	3,366	0.7370	0.42612
1,880	3,384	0.7420	0.42901
1,890	3,402	0.7460	0.43132
1,900	3,420	0.7500	0.43363
1,910	3,438	0.7550	0.43652
1,920	3,456	0.7590	0.43884
1,930	3,474	0.7640	0.44173
1,940	3,492	0.7680	0.44404
1,950	3,510	0.7720	0.44635
1,960	3,528	0.7770	0.44924
1,970	3,546	0.7820	0.45213
1,980	3,564	0.7870	0.45502
1,990	3,582	0.7920	0.45792
2,000	3,600	0.7960	0.46023

Data Quality

The estimated accuracy on this data is as follows:

100 to 400°K = 2%
400 to 1350°K = 5%
1350 to 2000°K = 15%

Specific Heat of Oxygen at 1 Atm

Temperature		Specific Heat	
(°K)	(°R)	(J/kg-°K)	(Btu/lb -°R)
255	459	914.0	0.2183
300	539	919.9	0.2197
350	629	929.5	0.2220
400	719	941.6	0.2249
450	809	955.6	0.2282
500	899	971.0	0.2319
550	989	987.0	0.2358
600	1,079	1,003.0	0.2396
650	1,169	1,018.0	0.2432
700	1,259	1,032.0	0.2465
750	1,349	1,044.0	0.2494
800	1,439	1,055.0	0.2519
850	1,529	1,065.0	0.2543
900	1,619	1,074.0	0.2566
950	1,709	1,083.0	0.2587
1,000	1,799	1,091.0	0.2605
1,050	1,889	1,098.0	0.2622
1,100	1,979	1,104.0	0.2637
1,150	2,069	1,110.0	0.2652
1,200	2,159	1,116.0	0.2665
1,250	2,249	1,121.0	0.2678
1,300	2,339	1,126.0	0.2689
1,350	2,429	1,131.0	0.2702
1,366	2,459	1,133.0	0.2705

Data Quality

The estimated accuracy on this data is 1.1%.

Thermal Conductivity of Oxygen at 1 Atm

Temperature		Thermal Conductivity	
(°K)	(°R)	(W/m-°K)	(Btu/hr-ft-°R)
100	180	0.00905	0.00523
110	198	0.00998	0.00577
120	216	0.01092	0.00631
130	234	0.01187	0.00686
140	252	0.01281	0.00741
150	270	0.01376	0.00796
160	288	0.01466	0.00848
170	306	0.01556	0.00900
180	324	0.01646	0.00952
190	342	0.01735	0.01003
200	360	0.01824	0.01055
210	378	0.01911	0.01105
220	396	0.01997	0.01155
230	414	0.02083	0.01204
240	432	0.02168	0.01254
250	450	0.02254	0.01303
260	468	0.02339	0.01352
270	486	0.02424	0.01402
280	504	0.02509	0.01451
290	522	0.02592	0.01499
300	540	0.02674	0.01546
310	558	0.02753	0.01592
320	576	0.02831	0.01637
330	594	0.02907	0.01681
340	612	0.02982	0.01724
350	630	0.03056	0.01767
400	720	0.03420	0.01977
450	810	0.03770	0.02180
500	900	0.04120	0.02382
550	990	0.04470	0.02584
600	1,080	0.04800	0.02775
650	1,170	0.05130	0.02966
700	1,260	0.05440	0.03145
750	1,350	0.05740	0.03319
800	1,440	0.06030	0.03486
850	1,530	0.06320	0.03654
900	1,620	0.06610	0.03822
950	1,710	0.06890	0.03984
1,000	1,800	0.07170	0.04146
1,050	1,890	0.07450	0.04307
1,100	1,980	0.07710	0.04458
1,150	2,070	0.07960	0.04602
1,200	2,160	0.08210	0.04747
1,250	2,250	0.08460	0.04891
1,300	2,340	0.08710	0.05036
1,350	2,430	0.08960	0.05180
1,400	2,520	0.09210	0.05325
1,450	2,610	0.09460	0.05470
1,500	2,700	0.09700	0.05608

Data Quality

The estimated accuracy on this data is as follows:

100 to 340°K = 0.5%
340 to 600°K = 2%
600 to 850°K = 4%
850 to 1500°K = 6%

Dynamic Viscosity (Absolute) of Oxygen

Temperature		Viscosity	
(°K)	(°R)	(10^{-6} Pa-s)	(10^{-6} lb_f-s/ft^2)
80	144	6.27	0.1310
100	180	7.68	0.1604
120	216	9.12	0.1905
140	252	10.56	0.2205
160	288	11.96	0.2498
180	324	13.33	0.2784
200	360	14.65	0.3060
220	396	15.93	0.3327
240	432	17.17	0.3586
260	468	18.37	0.3837
280	504	19.54	0.4081
300	540	20.67	0.4317
320	576	21.77	0.5457
340	612	22.84	0.4770
360	648	23.89	0.4990
380	684	24.91	0.5203
400	720	25.89	0.5407
420	756	26.87	0.5612
440	792	27.82	0.5810
460	828	28.74	0.6002
480	864	29.65	0.6193
500	900	30.54	0.6378
520	936	31.4	0.6558
540	972	32.3	0.6746
560	1,008	33.1	0.6913
580	1,044	33.9	0.7080
600	1,080	34.7	0.7247
620	1,116	35.5	0.7414
640	1,152	36.3	0.7581
660	1,188	37.1	0.7748
680	1,224	37.8	0.7895
700	1,260	38.5	0.8041
750	1,350	40.3	0.8417
800	1,440	42.1	0.8793
850	1,538	43.8	0.9148
900	1,620	45.4	0.9482
950	1,710	47.0	0.9816
1,000	1,800	48.5	1.0129
1,050	1,890	50.0	1.0443
1,100	1,980	51.4	1.0735
1,150	2,070	52.9	1.1048
1,200	2,160	54.2	1.1320
1,250	2,250	55.6	1.1612
1,300	2,340	56.9	1.1884
1,350	2,430	58.2	1.2155
1,400	2,520	59.5	1.2427
1,500	2,700	61.9	1.2928
1,600	2,880	64.3	1.3429
1,700	3,060	66.6	1.3910
1,800	3,240	68.8	1.4369
1,900	3,420	71.0	1.4829
2,000	3,600	73.1	1.5267

Data Quality

The estimated accuracy on this data is 2%.

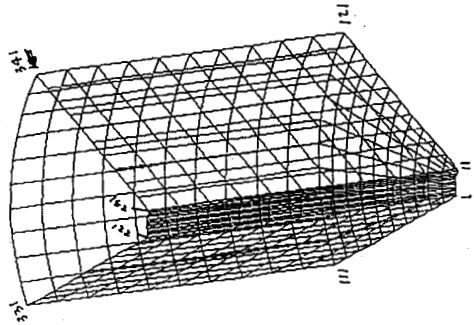

5/21/96
14:46:32

MARK IV SCRAP BASKET — SK-1-80209
Wireframe Plot

IMAGES-3D
Ver. 3.0
Geometry Plot